Macalester College Library
3 0527 02045 6915

WITHDRAWN FROM
MACALESTER COLLEGE
LIBRARY

PROGRESS IN LOW TEMPERATURE PHYSICS

II

SERIES IN PHYSICS

General Editors:

J. DE BOER, Professor of Physics, University of Amsterdam
H. BRINKMAN, Professor of Physics, University of Groningen
H. B. G. CASIMIR, Director of the Philips Laboratories, Eindhoven

Monographs:

B. BAK, Elementary Introduction to Molecular Spectra
H. C. BRINKMAN, Application of Spinor Invariants in Atomic Physics
W. ELENBAAS, The High Pressure Mercury Vapour Discharge
S. R. DE GROOT, Thermodynamics of Irreversible Processes
E. A. GUGGENHEIM, Thermodynamics
E. A. GUGGENHEIM, Boltzmann's Distribution Law
E. A. GUGGENHEIM and J. E. PRUE, Physicochemical Calculations
E. G. RICHARDSON, Relaxation Spectrometry
L. ROSENFELD, Nuclear Forces
L. ROSENFELD, Theory of Electrons
J. L. SYNGE, Relativity: The Special Theory
H. UMEZAWA, Quantum Field Theory

Edited Volumes:

J. BOUMAN (editor), Selected Topics in X-Ray Crystallography
J. M. BURGERS and H. C. VAN DE HULST (editors), Gas Dynamics of Cosmic Clouds. A Symposium
C. J. GORTER (editor), Progress in Low Temperature Physics. Volume I–II
Z. KOPAL (editor), Astronomical Optics and Related Subjects
K. SIEGBAHN (editor), Beta- and Gamma-Ray Spectroscopy
J. G. WILSON (editor), Progress in Cosmic Ray Physics. Volume I–II–III

PROGRESS IN LOW TEMPERATURE PHYSICS

EDITED BY

C. J. GORTER
Professor of Experimental Physics
Director of the Kamerlingh Onnes Laboratory, Leiden

VOLUME II

1957

NORTH-HOLLAND PUBLISHING COMPANY
AMSTERDAM

OLIN
QC 278
G6
v.2

Sole distributors for U.S.A.
Interscience Publishers Inc., New York

Printed in the Netherlands

PREFACE

The first volume of this book was largely devoted to three main fields of low temperature research: liquid helium, superconductivity and magnetism; and the announcement was made that some of the neglected subjects might be covered in a second volume.

In the present second volume due attention has been given again to the same main fields, and in particular different aspects of the problems of liquid helium have been considered. But also several other subjects have been reviewed here, such as various non-magnetic properties of solids.

No claim on completeness can be made, however. Important fields lacking are the cryogenic techniques and the magnetic resonances, for which it is possible to consult several other recent books and review papers.

C. J. Gorter

CONTENTS

Chapter Page

I J. DE BOER, Quantum effects and exchange effects on the thermodynamic properties of liquid helium 1

1. Introduction, 1. – 2. Liquid helium at zero absolute temperature, 11. – 3. Collective excitations, 25. – 4. Molecular excitations. – Order-disorder theory, 28. – 4a. Order-disorder theory, 29. – 4b. Fluctuation theory, 35. – 4c. Cell-theory, 35. – 4d. Other theories, 54.

II H. C. KRAMERS, Liquid helium below 1° K 59

1. Introduction, 59. – 2. Techniques, 60. – 3. The theory of elementary excitations and the two-fluid model, 61. – 4. Experiments on static and reversible properties, 65. – 5. Dissipative effects, 70. – 6. Large mean free path phenomena, 77. – 7. Miscellaneous experiments, 80.

III P. WINKEL and D. H. N. WANSINK, Transport phenomena of liquid helium II in slits and capillaries 83

1. Introduction, 83. – 2. The fountain effect and the mechanocaloric effect, 87. – 3. The frictional forces, 90. – 3.1. Isothermal flow, 91. – 3.2. Non-isothermal flow, with and without resulting flow of matter, 95. – 3.3. Conclusions, 100.

IV K. R. ATKINS, Helium films 105

1. Introduction, 105. – 2. Experimental difficulties, 108. – 3. Measurements of the thickness of the saturated film, 110. – 4. Unsaturated films, 113. – 5. The flow of the saturated film, 118. – 6. The flow of unsaturated films, 126. – 7. Theories of the formation of the film, 130.

V B. T. MATTHIAS, Superconductivity in the periodic system 138

1. Introduction, 138. – 2. The elements, 138. – 3. Alloys and compounds, 141. – 4. Transition temperatures, 141. – 5. Compounds, 145. – 6. The β–W structure, 148. – 7. Comparison of different crystal structures, 150.

VI E. H. SONDHEIMER, Electron transport phenomena in metals 151

1. Introduction, 151. – 2. The Bloch theory, 152. – 3. The matrix element for electron-phonon scattering, 164. – 4. The steady state of the lattice, 169. – 5. Special topics, 177.

VII V. A. JOHNSON and K. LARK–HOROVITZ, Semiconductors at low temperatures 187

1. Introduction, 187. – 2. Resonance phenomena, 189. – 3. Elec-

Page

trical measurements, 197. – 4. Thermal properties, 290. – 5. Optical properties, 216.

VIII D. SHOENBERG, The de haas–van alphen effect 226

1. Introduction, 226. – 2. Theory, 230. – 3. Comparison of theory with experiment, 238. – 4. Experimental methods, 245. – 5. Survey of the results for individual metals, 256.

IX C. J. GORTER, Paramagnetic relaxation 266

1. Introduction, 266. – 2. Description of the spin-lattice relaxation with the Casimir–Du Pré formulae, 271. – 3. Relaxation at very low temperatures, 274. – 4. Relaxation in the spin system, 279.

X M. J. STEENLAND and H. A. TOLHOEK, Orientation of atomic nuclei at low temperatures 292

1. Theoretical results on nuclear effects with oriented nuclei, 292. – 2. Methods for orienting nuclei, 301. – 3. Description of experiments and results, 316. – Discussion of possible further developments, 331.

XI C. DOMB and J. S. DUGDALE, Solid helium 338

Part I, 338. – 1. Introduction, 338. – 2. General thermodynamic properties of solid He^4, 340. – Thermal conductivity of solid helium, 346. – 4. Melting curve and melting parameters of He^4, 349. – 5. Melting parameters and general properties of solid He^3, 355. – *Part II*, 356. – Theoretical aspects, 356.

XII F. H. SPEDDING, S. LEGVOLD, A. H. DAANE and L. D. JENNINGS, Some physical properties of the rare earth metals 368

1. Introduction, 368. – 2. Lanthanum, 373. – 3. Cerium, 375. – 4. Praseodymium, 378. – 5. Neodymium, 378. – 6. Samarium, 380. – 7. Europium, 380. – 8. Gadolinium, 382. – 9. Terbium, 382. – 10. Dysprosium, 383. – 11. Holmium, 385. – 12. Erbium, 387. – 13. Thulium, 389. – 14. Ytterbium, 391. – 15. Lutetium, 391. – 16. Summary, 391.

XIII D. BIJL, The representation of specific heat and thermal expansion data of simple solids. 395

1. Introduction, 395. – 2. Solids at low temperatures, 397. – 3. The continuum (Debye) model, 399. – 4. Solids at high temperatures, 400. – 5. Methods of representing specific heat data, 403. – 6. Experimental data on the specific heat, 410. – 7. Discussion, 418. – 8. The representation of thermal expansion data, 422. – 9. Discussion, 426.

Page

XIV H. VAN DIJK and M. DURIEUX, The temperature scale in the liquid helium region 431

1. Introduction, 431. – 2. Thermodynamic pT-relation, 432. – 3. First measurements with the gas thermometer, 1908–1915, 433. – 4. The 1924-scale, 435. – 5. Use of the hot-wire manometer, 435. – 6. Measurements of 1927, 1928 and 1929, 437. – 7. Measurements of 1937, 440. – 8. The 1929- and the 1932-Scale, 443. – 9. The 1937- and the 1939-scale, 443. – 10. The 1948-scale, 445. – 11. Measurements of Kistemaker and Keesom, 445. – 12. Magnetic temperatures, 446. – 13. Confirmation of Kistemaker's results, 447. – 14. Measurements of Keller on helium isotherms, 451. – 15. pT-relation of Clement, Logan and Gaffney, 452. – 16. The temperature scale above 4.2° K, 452. – 17. Modification of the pT-relation of Clement *et al.*, 453. – 18. Accurate vapour pressure measurements of Ambler and Hudson, 454. – 19. Thermodynamic pT-relation. historical remarks, 456. – 20. Numerical calculation of the different terms in the pT-relation, 456. – 21. Calculation of the heat of vaporization, 458. – 22. Extension of the scale to the critical point, 460. – 23. The T_{L55}-scale, 462.

CHAPTER I

QUANTUM EFFECTS AND EXCHANGE EFFECTS ON THE THERMODYNAMIC PROPERTIES OF LIQUID HELIUM

BY

J. DE BOER

INSTITUTE FOR THEORETICAL PHYSICS, UNIVERSITY OF AMSTERDAM

CONTENTS: 1. Introduction, 1. — 2. Liquid helium at zero absolute temperature, 11. — 3. Collective excitations, 25. — 4. Molecular excitations — Order-disorder theory, 28. — 4a. Order-disorder theory, 29. — 4b. Fluctuation theory, 35. — 4c. Cell-theory, 35. — 4d. Other theories, 54.

1. Introduction

The influence which the quantum effects and in particular the exchange effects have on the equilibrium properties of liquid helium has been the object of a considerable number of theoretical investigations. In the beautiful and systematic exposition which the late F. London, in his book Superfluids II, gave on the whole subject of liquid helium, the exchange effects play an important role. Recent developments, however, have given new insight into this field and make it possible in some respects to obtain a better understanding of the influence of the exchange effects on the properties of liquid helium. It is for this reason that it may be justified to make this the object of a more detailed discussion. Recent theoretical survey articles in the same field are that of R. P. Feynman in Progress in Low Temperature Physics, vol. I, and of I. Prigogine [1] to which articles we shall refer later on in this chapter.

a) Intermolecular Potential Field

The point of view taken in this chapter is the molecular point of view, i.e. it will be attempted to give the considerations as far as possible a quantitative character, by basing them on the known interaction between helium atoms and trying to explain the experimental behaviour in terms of the parameters characterising the interaction between helium atoms.

The potential field of the intermolecular forces between helium atoms will be represented by the formula:

$$\varphi(r) = 4\varepsilon\{(\sigma/r)^{12} - (\sigma/r)^{6}\} \qquad (1)$$

The constants ε and σ have been obtained from the values of the second virial coefficient of the equation of state at low densities,

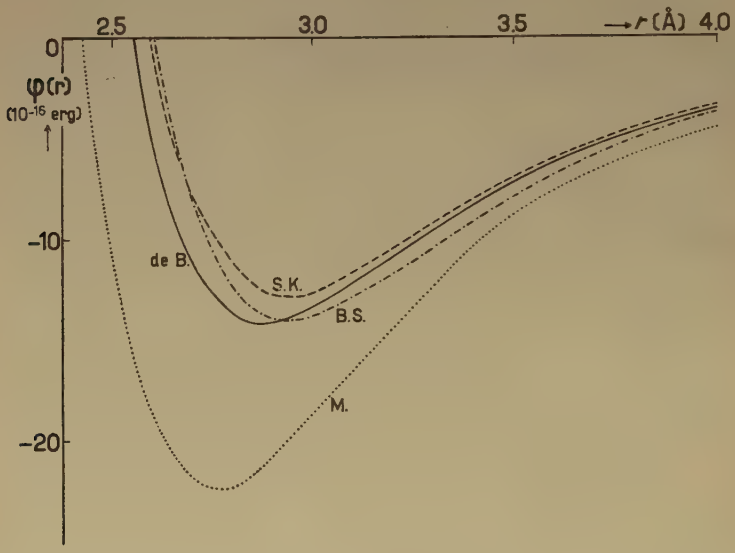

Fig. 1. Interaction potential of two helium atoms
Curve S.K: Theoretical curve calculated by Slater and Kirkwood
Curve M: Corrected curve from Margenau
Curve de B: Semi-experimental curve used by the author (Eq. (1))
Curve B.S: Semi-experimental curve obtained by Buckingham and Scriven.

which can be represented with the help of this expression in the temperature range from 200 – 300° C down to the lowest temperatures of a few °K where measurements have been made. The same expression gives also a satisfactory explanation of the second virial coefficient of ^{3}He gas and of the heat conductivity and viscosity of both the helium isotopes (see Vol. I, Ch. XIV for a survey article on this subject).

The values obtained for the constants are given in the table:

TABLE I

Constants of intermolecular field of helium:

$N\sigma^3 = 10.06$ cm^3/mole	$\varepsilon = 14.11 \quad 10^{-16}$ erg
$\varepsilon/k = 10.22$ °K	$\sigma = 2.556$ Å
$\varepsilon/\sigma^3 = 83.4$ atm.	$^4\mathrm{He}: \Lambda^* = \dfrac{h}{\sigma\sqrt{m\varepsilon}} = 2.68$
$N\varepsilon = 20.31$ cal/mole	
$= 84.9$ J/mole	$^3\mathrm{He}: \Lambda^* = \dfrac{h}{\sigma\sqrt{m\varepsilon}} = 3.08$

The values in the first column are directly derived from the experimental data or are obtained by using the value of R. The values in the second column are obtained from those of the first by using the present values of N, k, h, $m_{^4\mathrm{He}}$ and $m_{^3\mathrm{He}}$.

In the application of this potential field it is implicitly assumed that the intermolecular forces are additive. The justification for this assumption might be found in the fact that when a similar potential field is used in the case of the other noble gases Ne, A, Kr and Xe, in this case the *same field* can be used both in the dilute gas and in the solid state, where the number of nearest neighbours is even as large as 12: the potential field which fits the second virial coefficient gives a quite accurate description of the condensed state. We may assume therefore that the additivity assumption most probably will be also a reasonable working hypothesis in the case of liquid helium.

b) The Quantum Parameter

The small mass of the helium atoms and the small interatomic forces make helium a substance which is of the utmost interest for our insight into the effects of quantum theory of the thermodynamic properties. The small mass leads to a large de Broglie wavelength h/mkT, and the small interaction energy ε has the result that helium "has not much power to offer resistance" against the quantum effects. This finds its expression in the value of the quantum mechanical parameter $\Lambda^* = \Lambda/\sigma = (h/\sqrt{m\varepsilon})/\sigma = h/\sigma\sqrt{m\varepsilon}$, which has the physical meaning of being the ratio of the de Broglie wavelength for relative motion of two helium atoms with energy ε and the "diameter" σ of the atoms. It is clear that when $\Lambda^* = \Lambda/\sigma \ll 1$ one may expect that quantum effects are negligible, but that when $\Lambda^* = \Lambda/\sigma$ becomes of the order of magnitude 1 or larger, the quantum effects will play a

predominant role. From Table II, in which the values of Λ^* for the most important substances are given, it is clear that ^{4}He and ^{3}He must play a most exceptional role in this field.

TABLE II

Values of the quantum mechanical parameter

Substance	Λ^*	Substance	Λ^*
^{3}He	3.08	Ne	0.593
^{4}He	2.68	A	0.186
H_2	1.73	Kr	0.102
D_2	1.22	Xe	0.064

For the study of the quantum effects in general, but in particular also to appreciate the role which exchange effects play, it is important to consider very briefly the possibilities of the *quantum mechanical principle of corresponding states* [2]. When one assumes that the properties of the substances mentioned in Table II can be described on the basis of a potential field of the type (1), it follows from direct dimensional considerations that the partition function Z, which is a dimensionless quantity, *can* only be a function of the dimensionless "reduced" quantities i.e. the quantities expressed in the "molecular" units given in table 1: $T^* = T/(\varepsilon/k) = kT/\varepsilon$; $V^* = V/N\sigma^3$ and $\Lambda^* = \Lambda/\sigma$. This function should then, of course, be the same for all substances, however it may be different in the case of Fermi–Dirac (antisymmetrical wave functions) and Bose–Einstein (symmetrical wavefunctions) statistics. Thus

$$Z = f_{\text{B.E.}}(T^*, V, \Lambda^*) \text{ or } Z = f_{\text{F.D.}}(T^*, V^*, \Lambda^*). \tag{2}$$

Consequently the same holds for all the dimensionless quantities which can be obtained from the partition function: the reduced pressure $p^* = p\sigma^3/\varepsilon$, the reduced entropy $S^* = S/R$, the reduced energy $U^*/N\varepsilon$ as a function of V^*, T^* and Λ^* and also for characteristic temperatures, energies or volumes.

c) Quantum Effects and Symmetry Effects

This principle of corresponding states now offers an interesting tool for the empirical investigation of the quantum effects and for obtaining information about the relative importance of the symmetry effects: If symmetry effects are relatively unimportant for a property

of liquid He one may expect a smooth variation of this quantity as a function of Λ^* in particular for ^{4}He and ^{3}He. If, however, strong anomalies exist this might be an indication that the symmetry effects play an important role for that particular quantity.

We now first consider some properties which show a smooth variation as function of Λ^* and which therefore most probably are not influenced very much by the symmetry effects:

(1) The molar internal energy at temperature zero under zero pressure,

(2) The molar volume at temperature zero under zero pressure,

(3) The critical temperature,

and which are apparently not influenced very much by the exchange effects.

Molar Volume and Energy. In Fig. 2 and Fig. 3 we have plotted

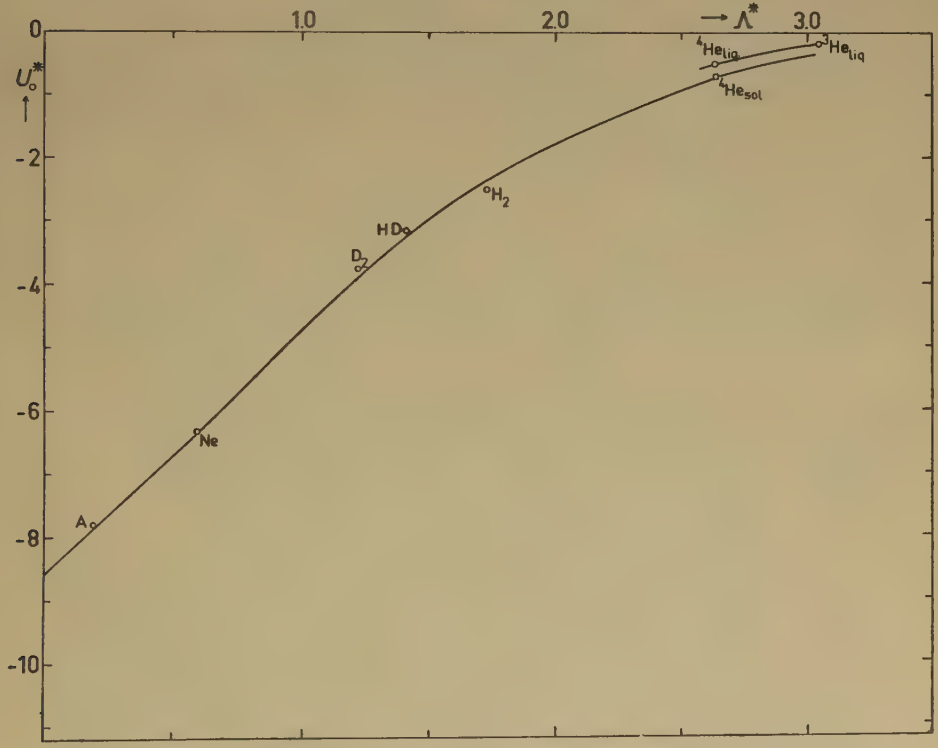

Fig. 2. Reduced value of the internal energy at the absolute zero of temperature under zero pressure as a function of the quantum mechanical parameter Λ^*.

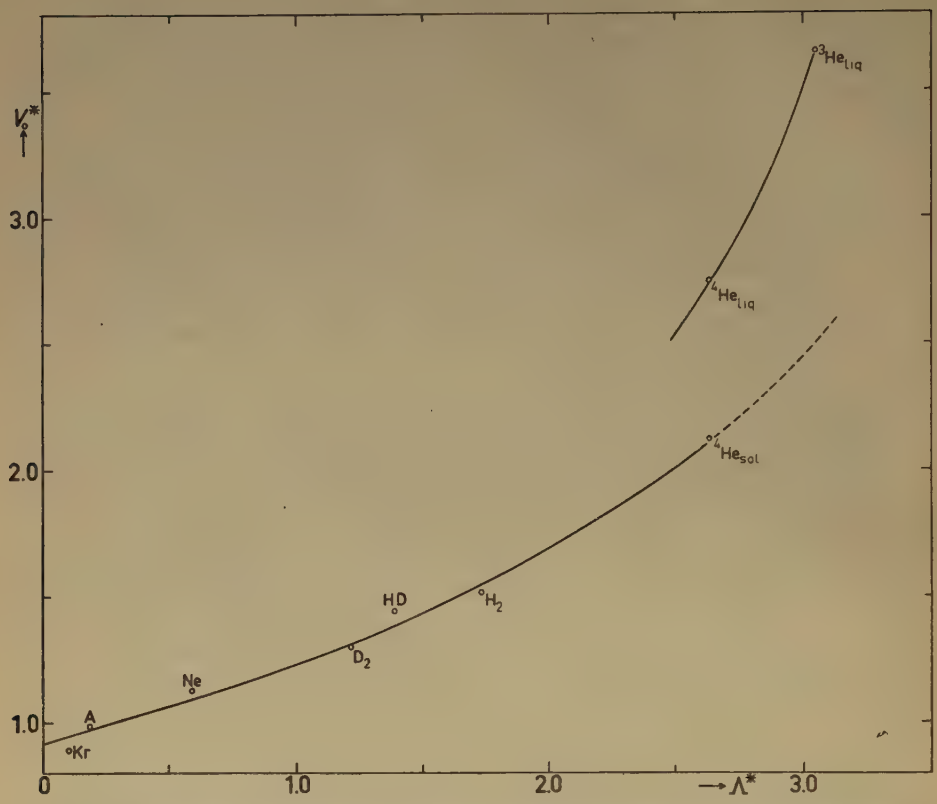

Fig. 3. Reduced value of the molar volume at the absolute zero of temperature under zero pressure as a function of the quantum mechanical parameter Λ^*.

the *internal energy and the molar volume* of different substances as a function of Λ^*. The fact that a rather smooth curve can be drawn through these points shows that at least in a first approximation the influence of the exchange effects is not very large. Some points need, however, more careful attention.

The principle of corresponding states assumes implicitly that e.g. in the solid state the "structure" is the same for all substances. Most probably all the noble gases crystallize in the close packed structure. This seems to be true also for the solid phase of helium, which can be realized under pressure (see J. S. Dugdale and F. E. Simon [3] and § 2.c). Helium at the absolute zero under zero pressure, however, has a structure with a very much smaller coordination number (4 to 6 instead of 12), which in principle makes liquid helium not very well

comparable to the other substances. In Fig. 2 and 3 we have therefore drawn separately the curves corresponding to the internal energy and volume of liquid helium at zero temperature. The fact that the curves are smooth functions of Λ^* suggests that for these properties the symmetry effects are not important.

Critical Temperature. In Fig. 4 we have plotted the reduced *critical temperature* as a function of Λ^*, showing that also in this case

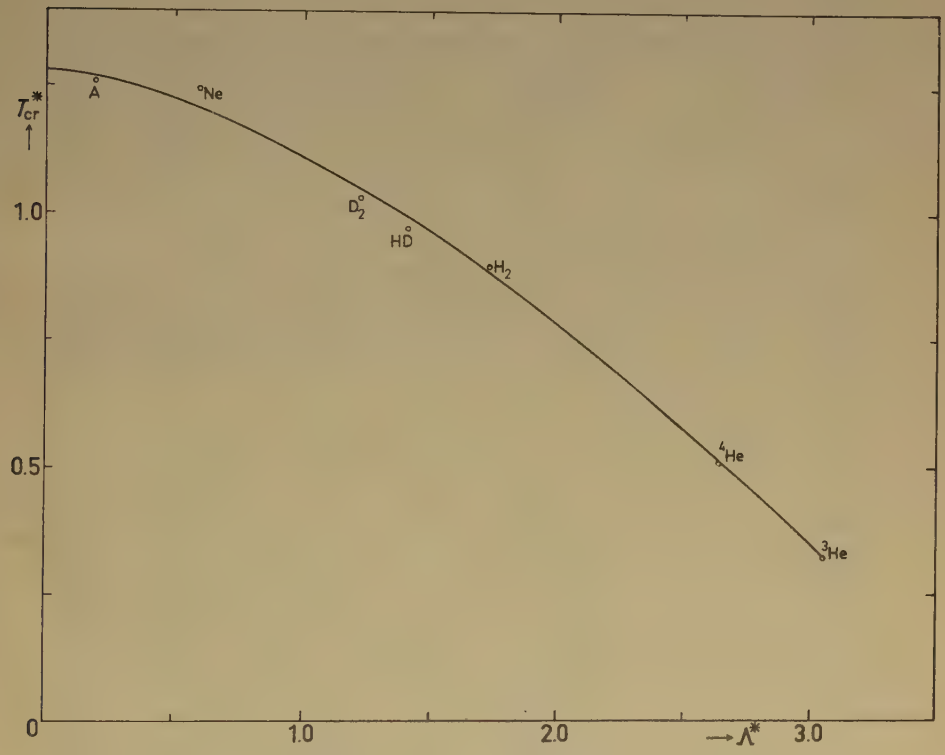

Fig. 4. Reduced critical temperatures as a function of Λ^*.

a smooth curve is obtained with no strong deviations in the case of liquid helium. It was even the assumption *that* this curve was a smooth curve, which made possible the approximate determination of the critical temperature of liquid ^{3}He before this could be measured [4].

In those thermodynamic properties which are more directly related to the *thermal motion of the molecules*, such as:

(1) the heat capacity and the entropy,
(2) the thermal expansion coefficient,

the deviations from the corresponding states-principle are larger and most probably here the exchange effects play a predominant role.

Heat Capacity. In liquid ^{4}He the most striking thermal effect is the *λ-transition* at 2.19° K. Below this temperature the *heat capacity*

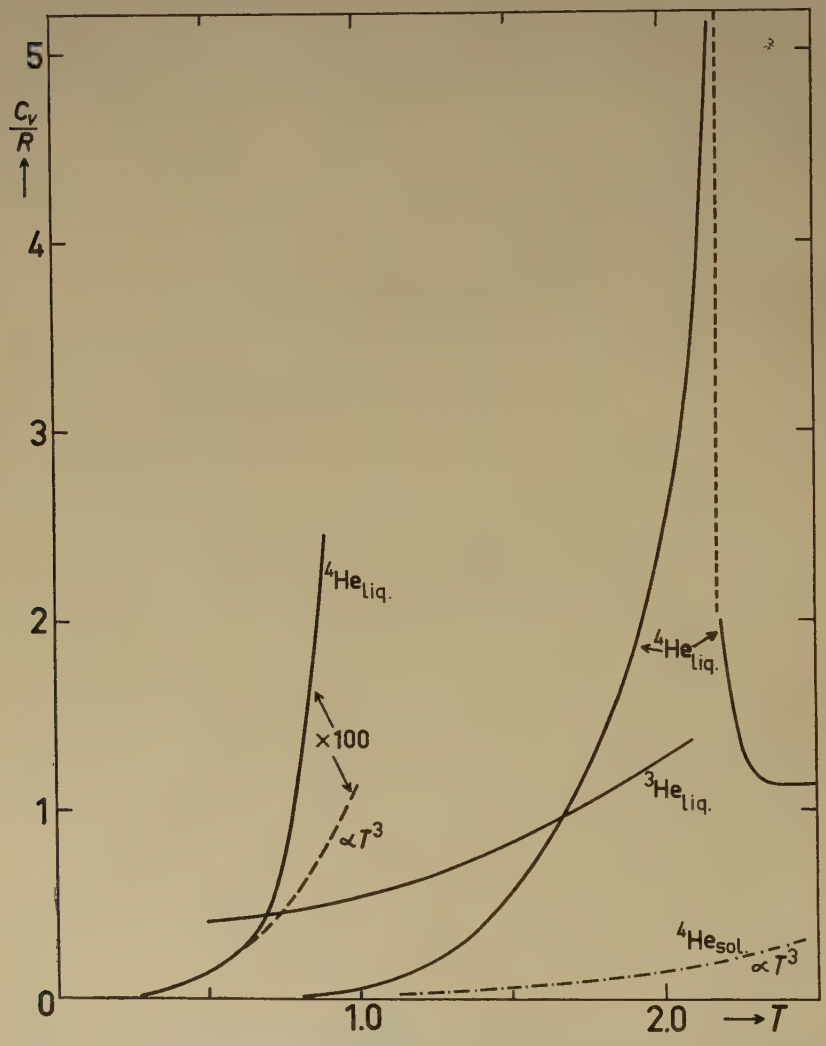

Fig. 5. Curves for molar heat capacity of ^{3}He, ^{4}He under vapour pressure and of solid helium at the solidification density.

falls off rapidly until at about 0.6° K the heat capacity approaches a Debye T^3-curve [5] (see Ch. II), with $\Theta = 18.9°$ K but only for one third of the degrees of freedom. This is usually explained by assuming that only longitudinal thermal waves are excited. In liquid ^{3}He the heat capacity is quite different: the values are much higher down to temperatures of about 0.5° K [6]. The curve shows an interesting flattening-off at the lowest temperatures, which might point in the direction of occurrence of a λ-point also in the case of ^{3}He, which, however, has not been observed so far. Both curves differ markedly from the normal heat capacity curve, which was measured in the case of solid ^{4}He by Keesom and Keesom [7], Webb, Wilkinson and Wilks [8] and by Dugdale and Simon [3]. This can be described at the solidification point by a Debye-curve having approximately $\Theta = 24°$ K with all degrees of freedom (see Fig. 5).

Debye-Temperature. It is interesting to apply to the values of the Debye-temperature observed for the sequence of substances listed in Table II the quantum mechanical principle of corresponding states again. The proper quantity which should be compared for the different substances is the ratio of the Debye-frequency $\nu_D = k\Theta_D/h$ to some frequency characteristic for the molecular field of the substance

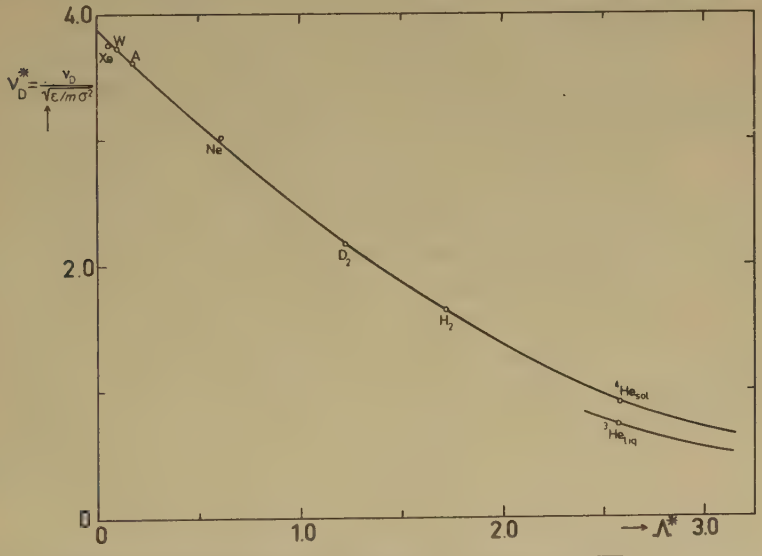

Fig. 6. Reduced values of Debye frequency $\nu_D^* = \nu_D/\sqrt{\varepsilon/m\sigma^2}$ as a function of the quantum mechanical parameter Λ^*.

considered. The only classical quantity of the dimension of a frequency to be built from ε, σ and m is $(\varepsilon/m\sigma^2)^{1/2}$. The reduced Debye-frequency may thus be written as $\nu_D^* = \nu_D/(\varepsilon/m\sigma^2)^{1/2}$. It is of interest that although the Θ_D itself varies quite irregularly as a function of Λ^*, the reduced Debye-frequencies ν_D^* vary smoothly as functions of Λ^*, as can be seen in Table III and Fig. 6.

TABLE III

Debye-temperature Θ_D and Debye-frequency ν_D for different substances

Substance	Λ^*	Θ_D (°K)	$\Theta_D^* = k\Theta_D/\varepsilon$	$\nu_D^* = \Theta_D^*/\Lambda^* = \nu_D/\sqrt{\varepsilon/m\sigma^2}$
^{4}He (liq.)	2.68	19	1.9	0.71
^{4}He (sol., 25 atm)	2.68	24	2.4	0.90
H_2	1.73	105	2.84	1.64
D_2	1.22	97	2.62	2.15
He	0.59	64	1.80	3.05
A	0.186	80	0.67	3.60
Kr	0.102	63	0.38	3.7
Xe	0.064	55	0.24	3.8

Thermal Expansion Coefficient. It is well known that a similar abnormal behaviour as is found for the heat capacity in liquid helium has also been observed for the *thermal expansion coefficient*. It was observed (comp. W. H. Keesom [7], p. 242) previously that below the λ-point the thermal expansion coefficient becomes negative. Recently Atkins [9] showed that at temperatures below 1.1° K the thermal expansion coefficient becomes positive again and approaches the normal T^3-curve, which can be expected from the behaviour of the heat capacity at temperatures below 1.1° K. In Fig. 7 this thermal expansion coefficient is plotted, together with the data for solid helium at the solidification point obtained by extrapolating the measurements from Dugdale and Simon [3] and using the thermodynamic relation: $(\partial V/\partial T)_p = (\partial S/\partial p)_T$. Unfortunately no data for ^{3}He are available so far in this case.

The behaviour of the heat capacity of liquid helium, differing so fundamentally from the behaviour according to the Debye-theory, and in particular also the remarkable difference between ^{4}He and ^{3}He will be studied in more detail in the next two sections. In § 2 we shall discuss the behaviour of liquid helium at the absolute zero

of temperature in order to have a basis for a discussion in § 3 of the thermal excitations and the λ-point. It will be shown that the differences between ^{3}He and ^{4}He which occur in the heat capacity are largely due to exchange effects.

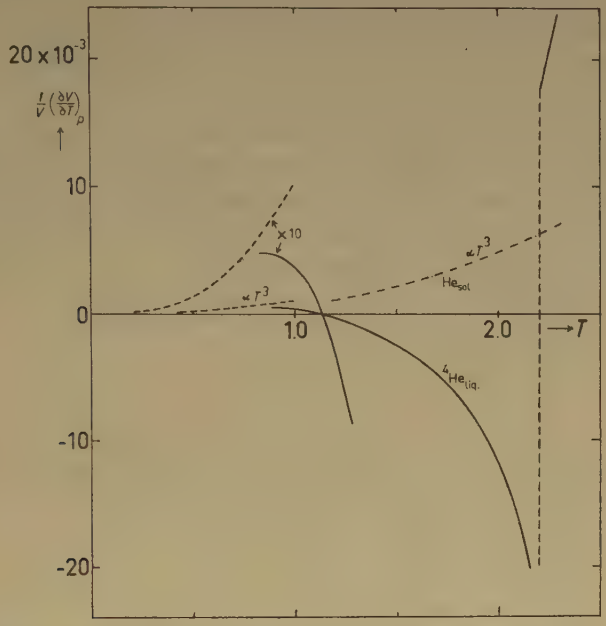

Fig. 7. Thermal expansion curve for liquid helium under vapour pressure and solid helium at the solidification density.

2. Liquid Helium at Zero Absolute Temperature

a) Lattice-structure Model Versus Ideal Gas Model

The theoretical attempts to describe the properties of liquid helium can be divided roughly into two fundamentally different approaches:

(a) The ideal gas approach,

(b) The solid state approach.

The main attraction of the *ideal gas model*, which has initially been advocated very much also by F. London in particular, comes from the following facts:

(1) It offers an explanation for the λ point in liquid ^{4}He in the transition due to the Bose–Einstein condensation which occurs in an ideal gas of helium atoms with the density of liquid helium at 3.15° K.

(2) It gives a possible explanation for the superfluid and normal component of liquid helium in terms of the "condensed atoms" and "excited atoms" of the B.E. gas below the transition point.

(3) The ideal gas model demonstrates very clearly the influence of the *symmetry-effects*: ^{4}He-atoms follow Bose–Einstein statistics and ^{3}He-atoms the Fermi–Dirac statistics and consequently an ideal ^{4}He gas shows the Bose-Einstein condensation phenomenon with an anomaly in the heat capacity at the "condensation" temperature and a curve proportional to $T^{3/2}$ below the point, whereas an ideal ^{3}He gas shows no anomaly at all and approaches at low temperatures a heat capacity curve proportional to T, as for the electrons in metals. This well known difference between these two gases is pictured in Fig. 8.

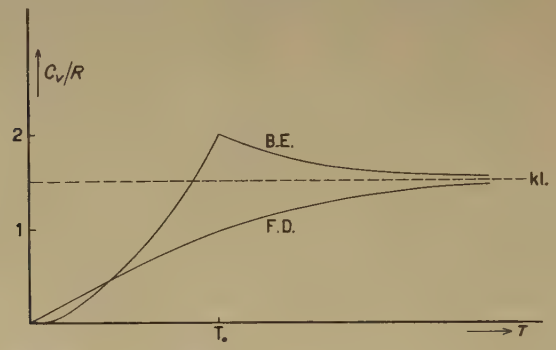

Fig. 8. Specific heat for an ideal:
a) Fermi Dirac gas $m = m_{^3\mathrm{He}}$, $V = 36.4$ cm^3/mole, $T_0 = 1.64°$ K.
b) Bose Einstein gas $m = m_{^4\mathrm{He}}$, $V = 27.3$ cm^3/mole, $T_0 = 3.15°$ K.

Later experiments have led to additional information, which makes it very difficult to consider the ideal gas model as a suitable first approximation:

(4) The $T^{3/2}$-law for the specific heat of a partly condensed B.E. gas could be modified only by assuming either an ad-hoc change of the statistical weights of the one particle states or by assuming the presence of an energy gap between the lowest and first excited state.

(5) The molar heat of liquid ^{3}He is in disagreement with the proportionality with T for an ideal Fermi–Dirac gas.

(6) Moreover the heat capacity approaches in the case of ^{4}He at

low temperatures a T^3-law which can directly be explained on the basis of a lattice model and is in contradiction with our expectations in the gas model.

The further development of our knowledge about liquid helium has given, however, many arguments in favour of an approach from the side of the solid state rather than the ideal gas state. According to this approach liquid helium at absolute temperature zero has to be considered as an ordered arrangement of helium atoms, resembling in principle that of a solid at temperature zero. Because of the uncertainty principle, however, the atoms cannot be located on definite sites of a lattice-structure. Therefore helium at temperature zero should be considered, according to such a model, as an ordered arrangement of wave packets instead of atoms. It may very well make sense, however, to speak about the "structure", this being the lattice according to which the wave packets are arranged.

Comparing such a "*lattice model*" with the ideal gas model, the following should be remarked:

(1) In such a lattice model *phase transitions* might occur which offer an explanation for that occurring in liquid helium: Very important in this connection is the early attempt of Fröhlich [10] to interpret the λ-point of liquid helium as an order-disorder transition in such a lattice model. But besides this one, other explanations are possible and will be discussed in next sections.

(2) In such a "lattice model" the two fluid model is given an entirely different basis, which is much closer to the original concepts of Landau [31]. The two fluids are no longer interpreted as two substantial components of the system or as two different states in which the atoms can be ("superfluid state" and "normal state"), but the two fluid model becomes only a mathematical description of the system of *thermal excitations* ("the normal fluid") moving in an ideally ordered system of helium atoms ("the superfluid") in the ground state as background.

The old language of "atoms in the normal or superfluid state" is typical for its origin: the ideal gas approximation with atoms in the condensed or in the normal state. Here however we consider the "gas" of excitations in analogy with developments in the field of solid-state physics. One is able to give a straight-forward derivation from first principles of the "equations of motion" of the two fluid-model (i.e. the equations of Landau) as has been

demonstrated by Kramers [11] by Kronig [12] and by Khalatnikov [13].

(3) The *symmetry effects* play in this model a less obvious role than for the ideal gas model: For a classical solid, in which interchange of atoms is practically impossible, the influence of the symmetry effects can be neglected entirely. For liquid helium, however, quantum effects have "blown up" the substance to a volume which is three times larger than that of a classical solid (see Fig. 3) and this allows the atoms to change place much easier than in a classical solid. Therefore in this model for liquid helium the exchange effects will also play a role; their influence will be in particular very large on the thermal excitations. It is, however, possible that in this model one obtains theoretically a λ-anomaly for liquid ^{4}He as well as for ^{3}He. This is not a drawback of the model, because it is by no means certain now that in ^{3}He no phase transition occurs: There are even strong indications that a transition occurs also in ^{3}He somewhat below 0.4° K.

(4) It has to be remarked, however, that important *investigations on the basis of different models* have been made e.g. the considerations of Feynman [14a], Chester [14b] and of Friedman and Butler [14c], among others. As it is the intention of this chapter to give the background for the recent cell theories the author felt that the approach from the side of the condensed state, making use of structure-considerations offers a better starting point for a satisfactory exposition than the gas model. It is for that reason that only very few of the researches made in the field of the liquid helium problem will be discussed in the present chapter, and that a large number of important contributions following different lines have to be disgarded, notwithstanding the fact that they may be very important for the whole problem.

In this section we first discuss the ground state of liquid helium, the discussion of the excitations being reserved for the next sections § 3 and 4.

b) Structure Analysis from Diffraction

The most direct information about the mutual arrangement of the helium atoms in liquid helium is obtained by X-ray-analysis or by elastic neutron-scattering experiments. The early experiments by Keesom and Taconis [7] have now been followed by three groups of experiments: The X-ray experiments of Reekie and collaborators [15a],

those of Gordon, Shaw and Daunt [15b] and the neutron elastic-scattering experiments of Hurst and Henshaw [15c]. Unfortunately the experiments have been done only at temperatures higher than 1.5° K, where an appreciable amount of disorder must exist and most probably not much detail of the structure at the absolute zero is left, but it may

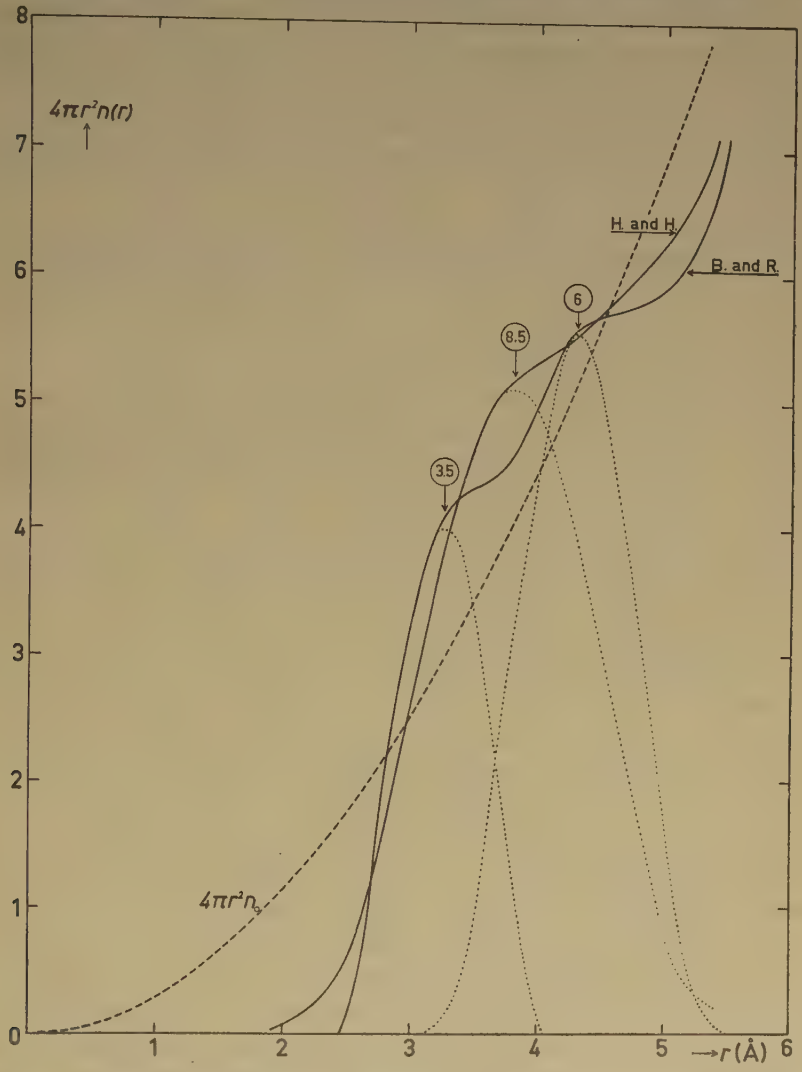

Fig. 9. Values of $4\pi r^2\, n(r)$, as a function of r at temperatures 2.06° K and 1.65° K according to the measurements of Beaumont and Reekie [13] and Hurst and Henshaw [15] respectively. The broken curve represents $4\pi r^2 n_0$.

still be of interest to compare the results with the "structures" which have been proposed for helium at the zero absolute temperature.

As is well known it is possible to derive with the method of Fourier transforms from the scattered intensity as a function of $s = (4\pi/\lambda)\sin(\vartheta/2)$ the average number of molecules which can be found at a distance between r and $r+\mathrm{d}r$ from a given molecule: $4\pi r^2 n(r)\mathrm{d}r$. Fig. 9 shows the curves obtained at temperatures below the λ-point for $4\pi r^2[n(r)-n_0]$ as a function of r measured in Å, where n_0 is the average number of molecules per Å ^{3}. Both groups of experiments show the large positive values between roughly $r=3$ and 4.5 Å and the minimum between 4.5 and 6.

In the neutron diffraction experiments this first maximum was assumed to be due to the scattering of a group of about 8.5 atoms at roughly 3.8 Å. The analysis of the X-ray experiments of Beaumont and Reekie pointed to a division of this first shell into two subshells at 3.3 and 4.3 Å, but it is highly probable that this division into two subshells is not real: From the X-ray scattering experiments one obtains only a Fourier composition of the quantity $4\pi r^2[n(r)-n_0]$ made by using a wavelength spectrum with a minimum wavelength of 1 Å, consequently a double maximum with a mutual distance of 1 Å as occurs in $n(r)-n_0$ according to Beaumont and Reekie can easily result from this composition without having any real significance. If, therefore, we do not take into account the splitting of the first maximum, both groups of measurements lead to the same conclusion that there exists a group of $8-9$ nearest neighbour atoms at roughly 3.8 Å.

In Fig. 10 we have compared the number of nearest neighbours with the different cubic structures which have been proposed for liquid helium at 0° K. It is obvious that the distribution of atoms above 1.5° K as found from this analysis does not agree with either the diamond or the T_d^2-structure, the number of nearest neighbours being much too large.

Instead, above 1.5° K the distribution of atoms is much more in agreement with the model which one very often makes of a liquid, i.e. *a partly occupied cubic close packed structure*, as has been suggested for this particular case by Hurst and Henshaw. One divides the liquid volume into L cells ordered according to a cubic close packed lattice, and one assume that only $N=xL$ of the cells are occupied and the remaining $(1-x)L$ cells are empty holes. The distance between

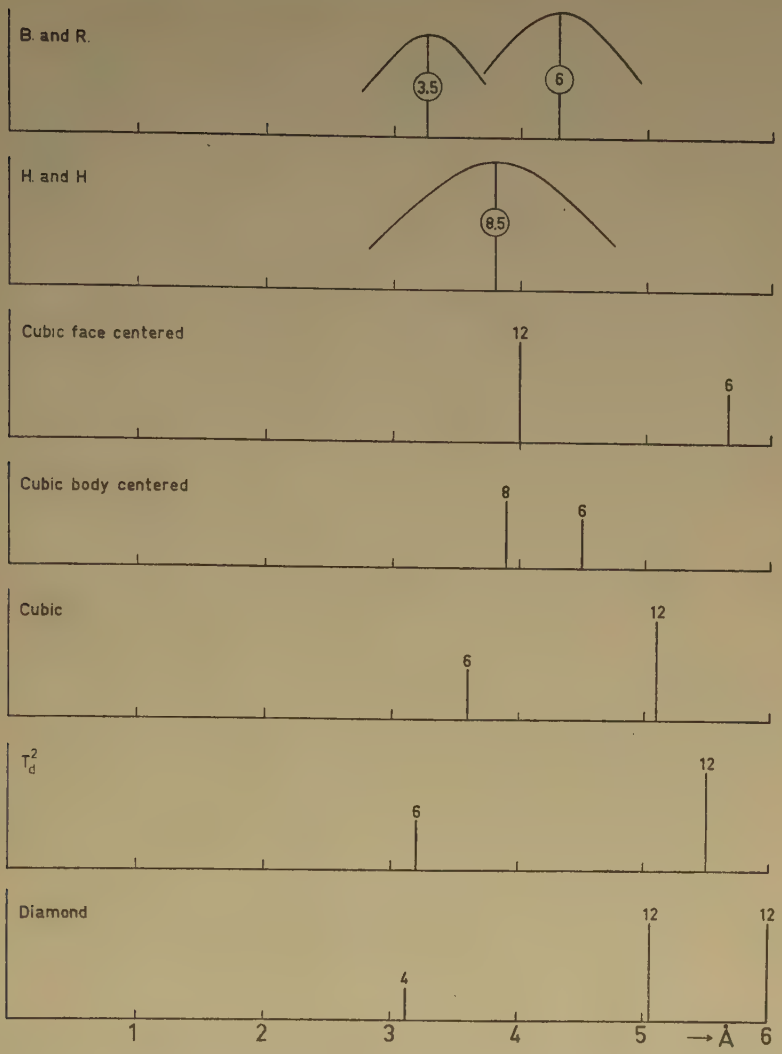

Fig. 10. Number of atoms at a distance r from a central atom according to scattering experiments compared with different structures.

nearest neighbours then becomes $a = (V/N)^{1/3} \cdot 2^{1/6} \cdot x^{1/3}$ and the average number of nearest neighbours or "coordination number" becomes $c = 12x$. In Fig. 11 we have plotted the change in average distance for the cubic face centered lattice for $x = 1$, $x = 5/6$, $x = 2/3$ and $x = 1/2$ respectively. This shows the regular shift of the nearest neighbour

distance to smaller values, the smaller the average coordination number c becomes. The situation at about 70 % occupation seems to be in good agreement with the experimental findings at temperatures above 1.5° K.

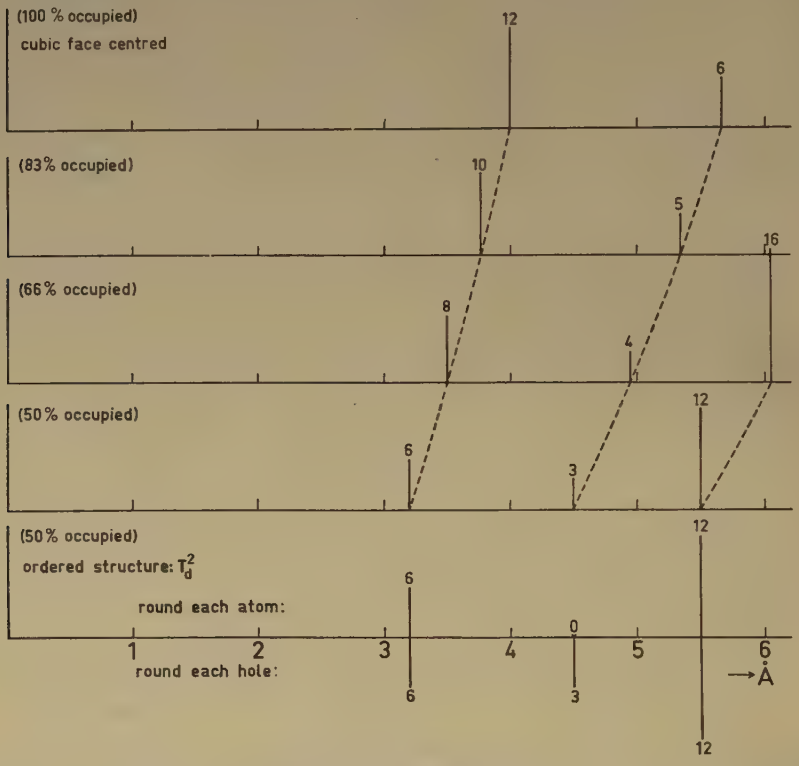

Fig. 11. Average number of atoms on different shells in partly occupied cubic close packed structure.

Still, one might expect that at 0° K an *ordered structure* is realized. It is nice that the present picture offers a possible indication for this structure: One might assume that at 0° K the atoms in liquid helium are "arranged" according to the T_d^2 structure, which, as is well known, can be considered as a close packed structure in which lattice sites are only 50 % occupied, but in *an ordered way*. The term "arranged" should be used, of course, with the considerable care needed in a picture which should be in agreement with quantum mechanical concepts as explained in § 2.1.

Increase of temperature then leads to disorder. Most probably this disorder becomes noticeable at temperatures above $0.8-1.0°$ K. Atoms then get enough kinetic energy to be displaced to the empty lattice sites of the T_d^2-structure and vice-versa. Such a disordered arrangement of a cubic close packed lattice which is 50 % occupied would have the same molar volume and nearest neighbour distance as the T_d^2 arrangement. However, when the open structure according to the ordered T_d^2-structure breaks down by raising the temperature it is rather improbable that the disordered structure also has a 50 % occupied lattice. Instead the number of holes decreases somewhat leading gradually to a 60 % or 70 % occupied close packed lattice. The decrease of the number of holes might then be accompanied by a decrease of the molar volume (because the decrease of the number of holes at constant volume leads to an increase of the distance a between nearest neighbours). This decrease in molar volume with rising temperatures demonstrates itself in the negative expansion coefficient which becomes noticeable in the temperature region above 0.8° K.

It should be stressed that this picture is largely the same as that put forward originally by Fröhlich, although for a different lattice arrangement. The only intention of the present remarks is to stress that the present results found with the diffraction experiments at temperatures above 1.5° K are by no means in conflict with the assumption of the existence of an ordered arrangement with coordination number 6 at 0° K. In § 3, where the temperature excitations are considered in more detail, we shall come back to these considerations, which had to be mentioned briefly in the present discussion of the diffraction experiments.

Also from the experimental data on the inelastic scattering of neutrons the conclusion has been drawn that a liquid structure model provides in principle the best model for a description of the scattering data. For a more detailed discussion of this point we refer however to the discussion of the experiments of Egelstaff and H. London [35], Somers, Dash and Goldstein and by Goldstein, Sweeney and Goldstein [35].

c) Energy and Volume at Absolute Zero

We come to the discussion of the energy-volume relationship of the ground state, and the influence which quantum effects and exchange effects have in this connection.

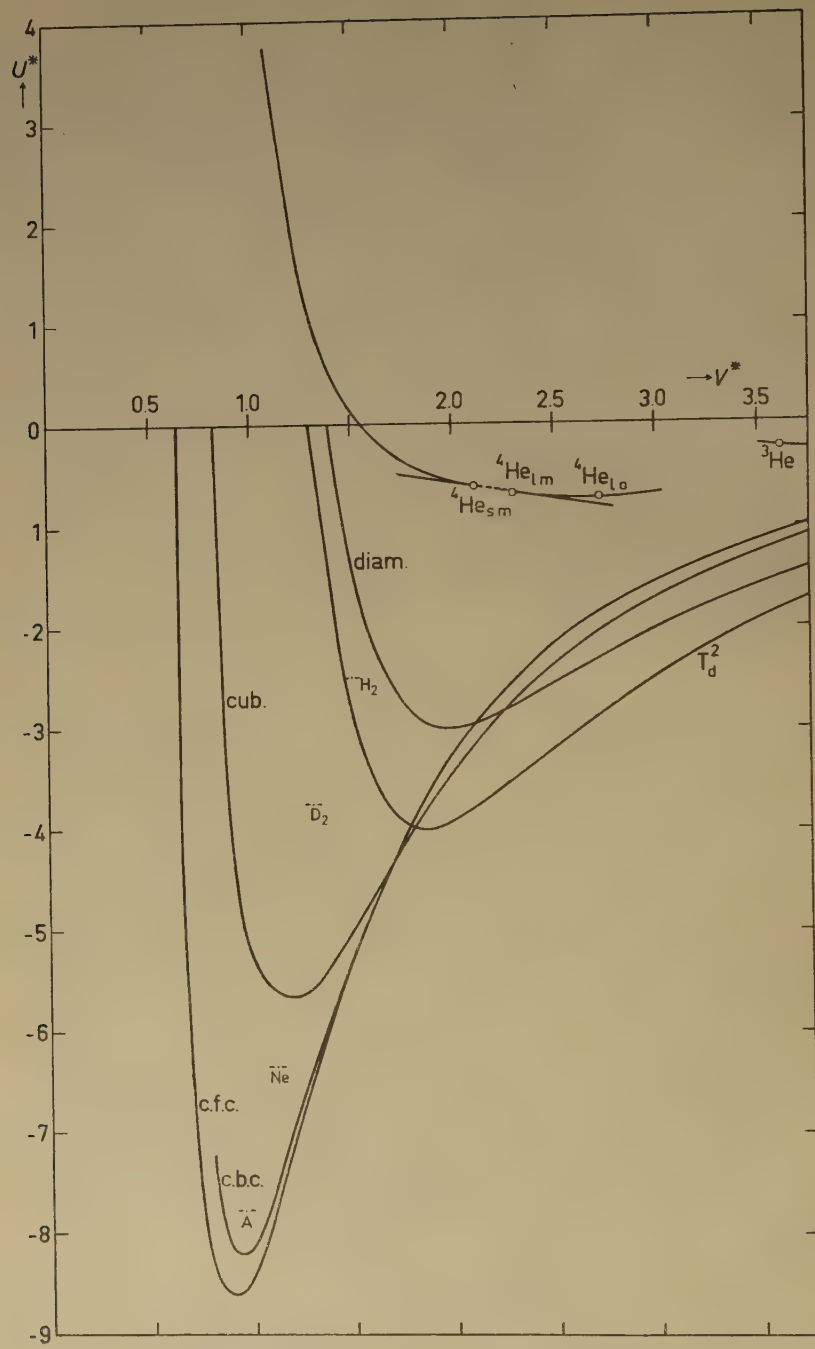

Fig. 12. Energy volume relationship for liquid and solid helium. The lattice energy for different lattice structures. The experimental values for the minimum of solid H_2, D_2, Ne and A are indicated as —·—.

In Fig. 12 we have given the values of energy and volume at the absolute zero of ^{4}He as well as ^{3}He. For liquid ^{3}He only the minimum of the energy curve is known.

In the case of ^{4}He much more data are available, viz. the energy and volume at the melting or solidification point both for the liquid l_m and the solid s_m. The pressure of solidification, being the slope of the line connecting the points s_m and l_m, is also known. In terms of the molecular units of Table I the values [17] of these quantities are:

TABLE IV
Condensed helium, experimental data

	$V^* = V/N\sigma^3$	$U^* = U/N\varepsilon$	$p^* = p\sigma^3/\varepsilon$
^{4}He: liq.	2.75	-0.70^5	0
liq. (solidif. pt.)	2.31	-0.65	0.30
solid (melt. pt.)	2.11	-0.58^5	0.30
^{3}He: liq.	3.862	-0.25	0
liq. (solidif. pt.)			0.5

Moreover, very much information is now available about the solid state of ^{4}He because of the extensive measurements and the detailed evaluation and discussion of these measurements by Dugdale and Simon [16] from which a very complete picture is obtained concerning the equation of state and the caloric properties of solid ^{4}He. As a result of these measurements it is now also possible to draw in Fig. 12 the $U^* - V^*$ curve at the absolute zero for the solid state as far as $V^* = 1.05$. These results are summarized in the Table V.

TABLE V
Solid helium, experimental data

$V^* = V/N\sigma^3$	$P^* = P\sigma^3/\varepsilon$	$U^* = U/N\varepsilon$	$\Theta_D^* = k\Theta_D/\varepsilon$ †
1.10	19.9	$+3.8$	11.1
1.3	8.34	$+1.1^5$	7.5
1.5	3.54	$+0.1^5$	5.3^3
1.7	1.63	-0.3	3.9^2
1.9	0.60	-0.5	2.9^9
2.1	0.30	-0.58	2.4

† The values of Θ_D are obtained by equating $\Theta_D = 1.1\ \phi$, ϕ being the "parameter" introduced by Dugdale and Simon. This conversion factor gives on the average a reasonable agreement of the C_v curve with the Debye curve.

We will now discuss the energy diagram from the point of view of the lattice structure model, which was also the basis of the discussions in the previous section. For the theoretical evaluation of the energy in this model one assumes that a first approximation for the energy can be obtained by assuming that all atoms are placed on the positions of the lattice. To this potential or "lattice" energy as a first approximation one should add the "*zero point*" *energy* due to the motion of the atoms round their lattice positions. It should be kept in mind that this division of the energy into a lattice energy and a zero-point energy becomes rather artificial when the amplitude of the zero-point motion round the equilibrium positions becomes of the same magnitude as the lattice distance, a. As this seems to be actually the case in liquid helium, the application of this procedure for calculating the energy has to be done with considerable scepsis. In Fig. 12 we have plotted the lattice-energy, calculated with the Lennard–Jones potential field (1) and expressed in units $N\varepsilon$, as a function of the reduced molar volume $V^* = V/N\sigma^3$ for the following lattice structures:

(a) cubic face centered structure (c.f.c.), (b) cubic body centered structure (c.b.c.), (c) simple cubic structure (c), (d) diamond structure and (e) the T_d^2 structure.

It seems to be certain that the *solid state of helium* is a cubic face centered structure. It can be seen from the figure that there is a very large difference between the lattice-energy curve for the cubic face centered lattice and the experimental energy curve for solid helium at $T = 0$, as determined by Dugdale and Simon [16]. The difference between these two curves, i.e. "the zero-point energy", can be determined empirically and the result has been plotted separately in Fig. 13 as function of V^*. As has been pointed out by these authors this zero-point energy can be explained quantitatively using the Debye theory, which gives the following expression for the total zero-point energy of all different heat waves:

$$K_0 = \tfrac{9}{8} Nk\Theta_D \qquad K_0^* = \tfrac{9}{8}\Theta_D^*. \tag{2}$$

In Fig. 13 the curve $\frac{9}{8}\Theta_D^*$ has been drawn for comparison with the "experimental" curve for K_0 using the experimental value as deduced from the calculations of Dugdale and Simon for Θ_D and the known dependence of Θ_D on volume (see Table V). The figure shows that

the two curves nearly coincide. It should be pointed out, however, that the zero-point energy can also be represented with reasonable accuracy by assuming that each helium atom moves as a hard sphere independently inside a spherical shell with radius $a-d$, a being the distance between nearest neighbours and d the diameter of the hard spheres. This gives for the zero point-energy:

$$K_0 = \frac{h^2}{8m(a-d)^2} \qquad K_0^* = \frac{\Lambda^{*2}}{8(a^*-d^*)^2}. \tag{3}$$

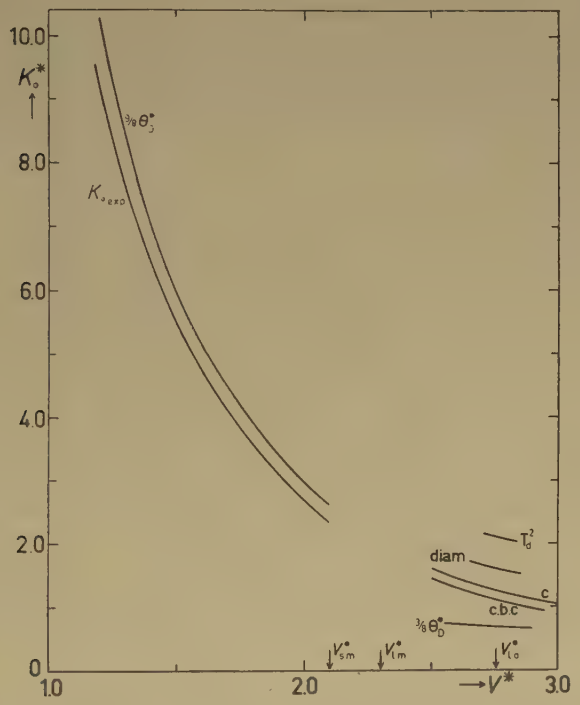

Fig. 13. The zero point energy of solid and liquid helium according to the Debye theory and the "empirical" values based on definite "lattice structures".

Taking $a^{*3} - V^* \cdot \sqrt{2}$, valid for a cubic face centered lattice, one obtains a reasonable agreement with the experimental data, when d^* is taken to be $d^* = 0.78$ or $d = 0.78\,\sigma$. Though this is a somewhat small value, it represents the effective diameter of an equivalent hard sphere which gives approximately the same wave function as the true potential field.

Although the quantum effects are obviously very large, the present method makes it very difficult to get insight into the exchange effects: for the Debye treatment this would require the knowledge of the interaction of different Debye waves, which is difficult to estimate and to take into account. In the single cell model used in connection with (3), taking into account of exchange effects is in principle impossible.

The situation in the *liquid phase of helium* is much more difficult to understand. In liquid helium only the longitudinal heat waves contribute to the T^3-law of Debye (see further § 4) because of the fact that transversal waves cannot be propagated in the liquid. Consequently the reduced zero-point energy is only $\frac{3}{8}\Theta_D^* = \frac{3}{8} \times 1.9 = 0.71$. The difficulty is that for the liquid state, because of the lack of knowledge about the "structure" of the liquid, no theoretical estimate for the lattice energy is available. In Fig. 12 we have plotted the value $K_0^* = \frac{3}{8}\Theta_D^*$ and its variation with V^* together with the zero-point energy which would be needed if the "structure" of the liquid state were as indicated. In any case it can be concluded that the zero-point energy due to the longitudinal Debye waves alone is *not* sufficient to explain the difference between the experimental energy curve and any of the lattice-energy curves. The discrepancy becomes even the more serious, the smaller the coordination number of the liquid state is assumed to be; and for a T_d^2-structure the "empirical" value for this reduced zero-point energy is even two or three times as large.

Of course one might bring forward in this connection the fundamental objections against the whole method of separating the total energy into lattice energy and zero-point energy, but in view of the fact that in the case of solid helium up to a reduced molar volume of $V^* = 2$ a reasonable description with this model is possible, one would expect that the situation in the liquid state at $V^* = 2.7$ is not so fundamentally different.

It seems therefore ineluctable to conclude that besides the zero-point energy of the longitudinal waves there must be another contribution to the zero-point energy in liquid helium, which undoubtedly is connected with transversal oscillations of some kind.

The explanation of this zero-point energy is, however, closely connected with the discussion of the excited states and their contribution to the thermodynamic properties of the system. We will therefore postpone the further discussion of the zero-point energy

to section § 4, where the excited states differing from the excitations of longitudinal waves will be discussed.

3. Collective Excitations

It is now generally assumed * that the excitations in liquid helium have to be divided into two different groups:

(a) *collective excitations*, which involve large groups of atoms and which can be described in terms of macroscopic physics as longitudinal elastic waves, and

(b) *molecular excitations*, which involve one or very few atoms and for which a molecular description is needed. The nature of these molecular excitations, about which still considerable uncertainty exists, will be considered in the next section § 4.

a) Collective Excitations in Solids and Liquids

In this section we shall first consider in somewhat more detail the *collective excitations*. As is well known, in the *amorphous solid state* the following excitations can be distinguished:

(1) longitudinal, or compressional waves, for which the velocity field is rotation-free: rot $\mathbf{v} = 0$, and the velocity of propagation c_l of which is determined by the formula: $c_l^2 = (\lambda + 2\mu)/\varrho$,

(2) transversal, or torsional waves, for which the velocity field is divergence-free: div $\mathbf{v} = 0$, which do not involve compressions, but only shear-deformations and for which the velocity of propagation is determined by the formula $c_t^2 = \mu/\varrho$.
Here λ and μ are the well-known elasticity coefficients of Lamé, $\mu = G$ being the shear modulus and $\lambda + \frac{2}{3}\mu = K$ being the compression modulus, which is the inverse of the compressibility $\varkappa$.

In the *liquid state* the shear modulus $\mu = G = 0$, leaving only the possibility for the propagation of longitudinal compression waves with a velocity of propagation $c^2 = K/\varrho = 1/\varrho\varkappa$ (K is the compression modulus and $\varkappa$ the compressibility). In general this velocity depends on the wave number σ, giving the dispersion relation: $\nu = \sigma \cdot c(\sigma)$.

According to the picture which we have made of liquid helium at $T = 0$ as a liquid but completely ordered state, the particle nature of the medium is taken into account by considering only wave-vectors σ

* See R. P. Feynman, Vol. I, Ch. I.

situated in the first Brillouin zone. According to the Debye picture one introduces a maximum wave vector σ_D, determined by the condition $V \cdot \int_0^{\sigma_D} 4\pi\sigma^2 d\sigma = N$ or $\sigma_D = (3N/4\pi V)^{1/3}$ which is of the order of magnitude $\sigma_D \approx 0{,}62\bar{a}^{-1}$, $\bar{a}$ being the average distance between molecules.

Usually the quanta of these longitudinal excitations are indicated as "phonons" and the distribution function $f(\sigma)$ for the phonons over the wave number then indicates that the state with wave number σ is excited corresponding to the quantum number $f(\sigma)$. Very often, however, and in particular when the transport properties are discussed, the phonon is identified with a wave packet with average wave number and frequency: $\bar{\sigma}$ and $\bar{\nu}$, which propagates with the group velocity $\bar{v} = \overline{d\nu/d\sigma}$. Of course the group velocity is approximately equal to the phase velocity c where $c(\sigma) = \text{constant}$. The spread $\delta\sigma$ in the wave number and the corresponding spread δx of the phonon in space are related by the uncertainty relation $\delta x \delta\sigma \approx 1$. If the extension in space is much larger than the lattice distance: $\delta x \gg a \approx \sigma_D^{-1}$, the spread in wave number is much smaller than the maximum wave number: $\delta\sigma \ll \sigma_D$. It thus makes sense to speak about the energy of phonons $\varepsilon = h\bar{\nu} = hc \cdot \bar{\sigma}$ and the distribution of the energy over different wave numbers characterized by the distribution function

$$f(\sigma)\, d\boldsymbol{\sigma} = \frac{d\boldsymbol{\sigma}}{\exp \beta\varepsilon(\sigma) - 1}, \tag{4}$$

this being equal to the number of phonons per unit volume in the element $d\boldsymbol{\sigma}$ of wave vector space at a temperature $T = 1/\beta k$.

b) Caloric Properties of Phonons

Using the methods of statistical mechanics one finds for the Gibbs free energy due to these excitations:

$$\tilde{F}^{(\mathrm{ph})} = \frac{F^{(\mathrm{ph})}}{V} = kT \int_0^{\sigma_D} \ln\{1 - \exp -\beta\varepsilon(\sigma)\}\, d\boldsymbol{\sigma} \tag{5}$$

and from the free energy all thermodynamic quantities can be obtained. They all are proportional to the volume and depend on the ratio T/Θ_D, Θ_D being the Debye temperature $\Theta_D = hc\,\sigma_D/k = h\nu_D/k$, which, using $c = 239\ m/s$ [18], gives $\Theta_D = 20.0°$ K.

In the temperature region which is of interest for liquid helium $T \ll \Theta_D$ always, and it is of particular interest that in this region the thermodynamic quantities obtained from $\tilde{F}^{(\mathrm{ph})}$ simplify consid-

erably because in this limit σ_D can be replaced by ∞. Then we obtain:

$$\tilde{F}^{(\mathrm{ph})} = -\frac{\pi^4}{15}\frac{N}{V}kT\left(\frac{kT}{h\nu_D}\right)^3 = -\frac{4\pi^5}{45}\frac{k^4}{h^3c^3}T^4 \tag{6}$$

which expression no longer contains particular reference to the discrete structures of the system, c being the limiting value for the velocity of sound at $T=0$.

From this one obtains for the caloric properties: *

$$\tilde{S}^{(\mathrm{ph})} = -\left(\frac{\partial \tilde{F}}{\partial T}\right)_V = \frac{16\pi^5}{45}\frac{k^4}{h^3c^3}T^3 \tag{7}$$

$$\tilde{U}^{(\mathrm{ph})} = -\left(\frac{\partial(\tilde{F}/T)}{\partial(1/T)}\right)_V = \frac{4\pi^5}{15}\frac{k^4}{h^3c^3}T^4 \tag{8}$$

which is – as is well known – in nice agreement with the experiments [5] on the specific heat of liquid ^{4}He below 0.6° K, where only this collective type of excitation is left (see Ch. II). As is shown in Fig. 5 deviations from this law occur at temperatures above 0.6° K which deviations are the result of the contribution of the molecular type of excitations to the entropy.

c) Thermal Pressure and Thermal Expansion due to Phonons

The contribution which these collective excitations give to the pressure is:

$$p^{(\mathrm{ph})} = -\left(\frac{\partial(\tilde{F}V)}{\partial V}\right)_T = \frac{4\pi^5}{45}\frac{k^4}{h^3c^3}\left[1-3\left(\frac{\partial \ln c}{\partial \ln V}\right)_T\right]T^4. \tag{9}$$

This "thermal pressure" clearly consists of two parts:

(1) the "kinetic" pressure of the phonons, which is equal to $\frac{1}{3}\tilde{U}^{(\mathrm{ph})}$, the relation which also holds in the photon gas, and

(2) the contribution $-(\partial \ln c/\partial \ln V)_T\tilde{U}^{(\mathrm{ph})}$, which is due to the dependence of the velocity of sound on density [19]. The last term is by far the most important, $(\partial \ln c/\partial \ln V)$ being roughly equal to: – 2.7.

This thermal pressure is the direct cause for the thermal expansion:

$$\alpha^{(\mathrm{ph})} = \frac{1}{V}\left(\frac{\partial V}{\partial T}\right)_p = \varkappa\left(\frac{\partial p}{\partial T}\right)_V = \frac{16\pi^5}{45}\frac{k^4}{h^3c^3}\left[1-3\left(\frac{\partial \ln c}{\partial \ln V}\right)_T\right]\varkappa T^3 \tag{10}$$

* Thermodynamic quantities per mole are indicated by capital characters. The quantities per unit volume are distinguished by a tilde $\sim$ on top: $\tilde{U}$, $\tilde{F}$, $\tilde{S}$, etc.

where $\varkappa = -(1/V)(\partial V/\partial p)_T$ is the isothermal compressibility. It has been shown by Atkins and Edwards [9], who have drawn attention to this interesting consequence of the thermal pressure exerted by the phonon gas, that such a behaviour is not in conflict with the experimental data. Although at temperatures above 1.1° K the thermal expansion coefficient is negative as the result of a large negative contribution due to the molecular type of excitations, the expansion coefficient becomes positive below 1.1° K and indeed approaches the positive T^3 curve in agreement with Eq. (10), as was shown in Fig. 7.

The exchange effects play only a very indirect role in this behaviour at very low temperatures, because this depends entirely on the bulk property: the velocity of sound and the dependence on density. There is no reason, therefore, that the behaviour in the case of liquid ^{3}He is different: also in that case there must be a contribution proportional to T^3 in the specific heat, entropy and thermal expansion, due to the collective phonon excitations. Assuming a value of Θ_D which is about 20 % smaller than that for liquid ^{4}He one would therefore expect also in the case of liquid ^{3}He a molar entropy contribution due to the collective excitations of the order of magnitude: $S/R = 0.008\, T^3$. This contribution is, however, largely dominated in the available temperature region by the contribution of the molecular excitations which for ^{3}He is much larger than for ^{4}He.

4. Molecular Excitations – Order-disorder Theory

The excitations of the molecular type will be the subject of discussion in this and the following section. It is well known that the nature of these excitations is not so very well understood. It is not the purpose of this article to review the existing literature in this connection. For this we may refer to existing review articles from Dingle [33], Wilks [33], Daunt [33] and others. Much attention to the nature of these excitations has been paid in particular by Feynman [30], who gave a very illuminating discussion in Prog. Low Temp. Physics, vol. I. We only discuss those theories which have a close relation to the cell theory:

(a) the *order-disorder theory* of H. Fröhlich [20] and H. Jones [21],

(b) the *fluctuation theory* of I. Prigogine [22],

(c) the *cell theory* connected with rational motions introduced by several authors independently: J. de Boer and E. G. D. Cohen [24], P. Price [26], O. K. Rice [25] and H. N. V. Temperly [27].

A) The Order-Disorder Theory

a) *General Principles*

The theory with which H. Fröhlich [20] and H. Jones [21] explained the phase transition of liquid He II into liquid He I goes entirely parallel with the theory of J. E. Lennard–Jones and A. F. Devonshire [23] for the melting process, i.e. the transition of the solid into the liquid state. It is not surprising that these different problems can be treated with the *same* theory: as we have pointed out in section 1 liquid helium II can be compared with the solid state of a heavier substance in the sense that in both a state of complete order is realized when the zero point of absolute temperature is approached. The existence of this ordering principle gives a close similarity between the behaviour of liq. He II and the solid state notwithstanding the fact that the density of liquid He II is so much smaller than that of an ordinary solid that the shear modulus happens to be zero in this case. According to these theories one considers the lattice of the substance at $T=0$, together with an interstitial lattice formed by the interlattice sites (see Fig. 14 *a*, *b*, *c*).

Lennard–Jones' theory of melting considers a simple cubic lattice of the NaCl type. The *cubic face centered lattice* of the solid substance

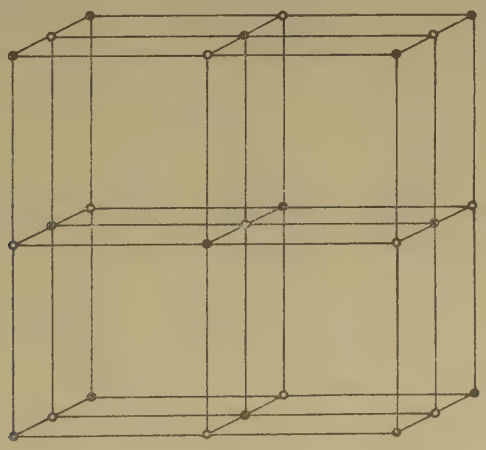

(a)

Fig. 14. Lattice ● and interstitial lattice o in:
(a) theory of melting of Lennard–Jones

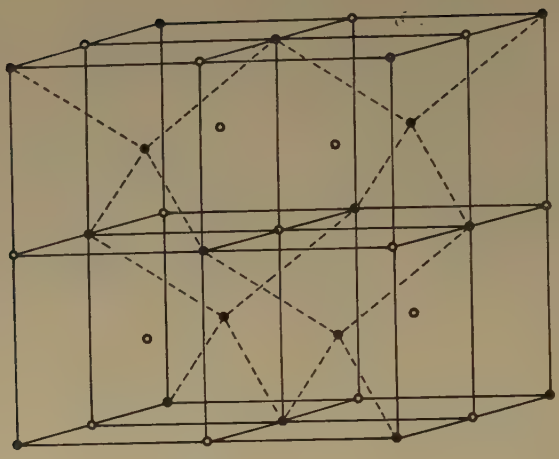

(b)

(b) theory of Fröhlich based on diamond lattice

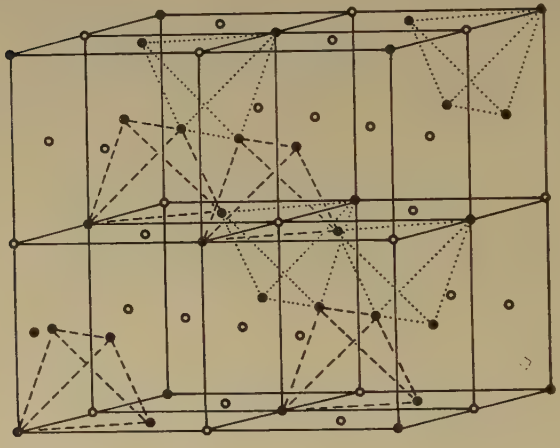

(c)

(c) theory of Fröhlich based on T_d^2 lattice.

at $T=0$ is identical with the lattice of the Na-sites and the interstitial lattice of empty sites are the Cl-positions.

Fröhlich's theory of the λ-transition considers a cubic body centered lattice, half the sites of which constitute a *diamond lattice* and the other half being the interlattice sites. When it became clear that liquid He at $T=0$ is not arranged according to a diamond lattice

Keesom and Taconis [28] generalized Fröhlich's theory for the λ-transition by considering a cubic face centered lattice, half the sites of which constitute the T_d^2-lattice considered in section 2 and the other half consists again of the interlattice sites.

The melting phenomenon, as well as the λ-transition, now is explained as a transition in the process of gradually distributing all the atoms over the lattice sites *and* the interlattice sites. The transition thus becomes entirely analogous to the order-disorder transition of very similar character occurring in binary metallic alloys like CuZn. The total entropy of disorder which is finally obtained when equal numbers of sites and inter-lattice sites are available is $2R \ln 2 = 1.38\, R$ per mole. It is well known that the transition in binary alloys sets in at a temperature where the entropy is still only about 65–70 % of this total disorder entropy, there still being some short range order left above the transition point which gradually disappears at higher temperatures. The fact that the entropy of liquid ^{4}He at the λ-point is only 60 % of this value is in rough agreement with this picture. It is also well known that the heat capacity curves for liquid ^{4}He and for β-brass closely coincide when both are plotted as function of T/T_λ.

It may be good to recall that according to the results concerning the atomic distribution in liquid ^{4}He, as discussed in section 2, such a concept of a partly occupied cubic face centered lattice for liquid Helium II is not in disagreement with experiment and is able to give an interpretation of some of the features of the scattering data

b) *Density Effects*

The present model is also able to throw some light on the relation between the anomaly in the heat capacity and that in the thermal expansion coefficient. If the anomaly in the heat capacity, which sets in at roughly 0.6° K, and the negative contribution to the thermal expansion coefficient, which becomes important in the same temperature region (both of which must be due to the molecular excitations), are indicated * by $C^{(\mathrm{mol})}$ and $\alpha^{(\mathrm{mol})}$, they seem to behave very similarly as a function of temperature (see Fig. 5 and Fig. 7) being roughly proportional according to: $\alpha^{(\mathrm{mol})} \approx -0.01\, C^{(\mathrm{mol})}/R$. According

* The contributions to C and α resulting from the molecular excitations are distinguished by an upper index (mol). Thus $C = C^{(\mathrm{ph})} + C^{(\mathrm{mol})}$ and $\alpha = \alpha^{(\mathrm{ph})} + \alpha^{(\mathrm{mol})}$.

to Jones this can be roughly understood by remembering that in order-disorder the entropy depends only on a quantity kT/W_0, where W_0 is the excitation energy needed for placing an atom on the interlattice position. On this basis straightforward thermodynamics shows that:

$$\alpha^{(\mathrm{mol})} = \varkappa \left(\frac{\partial p}{\partial T}\right)_V = \varkappa \left(\frac{\partial S}{\partial V}\right)_T = -\varkappa \frac{d \ln V}{d \ln W_0} \tilde{C}_v^{(\mathrm{mol})}, \qquad (11)$$

thus explaining the proportionality between $\alpha^{(\mathrm{mol})}$ and $C_v^{(\mathrm{mol})}$.

Using $\varkappa = 1.2 \times 10^{-8} \mathrm{cm}^2/\mathrm{dyne}$ one thus obtains $\mathrm{d} \ln W_0/\mathrm{d} \ln V \approx +0.3$.

An independent check on this is obtained from the change of the λ-temperature under pressure. As the λ-temperature should depend only on W_0/k this gives direct information on the change of W_0 under pressure, giving $\varkappa(\mathrm{d} \ln T/\mathrm{d} \ln V)_\lambda = (\mathrm{d} \ln W_0/\mathrm{d} \ln V)_\lambda = 0.40$ which is not very different from the figure obtained from the thermal-expansion coefficient.

To understand qualitatively the change of the excitation energy W_0 under pressure, we have to recall that the T_d^2-structure is an open structure with low coordination number. Increase of the temperature leads to an increasing number of atoms on interlattice sites, destroys the open structure, and is accompanied by a decrease in volume, which demonstrates itself in the negative expansion coefficient. In this respect there is a close similarity with the melting of ice in which also an open structure breaks down accompanied by a decrease in volume instead of the usual increase, although the total anomalous volume decrease of about 1.3 % is much smaller than in the case of ice. The increase of disorder, accompanying the increase of coordination number with rising temperature makes the excitation energy for placing atoms in interlattice positions gradually smaller and smaller than the $T = 0$ value W_0, a phenomenon which is characteristic for a cooperative phase transition. Decrease of volume at constant temperature, however, also results in an increase of coordination number, an increase in disorder and thus in a decrease of the excitation energy W_0. Decrease of volume and increase of temperature thus have in principle the same effect in liquid helium: increase of the coordination number, increase of disorder and thus *in*crease of entropy. Although it is possible to explain, some of the main features and to give some qualitative insight into the λ-transition, a more quantitative theory is rather difficult to give because of the difficulty of giving a more quantitative description of the increasing disorder.

c) *Role of Exchange Effects – Spin-Ordening*

It is important to discuss in this picture the influence of the exchange effects which might be of importance for a comparison of the behaviour of ^{4}He and ^{3}He. A molecular excitation in this theory places an atom on an interlattice position and thus brings this atom much closer to some of the neighbouring atoms. Now it may be expected that for atoms having antisymmetrical wave functions such a closer packing is more difficult to produce than for symmetrical wave functions. The argument is somewhat complicated, however, because of the fact that ^{3}He has a nuclear spin and ^{4}He has not. One may expect that two ^{3}He atoms with parallel spin have a *smaller* probability of being close to each other than ^{3}He atoms with anti-parallel spin, because the spatial wave function should be antisymmetrical in the first and symmetrical in the second case. As for ^{4}He atoms the wave function should be always symmetrical, there seems to be little doubt that the probability of finding two ^{4}He atoms close together is larger than for two ^{3}He atoms.

There is, however, an additional difference between liquid ^{4}He and ^{3}He, caused by two factors: the molar volume of ^{3}He is larger and the molecular mass is smaller. These two effects have a compensating influence on the excitation energy for an atom on an interlattice site and it is difficult to see which of these dominates. *If* these two effects compensate, however, one may conclude that in the case of ^{3}He most probably *the energy of an interlattice excitation* would be larger than in the case of He because of the statistics. One would conclude, therefore, that in liquid ^{3}He the spatial disordering process, which according to this theory is responsible for the λ-transition in liquid ^{4}He, would require somewhat higher temperatures in liquid ^{3}He and therefore is not observed.

There remains, however, according to this picture in liquid ^{3}He the necessity for ordering also the nuclear spins. The fact that at a temperature of 0.5° K the entropy is still of the order of magnitude of $S = R \ln 2 = 0.69\, R$ thus would indicate that the ordering process for the nuclear spins starts at temperatures below 0.5° K.

It is obviously difficult to develop in more detail a theory based on the order-disorder concepts and to make more quantitative statements about the role of the exchange effects. The general type of picture which might be expected on this basis is summarized *schematically*

in Fig. 15 in which are given the entropy contributions from the collective excitations $S^{(phon)}$, that from the molecular excitations $S^{(mol)}$ (where it has been assumed that for ^{3}He W_0 is somewhat larger than for ^{3}He) and the spin entropy $S^{(spin)}$. The experimental

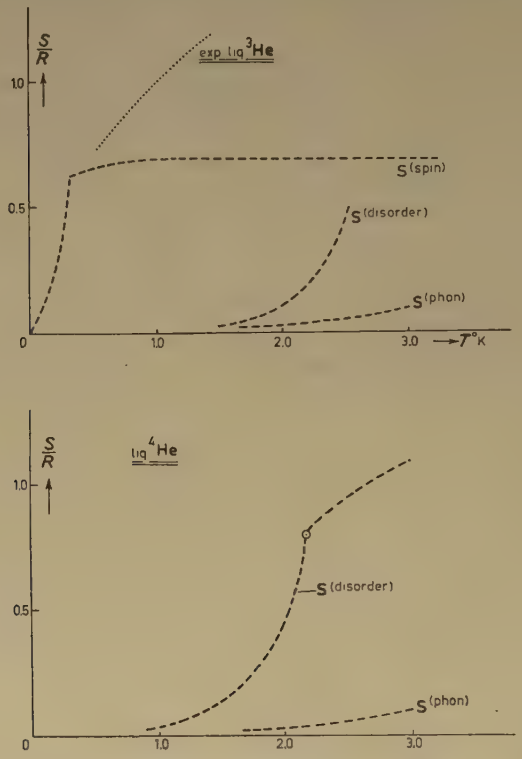

Fig. 15. Schematic picture of order-disorder treatment of liquid ^{4}He and ^{3}He.

curve for liq. ^{3}He suggests that this picture is insufficient: There must be some reason why the molecular excitations start at much lower temperatures. Another way of putting the question is to remark that obviously there is a much closer correlation between the spin-disorder and the spatial-disorder which becomes important in approximately the same temperature region in liquid ^{3}He. It will be shown that the cell treatment in which these two effects are treated at the same time gives somewhat better results in this respect.

B) Fluctuation Theory

Before starting the discussion of the cell theory we wish to stress the close relation between Fröhlich's order-disorder theory and the *fluctuation theory* of Prigogine [22]. In these considerations the molecular excitations are identified with density fluctuations. For the purpose of describing these density fluctuations Prigogine makes use of the cell picture: At $T = 0$ every molecule is moving in its cell, but at higher temperatures molecules gradually move, leave their cell empty and give rise to a doubly occupied cell somewhere else.

A molecular excitation of this type is thus very similar to a molecular "disorder" excitation to an interlattice site. The further thermodynamic treatment given by Prigogine is somewhat different, the result being that the entropy shows a sharp rise at that temperature at which the molecular excitations of this double-occupancy-type or density fluctuations become more and more probable. Of course the exchange effects have a big influence on the molecular fluctuation-excitations: the two atoms can be in the same quantum state in the doubly occupied cell in the case of ^{4}He, but for ^{3}He it is necessary to force one of the two into a more excited state when the spins are parallel, resulting in an excitation energy for ^{3}He which is so much higher that no excitation of these fluctuations appeared to be possible in liquid ^{3}He. This conclusion, which is similar to that drawn above for the molecular disorder excitations, is based, however, on rather qualitative arguments as was also the case with our discussion of the influence of the exchange effects on W_0. For further details concerning these calculations, the density effects and the application to mixtures, we refer to the original publications of Prigogine and Philippot [22].

C. The Cell-Theory

It was shown in the previous section A that the order-disorder treatment, although having the advantage of giving an explanation of the λ-transition, probably will have difficulties to explain the influence of the statistics: apparently the disorder in liquid ^{3}He starts at much lower temperatures than one would expect from purely theoretical considerations. This means that there must be molecular excitations of a somewhat different type which have the property that they can be excited much easier in ^{3}He than is the case in ^{4}He. In this connection the "cell-theories" which have been developed in recent years have made much progress. As the theories of this type

which have been proposed independently by J. de Boer and E. G. D. Cohen [24], P. Price [26], O. K. Rice [25] and by H. N. V. Temperley [27] are somewhat different in starting point and also in the further statistical treatment, we shall follow an argumentation which according to the author is the background for this procedure.

a) *Thermal Motion in Classical Liquids*

We first give an intuitive picture of this approach. In the discussion of the collective excitations which occur in liquid helium it was indicated that from the two types of collective excitations in a solid: the longitudinal or compressional excitations (with rot $\mathbf{v} - 0$) and the transversal or shear excitations (with div $\mathbf{v} = 0$), the latter do not occur in liquid helium because the shear modulus is zero. The different character of these two types of excitations is given in Fig. 16: arrows indicate the direction of simultaneous vibration in these modes of vibration; excess and deficit in pressure are indicated by + and −; no change in pressure is indicated by 0.

When in the liquid state the shear modulus is zero, the restoring force for the transversal motions is zero. This causes these motions

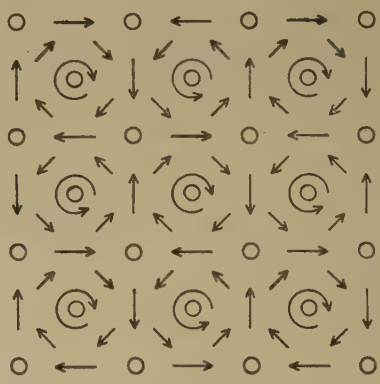

Figs. 16 and 17. Longitudinal (upper figure) and transversal modes (lower figure) in a two-dimensional solid. The phases have been chosen such that at the walls $v_\perp = \partial v_{\parallel}/\partial n = 0$ and σ_x has been chosen equal to σ_y.

The equations are:

$$v_x = A_x \sin 2\pi\sigma_x x \cos 2\pi\sigma_y y \exp i\omega t$$
$$v_y = A_y \cos 2\pi\sigma_x x \sin 2\pi\sigma_y y \exp i\omega t$$
$$\text{compr.mode:} \quad \text{rot } \mathbf{v} = 0 \quad A_x\sigma_y - A_y\sigma_x = 0$$
$$\text{transv.mode:} \quad \text{div } \mathbf{v} = 0 \quad A_x\sigma_x + A_y\sigma_y = 0.$$

to degenerate to rotational motions, damped by viscous forces as shown in Fig. 16, *b*. Brillouin [29] evaluated on this basis the *molar heat-capacity for a classical liquid* as follows:

The molar heat capacity due to the longitudinal, compressional waves, is in solid and liquid the sum of a kinetic and potential part, giving: $\frac{1}{2}R+\frac{1}{2}R=R$.

In a solid each of the transversal waves gives a similar contribution, making in total $2(\frac{1}{2}R+\frac{1}{2}R)=2R$ for the transversal waves because of the 2 degrees of freedom. One would expect that for a liquid from these transverse excitations only the *kinetic* contribution to the molar heat capacity: $2\cdot\frac{1}{2}R=R$ is left. One thus gets for a monoatomic solid a molar heat capacity $3(\frac{1}{2}R+\frac{1}{2}R)=3R$ and one would expect for a monoatomic liquid $1(\frac{1}{2}R+\frac{1}{2}R)+2\cdot\frac{1}{2}R=2R$. In fact, there is no abrupt change in heat capacity at the melting point, because of the fact that the transversal motions in the liquid state will be hindered rotations or librations, which still contain an appreciable potential energy contribution to the heat capacity. For the liquid state one would thus expect that for a classical liquid the molar heat capacity falls gradually from $3R$ at the melting point to $2R$ at the critical point. This is in fact the case for monoatomic liquids like Ne and A and one may consider this with some reserve as a rough confirmation of the concepts explained above.

b) *Molecular Excitations in Liquid Helium*

If we now consider this picture with *quantum mechanics*, we would expect that similar to the spectrum of possible longitudinal waves with wavelengths varying from very large values down to the value $\approx 2a$ at the boundary of the first Brillouin zone or the Debye-limit, we would have a spectrum of rotational motions with dimensions of the rotating groups varying from very large values down again to values of the dimension of the lattice distance a. Just as in the smallest longitudinal wave two neighbouring atoms vibrate in opposite phase, in the smallest rotational motion two neighbouring molecules would rotate round each other. Quantization has the effect that excitation of the longitudinal elastic waves requires an excitation energy hc/λ which thus becomes the smaller, the larger the wavelength is, and the maximum value $\approx hc/\lambda_D$ of which corresponds to the wavelength $\lambda_D \approx 2a$ at the Debye limit.

A similar spectrum of excitation energies could be expected for

the rotational motions, the quanta being of the order of magnitude $\hbar^2/ml^2$, when l is the diameter of the rotating group. From this picture it would then follow that not only the longitudinal modes, but also the rotational modes could easily be excited at very low temperatures, which is in conflict with the experimental findings at low temperatures.

The solution for this difficulty has been indicated by Feynman [30], who pointed out that the energy of excitation for rotational motions of a large number of atoms is very much larger than $\hbar^2/ml^2$ because of the large zero-point energy required for a synchronized rotational motion of a large group of molecules. In fact, it might be that the whole spectrum is *inverted* and the smallest excitation energy is that for the rotational motions corresponding to the Debye limit, i.e. the rotation or libration of a pair of neighbouring atoms; rotation of larger groups would then require a larger excitation energy.

We have thus arrived at the following picture for the possible excitations in liquid helium:

(1) one branch of *collective excitations*, corresponding to the longitudinal or compression waves with excitation energies $\varepsilon = hc\sigma = hc/\lambda$, starting from $\varepsilon = 0$ up to $\varepsilon \approx hc/2a$.

(2) various types of *molecular excitations* corresponding to rotational or rotation-vibrational (or librational) motions of small groups of molecules, requiring a finite excitation energy, the lowest value of which should be of the order of magnitude $\hbar^2/ma^2$.

For the evaluation of the contribution to the heat capacity due to these molecular excitations, we make an approximate calculation which is very similar to the Einstein procedure in the theory of solids: in the solid state, instead of considering all the different Debye-waves, with their frequencies, one divides the solid into N cells and one considers all the atoms as vibrating independently in their cells. The energy of excitation $h\nu_E$ in the cells is then not far from that at the Debye-limit of the vibrational spectrum.

We therefore replace the system of liquid helium by a system of N_c independent cells, each cell containing a small group of 2, 3 or 4 molecules which are moving independently of the neighbours.

We have thus to investigate what types of excitations are possible in these cells and it will be shown that the librational motions have the lowest excitation energy and thus are the only excitations which are of importance for the thermodynamic behaviour of liquid helium at low temperatures.

Moreover we will assume these cell excitations to be *localized*: when a single cell is excited, this excitation in general will have a certain probability to be transferred to neighbouring cells. In principle this state is therefore N_c-fold degenerate. Each excited state in the cell broadens to a narrow band of N_c states, to be distinguished by a wave vector $\boldsymbol{\sigma}$. The energy corresponding to this band r is $\varepsilon^{(r)}(\sigma) = \varepsilon_0^{(r)} + \hbar^2\sigma^2/2\mu_r$ where μ_r is the effective mass for the motion of a single excitation through the lattice. We will assume for simplicity that $\mu = \infty$ and thus neglect the motion of cell-excitations in the evaluation of the thermodynamic properties.

The free energy of this system of N_c independent cells then becomes:

$$F^{(\mathrm{mol})} = -N_c\, kT \ln Z^{(\mathrm{cell})}, \quad (12a) \qquad Z^{(\mathrm{cell})} = \sum_r \exp(-\beta\, \varepsilon_0^{(r)}) \quad (12b)$$

the quantum states in the cell being indicated by r.

If these molecular excitations are *nonlocalized*, the free energy is still given approximately by (12) as long as the effective mass is so large that the width of the band ($\approx \hbar^2/\mu_r a^2$) remains small compared to the mutual distance of the bands ($\approx \hbar^2/m_{\mathrm{He}} a^2$), i.e. when $\mu_r \gg m_{\mathrm{He}}$. When, however, the effective mass becomes comparable with m_{He} one has to use the expression (5), which is valid for any type of excitations and which in the case of molecular excitations, for which $kT \ll \varepsilon_0^{(r)}$. leads to:

$$F^{(\mathrm{mol})} = \sum_r F_r^{(\mathrm{mol})} \qquad F_r^{(\mathrm{mol})} = -kTV \int \exp -\beta\, \varepsilon^{(r)}(\sigma)\, d\boldsymbol{\sigma} \qquad (13)$$

Originally Landau [31] introduced a type of molecular excitations, the rotons, having an excitation energy: $\varepsilon^{(\mathrm{rot})}(\sigma) = \varepsilon_0^{(\mathrm{rot})} + \hbar^2\sigma^2/2\mu_{\mathrm{rot}}$ with $\varepsilon_0^{(\mathrm{rot})}/k = 8.5°$ K and having a large effective mass $\mu_{\mathrm{rot}} \approx 7.5\, m_{\mathrm{He}}$.

More direct information about the "mass" of the excitations could be obtained however from the "normal fluid density". This quantity, which according to the Landau [31]–Kramers [11]–Kronig [12] theory of the non-equilibrium phenomena is the mass per unit volume, which has to be attributed to the "gas of excitations", is expressed in terms of the distribution function $f(\sigma)$ of the excitations by the formula

$$\varrho_n = -\tfrac{1}{3} \int (\partial f/\partial \varepsilon)\, p^2\, d\boldsymbol{\sigma} = \int f(\sigma)\, [\tfrac{4}{3}\, p/w - \tfrac{1}{3}\, (p^2/w^2)\, d^2\varepsilon/dp^2]\, d\boldsymbol{\sigma}$$

where $w = d\varepsilon/dp$ is the group velocity of the excitations. For phonons for which $\varepsilon = cp$, one obtains sumply $p/w = \varepsilon/c^2$ or:

$$\varrho_n^{(\mathrm{phon})} = (4/3c^2) \int f(\sigma)\, \varepsilon\, d\boldsymbol{\sigma} = (4/3c^2)\, \tilde{U}^{(\mathrm{phon})} = 16\, \pi^5\, k^4\, T^4/45\, h^3 c^5$$

whereas for rotons, for which $\varepsilon = \varepsilon_0 + p^2/2\mu_{\text{rot}}$, one obtains

$$\varrho_n^{(\text{rot})} = \int f(\sigma)\, \mu_{\text{rot}}\, d\boldsymbol{\sigma} = \mu_{\text{rot}}\, n^{(\text{rot})}$$

$n^{(\text{rot})}$ being the number of rotons per unit volume. The values of ϱ_n can be determined from the experimental values of the velocity of second sound: $c_{\text{II}}^2 = (\varrho_n/(\varrho - \varrho_n))\tilde{S}^2 T/\tilde{C}_v \varrho$. At low temperatures, in the phonon region, the agreement between theory and experiment for $\varrho_n^{(\text{phon})}$ is satisfactory, but from an analysis of the available data between 1.3 and 1.8° K, Landau concluded [32] that a better agreement with the experimental data could be obtained by using an expression of the form $\varepsilon^{(\text{rot})}(\sigma) = \varepsilon_0^{(\text{rot})} + \hbar^2(\sigma - \sigma_0)^2/2\mu_{\text{rot}}$ where $\sigma_0 = 0.310 \times 10^8$ cm^{-1} and where now $\varepsilon_0^{(\text{rot})}/k = 9.6°$ K and $\mu_{\text{rot}} = 0.77\ m_{\text{He}}$. It should be mentioned, however, that in the region between 0.7 and 1.1° K, where these molecular excitations start playing a role, the agreement between theory and experiment is not yet convincing, whereas at higher temperatures where the agreement is good one would expect that the interaction between the excitations would spoil the independent-excitation picture on which these calculations of Landau are based.

c) *Quantum Mechanical Treatment of Collective and Molecular excitations on the Basis of the Cell-Model*

It is possible to give a more systematic quantummechanical treatment leading to the two types of thermal excitations. For full details we refer to an article to be published by J. de Boer and E. G. D. Cohen [24].

We divide the available liquid volume into $N_c = N/\nu$ cells each containing ν atoms, which cells will be indicated by letters α, β, ... Let the centre of mass of the ν atoms moving in any of these cells α be $\mathbf{R}_\alpha$ and let the coordinates of the ν atoms with respect to this centre of mass be indicated by the set $\mathbf{r}_\alpha \equiv \mathbf{r}_{\alpha 1}, \mathbf{r}_{\alpha 2}, \ldots \mathbf{r}_{\alpha,\nu-1}$ *.

The total Hamiltonian of the system can now be written as:

$$\mathscr{H} = \mathscr{K}_{\mathbf{R}} + \sum_\alpha \mathscr{K}_{\mathbf{r}_\alpha} + \sum_\alpha \Phi_\alpha + \tfrac{1}{2} \sum_\alpha \sum_\beta \Phi_{\alpha\beta}(\mathbf{r}_\alpha, \mathbf{r}_\beta; \mathbf{R}) \qquad (14)$$

where $\mathscr{K}_{\mathbf{R}} = \sum_\alpha (-\hbar^2/2m)\Delta_{\mathbf{R}_\alpha}$ is the kinetic energy operator of the centres of mass $\mathbf{R} \equiv \mathbf{R}_\alpha, \mathbf{R}_\beta, \ldots$; $\mathscr{K}_{\mathbf{r}_\alpha}$ is the kinetic energy operator corresponding to the motion of the atoms in cell α with respect to

* There are only $\nu - 1$ radius vectors to determine the positions of the ν atoms with respect to the centre of mass.

the centre of mass $\mathbf{R}_\alpha$; $\Phi_\alpha(\mathbf{r}_\alpha)$ is the mutual interaction of the molecules in cell α and $\Phi_{\alpha\beta}$ is the interaction between the atoms in cell α and those in β, which interaction depends on $\mathbf{R}_\alpha - \mathbf{R}_\beta$ as a parameter.

The quantum-mechanical treatment is based on the adiabatic method in which the motions connected with the centres of mass $\mathbf{R}_\alpha, \mathbf{R}_\beta, \ldots$ are considered to be slow, compared with those corresponding to the motions inside the cells, connected with the coordinates $\mathbf{r}_\alpha, \mathbf{r}_\beta, \ldots$. This treatment is justified when the excitation energies of collective motions connected with the centre of mass are small compared with the excitation energy of molecular motions in the cells. This in fact seems to be the case in liquid helium: the excitation energy of collective motions becomes smaller and smaller, the longer the wave lengths of the compressional waves; those of the molecular motions inside the cells are separated from the ground state by a finite gap corresponding to at least several degrees Kelvin.

According to the adiabatic method as developed by Born and Huang [34] we first consider the *centre of mass coordinates fixed*, i.e. the coordinates $\mathbf{R}$ are first treated as parameters. We then determine the eigenfunction for the motion of the ν molecules moving in the cell α, satisfying the equations:

$$\{\mathcal{H}_\alpha + \Phi_\alpha(\mathbf{r}_\alpha) + \sum_\beta [\bar{\Phi}^\beta_{\alpha\beta}(\mathbf{r}_\alpha) - \bar{\Phi}_{\alpha\beta}]\}\, \psi_{n_\alpha}(\mathbf{r}_\alpha) = \varepsilon_{n_\alpha} \cdot \psi_{n_\alpha}(\mathbf{r}_\alpha) \tag{15}$$

where

$$\bar{\Phi}^\alpha_{\alpha\beta}(\mathbf{r}_\alpha) = \int \psi_0^*(\mathbf{r}_\beta)\, \Phi_{\alpha\beta}(\mathbf{r}_\alpha\, \mathbf{r}_\beta)\, \psi_0(\mathbf{r}_\beta)\, \mathrm{d}\mathbf{r}_\beta \tag{15a}$$

is the interaction of the molecules in cell α with one of the surrounding cells β, averaged over the ground state in these cells β and where

$$\bar{\Phi}_{\alpha\beta} = \int\int \psi_0^*(\mathbf{r}_\alpha)\, \psi_0^*(\mathbf{r}_\beta)\, \Phi_{\alpha\beta}(\mathbf{r}_\alpha\, \mathbf{r}_\beta)\, \psi_0(\mathbf{r}_\alpha)\, \psi_0(\mathbf{r}_\beta)\, \mathrm{d}\mathbf{r}_\alpha\, \mathrm{d}\mathbf{r}_\beta \tag{15b}$$

is the average interaction between the cells α and β, both in the ground state. In this way $\varepsilon_{n_\alpha} - \varepsilon_0$ is the excitation energy of the cell α in the state n_α when ε_0 is the ground state energy.

The approximate eigenfunction for the whole system, still keeping the centre of mass coordinates $\mathbf{R} \equiv \mathbf{R}_\alpha, \mathbf{R}_\beta \ldots$ fixed as parameters, is:

$$\Psi_n(\mathbf{r}) = \prod_\alpha \psi_{n_\alpha}(\mathbf{r}_\alpha) \tag{16}$$

where $n \equiv n_\alpha, n_\beta \ldots$ and $\mathbf{r} \equiv \mathbf{r}_\alpha, \mathbf{r}_\beta \ldots$. The diagonal elements of the r-dependent part of the Hamiltonian (14) are then given by:

$$\left.\begin{aligned} W_n = \int \Psi_n^*(\mathbf{r}) \{ \sum_\alpha \mathcal{H}_{\mathbf{r}_\alpha} + \sum_\alpha \Phi_\alpha + \tfrac{1}{2} \sum_\alpha \sum_\beta \Phi_{\alpha\beta} \} \Psi_n(\mathbf{r})\, \mathrm{d}\mathbf{r} = \\ = \tfrac{1}{2} \sum_\alpha \sum_\beta \bar{\Phi}_{\alpha\beta} + \sum_\alpha \varepsilon_{n_\alpha} \end{aligned}\right\} \quad (17)$$

except for small terms which can be neglected when the number of cell excitations is small and the neighbouring cells of an excited cell can always be assumed to be in the ground state. This expression for W_n is clear from the physical point of view: the first term represents the average interaction energy between the cells and the second the sum of the energies inside the different cells.

There exist also *non-diagonal terms*, which shows that the function (16) is not a proper eigenfunction, but only an approximate one. Consider a state $\Psi(n, \alpha) = \psi_n(r_\alpha) \cdot \psi_0(r_\beta) \ldots$ in which cell α is excited in the state $n_\alpha = n$ and all other cells are in the ground state $n_\beta = n_\gamma = \ldots = 0$, then all different states $\Psi(n, \alpha)$ in which one of the other cells β is excited are degenerated with $\Psi(n, \alpha)$ so that the proper approximation for the eigenfunction should be:

$$\Psi_{n,k}(\mathbf{r}) = \sum_\alpha \Psi(n, \alpha)\, \mathrm{e}^{\mathrm{i}\mathbf{k}\cdot\mathbf{R}_\alpha}$$

which function satisfies the requirement of periodicity of the lattice of the centres of mass. The wave vector $\mathbf{k}$ may take all values in the first Brillouin zone of the lattice formed by these centres of mass. The motion of an excitation of cell α to neighbouring cells is caused by the matrix elements

$$\int \psi_n(\mathbf{r}_\alpha)\, \psi_0(\mathbf{r}_\beta)\, \bar{\Phi}_{\alpha\beta}\, \psi_0(\mathbf{r}_\alpha)\, \psi_n(\mathbf{r}_\beta)\, \mathrm{d}\mathbf{r}_\alpha\, \mathrm{d}\mathbf{r}_\beta$$

and gives rise to a broadening of the energy of an excited state into a narrow band. For the case of one single excitation at the bottom of this band (small k) the expression for the energy as function of the wave number k becomes $W_{n,k} = W_0 + (\varepsilon_n - \varepsilon_0) + \hbar^2 k^2 / 2\mu_{\mathrm{exc}}$ where μ_{exc} can be expressed in the matrix elements of $\Phi_{\alpha\beta}$ given above. This extra term thus corresponds to a kinetic energy of these excitations and μ_{exc} to their effective mass. The treatment thus gives in principle the possibility of calculating the effective mass of these molecular excitations. We will, however, neglect this kinetic energy of these cell-excitations and thus assume μ_{exc} to be infinite. The effect of the kinetic energy on the thermodynamic properties is most probably very small, the only effect being that all excited states due to molecular excitations broaden to a narrow band.

According to the adiabatic method as developed by Born and Huang [34] we now consider the *energy $W_n(R)$ as a function of the centre of mass coordinates* $\mathbf{R} \equiv \mathbf{R}_\alpha, \mathbf{R}_\beta, \ldots$, which occurred as a para-

meter in the previous treatment, and determine the eigenfunctions $\Xi(\mathbf{R})$ of the equation:

$$\{\mathscr{K}_{\mathbf{R}} + V(\mathbf{R})\}\,\Xi(\mathbf{R}) = E \cdot \Xi(\mathbf{R}) \tag{18}$$

where the potential energy in this equation is taken to be:

$$V(\mathbf{R}) = W_0(\mathbf{R}) + \int \Psi_0^*(\mathbf{r};\mathbf{R})\,\mathscr{K}_{\mathbf{R}}\,\Psi_0(\mathbf{r};\mathbf{R})\,\mathrm{d}\mathbf{r}. \tag{19}$$

In the integral, $\mathscr{K}_{\mathbf{R}}$ operates on $\mathbf{R}$ occurring in $\psi(\mathbf{r})$ as a parameter. The solution of this equation can be obtained by developing in the well-known way the total potential energy $V(\mathbf{R})$ in a power series in $\mathbf{R}-\mathbf{R}_0$ around the value of $\mathbf{R}-\mathbf{R}_0$ for which this potential energy is a minimum. After introducing normal coordinates $Q_{\boldsymbol{\sigma}}$ the equation can then be transformed into ($v \equiv v_{\boldsymbol{\sigma}}, v_{\boldsymbol{\sigma}'}, \ldots$).

$$\sum_{\boldsymbol{\sigma}} \left(-\tfrac{1}{2}\hbar^2 \frac{\partial^2}{\partial Q_{\boldsymbol{\sigma}}^2} + \tfrac{1}{2}\omega_{\boldsymbol{\sigma}}^2 Q_{\boldsymbol{\sigma}}^2 \right) \Theta_v(Q) = \left(E_v - V(R_0)\right) \cdot \Theta_v(Q) \tag{20}$$

where

$$\Theta_v(Q) = \prod_{\boldsymbol{\sigma}} \theta_{v_{\boldsymbol{\sigma}}}(Q_{\boldsymbol{\sigma}}) \tag{21}$$

and

$$E_v = \sum_{\boldsymbol{\sigma}} (v_{\boldsymbol{\sigma}} + \tfrac{1}{2})\,\hbar\omega_{\boldsymbol{\sigma}}. \tag{22}$$

Using the adiabatic method the problem has thus been separated into two distinct parts:

(1) the solution of the problem of the cell excitations or molecular excitations for given values of $\mathbf{R}-\mathbf{R}_\alpha, \mathbf{R}_\beta \ldots$, by Eq. (16),

(2) the solution of the problem of the vibrational motions given by Eq. (21) corresponding to the well-known system of vibrational modes in the harmonic approximation.

The *total eigenfunction* can now be written as approximately [34]:

$$\Omega_{v_{\boldsymbol{\sigma}};n}(R, r) = \prod_{\sigma} \theta_{v_{\boldsymbol{\sigma}}}(Q_{\boldsymbol{\sigma}}) \prod_{\alpha} \psi_{n_\alpha}(\mathbf{r}_\alpha). \tag{23}$$

The diagonal elements of the total Hamiltonian appear to be:

$$E_{\mathrm{tot}} = \int\int \Omega^*\,\mathscr{H}\,\Omega\,\mathrm{d}\mathbf{R}\,\mathrm{d}\mathbf{r} = V(\mathbf{R}_0) + \sum_{\boldsymbol{\sigma}} (v_{\boldsymbol{\sigma}} + \tfrac{1}{2})\hbar\omega_{\boldsymbol{\sigma}} + \sum_{\alpha} (\varepsilon_{n_\alpha} - \varepsilon_0) \tag{24}$$

where we have neglected small contributions resulting from the influence of cell excitations on the potential energy $V(\mathbf{R})$, which can

be neglected at low temperatures where the number of excitations is assumed to be small.

The wave function (23) is not a correct eigenfunction: there remain non-diagonal matrix elements of $\mathscr{H}$ of the type:

$$\int\int \Xi_{v'}^{*}(\mathbf{R})\, \Psi_{n'}^{*}(\mathbf{r};\mathbf{R})\, [\mathscr{K}_R,\, \Psi_n(\mathbf{r};\mathbf{R})]\, \Xi_v(\mathbf{R})\, \mathrm{d}\mathbf{R}\, \mathrm{d}\mathbf{r} \qquad (25)$$

(where $[a, b] = ab - ba$) which cause transitions between excitations of the elastic waves and internal excitations in the cells. The basic assumption of the adiabatic method is, however, that these effects are small and that the wave function (23) is a good approximation to the true eigenfunction (see for details Born and Huang [34]).

The adiabatic method thus allows a systematic quantum-mechanical treatment to be given, leading to the result that the total wave function of the system can be written as the product of a wave function corresponding to the elastic modes and a wave function corresponding to excitations in the different cells; and the energy can be written as the sum of two distinct contributions from the vibrations of the whole system and the cell excitations. Obviously the approximation is only good as long as the elastic modes have a wavelength long compared with the distance between cells. In this region $\omega_\sigma = 2\pi c \cdot \sigma$ where c is the macroscopic velocity of sound. In the particular case of liquid helium the transversal modes do not exist and thus the only excitations which have to be taken into account in the summation over σ are the longitudinal modes.

In this way the adiabatic method gives a division of the excitations in liquid helium into "*collective excitations*" connected with the elastic vibrations of the centres of mass of the cells and "*molecular excitations*" connected with motions of the atoms inside their cells with fixed centre of mass. The method gives also the formal expressions from which one may calculate the effective mass of the molecular excitations, as well as the expressions which allow the evaluation of the probability for transfer of excitation energy between collective excitations and molecular excitations, or in the language of Landau, between phonons and rotons.

In first instance one might think that the results obtained in this way depend very much on the size of the cells. In this connection it is important, however, to realize that the contribution of the collective excitations to the thermodynamic quantities as given in § 3, *b* did *not* depend on the molecular structure: the thermodynamic quantities

$\tilde{F}^{(\mathrm{ph})}$, $\tilde{S}^{(\mathrm{ph})}$, etc. per unit volume and the thermal pressure $p^{(\mathrm{ph})}$ depend only on the velocity of sound c, which is a macroscopic quantity which does *not* depend on the subdivision of the whole system into cells as long as these cells remain cells on a molecular scale. The contribution due to the collective excitations is thus largely independent of the subdivision into cells. The contribution from the molecular excitations depends on the size of the cells. Here one would expect that the larger the cell is chosen, the better the results will be (provided, of course, that the cell remains of molecular dimensions!). But of course for the treatment of more than two molecules in the cells we have to fall back on crude approximation methods which rather soon nullify the advantage of having taken a larger cell.

d) *Molecular Excitations in Cells with two Molecules*

We first consider a somewhat simplified model of a system of *spherical* cells with hard elastic walls in each of which move two atoms. Although the exact value of the radius of the cell will turn out to be not very important, we define the cell diameter as follows: The average distance $\bar{a}$ between neighbouring molecules in liquid ^{4}He is about 3.6 Å. Using for He-atoms an effective hard sphere diameter $d = 0.8\,\sigma = 2.05$ Å, the radius R_1 of a single cell is taken to be $R_1 = 3.6 - \frac{1}{2}(2.05) = 2.6$ Å. The radius of the double cell is then taken to be $R_2 = 2^{1/3} R_1 = 3.27$ Å.

We now consider the system of two helium atoms, with the centre of mass in the centre of the cell and moving under influence of their mutual interaction potential $\varphi(r)$ given by (1). According to Eq. (15) we then have to determine the eigenvalues of this system subject to the boundary condition that the radial wave function for the relative motion has a node at $r_0 = 2R_2 - d = 4.4$ Å.
The radial wave functions have been found by numerical integration of the Schrödinger equation:

$$(-\hbar^2/m)\mathrm{d}^2(r\psi)/\mathrm{d}r^2 + [\varphi(r) + \hbar^2 J(J+1)/mr^2](r\psi) = \varepsilon(J) r\psi \qquad (26)$$

for different values of the energy of relative motion ε and for different values of the angular momentum quantum number J. The values of the energy for which the corresponding wave-function has its first node at $r = r_0$ could be represented for the values $J = 0, 1, 2$, etc. by the well-known formula

$$\varepsilon(J) = \mathrm{const} + k\Theta \cdot J(J+1) \qquad (27)$$

corresponding to excited rotational states with constant moment of inertia $I_2 = \hbar^2/2k\Theta$. States with radial nodes, i.e. vibrational excitations in the double cell, have an energy which is much too high to be able to exist in this double cell. The excited states in the double cell thus behave as those of a rotation with constant moment of inertia which can be found from the value $k\Theta$ of the constant in (27). A determination of the distance of the atoms from these values of $I_2 = \frac{1}{2}ma_0^2$ gives $a_0 = 3.25$ Å, which compares nicely with the lattice distance for the T_d^2 lattice. A similar conclusion holds in the case of liquid ^{3}He. The data are summarized in the following table:

PARAMETERS FOR DOUBLE CELL

	liq. ^{4}He	liq. ^{3}He
$\bar{a} = (V/N)^{1/3}$	3.58 Å	3.99 Å
$R_1 = a - \frac{1}{2}d$	2.56 Å	2.97 Å
$R_2 = 2^{1/3}R_1$	3.23 Å	3.74 Å
$r_0 = 2(R_2 - \frac{1}{2}d)$	4.40 Å	5.42 Å
$\Theta = \hbar^2/2I_2k$	1.125 °K	1.248°K
a_0(from $I_2 = \frac{1}{2}ma_0^2$)	3.25 Å	3.62 Å
a_0(T_d^2-structure)	3.18 Å	3.54 Å

We now take into account the symmetry effects and the spin effects.

In the case of liquid ^{4}He there is *no* spin and the wave function should always be symmetrical, i.e. J should be even. Thus:

$$Z_{^4\mathrm{He}}^{(\mathrm{cell})} = \sum_{J=0,2,4\ldots} (2J+1) \exp\left(-\beta\varepsilon(J)\right) \tag{28}$$

where, of course, each state has the weight $2J+1$ because of the rotational degeneracy.

On the other hand, for liquid ^{3}He there *is* a spin $\frac{1}{2}\hbar$ and the total wave function including the spin state should be always antisymmetric. Thus when the total spin of the two ^{3}He atoms is equal to $S=1$, the angular momentum quantum number $J=$ odd; whereas for antiparallel nuclear spins ($S=0$) the angular momentum $J=$ even. The cell partition function thus becomes:

$$\left.\begin{aligned} Z_{^3\mathrm{He}}^{(\mathrm{cell})} &= \sum_J g_J (2J+1) \exp\left(-\beta\varepsilon_J\right) \\ g_0 = g_2 = g_4 &= \ldots = 1 \\ g_1 = g_3 = g_0 &= \ldots = 3. \end{aligned}\right\} \tag{29}$$

Thus the total weights for the states $J = 0, 1, 2, \ldots$ are in the case of ^{4}He: 1, 0, 5, 0, 9, ... and in the case of ^{3}He: 1, 9, 5, 21, 9, ... This results in the first excited state for ^{4}He corresponding to $6 \times 1.125 = 6.75°$ K, whereas in the case of ^{3}He the first excited state is $2 \times 12.48 = 2.5°$ K with a weight 9 (see Fig. 18). This difference in behaviour between ^{3}He and ^{4}He makes an enormous difference in the entropy, which for ^{3}He rises at very low temperatures to much higher values than is the case with ^{4}He. In fact, this is what is found experimentally as is shown in Fig. 19. The exchange effects thus explain directly the remarkable difference in entropy which exists between liquid ^{3}He and ^{4}He at very low temperatures.

It should be pointed out that the approximation which uses a spherical cell is somewhat artificial: The cell will be *ellipsoidal*

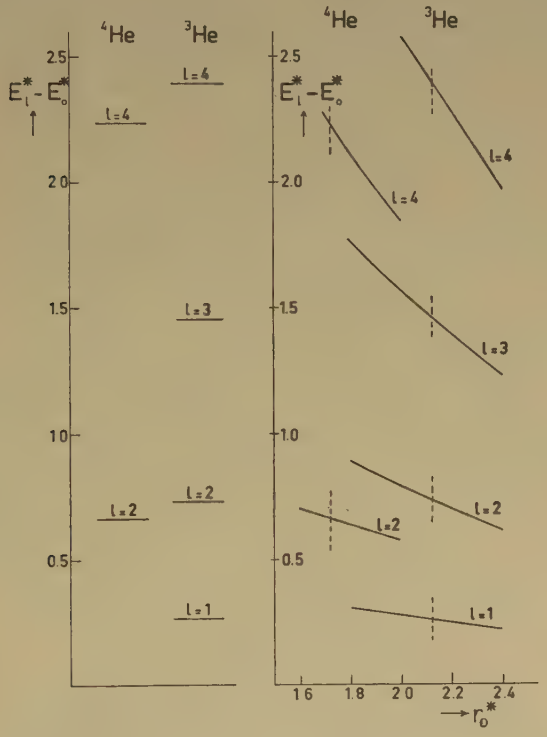

Fig. 18. Energy levels in double-cell as a function of the maximum distance $r_0^* = r_0/\sigma$ in the double cell and energy levels for $r_0 = 1.72\,\sigma = 4.40$ Å and $r_0 = 2.12\,\sigma = 5.42$ Å for ^{4}He and ^{3}He respectively.

having a hindering potential which prevents free rotation for small excitations. Such a hindering potential might be of the form:

$$V(\vartheta) = -A\left(\frac{3}{2}\cos^2\vartheta - \frac{1}{2}\right) \tag{30}$$

where ϑ is the angle which the axis of the pair of atoms makes with the symmetry axis of the cell.

The lowest excited states in the ellipsoidal cell are not of the rotational but of the rotation-vibrational type which are often indicated as "librational" because free rotation is prevented by the barrier. This, of course, has some influence on the evaluation of the partition function, because the hindering potential leads to a splitting up of each rotational level. The energy eigenvalues then are modified with somewhat changed weights, but as far as the order of magnitude is concerned, the calculations will remain correct. Another consequence of this librational motion in the ground state is that now also the

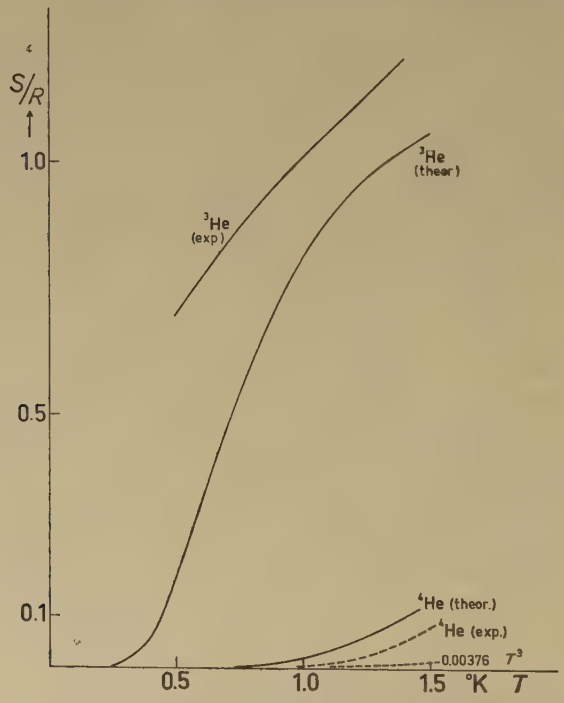

Fig. 19. Entropy of ^{4}He and ^{3}He at low temperatures according to the cell model.

zero-point energy obtains an additional contribution from the transversal oscillations of a pair of atoms in the double cell. This is important in connection with the fact which we found in section 2, viz. that the zero-point energy of the longitudinal modes alone was insufficient to explain the total zero-point energy which occurs obviously in the case of liquid helium.

e) *Molecular Excitations in Cells with more than two Atoms*

It is not too difficult to obtain some information as to the molecular excitations which would be obtained by considering cells of three or four molecules. In fact the structure of the type T_d^2, which might possibly be approximately the ordered arrangement of the helium atoms, makes plausible rotations of three molecules as well as of four molecules. In Fig. 20 it is shown how in this structure the surrounding atoms of a triangle of three atoms are arranged. This suggests that for a group of three molecules in a triangle a rotation of the triangle

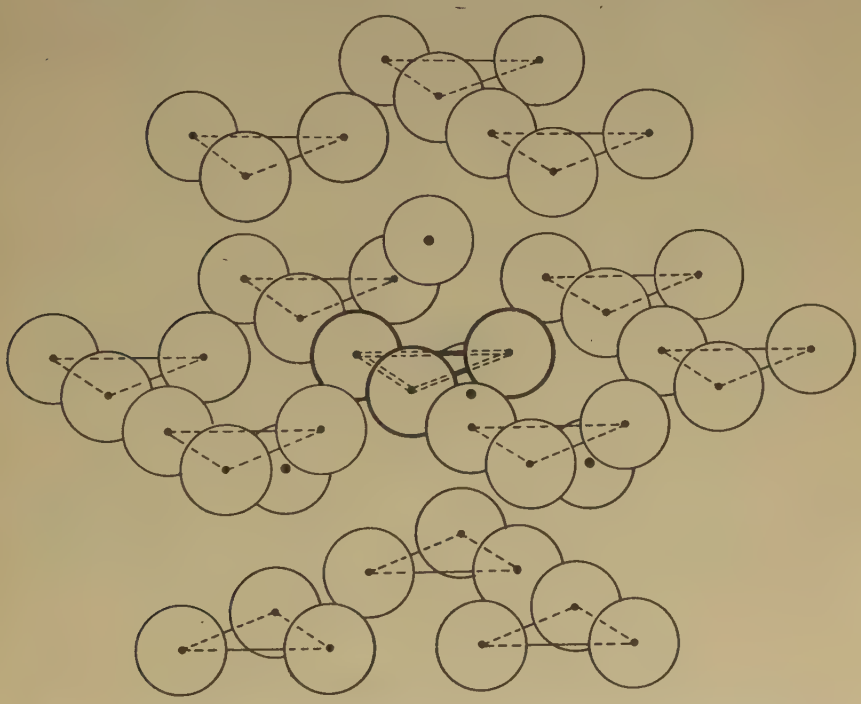

Fig. 20. The surrounding sites of a triangle of three sites in the T_d^2-structure.

as a whole in the plane could easily be excited. The excitation energies are then given approximately by:

$$\varepsilon(J) = (\hbar^2/2I_3)J^2 \tag{30}$$

where the moment of inertia is equal to half the value for a pair of molecules when the interatomic distance is taken to be the same, giving $\hbar^2/2I_3k = 2.25°$ K for ^{4}He and $\hbar^2/2I_3k = 2.50°$ K for ^{3}He.

In order to investigate the influence of the symmetry effects we have to investigate the symmetry properties of the eigenfunctions of a plane triangular rotator. The problem is very similar to that of the rotation of molecules like CH_3Cl around their symmetry axis, which problem has been considered by E. B. Wilson. The result is that for ^{4}He atoms with symmetrical wave functions and no spin only the states $J = 0, 3, 6$, etc. are allowed, giving:

$$Z^{(\text{cell})}_{^4\text{He}} = \sum_{J=0,3,6,\ldots} 2 \exp\left(-\beta\varepsilon(J)\right) \tag{31}$$

where of course each state has the weight 2 because of the rotational degeneracy.

On the other hand for ^{3}He atoms having antisymmetrical wave functions and a nuclear spin $\frac{1}{2}\hbar$ we have:

$$\left.\begin{array}{ll} Z^{(\text{cell})}_{^3\text{He}} = \sum g_J \cdot 2 \exp\left(-\beta\varepsilon(J)\right) & \\ g_0 = 2 \qquad\qquad g_1 = g_4 = g_7 = \ldots = 2 & \\ g_3 = g_6 = \ldots = 4 \qquad g_2 = g_5 = g_8 = \ldots = 2 & \end{array}\right\} \tag{32}$$

Figure 21 shows that one might also obtain a good approximation by considering groups of 4 atoms arranged in a tetrahedron. In fact, the structure of T_d^2 can be considered as a close-packed arrangement of tetrahedrons, and therefore an approximation in which the liquid is divided into a close packed arrangement of $N_c = \frac{1}{4}N$ spherical cells each of which contains a group of 4 He atoms, approximately arranged in a tetrahedral configuration, might offer a good approximation. During the motion of these 4 atoms in a spherical cell they will remain approximately arranged in the form of a tetrahedron and the energy levels will therefore be given approximately by

$$\varepsilon(J) = \frac{\hbar^2}{2I_4} J(J+1) \tag{33}$$

where $I_4 = I_3 = \frac{1}{2}I_2$. Thus for ^{4}He: $\hbar^2/2I_4k = 2.25°$ K and for ^{3}He: $\hbar^2/2I_4k = 2.50°$ K. Again we can apply to the investigation of the

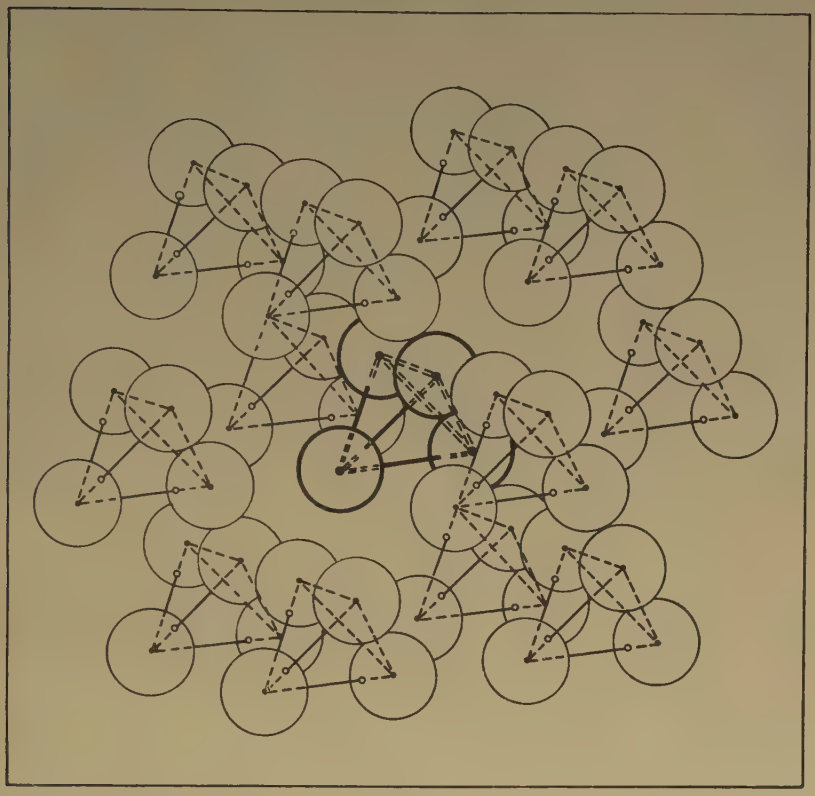

Fig. 21. The surrounding sites of a tetrahedron of four sites in the T_d^2-structure, showing the "close packed" surrounding by 12 tetrahedrons.

symmetry effects the results of molecular spectra, this time those of CH_4 investigated also by E. B. Wilson. In ^{4}He only the states with $J = 0, 3, 6, \ldots$ are allowed, giving:

$$Z_{^4\mathrm{He}}^{(\mathrm{cell})} = \sum_{J=0,3,6\ldots} (2J+1) \exp\left(-\beta\varepsilon(J)\right) \tag{34a}$$

whereas in the case of ^{3}He the nuclear spin gives rise to the following complicated set of weights:

$$Z_{^3\mathrm{He}}^{(\mathrm{cell})} = \sum_{J} g_J (2J+1) \exp\left(-\beta\varepsilon(J)\right) \tag{34b}$$

$$\begin{aligned} g_0 = g_6 = \ldots &= 5 & \qquad g_3 = g_9 = \ldots &= 11 \\ g_1 = g_7 = \ldots &= 3 & \qquad g_4 = g_{10} = \ldots &= 13 \\ g_2 = g_8 = \ldots &= 5 & \qquad g_5 = g_{11} = \ldots &= 11 \end{aligned}$$

In Fig. 22 we have compared the energy levels and the weights for the states in ^{3}He and ^{4}He for cells containing 2, 3 and 4 atoms respectively. The most important difference between these models is that in the cells with more than two atoms the lowest state is degenerate. Thus the entropy approaches at low temperatures the values

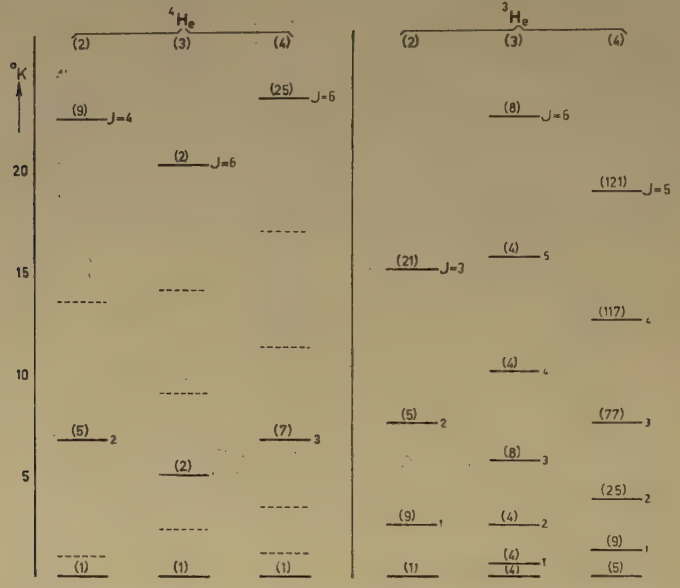

Fig. 22. Energy levels for cells containing 2, 3 or 4 He atoms, for the cases ^{3}He and ^{4}He.

$\frac{1}{3}R \ln 4 = 0.46\,R$ and $\frac{1}{4}R \ln 5 = 0.40\,R$ for cells with 3 or 4 atoms respectively. These models thus show in any case a much larger entropy for ^{3}He than in the case for ^{4}He. At somewhat higher temperatures above 0.5° K the behaviour between the different cell-occupations is not very different. At low temperatures, however, it is necessary to introduce the interaction between different cells so as to split up the lowest degenerate level.

f) *Discussion λ-Transition*

As has been indicated before, the idea of using the quantum states of pairs of helium atoms to explain why ^{3}He differs so remarkably from ^{4}He when we consider the behaviour of the entropy at low

temperatures has been put forward also independently by Temperley [27] and Rice [25]. Considerable discussion has been given by these authors to the system of levels which would explain the low temperature entropy of liquid ^{3}He. Thus Temperley suggests that a triplet at 0.4° K and an octet at 2.7° K are needed to give the experimental entropy curve, although a difficulty seems to be that in connection with these empirical levels a Debye entropy of $0.04\,RT^3$ would be necessary, which is about five times the value which seems reasonable in the case of ^{3}He. The question of the position of the lowest levels seems therefore still open and more measurements of the specific heat at very low temperatures will be needed to give more information about this point. The work of P. Price [26] had its origin in attempts to explain the magnetic susceptibility of liquid ^{3}He at very low temperatures. Also here the cell model proved to give interesting consequences in agreement with experiments, but the discussion of this point is considered to be outside the scope of this contribution.

The question remains to give on the basis of the cell theory an explanation of the *λ-transition*. The order-disorder theory gave directly an explanation of the λ-transition as being a cooperative transition at the temperature when the long range order becomes zero.

In the cell theory the λ-transition must also result from a cooperative effect, here, however, caused by the interaction between excitations in neighbouring cells. One of the approximations introduced in the present treatment is that the interaction with the neighbouring cells is the average interaction, averaged over the ground state of the neighbouring cell as shown in Eq. (15a). In fact, however, the interaction *depends* on the state in the neighbouring cells and just as the cooperative effect in the case of order-disorder transition results from the fact that existing disorder facilitates the creation of new disorder, one might expect in our picture that most probably *excitation in one cell is facilitated by the excitation of motions in neighbouring cells.* In this way again a cooperative transition results which then should be identified with the λ-point in liquid ^{4}He. It should be stressed, however, that it is by no means certain *that* this interaction leads to a phase transition. In the case of ^{3}He the cooperative process sets in at much lower temperatures, but it is not very well possible to predict whether this interaction causes a phase transition also in this case. If the cell excitations are of the rotational type the transition

we are describing here is a *rotational type of transition*, which in fact is based on the assumption that the rotation of one group is facilitated by that of the neighbouring groups. Unfortunately the statistical mechanics of transitions of this type is in a much more rudimentary state than that of the order-disorder transitions. The very great difficulty of treating the interaction properly and dealing with the spatial degeneracy have made the existing treatments unsatisfactory so far and it is not very well possible therefore at this moment to go into a more detailed discussion of the application of these types of phase transitions in the case of liquid helium.

The considerations given in this contribution only apply therefore to a temperature region far from the λ-point where the cooperative effects, disturbing the relatively simple situation at low temperatures, do not yet play an important role. Most probably, however, these kinds of effects are already important at temperatures between 0.5 and 1.0° K in liquid ^{3}He and this is the main reason why not very much attention has been paid to attempts to evaluate exactly the entropy of liquid ^{3}He from a detailed theory of the individual cell excitations.

As a concluding remark it may be good to mention that the treatment of the excitations in liquid helium, divided into the order-disorder (or also fluctuation) type of theory and into the cell theory does *not* mean that these two concepts are contradictory or that they exclude each other mutually. This division has been chosen only to make the exposition somewhat systematic, but these two types of excitations are rather similar in many respects. In fact, sometimes rotational transitions can be explained only slightly differently in terms of an order-disorder treatment. One may hope, therefore, that in the future it will be possible to make a proper synthesis of these considerations.

D. Other Theories

Extremely interesting progress in calculating the energy of excitations in liquid ^{4}He has been made by Feynman [30] and by Feynman and Cohen [30]. Although a complete discussion of their results falls outside the scope of this contribution, it may be useful to outline the relation with the results obtained with the cell theory approach. Following a suggestion originally made by A. Bijl, Feynman used

a trial wave function for the first excited state in liquid ^{4}He of the form

$$\Psi_{\boldsymbol{\sigma}}(\mathbf{r}_1 \ldots \mathbf{r}_N) = \varphi_0(\mathbf{r}_1 \ldots \mathbf{r}_N) \cdot \sum_{i=1}^{N} \exp 2\pi i\, \boldsymbol{\sigma} \cdot \mathbf{r}_i \tag{35}$$

where $\vartheta_0(\mathbf{r}_1 \ldots \mathbf{r}_N)$ is the groundstate eigenfunction and where the factor

$$Q_{\boldsymbol{\sigma}} = \int [\sum_{i=1}^{N} \delta(\mathbf{r}_i - \mathbf{r})] \exp(2\pi i\, \boldsymbol{\sigma} \cdot \mathbf{r})\, d\mathbf{r} = \sum_{i=1}^{N} \exp 2\pi i\, \boldsymbol{\sigma} \cdot \mathbf{r}_i, \tag{36}$$

being the Fourier transform of the microscopic density operator $\sum_i \delta(\mathbf{r}_i - \mathbf{r})$, is the normal coordinate corresponding to the wave vector $\boldsymbol{\sigma}$. In accordance with the fact that the eigenfunction of an harmonic oscillator in the first excited state is obtained from that of the ground state by multiplication with the coordinate (36), one may expect (35) to be a good approximation for the first excited state of the elastic waves. Using the variational principle the excitation energy turns out to be

$$\varepsilon(\sigma) = h^2 \sigma^2 / 2\, m S(\sigma) \tag{37}$$

where the normalizing factor $S(\sigma)$ may be transformed into:

$$\left.\begin{aligned} S'(\sigma) &= \int \ldots \int \varphi_0^2\, Q_{\boldsymbol{\sigma}} Q^*_{\boldsymbol{\sigma}}\, d\mathbf{r}_1 \ldots d\mathbf{r}_N = \\ &= 1 + n \int [g(r) - 1] \sin(2\pi\sigma r) \cdot (2\pi\sigma r)^{-1} d\mathbf{r} \end{aligned}\right\} \tag{38}$$

$g(r)$ being the pair correlation functions in the *ground state.* Assuming that these excitations for long wave lengths really describe the elastic (phonon-) excitations, $S(\sigma)$ should approach in the limit $\sigma \to 0$ to $S(\sigma) \to h\sigma/2mc$, which would give $\varepsilon = hc\sigma$, c being the velocity of sound. For higher values of σ the quantity $S(\sigma)$ can be obtained empirically from the X-ray scattering intensity as function of the scattering angle. Introduction of these values then leads to a curve for $\varepsilon(\sigma)$ having a maximum at $\sigma_{\max} \approx 0.25$ Å^{-1} and a subsequent minimum at $\sigma_{\min} = 0.32$ Å^{-1} with $(\varepsilon_{\min}/k) \approx 19.5°$ K. The general shape of the curve is in agreement with Landau's suggestion, that the two types of excitations: $\varepsilon = hc\,.\,\sigma$ (for σ small) and $\varepsilon = \varepsilon_0 + h^2(\sigma - \sigma_0)^2/2m$ (for $\sigma \approx \sigma_0$), can be considered as forming part of *one simple excitation curve.* The experimental value of ε_0/k is only 9.6° K, being half the value obtained at first by Feynman [30], whereas the experimental value of $\sigma_0 \approx 0.31$ to 0.36 Å^{-1} is in good agreement with the theory.

In a subsequent article Feynman and Cohen [30] used an improved trial function

$$\psi_{\sigma} = \varphi_0 \cdot \sum_{i=1}^{N} (1 + A \sum_{j \neq i} \mathbf{r}_{ij}/r_{ij}^3) \exp 2\pi i \, \boldsymbol{\sigma} \cdot \mathbf{r}_i \tag{39}$$

where the additional factor accounts for the "backflow" around a moving particle. With this wave function the minimum of the curve lowers to the value $\varepsilon_{\min}/k \approx 11.5°$ K but the curvature at the minimum seems still to be considerably higher than indicated by Landau.

A suggestion about the physical nature of the maximum and subsequent minimum in the $\varepsilon(\sigma)$ curve assumed by Landau and explained in principle by Feynman can be obtained by using again the lattice-structure model which was on the basis of the treatment in the previous chapters. In such a model the elastic waves show dispersion: the $\varepsilon(\sigma)$ curve has a maximum when the wave number is approximately at the Brillouin zone ($\sigma_{\text{Br.}} = 1/2a \approx 0.14$ Å^{-1} for a cubic lattice) in reciprocal space or what is roughly equivalent: near the Debye limit $\sigma_D = 0.62\, v^{-\frac{1}{3}} \approx 0.17$ Å^{-1}. The neighbouring atoms are then vibrating approximately in *opposite phase*, the wave length $\lambda = 1/\sigma$ being equal to twice the average distance a between the atoms. The fact that the maximum of the empirical curve of Landau also occurs at roughly $\sigma_{\max} \approx 0.16$ Å^{-1} seems to be in favour of this explanation. The minimum at about twice this value of σ can then be explained in principle by observing that there the wave length $\lambda \approx 3.2$ Å is of the order of the average distance of atoms $\bar{a} \approx 3.6$ Å in liquid helium. This however causes neighbouring atoms to move in the *same phase*, which obviously should lead to a minimum in the $\varepsilon(\sigma)$ curve.

The excitations considered by Feynman for liquid ^{4}He are thus in essence the long wave excitations and molecular excitations of the *longitudinal type*. The molecular excitations of the *transversal type*: i.e. the rotation-vibrational excitations considered in the previous sections, which show interesting exchange effects and require a finite excitation energy ε_0 of the same order of magnitude, should also play an important role. They have also to be taken into account so as to complete the picture of the thermal excitations of liquid helium.

REFERENCES

1 I. Prigogine, Advances in Physics, **3**, 131 (1954).
2 J. de Boer, Physica, **14**, 139 (1948).
3 J. S. Dugdale and F. E. Simon, Proc. Roy. Soc., A, **218**, 291 (1953).
4 J. de Boer and R. J. Lunbeck, Physica, **14**, 510 (1948).
5 H. C. Kramers, J. D. Wasscher, C. J. Gorter, Physica, **18**, 329 (1952), Comm. Leiden 288c.
G. R. Mercus, J. Wilks, Phil. Mag., **45**, 1163 (1954).
Z. Dokoupil, G. van Soest, D. H. N. Wansink, D. G. Kapadnis, Physica, **20**, 1181 (1954), Comm. Leiden 298a.
H. C. Kramers, T. van Perki–Tinbergen, J. Wiebes, F. A. W. van den Burg and C. J. Gorter, Physica, **20**, 743 (1954), Comm. Leiden 296b.
H. C. Kramers, Thesis Leiden 1956, Proc. Kon. Ak. Wet. Amsterdam, B, **58**, 302 (1955).
6 G. de Vries and J. G. Daunt, Phys. Rev., **92**, 1572 (1953); **93**, 631 (1954).
T. R. Roberts and S. G. Sidoriak, Phys. Rev., **93**, 1418 (1954).
D. W. Osborne, B. M. Abraham, B. Weinstock, Phys. Rev., **94**, 202 (1954).
7 W. H. Keesom, *Helium*, Elzevier, p. 227.
8 F. J. Webb, K. R. Wilkinson and J. Wilks, Proc. Roy. Soc., A, **214**, 546 (1952).
9 K. R. Atkins and M. H. Edwards, Phys. Rev., **97**, 1429 (1955).
10 H. Fröhlich, Physica, **4**, 639 (1937).
11 H. A. Kramers, Physica, **18**, 653 (1952), Comm. Leiden Suppl. 105a.
12 R. Kronig, Physica, **19**, 535 (1953).
13 I. M. Khalatnikov, Journ. Exp. Theor. Phys., U.S.S.R., 23, 8 (1952).
14a R. P. Feynman, Phys. Rev., **91**, 1291 (1953).
b G. V. Chester, Phys. Rev., 93, 606, 1412 (1954); 94, 246 (1954); 99, 1062 (1955).
c S. T. Butler and M. H. Friedman, Phys. Rev., **98**, 287, 294 (1955).
15a J. Reekie, T. S. Hutchison and C. F. A. Beamont, Proc. Phys. Soc., A, **66**, 409 (1953).
J. Reekie, T. S. Hutchinson, Phys. Rev., **92**, 827 (1953).
C. F. A. Beamont, J. Reekie, Proc. Roy. Soc., A, **228**, 363 (1955).
b W. L. Gordon, C. H. Shaw and J. C. Daunt, Phys. Rev., **96**, 1444 (1954).
c D. G. Hurst and D. G. Henshaw, Phys. Rev., **91**, 1222 (1953); **100**, 994 (1955).
16 J. S. Dugdale and F. E. Simon, Proc. Roy. Soc., A, **218**, 291 (1953).
17 London, Superfluids II, p. 23.
18 K. R. Atkins and C. E. Chase, Proc. Phys. Soc., London, A, **64**, 833 (1951).
C. E. Chase, Proc. Roy. Soc., A, **220**, 116 (1953).
A. van Itterbeek and G. Forrez, Physica, **20**, 133 (1954).
19 H. C. Kramers, J. D. Wasscher and C. J. Gorter, Physica, **18**, 329 (1952), Comm. Leiden 288c.
K. R. Atkins and R. A. Stasior, Can. J. of Phys., **31**, 156 (1953).
20 H. Fröhlich, Physica, **4**, 639 (1937).
21 H. Jones, Proc. Cambr. Phil. Soc., **34**, 253 (1938).
22 I. Prigogine, Advances in Physics, **3**, 131 (1954).
I. Prigogine and J. Philippot, Physica, **18**, 729 (1952); **19**, 227 (1953); **19**, 235 (1953).

[23] J. E. Lennard Jones and A. F. Devonshire, P. Roy. Soc., A, **163**, 53 (1937); A, **169**, 317 (1939); A, **170**, 464 (1939).
[24] J. de Boer, Proc. Int. Conf. Theor. Phys., Japan, 508 (1953).
J. de Boer and E. G. D. Cohen, Physica, **21**, 79 (1955); Proc. Int. Conf. on Low Temp., Paris, 1955, p. 113.
J. de Boer and E. G. D. Cohen, Physica (to be published).
[25] O. K. Rice, Phys. Rev., **97**, 263 (1955); Proc. Int. Conf., Paris, 1955, p. 117.
[26] P. Price, Phys. Rev., **97**, 259 (1955).
[27] H. N. V. Temperley, Proc. Phys. Soc., London, A, **67**, 495 (1954); Phys. Rev., **97**, 263 (1955), Proc. Int. Conf. Low Temp., Paris, 1955, p. 115.
[28] W. H. Keesom, *Helium*, Elsevier.
[29] L. Brillouin, Les tenseurs en mécanique et en élasticité, p. 349, Masson et Cie, Paris, 1938; J. de Physique, **6**, 337 (1935).
[30] R. P. Feynman, Phys. Rev., **91**, 1301 (1953); **94**, 262 (1954).
R. P. Feynman and M. Cohen, Phys. Rev., **120**, 189 (1956).
[31] L. Landau, J. Phys., U.S.S.R., **5**, 71 (1941).
[32] L. Landau, J. Phys., U.S.S.R., **11**, 91 (1947).
[33] R. B. Dingk, Advances in Physics, **1**, 112 (1952).
J. Wilks, Nuovo Cimento, **10**, Suppl. 4, 509.
J. G. Dannt and R. W. Smith, Rev. Mod. Phys., **26**, 172 (1954).
[34] M. Born and K. Huang, Dynamical theory of crystal lattices, Oxford, 1954.
[35] P. A. Egelstaff and H. London, Private communication.
H. S. Somers, J. C. Dash and L. Goldstein, N. S. At. En. Comm. Doc. 2855.
L. Goldstein, D. Sweeney and M. Goldstein, Phys. Rev., **77**, 319 (1950).
[36] S. T. Butler, J. M. Blatt, M. R. Schafroth, to be published.

CHAPTER II

LIQUID HELIUM BELOW 1° K

BY

H. C. KRAMERS

KAMERLINGH ONNES LABORATORIUM, LEIDEN

CONTENTS: 1. Introduction, 59. — 2. Techniques, 60. — 3. The theory of elementary excitations and the two-fluid model, 61. — 4. Experiments on static and reversible properties, 65. — 5. Dissipative effects, 70. — 6. Large mean free path phenomena, 77. — 7. Miscellaneous experiments 80.

1. Introduction

The distinction between liquid helium above and below 1° K was originally made only for a purely technical reason. As is well-known this temperature is roughly the limit which can be attained by ordinary pumping on the liquid. For experiments at lower temperatures usually recourse has to be taken to the magnetic cooling effect of paramagnetic substances. For temperatures below about 0.7° K this is actually the only method available.

However, the physical behaviour of the liquid also justifies this distinction. As will be shown in the following discussion most of the phenomena of the liquid below 1° K can be explained by means of the theory of elementary excitations (see Vol. I Ch. II). Actually the best evidence of the suitability of Landau's theory and its later extensions can be found in this region. The condition of the scarcity of low energy states, discussed by Feynman (Vol. I Ch. II) is here certainly fulfilled, in contrast to temperatures near the λ-point. Therefore the assembly of elementary excitations may be expected to behave truly gas-like. Consequently statistical methods may be applied to this gas to deduce thermodynamic quantities and to derive the equations of the two-fluid model. (For a somewhat different approach to the problem of liquid helium see Ch. I).

Although the interaction between the excitations should not be too large for this purpose, it should also not be too small, if this theory is to be applied without more ado to non-stationary phenomena. The rapidly decreasing number of excitations with diminishing

temperature leads to a similar decrease in their interaction. As a consequence equilibrium conditions are established only relatively slowly. This is indeed what will be shown to occur at the lowest temperatures: in a general way this can be expressed by saying that the mean free path becomes very large.

The temperature region can be divided into two parts. Below 0.6° K there are only phonons; above that temperature both phonons and rotons are present. Because of the small interaction between phonons the major part of the lower region (i.e. certainly below 0.4° K) roughly coincides with that where the mean free paths are comparable with the dimensions of the experimental equipment.

2. Techniques

The usual method of attaining low temperatures by reducing the pressure above the liquid can be extended to 0.8 or even 0.7° K [18, 20, 28]. A diffusion pump must be used and the film creep must be kept as small as possible by inserting a constriction in the pumping tube. Still lower temperatures have to be attained by demagnetizing a large enough paramagnetic sample in contact with the liquid.

A general disadvantage of this latter method is that no large thermostat is present and so the liquid is warming up during the experiment. Special care is therefore required to reduce the heat influx. The vessel is surrounded by a vacuum jacket and precautions against radiation are taken. The main source of heat influx with an open vessel is the film flow. The film can creep up, evaporate somewhere in the upper parts of the cryostat and recondense in the low temperature vessel, delivering a disastrous amount of condensation heat. On the other hand an open vessel is convenient because the helium can easily be condensed into it. A compromise can be found by using a narrow capillary (e.g. with an inner diameter of 0.2 mm). This method has been employed in many experiments [1, 2, 3].

Ashmead has introduced a different design, in which the inner vessel can be closed by means of a tightly fitting evacuated conical plunger. When it is open the inner helium is in direct contact with the outer bath. If a large amount of salt and helium can be used the rather considerable heat leak is not very awkward. This set-up has also been successfully used by some investigators [4, 5].

Some experiments have been done with a closed capsule technique. The helium is brought in beforehand, either at high pressure at room

temperature [6,7] or condensed at liquid helium temperature and then sealed off [8]. The advantage of the capsule technique is the very small warming-up rate but the, perforce, heavy metal apparatus hampers magnetic temperature meausrements, which are the most reliable ones in this range. The principles of the three main methods are shown in Fig. 1.

Finally, the continuous magnetic refrigerator of Daunt and Heer [9] may prove to be very convenient for these kinds of experiments.

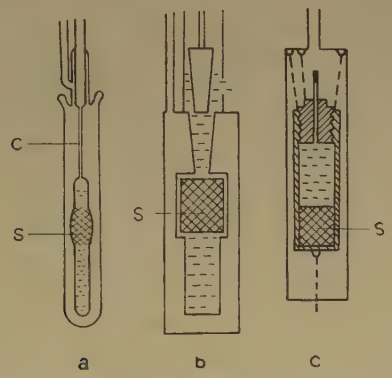

Fig. 1. Techniques.
a. capillary technique [1,2,3],
b. Ashmead plunger [4,5],
c. closed capsule (after Hull *et al.* [6]),
s = paramagnetic salt.

3. The Theory of Elementary Excitations and the Two-fluid Model

The theory of elementary excitations and Landau's interpretation of the two-fluid model on this basis have been expounded by Feynman in Vol. I, Ch. II, As has been argued there, it is supposed that there are two kinds of excitations: the phonons and the rotons. The energy-momentum relation for the phonons is $E = v_I p$ and for the rotons $E = \Delta + (p - p_0)^2/2\mu$ (see however Ch. I § 5b); v_I is the velocity of sound, Δ the zero-point energy of the rotons, p_0 their zero-point momentum and μ an effective mass [14]. One may now consider the assembly of excitations as a mixture of a phonon- and a roton gas. By applying statistics in the way indicated by Feynman in § 3 of Vol. I, Ch. II one can derive expressions for the thermodynamic quantities and for ϱ_n, the so-called normal density. All these quantities are sums of two contributing terms, one for the rotons and one for

the phonons. This is true as long as the interaction between the excitations is small, i.e. for temperatures not too near the λ-point.

In this way one finds for the specific heat per unit of mass:

$$c_v = c_{v\hbar} + c_r = \frac{16}{15}\pi^5 \frac{k^4}{\hbar^3}\frac{T^3}{v_I^3}$$

$$+ (2\pi)^{-1/2}\frac{m^{1/2}k^{3/2}}{\varrho\hbar}\left(\frac{p_0}{\hbar}\right)^2\left(\frac{\mu}{m}\right)^{1/2}\left(\frac{\Delta}{k}\right)^2\left[T^{-3/2} + \frac{k}{\Delta}T^{-1/2} + \frac{3}{4}\left(\frac{k}{\Delta}\right)^2 T^{1/2}\right]\exp(-\Delta/kT) \quad (1)$$

m being the mass of a helium atom, k the Boltzmann constant and h the Planck constant.

The two equations of motion of the two-fluid model follow immediately from the conservation laws of momentum for the gas of excitations and for the liquid as a whole. Further, the law of conservation of energy for this gas leads to the continuity equation of the entropy, reversibility being presupposed. Together with the mass conservation equation one has now four equations which determine the properties of the two-fluid model, provided irreversible effects may be neglected. Terms arising in this way which involve velocities to a higher order than the first are omitted in the equations of motion. The actually observed phenomena at large velocities can certainly not be accounted for by such serms following from the theory of excitations in its present form.

If one puts all velocities and accelerations in the equations equal to zero, the equation for the fountain effect follows immediately:

$$\text{grad}\, P = \varrho S\, \text{grad}\, T. \quad (2)$$

The mechano-caloric effect can also easily be derived:

$$Q = ST. \quad (3)$$

In the latter expression Q is the amount of heat produced per unit of mass of flowing liquid. All other thermodynamic quantities are also given per unit of mass.

For the inclusion of irreversible effects into the equations the problem has to be generalized in a way familiar from the kinetic theory of ordinary gases. This has been done by Khalatnikov [10] in a formal way. The treatment involves the setting-up of a non-equilibrium distribution function by means of the Boltzmann equation. The difference between this new function (f) and the distribution function valid in equilibrium (f_0) lies in terms depending on the derivatives with respect to the space coordinates of the temperature

and the velocities. Only the terms of the first order in these are preserved; therefore, the treatment is restricted to small deviations from equilibrium. The new distribution function, inserted into the conservation laws of the gas of excitations can now be used for a derivation of the equations of the two-fluid model, just as has been done in the case of equilibrium. The terms of $f-f_0$ lead to terms for first and second viscosity and heat conductivity in these equations.

The equations for the two-fluid model can now be written. Since there are two velocity fields ($\boldsymbol{v}_s$ and $\boldsymbol{v}_n$), one can choose any two lineair combinations of these to write down the equations of motion. For the purpose of a consideration of the propagation of ordinary and second sound it is useful to take $\boldsymbol{j}/\varrho = \varrho_n \boldsymbol{v}_n + \varrho_s \boldsymbol{v}_s$ and $\boldsymbol{w} = \boldsymbol{v}_n - \boldsymbol{v}_s$ as such. In the equations given here thermal expansion is neglected and a small transformation has been made to have only ϱ, T, $\boldsymbol{j}$, and $\boldsymbol{w}$ as variables. The result is:

$$\left.\begin{aligned} \frac{\partial \boldsymbol{j}}{\partial t} + \left(\frac{\partial P}{\partial \varrho}\right)_T \operatorname{grad} \varrho = \frac{\eta_n}{\varrho} \left(\nabla^2 + \tfrac{1}{3} \operatorname{grad} \operatorname{div}\right) (\boldsymbol{j} + \varrho_s \boldsymbol{w}) + \\ \frac{\zeta_{11}}{\varrho} \operatorname{grad} \operatorname{div} \boldsymbol{j} + \frac{\zeta_{12}}{\varrho} \operatorname{grad} \operatorname{div} (\varrho_s \boldsymbol{w}) \end{aligned}\right\} \tag{4}$$

$$\left.\begin{aligned} \varrho_n \frac{\partial \boldsymbol{w}}{\partial t} + \varrho S \operatorname{grad} T = \frac{\eta_n}{\varrho} \left(\nabla^2 + \tfrac{1}{3} \operatorname{grad} \operatorname{div}\right) (\boldsymbol{j} + \varrho_s \boldsymbol{w}) + \frac{\zeta_{12}}{\varrho} \operatorname{grad} \operatorname{div} \boldsymbol{j} \\ + \frac{\zeta_{22}}{\varrho} \operatorname{grad} \operatorname{div} (\varrho_s \boldsymbol{w}) \end{aligned}\right\} \tag{5}$$

$$\frac{\partial \varrho}{\partial t} + \operatorname{div} \boldsymbol{j} = 0 \tag{6}$$

$$\varrho \frac{c_v}{T} \frac{\partial T}{\partial t} + \varrho_s S \operatorname{div} \boldsymbol{w} = \frac{\lambda_n}{T} \nabla^2 T \tag{7}$$

where P is the pressure; η_n and λ_n are the coefficients for the viscosity and the heat conductivity of the normal fluid respectively; and ζ_{11}, ζ_{12} and ζ_{22} are three coefficients for the second viscosity.

It should be noted that the heat conductivity term has nothing to do with the heat transport observed in ordinary experiments, which is almost completely due to the motion of the normal fluid and the super-fluid. The heat conductivity term occurring in the equations is actually the heat conductivity of the normal fluid itself; as a rule its contribution is negligible in heat flow experiments.

Viscosity and heat conductivity terms were introduced much earlier [12]; the second viscosity terms arose for the first time from Khalatnikov's analysis. His interpretation of these will be given later.

Eq. (4) and (6) lead to the wave equation of ordinary sound; Eq. (5) and (7) to that of second sound. The nature of the latter is now also clear: the energy is oscillating between the kinetic energy connected with the relative motion of the two fluids and the potential energy connected with the local deviation of T from its equilibrium value. Since ϱ_n/ϱ is supposed to be dependent only on T, second sound can be thought of as a sound wave in the gas of excitations.

Neglecting dispersion, which is only an effect of the second order in the frequency, one gets for the velocities of ordinary and second sound

$$v_I^2 = \frac{\partial P}{\partial \varrho} \tag{8}$$

$$v_{II}^2 = \frac{\varrho_s}{\varrho_n} \frac{S^2 T}{c_v} \tag{9}$$

respectively. It is seen that measurements of v_{II} allow for a calculation of ϱ_n and a subsequent comparison with the theory. According to Landau [14] the phonon contribution to ϱ_n, which should be the only one at low enough temperatures, is

$$\varrho_{nph} = \frac{\varrho S T}{v_I^2} = \frac{16}{45} \pi^5 \frac{k^4}{h^3} \frac{T^4}{v_I^5}. \tag{10}$$

Consequently for temperatures near absolute zero one finds

$$v_{II}^2 = v_I^2/3. \tag{11}$$

The coefficients of absorption due to the irreversible terms can also immediately be derived from the plane wave solution of the Eq. (4), (5), (6), (7). This yields for the velocities expressions of the general form:

$$v^2 = v_0^2 + i\alpha\omega + \ldots, \tag{12}$$

higher order terms in the angular frequency ω being neglected. Since the absorption coefficient per cm (β) equals the imaginary part of ω/v, one finds easily [11, 13]

$$\beta_I = \frac{1}{2} \frac{\omega^2}{v_I^3} \frac{1}{\varrho} \left(\frac{4}{3} \eta_n + \zeta_{11} \right) \tag{13}$$

$$\beta_{II} = \frac{1}{2} \frac{\omega^2}{v_{II}^3} \left\{ \frac{\varrho_s}{\varrho \varrho_n} \left(\frac{4}{3} \eta_n + \zeta_{22} \right) + \frac{\lambda_n}{\varrho c_v} \right\}. \tag{14}$$

The coefficient ζ_{12} does not occur in these expressions; it enters into (12) only in terms proportional to ω^2.

It should be noted here that the type of two-fluid model which is yielded by the theory of excitations is less general than that proposed by Gorter (see Vol. I, Ch. I). The quantity S^* in that model has here been replaced by $\varrho S/\varrho_n$; this simplified model is identical with that obtained by H. London by a thermodynamic reasoning [15].

4. Experiments on Static and Reversible Properties

4.1. The Specific Heat

Below 0.6° K the specific heat proved indeed to be proportional to T^3 [16, 2], as would be expected, according to Debye, for a pure phonon gas and which is in agreement with Landau's predictions [14]. The temperature independent factor in the theoretical expression contains only (apart from general constants) the parameter v_I, which can be found from measurements on the velocity of sound. No very accurate measurements on this quantity are available in the low temperature region but a reliable extrapolation can be made from the range above 1° K, since just above that temperature v_I becomes practically temperature independent.

Atkins and Chase [17] deduced in this way $v_I = 239 \pm 2$ m/sec at $T = 0°$ K. This yields for the specific heat in the phonon region:

$$c_v = 0.0204\ (\pm\ 0.0006) \times T^3 \text{ joule/g deg.}$$

The experimental value of the coefficient originally published was about 15 % larger [2, 16]. However, new experiments in the Leiden laboratory, which will soon be published, indicate that this value was actually too large, and that there is no longer a discrepancy between the theoretical and the experimental value [43]. The error in the original data was probably due to an extra heat capacity of as yet unknown origin in the calorimeter. By using different amounts of liquid this effect could be eliminated. The correction is only of some importance in the range below 0.7° K.

Measurements of the specific heat in the region where rotons play also an important part allow for an evaluation of Δ/k. To find the roton contribution, the phonon part is first subtracted.

It appears that Eq. (1) gives a good representation of the experimentally found specific heat below 1.3° K with a value of Δ/k equal to 8.8 ($\pm$ 0.1)° K. At higher temperatures deviations occur because of the proximity of the λ-point (see Fig. 2).

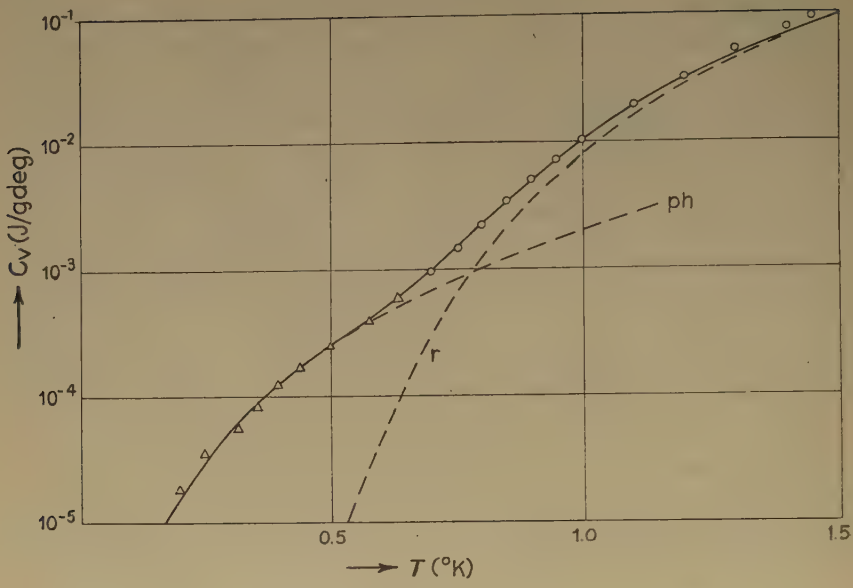

Fig. 2. The specific heat.

Fully-drawn line: total specific heat calculated from the energy spectra of phonons and rotons with $v_I = 239$ m/sec; $\Delta/k = 8.8°$ K; $p_0/\hbar = 1.96$ Å^{-1}; $\mu/m = 0.23$.

The phonon and roton parts are indicated by dashed lines separately.

○ data from Kramers *et al.* [2,16],

△ new Leiden measurements [43].

4.2. The Coefficient of Expansion

Data on the coefficient of expansion at constant pressure α_p were obtained down to 0.85° K by Atkins and Edwards [18]. Again there is a phonon and a roton contribution, the former being positive since v_I increases with pressure. The roton contribution is presumably negative, but at sufficiently low temperatures the phonon contribution should again predominate. This is indeed found experimentally: α_p is negative above 1.15° K and positive below this value. At the lowest temperatures α_p tends to approach very well the value for a phonon gas computed from v_I and its dependence on pressure [19] by means of well-known thermodynamic relations (see Fig. 3). It may be noted that the phonon influence on α_p persists at much higher temperatures than that on the specific heat (at 1° K: $c_{ph}/c_r \approx 0.25$ and $\alpha_{ph}/\alpha_r \approx 1$). For theoretical considerations one is referred to Ch. I, § 3c and 4b.

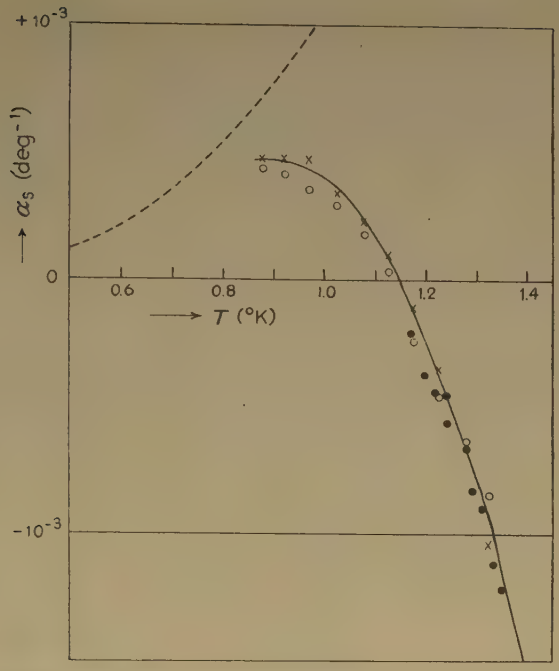

Fig. 3. The expansion coefficient at saturated vapor pressure (after Atkins and Edwards [17]).
Fully-drawn line and points: experimental data.
Dashed line: calculated phonon contribution.

4.3. The Fountain Effect

Fountain effect measurements were made by Peshkov [20] from 1.5 down to 0.82° K. By means of H. London's formula [Eq. (2)] a comparison can be made with entropy data calculated from the Leiden specific heat experiments [2]. The agreement is good.

Recently Bots and Gorter [21] published data on the fountain effect at still lower temperatures. In these measurements the so-called integral fountain effect was measured, i.e. one of the two vessels connected by a superleak of jeweller's rouge was kept at bath temperature (about 1.1° K), the other one being cooled magnetically. H. London's formula can now be tested by comparing the pressure heads with $\int_{T_1}^{T_2} S\,\mathrm{d}T$, calculated from the specific heat values. T_2 is a conveniently chosen reference temperature (e.g. 0.9°), and T_1 is the temperature of the cooled vessel. The agreement is good down to 0.70° K. Below this temperature deviations occur: the value of the

integral effect between 0.2 and 0.6° K is about 10 % lower than the calculated value. It should be noted, however, that the calculated value of the fountain height between 0.2 and 0.6° K is only 2.3 cm, while the actually measured integral effect (between 1.1° and the lower temperature) is of the order of 45 cm in this case. There seems therefore as yet no serious reason to distrust the H. London formula.

Unfortunately no experiments are available on the mechano-caloric effect in this region.

4.4. Second Sound

Of all the properties of liquid helium in the temperature range discussed the largest attention has been given by investigators to the propagation of heat pulses [22, 23, 24, 25, 26]. The preference given to pulses above sine waves is due to the small amount of heat developed with the former. Historically these experiments have played an important role, since they made possible a decision between the applicability of Landau's and Tisza's theories [14, 27]. The second author

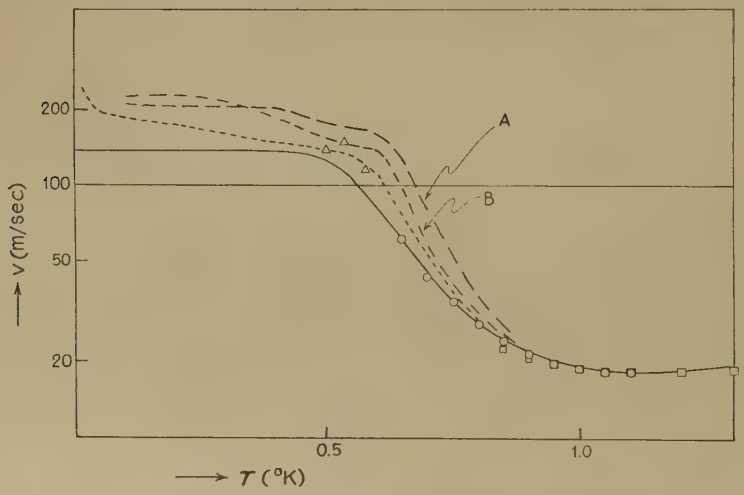

Fig. 4. Velocities of heat pulses and second sound.
Fully-drawn line: second sound velocity calculated with the parameters of Fig. 2.
□ Peshkov's data from standing waves [28];
○ Leiden data on top velocities of pulses [26];
. . . . . pulse front velocities (de Klerk *et al.* [3]); 5 cm tube.
– – – – – – – pulse front velocities from the Leiden experiments;
curve A: 1.5 cm tube,
curve B: 6.25 cm tube.
△ Osborne's data on the second sound velocity obtained from running waves.

expected the velocity of second sound to decrease from the 20 m/sec plateau at temperatures above 1° K to zero at 0° K. As has been shown, Landau's theory predicted a rise towards $v_I/\sqrt{3} = 138$ m/sec. When a rise of v_{II} was actually observed to occur below 1.1° K [22, 23, 24], it was a great triumph for the theory of phonons and rotons.

However, the interpretation of the results at low temperatures appears to be not as simple as Landau originally predicted. The shapes of the pulses are radically changed while passing through the liquid. Above 0.7° K this shape is still approximately symmetrical, but below that temperature a large tail develops and very little of the shape of the original pulse is preserved (see Fig. 5). These effects will be discussed later.

Since the pulses at low temperature do not remain narrow, it is

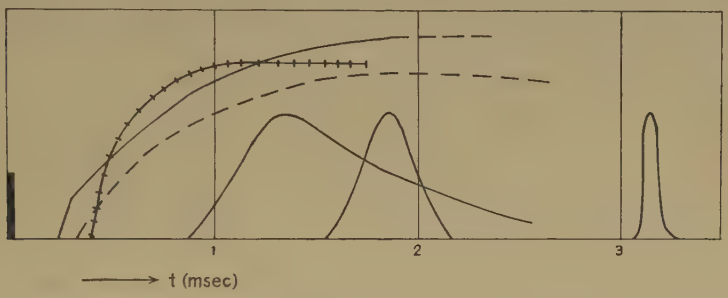

Fig. 5. Shapes of heat pulses for the 6.25 cm tube of the Leiden experiments [26]. The abscis indicates the time after the start of the heating pulse; the ordinate is arbitrary. In the order of the pulse fronts from right to left: $T = 1.1$; 0.75; 0.65; 0.55; 0.25; 0.15° K.

difficult to define a unique velocity of second sound. Most authors identified this with the velocity of the front of the signal, but this is rather an arbitrary choice. As long as the pulses are symmetrical and the original pulses have a negligible width, one should in the opinion of this author, identify the velocity of the top with v_{II}. This has been shown to occur only above 0.7° K [26]. A further condition is that surface attenuation, due to the presence of the tube can be neglected. In the experiments just mentioned [26], the velocity of the front depended clearly on the tube-length (see Fig. 4).

Standing wave measurements were extended by Peshkov [28] down to 0.81° K: the agreement with the Leiden data on v_{II} obtained from the top velocities is satisfactory.

The measurement of v_{II} allows for a calculation of ϱ_n, provided

Eq. (9) is valid. The result can be compared with the expression for ϱ_n obtained from the theory of excitations. Again there is a phonon and a roton contribution. The phonon contribution (ϱ_{nph}) has to be calculated from the theory since no direct measurements exist on either the normal density or v_{II} in the phonon region.

In view of the good agreement for the specific heat there is no reason to distrust such a calculation. ϱ_{nph} is proportional to T^4, the coefficient containing only v_I as a parameter. The roton contribution (ϱ_{nr}) can now be found by subtracting ϱ_{nph} from ϱ_n. Again one finds good agreement when $\Delta/k = 8.8°$ K. Moreover, by combining the data of ϱ_n with those of c_v it is possible to evaluate the other two parameters of the roton spectrum. One finds $p_0/\hbar = 1.96$ ($\pm$ 0.05) Å^{-1} and $\mu/m = 0.23$ ($\pm$ 0.1).

5. Dissipative Effects

A theoretical approach to the calculation of the coefficients of the irreversible processes from the kinetics of the phonon-roton gas has been made by Landau and Khalatnikov [29, 30, 13]. This has proved to be a very intricate problem: many types of collisions may occur. These collisions may even be inelastic in the sense that the number of excitations changes during the collision.

Moreover, only little is known about the nature of the rotons, though in general one may regard them as "heavy" particles in contrast to the "light" phonons since energy and momentum of the former are relatively much larger. To each type of collision one can attribute a characteristic time which determines the rate of approach to equilibrium in the gas by means of this process alone. Since the number of excitations (especially of the rotons) decreases rapidly with diminishing temperature, all these relaxation times show a substantial increase under the same condition. The temperature dependence is moreover different for all processes and consequently different types of collisions predominate at different temperatures.

A general consequence of this temperature dependence is that all irreversible coefficients increase towards low temperature. The increase of the relaxation times is actually equivalent to an increase in mean free paths.

The analysis shows that the energy and momentum transport below 1° K takes place only by the phonons. Between 0.7 and 1.0° K η_n and λ_n are determined only by elastic collisions of phonons with

rotons, i.e. transport in the phonon gas is almost exclusively limited by collisions of this type. Below 0.7° K elastic phonon-phonon collisions replace this process in limiting the momentum transport and consequently should determine η_n. According to Khalatnikov this latter process cannot affect the heat conductivity coefficient.

The second viscosity is supposed to be determined by two kinds of inelastic processes [30]: three phonons may be transformed into two, and two rotons into one roton and one phonon, or the reverse of both processes. The second viscosity terms with coefficients ζ_{11} and ζ_{22} give a contribution to the absorption of ordinary and second sound respectively; they cannot be measured in any other way. An alternative way of taking into consideration the influence of the inelastic collisions on the attenuation of the sounds, also due to Khalatnikov, is to regard the characteristic times as relaxation times in the ordinary sense and to express the absorption directly in terms of these. As long as the absorption coefficient is proportional to ω^2 [see Eq. (13) and (14)], this method is completely equivalent to the formal introduction of the coefficients ζ.

As to the actual calculation, the dependence on temperature can be found for all processes. An estimate of the actual magnitude is, however, only possible with the elastic phonon-roton collisions. Therefore, between 0.7 and 1.0° K η_n and λ_n can indeed be calculated in absolute value. Actually this calculation is not very accurate since some of the required parameters are only approximately known. The temperature-independent parts of the two inelastic relaxation times or, alternatively, of the ζ's cannot be evaluated from first principles. Two constants have to be found from experiments on the absorption of ordinary sound.

The result of these considerations is that in the case of ordinary sound the largest contribution to the absorption arises from the ζ_{11} term, while with second sound this is true for the λ_n term [see Eq. (13) and (14)]. The other contributions amount in both cases to about 15 % of the total absorption.

5.1. Absorption of Second Sound from Pulse Measurements

From the Leiden pulse measurements [26] in the range between 0.7 and 1.0° K it proved to be possible to deduce a value of the frequency-independent quantity β_{II}/ω^2, by measuring the width of the pulses. The deduction fails if the pulses lose their symmetry;

the method can therefore not be extended below 0.7° K. However, the lower region is more complicated also for other reasons (see § 6).

The agreement of the data on β_{II}/ω^2 with those calculated by Khalatnikov is quite good, in view of the many uncertainties (see Fig. 6). In the evaluation of β_{II}/ω^2 from the experiments, attenuation

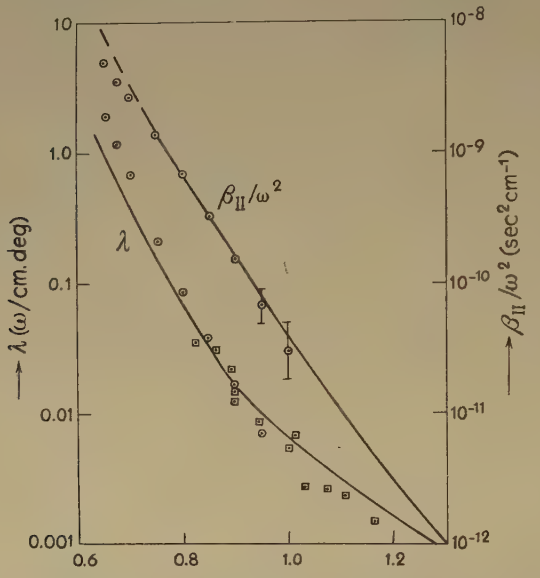

Fig. 6. Reduced absorption coefficient of second sound (β/ω^2) and the coefficient of heat conductivity (λ) as a function of temperature.
β/ω^2: line: calculated by Khalatnikov [13],
○ Leiden data [26].
λ: line: according to Khalatnikov [13],
○ Leiden data [26],
□ new data of Zinovieva [41].

effects originating from the presence of the walls of the tube have been neglected. This is not unreasonable, since the input pulses were narrow (20 μsec) and consequently the effective wavelength was small compared with the tube dimensions. Moreover no substantial change of the pulse widths was observed by reducing the tube diameter by a factor 0.5. A value of the coefficient of heat conductivity λ and from this a mean free path of the phonons (l_{ph}) can be obtained (see Fig. 7).

5.2. Attenuation Experiments of Second Sound from Sine Waves

According to a private communication [41] the attenuation experiments of Zinovieva [40] were recently extended down to 0.8° K. The method used is that of measuring resonance widths of standing waves. The attenuation is interpreted as being partly due to surface attenuation and partly to absorption in the bulk liquid; because of different frequency dependence separation is possible. The coefficient of

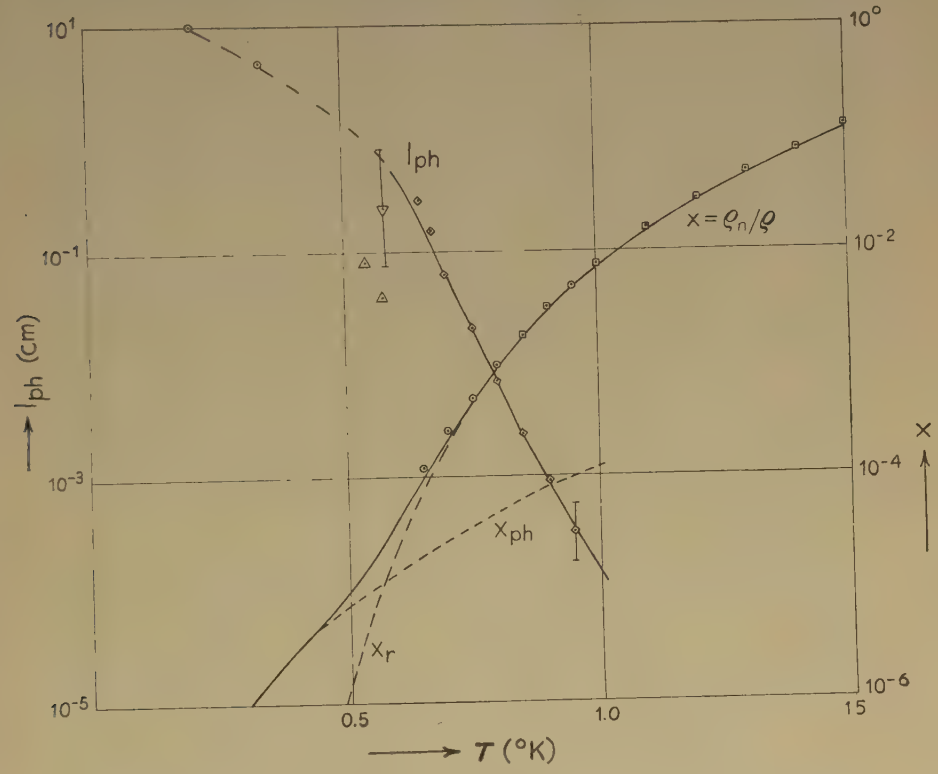

Fig. 7. Mean free paths of phonons (l_{ph}) and data on $x = \varrho_n/\varrho$.

l_{ph}: ◇ Leiden results above 0.7° K [26],
○ Leiden results from observations of the pulse front in the lower region [26],
▽ from heat conduction (Whitworth [32]),
△ from second sound attenuation of the Kirchhoff type (viscosity), according to Osborne.

x : line: calculated with the parameters of Fig. 2,
○ from Leiden data on v_{II} [26],
□ from Peshkov's data on v_{II} [28].

heat conductivity calculated from the latter part is shown in Fig. 6. The agreement with the Leiden pulse data is found to be very satisfactory *.

At still lower temperatures Osborne [5] recently published the first measurements on the propagation of heat, using a sine wave instead of a pulse method. The heat input could be kept low by using an amplifier with very narrow bandwidth (i.e. low noise level). It was not possible to employ a standing wave method because of the large attenuation in the temperature region investigated (below 0.6° K). However, velocity and attenuation can be found from the measurement of phase and amplitude as a function of tube length.

Since Osborne's experiments were performed only below 0.6° K, no direct comparision can be made with the pulse data just mentioned.

Osborne interprets the phenomena between 0.5 and 0.6° K as heavily damped second sound. He neglects bulk liquid absorption and attributes the observed damping completely to surface attenuation due to the presence of the walls of the tube. The old treatment of Kirchhoff of the propagation of sound in a narrow tube is applied to the phonon gas. It follows that the attenuation should almost com-

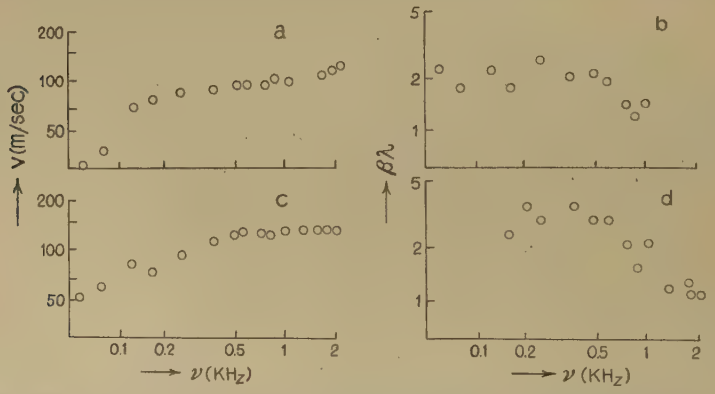

Fig. 8. Wave velocities (a and c) and attenuation per wavelength (b and d) as a function of the second sound frequency for two temperatures, according to Osborne [5]. a and b: $T = 0.58°$ K; c and d: $T = 0.50°$ K.

* The surface attenuation is mainly determined by the viscosity of the liquid. The new measurements of Zinovieva yield values for η_n which are in good agreement with those obtained by means of the rotating cylinder viscosimeter [44] (see Vol. I, Ch. IV) and with the theoretical predictions of Khalatnikov [29, 13].

pletely be due to the viscosity. For high frequencies the propagation is not very much hampered: only the layer of the medium just near the wall feels its presence. For low frequencies the whole liquid is affected and some kind of alternating flow of Poiseuille type should occur. The result is a very large attenuation and a considerable reduction of the velocity in the latter case. This is indeed found experimentally: the velocity increases with increasing frequency and tends to level off at a value near the theoretically expected value of v_{II}, while the attenuation decreases (see Fig. 8).

The supposition underlying this treatment is that the mean free path is still small compared with wavelength, geometrical dimensions etc. This is indeed found to be in agreement with the magnitude of the mean free path deduced from the viscosity which can be evaluated from the attenuation measured by Osborne. To what extent this is consistent with the Leiden pulse experiments will be discussed in § 6.

5.3. Absorption of Ordinary Sound

Chase and Herlin [4] published data on the absorption coefficient of ordinary sound at a frequency of 12.1 MHz down to 0.1° K (Fig. 9). They used a method of pulsed sound waves. The result shows two absorption maxima occurring just below 1° K. The absorption at higher temperatures can be explained by means of Eq. (13) or a similar expression using the relaxation times directly (see also Vol. I, Ch. XVII).

The maximum absorption should be attained at a temperature at which the relaxation times become equal to the reciprocal frequency. The two relaxation times of Khalatnikov should therefore correspond to the two maxima observed. Recently [31], however, Chase withdrew this explanation, since a more careful analysis of Khalatnikov's calculation yielded only one peak, not separated into two. Moreover it appears that the presence of two peaks instead of one was probably due to some experimental error.

The decrease of the absorption coefficient at lower temperatures should be due to the relaxation times becoming much larger than the reciprocal frequency. There is no longer a possibility of establishing equilibrium with respect to numbers of excitations and no energy can be dissipated in this way. However, the situation is even more complicated since also the ordinary viscosity gives a contribution to the absorption. The characteristic times connected with the viscosity

(i.e. of the phonon-roton and the phonon-phonon elastic collisions) may also become large. Actually one should take into account all these relaxation times in a theoretical approach to this problem. This has not yet been done.

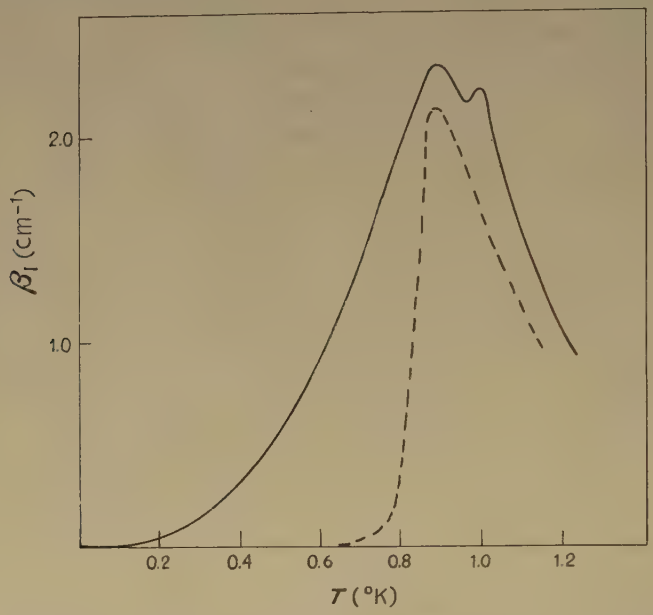

Fig. 9. Absorption coefficient per cm of ordinary sound at 12.1 MHz (after Chase [31]).
Fully-drawn line: experimental data of Herlin and Chase [4],
– – – – – calculated by Chase from Khalatnikov's theory.

It was not possible to measure the velocity with any accuracy in these experiments; therefore, no accurate data on the dispersion are available. Chase and Herlin gave a value of $v_I = 240$ ($\pm$ 5) m/sec at the lowest temperatures. Dispersion should therefore not be very significant, a conclusion which is also in agreement with the observed magnitude of the absorption.

The velocity of the thermal phonons (i.e. sound waves of 10^9 or 10^{10} Hz) which can be calculated from the specific heat below 0.6° K does not show a substantial difference from v_I at much smaller frequencies either. However, this does not imply the absence of dispersion at higher temperatures. The difference between the velocities of sound at infinite and zero frequencies ($v_\infty - v_0$) calculated by

Khalatnikov depends very much on temperature. In his evaluation $v_\infty - v_0$ increases from 0.175 cm/sec at 0.6° K to 37.5 cm/sec at 1.1° K and to 115 cm/sec at 1.5° K.

Very accurate measurements of the velocity of sound near 1.1° K at frequencies from 0.2 to 1.6 MHz were recently carried out by van Itterbeek [42] at Louvain. Preliminary results seem to point also to the absence of dispersion in this range.

6. Large Mean Free Path Phenomena

It may be expected from the foregoing that at low enough temperatures the mean free path of the phonons will become large and even comparable to the dimensions of the measuring apparatus. There are sufficient experimental data to support this picture.

6.1. Heat Conductivity

The conduction of heat should be equivalent to a Knudsen flow of phonons if the mean free path is much larger than the diameter of the measuring tube. The phonons only collide with the walls. The reflection may be diffuse or specular, though the wavelengths of the phonons in this region (e.g. at 0.2° K about 500 Å) suggest that at least a large part should be reflected diffusely from the relatively rough surface of the walls.

For a long and narrow tube, i.e. one in which the phonons are reflected many times, the propagation is determined by a differential equation of the heat-conductivity or diffusion type. The effective coefficient of heat conductivity in a tube of circular cross section is

$$\lambda_{\text{eff}} = \tfrac{1}{3} d v_l \varrho c_v \, (2-f)/f \qquad (15)$$

where d is the diameter of the tube and f the fraction of phonons scattered diffusely.

Measurements have been made on the stationary flow of heat by Fairbanks and Wilks [7] ($d = 0.029$ cm and 0.080 cm) and by Whitworth [32] ($d = 0.48$ cm). If f is equal to 1, λ_{eff} should be proportional to T^3. This is actually found approximately for temperatures between 0.4 and 0.6° K. At lower temperatures the heat conductivity is relatively too large, which would point to a decrease in f. This is not unreasonable, since the average wavelength of the phonons is inversely proportional to T. The quantitative agreement of the experimental results with one another and with Eq. 15 is fair; f may, however, be very much different for different tubes. The data on the narrowest tube appear

to be the most reliable ones; they are consistent with a decrease of f from 0.93 at 0.5° K to 0.75 at 0.2° K.

Above 0.6° K Fairbank and Wilks found a larger increase of λ_{eff} than given by a T^3 dependence. This points to the mean free path now becoming of the order of magnitude of the tube or smaller. The heat flow through the tube has now more the character of a Poiseuille flow of phonons, i.e. the flow is determined by the viscosity of the normal fluid. At still higher temperatures the conduction of heat shows the well-known complicated behaviour (see Ch. III).

In Whitworth's wider tube the increase began as low as 0.56° K. He concludes that, to an order of magnitude, the mean free path is 0.24 cm at 0.58° K.

6.2. Heat Pulses and Heat Waves

At temperatures below 0.4° K the general shape of the pulse in the Leiden experiments was found to be in agreement with the large free path picture, i.e. of the phonons being scattered only by the walls. For a long and narrow tube one would get a pulse shape similar to the temperature response found at the end of a heat conducting rod, when at the other end an amount of heat is supplied within a very short time. Though the tubes used were neither very long nor very narrow a satisfactory agreement was found for the longest tube (6.25 cm length, 0.95 cm diameter). The shorter tubes gave qualitatively the same result [26].

It should be emphasized that this propagation has nothing to do with second sound. The situation is analogous to the impossibility of propagating sound in a very dilute gas. If the mean free path of the excitations becomes larger than the wavelengths used, no local equilibrium can be built up, and some kind of phonon diffusion will occur [38]. Moreover, when the mean free path is even larger than the tube diameter, not even diffusion can occur, and the propagation is wholly determined by reflections at the walls. As has been shown, the analysis of the experiments in the latter case is relatively simple.

In the transition region from second sound to boundary scattering of phonons (from 0.7 to 0.4° K) the analysis is rather difficult, because of the coexistence of all effects. There are some indications in the pulse experiments that a trace of second sound still occurs down to 0.55° K: the velocity of the pulse front at that temperature is about 150 m/sec, i.e. not very far from v_{II} in the phonon region.

This latter supposition is also in agreement with the results of Osborne mentioned in 5.2. However, his estimate of the mean free path is rather small compared with the extrapolated value deduced from the pulse experiments at higher temperatures and from Whitworth's data in the same region. It should be noted, of course, that the mean free path is a very loosely defined quantity, which may be different for different processes. Actually, according to Khalatnikov, the mean free path which is characteristic for viscosity in this region is considerably smaller than that characterizing heat conductivity, but even so the deviations seem to be rather large (see Fig. 7). It is in general not surprising that Osborne's results are more second sound-like in the region between 0.5 and 0.6° K than the Leiden pulse results, since the wave-lengths in the former case were much larger. A strong point in favour of his data is the magnitude of the velocity at the highest frequency which is actually very near the value, deduced by Landau for the phonon region.

A very marked difference exists in the interpretation of the attenuation in the experiments of Osborne on the one hand and the pulse experiments above 0.7° K on the other hand. In the latter case the interpretation is that of absorption in the bulk liquid, in the former that of a Kirchhoff type of attenuation. This may not be inconsistent, however, since the effective wavelength in the pulse experiments is much shorter than the tube diameter, while in the wave measurements the reverse is true. Therefore it may be reasonable to neglect wall effects in the first case and the bulk effect (which is proportional to the square of the frequency) in the second case. On the other hand, the new results of Zinovieva seem to indicate that, at any rate near 0.8° K, the bulk liquid absorption cannot be neglected for frequencies of the order of magnitude which Osborne used.

Osborne's results at 0.25° K are in agreement with a very large mean free path picture. His estimate of the fraction of diffusely scattered phonons ($f = 0.26$) appears to be inconsistent with the heat conductivity data though the structure of the wall may play an important role. The value of f could not be evaluated from the pulse experiments.

Finally one other effect was found in the Leiden pulse experiments. A number of phonons may travel directly from heater to thermometer if the mean free path is larger than the length of the tube. Actually a sharp front was detected, traveling with the velocity of sound. The

way this front disappeared at higher temperatures was very curious: this occurred at a markedly different temperature for different tube lengths and at much lower temperatures than one would expect from Khalatnikov's estimate of the mean free path ($l_{ph} \approx 10$ m at $0.2°$ K$_0$). The conclusion should be that the mean free path increases not so fast as that and hence that yet another path-limiting process should exist.

A probable explanation is that this is due to a very small concentration of ^{3}He, which is always present (about 1 atom in 10^7). In agreement with this is one experiment with pulses in atmospheric helium which contains a 10 times larger amount of ^{3}He [26, 33]. These experiments showed clearly an extension of the transition region (with front velocities of about 150 m/sec) from 0.55 at the smaller to $0.35°$ K at the larger concentration, suggesting therefore that second sound may exist down to lower temperatures in the latter case because of a more limited mean free path. This is also in agreement with experiments using a much larger ^{3}He concentration [34].

7. Miscellaneous Experiments

Fairbank and Wilks [7] published data also on the magnitude of the Kapitza thermal resistance down to $0.3°$ K. They found a temperature dependence of T^{-2}, in the whole region below one degree, which appears at first sight to be rather surprising in view of the T^{-3} dependence found at higher temperatures. However, a similar dependence seems to exist for the boundary resistance between metal surface at low temperatures.

Mayper and Herlin [35] measured the velocity of heat pulses under pressure. They found for temperatures above $0.7°$ K (i.e. the proper second sound region) a decrease of v_{II} with increasing pressure. Below that temperature the interpretation of the results is not simple, since they measured the front velocity of the much broadened pulse. At low enough temperatures this velocity appeared to increase with increasing pressure. This is not surprising in view of the positive magnitude of $\partial v_I/\partial \varrho$. The velocity they measured should, according to the foregoing, be somewhere between v_I and $v_I/\sqrt{3}$. The quantitative results of these experiments may not be very reliable, since the total heating-up time was only a few minutes and therefore temperature equilibrium was probably not very well established.

Film flow experiments were performed by Ambler and Kurti [36]

and by Waring [37]. In the first experiment the flow was due only to a gravitational potential difference; an increase of flow amounting to 30 % was observed in passing from 0.85 to 0.15° K. Waring measured the flow due to a temperature gradient. At 1.4° K the magnitude was found to be about twice the gravitational potential value. It increased from this only by 10 % at 0.14° K.

REFERENCES

1 R. P. Hudson, B. Hunt and N. Kurti, Proc. Phys. Soc. London, A, **62**, 392 (1949).

2 H. C. Kramers, J. D. Wasscher and C. J. Gorter, Leiden Comm. No. 288c; Physica, **18**, 329 (1952); Proc. Kon. Ak. Wet. Amsterdam, B, **58**, 366, 377 (1955).

3 D. de Klerk, R. P. Hudson and J. R. Pellam, Phys. Rev., **93**, 28 (1954).

4 C. E. Chase and M. A. Herlin, Phys. Rev., **97**, 1447 (1955).

5 D. V. Osborne, Conférence de Physique des Basses Températures, Paris (1955) p. 48.
Phil. Mag. (8) **1**, 301 (1956).

6 R. A. Hull, K. R. Wilkinson and J. Wilks, Proc. Phys. Soc. London, A, **64**, 379 (1951).

7 H. A. Fairbank and J. Wilks, Proc. Royal Soc., A, **231**, 545 (1955).

8 Z. Dokoupil, G. van Soest, D. H. N. Wansink and D. G. Kapadnis, Leiden Comm. No. 298a; Physica, **20**, 1181 (1954).

9 C. V. Heer, C. B. Barnes and J. G. Daunt, Phys. Rev., **91**, 412 (1953).

10 I. M. Khalatnikov, Zh. Eksp. Teor. Fiz., **23**, 8 (1952).

11 For a more full review: H. C. Kramers, Proc. Kon. Ak. Wet. Amsterdam, B, **58**, 302, 313 (1955).

12 E.g.: R. Kronig, A. Thellung and H. H. Woldringh, Physica, **18**, 21 (1952). See also Vol. I, Ch. I of this issue.

13 I. M. Khalatnikov, Zh. Eksp. Teor. Fiz., **23**, 21 (1952).

14 L. Landau, J. Physics U.S.S.R., **5**, 71 (1941).
L. Landau, J. Physics U.S.S.R., **11**, 91 (1947).

15 H. London, Proc. Roy. Soc. London, A, **171**, 484 (1939).

16 H. C. Kramers, Proc. Kon. Ak. Wet. Amsterdam, B, **58**, 386, 396 (1955).

17 K. R. Atkins and C. E. Chase, Proc. Phys. Soc. London, A, **64**, 833 (1951).
C. E. Chase, Proc. Roy. Soc. London, A, **220**, 116 (1953).

18 K. R. Atkins and M. H. Edwards, Phys. Rev., **97**, 1429 (1955).

19 K. R. Atkins and R. A. Stasior, Can. J. Phys., **31**, 1156 (1953).

20 V. P. Peshkov, Zh. Eksp. Teor. Fiz., **29**, 351 (1954).

21 G. J. C. Bots and C. J. Gorter, Leiden Comm. No. 304b; Physica, **22**, 503 (1956).

22 V. P. Peshkov, Zh. Eksp. Teor. Fiz., **18**, 951 (1948).

23 J. R. Pellam and R. B. Scott, Phys. Rev., **76**, 869 (1949).

24 K. R. Atkins and D. V. Osborne, Phil. Mag., **41**, 1078 (1950).

25 D. de Klerk, R. P. Hudson and J. R. Pellam, Phys. Rev., 93, 28 (1954).

[26] H. C. Kramers, Tineke van Peski–Tinbergen, J. Wiebes, F. A. W. van den Burg and C. J. Gorter, Leiden Comm. No. 296b; Physica, **20**, 743 (1954).
H. C. Kramers, Proc. Kon. Ak. Wet. Amsterdam, B, **59**, 35, 48 (1956).
[27] L. Tisza, Journ. Phys. et Radium (8) **1**, 164 (1940).
L. Tisza, Phys. Rev., **72**, 838 (1947).
[28] V. P. Peshkov, Zh. Eksp. Teor. Fiz., **23**, 686 (1952).
[29] L. D. Landau and I. M. Kkalatnikov, Zh. Eksp. Teor. Fiz., **19**, 637, 709 (1949).
[30] I. M. Khalatnikov, Zh. Eksp. Teor. Fiz., **20**, 243 (1950).
[31] C. E. Chase, Amer. J. of Physics, **24**, 136 (1956).
[32] R. W. Whitworth, Conf. de Phys. des Basses Temp., Paris (1955), p. 56.
[33] H. C. Kramers, Conf. de Phys. des Basses Temp., Paris (1955), p. 51.
[34] J. C. King and H. A. Fairbank, Phys. Rev., **93**, 21 (1954).
[35] R. D. Mayper and M. A. Herlin, Phys. Rev., **89**, 523 (1953).
[36] E. Ambler and N. Kurti, Phil. Mag., **43**, 260 (1952).
[37] R. K. Waring, Phys. Rev., **99**, 1704 (1955).
[38] C. J. Gorter, Phys. Rev., **88**, 681 (1952).
[39] K. R. Atkins, Phys. Rev., **89**, 526 (1953).
[40] K. N. Zinovieva, Zh. Eksp. Teor. Fiz., **25**, 235 (1953).
[41] K. N. Zinovieva, Private Communication.
[42] A. van Itterbeek, Private Communication.
[43] J. Wiebes, C. G. Niels–Hakkenberg and H. C. Kramers, to be published in Leiden Comm. and Physica.
[44] W. J. Heikkila and A. C. Hullis–Hallett, Can. J. Phys., **33**, 420 (1955).

CHAPTER III

TRANSPORT PHENOMENA OF LIQUID HELIUM II IN SLITS AND CAPILLARIES

BY

P. WINKEL

PHILIPS' RESEARCH LABORATORIES, EINDHOVEN

AND

D. H. N. WANSINK

KAMERLINGH ONNES LABORATORY, LEYDEN

CONTENTS: 1. Introduction, 83. — 2. The fountain effect and the mechanocaloric effect, 87. — 3. The frictional forces, 90. — 3.1. Isothermal flow, 91. — 3.2. Non-isothermal flow, with and without resulting flow of matter, 95. — 3.3. Conclusions, 100.

This chapter deals with the transport phenomena of liquid helium II. We restrict ourselves to bulk flow through slits and capillaries under the influence of pressure and temperature gradients in the temperature region above 1° K. The transport phenomena in rotating cylinders and oscillating disks have been discussed already [1] in Vol. I, Ch. IV. Separate chapters are devoted to the properties of the helium film and the helium in the case of temperatures below 1° K (Ch. IV and II).

Both the flow of ^{4}He and of mixtures of ^{4}He with ^{3}He shall be discussed, although by far most experiments have been performed with practically pure ^{4}He.

1. Introduction

We shall discuss the experiments on the basis of the well-known two-fluid model for liquid helium II [2]. Although especially at high velocities its validity and application may become doubtful, it is still a convenient starting point.

Under the influence of a pressure and (or) a temperature gradient liquid helium II will flow, this flow being supposed to consist of a

contribution from the normal fluid (velocity v_n) and the superfluid (velocity v_s). The equations of motion for both fluids are written as follows:

$$\varrho(1-x)\mathrm{d}\mathbf{v}_s/\mathrm{d}t = -(1-x)\ \mathrm{grad}\ p + x(1-x)S^*\varrho\ \mathrm{grad}\ T - \mathbf{F} \qquad (1)$$

$$\varrho x\mathrm{d}\mathbf{v}_n/\mathrm{d}t = -x\ \mathrm{grad}\ p - x\,(1-x)S^*\varrho\ \mathrm{grad}\ T + \eta_n(\Delta\mathbf{v}_n + \tfrac{1}{3}\ \mathrm{grad\ div}\ \mathbf{v}_n) + \mathbf{F}' \qquad (2)$$

The symbols have the usual meaning [2] (see Vol. I, Ch. I), S^* being a quantity with the dimensions entropy/gram. Hence only the pressure gradient and the temperature gradient are stated explicitly in both equations. The former acts on both fluids independently but in the same direction, the latter has the form of a diffusion force. All other forces are formally included in $\mathbf{F}$ and $\mathbf{F}'$, except for the Poiseuille term. This force is supposed to be essentially absent in the superfluid equation. Numerically the acceleration terms (left-hand members) are always very small and can be neglected.

When $F=0$, Eq. (1) yields

$$\mathrm{grad}\ p = \varrho x S^*\ \mathrm{grad}\ T. \qquad (3)$$

This implies the possibility of a pressure gradient as a result of a temperature gradient, the so-called 'fountain effect' (after its discovery by Allen and Jones [3]). With $S^* = S/x$, Eq. (3) takes the form, derived by H. London [4]; with $S^* = \partial S/\partial x$, it becomes the equation derived by Gorter [5] and also by de Groot *et al.* [6] and Usui [7]. As will be seen in the next section, the H. London equation is a good numerical approximation in the temperature region under discussion.

By adding Eq. (1) and (2), one obtains in the case of a stationary state and F equal to F':

$$\mathrm{grad}\ p = \eta_n(\Delta\mathbf{v}_n + \tfrac{1}{3}\ \mathrm{grad\ div}\ \mathbf{v}_n), \qquad (4)$$

the well known Poiseuille equation for a normal fluid. For a slit with a width h, Eq. (4) becomes

$$\bar{\mathbf{v}}_n = -\frac{h^2}{12\,\eta_n}\ \mathrm{grad}\ p. \qquad (5)$$

In addition to Eq. (1) and (2), describing the flow through the slit, a third important one is the energy balance of the reservoirs, at both sides of the slit. Besides showing the quantities contributing to an

ordinary balance, helium II exhibits the property of the so-called 'mechanocaloric effect', i.e. a heat effect Q, caused by a displacement of superfluid [2]. This may be expressed as

$$Q = xTS^{**}, \tag{6}$$

where S^{**} is a quantity with the dimensions entropy/gram. From the first and second law of thermodynamics it follows in the case of small velocities [5] that $S^{**} = S^{*}$.

The mechanocaloric effect implies a special kind of heat conduction in helium II, caused by convection of the normal and superfluid, which in the case of a stationary state yields

$$\mathbf{I} = O\varrho xS^{*}T\mathbf{v}_n \tag{7}$$

where O denotes the cross-section of the slit or capillary. With Eq. (5) this becomes

$$\mathbf{I} \sim \operatorname{grad} p. \tag{8}$$

Apparently no such relation between I and grad T exists when $F \neq 0$ [cf. Eq. (1)]. The conservation of mass is always tacitly assumed.

Concerning the forces F and F' in the two equations of motion (1) and (2), it is generally believed that they depend on the velocities v_s and (or) v_n of the fluids. They can be considered as a correction to the original simple two-fluid model, apparently necessary in the case of high velocities. We shall return to this question in the last §. In the earlier measurements only more or less qualitative results concerning the $F - v$ relation [8, 9] were obtained. Later it was supposed that these forces were zero up to a certain velocity (the 'critical velocity'), above which these forces strongly increased with increasing velocity [10]. This notion of a critical velocity originated in experiments on film flow (see Ch. IV). Gorter and Mellink [11, 12] gave the first quantitative suggestion of these forces by writing

$$F = F' = Ax(1-x)\varrho^2(v_s - v_n)^m; \quad m = 3. \tag{9}$$

This accounts for the strong dependence of the velocity on the driving force, as is observed, whereas the small values of F and F' at low velocities are not necessarily in contradiction with a critical velocity. This expression was mainly based on the data available on heat conduction in slits and capillaries (I as a function of grad T), where

rather high velocities occurred. At present we are inclined to prefer the combination of a negligible friction up to a critical velocity and in many cases a cubical dependence of the friction on the velocity for the higher velocities [13, 14]. In many cases it is certain that the values of F and F' at velocities near the critical value are smaller than those given by the cubical relation [15].

We prefer to divide the experiments on helium II in slits and capillaries into two groups, one determining S^* and one determining qualitatively and quantitatively F and F'. This will be the classification of the following §§. Before doing so we wish to make some general remarks. Each apparatus, used for the experiments is essentially one of the four standard types given in Fig. 1. In Fig. 1a reservoir A is connected with a volume B by a slit or capillary, sometimes filled with a fine powder such as jewellers' rouge. The volume B

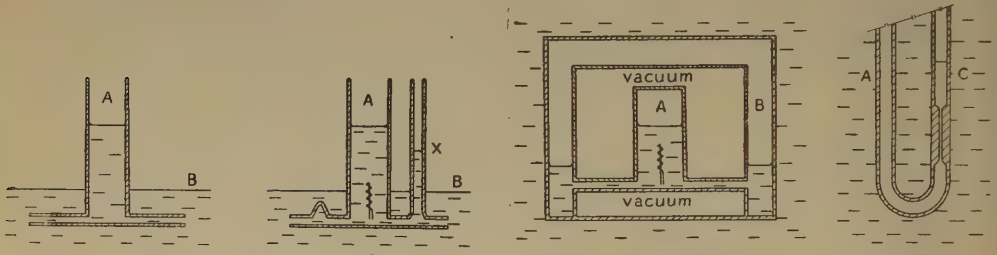

Fig. 1.

is the helium bath itself. The volume A is open or closed depending on whether isothermal or adiabatic flow is concerned, the glass being supposed to be a satisfactory insulator. The advantage of this arrangement is that pressure differences can be adjusted easily in the case of isothermal flow. The disadvantages are the lowering of the level of B during the experiments as a result of evaporation and the precautions which have to be taken in order to ensure isothermal conditions. In Fig. 1b the apparatus is similar to the previous one except that between A and B a manometer X is placed. As the diameter of X is necessarily much larger than the width h of the capillaries or slits one can also describe this as a situation with three reservoirs A, X and B connected by two slits or capillaries in series. In Fig. 1c a third type is given for application to truly adiabatic experiments. It combines the advantages of good thermal insulation and the use of a constant amount of helium. It is not possible, however,

to perform isothermal experiments with this system. A fourth type (see Fig. 1d) consists of a slit, connected to two tubes A and C, leading to manometers outside the cryostat. By condensing helium in A up to a level much higher than the bath level, pressures up to 1 atmosphere can be reached in A. The resulting flow of matter which is observed in C, is isothermal as both the liquid in C and the lower part of A are at bath temperature, since they are far below the bath level.

To describe the experiments it is convenient to introduce some symbols and to simplify the three equations mentioned above [14, 16]. Neglecting the left-hand member, Eq. (1) becomes

$$\tilde{F} = f\Delta T - \Delta p \equiv f\Delta T^{+}, \qquad (10)$$

where Δp and ΔT are the differences in pressure (in cm He) and temperature across the slit or capillary and f denotes the fountain effect in cm He/degree. ΔT^{+} is defined by this equation as a kind of 'surplus' ΔT, proportional to $\tilde{F}$, the integrated F, divided by $(1-x)\varrho g$. Eq. (2) can be reduced to

$$\bar{v}_n = \frac{G}{\eta_n}\Delta p, \qquad (11)$$

the constant G depending on the geometry of the slit or capillary. In the case of an apparatus of the type of Fig. 1c, one can reduce the energy balance of the vessel A approximately to

$$\frac{\mathrm{d}\Delta T^{+}}{\mathrm{d}t} = -b\,v_r + c, \qquad (12)$$

b and c being constants and v_r the relative velocity $v_s - v_n$ [14, 16]. With these three equations the behaviour of helium II is formally described. In the case of the Gorter–Mellink assumption, Eq. (9) gives $\Delta T^{+} \sim v_r^m$. Substituting this in Eq. (12) one obtains a differential equation for v_r, which has a special character when $m \neq 1$.

2. The Fountain Effect and the Mechanocaloric Effect

The values of xS^* are determined by measuring grad p and grad T under the condition that $F = 0$ [Eq. (1)]. As this condition is expected to be realised anyhow when $v_n = v_s = 0$, the measurement of the so-called ideal fountain effect is – mirabile dictu – a static problem. However, in view of the existence of a critical velocity, i.e. a velocity below which the force F is negligible, this requirement is not so stringent.

These measurements were carried out by Kapitza [10] and by Meyer and Mellink [17]. The apparatus is schematically drawn in Fig. 1c, although in Kapitza's arrangement the outer volume was the bath itself. In both cases an annular slit was used (width $h < 1\,\mu$). The results are given in Fig. 2. Below $T = 1.7°$ K good agreement between the two sets of data exists, but at higher temperatures more or less serious deviations occur. The reason for this is not clear. Perhaps it may be connected with the difference of experimental method.

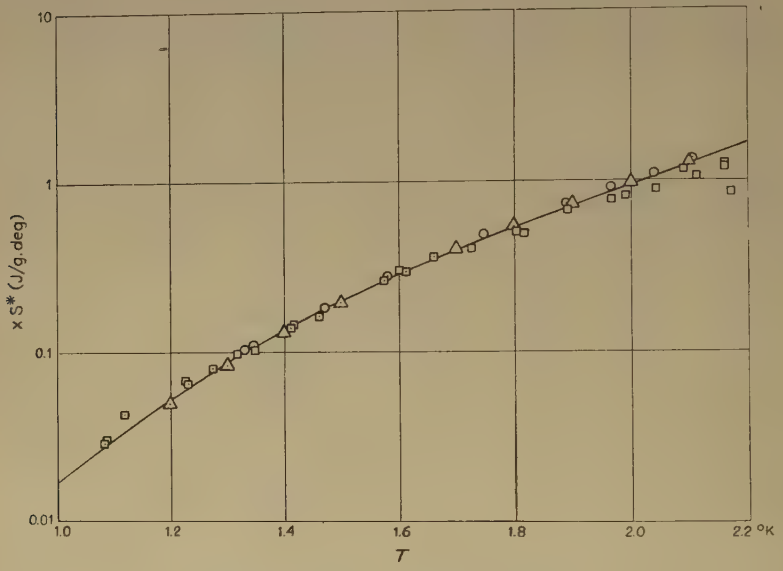

Fig. 2. xS^* as a function of T.
⊙: Kapitza. ⊡: Meyer and Mellink. △: Brewer, Edwards and Mendelssohn.
—: Kramers' entropy values.

Kapitza adjusted the height and measured the resulting temperature difference, whereas Meyer and Mellink adjusted the temperature difference and measured the corresponding level height. Also it can be mentioned that the length and the shape of both slits were rather different. Finally, as a result of the limited pressure differences the values at higher temperatures are inaccurate, which, however, cannot explain the systematic differences observed.

There also exist measurements on the integrated fountain effect carried out by Van den Meijdenberg, Taconis, Beenakker and Wansink [18]. In this case large pressure differences are measured as a

result of temperature differences of several tenths of a degree. We shall come back to these results below.

It is also possible to determine the quantity xS^* by measuring the mechanocaloric effect, $Q = TxS^*$ (cf. § 1). These data have been obtained by Kapitza [10] with the same apparatus as above by determining the flow of matter as result of a heat supply to volume A (at low velocities). His results agreed quite well with his measurements on the fountain effect (see Fig. 2). New measurements were carried out by Brewer, Edwards and Mendelssohn [19] with an apparatus like that of Kapitza but with a refinement in order to prevent the normal fluid flow. These results give lower values than those of Kapitza (see Fig. 2). In this respect we should like to mention that measurements on the mechanocaloric effect in film flow give much higher values (about 15 %) [20]. However, as has been pointed out [19], it is not necessary that film flow and bulk flow have the same thermal properties.

On the basis of H. London's equation, i.e. by putting $xS^* = S$, one can compare the results mentioned above with the data of the entropy available. At present the most reliable ones seem to be those of Kramers, Wasscher and Gorter [21], calculated from their measurements on the specific heat. These values are confirmed by other investigators [22], while they also agree partly with earlier data [23]. These entropy values are also given in Fig. 2.

On the basis of the measurements available at present and given in Fig. 2, it seems to be justifiable to sketch the present situation as follows: to a good approximation one can replace xS^* by S in the temperature region in discussion, using Kramers' data for S. This implies the validity of the H. London-equation in this temperature region and of the corresponding relation $Q = TxS^*$ for the mechanocaloric effect.

Direct support for this statement is presented by the measurements of Brewer, Edwards and Mendelssohn and by the measurements of Van den Meijdenberg *et al.* For, in this latter case the integrated values of the fountain effect were compared with different integrated curves based on the data given in Fig. 2. By far the best agreement was found with Kramers' curve. Finally the deviations of the points given by Mellink and Kapitza by chance approximately cancel each other. In this way the present situation seems to be satisfactory.

3. The Frictional Forces

The flow of the superfluid plays the most important role in many of the experiments, in agreement with the hypothesis of the absence of a Poiseuille friction. The flow of the normal fluid can even be suppressed completely by using small slits and low temperatures. The former implies high ordinary friction, the latter a small concentration of the normal fluid. Thus in general we get only information on the force F in Eq. (1). The force F' [Eq. (2)] can only be examined in experiments where the normal fluid flow is relatively high as a result of special conditions.

We shall divide the experiments into two groups, one concerning experiments where helium flows isothermally under the influence of a gravitational potential and one where the flow is caused by a thermal and a gravitational potential. The latter group can be split into two parts, one with and one without resulting flow of matter.

Before doing so we should like to make some remarks. Although v_n and v_s are not constant along the cross-section of the slit, one usually considers only the average velocity without even using special symbols. We shall do the same although in a detailed analysis the difference has to be remembered and can play an essential role.

It is convenient to introduce the velocity $\hat{v}$ by the equation

$$\frac{1}{O}\frac{\mathrm{d}V}{\mathrm{d}t} = \hat{v} = (1-x)\, v_s + x v_n \tag{13}$$

where V is a volume and O the cross-section of the slit. In the case of a normal liquid $\hat{v}$ is the ordinary flow velocity. In the helium II case it is proportional to v_s and to the relative velocity $v_r = v_s - v_n$ in the case of negligible v_n.

Concerning the isothermal experiments, the high values of the fountain effect imply the necessity of many precautions. Small temperature differences cause important errors in the results; such temperature differences arise easily as the flow itself is accompanied by heat effects. In discussing the isothermal results one must keep in mind this point in spite of all the (sometimes ingeneous) precautions taken.

A last point is related to the uniformity of the slits and capillaries. Usually the former consists of two annular optically flat glass surfaces, kept at a fixed distance by thin blades of some material. In the experiments on the fountain effect the exact shape of the slit is

unimportant as it only serves to suppress the flow of the normal fluid. But in determining the frictional forces F the exact shape of a slit or capillary is of fundamental importance. This makes these experiments rather awkward especially in the case of slits of the order of 1 μ and smaller. Also the shape of the entrance and the exit can be of importance. It is possible to get information about the homogeneity by determining the effective slitwidth in different ways. This can be done e.g. by comparing the results of a Poiseuille flow and a Knudsen flow through the slit or capillary, the former giving an effective value of h^3, the latter of h^2. Further informations are obtained by comparison of these results with those from optical interference methods and also from the thickness of the blades separating the glass surfaces. When carrying out the Poiseuille and Knudsen flow also at lower temperatures, another welcome control results. But nevertheless the actual shape of the slit still remains the most uncertain factor in the results of flow experiments.

3.1. Isothermal flow

The experiments are carried out with an apparatus of the type of Fig. 1a and partly of Fig. 1b. By lowering or raising the apparatus relative to the bath level a pressure difference is established. By measuring the level height as a function of time the flow is determined. In many cases these observations obey the relation

$$\text{grad}\, p \sim \hat{v}^m. \tag{14}$$

If $v_n = 0$ and $m = 3$ this would be identical with the formulation of Gorter and Mellink.

First we should remember that by this method Kapitza [24] tried to measure the viscosity of the liquid as a whole, which yielded an apparent viscosity of less than 10^{-9} P. The discrepancy between this viscosity value and the one, obtained from oscillating disk experiments, lead to the hypothesis of the two-fluid model.

An extensive study was made by Allen and Misener [8, 25, 26] using capillaries of different diameter ($0.1 - 400$ μ) and length ($0.1 - 40$ cm). Although the importance of these pioneering experiments cannot be underestimated we will mention at the moment only that a relation (14) is found with m varying between 1.6 and 4.5.

Much later a new set of careful experiments in wide capillaries (> 100 μ) was carried out by Atkins [27] at low temperatures (small

x-values, i.e. $\hat{v} \approx v_s$). Writing formally $\hat{v} = v_1(r) + v_2(\mathrm{grad}\, p) + v_3(r, \mathrm{grad}\, p)$, Atkins supposed the velocity to be divided into three parts. On the basis of the different widths used, his experimental data could be composed in this way. However, the velocity v_1 is found to be negligible as this has the character of a critical velocity and in these experiments no superfluidity was observed. Velocities of the type of v_2 and v_3 are both provided by the Gorter–Mellink hypothesis [12]. With respect to v_2 a satisfactory agreement with the values given in ref. 12 was observed even when calculating values of the constant of mutual friction [Eq. (9)]. However, comparison of the numerical v_3-values of Atkins with those of Gorter–Mellink [12] seems to suggest that still other forces are present. It must be mentioned that in these experiments for the first time the end-effects were studied carefully. As a result, for each capillary a correction of about ϱv^2 was applied. Also oscillations of the liquid around the equilibrium position were studied. With respect to amplitude and period, agreement was found with elementary formulae.

Narrow capillaries, such as those present in a porous membrane, were used by White [28]. The results gave a relation of the type (14) with $m = 3.3 - 4.5$.

A new idea was realised in another set of experiments [13, 29, 30, 31, 32] carried out in Oxford with different shapes of the apparatus of Fig. 1b. Operating in the same way as mentioned above one can now also observe the height at which the level X will adjust itself, i.e. one can determine the pressure at the position X. It was found that the level A went down according to Eq. (14), with different values of m. In the case of a slit the value $m = 3.7$ was observed; a capillary filled with jewellers rouge gave $m = 2 - 3.3$; while in the case of (two) membranes a value of $m = 10$ was realised. The level X always adjusted itself very rapidly near the bath level in case the flow resistance AX is larger than XB; in the opposite case the level X follows the level in tube A. Obviously all (or most) of the pressure drop exists across the highest resistance. This implies the possibility of a discontinuity in the (derivative of the) pressure along the flow channel. However, this is not necessarily the case, as follows from the high value of m and assuming the existence of a critical velocity. Also other experiments are in contradiction with the former idea.

Swim and Rohrschach [33] used the same apparatus, only with longer tubes A and X. These experiments are the only ones with level diffe-

rences exceeding 10 cm He. Nevertheless the same results as in the shorter tubes are obtained (with $m=3$), although at the highest pressure differences the accuracy is reported to be low.

The flow of He II under the influence of large pressure gradients has been measured at Leyden [34]. An apparatus of the type of Fig. 1d with a slit width of 0.33 micron was used. With pressure gradients varying between 25 and 3500 cm He/cm the relative velocity was found to obey the relation

$$\text{grad } p = \text{constant } (v_s - v_n)^{3.45}, \qquad (15)$$

the relative velocity obviously being independent of temperature.

In view of flow experiments with pure ^{3}He and ^{3}He$-^4$He mixtures we first have to mention Abraham, Osborne and Weinstock [35] and Hammel and Schuch [36], who studied the flow of pure ^{3}He and of a 3.9 % ^{3}He$-^4$He mixture resp. At one side of a slit a small amount of liquid was condensed, whereas the space at the other side of the slit was evacuated. By observing the pressure increase in this space (after switching off the pump) some information about the flow was obtained, such as the non-existence of superfluid ^{3}He. As, however, no values of $\hat{v}$ were obtained, whereas on the other hand the unsaturated liquid at the low-pressure side of the slit might have affected the flow rate, we shall not discuss their results further.

At Leyden measurements of the flow properties of ^{3}He$-^4$He mixtures [34] at concentrations up to 7 % have been performed with the same apparatus as used in the case of the ^{4}He-flow under high pressure gradients, mentioned above. Since a concentration gradient along the slit, which gives rise to an osmotic pressure gradient, is inevitable in experiments with mixtures, the equations of motion (1) and (2) have to be modified in the mixture case by inserting $(1-x)$ grad $p_{\text{osm}} = (1-x)\,\varrho RT$ grad X (where X denotes the ^{3}He-concentration in the liquid), a term rather similar to the fountain pressure term $x\ (1-x)\,\varrho S$ grad T. Hence the equations of motion become in the isothermal case

$$v_n \backsim \Delta p \qquad (16)$$

$$(v_r)^m \backsim (\Delta p - \Delta p_{\text{osm}}) = \Delta p_{\text{eff}} \qquad (17)$$

where Δp and Δp_{osm} are the pressure differences across the slit. By keeping the concentration larger at the high pressure side of the slit

both Δp and Δp_{osm} are positive. Hence v_n has to be positive always, whereas v_r can be either positive or negative, according to the sign of Δp_{eff}. Since v_r becomes much larger than v_n as soon as Δp_{eff} is not nearly zero, the observed velocity $\hat{v}=(1-x)v_r+v_n$ can be larger or smaller than zero too (see Fig. 3). At the same absolute value of

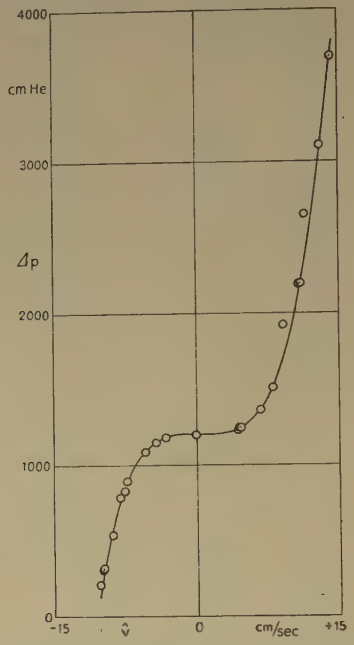

Fig. 3. The velocity $\hat{v}$ of a 4.1 % ^{3}He–^{4}He mixture at 1.7° K as a function of the pressure Δp.

Δp_{eff}, however, the modulus of the negative velocity $\hat{v}$ is smaller than the corresponding positive one. This is obviously caused by the normal fluid flow, which implies the possibility of calculating the normal fluid viscosity η_n directly from experiment. On the other hand, $(1-x)(v_s-v_n)$ can also be derived from $\hat{v}$, once η_n has been determined. The experiment yields the relation

$$\Delta p_{\mathrm{eff}}=\alpha(T, X)\,\{(1-x)(v_s-v_n)\}^{3.45}. \tag{18}$$

Since the value of the exponent is the same as for the ^{4}He-flow with the same apparatus, one is tempted to apply Eq. (14) once more to v_r, obtaining in this way the dependence of the normal fluid concentration x on the ^{3}He-concentration X. At temperatures near the

lambda-point values of $(\partial x/\partial X)_T$ somewhat smaller than four have been found, which is in good agreement with the latest determinations of the shift of the lambda-point of mixtures, dT_λ/dX [22, 37, 38]. At lower temperatures $(\partial x/\partial X)_T$ decreases to a value of about two tenths.

3.2. Non-isothermal flow

In this § we shall discuss only those experiments (with thermal and gravitational potential) in which the frictional forces were investigated qualitatively and quantitatively.

A. Experiments with Resulting Flow of Matter

The first measurements were carried out by Kapitza [10] who observed a strong increase of the temperature in volume A (see Fig. 1c) when the heat supply I exceeded a 'critical' value. An analogous result is reported by Meyer and Mellink [17] although most of their work belongs to section B, concerning the experiments without resulting flow of matter.

Extensive studies have been carried out in Oxford and Leyden by several investigators [13, 14, 15, 29, 30, 31, 32, 39, 40, 41]. The Oxford experiments have been performed in the apparatus of Fig. 1b with the volume A closed at the top; the Leyden experiments with an apparatus of the type of Fig. 1c. In this case also the temperature in A and B was measured. For this reason and because of the thermal isolation, it is possible to discuss the energy blance of the vessel A. These measurements will be described with the quantities discussed in § 1.

As a result of a heat supply I to A, the helium will flow with a velocity $\hat{v}$ (about $(1-x)v_s$) and the level in A will rise. Neglecting the flow of normal fluid and, for the time being, the force F, there will flow as much helium as is required to compensate the heat input. As a result, the velocity $\hat{v}$ will be proportional to I. Of course a (in practice small) part of I will be required for heating the volume A in order to obtain the (equilibrium) temperature difference corresponding to the pressure difference. Also as a result of this temperature difference some heat will leak away (see Fig. 1b). However, all these effects are propertional to each other and do not affect the proportionality of $\hat{v}$ and I.

The existence of the force F, however, implies that a great part of the heat will be necessary for creating the extra temperature difference ΔT^+, proportional to F, and the velocity $\hat{v}$ will be less than

proportional to I. Now the hypothesis of a critical velocity implies that below a certain value F is negligibly small whereas for large values F can also be rather large. Therefore the $\hat{v}$ vs. I-curve must have a discontinuity in its first derivative at $\hat{v} = v_{crit}$, which is actually observed. This is schematically drawn in Fig. 4. These considerations refer to the velocity $\hat{v}_a$, i.e. the value of $\hat{v}$ directly after the heat supply is started. For, during a constant heat supply I, the $\hat{v}$-values change as a function of time which makes the situation somewhat more complicated. But this $\hat{v}(t)$-function also can be calculated, and agreement with experiment is found [15].

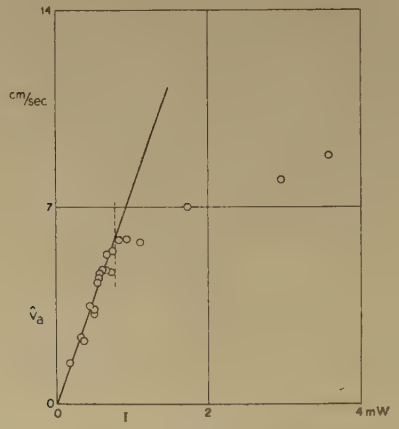

Fig. 4.
The initial velovity $\hat{v}_a$ as a function of the heat supply I ($T = 2.02°$ K).

The behaviour of the tube X is somewhat peculiar. The level remains at the height of the bath level until the critical value is reached, above which it first lowers and later increases. We are inclined to attribute this to temperature effects but as it is impossible to measure any temperature in the tube X it is not possible to test this supposition.

If one stops heating after some time, the helium will continue to flow in case $I > I_{crit}$. This is because Δp and ΔT are obviously not in equilibrium, the difference ΔT^+ being proportional to F or to v_r^m. On the other hand, if $I < I_{crit}$, $F = 0$ and no flow will occur after the heat supply is removed. So this 'overshoot' $\square$ as a function of I (or $\hat{v}_a$) will also exhibit the critical effect [13]. This has been confirmed by many careful experiments [15]. These relations can all be calculated

exactly with the formulae (10), (11) and (12), based on the equations of motion and the energy balance [16].

Finally in these experiments one can just measure the differences in temperature and pressure across the slit as a function of time and calculate at each instant the force F directly according to Eq. (1). This is the most direct way and a number of data are available [39, 40]. At low velocities, however, the overshoot method is more accurate, since $\square$ is proportional to F, whereas in the other experiments F is derived from the (small) difference between two large quantities. The value of m, obtained with this method, equals 3 for all slits with $h > 1\ \mu$. At lower h-values the m-values became somewhat higher. Numerical values of A, the proportionality factor in the mutual friction force, have been calculated. It was shown that these values vary as a function of temperature but that they do not depend on the length of the slit. This is a strong indication that the frictional processes occur in the whole slit, in contradiction to other possible assumptions (cf. § 3.1). More evidence is given below.

With an apparatus of the type of Fig. 1c (the slit of 0.2 micron width being made by fusing a gold wire into soft glass) the flow rate of He II as a function of large temperature differences [42] was measured at Leyden (see Fig. 5). In this case one can neglect v_n, because of the small pressure differences across the slit. When Eq. (9) is modified into $F = B\{(1-x)v_r\}^m = B\hat{v}^m$, integration of Eq. (10) along the slit yields

$$\int f \mathrm{d}T^+ = \hat{v}^m \int B \mathrm{d}z = \hat{v}^m \int B(\mathrm{d}z/\mathrm{d}T)\mathrm{d}T. \tag{20}$$

As the normal fluid flow was fully suppressed, the temperature distribution along the slit was determined by the gold wire, the heat conductivity of the glass being relatively poor. Hence Eq. (20) becomes

$$\int_{T_1}^{T+\Delta T} f_1 \mathrm{d}T^+ = \frac{\hat{v}^m L}{\bar{T}\,\Delta T} \int_{T}^{T+\Delta T} BT\,\mathrm{d}T \tag{21}$$

where L is the slit length, $\bar{T}$ the mean temperature of the slit and ΔT the applied temperature difference. By inserting the values of B as determined from isothermal flow with the same apparatus, complete accordance with experiment was found. All other types of distribution of the flow resistance along the slit failed to describe the experimental data correctly. Hence one has to conclude also in this case that the

flow resistance for the superfluid is distributed evenly over the whole length of the slit.

With the same apparatus the flow of $^3He-^4He$ mixtures under the influence of large fountain pressures [42] was studied by condensing pure ^4He at the warm side of the slit and mixture at the other. The results are analogous to the pure ^4He-flow, although the velocities observed were somewhat smaller. At high temperatures the decrease

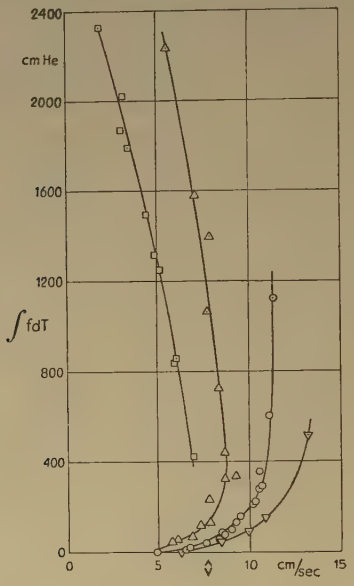

Fig. 5.

The flow rate of He II as a function of large temperature differences.
⊡ : $T = 1.95°$ K; △ : $T = 1.84°$ K; ⊙ : $T = 1.66°$ K; ▽ : $T = 1.48°$ K.

in velocity became so large that zero velocity could be attained. The results are not fully understood at the moment, as the mixture flow under pressure gradient is still under discussion. Furthermore, in contrast to the latter case, no ^3He passes the slit, making comparison of the two experiments rather difficult.

B. Experiments without Resulting Flow of Matter

In this case a stationary state with a temperature and a pressure difference is reached. This can be realised (i) without any heat supply to volume A (see Fig. 1c) when $v_n = 0$ (narrow slits) or (ii) with a heat supply which just compensates the energy loss by the outflow of the

normal fluid. The first method was used by Kapitza [10] and by Meyer and Mellink [17] (discussed in § 2). In the case (ii) we are dealing with 'ordinary' heat conduction which will be discussed here.

The pioneering experiments were carried out by Allen and Reekie [9,43] leading to Allen and Reekies' rule. This contends that in all circumstances (slitwidth and length) the heat flow is proportional to the pressure difference. This in complete agreement with Eq. (8).

An extensive study was made at Leyden [17, 44, 45, 46, 47]. The heat flow was observed as a function of slitwidth and diameter of capillaries over a wide range, and as a function of temperature and of temperature and pressure differences. Allen and Reekies' rule was confirmed ($I \sim \Delta p$). In the wider slits the heat flow (and so also Δp) was found to be proportional to the cube root of the temperature difference ($I \sim \Delta p \sim \Delta T^{1/3}$). On the other hand in narrow slits a direct linearity was observed ($I \sim \Delta p \sim \Delta T$). The proportionality factor depends strongly on the temperature. It should be mentioned that on these experiments the formulation of the mutual friction was based. Quantitatively this model was also a success.

Later experiments were carried out with an apparatus of the same type although with a geometrically better defined slit [39, 41]. The aim was a closer examination of the heat conduction below and around the critical velocity. It was found that the heat flow as a function of ΔT also showed the critical effect, the increase being much sharper than given by a cubical law. Thus at low values of I obviously $F = 0$ and $I = \alpha \Delta T$. As this factor α appears to be proportional to h^3 (as it should be in the case of an ordinary liquid when substituting $\Delta p = c \Delta T$), the calculation of η_n from the values of α seems to be reliable. At low values of h these results deviate from the earlier results of Mellink, where the decrease of the heat conduction was found to be less than according to h^3. The reason is not clear, but it may be connected with the special shape of the earlier slit, which has disadvantages at these low h-values. On the other hand, the recent calculations of Klemens [48] suggesting an additive heat conduction independent of slitwidth and giving more or less a description of the results of Mellink, are not confirmed by these later experiments directly. For, in this case only at the lower temperatures and slitwidths, deviations are observed, which are at least an order of magnitude smaller than calculated by Klemens.

The calculated values of η_n are given in Fig. 6 together with other

data [49, 50, 51, 52]. It should be remarked that with the experiments involving the viscometer and the slits, we are dealing with a stationary flow of the normal fluid in contrast with the experiments with the oscillating disk. The differences between the three η_n-curves, however, are all of the same order, although it is true that with regard to the temperature derivative of η_n, the data of the viscometer and the slits are in somewhat better agreement.

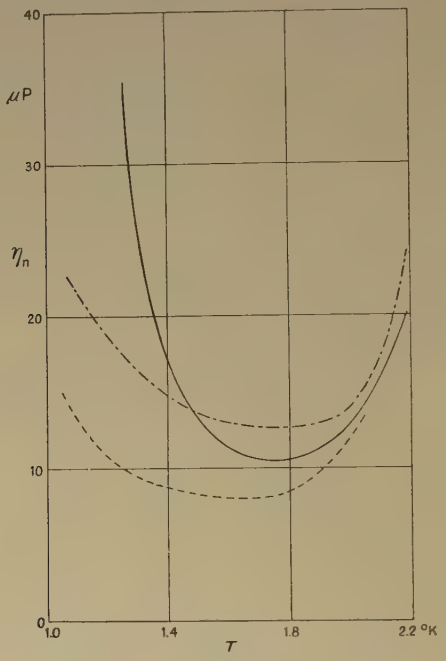

Fig. 6. The normal fluid viscosity η_n as a function of temperature.
————: oscillating disk-values
— - — - —: rotating viscometer-values
– – – – –: heat conduction-values.

3.3. Conclusions

Now that we have outlined the experimental material we are able to submit our picture of the dependence of F on the velocity, as mentioned in the first §, to a closer examination.

At low velocities we have found the frictional forces to be negligible. There are, however, indications that they are not exactly zero [15]. But as soon as the critical velocity is reached the situation is completely altered. We should like to discuss this velocity first.

As is obvious from experimental reasons, it will always be impossible to decide whether or not the first derivative of the $F-v$ curve really shows a discontinuity at $v=v^c$. One can only say that the derivative of F changes rather fast at $v=v^c$, which values v^c can be determined rather precisely. Furthermore it must be remarked that the critical effect is related to the superfluid velocity. For, although this velocity is about equal to the relative velocity in many experiments, in the case of the measurements on heat conduction these two velocities differ in such a way that this statement is justified.

The values of the critical velocity v_s^c can be calculated from all experiments mentioned in the previous § where critical behaviour was observed. Actually, the critical effect is observed only in experiments with slits, narrower than 3 μ. It is found that these values are of the order of 5 – 15 cm/sec and depend somewhat on temperature [15]. Also they are generally believed to depend on the slitwidth. Although we will not discuss this question we should mention a rather remarkable fact. The values obtained by very different experiments and h-values obey approximately a $h^{-1/2}$-relation over a wide range. This was first pointed out by Dash [53].

It is possible that accurate values of the critical velocity do not exist in principle. For, if the critical behaviour is from microscopic origin it is by no means certain that it is always related to the same macroscopic average velocity. Actually there are experimental indications that it is not so [14]. In this connection we should also comment on the question of the velocity profile of the superfluid. Up till now we have just considered the average velocity across the slit and the actual profile has not been in discussion. As a matter of fact the situation in this respect is not clear. It may be that the velocity is indeed a constant across the slit (rot $\mathbf{v}_s=0$). On the other hand sometimes a model is suggested including very large velocities along the wall over a depth δ, with zero velocity in the middle [9, 33]. However, as has been pointed out by Atkins [27], his oscillation experiments exclude such a possibility, admitting only a not-too-strong variation of v_s across the slit. This is, for example, provided by the mutual friction force, especially in the case of small velocity of the normal fluid [12]. We shall not discuss the question further. Anyhow it is likely that also in this respect the situation above and below v_s^c is different.

Now we return to the description of the $F(v)$-relation. As soon as

the critical velocity is passed the situation changes. A strong interaction with the normal fluid is revealed which at higher values can often be described by Eq. (9) ($F \sim (v_s - v_n)^m$). The value of m is found to be about 3, although using slits with low h-values somewhat higher values appear. This may be caused by the inhomogeneity of the slit or capillary which causes a higher effective friction giving a higher effective m. In the case of isothermal flow in wider slits described by the velocity $\hat{v}$, somewhat smaller values of m are observed. In this case the normal fluid flow is not completely suppressed and some average between $m=1$ and $m=3$ can be expected.

The value of A in Eq. (9) is of the order of 50 cgs units and depends on temperature.

If Allen Reekies' rule applies, i.e. $I \sim \Delta p$, the forces F and F' are obviously equal. However, this may be only a (fairly good) approximation, since closer examination suggests that small deviations from this rule occur [41].

Although this description of the behaviour of helium II in slits seems to be satisfactory, it must be kept in mind that in some other experiments [1] still other forces are found to be present than those given by a type of mutual friction. Also some experiments in slits lead to such a conclusion, as we have seen [27]. This may seem to be ambiguous, but on the other hand we may ask whether or not complete agreement could be expected in the present situation. The general flow mechanism of helium II reduces for small velocities to two independent sub-fluids, one of them behaving as a superfluid.

It may well be that at high velocities this reduction has an arbitrary character and that the usual introduction of a mutual friction in the two-fluid model has only sense as a reasonable approximation for narrow slits. It is quite possible that in different experimental arrangements other formal descriptions are required. A real synthesis can only be expected on the basis of a general theory of the flow phenomena in liquid helium II.

Perhaps we can illustrate this with measurements on the viscosity of gases. Suppose one knows the Poiseuille-formula but does not know the existence of mean free path effects. This implies that one will observe deviations of the formulae in the case of experiments at low pressure. To explain these one can assume a variable effective radius. As in the case of the F-force in liquid helium, this has the advantage of a formal description of the experiments, but it is unsatis-

factory from a theoretical point of view and it may be a source of confusion when using different kinds of experimental arrangements.

The present situation suggests that a better knowledge of microscopic details will be of extreme importance. Probably it is one of the most interesting directions for futher research. How far this field will be accessible to experimentation without losing the real bulk flow, will be a subject of closer investigations.

REFERENCES

[1] A. C. Hollis Hallett, Progr. Low Temp. Phys., Vol. I, Ch. IV (1955).
[2] C. J. Gorter, Progr. Low Temp. Phys., Vol. I, Ch. I (1955).
[3] J. F. Allen and H. Jones, Nature, **141**, 243 (1938).
[4] H. London, Nature, **142**, 612 (1938); Proc. Roy. Soc. **A, 171**, 484 (1939).
[5] C. J. Gorter, Physica, **15**, 523 (1949); Comm. Leiden Suppl. 99a.
[6] S. R. de Groot, L. Jansen and P. Mazur, Physica, **16**, 421 (1950).
[7] T. Usui, Physica, **17**, 694 (1951).
[8] J. F. Allen and A. D. Misener, Nature, **141**, 75 (1938).
[9] J. F. Allen and J. Reekie, Nature, **144**, 475 (1939).
[10] P. Kapitza, J. Phys. U.S.S.R., **5**, 59 (1941).
[11] C. J. Gorter, Phys. Rev., **74**, 1544 (1948).
[12] G. J. Gorter and J. H. Mellink, Physica, **15**, 285 (1949); Comm. Leiden Suppl. 98a.
[13] R. Bowers and K. Mendelssohn, Proc. Roy. Soc. A, 213, 158 (1952).
[14] P. Winkel, Thesis, Leiden (1954).
[15] P. Winkel, A. M. G. Delsing and J. D. Poll, Physica, 21, 332 (1955); Comm. Leiden 299b.
[16] P. Winkel, Physica, 21, 322 (1955); Comm. Leiden Suppl. 109d.
[17] L. Meyer and J. H. Mellink, Physica, 13, 197 (1947); Comm. Leiden 272b.
[18] C. J. N. van den Meijdenberg, K. W. Taconis, J. J. M. Beenakker and D. H. N. Wansink, Physica, 20, 157 (1954); Comm. Leiden 295c.
[19] D. F. Brewer, D. O. Edwards and K. Mendelssohn, Comm. Confér. de Phys. de Basses Temp., p. 40 (1955).
[20] B. S. Chandrasekhar and K. Mendelssohn, Proc. Phys. Soc. London A, **68**, 857 (1955).
[21] H. C. Kramers, J. D. Wasscher and C. J. Gorter, Physica, 18, 329 (1952); Comm. Leiden 288c.
[22] Z. Dokoupil, G. van Soest, D. H. N. Wansink and D. G. Kapadnis, Physica, 20, 1181 (1954); Comm. Leiden 298a.
[23] R. A. Hull, K. R. Wilkinson and J. Wilks, Proc. Phys. Soc. London A, **64**, 379 (1951).
[24] P. Kapitza, Nature, **141**, 74 (1938).
[25] J. F. Allen and A. D. Misener, Nature, **142**, 643 (1938).
[26] J. F. Allen and A. D. Misener, Proc. Roy. Soc. A, 172, 467 (1939).
[27] K. R. Atkins, Proc. Phys. Soc. London A, **64**, 833 (1951).

[28] G. K. White, Proc. Phys. Soc. London A, **64**, 554 (1951).
[29] R. Bowers and K. Mendelssohn, Proc. Phys. Soc. London A, **63**, 178 (1950).
[30] R. Bowers, B. S. Chandrasekhar and K. Mendelssohn, Phys. Rev., **80**, 856 (1950).
[31] R. Bowers and G. K. White, Proc. Phys. Soc. London A, **64**, 558 (1951).
[32] B. S. Chandrasekhar and K. Mendelssohn, Proc. Roy. Soc. A, **218**, 18 (1953).
[33] R. T. Swim and H. E. Rohrschach Jr., Phys. Rev., **97**, 25 (1955).
[34] D. H. N. Wansink and K. W. Taconis, to be published in Physica.
[35] D. W. Osborne, B. Weinstock and B. M. Abraham, Phys. Rev., **75**, 988 (1949).
[36] E. F. Hammel and A. F. Schuch, Phys. Rev., **87**, 154 (1952).
[37] J. C. King and H. A. Fairbank, Bull. Am. Phys. Soc., **28**, 65 (1953).
[38] J. G. Dash and R. D. Taylor, Phys. Rev., **99**, 598 (1955).
[39] C. S. Hung, B. Hunt and P. Winkel, Physica, **18**, 629 (1952); Comm. Leiden 289c.
[40] P. Winkel, A. M. G. Delsing and C. J. Gorter, Physica, **21**, 312 (1955); Comm. Leiden 299a.
[41] P. Winkel, A Broese van Groenou and C. J. Gorter, Physica, **21**, 345 (1955); Comm. Leiden 299c.
[42] D. H. N. Wansink and K. W. Taconis, Comm. Confér. de Phys. de Basses Temp., p. 33 (1955).
[43] J. F. Allen and J. Reekie, Proc. Cambr. Phil. Soc., **35**, 114 (1939).
[44] W. H. Keesom and B. F. Saris, Physica, **7**, 241 (1940); Comm. Leiden 257d.
[45] W. H. Keesom, B. F. Saris and L. Meyer, Physica, **7**, 817 (1940); Comm. Leiden 260a.
[46] W. H. Keesom and G. Duyckaerts, Physica, **13**, 153 (1947); Comm. Leiden 271c.
[47] J. H. Mellink, Physica, **13**, 197 (1947).
[48] P. G. Klemens, Austr. J. Phys., **8**, 206 (1955).
[49] E. L. Andronikashvilli, J. Exp. Theor. Phys., **18**, 429 (1948).
[50] A. de Troyer, A. van Itterbeek and G. J. van den Berg, Physica, **17**, 50 (1951); Comm. Leiden 284c.
[51] A. C. Hollis Hallett, Proc. Roy. Soc. A, **210**, 404 (1952).
[52] W. J. Heikkila and A. C. Hollis Hallett, Canad. J. Phys., **33**, 420 (1955).
[53] J. G. Dash, Phys. Rev., **94**, 825, 1091 (1954).

CHAPTER IV

HELIUM FILMS

BY

K. R. ATKINS

DEPARTMENT OF PHYSICS, UNIVERSITY OF PENNSYLVANIA

CONTENTS: 1. Introduction, 105. — 2. Experimental Difficulties, 108. — 3. Measurements of the Thickness of the Saturated Film, 110. — 4. Unsaturated Films, 113. — 5. The Flow of the Saturated Film, 118. — 6. The Flow of Unsaturated Films, 126. — 7. Theories of the formation of the Film, 130.

1. Introduction

Helium films present a clear cut case of physical adsorption. The helium atom is chemically inert and there can be no question of chemical bonding between the atoms of the film and the atoms of the wall. Offsetting this initial simplification, however, are the complications associated with the existence of the films at low temperatures — the importance of a large zero point energy and the quantum effects which give rise to the λ-transition in the liquid. The superfluidity of the liquid also gives the films unique properties and the flow of the films draws attention to their existence in a dramatic fashion. Thick films of helium are particularly easy to study, because, whereas a thick film of an ordinary substance is readily evaporated by a small amount of stray heat, a helium film under the same circumstances can be replenished by superfluid flow. Multimolecular adsorption is therefore unusually prominent in the case of helium.

The flow of the film was probably first observed by Kamerlingh Onnes [1] who had built an apparatus in which an open Dewar vessel containing liquid helium II was partially immersed in liquid helium contained in an outer Dewar vessel. He noticed that, whatever the initial relative positions of the two liquid levels, the inner level always rose or fell until it reached the height of the outer level. We now believe that a thick helium film had formed on the walls of the inner vessel and flow took place through this film until the two levels were equal, but this explanation was first advanced many years later by

Rollin and Simon [2], when they observed that a thermally isolated vessel connected to a region at a higher temperature via a narrow tube warmed up much more rapidly when the liquid helium inside it was below the λ-point. They attributed this to the formation of a thick film on the wall of the connecting tube, flow through this film towards the high temperature region, evaporation of the film there,

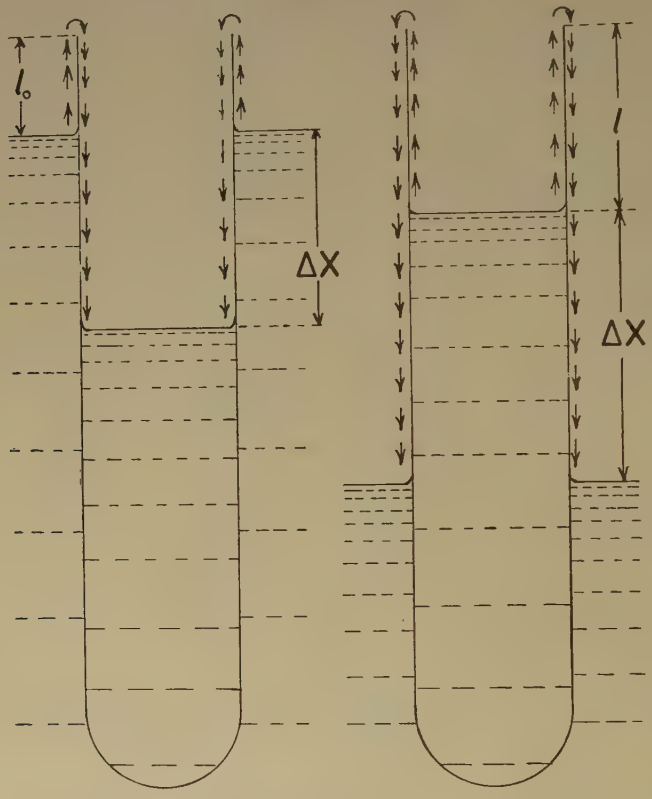

Fig. 1. The pioneer film flow experiments of Daunt and Mendelssohn.

and a backward flow of gas to the inside of the vessel where it condensed, giving up its latent heat. Some pioneer work on the film was performed by Kikoin and Lasarew [3, 4] but the existence of the film was firmly established and its basic properties discovered in an elegant series of experiments by Daunt and Mendelssohn [5, 6]. Their basic experiment is illustrated in Fig. 1. As the beaker was raised or lowered, liquid flowed through the film on the exposed part of the

wall so that the inner level always moved towards the outer level. The rate of transfer was found to be almost, but not quite, independent of the level difference Δx and almost, but not quite, independent of the height of the film l. In support of the hypothesis of film flow, the volume of liquid transferred per second was found to be proportional to the circumference of the beaker and in an arrangement such as that of Fig. 2(a) was proportional to the perimeter at the point of constriction. The transfer rate of the film is therefore usually expressed as cm^3 of bulk liquid per second per cm of perimeter. In the arrangement of Fig. 2(b) the abnormally long path over which the film had to flow had no detectable effect on the rate of transfer. Daunt and

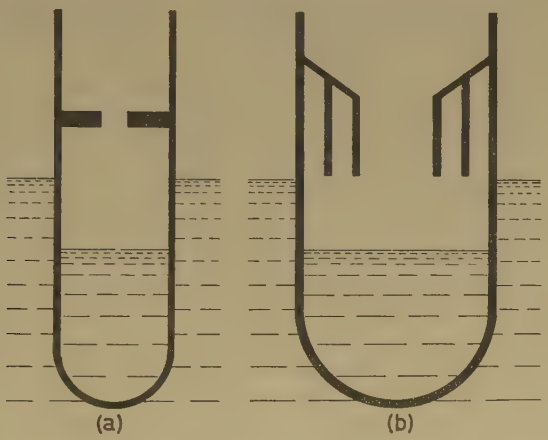

Fig. 2. Further film flow experiments of Daunt and Mendelssohn.

Mendelssohn therefore proposed that, apart from secondary effects, the phenomena could be explained by assuming that the flowing film attains a 'critical velocity' independent of everything, except possibly temperature.

The thick film studied in this type of experiment has been called the saturated film because it exists in equilibrium with the saturated vapour. It is also possible to perform a more conventional type of adsorption experiment in which the film is in equilibrium with gas at a pressure p less than the vapour pressure p_0, and films of this type are called unsaturated films. There is a possible connection between the two cases. Imagine the ideal case of a static saturated film formed on a perfectly smooth, clean surface in an accurately isothermal

enclosure, as in Fig. 3. The thickness d of the film is a function of the height H above the free surface of the bulk liquid. However, at this height the film is in equilibrium with gas whose pressure p at large distances from the wall is not p_0 but

$$p = p_0 \, e^{-MgH/RT}. \tag{1}$$

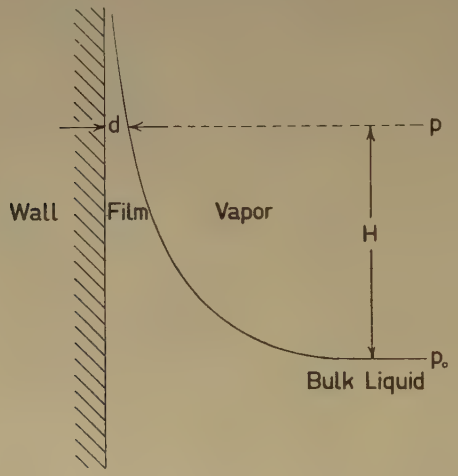

Fig. 3. The contour of the saturated film.

This seems to imply that an unsaturated film being studied in an adsorption experiment at a relative pressure p/p_0 has identical properties with a saturated film in equilibrium at a height H above the surface of the bulk liquid given by

$$H \equiv \frac{-RT}{Mg} \ln (p/p_0). \tag{2}$$

2. Experimental Difficulties

It is extremely doubtful whether the ideal case just discussed can be realized, or even approached, in practice. Atkins [7] and, independently, de Haas and van den Berg [8] observed that, occasionally, the rate of transfer through the saturated helium film is many times greater than normal. Bowers and Mendelssohn [9] were able to show that this is a consequence of contamination of the surface by a deposit of some solidified gas, such as solid air, solid hydrogen or ice. Perhaps the deposit is granular and either increases the effective perimeter of the beaker on a micro-scale or else liquid is held in the spaces between

the grains, so that the effective thickness of the film is increased. Possibly, even a thin deposit of some impurity is able to modify the forces between the wall and the helium in such a way that the film thickness is increased. The views of McCrum and Eisenstein [10] on this point will be discussed later. From a practical point of view, it is extremely difficult to avoid accidental contamination of the surface and even the most careful of experiments can be suspect in this connection.

No surface is perfectly smooth and even the surface of glass probably contains the so-called Griffith's cracks which are important in determining its strength. For every helium film experiment, therefore, it is relevant to ask whether the results are entirely determined by the film or whether they are significantly influenced by liquid which is held in the cracks by surface tension effects. Recent experiments of Dyba, Lane and Blakewood [11] and Brewer and Mendelssohn [12] confirm that surface tension effects can fill such cracks with liquid, particularly below the λ-point where any liquid evaporated out of the crack by stray heat can be quickly replenished by film flow.

Consider an adsorption experiment on an unsaturated helium film with a gas pressure p and with the surrounding liquid helium bath at a temperature T, where the vapour pressure is $p_0(T)$. A small amount of heat falling on the surface holding the film will raise the temperature in that vicinity to $T+\mathrm{d}T$, where the vapour pressure is $p_0(T+\mathrm{d}T)$. The experimenter will therefore relate the thickness of the film to the relative pressure $p/p_0(T)$ whereas he should use $p/p_0(T+\mathrm{d}T)$. If $\mathrm{d}T$ is not too large, this does not matter when p/p_0 is appreciably less than 1, but when p is close to p_0 the thickness of the film is very sensitive to p_0-p (see Fig. 6) and a film which might be expected to be thick because $p \quad p_0(T)$ is small remains thin because $p-p_0(T+\mathrm{d}T)$ is large. For this reason, thick films were not observed above the λ-point until care was taken to reduce extraneous radiation. Below the λ-point the situation is somewhat different. The superfluid film is able to flow towards the source of heat and prevent the formation of large temperature differences, but there is then a dynamic type of equilibrium in which the film arriving at the hot region evaporates, returns as vapour to the cold region, condenses as bulk liquid or film and flows back to the hot region. It is relevant to inquire whether a film behaving in this way has the same properties as a static film. Meyer [13] has suggested, for example, that when the super-

fluid component in the film is flowing with a velocity v_s, the kinetic energy of the film must be included in its free energy and the thermodynamic equilibrium is thereby disturbed in such a way that the film thickness is increased and has a different variation with height.

For saturated films of liquid helium II, there is another disturbing possibility if a vertical temperature gradient exists. In accordance with the well-known thermo-mechanical effect, if two volumes of liquid communicate with one another through a narrow channel and there is a temperature difference ΔT between them, the level in the warmer vessel is raised above the other level by an amount

$$\Delta h = \frac{S}{g} \Delta T. \qquad (3)$$

If a vertical surface dips into liquid helium II and the temperature increases upwards, one might wonder if the effective height H determining the formation of the film ought to be reduced by Δh. At 2.0° K a temperature gradient of only 10^{-4} deg/cm would be sufficient to counteract the effect of gravity!

This is a formidable array of possible difficulties and it is clear that the perfect film experiment would be difficult to perform. It is therefore not surprising that the experiments which have so far been performed are mutually contradictory. Moreover, no single experiment can be said to be absolutely free from suspicion on one or more of the counts presented above.

3. Measurements of the Thickness of the Saturated Film

Jackson and his co-workers [14, 15, 16] have measured the thickness of the saturated film by an optical method, depending upon the fact that, if plane polarized light is reflected from a polished metal surface covered by a film, then the reflected light is elliptically polarized and the angle between the initial plane of polarization and the major axis of the ellipse can be related to the thickness of the film. Referring to Fig. 4, light from a sodium lamp S.L. was collimated by the slits S_1 and S_2, passed through a heat absorbing filter F and was plane polarized at 45° to the vertical by the polaroid slab P. After reflection from the surface M, the elliptically polarized light was converted back into plane polarized light by the compensating plate, $\lambda/4$, and the plane of polarization was determined by rotating the nicol prism N. The upper part of the polished stainless steel mirror M was coated with a

monomolecular layer of barium stearate (2.4×10^{-7} cm thick) whereas the lower part had a coating three molecules thick. Different settings of the Nicol prism N were therefore needed to make the two regions appear dark, but an intermediate setting could be found at which the upper and lower sides of the $1-3$ boundary appeared equally bright. When the helium film formed on top of the barium stearate layers, this halfshade setting was destroyed, but could be restored by rotating the Nicol prism through a small angle of a few degrees, measurable to within $\pm$ 8 min of arc, and from this angle the film thickness at the $1-3$ boundary could be deduced. The lower part of the mirror M dipped into a liquid helium bath and the film thickness measured therefore corresponded to the height H of the $1-3$ boundary above the surface of the bath.

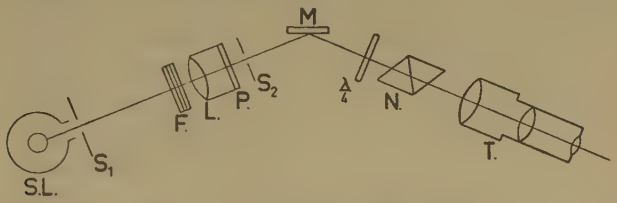

Fig. 4. The optical method of measuring film thickness. S.L., sodium lamp; S_1, S_2, slits; F, filter of heat absorbing glass; L, lens; P, polaroid; M, mirror; $\lambda/4$, mica compensating plate; N, nicol prism; T, telescope. (after Burge and Jackson).

As the technique has been developed and some of the difficulties mentioned in § 2 appreciated, the results have been progressively modified, so we shall discuss only the latest measurements [16], though these may still not be final. Below the λ-point the film thickness d may be expressed in the form

$$d = \frac{k}{H^n} \text{ cm} \tag{4}$$

k varied from 2.96×10^{-6} at 1.32° K to 3.15×10^{-6} at 2.05° K and n remained constant at 0.435 over this temperature range. At a height of 1 cm the film was therefore about 80 layers thick. Above the λ-point, when extraneous heat was avoided there was still a thick film of about 10 layers (4×10^{-7} cm). Within a temperature range of only 0.005 deg K just below the λ-point, the thickness rapidly decreased from 80 layers to 10 layers, but this may be connected with the falling out of the flow mechanism. When a heating coil

was attached to the top of the mirror and a small heat input of 7.75 μW applied, the film thickness increased by about 20 % and varied less rapidly with height. At 300 μW the flow mechanism probably saturated, because then the film was observed to have a sharp upper boundary which slowly retreated down the mirror as the power was increased. At about 30 mW a very thick film, similar to a surface tension meniscus, was formed and rose to a height of 8 mm above the bulk liquid. In another experiment the mirror M formed part of the outer wall of a beaker and it was found that the film thickness did not change noticeably when there was film flow out of the beaker.

Bowers [17] has used a microbalance to weigh the film formed on a roll of aluminium foil. A wire tail hanging from the foil dipped into bulk liquid and the variation in the weight of the film was studied as the distance between the liquid surface and the bottom of the foil was varied. Interpreting the results in terms of Eq. (4), k was 11.8×10^{-6} and n was 0.5 ± 0.07, so that the height dependence was not inconsistent with the optical method but the absolute thickness of the film was about three times greater. The thickness was almost independent of temperature below the λ-point, but within a few thousandths of a degree of the λ-point suddenly fell to about 4×10^{-7} cm. The weight of the film was very sensitive to radiation influx and when the wire tail did not dip into the bulk liquid, so that the heat contact of the creeping film was lost, the thickness fell to about 2.2×10^{-6} cm and was independent of the height of the foil above the liquid surface and almost independent of temperature.

Atkins [18] has employed the oscillation method illustrated in Fig. 5. As the beaker empties through the film, the rate of film transfer is almost independent of the level difference and so, when the inner level reaches the outer level, the film is still moving rapidly and its momentum causes the level to overshoot and then oscillate about its equilibrium position. This oscillation involves a periodic interchange of energy between the kinetic energy of the film and the potential energy of that liquid inside the vessel which is raised above the outer level, and the period therefore depends primarily on the thickness of the film. To interpret the results it is necessary to make certain assumptions about the nature of the flow, such as that the velocity in the film at a fixed height is independent of distance from the wall, and that the thickness of the film is independent of its

velocity. The period of an oscillation can then be shown to be

$$\tau = 2\pi \left[\frac{\varrho}{\varrho_s} \frac{r}{2g} \left(1 + \frac{r}{R} \right) \int_0^l \frac{dH}{d} \right]^{1/2} \tag{5}$$

where r and R are the inner and outer radii of the beaker and l is the height of the rim of the beaker above the bath level. Measurements of the period τ over a range of values of l therefore enable d to be deduced as a function of H.

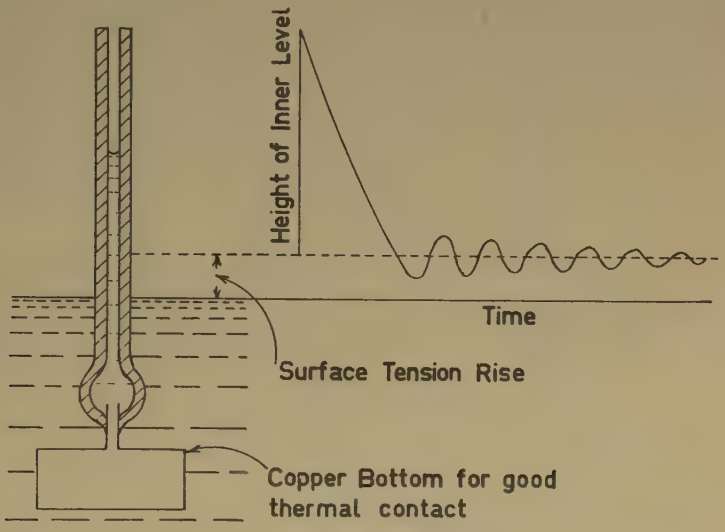

Fig. 5. The oscillation method of measuring film thickness.

Over a range of heights from 1 cm to 5 cm, the results could be represented by Eq. (4), with k varying from 1.5×10^{-6} at 1.1° K to 2.2×10^{-6} cm at 2.0° K, more in agreement with the optical method than the weighing method. The value of n was 0.14, which is much less than the other two methods give, but there was some evidence that the effective value of n was greater at heights less than 1 cm. However, when the experiment was repeated with a slightly different beaker, the film appeared to be about 30 percent thicker, so there were obviously some unexplained effects.

4. Unsaturated Films

The basic experiment on unsaturated films is the plotting of an adsorption isotherm, showing how the mass of gas held on a surface

varies with the relative pressure p/p_0 at constant temperature. This has been done by the usual volumetric method of introducing measured volumes of gas into a system containing a powder of large surface area, such as carbon [19], jeweller's rouge [20, 21, 22] or rutile [23]. Bowers [24] has used the microbalance technique described in the previous section, weighing the film formed on a roll of aluminium foil in an

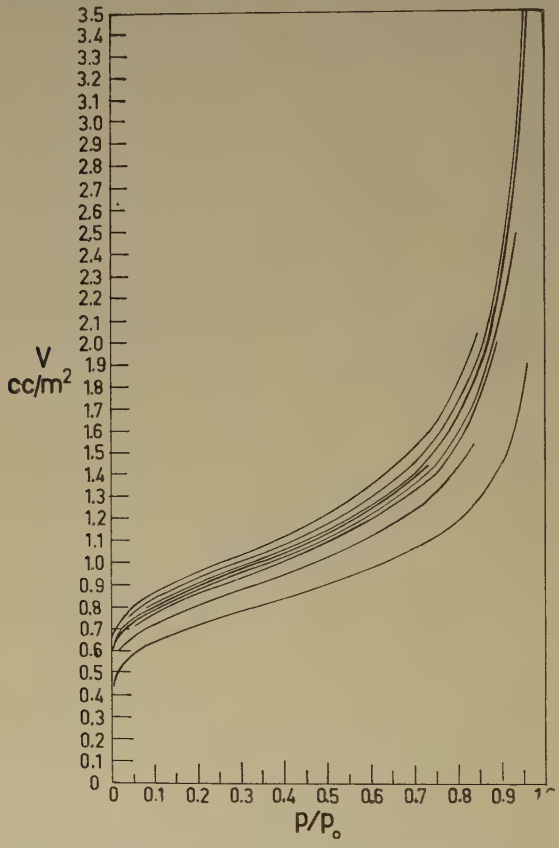

Fig. 6. Adsorption isotherms of helium on jeweller's rouge in cm³ (S.T.P.)/m² as a function of saturation at 4.21° K-lowest curve; 3.02° K, 2.42° K, 2.25° K, 2.14° K, 2.01° K, 1.80° K and 1.59° K-top curve (after Strauss).

atmosphere of helium gas at a pressure p less than the vapour pressure p_0. The optical method of Jackson has been adapted to the unsaturated film by McCrum and Mendelssohn [25]. A typical set of isotherms

obtained by Strauss [22], is shown in Fig. 6. At values of p/p_0 near 0.1 there is a 'knee' in the curve which is usually taken to indicate the completion of the first layer. This region of the curve is conventionally treated in terms of a theory due to Brunauer, Emmett and Teller [26] (the BET theory), and although the principles of this theory are now being questioned there is some experimental and theoretical evidence that its formalism may be applicable at low values of p/p_0 [27]. Application of the BET equations to the helium isotherms gives a very high density for the first layer, corresponding to an interatomic separation of 2 Å as compared with 3.7 Å in the liquid. The first layer is undoubtedly solid and it may even be that the first two or three layers are solid [23, 28]. The density of the first layer appears to decrease with increasing temperature [22].

At larger values of p/p_0, the thickness d of the film can be expressed [24] in the form

$$d = \varkappa/(\ln p_0/p)^{1/3}. \qquad (6)$$

Using Eq. (2) to express this as a variation of film thickness with height, it is equivalent to

$$d = k/H^{0.333} \qquad (7)$$

with values of k similar in order of magnitude to those quoted in § 3, but varying more markedly with temperature. It is interesting to note that the thickest film studied in an adsorption experiment had about 20 layers, and the corresponding value of p/p_0 was equivalent to a height of about 25 cm in a saturated film experiment.

Brewer and Mendelssohn [29], studying adsorption on glass at high relative pressures, observed discontinuities at the λ-point. Long and Meyer [30] have argued that this is thermodynamically impossible. Brewer and Mendelssohn ascribe the results to an 'anomalous surface tension effect' [12, 31] producing bulk liquid in their apparatus. Tjerkstra, Hooftman, and van den Meydenberg [67] have also studied adsorption on glass.

From a set of adsorption isotherms at different temperatures, standard thermodynamic arguments can be used to derive the heat of adsorption and the differential entropy of the film. The heat of adsorption, shown in Fig. 7, is high for the first one or two layers but soon falls to a value near the latent heat of vaporisation of the bulk liquid. Similarly, the differential entropy of the film, S_f, is very close

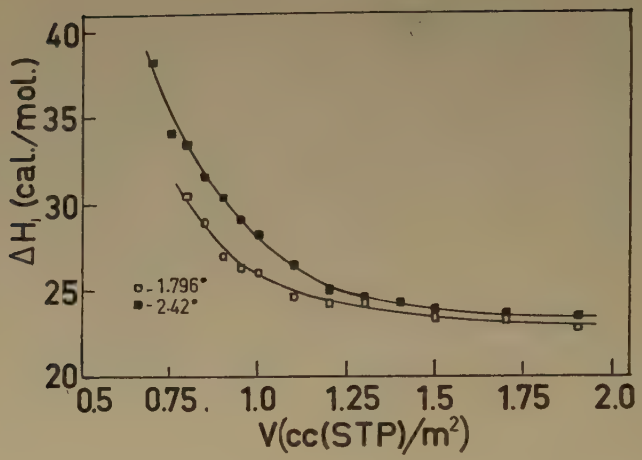

Fig. 7. Heat of adsorption ΔH_f of helium adsorbed on jeweller's rouge in cal/mol as a function of the amount adsorbed, at constant temperature (after Strauss).

to the entropy of the bulk liquid, S_l, for films more than one or two layers thick (Fig. 8). Both these facts suggest that, apart from a few layers near the wall, the liquid in the film is very similar to the bulk liquid. It is interesting to note that $S_f - S_l$ is negative above the

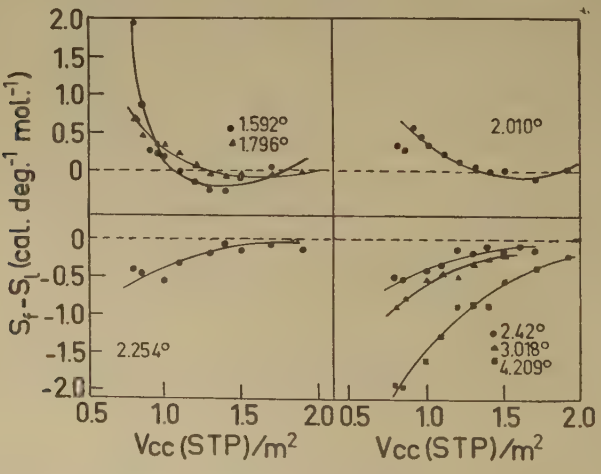

Fig. 8. Difference between differential entropy S_f of helium adsorbed on jeweller's rouge and the entropy S_l of bulk liquid as a function of the amount adsorbed for different temperatures (after Strauss).

λ-point and positive below the λ-point (but with a suggestion of negative values for intermediate coverages). The specific heat of films of various thicknesses on jeweller's rouge has been measured by Frederikse [32, 33] (Fig. 9). The results suggest that some sort of smeared out λ-transition occurs at temperatures lower than the bulk λ-point. Band [34] has pointed out that the specific heat of the first layer follows roughly a T^2 law, as for a two dimensional solid with a Debye temperature of 18°K. There is order of magnitude agreement between the specific heat curves and the entropies deduced from the adsorption isotherms.

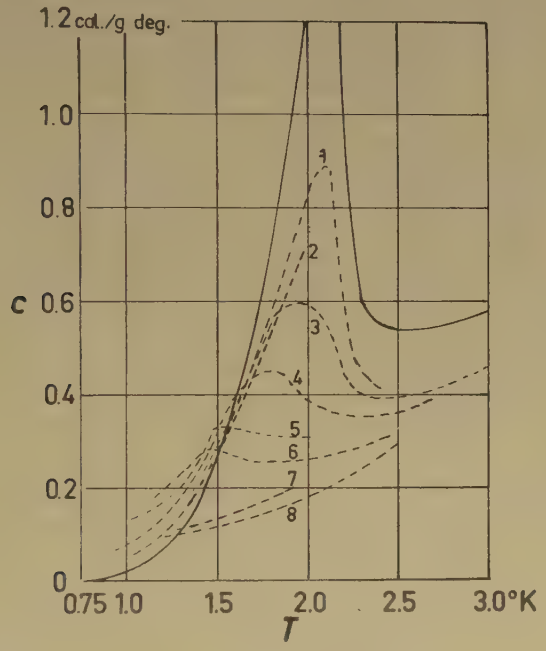

Curve	1	2	3	4	5	6	7	8
p/p_0	0.82	0.76	0.70	0.48	0.40	0.28	0.13	0.11
No. layers n	~8	~6	~5	~3	~2	~1.5	~1	~1

Fig. 9. Average specific heat of helium adsorbed on jeweller's rouge in cal/g-deg as a function of temperature for different amounts adsorbed. Number of statistical layers estimated as: 1st layer = v_m; 2nd layer = $1/2v_m$; 3rd and higher layers = liquid density = $1/4v_m$. Drawn line specific heat of bulk liquid helium (after Frederikse).

5. The Flow of the Saturated Film

The broad outlines of film flow phenomena were presented in the Introduction and we shall now discuss the finer details. The flow of the film is frequently taken to represent the best available case of pure superfluidity in which the flow of the superfluid component is not accompanied by viscous flow of the normal component. Several experiments have been conducted to demonstrate the absence of any frictional forces opposing this flow. The ingenious double beaker experiment of Daunt and Mendelssohn [35] is illustrated in Fig. 10 (a). In such an arrangement of two coaxial beakers, it is obvious that the level in the inner beaker cannot fall below the level in the annulus or there would be film flow from the annulus back into the inner

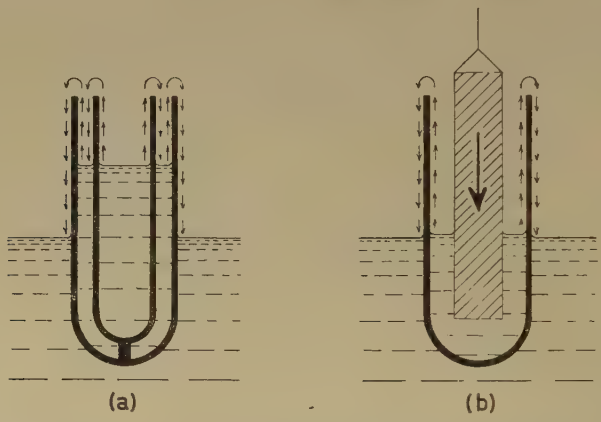

Fig. 10. Experiments to detect frictional forces opposing the flow of the film. (a) The double beaker experiment of Daunt and Mendelssohn. (b) The moving plunger experiment of Picus.

beaker. What happens therefore is that the levels fall at the same rate with the film velocity on the wall of the outer beaker assuming its critical value but with the film velocity on the wall of the inner beaker needing to be only about 90 % of the critical value in order to keep up. The important question then is whether this subcritical velocity is opposed by any frictional forces, so that the inner level has to be raised above the annulus level in order to provide the pressure head needed to maintain the flow against such dissipative forces. In the experiment the two moving levels were observed to stay together to within the accuracy of measurement, which was

about 10^{-2} cm, and it was concluded that the frictional forces must be extremely small.

Picus [36] has conducted another ingenious experiment bearing on the same point (see Fig. 10 (b)). A plunger was slowly lowered into a beaker of liquid helium II so that the level inside the beaker rose and film flow took place into the surrounding bath. The motion of the plunger was slow enough to permit the film to maintain the inner and outer levels at the same height while flowing with a sub-critical velocity. When the motion was first started, there were complicated effects which can probably be explained by using the same equations which describe the film oscillations discussed in § 3, but eventually the flow settled down with the inner level about 0.02 mm above the outer level. This suggests that a small pressure head is needed to maintain the flow but it is also possible that the level difference was a thermomechanical effect, consequent upon a small temperature difference of the order of 10^{-7} °K.

From a study of the oscillatory effects, Picus concluded that as the motion got under way the film became thicker and its shape altered. This is in direct conflict with the experiment of Jackson and Henshaw [15] (see § 3) in which the thickness of a moving film was found to be the same as that of a static film.

An upper limit to the size of the frictional forces can be deduced from the damping of the film oscillations [18] (see Fig. 5). This damping may have been caused by secondary effects not connected with the forces opposing the film flow, but, in any case, the damping was so small that it was possible to conclude that, in experiments of the type performed by Daunt and Mendelssohn and Picus, the pressure head could not have exceeded 2×10^{-4} cm. Another way of expressing this is that, as an element of the liquid flows along several cm of film, it does not lose more than 0.05 % of its kinetic energy of flow.

Although the resistance to flow is negligible at sub-critical velocities it is clear that, once the critical velocity is reached, strong dissipative processes come into play to prevent the velocity increasing further. In this connection it is interesting to note that the transfer rate of the film has a tendency to decrease when the level difference falls below about 0.5 cm [37] (see Fig. 11). Eselson and Lasarev [38] suggest that the mechano-caloric effect consequent upon film flow produces a temperature excess inside the beaker during emptying and a temperature defect during filling. As a consequence of the thermo-

mechanical effect, the inner level then reaches an equilibrium position displaced slightly from the outer level and subsequently approaches the outer level at a rate depending upon inertial effects and the rapidity with which the temperature difference can be dissipated. They support this with an experiment in which the effect was made to disappear by improving the thermal contact between the inside and outside of the beaker by means of a copper bottom. However, Atkins [37] has pointed out that, even without a copper bottom, the possibility of distillation between the inner and outer liquid surfaces restricts possible temperature differences to less than 10^{-6} °K, which

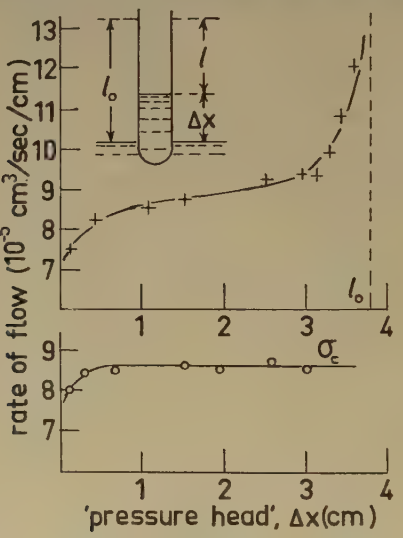

Fig. 11. Dependence of the rate of flow of the film on the level difference. + empting, $l_0 = 3.78$ cm; o, filling, $l_0 = 0.82$ cm.

would give a negligible thermomechanical effect. The issue may be a fundamental one, because, if the level difference is really a measure of the frictional forces opposing the flow, there is a suggestion that these forces vary with velocity in the region of the critical velocity. Fig. 12 shows various possibilities. Curve 1 is the ideal case of zero friction below v_c and infinite friction above v_c. Curve 2 is the case where no velocity is truly frictionless, but there is a very marked non-linearity. Curve 3 represents a combination of frictionless flow and non-linear frictional flow. If this last represents the true situation, we must always bear in mind the possibility that the frictional compo-

nent has nothing to do with the film but represents, for example, flow in cracks.

The transfer rate varies in a complicated way with the level difference and the height of the film [6, 37, 38, 39]. During a filling the transfer rate is practically constant (see Fig. 11), except at very small pressure heads, but the constant rate thus determined depends markedly upon the height of the rim of the beaker above the outer level (see Fig. 13). When the beaker is emptying (Fig. 11 again), the transfer rate now depends on the level difference, but the various observations can be

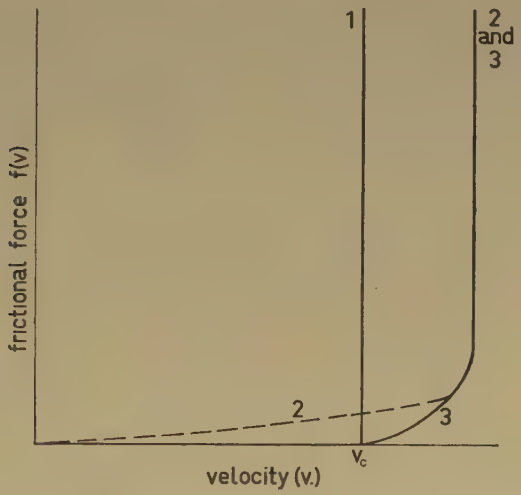

Fig. 12. Possible forms of the frictional force in film flow. 1, simple critical velocity; 2, flow which is never completely frictionless; 3, mixed flow.

correlated if we assume that the important factor is the height of the rim of the beaker above the *higher* of the two liquid levels. Atkins [37] has pointed out that, since the film thickness varies with height and since the transfer rate through a channel is known to vary slightly with its width, one might expect the rate of transfer to depend upon the thickness of the film at the rim of the beaker. Although such an effect may exist, it is also possible that the observed variations are largely caused by secondary factors, such as capillary flow in cracks [40].

When the inner and outer levels are at very different heights, it is pertinent to ask whether the thickness of the film is determined by its height above the inner level, the outer level, or neither. Jackson,

Henshaw and Ham [15, 41] used their optical method (Fig. 4) to observe the thickness of the film on the outer surface of the stainless steel beaker shown in Fig. 14 (a). They found that this thickness was uniquely determined by the height above the outer level and was quite independent of the position of the inner level. When the inner level was in the wide part of the beaker, A, but the outer level was in the region of the narrow part, B, the transfer rate was still determined by the perimeter of A, but on the outside of B droplets were observed to form and run down the wall, carrying away the excess liquid which

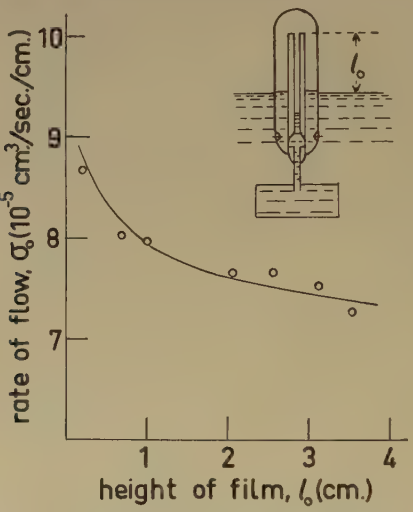

Fig. 13. Variation of the rate of filling with the height of the film. Temperature = 1.47° K.

could not be transferred by the film in this constricted region. However, in the apparatus of Fig. 14 (b), although the droplets were again observed in the waist region, B, they merged into the film again and were not observed on the outside of C where the transfer was again supported wholly by the film. Using the complicated beaker shown in Fig. 15, Chandrasekhar and Mendelssohn [42] observed that the formation of drops occurred in a manner which can be understood by studying the figure. From these experiments we may conclude: firstly, that the transfer rate is determined by the smallest perimeter lying above the higher of the two liquid levels; secondly, that, if there is a still smaller perimeter below this level, then drops form there to carry away the excess flow; thirdly, that no drops are formed

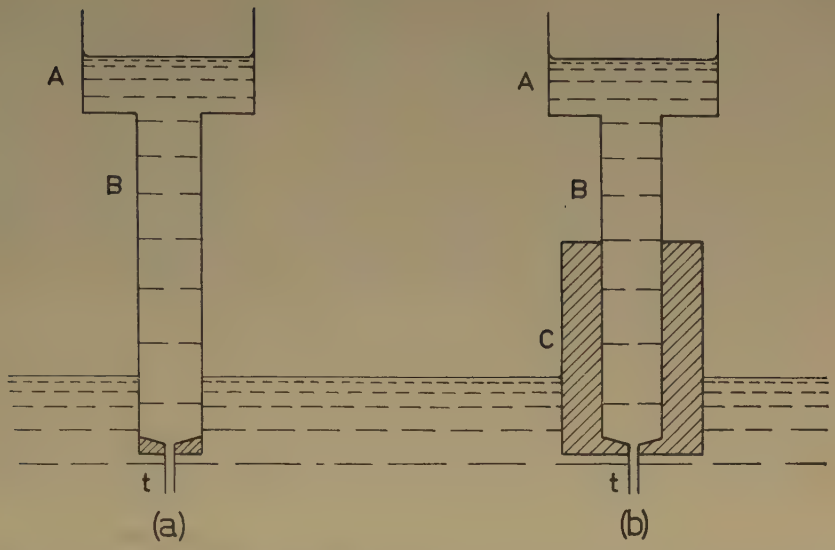

Fig. 14. An experiment to observe the formation of droplets out of the film. The tube *t* communicates with a glass monitoring tube (after Jackson and Henshaw).

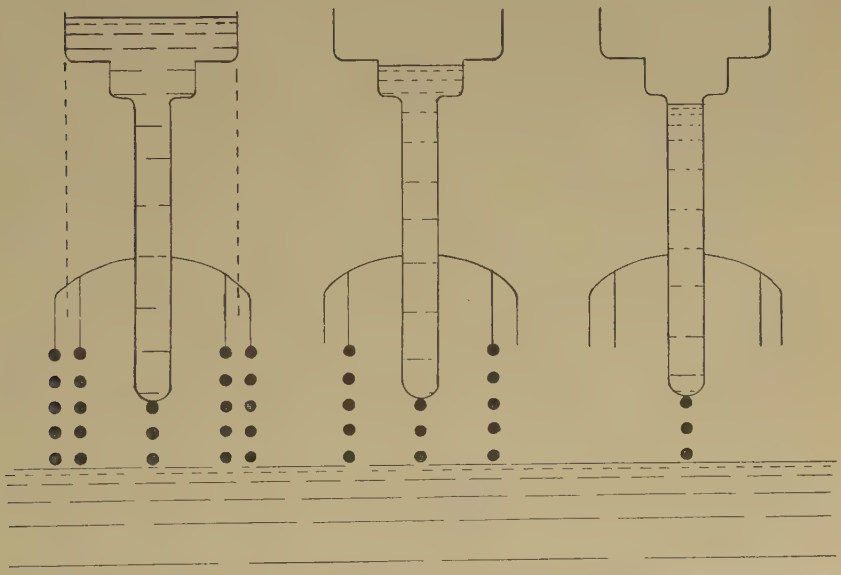

Fig. 15. The formation of droplets out of the film (after Chandrasekhar and Mendelssohn).

below the higher level if the perimeter is sufficient to enable the film to carry all the flow. Ham and Jackson [42] estimated the size and velocity of the drops and found them to be in agreement with a theory advanced by Frenkel [43].

When the surface is contaminated by a solid deposit, the transfer rate is increased and its dependence on the height of the rim above the liquid level is accentuated [7, 8, 9]. In such cases, the oscillation method [18] (Fig. 5) gives a period linearly proportional to the height l_0 of the film, and, if this is interpreted in terms of Eq. (5), it implies an equivalent film thickness of the form

$$d = k/H \tag{8}$$

with k several times greater than for a clean surface. The detailed explanation of this is still obscure, but might well reward further study. The transfer rate is also increased when the surface is deliberately roughened [40, 44, 45, 46, 47], but again it is not clear whether this should be ascribed to an increase in the micro-perimeter or to bulk liquid held in grooves. At this stage, one might reasonably ask whether all secondary effects, such as the variation of the rate of transfer with the height of the rim, are caused by contamination or surface irregularities, and the experimental difficulties are such that it is not yet possible to give a dogmatic answer. However, these effects have always been present in the most carefully conducted experiments and Smith and Boorse [39] found that the height dependence was just as marked for a highly polished metal surface as for an unpolished metal surface or a glass surface. Another interesting question is whether the transfer rate depends on the chemical nature of the surface. Smith and Boorse [48] have made a careful study of this point with beakers of aluminium, silver, copper, nickel, nickel-silver, stainless steel, Pyrex, quartz and Lucite. They conclude that, even with the same surface, the transfer rate is not reproducible from run to run to better than 10 % and any differences between the various surfaces were less than this.

Eselson and Lasarev [38] have complicated still further an already complex situation by observing that a beaker which had been filled by complete submersion in the bath emptied more rapidly than if it had initially been partially immersed in the bath and allowed to fill through the film.

The variation of transfer rate with temperature is shown in Fig. 16.

Different experiments give slightly different curves and the maximum near 1.5° K is not always reproduced [49]. The transfer rate per unit width of perimeter is, of course,

$$\sigma_c = \frac{\varrho_s}{\varrho} v_c d \tag{9}$$

where v_c is the velocity of the superfluid component. The variation between 1° K and the λ-point is mainly caused by the factor ϱ_s/ϱ, although the weight of the evidence suggests that the product $v_c d$

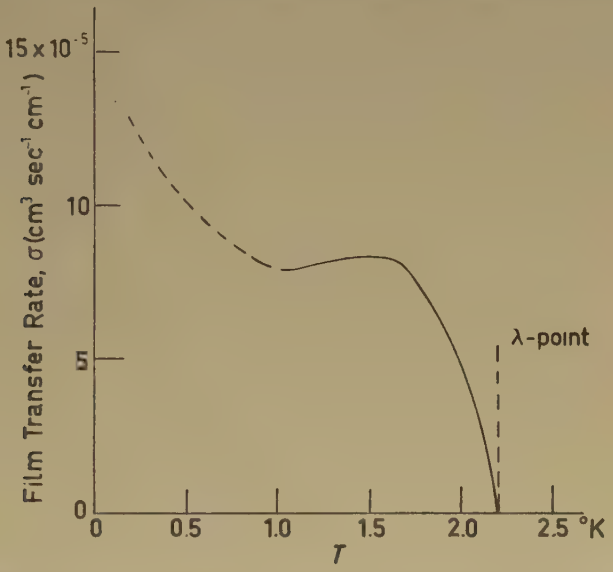

Fig. 16. Variation of the transfer rate of the saturated film with temperature (schematic).

also varies with temperature. Ambler and Kurti [50] have measured transfer rates below 1° K and find an increase of about 30 % as the temperature is lowered from 1° K to 0.15° K. Experiments of Lesensky and Boorse [51] and Waring [52] support this conclusion.

In order of magnitude

$$v_c d \approx \frac{h}{4\pi m} \tag{10}$$

where m is the mass of the helium atom, but there is no clear evidence that $v_c d$ is constant and it probably varies with both temperature and the height of the film. It should be noted, however, that because

$v_c d$ is approximately constant, the transfer rate of the film is a very insensitive measure of its thickness and the fact that the transfer rate is approximately the same for different substrates, for example, does not imply that the film thickness is correspondingly invariant. Eq. (10) is obviously of fundamental significance. For a possible explanation, see the article by Feynman in Vol. I [53].

Some recent results of Dillinger and his co-workers [54] suggest that the film has a step-like structure, changing its thickness abruptly at certain heights. It is perhaps too early to appreciate the full significance of these experiments.

6. The Flow of Unsaturated Films

The discovery by Long and Meyer [55, 56] of superfluid flow through the unsaturated film opened up the possibility of extending our knowledge of superfluidity to much narrower channels and also gave valuable information about the nature of these very thin films. In their excellent review article Long and Meyer [57] state: – 'The flow measurements and the heat transport experiments show that only $\sim 1/2$ statistical layer on top of the densely packed first monolayer is sufficient to produce He II phenomena' (that is, film flow). The apparatus used in their initial investigations consisted of an adsorption chamber A connected to a measuring chamber B through a superleak, which was either a platinum wire sealed into a Pyrex capillary or two optically ground stainless steel plates pressed together. They adopted two different procedures, which they call Method I and Method II, and which gave apparently contradictory results. In Method I chamber A contained gas at a pressure p/p_0 and there was therefore a thin unsaturated film on the walls of this chamber and on the surface of an adsorbent (Fe_2O_3) which was sometimes present to act as a reservoir of film. Chamber B was initially evacuated, then closed off, and the initial rate of rise of pressure in B was taken to represent the rate of flow of the unsaturated film through the superleak. The results are shown in Fig. 17, which gives the rate of flow as a function of temperature at the constant relative pressure p/p_0 indicated by the figure adjacent to each curve. The range of values of p/p_0 covered corresponds to film thicknesses from 2 up to 20 atomic layers. The striking feature of these results is that superfluidity sets in sharply at a temperature well below the normal λ-point, and the thinner the film the lower the onset temperature.

In Method II the pressure in chamber B was only slightly less than in chamber A so that the flow took place under a small pressure differential. Under these conditions, for all thicknesses of film, flow occurred at all temperatures up to the normal λ-point. A type of thermo-mechanical effect was also observed. When there was a temperature difference between the two chambers, the film flowed into the chamber at the higher temperature, even though the pressure

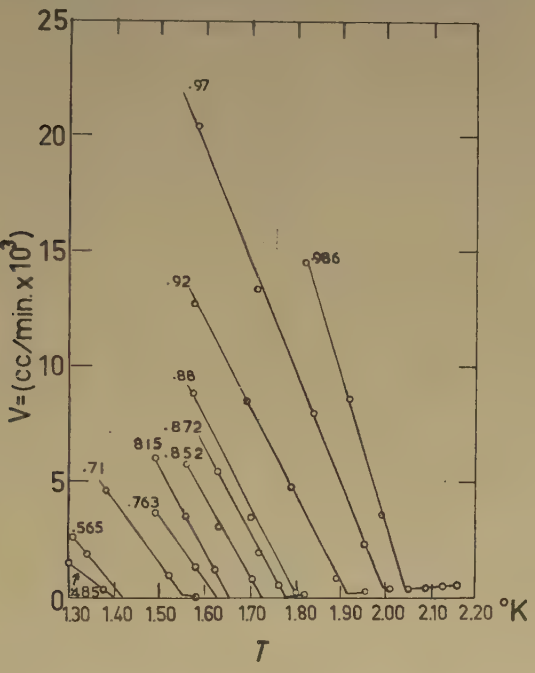

Fig. 17. Flow rate of the unsaturated film as a function of temperature for different relative pressures (Long and Meyer, Method I).

there was higher. The discrepancy between Methods I and II has not yet been resolved, but the heat transport experiments described below favour the conclusions of Method I.

The experiment performed by Bowers, Brewer and Mendelssohn [58] is illustrated in Fig. 18. The lower part of the chamber was in contact with a helium II bath and the upper part was thermally isolated. The chamber contained helium gas at a relative pressure p/p_0. Heat at a rate Q was supplied to a heater near the top of the chamber and a thermometer registered the temperature in the vicinity of the

heater. When the heat input was small no temperature rise was observed, probably because the heat was dissipated by flow of the unsaturated film up the walls of the chamber, evaporation of the

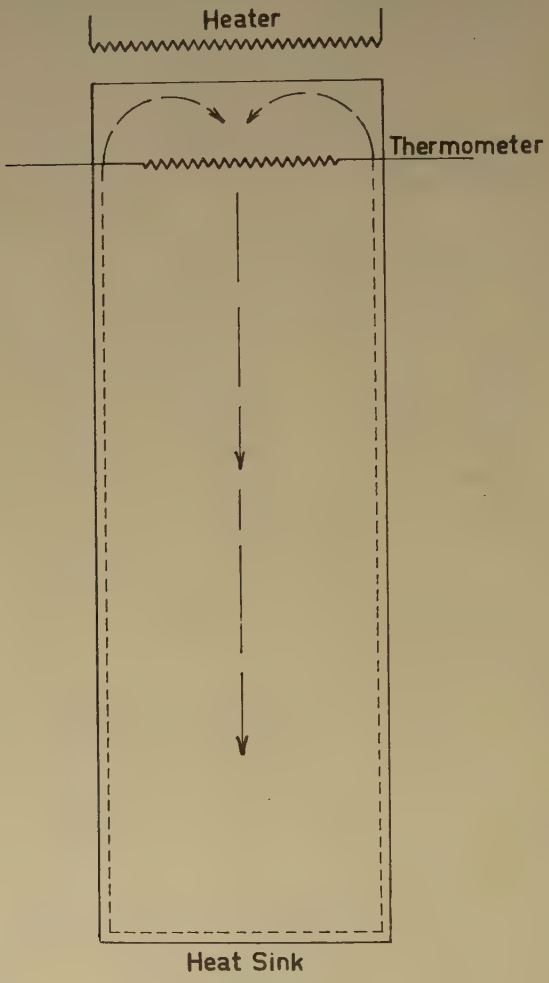

Fig. 18. Apparatus to investigate heat transport in the unsaturated film (after Bowers, Brewer and Mendelssohn).

film near the heater and flow of the gas down to the bottom of the chamber where it condensed again. However, at a critical heat input, $\dot{Q}_c$, a large rise in temperature suddenly occurred and $\dot{Q}_c$ was therefore taken to be a measure of the critical rate of transfer of the unsaturated

film. The total rate of transfer over the whole perimeter in gm sec^{-1} must in fact have been $\dot{Q}_c/(L_B+TS)$, where L_B is the latent heat of the film, which is known to be approximately the same as the latent heat of the bulk liquid. When the pressure in the chamber was raised to the saturated vapour pressure p_0, the saturated film was studied and the critical heat input $\dot{Q}_S$ was found to vary with temperature in the same way as the transfer rate of the saturated film (Fig. 16). The quantity $r_c/r_s=\dot{Q}_c/\dot{Q}_S$ plotted against p/p_0 at various temperatures in Fig. 19 is therefore the ratio of the critical transfer rates in the unsaturated and saturated films. The rate of flow of the unsaturated film is seen to be only a small fraction of that of the saturated film.

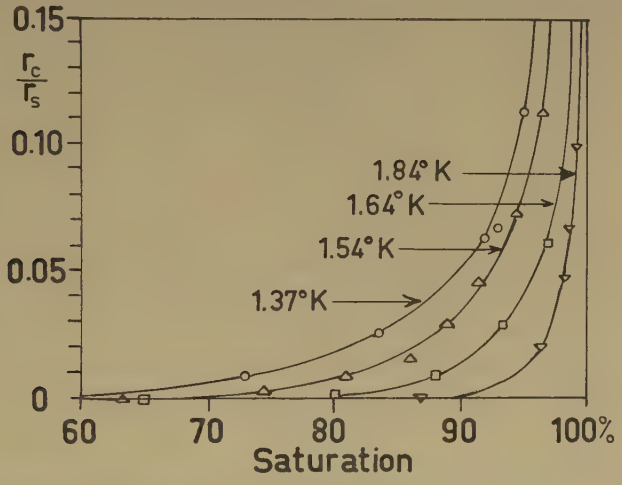

Fig. 19. The relative rate of flow of the unsaturated film plotted against relative pressure p/p_0 at constant temperature (after Bowers, Brewer and Mendelssohn).

This is important, because it establishes without any doubt that σ_c must vary with d in this region of film thicknesses. Examination of Fig. 19 reveals that, for every relative pressure p/p_0, there is an onset temperature for superfluidity which is well below the normal λ-point. In fact the onset temperatures deduced in this way agree satisfactorily with those found by Method I of Long and Meyer.

Long and Meyer [59] have repeated and extended these heat transport measurements. They noted, however, that even when the heat input was less than the critical value $\dot{Q}_c$, there was a small temperature gradient along the film, varying approximately as the cube of the

heat input. Using the adsorption isotherm data of Strauss [22] they were able to express their measurements in terms of the film thickness in atomic layers. They conclude that the critical velocity of the unsaturated film is approximately independent of its thickness, varying from 21 cm/sec at 2.0° K to 48 cm/sec at 1.3° K. Fig. 20 gives their data for the variation of onset temperature T_0 with film thickness, expressed as a number n of atomic layers. They interpet Fig. 20 to mean that, whatever the thickness of the film at a temperature T_0,

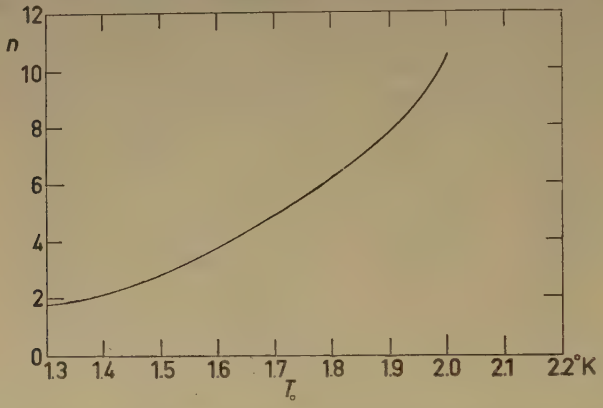

Fig. 20. The onset temperature of superfluidity as a function of film thickness (after Long and Meyer).

the first n layers near the wall are immobile and the outer layers are mobile. Another possible interpretation, of course, is that a film n layers thick is completely mobile below T_0 and completely immobile above T_0 (ignoring the solid layers very close to the wall). They point out that n varies approximately as ϱ_n/ϱ, which would extrapolate to give a film 20 layers thick an onset temperature at the bulk λ-point, 2.182° K. Some of their experiments suggest that films thicker than 20 layers have onset temperatures slightly above the bulk λ-point.

7. Theories of the Formation of the Film

Schiff [60] and Frenkel [61] have discussed the formation of the film solely in terms of the forces of attraction between the helium atoms and the wall. At large distances the force between a helium atom and an atom of the wall is of the van der Waals type and varies as the inverse seventh power of the distance. Integrating over all the atoms of the wall, the force on a helium atom varies as the inverse

fourth power of its distance z from the wall, and the potential energy of the helium atom therefore varies as the inverse third power of z. If the atom is also at a height y above the surface of the bulk liquid, its total potential energy may be expressed as

$$\phi = mgy - \frac{m\alpha}{z^3} \tag{11}$$

where m is the mass of the helium atom and α is a constant depending on the strength of the interatomic forces. If, in equilibrium, a small quantity of fluid is removed from the surface of the bulk liquid and placed on the surface of the film, the total change in energy must be zero, and so the relationship between film thickness d and height H is

$$\left.\begin{aligned} mgH - \frac{m\alpha}{d^3} &= 0 \\ d = \left(\frac{\alpha}{gH}\right)^{1/3} &= \frac{k}{H^{0.33}} \end{aligned}\right\} \tag{12}$$

Schiff [60] has calculated the magnitude of the van der Waals forces for several surface materials and the resulting values of k are given in Table I. Comparing these theoretical predictions with the somewhat uncertain experimental results described in § 3, it will be seen that the order of magnitude of the film thickness is correctly predicted

TABLE I

The Constant k in Eq. (12) as calculated by Schiff

Material of Wall	Copper	Silver	Glass	Rocksalt
$k \times 10^6$	4.3	4.7	4	2.2

but that there is some evidence that the exponent of H is actually slightly larger than 0.33. An important prediction of the Schiff–Frenkel theory is that the film thickness should be independent of temperature and should be the same above the λ-point as below, the peculiarities of He II being quite irrelevant to the theory. The latest experimental results are not inconsistent with this. Hill [62] has made a detailed analysis of multilayer physical adsorption and his results are essentially in agreement with Eq. (12) for thick films.

Atkins [28] has extended these ideas by treating the film as a continuous fluid distributed over the potential field given by Eq. (11).

It is a well known classical result that the hydrostatic pressure of a fluid varies from point to point in such a field, and in this particular instance the pressure is given approximately by

$$p = p_0 + \varrho\left(\frac{\alpha}{z^3} - gy\right). \tag{13}$$

The pressure therefore increases as one goes inwards from the surface of the film towards the wall, for exactly the same reason that the hydrostatic pressure increases as one goes downwards in any fluid in the earth's gravitational field. The analysis is permissible as long as the pressure does not change appreciably over a distance equal to the interatomic separation, since the assumption of a continuum is then a reasonable approximation. The argument therefore breaks down near the wall where the atomistic nature of the film must be taken into account, but even here the continuum approach might be expected to give a qualitative understanding of some of the important characteristics of the film. The first important consequence of Eq. (13) is that, if we put p equal to the vapor pressure p_0, we obtain Eq. (12) for the contour of the surface of the film. The pressure inside the film may then be rewritten as

$$p = p_0 + \varrho\alpha\left(\frac{1}{z^3} - \frac{1}{d^3}\right). \tag{14}$$

At a distance of about 7×10^{-8} cm from the wall p becomes equal to the solidification pressure of 25 atm. As the interatomic distance in the solid is about 3.3 Å, this suggests that there may be two solid layers near the wall. Even outside these solid layers the increasing pressure implies that the density of the liquid film increases towards the wall. Just below the λ-point, there is a point in the film where the pressure rises above the λ-curve, and the film therefore divides up into three regions, an outer region of He II, an intermediate region of He I and the solid region near the wall.

Bijl, de Boer and Michels [63] adopted an entirely different approach. At the time it was popular to treat helium as an ideal Bose–Einstein gas and they pointed out that for such a model the ground state wave function has a node at the wall and at the surface of the film, with a wavelength $\lambda = 2d$. The zero-point energy per atom would then be $h^2/8md^2$ and the total energy per cm^2 of film would be

$$U = nd\,mgH + nd\,\frac{h^2}{8\,md^2} \tag{15}$$

n being the number of atoms per cm^3 of film. Varying the film thickness d in order to minimize this energy, one readily obtains

$$\left.\begin{aligned} & n\,mgH - n\,\frac{h^2}{8md^2} = 0 \\ & d = \frac{h}{2m}\left(\frac{1}{2gH}\right)^{1/2} \\ & \quad = \frac{11.2\times 10^{-6}}{H^{0.50}}. \end{aligned}\right\} \tag{16}$$

This is consistent with the experiments of Bowers [17] but with none of the other measurements of film thickness. In this treatment the forces of attraction to the wall have been ignored, but this is readily seen to be untenable, since the excess energy given by equation 15 is always positive, so that the film would be metastable. Moreover, Mott [64] has pointed out that the ground state wave function assumed in the theory implies a peculiar variation of density from a maximum at the center to zero at the wall and at the surface.

Actually, it is now well established that the zero point energy of liquid helium is not $h^2/8md^2$ but the much larger quantity $h^2/8m\delta^2$ where δ has the order of magnitude of the interatomic distance. Atkins [28, 65] has based a theory upon the fact that the properties of the film would be seriously influenced if this large zero point energy varied with film thickness by only 1 part in 10^6. To illustrate this, he considers the longitudinal Debye modes which are known to exist in liquid helium and shows that the zero point energy of these modes for a slab of thickness d has the form

$$Z = Z_\infty\left[1 - \frac{1}{6}\frac{\lambda_c^\infty}{d} + \frac{1}{32}\left(\frac{\lambda_c^\infty}{d}\right)^2 + \ldots\right] \tag{17}$$

where Z_∞ is the zero-point energy of the bulk liquid and λ_c^∞ is the cut-off wavelength of these normal modes in the bulk liquid. The next step is to write down the total energy of the film, including gravitational energy, van der Waals energy and zero-point energy, and then to minimize this by varying both the density and thickness of the film. The mean density is found to be slightly greater than that of the bulk liquid.

$$\frac{\varrho(d) - \varrho(\infty)}{\varrho(\infty)} = \frac{1}{6}Z_\infty K\varrho\left(1 + \frac{\varrho}{c}\frac{\partial c}{\partial \varrho}\right)\frac{\lambda_c^\infty}{d} \tag{18}$$

where K is the compressibility and c is the velocity of first sound. The

equilibrium thickness of the film is given by

$$gH = \frac{\alpha}{d^3} + \left(\frac{\lambda_0^\infty}{d}\right)^2 \left[\frac{1}{32} Z_\infty - \frac{1}{72} K \varrho Z_\infty^2 \left(1 + \frac{\varrho}{c}\frac{\partial c}{\partial \varrho}\right)^2\right]. \qquad (19)$$

The results of Jackson (§ 3) can be expressed in this form

$$H = \left(\frac{2.07 \times 10^{-6}}{d}\right)^3 + \left(\frac{2.47 \times 10^{-6}}{d}\right)^2. \qquad (20)$$

The order of magnitude of the term in $1/d^2$ is correctly predicted by Eq. (19).

The increased density suggested by Eq. (18) may be very important in the case of unsaturated films. The effect, which varies as $1/d$, becomes quite large for thin films and is further augmented by the large increase in pressure very close to the wall (Eq. 14). It provides a ready explanation of the differential entropy (see Fig. 8). For He I the entropy of the liquid is known to decrease with increasing density, whereas for He II the entropy increases with increasing density and this is mirrored in the behaviour of the differential entropy of the film. The increase in density may also explain the low temperatures for the onset of superfluidity observed in thin films (see Fig. 20). The negative slope of the λ-curve means that the λ-point of the bulk liquid decreases with increasing density and it is therefore very plausible that the λ-point of a thin film should be lower if its density is higher. One might object that the λ-curve meets the solidification curve at 1.75° K, whereas onset temperatures have been observed down to 1.3° K, but it is not necessarily permissible to apply the phase diagram of the bulk liquid to extremely thin films. A more serious objection is that, even for thick films, the increase in density given by Eq. (18) seems to be too small by a factor of about ten. This may be because the spectrum of normal modes has been oversimplified, or because only the zero-point energy has been considered and the thermal excitations have been ignored. It is also possible that the λ-transition involves long range effects [53] which are modified in a thin film. Franchetti [66] has advanced a theory based upon the fact that the thickness of the film is comparable with the wavelength of the excitations, but full details are not yet available.

McCrum and Eisenstein [10] have drawn attention to the possibility that the surface might be contaminated by small quantities of a polar substance and that the dipoles might become aligned perpendicular

to the surface, particularly in the case of a metal surface. Even a small non-uniformity of the dipole density would produce strong electric fields near the wall and would thereby play an important role in determining the film thickness. Full details of this treatment have not yet been published.

There is obviously much still to be done to straighten out the theory of helium films. From what has already been said, it can be seen that the following factors should all be given serious consideration:

(1) The basic factor is probably the force between the wall and a helium atom in the film. This may be a simple van der Waals type of force or something more complicated, as in the theory of McCrum and Eisenstein.

(2) The zero-point energy per gm of the film may vary with its thickness. More generally, one should consider, not only the zero point energy, but the total free energy.

(3) It is possible that the density of the film is not the same as that of the bulk liquid, even at points remote from the wall.

(4) The density of the film probably increases towards the wall. This also suggests that, under some circumstances, the outer region of the film may be superfluid while the region nearer the wall is not. In flow phenomena, the fraction of superfluid ϱ_s/ϱ may have to be taken to be a function of distance from the wall.

(5) Looming in the background of any theory of a perfect film is the possibility that the properties of an experimentally realizable film may be determined primarily by surface imperfections, surface roughness, surface contamination, temperature inhomogeneity or flow effects.

REFERENCES

1 H. Kamerlingh Onnes, Trans. Faraday Soc., 18, No. 53 (1922); Leiden Comm. 159.
2 N. Kurti, B. V. Rollin and F. Simon, Physica, 3, 269 (1936).
3 A. K. Kikoin and B. G. Lasarew, Nature, 141, 912 (1938).
4 A. K. Kikoin and B. G. Lasarew, Nature, 142, 289 (1939).
5 J. G. Daunt and K. Mendelssohn, Nature, 141, 911 (1938).
6 J. G. Daunt and K. Mendelssohn, Proc. Roy. Soc., A, 170, 423, 439 (1930).
7 K. R. Atkins, Nature, 161, 925 (1948).
8 W. J. de Haas and G. J. van den Berg, Rev. Mod. Phys., 76, 609 (1949).
9 R. Bowers and K. Mendelssohn, Proc. Phys. Soc. A, 63, 1318 (1950).
10 N. G. McCrum and J. C. Eisenstein, Phys. Rev., 99, 1326 (1955).

[11] Dyba, Lane and Blakewood, Phys. Rev., **95**, 1365 (1954).
[12] D. F. Brewer and K. Mendelssohn, Phil. Mag., **44**, 559 (1953).
[13] L. Meyer, Conférence de Physique des Basses Temperatures, p. 95, Paris (1955).
[14] E. J. Burge and L. C. Jackson, Proc. Roy. Soc. A, **205**, 270 (1951).
[15] L. C. Jackson and D. G. Henshaw, Phil. Mag., **44**, 14 (1953).
[16] A. C. Ham and L. C. Jackson, Phil Mag., **45**, 1084 (1954).
[17] R. Bowers, Phil. Mag., **44**, 1309 (1953).
[18] K. R. Atkins, Proc. Roy. Soc. A, **203**, 119 (1950).
[19] W. D. Schaeffer, W. R. Smith and C. B. Wendell, J. Chem. Soc., **71**, 863 (1949).
[20] H. P. R. Frederikse and C. J. Gorter, Physica, **16**, 403 (1950); Leiden Comm. 281.
[21] E. A. Long and L. Meyer, Phys. Rev., **76**, 440 (1949).
[22] A. J. Strauss, Thesis, Chicago University (1952).
[23] S. V. R. Mastrangelo and J. G. Aston, J. Chem. Phys., **19**, 1370 (1951).
[24] R. Bowers, Phil. Mag., **44**, 485 (1953).
[25] N. G. McCrum and K. Mendelssohn, Phil. Mag., **45**, 102 (1954).
[26] Brunauer, Emmett and Teller, J. Amer. Chem. Soc., **60**, 309 (1938).
[27] W. G. McMillan and E. Teller, J. Chem. Phys., **19**, 25 (1951).
[28] K. R. Atkins, Canad. J. Phys., **32**, 347 (1954).
[29] D. F. Brewer and K. Mendelssohn, Phil. Mag., **44**, 340 (1953).
[30] E. A. Long and L. Meyer, Phil. Mag., **44**, 788 (1953).
[31] D. F. Brewer and K. Mendelssohn, Phil. Mag., **44**, 789 (1953).
[32] H. P. R. Frederikse, Physica, **15**, 860 (1949); Leiden Comm. 278.
[33] H. P. R. Frederikse and C. J. Gorter, Physica, **16**, 403 (1950); Leiden Comm. 281.
[34] W. Band, Phys. Rev., **76**, 441 (1949).
[35] J. G. Daunt and K. Mendelssohn, Nature, **157**, 829 (1946).
[36] G. S. Picus, Phys. Rev., **94**, 1459 (1954).
[37] K. R. Atkins, Proc. Roy Soc., A, **203**, 240 (1950).
[38] B. N. Eselson and B. G. Lazarev, J. Exp. Theor. Phys. (U.S.S.R.), **23**, 552 (1952).
[39] B. Smith and H. A. Boorse, Phys. Rev., **99**, 358 (1955).
[40] B. S. Chandrasekhar, Phys. Rev., **86**, 414 (1952).
[41] A. C. Ham and L. C. Jackson, Phil. Mag., **44**, 214 (1953).
[42] B. S. Chandrasekhar and K. Mendelssohn, Proceedings of the International Conference on Low Temperature Physics, p. 66, Oxford 1951.
[43] J. Frenkel, J. Exp. Theor. Phys. (U.S.S.R.), **18**, 659 (1948).
[44] B. S. Chandrasekhar and K. Mendelssohn, Proc. Phys. Soc. A, **65**, 226 (1952).
[45] J. G. Dash and H. A. Boorse, Phys. Rev., **82**, 851 (1951).
[46] K. Mendelssohn and G. K. White, Proc. Phys. Soc. A, **63**, 1328 (1950).
[47] B. Smith and H. A. Boorse, Phys. Rev., **99**, 346 (1955).
[48] B. Smith and H. A. Boorse, Phys. Rev., **99**, 328 (1955).
[49] B. Smith and H. A. Boorse, Phys. Rev., **99**, 367 (1955).
[50] E. Ambler and N. Kurti, Phil. Mag., **43**, 260 (1952).

[51] L. Lesensky and H. A. Boorse, Phys. Rev., **87**, 152 (1952).
[52] R. K. Waring, Phys. Rev., **99**, 1704 (1955).
[53] R. P. Feynman, Progress in Low Temperature Physics, Vol. I, Ch. II (1955).
[54] J. R. Dillinger, Conference de Physique des Basses Temperatures, p. 97, Paris (1955).
[55] E. Long and L. Meyer, Phys. Rev., **79**, 1031 (1950).
[56] E. Long and L. Meyer, Phys. Rev., **85**, 1030 (1952).
[57] E. Long and L. Meyer, Phil. Mag., Suppl. **2**, 1 (1953).
[58] R. Bowers, D. F. Brewer and K. Mendelssohn, Phil. Mag., **42**, 1445 (1951).
[59] E. Long and L. Meyer, Phys. Rev., **98**, 1616 (1955).
[60] L. Schiff, Phys. Rev., **59**, 838 (1941).
[61] J. Frenkel, J. Phys. U.S.S.R., **2**, 345 (1940).
[62] T. L. Hill, J. Chem. Phys., **17**, 580, 668 (1949).
[63] A. Bijl, J. de Boer and A. Michels, Physica, **8**, 665 (1941).
[64] N. F. Mott, Phil. Mag., **40**, 61 (1949).
[65] K. R. Atkins, Conference de Physique des Basses Temperatures, p. 100, Paris (1955).
[66] S. Franchetti, Il Nuovo Cimento, **10**, 1127 (1955).
[67] Tjerkstra, Hooftman and van den Meijdenberg, Physica, **19**, 935 (1953); Leiden Comm. 293.

CHAPTER V

SUPERCONDUCTIVITY IN THE PERIODIC SYSTEM

BY

B. T. MATTHIAS

BELL TELEPHONE LABORATORIES, INC., MURRAY HILL, N.J.

CONTENTS: 1. Introduction, 138. — 2. The Elements, 138. — 3. Alloys and Compounds, 141. — 4. Transition Temperatures, 141. — 5. Compounds, 145. — 6. The β—W Structure, 148. — 7. Comparison of Different Crystal Structures, 150.

1. Introduction

Many attempts have been made to state the necessary and sufficient conditions for the occurrence of superconductivity among the elements. As yet, however, no efforts have been made to find the corresponding conditions for superconducting compounds or alloys. The purpose of the present work is to indicate those features which, through the discovery and study of a large number of superconducting compounds and alloys, have been found to be common to all superconductors, elements, compounds and alloys alike. This, however, was done by an oversimplification which went so far as to consider only properties of the single atom, and to take the averages in the case of composite systems. From the available experimental data, a necessary condition for the occurrence of superconductivity above 0.1° K appears to be that the average number of valence electrons per atom cannot be smaller than two or larger than eight. Between these limits the actual transition temperature is determined by the number of valence electrons per atom [1], in a manner that can be traced in the various parts of the periodic system as will be shown in the following paragraphs.

2. The Elements

Fig. 1 gives the periodic system of the elements. The superconduction transition temperatures are taken from Shoenberg's book [2]. Elements in the same column are considered as having the *identical*

Fig. 1. The superconducting elements in the periodic system.

H																He
Li 0.08 cub.	Be 0.06 hex.		Rare earths	Ce 0.25 cub.	Pr 0.25 hex.	Nd 0.25 hex.	Pm	Sm	Eu cub.	Gd hex.	B 1.3 hex.	C 1.2 hex.	N	O	F	Ne
				Tb hex.	Dy hex.	Ho hex.	Er 0.8 hex.	Tm hex.	Yb cub.	Lu hex.						
Na 0.09 cub.	Mg 0.05 hex.										Al 1.20 cub.	Si 0.07 cub.	P 2.0 orth	S	Cl	A
K 0.08 cub.	Ca 1.3 cub.	Sc cub.	Ti 0.53 hex.	V 5.1 cub.	Cr 0.08 cub.	Mn 0.15 cub.	Fe 0.75 cub.	Co 0.06 hex.	Ni 0.75 cub.	Cu 0.05 cub.	Zn 0.91 hex.	Ga 1.10 orth	Ge 0.05 cub.	As 0.8 rhom	Se 1.3 hex.	Br	Kr
Rb 0.8 cub.	Sr 1.4 cub.	Y 0.10 hex.	Zr 0.70 hex.	Nb 8 cub.	Mo 0.05 cub.	Tc 11.0 hex.	Ru 0.47 hex.	Rh 0.09 cub.	Pd 0.10 cub.	Ag 0.05 cub.	Cd 0.56 hex.	In 3.37 tetr.	Sn 3.730 tetr.	Sb 0.15 rhom	Te 1.2 hex.	I	Xe
Cs 0.8 cub.	Ba 0.15 cub.	La 4.37 hex.	Hf 0.35 hex.	Ta 4.4 cub.	W 0.06 cub.	Re 1.7 hex.	Os 0.71 hex.	Ir 0.10 cub.	Pt 0.10 cub.	Au 0.05 cub.	Hg 4.152 rhom	Tl 2.38 hex.	Pb 7.22 cub.	Bi 0.05 rhom	Po mono.	At	Rn
Fr	Ra	Ac	Th 1.39 cub.	Pa	U 0.8 orth	Np	Pu	Am	Cm								

From Shoenberg's book [2]. The framed elements are superconducting. The transition temperatures are given. For the normal elements, the lowest tested temperatures are indicated.

number of valence electrons. Their transition temperatures can be roughly represented by

$$T_c \backsim \frac{r^{13}}{M} \tag{1}$$

where r is the radius of the neutral atom and M its mass. The proportionality (1) does not hold at all well for those elements with two or eight electrons which are at the boundary of the superconducting region. The elements Ru–Os and Zn–Cd–Hg do therefore not fit (1). The variation of transition temperature due to the change in the number of valence electrons can be accounted for by a function

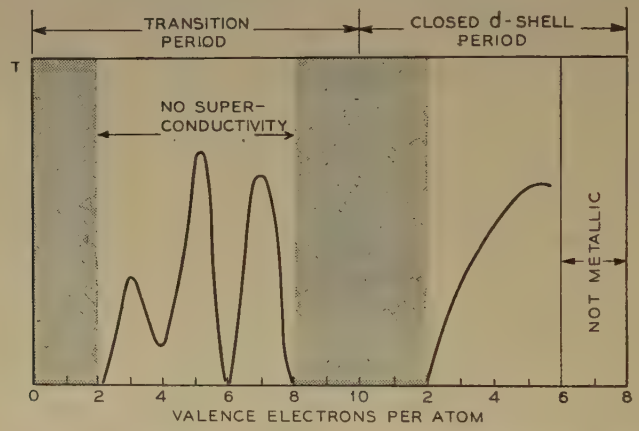

Fig. 2. Qualitative behavior of superconducting transition temperatures throughout the periodic system.

of purely qualitative nature as shown in Fig. 2 which shows its variation throughout the periodic system. One can therefore represent the transition temperatures of the elements, except those mentioned above, by the following equation

$$T_c \backsim c \frac{V^x}{M} T(n) \quad 4 < x < 5 \tag{2}$$

where c varies between 20 and 30 % for the different crystal systems. V is the atomic volume.

The linear variation with the atomic mass is probably best demonstrated by the two pairs Zr–Hf and Nb–Ta which are isomorphous respectively and have the *same* atomic volume. The major difference between the two members of every pair is an increase of the atomic mass by a factor 2.

Eq. (2), as well as it may represent the connection among most of the elements, does not give correctly the pressure variation of the transition temperature [3] for a single element, being the variation of one element in itself, nor does it explain the differences in transition temperatures between isotopes [4]. In these cases the volume exponent is close to 7 and the mass dependence $1/\sqrt{M}$. The explanation of this discrepancy is not entirely clear although general suggestive possibilities exist. Throughout the periodic system, among comparable elements however, no volume dependence of more than the 5th power can be found.

3. Alloys and Compounds

If one turns from the superconducting elements to superconducting compounds, a much larger variation of crystal structures and lattice sizes is available. The occurrence of superconductivity here again follows the rule outlined above. The valence electron per atom concentration, favorable to superconductivity, again varies between two and eight for *all* alloys. Transition temperatures also follow qualitatively the electron concentration in the manner outlined for the elements in Fig. 2. There are slight shifts of the peaks for different crystal symmetries. While here volume exponents between five and ten can be found, seven is the dominant one. As far as the variation with mass is concerned, not too many comparative data are available but results in the β–W crystal structure indicate that a value intermediate between the reduced mass of the components and the geometric mean of the two seems in Eq. (2) to be most likely to lead to more or less consistent results. Average mass values do not give any agreement at all.

4. Transition Temperatures

For a systematic treatment of all superconductors known today, they shall be divided into first the elements and alloys and then the compounds.

As outlined above those elements which have fewer than two or more than eight valence electrons per atom are not superconducting above the temperatures available. Elements with two valence electrons are the borderline cases. Those among them which crystallize in a close packed arrangement are normal down to between 1° and 0.1° K, as not all of these elements have been measured to 0.1° K. If the

crystallographic symmetry begins to deviate from a close or b.c.c. packing, elements with two electrons become superconducting. Zn and Cd achieve this by a c/a ratio of 1.84 which deviates considerably from the 1.633 required by a hexagonal close packed structure. Hg crystallizes in an even less simple hexagonal system. For these three elements as well as for Ru and Os, which have eight electrons and are on the other end of our boundary the relation (1) fails completely from a quantitative viewpoint.

Elements for which no superconductivity has as yet been reported but which should however become superconducting above 0.1° K are Sc, Y and Pa. Y was measured by Goodman [2] to 0.1° K and was found to be normal. This we think can be blamed easily on the insufficient purity of this sample. Ferromagnetic and antiferromagnetic elements do not appear to become superconductors and therefore, less than 0.1 % of a paramagnetic or ferromagnetic element as impurity, such as a rare earth or iron, might easily inhibit superconductivity.

Among the closed d-shell metals, As, Sb and Bi do not become superconducting in their semimetallic rhombohedral crystal form, but Bi can be transformed into a superconducting modification which most likely is cubic. This can be done either by high pressure [5] or condensation at low temperatures [6]. Higher symmetric polymorphs of Sb and As would be expected to do the same.

The closed d-shell elements unfortunately do not form alloys as easily as do the transition elements. For the latter it is possible to complement our information by the consideration of some of their alloys. As mentioned above the antiferromagnetism and ferromagnetism of Cr, Mn, Fe, Co and Ni, as well as that of the rare earth, renders them rather unlikely of ever becoming superconducting. While thus the first long row of the periodic system is not favorable for the study of its alloys, those of Mo and W proved to be quite informative. Mo as well as W are at the bottom of the center gap in Fig. 2. This of course indicates that any configuration of six valence electrons is unfavorable to superconductivity. But the gap is a very narrow one and therefore most alloys and compounds with Mo and, to a minor extent with W, which cause a deviation in the number of electrons will therefore introduce superconductivity. The compounds of Mo and W will be discussed later, but their alloys can help us now to understand better the elements, as they cover more or less continuously some parts of the periodic system. Alloys of Mo and W with

the noble metals of the VIIIth column were first reported by Raub [7]. He found that nearly all combinations of Mo and W with the noble elements such as Ru, Os, Rh, Ir, and Pt include the formation of a hexagonal close packed phase with a very large homogeneity range. For a valence electron concentration between 6.5 and 7.5 these alloys do have lattice constants as well as superconducting transition temperatures closely resembling those of the corresponding hexagonal elements: Tc [8], Re, Ru and Os. The virtue of the averaging over the

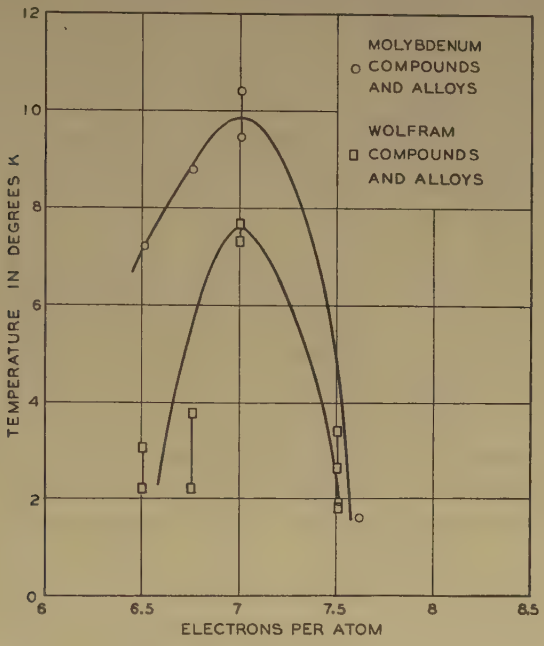

Fig. 3. Superconductivity in Mo and W systems.

periodic system here is self evident. In Fig. 3 the variation of the transition temperature with electron concentration of some of these alloys is shown. At the same time the lowering of the transition temperature with increasing mass (by going from Mo to W alloys) can be verified. Though neither Mo nor W have ever been found to be superconductors by themselves one may conclude that if they would do so at extremely low temperatures, the transition of W would be half that of Mo, which is about the same ratio as among their alloys — or for that reason like that between Zr and Hf or Nb and Ta.

The minimum transition temperatures for four valence electrons per atom can be shown in a rather picturesque way by alloying any

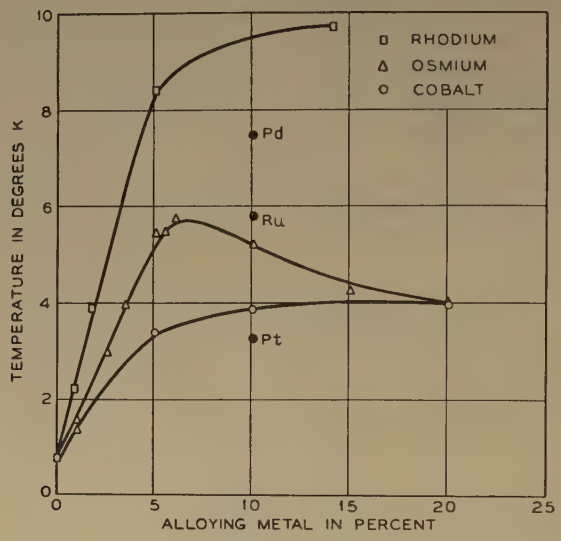

Fig. 4a. Superconductivity of zirconium alloys.

element of the IVth column in the long period, i.e., Ti, Zr or Th (we did not have enough Hf) with small percentages of the VIIIth column elements. Any one of the latter will dissolve somewhat in the IVth

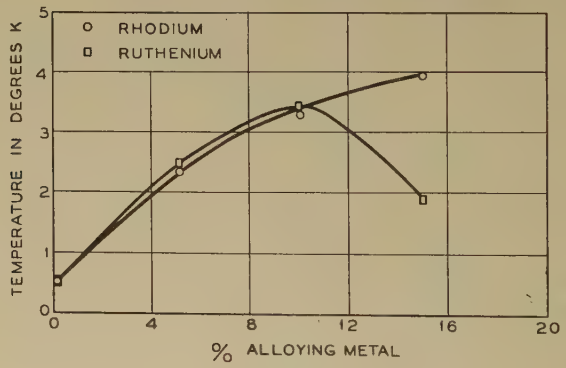

Fig. 4b. Superconductivity of titanium alloys.

column element, thus raising the average number of its valence electrons per atom and with it the transition temperature. The most spectacular effect is obtained with Rh which raises the superconducting

transition temperature of Zr by more than an order of magnitude (Fig. 4).

From these alloys and the elements the course of the transition temperature had become rather apparent. It is a periodic function in the long period with maxima near three, five and seven valence electrons per atom and minima in between and seeming to vanish at two and above eight electrons. The picture in the short period or closed d-shell subgroup is that of a gradual rise from two to a maximum between four and five (Fig. 2). A similar picture is obtained by Daunt's specific heat considerations [9].

5. Compounds

The average electron concentration of all superconducting compounds, as was pointed out earlier, varies between two and eight electrons per atom, though it is usually not possible to decide whether they fall in the transition element or closed d-shell subgroup. Their maximum transition temperatures are nevertheless again in the neighborhood of five and seven electrons per atom. Nearly all compounds crystallize in crystal classes which usually do not contain any elements. A few of these crystal systems and elements are considerably more favorable to form superconducting compounds. We want to outline here only some of those of the two which have a rather preferred tendency to become superconductors.

α) *Bismuth Compounds:* Probably the first superconducting compound to be discovered was Au_2Bi [10]. Meissner [11] came perhaps closest to the correct explanation of this compound's superconductivity by postulating that there might be a superconducting metallic modification of Bi responsible for it. The connection is not quite obvious however. Though this new modification has since been found, as pointed out earlier, and many more superconducting compounds of non-superconducting metals with bismuth have been discovered, all these compounds have complicated structures as compared to those of the metallic elements. They include compounds of Bi with [2]

TABLE I

LiBi 2.5	$CaBi_3$ 2.0		Ni–Bi 3.6–4.2	
NaBi 2.2	$SrBi_3$ 5.5	Rh–Bi 2.1–3.4	Pd–Bi 2–3.5	
KBi_2 3.6	$BaBi_3$ 6		PtBi 1.21	
Rb–Bi 4.25				Au_2Bi 1.7
Cs–Bi 4.75				

The one with Ir undoubtedly exists, but experimentally the difficulties have been too great to prove it. The highest transition temperature occurs for $BaBi_3$ at 6° K [12].

β) Molybdenum Compounds: Compounds of molybdenum form the next most varied arrangement [13, 14]:

TABLE II

Mo_2B 4.74	Mo_2C 2.78		MoC 9.76
Mo_2N 5.0	MoN 12.0	Mo_3P 7	Mo_3Si 1.3
Mo_3Ge 1.43	$MoGa_2$ 9.5		Mo_3Sb_4 2.1

The highest transition temperature is here found for MoN at 12.0° K [13]. Apart from these compounds there are the superconducting alloys with Ru, Os, Rh and Ir. Some of these elements form superconductors with W as well but due to generally lower temperatures, they are not quite as informative.

γ) Rhodium Compounds: Though Rh metal is just outside the boundary within which the superconducting elements are found, the formation of compounds can push Rh easily into the superconducting region. Here then are the superconducting Rh-compounds Rh_9S_8, $RhSe_{1.75}$, $RhTe_2$, Rh_5P_4 and Rh_5Ge_3 [1, 15].

δ) $CoSi_2$: This is the only superconductor among the intermetallic compounds of the $\langle CaF_2 \rangle$ system. $RhSi_2$, due to the larger radius of Rh is not isomorphous. However (Co, Rh) Si_2 solid solutions still crystallize in the fluorite structure and due to the increase in volume the transition temperature can be raised from 1.4° K for pure $CoSi_2$ [16] to near 3.6° for mixed crystals with Rh.

ε) The NiAs Structure: The superconductivity of CuS was discovered by Meissner [17]. No even remotely similar compound was found for the next twenty years and the opinion prevailed that CuS was an isolated case. The crystal structure of CuS is a very complicated distortion of NiAs. NiAs itself does not show any transition above 1° K. We have now demonstrated [1] that the NiAs structure is really quite favorable to the occurrence of superconductivity by detecting the phenomenon in a number of more or less isomorphous compounds:

NiBi (Ni,Pd)As

PdSb PdBi PdTe

IrGe PtSb PtBi

Many other compounds in this system unfortunately are either ferromagnetic or antiferromagnetic. The question of NiAs which

itself does not seem to be superconducting above 1° K could be solved in a way by widening the crystal lattice through the partial replacement of nickel by palladium and thus obtaining a mixed crystal which was superconducting. The maximum transition temperature of 1.6° K corresponds to $Ni_{0.12}Pd_{0.82}As$. (PdAs does not exist.)

Apparently superconductivity is not linked to a perfect NiAs lattice but instead is favored by a deviation from either the proper stoichiometry or symmetry. So is the highest transition temperature in PdTe obtained for a compound of the composition $PdTe_{0.85}$. It is well known that the NiAs structure is distinguished by just this continuous transition in composition and therefore of a simultaneous change in metallic properties. In this light the superconducting CuS does not any longer appear as a lonely compound. An orthorhombic deviation of the NiAs structure is the ⟨MnP⟩ system, in which the compound IrGe was found to be superconducting.

Those systems in which superconductors possessing the highest transition temperatures have been found, however, usually show cubic symmetries. The first one to be discovered was the NaCl structure.

ζ) *The NaCl Structure:* Many of the interstitial carbides and nitrides have been found to become superconducting. The highest among them is NbN: ≈ 15° K. Even Mo_2N crystallizing with 25 % vacancies in this class becomes superconducting. There is no point in repeating the superconducting behavior of this class as it is so well described in the paper by Hardy and Hulm [18]. All that we would like to show here is that this symmetry is more favorable than a hexagonal one. MoC, which becomes superconducting at 9.26° K [18] is hexagonal with a c/a ratio quite close to unity. Kieffer *et al.* [19] have shown by studying extended series of mixed crystals that there may be also a not too stable cubic modification of MoC, and they find that this cubic modification can however be stabilized by as little as 10 % (at) of some of the cubic carbides. One is thus able to explore the influence of the crystal structure on the transition temperature. Until now lanthanum had been the only case of a superconductor having two different crystal modixcations, *both* of which were superconductors. According to Spedding [20] the hexagonal modification had a transition point about 1/2° above that of the cubic phase. As both forms are nearly closed packed one would not have expected a very big change.

It has now been possible to dissolve up to about 80 % (at) MoC in TiC, ZrC, VC and NbC. Of these four carbides only NbC is a super-

conductor. In every instant there is an asymptotic approach to 10.4° K, the apparent transition temperature of cubic MoC (Fig. 5).

It is easy to obtain mixed crystals in this system of cubic interstitial compounds and a few do sometimes show higher transition temperatures than either of the two constituent compounds. $(NbC)_{0.33}(MoC)_{0.66}$ is superconducting near 12.5° K and $(NbN)_{0.85}(NbC)_{0.15}$ exceeds 17° K. Strain and small imperfections in this structure usually are advantageous as can be seen by a rise in temperature after quenching or a decline following prolonged annealing. It is the opposite to what is found in the following cubic structure, which exhibits even higher transition temperatures, the $\beta-W$ structure.

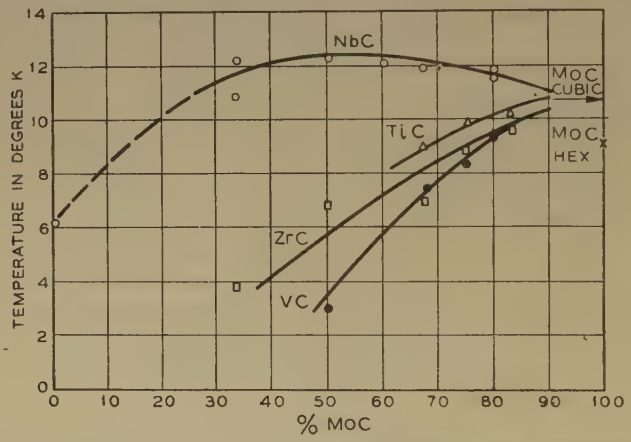

Fig. 5. Superconductivity of cubic solid solutions between MoC and cubic carbides.

6. The β−W Structure

The $\beta-W$ structure received its name from the low temperature modification of what was thought to be Wolfram. Only recently It has been [21] shown that this was not the pure metal but W_3O instead. Several A_3B compounds isomorphous to W_3O (or $\beta-W$) have been known for some time and four among them have been found by Hardy and Hulm [18] to be superconductors. The outstanding one of these is V_3Si with a transition temperature of 17° K, thus indicating the possibilities of this structure. We subsequently discovered about 20 more representatives of this symmetry class, some of them shown in Fig. 6, and reached a new maximum transition temperature of 18° K with Nb_3Sn. The transitions cover the temperature range from

1° to 18° and the average number of valence electrons/atom in the compounds varies from 4 to 6.75. It is in this structure that it has been possible to obtain the maximum variation of transition temperature with the electron concentration within a strictly isomorphous

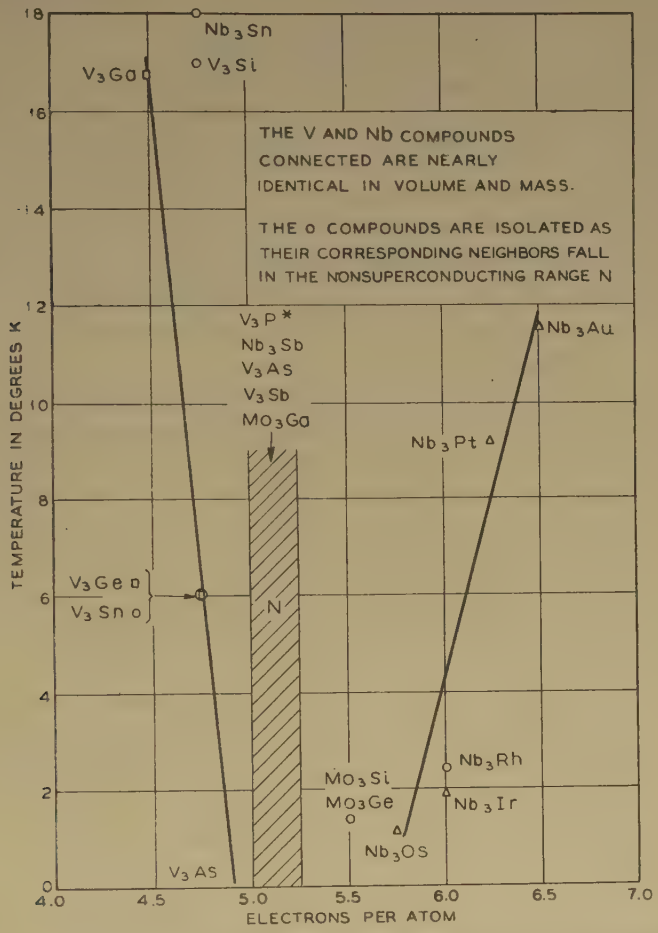

Fig. 6. Superconductivity in the β–W structure. V_3P is distorted.

group of compounds. The peaks have been shifted from those for the elements by about half an electron per atom to lower values, but the same qualitative pattern remains. In order to compare all $\beta-W$ compounds one would have to account not only for the change in mass but for the one in volume as well, because otherwise points for

a given electron concentration will scatter. By plotting, however, only the transition temperatures without taking into consideration any variation of lattice constant or valence, one nevertheless gets a qualitative picture of the variation of transition temperature with electron concentration (Fig. 6).

7. Comparison of Different Crystal Structures

It has become apparent that the simple cubic and hexagonal system as well as the $\beta-$W structure all are favorable for superconductivity. The latter, however, shows one remarkable difference as compared to the comparative simple structures: The formation of any mixed crystals as well as the introduction of any imperfections or strain causes a *lowering* of the transition temperature. This is a behavior opposite from that found for the simple structures. In it the $\beta-$W system resembles closely CuS, in which equally any impurity will lower the transition temperature [22]. From our strictly empirical viewpoint, this sensitivity to all disturbances of the crystal lattice is observed only in those structures which have a rather large unit cell.

REFERENCES

1 B. T. Matthias, Phys. Rev., **92**, 874 (1953); Phys. Rev., **97**, 74 (1955).
2 D. Shoenberg, Superconductivity, Cambr. Univ. Press (1952).
3 D. H. Bowen and G. O. Jones, Conf. Phys. Basses Temp., p. 514, Paris (1955).
4 For a complete list of references to pressure and isotope effects see Vol. I, Ch. VII, VIII and ref. 2.
5 P. F. Chester and G. O. Jones, Phil. Mag., **44**, 1281 (1954).
6 R. Hilsch, Proc. Int. Conf. Low Temp. Physics p. 119 (1951).
7 E. Raub, Z. Metallk. **45**, 23 (1954).
8 L. G. Daunt and L. W. Cobble, Phys. Rev., **92**, 507 (1953).
9 L. G. Daunt, Progress of Low Temperature Physics, Vol. I, Ch. XI.
10 W. J. de Haas *et al.*, Comm. Leiden, No. 197a.
11 W. Meissner, H. Franz and H. Westerhoff, Ann. d. Phys., 13, 553 (1932).
12 See reference 6, p. 69.
13 J. K. Hulm and B. T. Matthias, Phys. Rev., **82**, 273 (1951).
14 B. T. Matthias and J. K. Hulm, Phys. Rev., **89**, 439 (1953).
15 B. T. Matthias, E. Corenzwit and C. E. Miller, Phys. Rev., **93**, 1415 (1954).
16 B. T. Matthias and J. K. Hulm, Phys. Rev., **89**, 439 (1953).
17 W. Meissner, Z. Phys., **58**, 570 (1929).
18 G. F. Hardy and J. K. Hulm, Phys. Rev., **93**, 1004 (1954).
19 R. Kieffer and P. Schwarzkopf, Hartstoffe und Hartmetalle, (1953).
20 N. R. James, S. Legvold and F. H. Spedding, Phys. Rev., **88**, 1092 (1952).
21 G. Hägg and N. Schönberg, Acta Cryst., **7**, 351 (1954).
22 W. Buckel and R. Hilsch. Z. Phys., **128**, 324 (1950).

CHAPTER VI

ELECTRON TRANSPORT PHENOMENA IN METALS

BY

E. H. SONDHEIMER

DEPARTMENT OF MATHEMATICS, QUEEN MARY COLLEGE, LONDON

CONTENTS: 1. Introduction, 151. — 2. The Bloch theory, 152. — 3. The matrix element for electron-phonon scattering, 164. — 4. The steady state of the lattice, 169. — 5. Special topics, 177.

1. Introduction

The most striking characteristic of a metal is its high electrical conductivity, and from the earliest days of the theory of metals one of its chief aims has been to explain the electrical and the associated thermal conduction phenomena. Within a few years of the discovery of quantum mechanics it had become possible to give what seemed to be a satisfactory account, at least in qualitative terms, of the main feature of metallic conduction behaviour, with the exception of the phenomenon of superconductivity. This account was based on the theory originated by Sommerfeld and Bloch, discussed in § 2. At that time, however, only meagre experimental data were available for the region of very low temperatures, where the phenomena are particularly interesting and varied in view of the importance of quantum effects and of effects arising from the combined influence of lattice vibrations and of static lattice defects of various types. In recent years much more extensive experimental data have become available; these, together with a more complete evaluation of the predictions of the Bloch theory, have made it possible to subject the theory to a much more searching test, and it has become clear that it can be regarded only as a rough first approximation. Many of the assumptions underlying this theory have, in fact, long been recognized as obvious oversimplifications, and it seems likely that many of the discrepancies with experiment will disappear when a more realistic theory has been developed. Some of the necessary refinements, such as

the extension of the theory to deal with general forms of energy spectrum for electrons and lattice vibrations, are in principle simple to introduce; others, such as the influence of electron exchange and correlation effects, and the role played by the emission and absorption of virtual phonons (which may be the key to the explanation of superconductivity), are more difficult to take into account, and at present only some preliminary studies have been made of these questions, which present great mathematical difficulties. In spite of all its shortcomings, however, the theory in its present form has been sufficiently successful in explaining the properties of normal metals that its main features are unlikely to be lost entirely in the more general theory of the future.

In this review it is, of course, impossible to give a complete account of the subject, which forms a major and complex branch of present-day physics. I have therefore confined myself to an outline of the central predictions of the Bloch theory, followed by a discussion of some of the more interesting discrepancies with experiment, together with some account of the progress that has been made so far in bringing the conduction theory more closely into line with reality. The emphasis throughout is on the low-temperature behaviour, and I have tried to select those aspects which seem to be most important from the point of view of the future development of the subject.

2. The Bloch Theory

The basic theory of the transport phenomena in metals is described in full detail by Wilson [1]; this book will be referred to as T.M., and the theory given there as the standard theory. The standard theory is essentially an elaboration of that first given by Bloch [2] and, in spite of its many oversimplifications, it is likely to remain for a long time to come the basis of all detailed theoretical attempts to understand the conduction properties of normal metals.

The calculation of the standard theoretical formulae for the conduction magnitudes proceeds in three stages which, together with the approximations made at each stage, can be briefly summarized as follows (see also Ziman [3]):

(a) It is assumed that the state of a metal can be described by one-electron wave functions, so that any electron can be regarded as moving in the field produced by the lattice ions and the self-consistent field of all the other electrons; in calculating the self-consistent field,

correlations in electronic positions due to Coulomb interaction and exchange effects are neglected. In a perfectly periodic, static crystal lattice an electron can move freely without resistance; finite resistance to the transport of electricity and heat by electrons is due to two causes, the thermal vibrations of the lattice ions and the presence of static lattice imperfections (impurity atoms, strains, dislocations etc.), which destroy the regularity of the lattice and thus lead to electron scattering. In a commercially pure metal (but not necessarily in an alloy) the scattering by lattice waves predominates at all except very low temperatures and leads to a strongly temperature-dependent resistance. An electron in a state described by the wave vector $\mathbf{k}$, interacting with a quantized lattice wave (phonon) of wave vector $\mathbf{q}$, can make a transition to a state of wave vector $\mathbf{k} \pm \mathbf{q}$; the probabilities of transition are calculated by quantum-mechanical second-order perturbation theory, various simplifying assumptions being made in choosing the form of the perturbation potential and in performing the integrations to evaluate the matrix element of the perturbation. The result is that the transition probability is zero unless the lattice wave is longitudinally polarized, and in this case it is proportional (amongst other factors) to the square of a quantity C whose value is not known exactly, but which is of the order of magnitude of the Fermi energy ζ in the metal; C is assumed to be independent of $\mathbf{k}$ and $\mathbf{k} \pm \mathbf{q}$. The elastic scattering by static lattice imperfections is most simply taken into account by introducing a temperature-independent mean free path which, for the case of scattering by randomly distributed impurity atoms for example, will be of the order of the mean distance between the impurities.

(b) Statistical mechanics is now applied to the problem: the integral which gives the rate of change of the electron velocity distribution function due to collisions is evaluated, taking into account the restrictions imposed by the Pauli exclusion principle on the number of electrons in each state. In the reduction of the (triple) collision integral to a single integral it is assumed that the energy spectrum of the lattice vibrations is that given by the simple Debye theory, and also that the energy spectrum of the electrons is that of quasi-free electrons, i.e., of the same form as that of perfectly free electrons except that an effective mass replaces the mass of a free electron. It is also supposed that the distribution function of the lattice vibrations may be replaced by its value for thermal equilibrium of

the lattice, i.e. that any possible non-equilibrium of the lattice may be ignored in deriving the non-equilibrium electron distribution (but see § 4).

The Boltzmann transport equation can now be set up. This integral equation expresses the condition that the electron distribution function be stationary under the combined influences of the collision mechanisms and of the externally applied forces (electric field and temperature gradient). It is sufficient to suppose here that the stationary distribution differs by terms linear in the applied forces from the equilibrium Fermi distribution.

(c) The final problem is the pure mathematical one of solving the integral equation to obtain the stationary electron distribution function. The associated electric and heat currents can then be calculated, and from them all the transport quantities of interest. In the absence of magnetic fields there are three independent transport magnitudes to be determined by the theory: the electrical conductivity σ, the (electronic) thermal conductivity $\varkappa$, and the absolute thermoelectric force per degree (or thermoelectric power) Q. The other thermoelectric quantities, such as the Peltier and Thomson coefficients, may be derived from Q by applying the Kelvin thermodynamic relations, which are a consequence of a symmetry property (a special case of the so-called Onsager reciprocal relations) associated with the relations connecting the electric and heat currents with the applied electric field and temperature gradient. This symmetry provides a useful check on the consistency of the approximations adopted in the electron theory, but, since it must be maintained in all versions of the theory, it is of course not relevant to the discussion of the merits or otherwise of any particular version.

A powerful and convenient method of solving the transport equation is to reformulate the condition for a stationary state of the electron distribution as a variational principle, which can be shown to be a special case of the general theorem of maximum entropy production in irreversible thermodynamics (Ziman, unpublished). A convergent sequence of solutions can then be constructed by expanding the distribution function in terms of some suitable complete set of functions; it should be noted, however, that this method determines only the transport magnitudes and does not pretend to give the distribution function itself to any high degree of accuracy. In metals the electron gas is highly degenerate, and it is generally sufficient to

evaluate the results by retaining only terms of the lowest non-vanishing order in the degeneracy parameter kT/ζ. Even with this approximation the complete solutions are very complicated, but fortunately the first-order variational solution is in general already close to the exact solution.

The first-order results of the Bloch theory may be expressed as follows. The electrical resistivity $\varrho = 1/\sigma$ is the sum of a residual resistivity ϱ_r, due to scattering by static lattice defects, and an ideal resistivity ϱ_i due to scattering by the lattice vibrations; thus

$$\varrho = \frac{1}{\sigma} = \varrho_r + \varrho_i, \tag{1}$$

where ϱ_r is independent of T and varies from specimen to specimen, while ϱ_i is characteristic of the ideally pure metal, and is given by

$$\varrho_i = \frac{1}{\sigma_i} = 4A \left(\frac{T}{\Theta}\right)^5 \mathcal{J}_5. \tag{2}$$

Here A is a constant proportional to the square of the electron-lattice interaction constant C, Θ is the Debye temperature and $\mathcal{J}_5$ belongs to the class of functions of Θ/T defined by

$$\mathcal{J}_n(\Theta/T) = \int_0^{\Theta/T} \frac{z^n \, dz}{(e^z - 1)(1 - e^{-z})}. \tag{3}$$

The corresponding result for the thermal resistivity $1/\varkappa$ is

$$\frac{1}{\varkappa} = \frac{1}{\varkappa_r} + \frac{1}{\varkappa_i}, \tag{4}$$

where the residual thermal resistivity $1/\varkappa_r$ is related to ϱ_r by the Wiedemann–Franz law, i.e.

$$\frac{1}{\varkappa_r} = \frac{\varrho_r}{L_n T}, \tag{5}$$

$L_n = \frac{1}{3}(\pi k/e)^2$ being the Lorenz number. The ideal resistivity may be expressed in the form

$$\frac{1}{\varkappa_i} = \frac{4A}{L_n T} \left(\frac{T}{\Theta}\right)^5 \left[\left\{1 + \frac{3}{2\pi^2} \frac{\zeta}{D} \left(\frac{\Theta}{T}\right)^2\right\} \mathcal{J}_5 - \frac{1}{2\pi^2} \mathcal{J}_7\right], \tag{6}$$

where ζ/D is a numerical parameter given by

$$\zeta/D = 2^{1/3} N_a^{2/3}, \tag{7}$$

N_a being the number of conduction electrons per atom.

The expression for the thermoelectric power, finally, may be written in various practically equivalent forms, one of which is

$$Q = -\frac{\pi^2 k^2 T}{3e\zeta} \frac{\varrho_r + 3\varrho_i \left\{1 - \frac{\mathscr{J}_7}{4\pi^2 \mathscr{J}_5} + \frac{1}{2\pi^2} \frac{\zeta}{D} \left(\frac{\Theta}{T}\right)^2\right\}}{\varrho_r + \varrho_i \left\{1 - \frac{\mathscr{J}_7}{2\pi^2 \mathscr{J}_5} + \frac{3}{2\pi^2} \frac{\zeta}{D} \left(\frac{\Theta}{T}\right)^2\right\}}. \tag{8}$$

It should be noted that the formulae (1), (4) and (8), although in general not exact solutions of the Bloch transport equation, can be shown to pass over into the exact solutions both at sufficiently high and at sufficiently low temperatures, and they therefore have the status of interpolation formulae valid at least approximately over the whole temperature range.

We now discuss the principal features of the behaviour predicted by these interpolation formulae, with particular emphasis on the behaviour at low temperatures, and point out some of the principal discrepancies between theory and experiment. The general conclusion to be drawn from the experimental data, which are much too extensive to be considered in full detail within the scope of this article, is that the actual behaviour of metals is much more varied than is envisaged by the standard theory, so that the theory is only a rough first approximation and cannot account in detail for the variations in behaviour from one individual metal to another. Indeed, the approximations made in the theory (in particular, the assumption that the electronic energy spectrum is that of quasi-free electrons) are such that quantitative agreement between theory and experiment can be expected, if at all, in the case of monovalent metals only, and amongst these in particular for sodium, which appears to provide the closest approximation to an ideal free-electron metal. The first aim of the theory must be, therefore, to provide a satisfactory interpretation of the conduction properties of this metal; these properties, which have only recently been investigated in detail at low temperatures, are thus of particular interest and importance. (These are indications, however, that sodium undergoes a partial phase transition below 36° K [3a], and this casts some doubt on the precise interpretation of results obtained below that temperature.)

(a) The electrical conductivity

The integrals $\mathscr{J}_n(\Theta/T)$ required for the evaluation of the theoretical formulae are discussed and tabulated in T.M. For present purposes it

is sufficient to note that $\mathscr{J}_n$ tends to a constant limiting value as $T \to 0$, and that, when $T \gg \Theta$,

$$\mathscr{J}_n \approx \frac{1}{n-1}\left(\frac{\Theta}{T}\right)^{n-1} \qquad (9)$$

ϱ_i should therefore be proportional to T at high temperatures ($T \gg \Theta$) and to T^5 at low temperatures ($T \ll \Theta$); further, the additivity of ϱ_i and ϱ_r (Matthiessen's rule) implies that the resistance curves of different specimens should all be parallel to each other and to the resistance curve of an ideally pure metal. Since the numerical value of the constant A in (2) is left undetermined in the Bloch theory, comparison between theory and experiment must be made by choosing A and ϱ_r so as to fit the observed resistivity ϱ at some arbitrary high temperature (when $\varrho \approx AT/\Theta$) and in the limit $T \to 0$ (when $\varrho = \varrho_r$); the theoretical shape of the ϱ/T curve over the whole range of temperature can then be compared with the experimental form.

It has been known for a long time [4] that a formula of the type (1) gives a good representation of the general trend of the resistance-temperature curves of many metals; but recent detailed measurements [5, 7] in the temperature range between about 0.4 Θ, where deviations from the linear high-temperature law begin to be appreciable, and very low temperatures where ϱ is independent of T have shown that there are many divergences from the theoretical law in the detailed behaviour of individual metals. For sodium, however, it is found [5] that the ideal resistivity is in close agreement with formula (2) over a wide temperature range if Θ is taken as 202° K. This value of Θ is appreciably higher than the Debye temperature 160° K obtained from specific heat data; but, as has been emphasized by Blackman [6], there is no reason to expect that all the different phenomena which depend upon the lattice vibration spectrum should necessarily lead to identical values of Θ, since in general different averages of the lattice frequencies are involved. In the standard theory of the transport phenomena, in particular, Θ should be a 'Debye' temperature associated with the longitudinal lattice modes only; according to Blackman, this would be expected to be about 280° K for sodium, a value considerably larger than the value of Θ derived from either the specific heat or the electrical resistivity data. In view of all the uncertainties in the theory, particularly as regards the true frequency spectrum of the lattice vibrations in any given metal, it seems that Θ must at present be regarded as a parameter

whose value cannot be predicted a priori except as regards orders of magnitude (but see also § 3). It might be hoped, however, that a single value of Θ should suffice to account for all the electron transport phenomena in a given metal; but even this seems in general to be an overoptimistic expectation.

For metals other than sodium, in fact, the observed resistivities cannot be fitted to an expression of the form of (2) with any single value of Θ [5,7]. The data may be analyzed, in a manner similar to that often used in the discussion of specific heat data, by treating Θ as a function of T and by choosing its value at any particular temperature so as to obtain agreement with (2); but, if wide variations of Θ are obtained in this way, it is simply an indication that a formula of the type of (2) cannot be applied at all. Moreover, various different methods can be used in practice to deduce Θ from the observed resistance data, and these do not in general lead to identical results [8].

For the alkali metals other than sodium it is found, in general, that the temperature variation of ϱ_i approaches the T^5 law, if at all, only at temperatures much lower than expected on the basis of the behaviour at higher temperatures, which means that the apparent value of Θ decreases markedly with decreasing temperature. In caesium, however, ϱ_i does not seem to vary faster than T^3 even below 4° K. (Very recently it has been reported [9] that ϱ_i for sodium varies as T^6 below 8° K). Similar anomalies are observed in the behaviour of the alkaline earth metals [7].

The behaviour of the transition-element metals is also at variance with the predictions of the standard theory, the ideal resistivity of platinum being proportional to T^2 and that of palladium varying approximately as T^3 at sufficiently low temperatures [10]. In these metals the conduction electrons occupy two incompletely filled, overlapping energy bands, the s- and d-bands, and the theory of the electron-lattice collisions must take into account the possibility of electron transitions from one band into the other. The most detailed theory of this effect has been given by Wilson [11], who finds that the resistivity arising from $s-d$ transitions should, at low temperatures, be proportional either to $\exp(-\Theta'/T)$ or to T^3, depending on whether or not there is a non-zero lower limit $k\Theta'$ to the energy of the lattice waves which can induce $s-d$ transitions. The choice between the two theoretical possibilities depends upon the detailed configuration of the electronic energy surfaces; for spherical surfaces, in particular,

the exponential law is expected to hold, in disagreement with experiment. To settle the question the theory must be extended to take into account the detailed band structure of the transition metals more fully than has been done hitherto.

The experimental results indicate, finally, that Matthiessen's rule concerning the separability of the resistance of metals into the sum of independent ideal and residual parts is only valid as a first approximation, and deviations from the rule are observed to occur particularly in the temperature range where the ideal and residual resistances are of the same order of magnitude. And indeed, although it is assumed in the theory that the collision integral in the transport equation can be written as the sum of separate terms referring to the ideal metal and to the impurities respectively, and although Matthiessen's rule holds in the approximation represented by equation (1), there is no reason why the additivity of the collision integrals should necessarily lead to additive resistivities unless special conditions are satisfied. In fact Matthiessen's rule is no longer strictly valid when the higher order terms in the standard theory are taken into account, although the deviations are found to be very small [21]. More generally, it can be shown from arguments based upon the variation principle [12], or by considering specific models more general than that of quasi-free electrons [13], that the deviation $\Delta = \varrho - (\varrho_r + \varrho_i)$ from Matthiessen's rule should be positive and of the form

$$\Delta = \frac{\varrho_i \varrho_r}{\alpha \varrho_i + \beta \varrho_r}, \tag{10}$$

where ϱ_i is the resistivity of the ideally pure metal, ϱ_r is the resistivity due to static lattice defects, and α and β are quantities of the order of unity. Δ should therefore be zero when $T = 0$, should increase as T increases, and finally (when $\varrho_i \gg \varrho_r$) it should approach a constant value proportional to ϱ_r. These predictions have been confirmed in recent careful measurements [14] of the resistance of tungsten wires, in various states of cold-work, as a function of temperature and of ϱ_r.

Some other aspects of the resistive behaviour of metals, which seem to fall entirely outside the theoretical scheme considered here, are discussed briefly in § 5.1 below.

(b) The thermal conductivity

According to equations (2) and (6), $\varkappa_i$ at high temperatures is independent of T and is related to σ_i by the Wiedemann–Franz law,

in agreement with observation. As T decreases, $\varkappa_i$ decreases at first, but at very low temperatures $\varkappa_i$ is proportional to T^{-2}, whereas $\varkappa_r$ is proportional to T. The qualitative behaviour of the thermal conductivity of a pure metal is therefore predicted to be as follows. As T decreases below Θ, $\varkappa$ decreases initially from its constant high-temperature value, passes through a minimum (which occurs near $T = \Theta/4$), and then it increases rapidly until, at temperatures when the impurity scattering begins to predominate, $\varkappa$ passes through a maximum and finally decreases linearly towards zero. A typical curve is shown in Fig. 1 (curve 2). (These results refer only to the conductivity associated with heat transport by the conduction electrons. The lattice vibrations in metals must also be responsible for some heat transfer, but in good metals – though not in general in poor conductors and in alloys – the lattice thermal conductivity is so small compared with the electronic conductivity that it can nearly always be neglected. The heat transfer by the lattice is considered further in § 4 below.)

Much experimental work has recently been carried out on the thermal conductivity of metals at low temperatures [15]; we refer, in particular, to the extensive investigation by Rosenberg [16]. The observations are in general qualitative agreement with the theoretical formula for $\varkappa$; thus the graph of $T/\varkappa$ against T^3 is usually a straight line at sufficiently low temperatures, in agreement with the law

$$\frac{1}{\varkappa} = \alpha T^2 + \frac{\beta}{T} \tag{11}$$

predicted by the theory, and in most cases $\varkappa$ passes through a maximum. On the other hand, the predicted minimum in $\varkappa$ at higher temperatures is not observed to occur. Further, the theoretical values of α and β in (11) are

$$\alpha = 95.3 \frac{N_a^{2/3}}{\varkappa_\infty \Theta^2}, \qquad \beta = \varrho_r / L_n, \tag{12}$$

where $\varkappa_\infty$ is the limiting value of $\varkappa$ at high temperatures; and in most cases it is found that, whereas the calculated and observed values of β are in good agreement, the theoretical values of α (even allowing for uncertainties in the values of N_a and Θ) are much too large.

It is of particular interest that this type of departure from the theoretical behaviour is shown even by the free-electron metal sodium,

the results for which are worth considering further as a typical example. In Fig. 1 we show the observed thermal conductivity of a pure sample of sodium (Berman and MacDonald [17]), and also the curve predicted by the standard theory. The adjustable constants A and ϱ_r in the theoretical formulae (4) to (6) have been chosen to give agreement with experiment at high temperatures and in the residual resistance region; further, since $N_a = 1$ for a monovalent metal, we have $\zeta/D = 2^{1/3}$, and Θ has been assumed to have the value 202° K obtained from the electrical resistance measurements. The

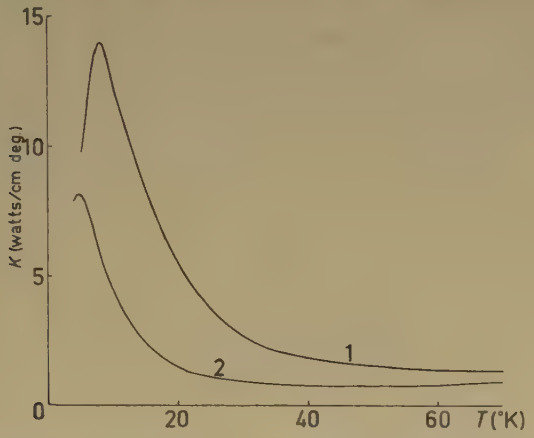

Fig. 1. The thermal conductivity of a sample of sodium at low temperatures. 1, experimental curve (after Berman and MacDonald [17]); 2, theoretical curve (standard theory).

discrepancy between theory and experiment at intermediate temperatures is seen to be considerable. Further, the theoretical value of α is 18×10^{-4}, while the observed value is 3.8×10^{-4} ($\varkappa$ being measured in watts/cm–deg) and, even if it is supposed that N_a and Θ may have values somewhat different from those adopted here, the values required to give agreement with experiment are too highly anomalous to be acceptable. The standard theory therefore over-estimates the effect on the thermal conductivity of the interaction between the conduction electrons and the lattice vibrations at low temperatures.

(c) The thermoelectric power

Eq. (8) is equivalent to the formula

$$Q = -x\pi^2 k^2 T/(e\zeta), \tag{13}$$

where x is a numerical factor which has the value $\frac{1}{3}$ at very low temperatures (independently of the degree of purity of the metal), and which increases monotonically to the value 1 at high temperatures. The experimental data on the thermoelectric effects in metals, however, are highly complex, particularly at low temperatures, and show a much greater variety of behaviour than is predicted by the simple expression (13). It is known, in fact, that the thermoelectric phenomena depend much more sensitively on the details of the electronic energy levels in metals than do the electrical and thermal conductivities, and there is therefore even less reason to expect the theory to apply to any but the monovalent metals; but even these do not behave in the expected manner. At ordinary temperatures [18], indeed, Q varies approximately linearly with T for monovalent metals, as predicted, and the observed value of Q for the alkali metals (except lithium) is in fair agreement with the value given by (13); but in lithium, copper, silver and gold the observed value of Q has a positive sign. Detailed measurements on monovalent metals at low temperatures have recently been carried out by Pullan [19] for silver and by MacDonald and Pearson [20] for the alkali metals and copper. The thermoelectric powers of Li, Cs, Cu, Ag all have the anomalous positive sign at low temperatures, while Rb shows a change of sign at about 30° K. For sodium and potassium, however, Q is negative; in sodium Q is approximately linear in T over the lower part of the temperature range investigated (4 to 80° K), but with a trend towards a higher power law below 15° K, while pure potassium seems to follow a square law below about 30° K. Again choosing sodium for quantitative comparison between theory and experiment, we show in Fig. 2 MacDonald and Pearson's experimental results (curve 1) for the absolute thermoelectric force (defined by $E = \int_0^T Q \, dT$) of pure sodium, and also the result (curve 2) obtained from the standard theory, taking $\Theta = 202°$ K, $\zeta = 3.2$ eV (T.M., p. 270), and (to sufficient accuracy) $\varrho_r = 0$. It is seen that the observed values of E are greater by a factor of the order of three than those predicted by the theory.

The simple theory also fails to account for the observed effects of impurities and strains on the thermoelectric power [19, 20]. According to (13) Q should, to a first approximation, be entirely independent of the residual resistance ϱ_r at low temperatures; observations on dilute alloys show, on the other hand, that Q in general varies markedly, and sometimes in a most striking manner (see Fig. 6),

with the amount and nature of the impurities, even when the concentration of foreign atoms is very small. Anomalous impurity effects are considered further in § 5.1.

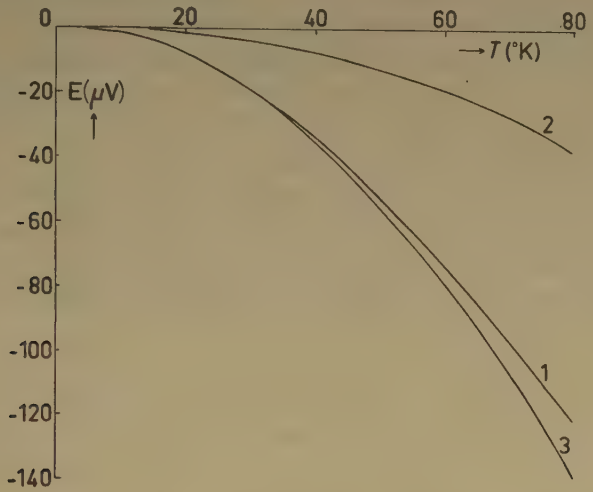

Fig. 2. The absolute thermoelectric force of sodium at low temperatures. 1, experimental curve (after MacDonald and Pearson [20]); 2, standard theory; 3, theoretical curve, taking into account non-equilibrium of lattice (see § 4).

Higher approximations. As has already been mentioned, the theoretical formulae discussed above are only approximate solutions of the integral equation of the standard theory. The calculation of more accurate expressions, either by including higher-order terms in the variational solution [21] or by direct numerical solution of the integral equation [22], shows that the correction terms are in general small and do not materially affect the comparison between theory and experiment. The main results of the more accurate calculations are that (i) the residual and ideal electrical and thermal resistivities are in general no longer strictly additive (as already remarked), (ii) the ideal electrical conductivity exceeds the value given by (2) by up to 10 % at intermediate temperatures, and (iii) the factor 95.3 in the expression for the ideal thermal conductivity at low temperatures (see Eqs. (11) and (12)) is to be replaced by a factor of the order of 60. (The higher-order terms in the thermoelectric power, which have not so far been evaluated numerically, would also be of interest.) There are some features of the experimental data, such as

certain departures from linearity of the graph of $T/\varkappa$ against T^3 at low temperatures [16] *, and the fact that the value of α in (11) appears to vary with impurity content [23], which are in qualitative agreement with these theoretical results; however, serious quantitative discrepancies remain, even for sodium, between the observed and calculated values of the thermal conductivity, and presumably also of the thermoelectric power. It must therefore be concluded that the problem of removing the discrepancies between theory and experiment is, essentially, not the mathematical one of improving the accuracy of the first-order solutions of the transport equation in the standard theory, but the physical one of examining the nature of the simplifying assumptions underlying the derivation of the transport equation itself, and of finding a more realistic form of the equation and hence of its solutions.

3. The Matrix Element for Electron-Phonon Scattering

The various generalizations required to bring the conduction theory more into line with reality can be classified, broadly speaking, under the following three main headings:

(a) It is necessary to refine the calculation of the perturbing potential which determines the scattering of electrons by lattice waves, and to obtain more accurate expressions for the transition probabilities.

(b) It is necessary to free the theory from the over-restrictive assumptions that the energy spectrum of the conduction electrons is that of quasi-free electrons, and that the energy spectrum of the lattice waves is that given by the Debye theory.

(c) The validity of the assumption that the lattice is always in thermal equilibrium must be investigated.

These questions are, in fact, not independent of each other; for example, the form of the matrix element for electron-phonon scattering must depend on the wave functions and energy levels of the conduction electrons. The development of a completely rigorous theory which takes all the relevant factors into account simultaneously is, however, a task of such forbidding magnitude that we are, in practice, forced to develop the detailed theory on the basis of simplified models, amongst which the model underlying the standard theory is only a specially simple example, and which can, at best, take the various

* But not the behaviour shown in Fig. 7 below!

factors mentioned above only partially into account. But it must be remembered that the features of a given model often correspond to reality much more closely for certain metals than for others; furthermore, it seems that some, at least, of the discrepancies between experiment and the standard theory can be ascribed specifically to one or other of the shortcomings of that theory, so that there is some justification for studying the effect of the various generalizations separately. In the present section we briefly review some of the attempts that have been made to deal with the topics (a) and (b) mentioned above, leaving (c) for separate discussion in § 4.

In the standard theory it is assumed that the conduction electrons move, to the first order, independently of the lattice ions; the coupling between electrons and lattice is caused by the alteration in the potential energy due to the displacement of the lattice, and the ions are supposed to be displaced without being deformed. It is evident that this picture must be over-simplified, since account must be taken of the way in which the self-consistent field of the electrons is affected by the displacement of the lattice. An exact treatment of this problem is necessarily very complicated, but approximate methods have been developed by several authors, and in particular detail by Bardeen [24]. The main result of the calculations is that the matrix element which corresponds to a transition between two electron states of wave vectors $\mathbf{k}$ and $\mathbf{k}'$ must contain, instead of the interaction constant C of the standard theory, a function $C(\mathbf{k}, \mathbf{k}')$ which decreases rapidly with increasing values of $|\mathbf{k}-\mathbf{k}'|$, i.e., with the angle through which the electron is scattered. Further [25], it is necessary to extend the theory to include, in addition to the normal collisions for which $\mathbf{k}'=\mathbf{k}\pm\mathbf{q}$, the so-called Umklapp collisions for which

$$\mathbf{k}'=\mathbf{k}\pm\mathbf{q}\pm 2\pi\mathbf{g}_b, \tag{14}$$

where $\mathbf{q}$ is the wave vector of the phonon absorbed or emitted, and $\mathbf{g}_b$ is an arbitrary non-zero vector of the reciprocal lattice. Such collisions can be regarded as two-stage processes, involving a collision with the lattice and a reflection at a zone boundary, and, in view of the large change in momentum involved, these collisions have a considerable effect on the electrical and thermal resistivities at high temperatures. At low temperatures, however, only the longest lattice vibrations are excited, so that both $|\mathbf{q}|$ and the phonon energy are small; it is then impossible to conserve energy in a transition of the

type (14) unless the surface of the Fermi distribution intersects a zone boundary. For monovalent metals, then, in which there is much evidence to show that the Fermi surface is approximately spherical and therefore well inside the first Brillouin zone, the part of the resistance which arises from Umklapp collisions will be frozen out at low temperatures, decreasing to zero according to an exponential law.

The influence of these modifications in the theory on the electrical and thermal conductivities of metals has recently been examined in detail by Ziman [3] for the case of sodium. He finds that, if the function $C(\mathbf{k}, \mathbf{k}')$ is assumed to have the form given by Bardeen, the electrical and thermal resistivities at high temperatures due to Umklapp processes are nearly three times as large as the normal resistivities; and the absolute values of the total resistivities, which can be related to numerical calculations of the energy levels and wave functions of the conduction electrons in sodium, are in fair agreement with the observed values. Further, it is found that the theoretical thermal conductivity is now in much better agreement with experiment over the whole temperature range. It appears, at first sight, that any improvement in the theory which removes the discrepancies between theory and experiment in the case of the thermal conductivity must also modify the expression for the electrical conductivity in such a way as to disturb the excellent agreement with the standard theory found for the electrical conductivity of sodium by MacDonald and Mendelssohn [5]. In fact, however, over most of the temperature range the new expression for the ideal electrical conductivity approximates closely to an expression of the form $\alpha\sigma_i(\beta T/\Theta)$, where σ_i is the function (2) and where α and β are constants, with $\beta > 1$. The shape of the resistance-temperature curve is therefore the same as in the standard theory, but with an apparent Debye temperature Θ/β smaller than the true characteristic temperature Θ; thus the agreement with experiment in the case of σ_i is unaffected, and, in addition, the new formula is in the right direction to explain the discrepancies between the various values of Θ obtained for sodium (see § 2 above).

The scattering function $C(\mathbf{k}, \mathbf{k}')$ calculated by Bardeen is shown in Fig. 3 (which actually shows the dimensionless quantity C^2/ζ^2), as a function of the scattering parameter

$$u = \tfrac{1}{2}|\mathbf{k}' - \mathbf{k}|/|\mathbf{k}| = \sin \tfrac{1}{2}\phi,$$

where ϕ is the angle of scattering. (In an ideal monovalent metal the

collisions are of the normal or Umklapp type, according as u is less or greater than $2^{-2/3}$.) Although the use of Bardeen's function in the theory of the transport phenomena leads to much better agreement with experiment, various small discrepancies remain; but, according to Ziman, complete agreement with experiment may be obtained for the electrical and thermal conductivities of sodium by using a somewhat modified scattering function in which the forward peak is even stronger but narrower, and in which the backward scattering

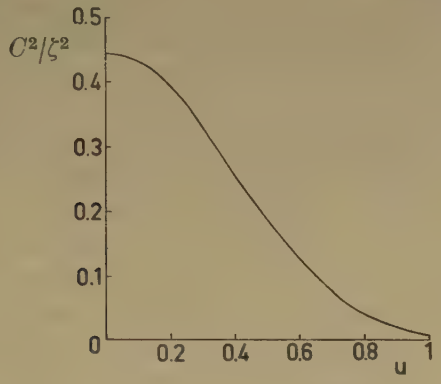

Fig. 3. The Bardeen scattering function.

is rather larger, than in the function shown in Fig. 3. It should be noted, however, that at the very lowest temperatures the predictions of the theory are essentially independent of the form of the scattering function: as $T \to 0$, the resistivities due to Umklapp collisions tend to zero as $\exp(-a\Theta/T)$, where a is a constant whose value is determined by the lattice structure, and the ideal electrical and thermal conductivities, which are now determined by normal collisions only, satisfy the simple relation (true also in the standard theory)

$$\frac{\varkappa_i}{\sigma_i T^3} = \frac{2\pi^2}{3} L_n (D/\zeta) \Theta^{-2}, \tag{15}$$

which may be contrasted with the Wiedemann–Franz law (5) relating the high-temperature ideal and also the residual conductivities.

Ziman's work shows that the formula for the cross-section for scattering of electrons by phonons plays an important role in the conduction theory, and suggests that it should be possible to use the experimental data on the transport phenomena to provide valuable information on the basic interaction processes in metals. A general

and systematic investigation of the dependence of the temperature variation of the transport coefficients on the form of the function $C(\mathbf{k}, \mathbf{k}')$ would be of considerable interest.

Particularly important amongst other investigations of the electron-lattice interaction problem are the attempts that have been made to deal with various fundamental difficulties in the theory, which throw doubt on the validity of the usual semi-classical formulation of the conduction problem in terms of a distribution function in phase space which satisfies a Boltzmann equation. There is, first, the question of the justification of the usual independent-particle model, in which the electrostatic interactions between electrons are treated in a highly over-simplified way. A more exact theory, which takes the correlations in electronic positions due to electrostatic interactions properly into account, is necessarily very difficult, since it involves the solution of a complex many-body problem; recent discussions of the problem [26] appear to show that electron correlation effects do not, in fact, affect the transport phenomena in normal metals in any significant way, but the question is by no means finally settled. Another question is that of the applicability of ordinary second-order time-dependent perturbation theory to the electron-lattice interaction; this is not easy to justify directly, since we are usually dealing with processes which occur so frequently that the initial and final states are not well defined. Arguments have been given [27] to show that the usual approach does, in fact, give correct results in the ordinary theory of conduction; but it is probable that a fully satisfactory treatment of the electron-lattice interaction, which will in all likelihood include also an explanation of the phenomenon of superconductivity [28], must await the development of more powerful and general methods of dealing with the interaction problem. Questions such as these, which are basic to the further development of the subject, cannot be discussed further here, and we remark only that they will probably find their eventual solution within the framework of a future theory, of which only rudimentary forms exist so far [29], in which attention is focussed from the start on the dynamical properties of electrons and lattice treated as a single quantum-mechanical system.

On the other hand, it may well be that the extension of the usual conduction theory to deal with more general forms of energy spectrum for both conduction electrons and lattice vibrations, which is quite straightforward in principle although few detailed calculations have

been made as yet, will be able to account to a large extent for the detailed variations in behaviour from one metal to another. This type of generalization is required to show how, and to what extent, the conduction properties of any given metal depend upon its crystal structure, and it is, of course, essential for the study of anisotropy effects in single crystals. Approximate solutions of the transport equation for a general anisotropic medium can be constructed by means of the variational principle (T.M., § 10.6), but much numerical work is required, making use of the considerable amount of information [30] that has become available recently on the form of the actual lattice frequency spectrum (see Ch. XIII) and the actual electronic energy levels in real metals, in order to decide to what extent the peculiarities of individual metals can be understood within the limits of the present theoretical scheme. Preliminary investigations indicate, for example, that some of the anomalies in the resistive behaviour of the alkali metals may arise from anomalies in the lattice frequency spectrum [31], and that, in the noble metals, departures from the model of quasi-free electrons may have a significant influence on the conduction phenomena [32] and may, in particular, account for the anomalous sign of the thermoelectric power [33]. Up to the present, however, the subject remains largely unexplored, particularly as regards the behaviour of multivalent and transition metals, and a much more extensive and systematic treatment is required.

4. The Steady State of the Lattice

The theory of the electronic conduction phenomena given so far rests upon the assumption that the lattice vibrations may be treated as being in thermal equilibrium. Since the lattice is itself capable of conducting heat, the lattice distribution must, in any case, depart from equilibrium when a temperature gradient is present; but the effect of this on the electronic distribution is usually ignored, and the heat transport by the lattice is taken into account [34] by setting up a separate Boltzmann equation for the phonon distribution, calculating, in this case, the collision integral for scattering of phonons by electrons on the supposition that the conduction electrons have their equilibrium distribution. The solution of the phonon Boltzmann equation then gives the lattice thermal conductivity, and this is added to the electronic conductivity to give the total thermal conductivity of the metal. The electrical conductivity and thermoelectric power

are of course unaffected by these considerations, since the phonons do not carry any electric charge.

It has been realised for a long time, however, that the procedure of calculating the steady-state electron and phonon distributions separately in this way cannot be strictly correct, since the collision integrals which give the rate of change either of the electron distribution function or of the phonon distribution function, due to electron-phonon collisions, themselves depend upon the actual (non-equilibrium) values of both the distribution functions, and neither of these are known until the steady-state equations have been solved. It is therefore necessary to determine the two distribution functions simultaneously as the solutions of two coupled linear integral equations. In setting up these equations, care must be taken to treat the electron-lattice interaction symmetrically, in such a way that the non-equilibrium phonon distribution function enters into the electron Boltzmann equation in the same way that the non-equilibrium electron distribution function enters into the phonon Boltzmann equation; this symmetry requirement, to which insufficient attention has sometimes been paid in the past [34, 35], is needed, for example, in order to ensure the validity of the Kelvin relations among the thermoelectric effects [36]. (A useful alternative statement of the problem (Ziman, unpublished) is to formulate the condition for a stationary state of the electron-lattice system in terms of a single variational principle, in which the symmetry properties are immediately evident.) It should be noted, also, that, although the total heat current carried by a metal is always the sum of separate electronic and lattice heat currents, it does not necessarily always follow that the conduction magnitudes should be separable, uniquely, into the sum of terms associated with the conduction electrons only and with the lattice only, and in general they will represent the resultant transport properties of electrons and lattice together.

A number of authors have considered different aspects of the theory at various times, but it will be sufficient to discuss here the results of a recent detailed treatment [37] in which the symmetry considerations mentioned above have been taken into account and in which all the (non-magnetic) conduction phenomena have been treated together from a unified point of view. For simplicity all the assumptions of the standard theory have been retained (except, of course, that the lattice is not supposed to be in equilibrium), with

the slight but important generalization that both transverse and longitudinal lattice waves are assumed to interact with the conduction electrons. The simplest way to take this generalization into account (see T.M., § 9.81) is to introduce free paths l_j for the scattering of a conduction electron by lattice waves of polarization j ($j=1$ for longitudinal and $j=2,3$ for transverse waves); such free paths may be defined at high temperatures ($T>\Theta$; see T.M., p. 264), and are assumed to be of the same form as the single free path l of the standard theory, but involving different interaction constants C_j for the three different directions of polarization of the lattice waves. It is convenient to write $l_j=l/\alpha_j$, where l is the resultant electron free path at high temperatures for scattering by all types of lattice waves; then, since $l^{-1}=\sum_j l_j^{-1}$, we must have $\sum_j \alpha_j=1$. We must also introduce the various free paths which characterize the various mechanisms whereby lattice vibrations may be scattered. The scattering by conduction electrons is, of course, described by the same transition probabilities as occur in the standard theory; to describe the scattering by all causes other than conduction electrons we introduce an effective free path $L(z, T)$, which in general will be an explicit function both of T and of $z=h\nu/kT$, where ν is the frequency of the lattice wave.

With these assumptions it is possible to obtain relatively simple solutions of the simultaneous transport equations for the electron and phonon distribution functions. The resulting expressions for the transport magnitudes, like the first-order results of the standard theory, are exact at sufficiently high and sufficiently low temperatures, and have the status of approximate interpolation formulae at intermediate temperatures. The expressions which replace (1), (4) and (8) of § 2 are found to be as follows:

$$\frac{1}{\sigma}=\frac{1}{\sigma^{(0)}}-\frac{F_1}{\sigma_i}, \qquad \varkappa=\varkappa^{(0)}+\varkappa_i F_2, \qquad Q=Q^{(0)}+Q^{(1)}, \tag{16}$$

where $\sigma^{(0)}$, $\varkappa^{(0)}$ and $Q^{(0)}$ are the expressions for σ, $\varkappa$ and Q when the lattice is in equilibrium, σ_i and $\varkappa_i$ are the ideal conductivities given by Eqs. (2) and (6), and where

$$F_1=\mathscr{J}_5^{-1}\sum_j \alpha_j^2 \mathscr{K}_{j,6}, \tag{17}$$

$$F_2=\frac{6}{\pi^2}\left(\frac{D}{\zeta}\right)^3\left(\frac{T}{\Theta}\right)^6\left[\left\{1+\frac{3}{2\pi^2}\frac{\zeta}{D}\left(\frac{\Theta}{T}\right)^2\right\}\mathscr{J}_5-\frac{1}{2\pi^2}\mathscr{J}_7\right]\sum_j \mathscr{K}_{j,4}, \tag{18}$$

$$Q^{(1)}=-\sqrt{2}\,\frac{k}{e}\left(\frac{D}{\zeta}\right)^{3/2}\left(\frac{T}{\Theta}\right)^3\sum_j \alpha_j \mathscr{K}_{j,5}. \tag{19}$$

The notation here is the same as in § 2, with

$$\mathscr{K}_{j,n} = \int_0^{\Theta/T} \left\{ \alpha_j z + \frac{1}{2}\left(\frac{D}{\zeta}\right)^2 \frac{T_0}{T} \frac{l}{L(z,T)} \right\}^{-1} \frac{z^n \, \mathrm{d}z}{(\mathrm{e}^z - 1)(1 - \mathrm{e}^{-z})}; \qquad (20)$$

l is the electron free path at some temperature $T_0 > \Theta$, and is such that lT_0 is independent of T_0.

The behaviour of the new terms in the conduction magnitudes is determined by the integrals $\mathscr{K}_{j,n}$, which, in turn, depend upon the free path $L(z, T)$. The various factors which determine the form of $L(z, T)$ in different ranges of temperature have been considered in detail by Makinson [34]. At high temperatures $L(z, T)$ is the effective free path for phonon-phonon scattering, which arises from the anharmonic terms in the equations of motion of the lattice vibrations; this free path, however, increases exponentially with decreasing temperature at temperatures below Θ, and in the low temperature region $L(z, T)$ is determined by scattering of phonons by static lattice defects of various types. A complete discussion of all possible cases of interest is out of the question here, and we shall confine ourselves to pointing out some of the features of particular interest in the low temperature region. We first consider the thermoelectric power, for which the results are particularly striking.

Qualitative discussions of the term $Q^{(1)}$ in Q which arises from the non-equilibrium of the lattice have been given by Gurevich, MacDonald and Klemens [38]. If phonons are supposed to be scattered by electrons only, we have $\mathscr{K}_{j,n} = \alpha_j^{-1} \mathscr{J}_{n-1}$; in this case, therefore, $Q^{(1)}$ varies as T^3 when $T \ll \Theta$, and increases with increasing temperature to a limiting value of the order of $-k/e$. Further, in this case $Q^{(1)}$ is very much greater than $Q^{(0)}$ for all except extremely low temperatures, and, although the low-temperature experimental value of Q for sodium (see § 2) is also greater than $Q^{(0)}$, the values of $Q^{(1)}$ are far in excess of the required corrections. It therefore seems clear that scattering of phonons by causes other than conduction electrons must be taken into account. In general, the most important of these causes at low temperatures will be the elastic scattering by impurities and other irregularities of atomic dimensions; this type of scattering varies as the fourth power of the frequency (Rayleigh's law), so that the corresponding free path may be written

$$L(z, T) = \{\mathscr{I} z^4 (T/\Theta)^4\}^{-1}, \qquad (21)$$

where $\mathscr{I}$ is a constant. (A detailed discussion of the scattering of lattice waves by static imperfections, including dislocations and grain boundaries, has recently been given by Klemens [39]; it should be noted, in particular, that at sufficiently low temperatures L will be limited by grain boundaries and the external boundaries of single crystal specimens, and will then be independent of frequency and temperature. We assume here that the temperature is high enough for boundary scattering to be negligible).

To fix the values of the α_j's in Eqs. (17) to (20) we may assume, as in the standard theory, that the transverse lattice waves do not scatter conduction electrons at all, so that $\alpha_1 = 1$, $\alpha_2 = \alpha_3 = 0$; or we may assume, with Makinson [34], that all types of waves scatter equally, so that $\alpha_1 = \alpha_2 = \alpha_3 = \frac{1}{3}$. In view of the oversimplified nature of the model, the choice between the various possible assumptions is to a large extent arbitrary (in a more exact theory the quantities corresponding to the α_j's would be functions of the temperature); as a rough compromise we shall here adopt the arithmetic means of the values quoted above, i.e. we take

$$\alpha_1 = \tfrac{2}{3}, \quad \alpha_2 = \alpha_3 = \tfrac{1}{6}. \tag{22}$$

From (20) we obtain, when $L(z, T)$ is given by (21),

$$\mathscr{K}_{j,n} = \int_0^{\Theta/T} \left\{ \alpha_j z + p \left(\frac{T}{\Theta}\right)^3 z^4 \right\}^{-1} \frac{z^n \, dz}{(e^z - 1)(1 - e^{-z})}, \tag{23}$$

where

$$p = \frac{1}{2} \left(\frac{D}{\zeta}\right)^2 \frac{T_0}{\Theta} \, l \mathscr{I}; \tag{24}$$

with the α_j's given by (22), the theory thus contains only the parameter p additional to those appearing in the standard theory. The appropriate value of p in any given case is difficult to estimate a priori, and we therefore adjust it to fit the experimental data. $Q^{(1)}$ has been evaluated for sodium from Eqs. (19), (22) and (23), taking $p = 70$; the total thermoelectric force $\int_0^T (Q^{(0)} + Q^{(1)}) \, dT$ obtained in this way is shown as curve 3 in Fig. 2, and is seen to be in good agreement with MacDonald and Pearson's experimental curve [20] for the low temperature region. The value of p required to obtain agreement with experiment corresponds to a free path (21) of the same order of magnitude as the free path required to account for the thermal resistance of

alkali halide crystals in the liquid hydrogen region, where scattering of phonons by lattice defects is also the predominant scattering mechanism [40].

It would, of course, be wrong to attach much importance to the quantitative agreement with experiment obtained here, but it seems clear that the non-equilibrium of the lattice plays an important part in determining the thermoelectric effects in metals *. Further, the behaviour of the new terms arising from this cause depends sensitively on the interaction mechanism whereby lattice vibrations are scattered, and is likely to be much more varied and complicated than the behaviour predicted by the standard theory, which is relatively insensitive to the nature of the electron scattering mechanisms; it seems, therefore, that we have here at least a partial clue towards the understanding of the complicated thermoelectric behaviour of real metals. It should be noted, however, that the expression obtained here for the new term in Q has always the same sign as the standard term, and it cannot therefore be invoked to explain the anomalous sign of Q in the noble metals.

Turning to the electrical conductivity, we find from (17) and (20) that, if phonons are supposed to be scattered by electrons only, $F_1 = 1$, so that $\sigma = \sigma_r$ and the ideal electrical resistivity is identically zero. This remarkable result, which has been known for a long time [41], arises from the fact that collisions between electrons and phonons which satisfy the condition $\mathbf{k}' = \mathbf{k} \pm \mathbf{q}$ cannot affect the total sum of the wave vectors of electrons and lattice, so that the total wave vector must increase continually in the presence of an electric field, and no stationary state is possible. It is therefore clear that there must be other scattering processes which prevent the phonon distribution from departing too far from thermal equilibrium. At high temperatures we can invoke both the Umklapp processes and the anharmonic phonon-phonon scattering, but at low temperatures the most important process is probably the scattering of phonons by lattice defects. Evaluation of F_1 for sodium by means of (17) and (23), using the same values of the parameters as in the calculation of $Q^{(1)}$ above, gives $F_1 = 0.03$ when $T/\Theta = 0.25$, and $F_1 = 0.09$ when $T/\Theta = 0.1$; these small values suggest, if the picture adopted here is

* For the corresponding effect in semi-conductors, where $Q^{(1)}$ appears to be of even greater importance for the thermoelectric behaviour at low temperatures, see Ch. VII.

correct, that the correction to the electrical conductivity due to the non-equilibrium of the lattice is likely to remain small down to temperatures where the ideal electrical resistance is in any case, in practice, very small compared with the residual resistance. However, a more detailed examination of the conditions under which significant deviations from the usual formula are to be expected might well prove of interest (see also § 5.1 below). The electrical conductivity of metals has been discussed from a similar point of view by Klemens [40].

In the case of the thermal conductivity, finally, it turns out that the term $\varkappa_i F_2$ in $\varkappa$ which arises from the non-equilibrium of the lattice is identical with the expression for the lattice thermal conductivity of a metal (usually denoted by $\varkappa_g$) calculated by Makinson [34] on the assumption that the electron distribution is in equilibrium (see also T.M., § 9.81, and Klemens [42]). To the approximation considered here, therefore, the thermal conductivity is the same as that obtained by supposing that the lattice non-equilibrium has no influence at all on the electron distribution, and that the electron non-equilibrium has no influence on the lattice distribution. The lattice thermal conductivity is generally considered to be negligibly small in good metallic conductors, and this is confirmed (for low temperatures) by the present calculations; with the values of the parameters used above in discussing Q and σ, we find that, for sodium, $F_2 = 0.032$ when $T/\Theta = 0.25$, and $F_2 = 0.013$ when $T/\Theta = 0.1$, so that in pure specimens, where $\varkappa^{(0)} \approx \varkappa_i$ at the temperatures considered, the lattice conductivity $\varkappa_i F_2$ is very small compared with the electronic conductivity $\varkappa^{(0)}$. Since the standard formula for $\varkappa^{(0)}$ disagrees with the observed thermal conductivity of pure sodium (§ 2), we must therefore conclude that some generalization of the theory outlined here, probably along lines similar to those considered by Ziman [3], is required to give a completely satisfactory account of the thermal conduction phenomena in monovalent metals.

In alloys and impure metallic elements, and in poor conductors (such as bismuth) with a small free-electron density, the lattice thermal conductivity may form an appreciable fraction of the observed thermal conductivity. As an example we consider the results, shown in Fig. 4, obtained by White and Woods [43] for a specimen of copper containing 0.056 % iron. At sufficiently low temperatures we have $\varkappa^{(0)} = \varkappa_r$ and $\varkappa = \varkappa_r + \varkappa_i F_2$, where $\varkappa_r$ is proportional to T and

$\varkappa_i F_2$ varies as some power of T higher than the first (the precise form depending upon the dominant phonon scattering mechanism). Extrapolation to $T=0$ of the graph of $\varkappa/T$ against T therefore gives $\varkappa_r$, and the total electronic conductivity $\varkappa^{(0)}$ at higher temperatures is given by $(\varkappa_r^{-1}+\varkappa_i^{-1})^{-1}$, the values of $\varkappa_i$ being taken from measurements on pure copper. This gives curve 2 in Fig. 4; the lattice conductivity $\varkappa_i F_2$ can now be obtained as the difference $\varkappa-\varkappa^{(0)}$, and is shown as curve 3 in Fig. 4. Below 15° K $\varkappa_i F_2$ follows the T^2 law to be expected

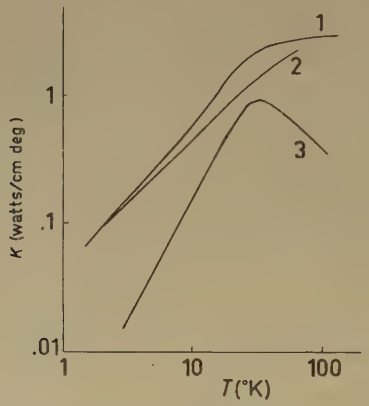

Fig. 4. The thermal conductivity of a dilute copper-iron alloy at low temperatures (after White and Woods [43]). (Logarithmic scale.) 1, measured conductivity; 2, electronic conductivity; 3, lattice conductivity.

if the lattice waves are scattered predominantly by conduction electrons; the general behaviour of $\varkappa_i F_2$ is in accordance with the qualitative predictions of Makinson [34]. In the T^2 region the ratio F_2 of the lattice to the ideal electronic thermal conductivity is proportional to $\sum_j \alpha_j^{-1}$, and its value can thus be used to derive information on the extent to which the conduction electrons interact with the transverse lattice waves [42]; considerable uncertainty arises, however, from possible variations in the effective value of Θ to be used for different coupling schemes. On the whole the evidence indicates that the interaction of conduction electrons with transverse lattice waves is comparable in magnitude with the interaction with longitudinal waves.

Results similar to those of White and Woods [43] have been obtained for silver-palladium and silver-cadmium alloys [44], indium-thallium

alloys [45] and for beryllium [46]; in bismuth [46], however, the lattice conductivity is found to be size-dependent and proportional to T^3 at very low temperatures, thus showing the behaviour characteristic of boundary scattering of lattice waves. For references to earlier work on the lattice thermal conductivity in metals we refer to the review article by Olsen and Rosenberg [15].

5. Special Topics

We finally consider briefly some aspects of the subject which fall outside the theoretical framework outlined above, either because no satisfactory theory exists or because the effects concerned are of a more specialized kind.

5.1. Anomalous impurity scattering

It was found by de Haas, de Boer and van den Berg [47] in 1934 that the electrical resistance of some pure specimens of gold passed through a minimum at liquid helium temperatures. A similar effect has been observed in other metals, among them copper, silver [48] and magnesium [7], and the phenomenon has been investigated intensively in recent years (see, in particular, the detailed study by MacDonald and collaborators [49] of copper and dilute copper alloys; references to earlier work may be found in these papers). It seems to be well established that the occurrence of the resistance minimum is always associated with the presence of impurities, the minimum moving to higher temperatures as the impurity content is increased. The factors which determine the details of the behaviour are, however, complicated and involve the specific nature of the impurity atoms as well as their concentration (for example, the effect of small amounts of manganese as an impurity in specimens of the noble metals is to produce a maximum as well as a minimum in the resistance-temperature curve [50]); and there is some evidence [51] that structural lattice defects such as grain boundaries must also be taken into account. The anomalies in electrical resistance are often associated with anomalies in other conduction properties; thus Fig. 5 shows the electrical resistance and Fig. 6 the absolute thermoelectric force of dilute copper-tin alloys at low temperatures [20], the latter figure showing dramatically how profound may be the effect of very small quantities of impurity on the more complicated conduction properties. In magnesium there is a clearly marked abnormality in the thermal conductivity accom-

panying the electrical resistance minimum [16]; the effect is best shown up by plotting $T/\varkappa$ against T^3 (Fig. 7), and the curve so obtained is interesting since it suggests that the effect is to be ascribed to a decrease of the electrical and thermal resistivities below their normal values in the neighbourhood of the resistance minimum, rather than to an abnormally enhanced resistivity at temperatures below the minimum.

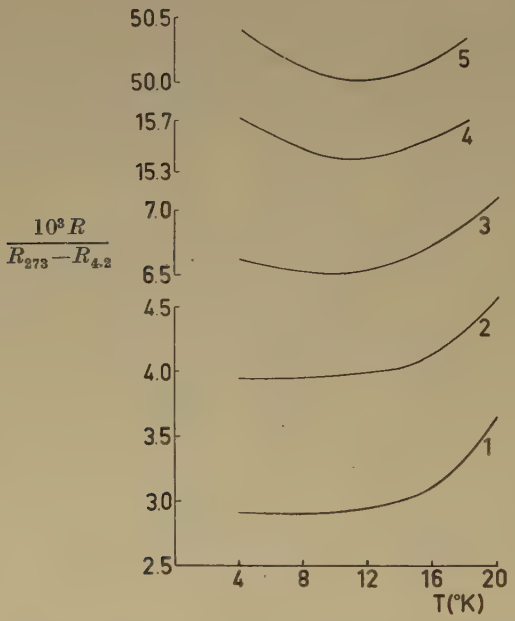

Fig. 5. Relative electrical resistance of copper and copper-tin alloys at low temperatures (after MacDonald and Pearson [20]). 1, pure copper; 2, Cu + 0.0009 atomic % Sn; 3, Cu + 0.0026 atomic % Sn; 4, Cu + 0.0054 atomic % Sn; 5, Cu + 0.026 atomic % Sn.

Various tentative suggestions have been put forward [52] to explain the resistance minimum, and a detailed theory has been developed (Korringa and Gerritsen [53]) which pictures the effect in terms of resonance scattering processes arising from impurity levels at the Fermi surface. None of these ideas has, however, found general acceptance so far, and it cannot be pretended that we have as yet any real understanding of the phenomenon. It is perhaps worth pointing out that the theory of § 4 may, in certain circumstances, lead to an anomalous temperature variation of the effective ideal

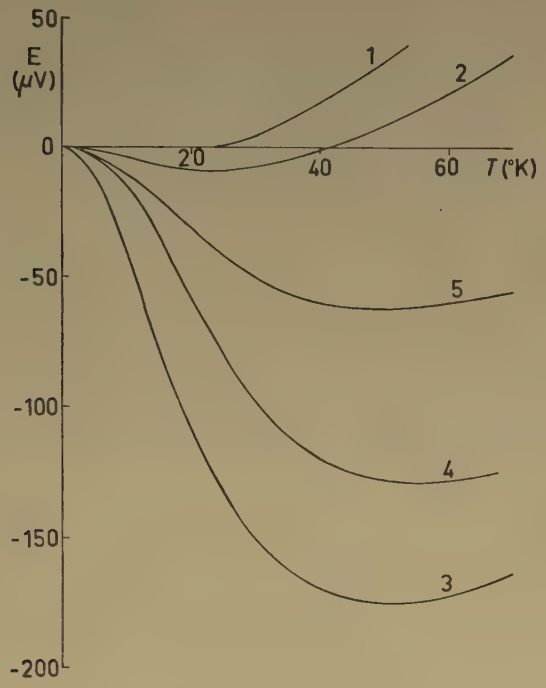

Fig. 6. The absolute thermoelectric force of copper and copper-tin alloys at low temperatures (after MacDonald and Pearson [20]). Legend as for Fig. 5.

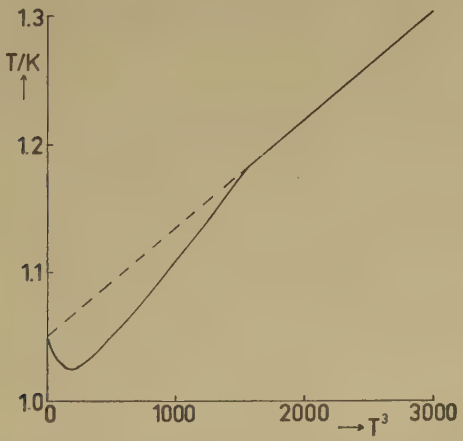

Fig. 7. The graph of $T/\varkappa$ against T^3 for a magnesium specimen at low temperatures (after Rosenberg [16]).

resistivity at low temperatures, and it might perhaps be possible to choose the parameters in the general expression (Eqs. (17) and (20)) for F_1 so as to lead to a resistivity which decreases with increasing temperature over some temperature range. However, while this suggests a possible physical mechanism for the effect (in terms of the depression of the ideal resistance arising from the non-equilibrium of the lattice), the suggestion is a highly tentative one and much further work is required in order to decide whether this possibility or any of the other ideas that have been proposed can really provide an adequate explanation. In any case, the effects discussed here form only one (particularly striking) part of the evidence which indicates that a much more detailed theory of the effect of specific types of lattice imperfection on the electron transport phenomena in metals is required.

5.2. Magnetic effects

When a magnetic field is present as well as electric and thermal currents the conduction phenomena in metal are highly variegated and complex; for a classification of the effects and reviews of the subject we refer to T.M. and to MacDonald and Sarginson [54]. In order to obtain appreciable magneto-resistance effects the magnetic field must be large enough to make the radius of curvature of the path of a conduction electron comparable with the mean free path at the temperature in question; for a given magnetic field, therefore, the largest effects are obtained in experiments on very pure specimens at very low temperatures, and in fact it is often under these conditions only that the effects become large enough to be readily observable.

The magnetic effects depend essentially upon the finer details of the energy-level structure of the conduction electrons, and the usual model of quasi-free electrons is quite inadequate for even a qualitatively correct theoretical account. The more general model in which there is a number of overlapping energy bands, each of which has spherical symmetry, is somewhat more realistic in giving the right order of magnitude both for the Hall effect and for the transverse magneto-resistance effect, and in showing that the sign of the Hall effect may be either positive or negative [55]; but there are some magnetic effects, such as the change in resistance in a longitudinal magnetic field, which cannot be understood at all except on the basis of models which take the anisotropy of the energy surfaces explicitly into account.

It is, however, possible to show [56] without explicitly solving the Boltzmann equation that, for a given metal, whatever the form of the energy surfaces, the relative change of resistance produced by a magnetic field H is of the functional form

$$\Delta\varrho/\varrho = \{\varrho(H)-\varrho(0)\}/\varrho(0) = F\{H/\varrho(0)\}, \qquad (25)$$

where, for small x, $F(x) = Bx^2$, with B a positive number which depends only upon the orientation of H relative to the electric current (in general B is larger for transverse than for longitudinal fields). This rule, and an analogous rule for the thermal conductivity [57], are useful in correlating experimental results for specimens at different temperatures and in different states of purity, and are found to be reasonably well obeyed in practice. For strong fields the theory predicts that, in general, $\Delta\varrho/\varrho$ should tend to a constant limiting value, although in special cases $\Delta\varrho/\varrho$ may continue to increase as H^2 for all values of H; there is experimental evidence for both types of behaviour, although $\Delta\varrho/\varrho$ (and also the relative change in thermal conductivity) are often almost linear in H over a wide range of values of H — too wide, it seems, to be ascribable simply to the transition from an H^2 law to a saturation region. It seems probable, however, that with better knowledge of the electronic energy levels it will be possible to account for such discrepancies on the basis of the existing fundamental theoretical scheme, and also to explain the complex influence on the magnetic effects of the anisotropy of the crystalline field in metals; but the detailed calculations required are certain to be highly complicated.

There are some anomalies in the magnetic effects at low temperatures which seem to be of a more fundamental kind. For example, the quantization of the electron orbits in a magnetic field, which is responsible for the oscillatory diamagnetic behaviour of metals at low temperatures (see Ch. VIII), leads to an analogous, though usually less strongly marked, oscillatory dependence of the electronic transport phenomena upon magnetic field which has attracted much attention recently (see, e.g., Alers [58], where references to earlier work may be found). Amongst other anomalies, of more uncertain origin, we may note that the resistance of some of the dilute alloys discussed in § 5.1 is found to decrease at very low temperatures when a magnetic field is applied [59]. Finally, the electrical resistance of a single crystal of antimony has been found [60] to vary with a longitudinally applied

magnetic field in the curious manner shown in Fig. 8, which has been tentatively ascribed to the influence at low temperatures of a surface scattering effect of the type discussed in § 5.3.

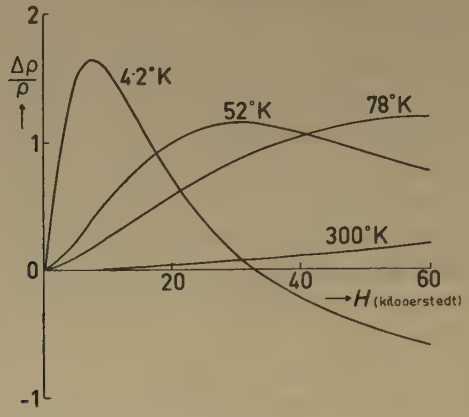

Fig. 8. Change of resistance of an antimony single crystal in a longitudinal magnetic field (after Steele [60]).

5.3. Mean-free-path effects

Interesting surface effects occur in metals under conditions where the free path of the conduction electrons is large compared with a linear dimension of the specimen (conduction in thin films or wires), or, at high frequencies, when the free path is large compared with the depth of penetration of an electromagnetic field into the metal (the anomalous skin effect). Under these conditions, the realization of which in general requires measurements extending to very low temperatures, the resistance depends explicitly upon the ratio of the free path to the other characteristic length concerned, and measurements of the resistance can thus be used to obtain a direct estimate of the magnitude of the free path. For reviews of the subject we refer to articles by Sondheimer [61] and Pippard [62] (see also Mac-Donald and Sarginson [54] for a discussion of the effect of a magnetic field).

The chief interest of these effects in the study of metals arises from the fact that they make it possible, at least in principle, to use measurements on single crystals in order to obtain detailed information on the shape of the electronic energy surfaces. Ordinarily, the electrical conductivity of an anisotropic metal crystal is represented by a symmetric second-order tensor, and the form of its anisotropy is

determined completely by the crystal symmetry. When surface effects are dominant, however, the conduction process is more complicated, and may be visualized most readily by supposing that the electric current is carried entirely by electrons whose paths are nearly parallel to the surface of the specimen [63, 61]; it follows that, when the direction of the crystal axes relative to the surface is varied, different groups of electrons corresponding to different portions of the Fermi surface become dominant in determining the resistance, and in this way the anisotropy of the resistance reflects the local geometry of the Fermi surface.

Detailed calculations have been carried out for models in which the Fermi surface is represented by a superposition of ellipsoids, both for the high-frequency effects [64] and for d.c. conduction in thin films [65]; and Pippard [66] has used more general, but less rigorous, methods to show that, subject to certain limitations, the actual shape of the Fermi surface may be deduced from the observed anisotropy of the surface resistance at high frequencies when the skin effect is highly anomalous. The experimental aspects of the problem present obvious practical difficulties, and little work has been done so far; the most detailed measurements available, on the anomalous skin effect in plane single crystals of tin [67], have not so far proved easy to interpret, but there is every hope that future experimental and theoretical work on these effects will do much to further our knowledge of the electronic structure of metals.

My best thanks are due to Dr. R. G. Chambers for reading the article in typescript and for suggesting a number of improvements.

REFERENCES

1 A. H. Wilson, The Theory of Metals, 2nd ed. (1953).
2 F. Bloch, Z. f. Phys., **52**, 555 (1928), **59**, 208 (1930).
3 J. M. Ziman, Proc. Roy. Soc. A, **226**, 436 (1954).
3a C. S. Barrett, J. Inst. Metals, **84**, 43 (1955).
4 E. Grüneisen, Ann. d. Physik, **16**, 530 (1933).
5 D. K. C. MacDonald and K. Mendelssohn, Proc. Roy. Soc. A, **202**, 103 (1950).
6 M. Blackman, Proc. Phys. Soc. A, **64**, 681 (1951).
7 D. K. C. MacDonald and K. Mendelssohn, Proc. Roy. Soc. A, **202**, 523 (1950).
8 F. M. Kelly and D. K. C. MacDonald, Can. J. Phys., **31**, 147 (1953); F. M. Kelly, Can. J. Phys., **32**, 81 (1954).

[9] S. B. Woods, Can. J. Phys., **34**, 223 (1956).
[10] W. J. de Haas and J. de Boer, Physica, **1**, 609 (1934); Comm. Leiden 231c. W. R. G. Kemp, P. G. Klemens, A. K. Sreedhar and G. K. White, Phil. Mag., **46**, 811 (1955).
[11] A. H. Wilson, Proc. Roy, Soc. A, **167**, 580 (1938).
[12] M. Kohler, Z. f. Phys., **126**, 495 (1949).
[13] E. H. Sondheimer and A. H. Wilson, Proc. Roy. Soc. A, **190**, 435 (1947).
[14] E. Krautz and H. Schultz, Z. f. Naturforsch. **9a**, 125 (1954).
[15] J. K. Hulm, Proc. Roy. Soc. A, **204**, 98 (1950); F. A. Andrews, R. T. Webber and D. A. Spohr, Phys. Rev., **84**, 994 (1951); K. Mendelssohn and H. M. Rosenberg, Proc. Phys. Soc. A, **65**, 385 (1952); R. Berman and D. K. C. MacDonald, Proc. Roy. Soc. A, **211**, 122 (1952); J. L. Olsen and H. M. Rosenberg, Advances in Physics, **2**, 28 (1953); G. K. White, Proc. Phys. Soc. A, **66**, 559, 844 (1953); Aust. J. Phys., **6**, 397 (1953); W. R. G. Kemp, P. G. Klemens, A. K. Sreedhar and G. K. White, Phil. Mag., **46**, 811 (1955).
[16] H. M. Rosenberg, Phil. Trans. A, **247**, 441 (1955).
[17] R. Berman and D. K. C. MacDonald, Proc. Roy. Soc. A, **209**, 368 (1951).
[18] G. Borelius, Handbuch der Metallphysik, **1.1**, 385 (1935); A. Sommerfeld, Naturwiss., **22**, 49 (1934).
[19] G. T. Pullan, Proc. Roy. Soc. A, **217**, 280 (1953).
[20] D. K. C. MacDonald and W. B. Pearson, Proc. Roy. Soc. A, **219**, 373 (1953), **221**, 534 (1954).
[21] E. H. Sondheimer, Proc. Roy. Soc. A, **203**, 75 (1950).
[22] P. Rhodes, Proc. Roy. Soc. A, **202**, 466 (1950); P. G. Klemens, Aust. J. Phys., **7**, 64 (1954). See also R. E. B. Makinson, Proc. Phys. Soc. A, **67**, 290 (1954); T. Kasuya, Progr. Theor. Phys. **13**, 561 (1955).
[23] G. K. White, Proc. Phys. Soc. A, **66**, 559, 844 (1953).
[24] J. Bardeen, Phys. Rev., **52**, 688 (1937). See also, e.g., N. F. Mott and H. Jones, The Theory of the Properties of Metals and Alloys, Ch. 7 (1936); F. G. Serova, J. exp. theor. Phys. U.S.S.R., **19**, 126 (1949); S. C. Hunter and F. R. N. Nabarro, Proc. Roy. Soc. A, **220**, 542 (1953); C. A. Busse and F. Sauter, Z. f. Phys., **139**, 440 (1954).
[25] R. Peierls. Ann. d. Physik, **12**, 154 (1932).
[26] D. Bohm and T. Staver, Phys. Rev., **84**, 836 (1952); E. Abrahams, Phys. Rev., **95**, 839 (1954); J. Bardeen and D. Pines, Phys. Rev., **99**, 1140 (1955); F. J. Blatt, Phys. Rev., **99**, 1735 (1955). See also S. V. Vonsovskii, Uspekhi Fiz. Nauk., **48**, 289 (1952) and references given there; J. M. Ziman, Proc. Camb. Phil. Soc., **51**, 707 (1955); V. L. Ginzburg and V. P. Silin, J. exp. theor. Phys. U.S.S.R., **29**, 64 (1955).
[27] J. S. van Wieringen, Proc. Phys. Soc. A, **67**, 206 (1954); R. E. Peierls, Quantum Theory of Solids, Oxford (1955).
[28] H. Fröhlich, Phys. Rev., **79**, 845 (1950); J. Bardeen, Rev. Mod. Phys., **23**, 261 (1951).
[29] See, e.g., H. Fröhlich, Proc. Roy. Soc. A, **215**, 291 (1952).
[30] See the reviews by M. Blackman, Handb. d. Phys., **7/1**, 325 (1955); J. R. Reitz, Solid State Physics, **1**, 1 (1955); F. S. Ham, Solid State Physics, **1**, 127 (1955).

[31] F. H. J. Cornish and D. K. C. MacDonald, Phil. Mag., 42, 1406 (1951).
[32] P. G. Klemens, Aust. J. Phys., 7, 70 (1954).
[33] H. Jones, Proc. Phys. Soc. A, 68, 1191 (1955).
[34] R. E. B. Makinson, Proc. Camb. Phil. Soc., 34, 474 (1938).
[35] D. ter Haar and A. Neaves, Proc. Roy. Soc. A, 228, 568 (1955).
[36] E. H. Sondheimer, Proc. Roy. Soc. A, 234, 391 (1956); A. G. Samoylovich and L. L. Korenblit, Uspekhi Fiz. Nauk, 49, 337 (1953).
[37] I. I. Hanna and E. H. Sondheimer, to be published.
[38] L. Gurevich, J. Phys. U.S.S.R., 9, 477 (1945), 10, 67 (1946); D. K. C. MacDonald, Physica, 20, 996 (1954); P. G. Klemens, Aust. J. Phys., 7, 520 (1954).
[39] P. G. Klemens, Proc. Phys. Soc. A, 68, 1113 (1955).
[40] P. G. Klemens, Proc. Phys. Soc. A, 64, 1030 (1951); W. J. de Haas and Th. Biermasz, Physica, 4, 752 (1937); Comm. Leiden, 249a; Physica, 5, 47, 320 (1938); Comm. Leiden, 251a.
[41] R. Peierls, Ann. d. Physik, 4, 121 (1930).
[42] P. G. Klemens, Aust. J. Phys., 7, 57 (1954).
[43] G. K. White and S. B. Woods, Phil. Mag., 45, 1343 (1954).
[44] W. R. G. Kemp, P. G. Klemens, A. K. Sreedhar and G. K. White, Proc. Roy. Soc. A, 233, 480 (1956).
[45] R. J. Sladek, Phys. Rev., 97, 902 (1955).
[46] G. K. White and S. B. Woods, Can. J. Phys., 33, 58 (1955).
[47] W. J. de Haas, J. de Boer and G. J. van den Berg, Physica, 1, 1115 (1934); Comm. Leiden, 236a; G. J. van den Berg, Thesis, Leiden (1938).
[48] W. J. de Haas and G. J. van den Berg, Physica, 3, 440 (1936); Comm. Leiden, 241d; W. H. Keesom, Comm. Leiden Suppl., 80a; E. Mendoza and J. G. Thomas, Phil. Mag., 42, 291 (1951).
[49] D. K. C. MacDonald and W. B. Pearson, Acta Metallurgica, 3, 392, 403 (1955); W. B. Pearson, Phil. Mag., 46, 911, 920 (1955); G. K. White, Can. J. Phys., 33, 119 (1955).
[50] A. N. Gerritsen and J. O. Linde, Physica, 17, 573 (1951), 18, 877 (1952); Comm. Leiden, 285 and 290.
[51] T. H. Blewitt, R. R. Coltman and J. K. Redman, Phys. Rev., 93, 891 (1954); W. B. Pearson, Phys. Rev., 97, 666 (1955).
[52] E.g. J. C. Slater, Phys. Rev., 84, 179 (1951); D. K. C. MacDonald, Phil. Mag., 42, 756 (1951); A. B. Bhatia, Phys. Rev., 95, 914 (1954); W. B. Pearson, Phil. Mag., 45, 1087 (1954).
[53] J. Korringa and A. N. Gerritsen, Physica, 19, 457 (1953); Comm. Leiden Suppl., 106.
[54] D. K. C. MacDonald and K. Sarginson, Rep. Progr. Phys., 15, 249 (1952).
[55] R. Peierls, Z. f. Phys., 53, 255 (1929).
[56] R. Peierls, Ann. d. Physik, 10, 97 (1931); M. Kohler, Ann. d. Physik, 32, 211 (1938).
[57] M. Kohler, Naturwiss., 36, 186 (1949); K. Mendelssohn and H. M. Rosenberg, Proc. Roy. Soc. A, 218, 190 (1953).
[58] P. B. Alers, Phys. Rev., 101, 41 (1956).
[59] N. M. Nakhimovich, J. Phys. U.S.S.R., 5, 141 (1941); A. N. Gerritsen

and J. O. Linde, Physica, **17**, 584 (1951); Comm. Leiden, 285; A. N. Gerritsen, Physica, **19**, 61 (1953); Comm. Leiden, 291.

[60] M. C. Steele, Phys. Rev., **97**, 1720 (1955).

[61] E. H. Sondheimer, Advances in Physics, **1**, 1 (1952).

[62] A. B. Pippard, Advances in Electronics and Electron Physics, **6**, 1 (1954).

[63] A. B. Pippard, Proc. Roy. Soc. A, **191**, 385 (1947).

[64] E. H. Sondheimer, Proc. Roy. Soc. A, **224**, 260 (1954).

[65] F. S. Ham and D. Mattis, Tech. Rep. No. 4, Dept. of Physics, University of Illinois (1955); R. Englman and E. H. Sondheimer, Proc. Phys. Soc. B, **69**, 449 (1956).

[66] A. B. Pippard, Proc. Roy. Soc. A, **224**, 273 (1954); see also M. I. Kaganov and M. Ya. Azbel', J. exp. theor. Phys. U.S.S.R., **27**, 762 (1954); Dokl. Akad. Nauk. S.S.S.R., **102**, 49 (1955).

[67] E. Fawcett, Proc. Roy. Soc. A, **232**, 519 (1955).

CHAPTER VII

SEMICONDUCTORS AT LOW TEMPERATURES*

BY

V. A. JOHNSON AND K. LARK-HOROVITZ

DEPARTMENT OF PHYSICS, PURDUE UNIVERSITY LAFAYETTE, INDIANA

CONTENTS: 1. Introduction, 187. — 2. Resonance phenomena, 189. — 3. Electrical measurements, 197. — 4. Thermal properties, 209. — 5. Optical properties, 216.

1. Introduction

Measurements made in the liquid hydrogen and liquid helium temperature ranges are useful in obtaining information about the basic nature of semiconductors. The investigations to be considered are resonance phenomena, electrical properties, including resistivity, magnetoresistance, Hall coefficient, and thermoelectric power, thermal properties such as specific heat and thermal conductivity, and optical properties such as absorption and photoconductivity.

The basic properties of a semiconductor may be understood from the band structure, that is, by consideration of the arrangement of allowed and forbidden bands of electron energies [1-4]. In a semiconductor or insulator there is a *forbidden gap* between the highest band of completely occupied electronic energy levels (the valence band) and the empty band of allowed energy levels above (the conduction band).

The main distinction between semiconductors and insulators arises from the forbidden gap in semiconductors being smaller than in insulators. In most semiconductors additional energy levels are present in the forbidden gap arising from the presence of impurities or crystal imperfections. Fig. 1 gives a schematic energy diagram of a typical semiconductor. Electrons may readily be excited from impurity donor levels to the conduction band and from the valence band to the impurity acceptor levels at normal temperatures. On the basis of this simple model at least a few milli-electronvolts of thermal energy are required to raise an electron from a donor level to the

* Work supported in part by contract with U.S. Signal Corps.

conduction band (or to raise an electron from the valence band to an acceptor level and thus create a hole in the valence band). From

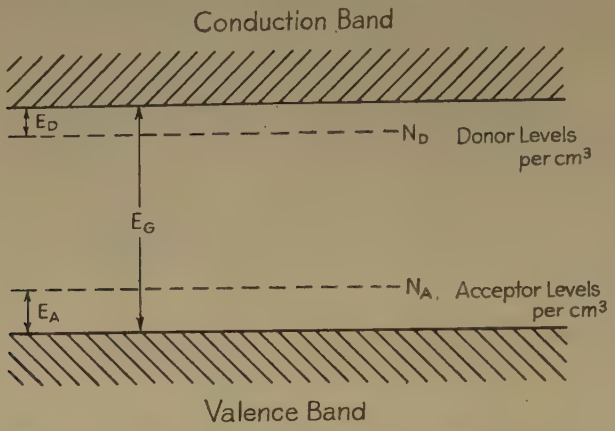

Fig. 1. Simplified representation of the energy band structure of a semiconductor.

this idealized picture one expects the resistance of a semiconducting sample to become infinite as the temperature approaches 0° K.

There are a number of semiconductors with constant numbers of carriers, as deduced from the constancy of the Hall coefficient over a large range of temperatures down to very low temperatures, while the resistivity decreases with temperature as in a metal (metallic type of semiconductor); lead sulfide with excess lead is such a semiconductor * [5]. There also are semiconductors with constant carrier concentrations and constant conductivity down to 1° K as observed (3, 1 and 2) in germanium and silicon at high carrier concentrations. These observations prompted the extension of semiconductor theory and measurements to low temperatures.

The behavior of a semiconductor depends not only upon the charge carrier density, but also upon the mechanism of the scattering encountered by the carriers. In an ideal semiconductor one would expect the scattering due to collisions between the carriers and the lattice phonons to vanish and the mobility thus to become very large as 0° K is approached. Lattice scattering does become negligible in

* In some samples of lead sulfide even super-conductivity has been suspected to occur [6]. Present evidence seems to indicate that the transition curves are different from the ones of true superconductors and may be due to bridges between superconducting islands in the semiconductor.

the low temperature range, but it is usually replaced by scattering of the carriers by ionized and neutral impurities. Information about these processes is found from plots of the mobility as a function of temperature as obtained from measurement of the conductivity, Hall effect, and magnetoresistive ratio as functions of temperature.

In the simplest case one assumes that the energy relative to a band edge can be written as

$$E = \frac{\hbar^2 K^2}{2m^*}, \qquad (1)$$

where effective mass m^* is a scalar quantity and **K** the electronic wave number.

Theoretical considerations, extended by cyclotron resonance investigations, show that the band structure may be more complicated. The surfaces of constant energy in **K**-space are not spherical in the several cases investigated in detail so far. The lack of sphericity in the energy surfaces implies that the effective mass is not scalar but is a tensor quantity. Resonance experiments determine the principal mass values of the mass tensor. These principal mass values lead to predictions for the "conductivity" mass, which appears in the mobility, and the "density-of-states" mass, which appears in the electron distribution function. The density-of-states mass can be determined from measurements of thermoelectric power and the electronic contribution to the specific heat.

Optical measurements of absorption coefficient and photoconductivity give direct information about various activation energies. These in turn may be employed to obtain information about the band structure.

2. Resonance Phenomena

1. Cyclotron Resonance

The diamagnetic or cyclotron resonance measurement in semiconductors is the experiment which directly measures the effective mass of the charge carriers. The concept of cyclotron resonance as applied to solids is relatively recent [7, 8, 9]. It was suggested [9] that conditions in germanium at low temperatures are favorable for the observation of the effect.

A microwave electric field, of frequency in the range 8000–48000 Mcps, is applied to a semiconducting sample in a direction perpendicular to an external magnetic field H. A sufficiently strong magnetic

field causes the charge carriers to move in circles [10, 11]. If the angular frequency of the carriers in their orbits is equal to the frequency of the microwave field, resonance occurs and the carriers absorb energy from the electric field. This occurs at an angular frequency

$$\omega = \pm \frac{eH}{m_c c}, \tag{2}$$

where m_c is the "cyclotron" effective mass and $\pm$ indicates that the holes and electrons rotate in opposite directions. The resonance condition is observed by measuring the absorption of microwave power in a cavity containing the sample as H is allowed to vary.

The two essential requirements for the existence of cyclotron resonance are (a) a sufficiently large number of free charge carriers so that a detectable signal is produced, and (b) the collision time τ of the charge carriers must be long enough that the carriers make at least one revolution between collisions. It has been estimated [11] that at least 10^5 to 10^7 free carriers are required *, depending on the frequency used and the sensitivity of the measuring devices. The collision time requirement, $\omega\tau \geqslant 1$, demands that high purity material be used so as to reduce collisions between carriers and neutral or ionized impurities. The carrier-phonon collisions are reduced by making the measurements at very low temperatures. E.g., in germanium of high purity, $\omega\tau$ slightly exceeds unity at 4.2° K for ω of the order 10^4 Mcps. More favorable $\omega\tau$ values may be obtained by further reduction of temperature. All of the measurements to be discussed in this section were made in the liquid helium temperature range. At such temperatures, the equilibrium number of free carriers is too small to give a detectable resonance. This difficulty is overcome by using microwave or infrared radiation to excite electrons and holes into the conduction band.

The first measurements [10] were made at 4° K with a microwave frequency of 9050 Mcps and with the [100] axis of the crystal parallel to the magnetic field. In an n-type germanium sample having a room temperature resistivity of 38 ohm-cm, a cyclotron effective mass of 0.11 m_0, where m_0 is the free electron mass, was observed. A p-type germanium sample of similar purity yielded hole cyclotron masses of about 0.04 m_0 and 0.3 m_0.

N-type germanium [12–15]. The samples investigated [12, 13] were rods

* Too high a carrier concentration produces depolarization.

mounted with their axes parallel to the microwave electric field. The axis of each rod was cut along a [110] direction; hence the rotation of the sample orients the magnetic field successively along all the directions in the (110) plane, including a [100], a [111], and a [110] direction. The resonance curves obtained show a marked dependence on sample orientation. In this way, cyclotron effective mass values are obtained as a function of the angle between the magnetic field and the [100] direction. A theoretical dependence [9] of cyclotron mass upon orientation can be computed for any chosen model of the Brillouin energy surfaces. In n-type germanium, there are four or eight ellipsoids of revolution lying along [111] axes with a longitudinal mass m_l and a transverse mass m_t. This leads to the equation, for a single ellipsoid,

$$m_c = m_t \left\{ \frac{m_l}{m_l \alpha^2 + m_t(1-\alpha^2)} \right\}^{1/2}, \tag{3}$$

where α is the direction cosine of the magnetic field with respect to the major axis of the ellipsoid. From the resonance peaks in the [110] direction m_l and m_t have been calculated:

$$m_l = (1.600 \pm 0.008)\, m_0, \quad m_t = (0.0813 \pm 0.002)\, m_0. \quad \text{(ref. 15)}$$

P-type germanium [13–16]. When p-type germanium rods are mounted and rotated so as to produce variation in the angle between the magnetic field and the crystal axes, only slight anisotropy is detected. Two resonances occur, corresponding to cyclotron masses $m_1 = 0.042\, m_0$ and $m_2 = 0.290\, m_0$, with H along the [001] direction. The two resonances are interpreted on the basis of a warped sphere model [13, 17, 18] for the top of the valence band in germanium. According to this model, the energy E is related to the components of the wave vector $\mathbf{K}$ by

$$E = \frac{-\hbar^2 K^2}{2m^*} = \frac{-\hbar^2}{2m_0}\{aK^2 \pm [b^2K^4 - c^2(K_x^2 K_y^2 + K_y^2 K_z^2 + K_z^2 K_x^2)]^{1/2}\}. \tag{4}$$

The value of m_1 changes only by about 2.5 % as θ, the angle between H and the [001] axis, varies from 0° to 90°. In summary, the top of the valence band consists of two sets of constant energy surfaces in the Brillouin zone; these are centered at $\mathbf{K} = 0$. The surfaces are almost spherical for the holes of lower effective mass, but are warped spheres for the holes of higher effective mass with eight maxima along the [111] directions and six minima along the [100] directions *.

* Additional cyclotron resonance lines associated with the valence band of germanium have been observed [15] upon cooling the samples to temperatures

N-type silicon [14, 22]. The experiments were carried out on single crystal silicon samples at temperatures in the liquid helium range. Optical excitation was necessary to provide sufficient carriers. The fact that two resonance peaks are observed when H is in the [001] and [110] directions and only one for H in the [111] direction suggests that the constant energy surfaces for the conduction band in silicon are ellipsoids of revolution along the cubic axes in the Brillouin zone. In a manner analogous to that described for n-type germanium, the cyclotron effective mass can be expressed in terms of a longitudinal mass, a transverse mass, and the orientation of H relative to the ellipsoid major axes. Thus the measured values of effective mass lead to the principal values:

$$m_l = 0.98\, m_0,\ m_t = 0.19\, m_0.$$

P-type silicon [14, 23]. Cyclotron resonance experiments have also been carried out on p-type silicon. Two resonance peaks were observed. From this it is deduced that there are light and heavy holes with masses m_1 and m_2, where m_1 is near 0.16 m and m_2 around 0.5 m_0. These cyclotron masses m_1 and m_2 vary only slightly with the orientation H relative to the crystal axes. Measurements have also been made on germanium-silicon alloys [24].

Indium antimonide [25]. Investigations have been initiated in the case of indium antimonide, and preliminary results have been obtained. Measurements have been made at temperatures down to 2.2° K. One resonance line, associated with conduction electrons, corresponds to a cyclotron effective mass of $(0.013 \pm 0.001)\, m_0$. Thus resonance appears to be isotropic under rotation in a (100) plane, within the experimental error limits. Preliminary work indicates two resonance lines corresponding to light and heavy holes. There is some indication of anisotropy. These resonances are rather poorly resolved, but from them one obtains the effective mass values

$$m_1 \approx 0.18\, m_0,\ m_2 > 1.2\, m_0.$$

---

as low as 1.3° K ($\omega\tau \approx 80$ for electrons at this temperature). A quantum mechanical treatment [19, 20, 21] of cyclotron resonance, for holes, predicts a non-uniform spacing between the lower energy levels. Thus, new resonances are expected if these energy levels can be preferentially populated at sufficiently reduced temperatures. These additional resonances are clearly seen [15] in p-type germanium upon comparing heavy-hole resonance plots, for the [100], [111], and [110] directions of H, taken at 4.2° K and 1.3° K, respectively.

It should be noted that, because of the high conductivity of indium antimonide the skin depth in this material is of the order of, or smaller than, practical sample dimensions. Under such conditions, dimensional effects diminish or mask the resonances [26].

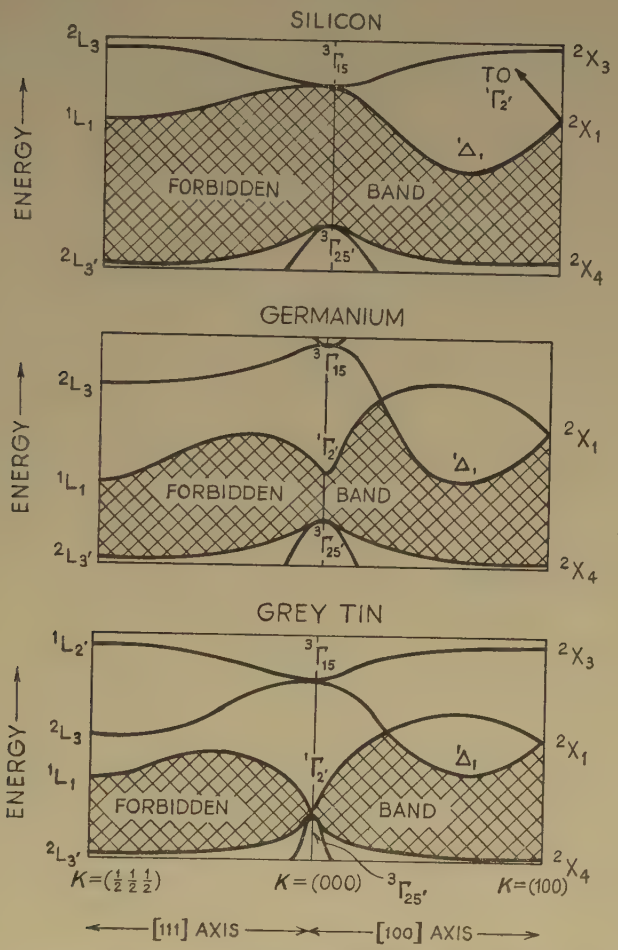

Fg. 2. Schematic diagrams of the energy band structure of silicon, germanium, and gray tin (taken from F. Herman, ref. 31). The spin-orbit splitting is not shown. The symmetry classification of the various band states is indicated in the notation of refs. 27, 28, and 29. The superscripts to the symmetry symbols denote the spatial degeneracy of the corresponding band states. Discrepancies exist between the details of these calculated curves and the actual band structure determined by experimental means.

2. Energy Band Structure

The simple diagram of Figure 1 gives no information about the detailed band structure of an actual semiconductor such as germanium or silicon. A more complete diagram should indicate the behavior of the band edge energy as a function of wave vector **K**.

Theoretical calculations [27, 28, 29] gave a picture of the conduction band edge in germanium. In particular, the computations indicated that the conduction band edge in diamond-type crystals does not lie at the $\mathbf{K}=(0, 0, 0,)$ point, but at a number of equivalent points away from the zone center. In the discussion of cyclotron resonance, it has been seen that the experimental results can best be explained in n-type germanium by taking the constant energy surfaces to be ellipsoids lying along the [111] axes and in n-type silicon by taking the corresponding surfaces to be ellipsoids along the [100] axes. Such an arrangement is consistent with the calculations mentioned above.

The valence band edge in germanium and silicon, on the basis of calculations reinforced by cyclotron resonance measurements, lies at the $\mathbf{K}=(0, 0, 0)$ point and is defined by two bands which touch at this central point. Fig. 2 shows a schematic arrangement of the energy band structure * for silicon, germanium, and gray tin without showing the fine structure due to spin-orbit splitting [30]. (The structure for gray tin is based upon calculation alone.)

3. Paramagnetic Resonance and Impurity States

In the diamagnetic or cyclotron resonance, transition probabilities are due to interaction with an electric microwave field and are proportional to the square of the electric dipole moment. In paramagnetic or electron spin resonance, one observes transitions produced by a magnetic microwave field which are proportional to the square of the magnetic moment. In the constant magnetic field the spins can be oriented parallel or antiparallel to the field [14]. The resonance relation is

$$h\nu_0 = g\mu_B H, \tag{5}$$

* Theoretical schemes for the energy band structures have been roughly calculated [31] for some of the III–V compounds (aluminum phosphide, gallium arsenide, and indium antimonide) on the basis of their respective resemblances to silicon, germanium, and gray tin. So far, experimental evidence, such as cyclotron resonance mass values, has not become available for the III–V compounds other than the preliminary data available for indium antimonide.

where ν_0 is the resonance frequency, g the spectroscopic splitting factor, and μ_B the Bohr magneton. The g shift,

$$\Delta g = g_{\text{obs}} - 2.0023, \qquad (6)$$

measures the spin-orbit interaction. According to Kittel [32], Δg is positive for holes and negative for electrons [33].

The semiconducting sample, silicon in experiments carried out to date, either in the form of a single crystal or fine powder from a crushed single crystal, is mounted on the wall of a resonant cavity in a rectangular wave guide and maintained at a low temperature, usually 4.2° K. Microwave power in the frequency range 9000–24000 Mcps is directed down the guide and coupled into the cavity containing the specimen.

The paramagnetic resonance investigations in semiconductors [34–39] have involved the study of silicon samples containing donor impurities from group V of the periodic table (phosphorus, arsenic and antimony) *. In most cases more than one resonance line is observed due to the hyperfine structure.

Paramagnetic resonance observations, at 4.2° K, of arsenic-doped silicon [35] showed four fairly sharp absorption lines (see Fig. 3). Plastic deformation of the sample by compression at 1000° C enhances the resonance lines. The same four resonance lines are found in silicon crystals in which the arsenic donors are compensated by boron acceptors as long as one uses parts of the crystal in which the arsenic concentration exceeds the boron concentration. No lines are found in silicon doped with boron or aluminum.

The fact that four lines are associated with arsenic suggests that these lines represent a hyperfine structure due to interaction of the electrons with the As^{75} nucleus which has spin 3/2. Therefore, in phosphorus with the single isotope P^{31} and a nuclear spin of 1/2, one expects the hyperfine splitting to give two lines. A silicon sample doped with 4×10^{17} phosphorus atoms per cm^3 was compressed and measured. Two strong resonance lines of equal amplitude were observed, in support of the hypothesis of a hyperfine splitting into $2I+1$ lines, where I is the nuclear spin. It has been shown [36] that in silicon doped with phosphorus, arsenic, or antimony the hyperfine

* The problem of an absolute determination of ν_0 is avoided by calibrating against a sample of diphenyl picryl hydrazyl, a paramagnetic organic compound for which the g-factor is known [40, 41] to be $g = 2.0036 \pm 0.0002$.

splitting disappears when the donor concentration rises to a value greater than about 1×10^{18} atoms per cm^3, and is replaced by a single narrow line [34]. *

A recent application of paramgnetic resonance has been the study

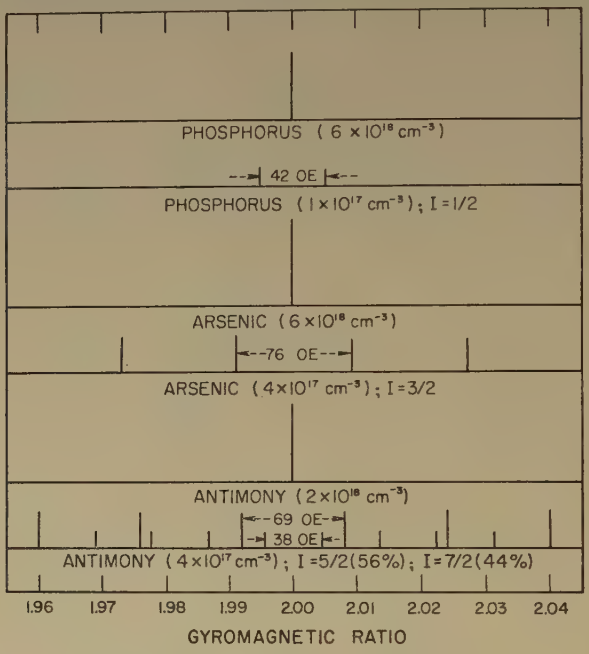

Fig. 3. A schematic representation of the paramagnetic resonance absorption lines observed in silicon doped with various amounts of phosphorus, arsenic, and antimony (taken from Fletcher *et al.*, ref. 36).

of the effect of neutron irradiation upon boron-doped silicon [43]. Three pure samples were cut from an ingot of *p*-type silicon with a room temperature resistivity of about 50 ohm-cm. No paramagnetic resonance was found before irradiation. The samples were exposed to neutron fluxes of 2×10^{17}, 7×10^{17}, and 20×10^{17}. In each sample the room temperature resistivity rose to 10^5 ohm-cm with correspondingly extremely high resistivities at 4.2° K. The two more heavily bombarded samples showed resonance. From the amplitudes the densities of paramagnetic centers were estimated and found to be proportional to the incident fluxes **. This type of investigation may

* For details see references 36, 38, 42.

** More recent observations [44] on high conductivity *n*- and *p*-type samples before and after bombardment seem to indicate that not all centers introduced by bombardment become effective in spin resonance.

well help in attaining an understanding of the nature of the centers introduced by irradiation.

3. Electrical Measurements

1. Hall Coefficient, Conductivity, and Degeneracy

At the low temperatures being considered, extrinsic, or impurity conduction takes place with charge carriers strongly predominant in one sign, either negative (n-type) or positive (p-type). Then the carrier density n is found from

$$n = \pm \frac{r}{Re}, \tag{7}$$

where R is the Hall coefficient (usually given in cm^3/coulomb), e is the magnitude of the electronic charge, and r is a factor, usually between 1 and 2, which depends on the statistics of the electron gas and the energy dependence of the carrier relaxation time.

For electrons released from donors with a definite activation energy E_D, n_e is given by a dissociation equation of the type

$$\frac{n_e(n_e+N_A)}{N_D-N_A-n_e} = \frac{f_c}{g_D} \exp\left(-\frac{E_D}{kT}\right), \tag{8}$$

where N_D is the donor level density, N_A the acceptor level density, E_D the energy required to lift electrons from donor levels to the conduction band, and g_D is the degeneracy of the ground state. For classical statistics,

$$f_c = 2\,(2\pi m_e kT\, h^{-2})^{3/2}, \tag{9}$$

and g_D is taken as 2; a corresponding expression applies to the hole distribution.

The effective mass which enters into Eq. (9) as well as other expressions derived from the distribution function is the "density of states" mass. In the case of n-type material that is characterized by the equivalent ellipsoids in reduced momentum space (see Ch. II. 1), the density-of-states mass [45] is given by

$$(m_e)_d = N_v^{2/3}\,(m_t^2\, m_l)^{1/3}, \tag{10}$$

where N_v is the number of equivalent ellipsoids. If there are four equivalent ellipsoids in germanium $(m_e)_d = 0.57\, m_0$ on the basis of the cyclotron resonance values of m_l and m_t. The assumption of six equivalent ellipsoids in silicon yields $(m_e)_d = 1.08\, m_0$. p-type material is not characterized by ellipsoidal energy surfaces, but appropriate

weighting must be given to the light and heavy holes. The density-of-states masses for holes in germanium and silicon [46] are, respectively, $(m_h)_d = 0.37\ m_0$ and $0.59\ m_0$.

When the activation energy is below 0.01 eV, the sample must be lowered well into the liquid hydrogen range before log $(nT^{-3/4})$ becomes proportional to $1/T$ and the activation energy may be determined from the slope. The activation energy of a given impurity in a semiconductor is found to be dependent upon the nature of the impurity and only slightly dependent upon the impurity concentration for concentrations less than about 10^{16} per cm^3. * The observed decrease of ionization energy as the charge carrier density becomes high can be at least partially accounted for on theoretical grounds [56].

Since the conductivity σ in a sample containing only one kind of carrier is given by

$$\sigma = ne\mu, \tag{11}$$

where μ is the "conductivity" mobility of the carrier, a combination of this equation with Eq. (7) yields an expression for the mobility

$$\mu = |R|\sigma/r. \tag{12}$$

A related quantity frequently encountered in the literature is the "Hall" mobility, defined by

$$\mu_H = |R|\sigma. \tag{13}$$

The ratio r then is equal to μ_H/μ. From the equation of motion of a conduction electron, it follows that

$$\mu = e\tau/m_\sigma, \tag{14}$$

where τ is the relaxation time, which depends on the mechanism of the scattering encountered by the carrier. The effective mass m_σ is

* Typical values for activation energies: E_D (for arsenic in germanium [47]) $= 0.010-0.012$ eV for $N_D < 10^{16}$ cm^{-3}, E_A (for boron in germanium [48]) $= 0.0104$ eV. For other low temperature determinations see refs. 49, 50, 51. Recent work on indium antimonide [52] yields $E_A \approx 0.008$ eV for a p-type impurity in relatively pure material, while another study [53] on this material yields an estimated E_A of about 0.005 eV. On the other hand, p-type gallium antimonide with unknown impurity appears to have two acceptor levels [54] with activation energies of 0.024 eV and 0.037 eV. Cadmium sulfide, pure and doped with either chlorine or gallium, is an n-type conductor. At low carrier concentration, the donor activation energy is found [55] to fall in the $0.01-0.02$ eV range.

called the "conductivity" mass, which is derived from the characteristic masses determined by cyclotron resonance. For n-type germanium and silicon, the conductivity mass is given [45] by

$$m_\sigma = \frac{3m_l m_t}{2m_l + m_t}, \tag{15}$$

an expression which yields 0.12 m_0 for germanium and 0.26 m_0 for silicon. In p-type material the conductivity mass is found by a weighting of the light and heavy hole masses and comes out [46] to be 0.25 m_0 for germanium and 0.38 m_0 for silicon.

Generally speaking, the temperature dependence of τ depends upon the nature of the scattering processes and thus determination of τ by measurement of R and σ indicates the dominant scattering process and even the details of the mixing of two or more processes [57, 58, 59]. For classical statistics, the lattice mobility is proportional to $T^{-3/2}$. While such mobility behavior is often observed near room temperature, frequently the mobility differs very widely from a $T^{-3/2}$ law as temperature is lowered. The conductivity behavior indicates that an additional source of scattering is present, an effect attributed to the scattering of conduction electrons by ionized impurity ions. The mean free path associated with ionized impurity scattering was estimated [59], on the basis of Rutherford scattering, to be

$$l_I = \frac{\alpha E^2}{\ln(1+\beta E^2)}, \tag{16}$$

where subscript I denotes impurity scattering, and α and β are factors determined by temperature, impurity ion concentration, and dielectric constant *. Detailed studies of this type of scattering have been made for n-type germanium [47] and silicon [51]. In order to fit Eq. (16) to observed low temperature resistivities in germanium, it is necessary to take the effective mass to be $m_0/4$ or smaller [47, 48].

At relatively high temperatures, the impurity ion concentration N_I can be taken as equal to the carrier density, which is found from the Hall coefficient. Such agreement is usually not found when one analyzes resistivity curves in the 15° K–50° K range. Here N_I usually appears to be substantially greater than the carrier density. This

* A quantum mechanical consideration of scattering by impurity ions with screening taken into account, leads to a form [60,61] somewhat different from Eq. (16).

result is interpreted [62] as evidence for the simultaneous existence of donor and acceptor levels *.

For samples having carrier concentrations greater than about 10^{18} per cm^3, the Hall coefficient is observed to be constant or almost constant from the intrinsic range down to temperatures in the liquid helium range, even as low as 1° K. Also the mobilities are practically independent of temperature. The flat Hall curves imply activation energies of zero or less, i.e. impurity levels lying at the boundary of or within the conduction or valence band. Such behavior has been observed in n- and p-type germanium [47, 63, 64, 65, 66], n- and p-type silicon [51], indium antimonide [67, 68], cadmium sulfide [55], and cadmium oxide [69]. Formally this behavior of the conductivity and mobility can be understood as arising from the degeneracy of the electron gas [70, 71]. A simple criterion for the onset of degeneracy is found [70] by setting the Fermi energy equal to kT_D, where T_D is the degeneracy temperature. Then

$$T_D = \frac{h^2}{8km^*}\left(\frac{3n}{\pi}\right)^{2/3}. \tag{17}$$

This is almost identical with letting the Fermi space level ζ coincide with the bottom of the conduction band in n-type material or top of the valence band in p-type material. If $m^* = m_0$, then $T_D = 42°$ K for $n = 10^{18}$ cm^{-3} and 4.2° K for 3×10^{16} cm^{-3}. From Eq. (17) it may be seen that if n is known and T_D is determined experimentally, then the effective mass m^* may be calculated. The effective mass determined in this manner is the density-of-states mass.

At temperatures below T_D, Fermi–Dirac statistics must be applied For example, the Fermi level is found from the conduction electron density by use of

$$n_e = \frac{4\pi(2m^* kT)^{3/2}}{h^3} J_{1/2}(\zeta^*), \tag{18}$$

where $\zeta^* = \zeta/kT$ (ζ measured negative downward and positive upward from the bottom of the conduction band) and $J_{1/2}(\zeta^*)$ is one of the Fermi–Dirac integrals.

* For $N_D > N_A$, at 0° K N_A electrons from the donor level fill the N_A acceptor levels and so $N_I = 2N_A$ while the carrier density $n = 0$. As temperature rises, n electrons are excited from donor levels into the conduction band and $N_I = n + 2N_A$. The separate valves of N_D and N_A may be found since $N_D - N_A$ is given by the exhaustion range Hall coefficient and N_A by the low temperature resistivity.

At temperatures low enough to be in the degeneracy range, one can assume that scattering arises almost entirely from the impurity ions. Then the resistivity or mobility is calculated by using Fermi–Dirac statistics in the derivation of l_I and thus finding an expression to replace Eq. (16). This leads to a mobility having a small temperature dependence at intermediate temperatures [73] and a constant value at very low temperatures [71].

Ehrenberg * and, independently, Schottky * have shown sometime ago that any semiconductor model based upon Eq. (8) with $E_D > 0$ can not give degeneracy at very high or very low temperatures; therefore, depending upon the number of impurity centers and their activation energy, at a certain low temperature the material must become non-degenerate again. The analysis of the Fermi level in semiconductors by Hutner *et al.* [72] leads to the same conclusion.

In a detailed analysis of this problem Schottky [85] came to the conclusion that the experimental observations down to 1° K, with the number of carriers independent of temperature, cannot be explained by any theory which assumes ionization of impurities with a finite activation energy.

2. Impurity Band Phenomena

In non-degenerate samples of germanium, as temperatures approach or enter the liquid helium range, the Hall coefficient deviates from exponential behavior, passes through a maximum. and drops by orders of magnitude as temperature is lowered further. At a temperature corresponding to the Hall maximum, the resistivity slope sharply changes to a much smaller value **; the resistivity continues to increase at this small constant rate as temperature is decreased further [63, 64]. Systematic observations followed, with the anomalies being observed not only in germanium [49, 65, 66, 76], but also in silicon [50, 51], indium antimonide [52, 53, 67, 77], and cadmium sulfide [55]. These anomalies are illustrated for gallium-doped germanium in Fig. 4.

For germanium samples having less than about 2.5×10^{16} carriers

---

* Private communication.

** The sharp break in the resistivity curve was first observed in 1949 during the course of an investigation [74] of the resistivity of a germanium rod; the break occurred near 5° K.

per cm^3 the maximum occurs in the neighborhood of 5° to 6° K. The maximum shifts toward higher temperatures as the carrier concentrations increase. This shift is particularly noticeable in germanium samples having concentrations above 10^{17} per cm^3. Qualitatively, the behavior of the Hall curves in silicon, indium antimonide, cadmium

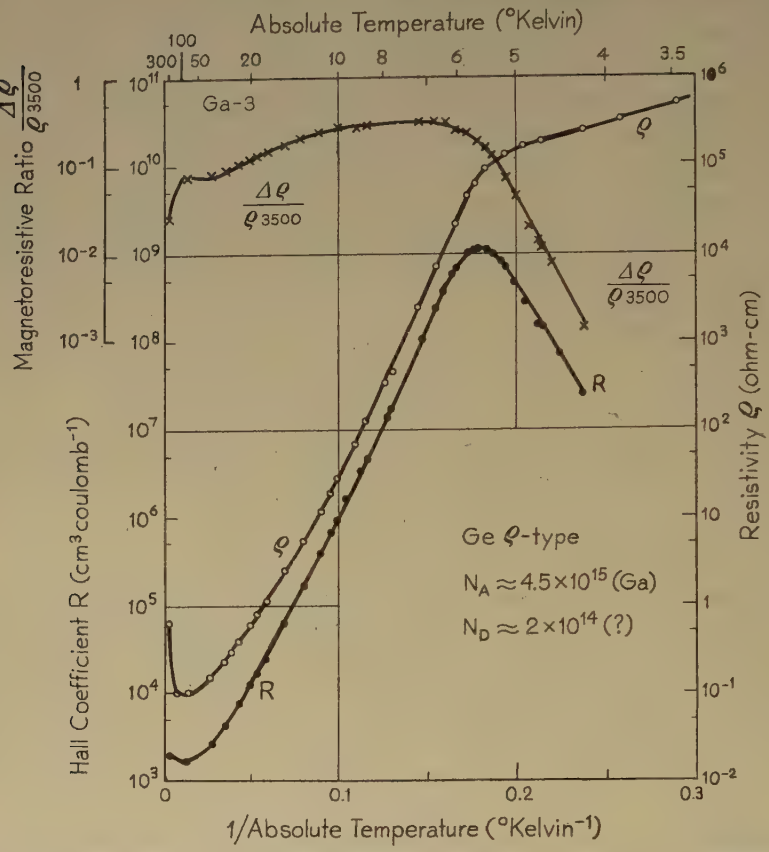

Fig. 4. Comparison of the temperature behaviors of the Hall coefficient, resistivity, and magnetoresistive ratio for a P-type (gallium-doped) germanium sample (taken from H. Fritzsche and K. Lark–Horovitz, ref. 65).

sulfide, and silicon carbide is the same, except that the maxima occur at higher temperatures than in germanium.

The conductivity of germanium in the low temperature range may be represented empirically by an equation of the type [66]:

$$\sigma = C_1 e^{-E_1/kT} + C_2 e^{-E_2/kT} + C_3 e^{-E_3/kT}, \qquad (19)$$

with subscript 1 referring to the exponential section at high temperatures, 2 to the middle portion (observed only for samples having concentrations between 2.5×10^{16} cm^{-3} and 1.2×10^{17} cm^{-3}), and 3 to the lowest temperature portion. E_1 is practically constant for all germanium samples having the same kind of impurity but changes somewhat with the nature of the impurity. C_1 depends on the amount of impurity present. C_2 is practically constant from sample to sample, but E_2 decreases strongly with increasing impurity concentration. E_3 *, corresponding to the slope at the lowest temperatures, is practically independent of concentration and is very much smaller than E_1. C_3 increases markedly with increasing impurity content.

In order to explain the low temperature anomalies in germanium. Hung [79] used the concept of conduction in an impurity band. Conduction is supposed to occur in parallel in the conduction (or valence) band and a band formed by the overlapping states of the impurity centers. As temperature approaches very low values, the carrier density in the conduction band drops markedly and thus the impurity band conduction dominates. Although several authors [78, 80, 83, 88] have considered impurity band conduction, the theory of this type of conduction is not well developed. The Hung model is based upon the assumptions that (1) the conductivity may be represented by

$$\sigma = n_C e \mu_C + n_D e \mu_D, \tag{20}$$

where suscript C refers to the conduction (or valence) band and D to the donor (or acceptor) band, and (2) the Hall coefficient may be written

$$R = \frac{1}{e} \frac{r_C n_C \mu_C^2 + r_D n_D \mu_D^2}{(n_C \mu_C + n_D \mu_D)^2}, \tag{21}$$

where it is expected that r_C and r_D do not differ widely from unity. If $r_C \approx r_D$, it may be seen that the maximum in the Hall curve occurs when

$$n_C \mu_C = n_D \mu_D. \tag{22}$$

At higher temperatures $\mu_D \ll \mu_C$ and n_C is comparable with or greater than n_D, so that

$$\sigma = n_C e \mu_C, \quad R = \frac{r_C}{n_C e}. \tag{23}$$

* According to the latest experiments E_3 is, within the experimental error, the same for gallium- and antimony-doped germanium samples of comparable impurity concentrations.

However, at temperatures lower than that at which the Hall maximum occurs, $n_C \ll n_D$ becuase there is not sufficient thermal energy available to excite an appreciable number of electrons into the conduction band. Below the Hall maximum $n_C e\mu_C < n_D e\mu_D$ and at exceedingly low temperatures

$$\sigma = n_D e \mu_D, \quad R = \frac{r_D}{n_D e}. \tag{24}$$

Since n_D at $T \to 0°$ K equals n_C in the exhaustion range, one expects R near 0° K to be close in value to the exhaustion range value of R [63, 64]. Estimates of μ_D from the very low temperature conductivity indicate that μ_D increases with increasing impurity concentration. In all experiments in germanium and indium antimonide the sign of the Hall coefficient is preserved *.

The impurity band model is not the only possible way of explaining the observed phenomena. Models based upon surface levels, dislocation levels, or crystal inhomogeneities have been briefly discussed [65, 55]. In 1935 Gudden and Schottky [87] pointed out that there is a finite probability of carriers tunneling from a full level to an empty level without being excited into the conduction band. The transition probability increases with the concentration of levels. At high carrier concentrations this process can be linked to the overlapping of wave functions and the forming of an impurity band [78, 80]. At low impurity concentrations the overlap of the wave functions is so small that band formation is not conceivable. One could still calculate an exchange term giving the frequency with which carriers are exchanged between impurity atoms. However, exchange of carriers does not transport charge. The transfer of charge requires a probability that the electrons can jump from occupied to unoccupied impurity centers. Thus the probability of jumping depends both on the separation and concentration of unoccupied centers. It is reasonable to take this concentration as equal to the concentration of compensated minority impurities (i.e. N_A in an n-type sample). Schottky [85] pointed out that, since the polarization of the lattice in the neighborhood of an occupied impurity center differs from that in the neighborhood of an unoccupied center, one of the centers must be excited by an amount

* The thermoelectric power of a silicon sample reverses sign at a temperature for which impurity band conduction is suspected [84]. However, in compensated samples such a reversal was not observed.

equal to the difference in polarization energies before a carrier jump is possible. Tentatively he identifies the three activation energies [Eq. (19)] as: E_1 with ionization into the conduction band, E_2 with excitation to excited states, and E_3 with the lattice activation energy (also ref. 90).

In this range the transverse magnetoresistive ratio shows an unusual behavior. Since the mobility becomes quite low in the impurity band conduction range and the transverse magnetoresistive ratio is, in first approximation, proportional to the square of the mobility, the magneto-resistivity of germanium and indium antimonide was investigated in the neighborhood of the Hall maxima. Fig. 4 shows a typical result for germanium [65, 66]; the magnetoresistive ratio passes through a maximum at about the temperature of the Hall maximum and resistivity break and then decreases as temperature decreases still further. The behavior in indium antimonide [52] (Fig. 5) is still more peculiar: the magnetoresistive ratio passes through a maximum at a temperature a little higher than that of the Hall maximum and then, with lowered temperature, not only decreases but reverses sign to become negative. However, applying higher electric fields ($E \approx 40$ V/cm) and producing breakdown in this region [95] leads to positive magnetoresistance in p-type indium antimonide. This is understandable if one assumes that free carriers (holes) are excited into the valence band by a multiplication process. The ratio of longitudinal to transverse magnetoresistances varies with temperature: at 78° K, when the carriers are all free, the longitudinal effect is only 9 % of the transverse effect. At 4.2° K the longitudinal effect is almost equal to the transverse effect and both are negative *. In n-type indium antimonide the longitudinal and transverse magnetoresistance are also of the same order of a magnitude at 4.2° K, but they are positive **.

* An attempt to understand the negative magnetoresistance by assuming a change in population of levels [91, 92] in the magnetic field is hardly applicable to the observed case, since it deals with carriers in the conduction band, not in the impurity band.

** Entirely different magnetoresistive anomalies not in the impurity band have been observed in very pure germanium at low temperature and high magnetic field [93, 94]. At 20000 gauss a magnetoresistive ratio of 1200 % was observed. Even oscillations of magnetoresistance were observed at 10° K, equidistant if plotted against $1/H$. On the other hand, magnetic susceptibility measurements on pure samples give a constant susceptibility in this temperature range [89].

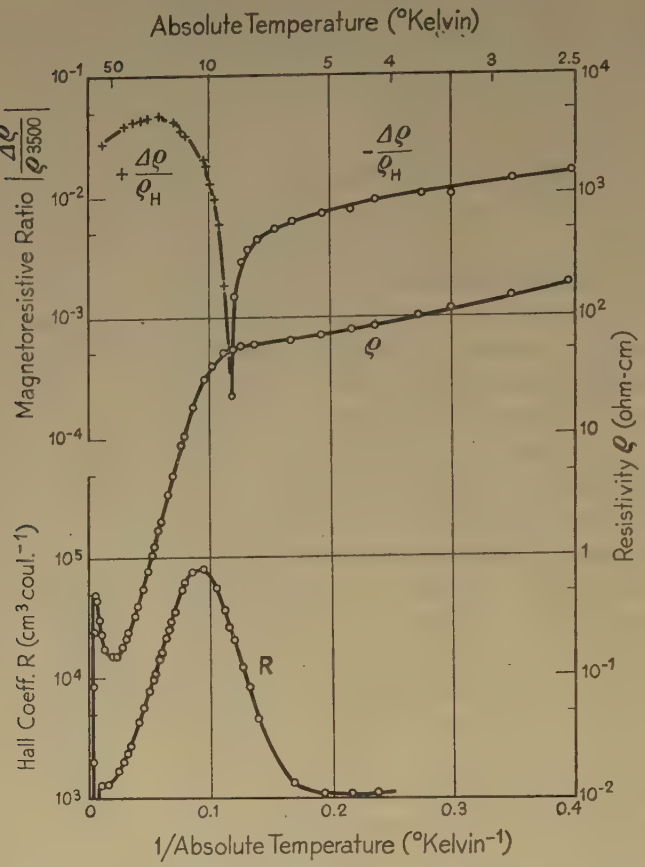

Fig. 5. Comparison of the temperature behaviors of the Hall coefficient, resistivity, and magnetoresistive ratio for a p-type sample of indium antimonide. The sign of the magnetoresistive ratio reverses in the same temperature range in which the Hall coefficient and resistivity deviate from their normal behaviors. (Curves taken from H. Fritzsche and K. Lark-Horovitz, ref. 52).

3. Microwave Absorption

The experimental arrangement [96] can be briefly described as follows: Germanium single crystal samples of suitable thickness (1 mm to 1 cm) are prepared to closely fit the cross section of a rectangular wave guide. Power attentuation in the sample can be found by adjusting a calibrated attentuator to give the same detected power with and without the sample in the guide. A bridge circuit is used to measure the phase shift. From the measured phase shift and

attentuation it is possible to calculate [97] the dielectric constant and conductivity at the microwave frequency.

It should be mentioned that various investigators [99, 100, 101] have studied microwave transmission in germanium at the higher temperatures (200°–300° K), but to date only the measurements of D'Altroy and Fan [98, 102, 103] have been extended to temperatures as low as 4.2° K. The dielectric constant of high purity germanium is found to be $\varepsilon_0 = 16.2 \pm 0.3$. For a p-type sample of 3 ohm-cm resistivity, the conductivity ratio $\sigma(0)/\sigma(\omega)$, i.e. the ratio of dc conductivity to conductivity at the microwave frequency ω, is unity at 200° K and 300° K, rises to 1.2 at 77° K, and to values up to 2.0 at 20° K. The free carrier contribution to the dielectric constant is negligible at 300° K, small at 200° K, but as large as -40 at 20° K. In order to make effective mass estimates, mobility values for the various samples were determined by making conductivity and Hall coefficient measurements. For the p-type samples the weighted effective mass obtained at each temperature (300°, 200°, 77°, 20° K) is about 0.33 m_0. The corresponding theoretical value is computed [98] from conductivity masses and density-of-states masses, for the two kinds of holes, which in turn are estimated from cyclotron resonance mass values. The result is 0.13 m_0, a value some 2.5 times smaller than the observed value.

The microwave effective mass value for n-type germanium is 0.16 m_0 at 20° K. This value compares well with 0.15 m_0, the computed value based on the 4.2° K cyclotron resonance mass values.

Microwave measurements in samples with high impurity content were made near 4.2° K in order to observe the effect of carriers in impurity states. Both n-type and p-type germanium samples were studied [103]. Values of dielectric constant have been obtained which are much higher than in pure crystals. The effect is attributed to the polarization of neutral impurity atoms and gives an estimate of the impurity ionization energy. The values obtained for the ionization energies in gallium- and antimony-doped samples are in fair agreement with the known ionization energies. The ratio of dc and microwave conductivities gives an estimate of the relaxation time for conduction. From the relaxation time and dc conductivity, the values of the effective mass in the impurity band were found to be of the order of 1000 m_0, a result consistent with the marked decrease in mobility observed as the conduction process shifts from the conduction to the impurity range.

4. Thermoelectric Power

The thermoelectric power of a semiconductor may be calculated from the position of the Fermi level ζ and is determined by the kind of statistics applicable and the energy dependence of the mean free path [104, 105]. If classical statistics are applicable and the mean free path independent of energy (lattice scattering), one obtains for an n-type semiconductor

$$Q = \frac{\zeta}{eT} - \frac{2k}{e}, \tag{24}$$

where Q represents the thermoelectric power and ζ the Fermi level, measured negative downard from the bottom of the conduction band. If impurity scattering dominates so that the mean-free-path may be taken as proportional to the square of the carrier kinetic energy, Eq. (24) is replaced by

$$Q = \frac{\zeta}{eT} - \frac{4k}{e}. \tag{25}$$

However, as was pointed out first by Gurevich [106], there exists an additional contribution to the thermoelectric power, a term due to the "drag" of electrons by the phonon current created by the temperature gradient, a phenomenon frequently referred to as the Gurevich effect. This effect is due to the asymmetrical scattering of the electron current by the lattice vibrations as perturbed by the temperature gradient, so that the electrons are preferentially pushed toward the cold end. The direction of the thermoelectric field caused by the Gurevich effect is such as to increase the magnitude of the thermoelectric power. Thus the thermoelectric power at low temperatures may be written as

$$Q = Q_e + Q_\phi, \tag{26}$$

where Q_e is the electronic contribution of the type given in Eq. (24) and (25) and Q_ϕ is the contribution arising from the phonon drag. Gurevich derived an expression for metals, not for semiconductors. An early estimate [107] of the importance of the Gurevich effect for semiconductors leads to

$$\frac{Q_\phi}{Q_e} \approx \frac{3 l_\phi u k T}{l_e \bar{v} |\zeta|}, \tag{27}$$

where l_ϕ is the phonon mean free path as a result of the interaction of phonons with each other, l_e is the electron mean free path, u the sound velocity and $\bar{v}$ the average electron velocity. This result is difficult to apply because of the uncertainty in the ratio l_ϕ/l_e.

Recent measurements [84, 108, 109, 110] of the thermoelectric power of

germanium and silicon samples between 300° K and 10° K show that below about 200° K the magnitude of the thermoelectric power is much greater than the Q_e value predicted by Eq. (25), and thus one is led to the belief that the Q_ϕ term is important in semiconductors and even dominant at the lower temperatures.

Theoretical discussions [108, 111, 112] give results for Q_ϕ/Q_e that are more complicated than Eq. (27) but still depend on l_ϕ/l_e as the quantity determining the relative importance of Q_ϕ. Herring [113] has made an extensive study of phonon-phonon collisions, from which he is able to ascertain the temperature and momentum dependences of l_ϕ. The temperature dependence of Q_ϕ is estimated as proportional to $T^{-7/2}$. This is in good agreement with the experiments of Geballe and Hull [109], who find that Q_e is practically negligible and $Q = Q_\phi$ increases in proportion to $T^{-3.2}$ as temperature drops from about 100° K in a group of high purity p-type germanium samples *.

At very low temperatures, the relaxation time associated with the scattering of phonons at the boundaries of the sample becomes shorter than the relaxation time for phonon-phonon scattering. Estimates [111] of the effect of boundary scattering yield a sharp decrease in Q_ϕ at low temperatures with the asymptotic expression for Q_ϕ approximately proportional to $T^{1/2}$. Thus Q approaches zero as temperature approaches 0° K.

Experiments [84, 108, 109, 110] show that the thermoelectric power has a maximum, usually in the 30° to 50° K range, and then decreases sharply as the temperature drops further. The theory of thermoelectric power in the region of electron drag by phonons has to be formulated [114] so that the phonon current is introduced so as to obey the Onsager reciprocal relations [115, 116].

4. Thermal Properties

1. Specific Heat

Germanium. Early measurements [117] showed a peak in the specific heat curve of germanium in the neighborhood of 80° K. Later specific

* In a discussion of the role of low frequency phonons in thermoelectricity and thermal conduction, C. Herring (International Semiconductor Conference, Garmisch, 1956) pointed out that the deviation of the experimentally observed T dependence from the ideal theoretical value $T^{-3.5}$ is due mainly to the fact that the temperature is not sufficiently small compared with the Debye temperature.

heat measurements [118] were made in the range from 4° K up to 170° K for two samples of high purity germanium, one consisting of granules and the other of a polycrystalline ingot. The results coincided with each other over the temperature range investigated and failed to disclose any peak. It was found that Θ, the Debye temperature, shows a rather large temperature variation. The behavior is similar to that

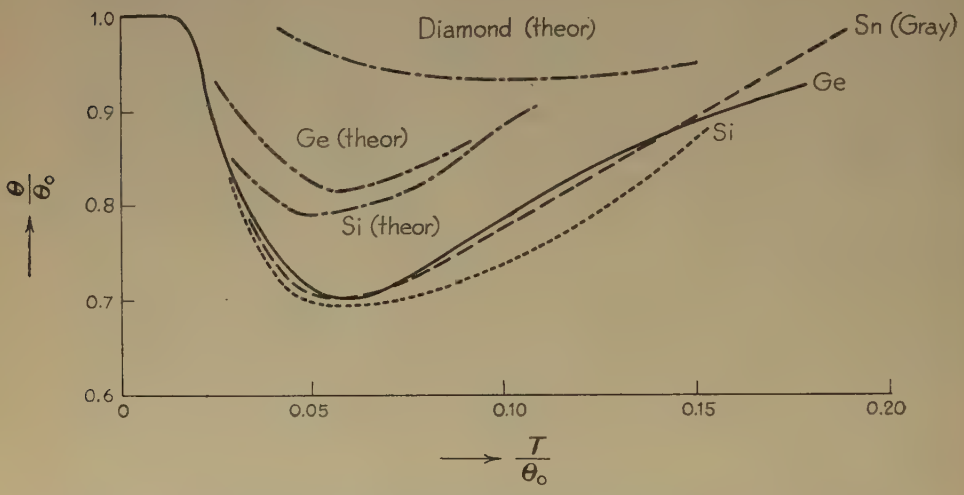

Fig. 6. Θ/Θ_0 vs T/Θ_0 for elements having the diamond lattice (The theoretical curve for diamond is from H. M. J. Smith, ref. 130, and the theoretical curves for germanium and silicon from Y. C. Hsieh, ref. 131. The experimental curves are as given by P. H. Keesom and N. Pearlman, ref. 123.)

observed in diamond *, silicon, and gray tin and is thought to be a characteristic of the diamond lattice. Figure 6 shows a plot of Θ/Θ_0 vs. T/Θ_0 for various elements having the diamond structure.

Specific heat was measured [119] from 20° K to 200° K for each of three germanium samples having, respectively, high, intermediate, and low purity. The results are identical except in the temperature range 60°–120° K, where a very small difference, just outside the experimental accuracy, was found.

Keesom and Pearlman [120, 121] extended the specific heat measurements on germanium down to 1.42° K. Their results show that the

* The minimum Θ for diamond is only about 10 % less than Θ_0, the value approached as $T \to 0°$ K, whereas the minimum Θ for silicon, germanium, and gray tin is about 30 % less than Θ_0.

true T^3 region extends up to 4° K, a value in agreement with Blackman's prediction [122] that the upper limit of the true T^3 region is at least $\Theta_0/100$. The measurements on the ingots are in substantial agreement with one another *.

Keesom and Pearlman analyzed their data on the basis that the observed specific heat C_v is the sum of a lattice specific heat proportional to T^3 and an electronic specific heat proportional to T:

$$C_v = \alpha T^3 + \gamma T. \tag{28}$$

The method of least squares was applied to the data for each sample to calculate the values of α and γ. The average value of α corresponds [123] to $\Theta_0 = (366 \pm 5)°$ K, a value in rather good agreement with the Θ value of 374° K which is calculated from the elastic constants [124, 125] of germanium. The values of γ are obtained from the intercepts of C_v/T vs T^2 plots. (Fig. 7 shows such a plot for a silicon

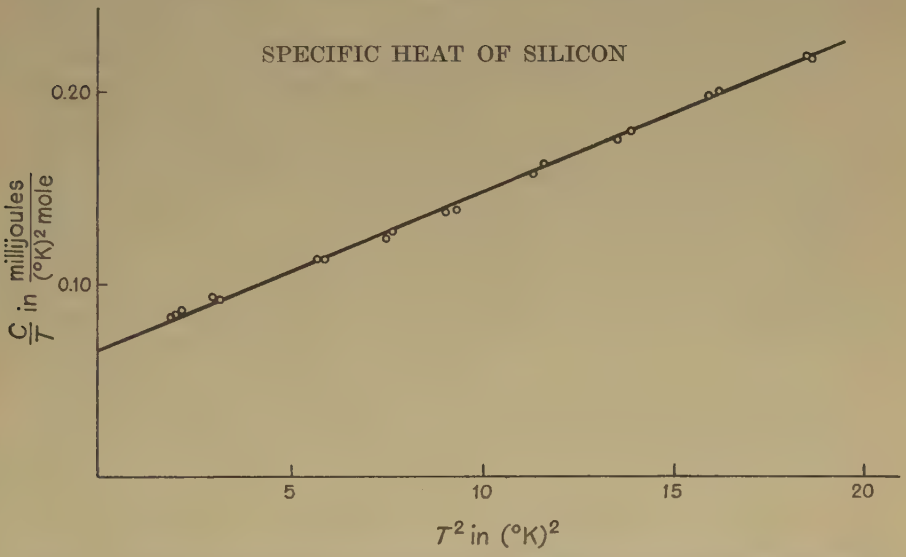

Fig. 7. C_v/T versus T^2 for a typical silicon sample. The straight line obtained indicates the validity of Eq. (28). (Plot from unpublished data of P. H. Keesom and G. M. Seidel.)

* Above 3° K there is no difference between the data for the ingots and that for the crushed germanium, but below 3° K the specific heat values for the crushed material are higher than for the ingots, a difference which is ascribed to the desorption of exchange gas from the small bits of germanium during the heating periods.

sample.) In the case of germanium these values do not differ significantly from zero and thus, even in a sample with a carrier concentration of about 10^{18} per cm^3, the electronic specific heat is negligible compared with the lattice specific heat.

Silicon. The lattice specific heat of silicon [126] shows a behavior very similar to that of germanium. Measurements made at temperatures down to 1.5° K show that the true T^3 region extends upward to about 5° K. The best current value [127] of Θ_0 for silicon is (630 ± 5)° K. This value is somewhat lower than the formerly published values [126]. Part of the discrepancy is explained on the basis of the temperature scale used in the measurements *. A value $\Theta = 648$° K is calculated from the elastic constants of silicon [129, 125].

The least squares fit of the data for a particular silicon sample yields a γ value [127] of about 6×10^{-6} joule/mole-deg^2. Since γ is a measure of the electronic contribution to the specific heat, it should increase with increasing carrier density. The theoretical expression for γ, found by treating the carriers as a degenerate electron gas, is

$$\gamma = 1.6 \times 10^{-12} N_c^{2/3} V_m n^{1/3} \mu \text{ Joule/mole-deg}^2, \qquad (29)$$

where n is the number of carriers per cm^3, N_c the number of absolute minima (or maxima) of the energy band having a multiple ellipsoid structure, V_m the molar volume in cm^3 and $\mu = (m_t^2 m_l)^{1/3}/m_0$. For p-type silicon $N_c = 1$, and, although the values of γ and n are not known sufficiently well to make an accurate determination of m^* from Eq. (29), the result is consistent with the density-of-states mass given in III, 1. In the case of n-type silicon, Eq. (29) offers an opportunity for determining whether the constant energy surface is composed of three or six ellipsoids. Substitution of the best available values of γ and n, and taking $\mu = 0.33$ indicate that N_c is more likely to be 6 than 3.

The temperature dependence ** of Θ for silicon is indicated in Fig. 6.

---

* Clement [128] pointed out that deviations of the adopted temperature scale of 1948 from the true thermodynamic scale may cause significant anomalies in calorimetric results. Consideration of the deviations led to the adoption of a 1955 temperature scale having an improved agreement with the true thermodynamic scale. The older data, reconsidered on the basis of the 1955 temperature scale, show that the originally indicated Debye temperature of 658° K should be lowered to about 630° K.

** Theoretical explanations of the temperature dependence of Θ have been attempted for elements having the diamond lattice, including diamond [130],

Gray Tin. The specific heat of gray tin has been measured [118] from 4.2° K to 110° K, and its value of Θ_0 has been found [132] to be 212° K. As may be seen from Fig. 6, the Θ/Θ_0 vs. T/Θ_0 curve for gray tin is very similar to the curves for germanium and silicon *

Graphite. Graphite crystallizes in a layer lattice, and this arrangement produces considerable anisotropy in the interatomic forces responsible for binding in the crystal. The effect of this anisotropy upon the specific heat behavior has been the subject of a number of theoretical investigations [133–142]. The general result of these computations is that the anisotropy should produce a specific heat that is directly proportional to the square of the temperature over a temperature range the predicted limits of which vary from one computation to another. At sufficiently low temperatures the specific heat should become proportional to the cube of the temperatures, but there is not agreement among calculated values of the upper limit of the T^3 region.

A number of experimental investigations [143–148] have been made in attempts to clarify the specific heat behavior of graphite. One set of data [143], when plotted as $\log C_v$ against $\log T$, yields a line of slope 2 between temperatures of 13° K and 55° K. However, another set of data [146] plotted in the same manner shows that slope changes from about 1.8 at 90° K to 2.4 at 4° K. This changing slope is also observed by Keesom and Pearlman [147, 148], who also show that below 2° K the data can be represented by an equation of the form of (28), hence presumably a lattice term proportional to T^3 and a linear term representing an electronic specific heat.

Rutile (TiO_2). The specific heat of rutile has been measured [123] down into the liquid helium region and found to be proportional to

---

germanium and silicon [131]. The method involves calculation of the vibrational frequency spectra from the elastic constants of the elements, taking into account the interaction between each atom and its nearest neighbors and, in some cases, the central-force interaction between each atom and its second neighbors. Then the specific heat and characteristic temperature may be computed as functions of temperature from the frequency spectrum. Fig. 6 includes the calculated Θ/Θ_0 plots for diamond, germanium and silicon.

* The Θ_0 value of gray tin, 212° K, is close to that of indium antimonide, which is 200° K [ref. 123]. This result is accounted for by the fact that indium antimonide has the diamond crystal structure with a lattice constant almost identical with that of gray tin, and the atomic masses of indium and antimony are both close to that of tin.

T^3 at the very low temperatures. When the rutile is slightly reduced, the specific heat in the liquid helium range is increased by a large constant term. A possible explanation of this behavior is that the conduction electrons behave as a classical gas and supply a heat capacity of $3k/2$ per electron. On this basis one can estimate a lower limit of 300 for the m^*/m_0 ratio of the conduction electrons in rutile.

2. Thermal Conductivity

In semiconductors heat is conducted by the lattice rather than by the conduction electrons. Thus one expects to correlate the thermal conductivity of a semiconductor with its lattice properties, in particular with phonon-phonon scattering, and with the limitation of mean-free-path by the size of the sample. Electronic effects are superimposed upon the lattice phenomena.

Generally speaking, as a semiconducting sample is cooled, the thermal conductivity increases with decreasing temperature until a maximum is reached at a temperature of the order of one-thirtieth of the Debye temperature; at still lower temperatures, the thermal conductivity drops sharply with falling temperatures, and appears to approach zero as the temperature approaches 0° K. Briefly, thermal resistance [149–153] arises from phonon-phonon processes and from boundary scattering, with the former dominating at high temperatures, the latter at low temperatures; and the two contributions are comparable in the neighborhood of the thermal conductivity maximum. In a crystal, for $T > \Theta$, $\varkappa$ is proportional [149, 150, 154] to $1/T$. At very low temperatures, $\varkappa$ is proportional to aT^3 if one assumes that C_v is proportional to T^3 and takes a, the mean radius of the sample, as determining the mean free path [155]. In between these extremes a more complex behavior is expected. It has also been pointed out that elastic anisotropy has a major effect in limiting the thermal conductivity of a hypothetical perfect crystal of very large size [113]. Experimental studies of the thermal conductivity of quartz, diamond, and other dielectrics confirm the major aspects of the theory [153, 156, 157].

The measurements of Rosenberg [158] made on one sample each of pure germanium and silicon produced curves of the type described in the preceding paragraph. At very low temperatures $\varkappa$ is proportional to $T^{2.4}$ for germanium * and $T^{2.5}$ for silicon. The mag-

* K. Mendelssohn pointed out to us that, for pure germanium between 0.2 and 0.7° K, the T^3 law is fulfilled.

nitude agreed sufficiently well with the prediction of Casimir [137] that $\varkappa$ depend on aT^3 so that no appreciable electronic contribution is indicated. The Purdue group [159] found that $\varkappa$ of a low purity n-type germanium sample is proportional to T^4 from 1.5° K to 4.2° K. Such a steep slope has also been found recently by Rosenberg [161]. It now appears that the most effective way of detecting electronic contributions to the thermal conductivity is to make measurements on several

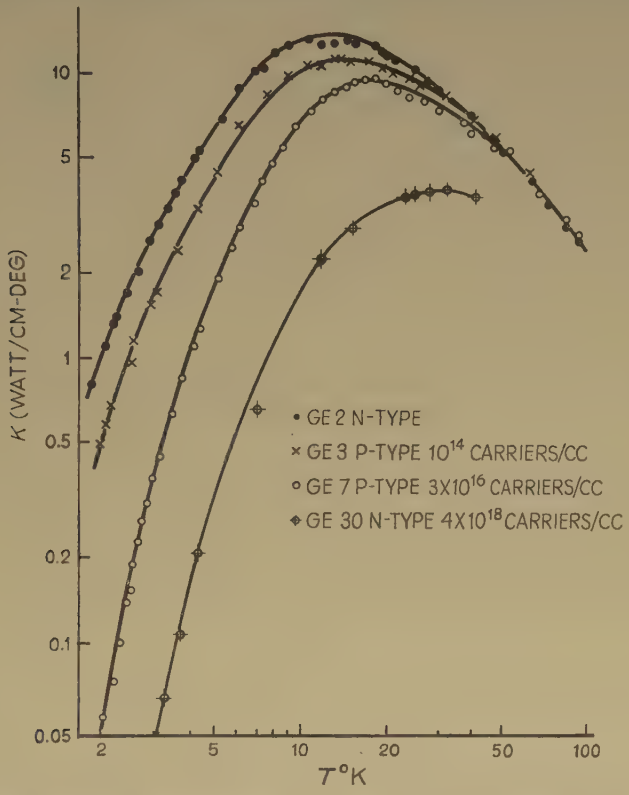

Fig. 8. The thermal conductivity of n- and p-type germanium samples of varying impurity concentrations, shown as a function of temperature. The curves of samples 2, 3, and 7 are from H. M. Rosenberg, ref. 161 and the curve for sample 30 from unpublished data of N. Pearlman and J. Goff, Purdue University.

samples of single crystal germanium or silicon, cut to the same dimensions and doped with varying amounts of the same impurity. Preliminary results [160, 161] show that both the heights of the maxima and the low temperature slopes are dependent on the impurity contents

(Fig. 8). It appears that, with increasing impurity content, the height of the maximum decreases and the low temperature slope steepens.

5. Optical Properties

1. Introduction

Low temperatures are employed in the study of optical properties primarily for the determination of energy level separations and for increased sensitivity in photoconductivity studies. The electrons which are optically excited to conduction states give a photocurrent that is large in comparison with the dark current. For example, it has been found [162] that, in indium antimonide, the photoconductive response at 5° K is about eight times the response at 85° K.

Almost all the low temperature optical investigations are concerned with the determination of the forbidden gap E_G or of the activation energy of impurity levels (ground state or excited levels). Either absorption or photoconductivity measurements may be made.

2. Forbidden Band Width

The thermal activation energy, E_G, which is measured from the temperature dependence of the intrinsic electrical conductivity, is the energy difference between the highest point of the valence band profile and the lowest point of the conduction band profile. Since these two points (Fig. 2) do not in general occur at the same momentum value, an electron must change its momentum in order to make such a transition. This is referred to as an indirect or non-vertical transition and occurs in the thermal activation case because of the transfer of momentum from or to phonons. When optical excitation involves an electron and a photon only, conservation of momentum requires that the K value remain unchanged and the transition be vertical [163]. Reference to Fig. 2 shows that the energies required for such vertical transitions are greater than E_G and the maximum wavelength of the illumination which can produce a vertical transition is correspondingly less than the wavelength corresponding to E_G. However, if a phonon is emitted or absorbed in the optical excitation process, the transition need not be vertical [163, 164].

It is known from the temperature dependence of the fundamental absorption edge, associated with the excitation of a valence electron to the conduction band, at elevated temperatures, that E_G is an approximately linear function of temperature [165, 166, 167]. It has been

found [168] that, in the range 90° K to 600° K, the energy gap can be expressed * by

$$E_G = E_0 + \beta T, \qquad (30)$$

where $E_0 = 0.77$, 1.19 eV and $\beta = -4.4 \times 10^{-4}$, -4.0×10^{-4} eV/deg for germanium and silicon, respectively. The energy gap varies quadratically with T at low temperatures as actually observed in silicon [174] and germanium [175]; also, in indium antimonide and gallium antimonide, dE_G/dT, which is approximately linear between 290° K and 100° K, falls off considerably, just as in germanium and silicon, at very low temperatures [176]. Measurement of E_G in the liquid hydrogen or liquid helium range permits extrapolation to the E_0 value if many observations at various low temperatures are available.

Indium Antimonide. One investigation [169] found the fundamental absorption edge at 5° K corresponding to about 0.25 eV, and the comparison of absorption edge positions over the range 5° K to 520° K yielded $\beta = -2.8 \times 10^{-4}$ eV/°K. Another group [170] found $E_G = 0.23$ eV at 15° K and $\beta = -2.5 \times 10^{-4}$ eV/°K over the range 15° K to 307° K. Measurements down to 9.2° K show at no temperature a difference between very high purity n- and p-type indium antimonide.

Gallium antimonide. Measurement [171] of the absorption spectrum at 300° K, 80° K, and 10° K yielded $\beta = -3.5 \times 10^{-4}$ eV/°K and $E_0 \approx 0.77$ eV. Measurements to 4.2° K yields 0.787 eV for pure and 0.798 eV for impure material; however, experimental errors make further experiments necessary before definite conclusions can be reached.

Aluminium antimonide. Absorption measurements [172] at 300° K, 85° K, and 14° K indicated that $E_0 = 1.6$ eV and $\beta = -3.5 \times 10^{-4}$ eV/°K.

Magnesium stannide. Infrared absorption [173] at 5° K, 85° K and 300° K gave $E_0 = 0.33$ eV for two samples and 0.30 eV for a third. The shift of the absorption edge with temperature indicated that $\beta = -3.5 \times 10^{-4}$ eV/°K. An E_G value of 0.30 eV corresponds, in all three samples, to the wavelength at which the photoresponse has fallen to one-half of its maximum value.

Silicon and germanium. Recent measurements [174] of the infrared absorption of fairly high purity silicon in the neighborhood of the

* In most cases β is negative, but in the lead compounds and tellurium it is positive.

fundamental absorption edge at seven temperatures between 20° K and 333° K yields a plot of E_G vs. T which extrapolates to $E_0 = 1.14$ eV. Similar absorption measurements [175] were made on germanium at seven temperatures from 4.2° K to 291° K and give an E_0 value of about 0.73 eV. In both cases dE_G/dT drops sharply at low temperatures.

In both germanium and silicon radiation has been obtained [177, 178] by carrier injection. Since the radiation at room temperature is sharply peaked at a wavelength which corresponds to estimates of the E_G value, it is assumed that this radiation is due to the direct recombination of excess electrons and holes. In the case of germanium [177] the recombination radiation has been observed at temperatures down into the liquid hydrogen range. This data yields $E_G = 0.72$ eV and an average β of the order of -10^{-4} eV/°K.

3. Activation Energies Associated with Impurity Levels

If optical excitation of carriers to conducting states from impurity levels is to exist, the sample must be at a temperature low enough so that carriers are bound to impurity levels in the absence of radiation. This may well require cooling to temperatures in the liquid hydrogen or helium ranges if the impurity ionization energies are very small.

One group [179] has studied photoconductivity, arising from photoionization of bound charge carriers, at liquid helium temperature in germanium doped with antimony, copper, indium, and zinc. The wavelength used did not exceed 38 micron and so the results were limited to detection of impurity activation energies greater than 0.033 eV. On the basis of electrical measurements of E_D or E_A, one expects the long-wavelength-limit of photoconductive response to occur near 120 micron for germanium doped with group III or V impurity elements (E_A or $E_D \approx 0.01$ eV), near 40 micron for zinc-doped germanium ($E_A \approx 0.031$ eV), and near 31 micron for copper-doped germanium. In the case of the copper-doped material, the photoresponse extends only to 29 microns, corresponding to $E_A \approx 0.043$ eV, a value in good argument with the electrical value [180]. Another group [181] studied the absorption as well as the photoconductivity in copper-doped germanium at liquid helium temperature, both of which gave a long wave-length threshold corresponding to the value of E_A determined electrically. Photoconductivity in gold-doped p-type germanium was also studied in the liquid helium range,

showing a threshold attributable to an energy level 0.15 eV above the valence band as found by Dunlap [49] and the Purdue group [181]. Dunlap also found an energy level 0.2 eV below the conduction band. The 0.15 eV ionization energy has also been detected as the cut-off in a photoconductivity curve measured [182] at 22° K.

Resistivity-temperature measurements [183] have shown that gold acts as a donor or hole trap in silicon and produces a level at 0.33 eV above the filled band. The photoconductivity of gold-doped silicon has been studied [184] at 195° K, 77° K and 20° K. The form of the curves at both 77° K and 20° K suggests a simple photoionization process with an optical activation energy of 0.32–0.33 eV. Resistivity-temperature measurements [185] yield ionization energies near 0.05 eV for all III and V impurities in silicon except for indium, which produces an acceptor level 0.16 eV above the valence band. The absorption spectrum of an indium-doped silicon sample [186] at 21° K shows an impurity level at about 0.16 eV above the valence band.

Optical absorption by neutral impurities may produce transitions from the ground state of the impurity center to higher energy states, corresponding to optical excitations of the bound charge carriers in addition to transitions from the ground state to the conduction band, which correspond to photoionization of bound charge carriers [179]. The detection of these excited states is most readily accomplished through low temperature optical investigations. On the basis of the hydrogen-like model, one predicts the existence of discrete excited levels. Such levels are indicated by the presence of relatively sharp absorption lines in the spectra of doped materials at low temperatures. Newman [186] found two such lines in indium-doped silicon at 0.147 eV and 0.152 eV. These lines are scarcely resolvable at 74° K but quite sharp at 22° K. The broadening, with rising temperature, of lines associated with optical transitions between bound states of trapped holes or electrons that are approximately hydrogenic in character has been discussed at length [187].

Kaiser and Fan [180] introduce the excitation of electrons or holes to such excited states as a possible mechanism for the explanation of the transmission vs wave number curves observed at long wavelengths in both *n*- and *p*-type indium antimonide.

Exciton absorption, which appears as a series of lines near the main optical absorption edge occurring in the red end of the visible region, has been observed [188, 189] in cuprous oxide crystals at tempera-

tures from 2° K to 77° K. The observed lines may be fitted empirically to a hydrogen-like series formula with high accuracy [189]. *

Another phenomenon is the appearance of structure in the absorption curve for p-type germanium due to transitions between the degenerate bands composing the valence band (c.f. Fig. 2). Such transitions are used by Kahn [190] to explain the absorption vs wavelength plots of Kaiser, Collins, and Fan [191], especially the curve measured near 5° K. The theory of this effect, as well as of other absorption phenomena, is discussed at length by Fan [192].

The authors are indebted to the members of the Solid State group at Purdue University for discussion and criticism of the manuscript and for making available unpublished results.

GENERAL REFERENCES

1 Harvey Brooks, Theory of the Electrical Properties of Germanium and Silicon, Advances in Electonics, **7**, 87 (1955).
2 E. Burstein and Paul H. Egli, The Physics of Semiconductor Materials, Advances in Electronics, **7**, 1 (1955).
3 G. Busch and U. Winkler, Bestimmung der Charakteristischen Grössen eines Halbleiter aus Elektrischen, Optischen, und Magnetischen Messungen, Ergeb. d. exakt. Wissensch., **29**, 145 (1956).
4 H. Y. Fan, Valence Semiconductors in Vol. I of Solid State Physics, edited by F. Seitz and D. Turnbull, Academic Press, New York, (1955).
5 Charles Kittel, Introduction to Solid State Physics, John Wiley and Sons, New York, (1953).
6 K. Lark-Horovitz, The New Electronics in The Present State of Physics, Am. Assoc. Adv. of Sci., (1954).
7 O. Madelung, Semiconductors, Vol. 20, Encyclopedia of Physics, Springer, Berlin, (1956).
8 W. Shockley, Electrons and Holes in Semiconductors, D. van Nostrand Co., New York, (1950).
9 E. Spenke, Elektronische Halbleiter, Springer, Berlin, (1955).
10 J. E. Wertz, Nuclear and Electron Spin Resonance, Chem. Rev., **55**, 901 (1955).
11 A. H. Wilson, The Theory of Metals, Cambridge, University Press, (1953).

TEXT REFERENCES

1 W. Shockley, Electrons and Holes in Semiconductors, D. Van Nostrand Co., New York, (1950) pp. 119–134.
2 Charles Kittel, Introduction to Solid State Physics, John Wiley and Sons, New York, (1953), pp. 249–385.

* For a complete survey of exciton optical spectra down to 1.3° K, see E. F. Gross, Supplement, Nuovo Cimento III, 672–707 (1956).

[3] A. H. Wilson, The Theory of Metals, Cambridge, University Press, (1953), Chapters II and V.
[4] F. Herman, Proc. IRE, **43**, 1703 (1955).
[5] J. A. Dunajew and J. P. Maslekovitz, Zh. Eksp. Teor. Fiz., **17**, 901 (1947).
[6] For a summary of the literature up to 1953 and additional experiments, see E. Justi and H. Schulz, Zeits. f. Naturforschung, **8a**, 149 (1953).
[7] J. D. Dorfman, Dokl. Akad. Nauk USSR, **81**, 765 (1951).
[8] R. B. Dingle, Proc. Roy. Soc., A, **212**, 38 (1952).
[9] W. Shockley, Phys. Rev., **90**, 491 (1953).
[10] G. Dresselhaus, A. F. Kip and C. Kittel, Phys. Rev., **92**, 827 (1953).
[11] A. F. Kip, Physica, **20**, 813 (1954).
[12] Benjamin Lax, H. J. Zeiger, R. N. Dexter and E. S. Rosenblum, Phys. Rev., **93**, 1418 (1954).
[13] Benjamin Lax, H. J. Zeiger and R. N. Dexter, Physica, **20**, 818 (1954).
[14] G. Dresselhaus, A. F. Kip and C. Kittel, Phys. Rev., **98**, 368 (1955).
[15] R. C. Fletcher, W. A. Yager and F. R. Merritt, Phys. Rev., **100**, 747 (1955).
[16] R. N. Dexter, H. J. Zeiger and Benjamin Lax, Phys. Rev., **95**, 557 (1954).
[17] W. Shockley, Phys. Rev., **78**, 173 (1950).
[18] G. Dresselhaus, A. F. Kip and C. Kittel, Phys. Rev., **95**, 568 (1954).
[19] W. Kohn and J. M. Luttinger, Phys. Rev., **96**, 529 (1954).
[20] J. M. Luttinger and W. Kohn, Phys. Rev., **97**, 869 (1955).
[21] J. M. Luttinger, Phys. Rev., **102**, 1030 (1956).
[22] R. N. Dexter, Benjamin Lax, A. F. Kip and G. Dresselhaus, Phys. Rev., **96**, 222 (1954).
[23] R. N. Dexter and Benjamin Lax, Phys. Rev., **96**, 223 (1954).
[24] G. Dresselhaus, A. F. Kip, Han-Ying Ku, G. Wagoner and Schuyler M. Christian, Phys. Rev., **100**, 1218 (1955).
[25] G. Dresselhaus, A. F. Kip, C. Kittel and G. Wagoner, Phys. Rev., **98**, 556 (1955).
[26] Laura M. Roth and Benjamin Lax, Lincoln Laboratory Quarterly Progress Report on Solid State Research (Nov. 1, 1955), p. 37.
[27] F. Herman, Phys. Rev., **88**, 1210 (1952).
[28] F. Herman and J. Callaway, Phys. Rev., **89**, 518 (1953).
[29] F. Herman, Phys. Rev., **93**, 1214 (1954).
[30] For a discussion of spin-orbit splitting, see e.g. pp. 1719 of ref. 4.
[31] Frank Herman, J. of Electronics, **1**, 103 (1955).
[32] C. Kittel, Proc. Tenth Solvay Conf., Brussels, (1954).
[33] R. J. Elliott, Proc. Bristol Conf., p. 121, Phys. Soc., London, (1954).
[34] A. M. Portis, A. F. Kip, G. Kittel and W. H. Brattain, Phys. Rev., **90**, 988 (1953).
[35] R. C. Fletcher, W. A. Yager, G. L. Pearson, A. N. Holden, W. T. Read and F. R. Merritt, Phys. Rev., **94**, 1392 (1954).
[36] R. C. Fletcher, W. A. Yager, G. L. Pearson and F. R. Merritt, Phys. Rev., **95**, 844 (1954).
[37] A. Honig and A. F. Kip, Phys. Rev., **95**, 1686 (1954).
[38] G. Feher, R. C. Fletcher and E. A. Gere, Phys. Rev., **100**, 1784 (1955).
[39] A. Honig and J. Combrisson, Phys. Rev., **102**, 917 (1956).

[40] A. N. Holden, C. Kittel, F. R. Merrit and W. A. Yager, Phys. Rev., **77**, 147 (1949).
[41] C. H. Townes and J. Turkevich, Phys. Rev., **77**, 148 (1949).
[42] Charles P. Slichter, Phys. Rev., **99**, 479 (1955).
[43] E. Schulz–DuBois, M. Nisenoff, H. Y. Fan and K. Lark–Horovitz, Phys. Rev., **98**, 1561 (1955).
[44] H. Y. Fan and M. Nisenoff, Purdue University Progress Report, 1956 (unpublished).
[45] C. Herring, Bell System Tech. J., **34**, 237 (1955).
[46] R. N. Dexter, B. Lax and H. J. Zeiger, Lincoln Laboratory Quarterly Progress Report on Solid State Research, p. 74 (May 1, 1955).
[47] P. P. Debye and E. M. Conwell, Phys. Rev., **93**, 693 (1954).
[48] T. H. Geballe and F. J. Morin, Phys. Rev., **95**, 1085 (1954).
[49] W. C. Dunlap, Jr., Phys. Rev., **96**, 40 (1954).
[50] R. O. Carlson, Phys. Rev., **100**, 1075 (1955).
[51] F. J. Morin and J. P. Maita, Phys. Rev., **96**, 28 (1954).
[52] H. Fritzsche and K. Lark–Horovitz, Phys. Rev., **99**, 400 (1955).
[53] B. V. Rollin and A. D. Petford, J. Electronics, **1**, 171 (1955).
[54] H. N. Leifer and W. C. Dunlap, Jr., Phys. Rev., **95**, 51 (1954).
[55] F. A. Kroger, H. J. Vink and J. Volger, Philips Res. Rep., **10**, 39 (1955).
[56] Guy W. Lehman and Hubert M. James, Phys. Rev., **100**, 1698 (1955).
[57] H. Jones, Phys. Rev., **81**, 149 (1951).
[58] V. A. Johnson and K. Lark–Horovitz, Phys. Rev., **82**, 977 (1951).
[59] E. Conwell and V. F. Weisskopf, Phys. Rev., **77**, 388 (1950).
[60] H. Brooks and C. Herring, unpublished but result reported in ref. 47.
[61] R. B. Dingle, Phil. Mag., **46**, 831 (1955).
[62] C. S. Hung and V. A. Johnson, Phys. Rev., **79**, 535 (1950).
[63] C. S. Hung and J. R. Gliessman, Phys. Rev., **79**, 726 (1950).
[64] C. S. Hung and J. R. Gliessman, Phys. Rev., **96**, 1226 (1954).
[65] H. Fritzsche and K. Lark–Horovitz, Physica, **20**, 834 (1954).
[66] H. Fritzsche, Phys. Rev., **99**, 406 (1955).
[67] H. J. Hrostowski, F. J. Morin, T. H. Geballe and G. H. Wheatley, Phys. Rev., **100**, 1672 (1955).
[68] D. N. Nasledov and A. Khalilov, Zh. Tekh. Fiz., **26**, 6 (1956).
[69] J. A. Bastin and R. W. Wright, Proc. Phys. Soc. London, A, **68**, 312 (1955).
[70] K. C. Shifrin, J. Phys. USSR, **8**, 242 (1944).
[71] V. A. Johnson and K. Lark–Horovitz, Phys. Rev., **71**, 374, 909 (1947).
[72] R. A. Hutner, E. S. Rittner and F. K. DuPre, Philips Res. Rept., **5**, 188 (1950).
[73] V. A. Johnson and K. Lark–Horovitz, Phys. Rev., **72**, 531 (1947).
[74] A. N. Gerritsen, Physica, **15**, 427 (1949).
[75] I. Estermann and A. Foner, Phys. Rev., **79**, 365 (1950).
[76] W. C. Dunlap, Jr., Phys. Rev., **94**, 1419 (1954).
[77] J. Hatton and B. V. Rollin, Proc. Phys. Soc. London, A, **67**, 385 (1954).
[78] G. Busch and H. Labhardt, Helv. Phys. Acta, **19**, 463 (1946).
[79] C. S. Hung, Phys. Rev., **79**, 727 (1950).
[80] H. M. James and A. S. Ginzbarg, J. Phys. Chem., **57**, 840 (1953).

[81] C. Erginsoy, Phys. Rev., **80**, 1104 (1950); **88**, 893 (1952).
[82] W. Baltensperger, Phil. Mag., **44**, 1355 (1953).
[83] P. Aigrain, Physica, **20**, 978 (1954).
[84] T. H. Geballe and G. W. Hull, Phys. Rev., **98**, 940 (1955).
[85] W. Schottky, private communication (1952).
[86] W. Schottky, Manuscript of Zurich Seminar (unpublished), 1955.
[87] B. Gudden and W. Schottky, Z. Tech. Phys., **16**, 323 (1935).
[88] F. Stern and R. M. Talley, Phys. Rev., **100**, p. 1638 (1955).
[89] A. van Itterbeck, L. DeGreve and W. Duchateau, Appl. Sci. Res., B, **4**, 300 (1955).
[90] S. Koshino, J. Phys. Soc., Japan, **11**, 608 (1956).
[91] I. M. Mackintosh, Proc. Phys. Soc. London, B, **69**, 403 (1956).
[92] K. W. H. Stevens, Proc. Phys. Soc. London, B, **69**, 406 (1956).
[93] G. Lautz and W. Ruppel, Z. f. Naturforschung, **10a**, 521 (1955).
[94] G. Lautz and W. Ruppel, Physikalische Verhandlungen, **6**, 193 (1955).
[95] R. Bray, Phys. Rev., **100**, 1262 (1955).
[96] F. A. D'Altroy and H. Y. Fan, Proc. Nat'l Electronics Conf., **8**, 522 (1952).
[97] See, e.g., C. G. Montgomery, Techniques of Microwave Measurement, Radiation Laboratory Series, Vol. 11, Ch. 10, McGraw–Hill, New York (1947).
[98] F. A. D'Altroy and H. Y. Fan, Purdue University Quarterly Report to the U.S. Signal Corps (1956).
[99] T. S. Benedict and W. Shockley, Phys. Rev., **89**, 1152 (1953).
[100] T. S. Benedict, Phys. Rev., **91**, 1565 (1953).
[101] J. M. Goldey and S. C. Brown, Phys. Rev., **98**, 1761 (1955).
[102] F. A. D'Altroy and H. Y. Fan, Phys. Rev., **94**, 1415, 1405 (1954).
[103] F. A. D'Altroy and H. Y. Fan, Phys. Rev., **100**, 1260 (1955).
[104] M. Bronstein, Physik. Zeits. Sowjetunion, **2**, 28 (1932).
[105] R. H. Fowler, Proc. Roy. Soc. London, A, **140**, 505 (1933); Statistical Mechanics, Cambridge, (1936), Sec. 11.74–11.81.
[106] L. Gurevich, J. Physics (USSR), **9**, 477 (1945); **10**, 67, 174 (1946).
[107] G. E. Pikus, Zh. Eksp. Teor. Fiz., **21**, 852 (1951).
[108] H. P. R. Frederikse, Phys. Rev., **92**, 248 (1953).
[109] T. H. Geballe and G. W. Hull, Phys. Rev., **94**, 1134 (1954).
[110] E. Mooser and S. B. Woods, Phys. Rev., **97**, 1721 (1955).
[111] C. Herring, Phys. Rev., **96**, 1163 (1954).
[112] D. ter Haar and A. Neaves, Physica, **20**, 995 (1954); Proc. Roy. Soc. London, A, **228**, 575 (1955).
[113] C. Herring, Phys. Rev., **95**, 954 (1954).
[114] E. H. Sondheimer, Proc. Roy. Soc. London, A, **234**, 391 (1956).
[115] L. Onsager, Phys. Rev., **37**, 405 (1931); **38**, 2265 (1931).
[116] S. R. de Groot, Thermodynamics of Irreversible Processes, Interscience Publishers, New York, (1951), Ch. VIII.
[117] S. Cristesu and F. Simon, Z. Physik Chem., B, **25**, 273 (1934).
[118] R. W. Hill and D. H. Parkinson, Phil. Mag., **43**, 309 (1952).
[119] I. Estermann and J. R. Weertman, J. Chem. Phys., **20**, 972 (1952).
[120] P. H. Keesom and N. Pearlman, Phys. Rev., **85**, 730 (1952).

[121] P. H. Keesom and N. Pearlman, Phys. Rev., 91, 1347 (1953).
[122] M. Blackman, Rept. Progr. Phys., 8, 11 (1941).
[123] P. H. Keesom and N. Pearlman, Low Temperature Heat Capacity of Solids, Vol. 14, p. 282, Encyclopedia of Physics, Springer, Berlin, (1956).
[124] W. L. Bond, W. P. Mason, H. J. McSkimin, K. M. Olsen and G. K. Teal, Phys. Rev., 78, 176 (1950).
[125] Jules DeLaunay, J. Chem. Phys., 24, 1071 (1956).
[126] N. Pearlman and P. H. Keesom, Phys. Rev., 88, 398 (1952).
[127] P. H. Keesom, private communication; P. H. Keesom and G. Seidel, Purdue University Quarterly Progress Report to the U. S. Signal Corps., 1956, p. 61.
[128] J. R. Clement, Phys. Rev., 93, 1420 (1954).
[129] An earlier value of 653° K was obtained by H. J. McSkimin, W. L. Bond, E. Buehler and G. K. Teal, Phys. Rev., 83, 1080 (1951).
[130] H. M. J. Smith, Trans. Roy. Soc. London, A, 241, 105 (1948).
[131] Y. C. Hsieh, Phys. Rev., 85, 730 (1952); J. Chem. Phys., 22, 306 (1954).
[132] F. J. Webb and J. Wilks, Proc. Roy. Soc. London, A, 230, 549 (1955).
[133] K. Komatsu and T. Nagamiya, J. Phys. Soc. Japan, 6, 438 (1951).
[134] V. V. Tarassov, C. R. Acad. Sci. USSR, 46, 20, 110 (1945).
[135] R. W. Gurney, Phys. Rev., 88, 465 (1952).
[136] P. G. Klemens, Australian J. Physics, 6, 405 (1953).
[137] J. Krumshansl and H. Brooks, J. Chem. Phys., 21, 1663 (1953).
[138] H. B. Rosenstock, J. Chem. Phys., 21, 2064 (1953).
[139] T. Nagamiya and K. Komatsu, J. Chem. Phys., 22, 1457 (1954).
[140] K. Komatsu, J. Phys. Soc. Japan, 10, 346 (1955).
[141] G. F. Newell, J. Chem. Phys., 23, 2431 (1955).
[142] Akio Yoshimori and Yoshiharu Kitano, J. Phys. Soc. Japan, 11, 352 (1956).
[143] W. DeSorbo and W. W. Tyler, J. Chem. Phys., 21, 1660 (1953).
[144] W. DeSorbo, J. Chem. Phys., 23, 1970 (1955).
[145] W. DeSorbo and W. W. Tyler, Bull. Am. Phys. Soc., 1, 31 (1956).
[146] U. Bergenlid, R. W. Hill, F. J. Webb and J. Wilks, Phil. Mag., 45, 851 (1954).
[147] N. Pearlman and P. H. Keesom, Phys. Rev., 98, 1539 (1955).
[148] P. H. Keesom and N. Pearlman, Phys. Rev., 99, 1119 (1955).
[149] P. Debye, Vorträge uber die Kinetische Theorie der Materie und der Elektrizität, Teubner, Berlin, (1914), pp. 19–60.
[150] R. Peierls, Annalen der Physik, Leipzig, 3, 1055 (1929).
[151] I. Pomeranchuk, J. Phys. USSR, 4, 259, 357 (1941); 6, 237 (1942); Phys. Rev., 60, 820 (1941).
[152] P. G. Klemens, Proc. Roy. Soc. London, A, 208, 108 (1951).
[153] R. Berman, Advances in Physics, 2, 103 (1953); an extensive review.
[154] Leibfrid and Schloemann, Gottingen Akad II A, No. 4, p. 71 (1954).
[155] H. B. G. Casimir, Physica, 5, 495 (1938).
[156] R. Berman, Proc. Phys. Soc. London, A, 65, 1029 (1952).
[157] R. Berman, F. E. Simon and J. M. Ziman, Proc. Roy. Soc. London, A, 220, 171 (1953).
[158] H. M. Rosenberg, Proc. Phys. Soc. London, A, 67, 837 (1954).
[159] E. Fagen, J. Goff and N. Pearlman, Phys. Rev., 94, 1415 (1954).

160 G. W. Hull and T. H. Geballe, Phys. Rev., **96**, 846 (1954).
161 H. M. Rosenberg, Conférence de Physique des Basses Températures, p. 464, Paris, (1955).
162 H. P. R. Frederikse and R. F. Blunt, Proc. I.R.E., **43**, 1828 (1955).
163 L. H. Hall, J. Bardeen and F. J. Blatt, Phys. Rev., **95**, 559 (1954).
164 J. Bardeen, F. J. Blatt and L. H. Hall, paper presented to the Conference on Photoconductivity held in Atlantic City, 1954, to be published in the Conference Proceedings.
165 H. Y. Fan, Phys. Rev., **78**, 808 (1950); **82**, 900 (1951).
166 T. S. Moss, Phys. Rev., **79**, 1011 (1950).
167 H. Y. Fan and M. Becker, Semiconducting Materials, p. 132, Butterworth's, London, (1951).
168 H. Y. Fan, M. Shepherd and W. Spitzer, paper presented to the Conference on Photoconductivity held in Atlantic City, 1954, to be published in the Conference Proceedings.
169 W. Kaiser and H. Y. Fan, Phys. Rev., **94**, 1431 (1954); **98**, 966 (1955).
170 R. G. Breckenridge, R. F. Blunt, W. R. Hosler, H. P. R. Frederikse, J. H. Becker and W. Oshinsky, Phys. Rev., **96**, 571 (1954).
171 R. F. Blunt, W. R. Hosler and H. P. R. Frederikse, Phys. Rev., **96**, 576 (1954).
172 R. F. Blunt, H. P. R. Frederikse, J. H. Becker and W. R. Hosler, Phys. Rev., **96**, 578 (1954).
173 R. F. Blunt, H. P. R. Frederikse and W. R. Hosler, Phys. Rev., **100**, 663 (1955).
174 G. G. Macfarlane and V. Roberts, Phys. Rev., **98**, 1865 (1955).
175 G. G. Macfarlane and V. Roberts, Phys. Rev., **97**, 1714 (1955).
176 V. Roberts and J. E. Quarrington, J. Electronics, **1**, 153 (1955).
177 J. R. Haynes and H. B. Briggs, Phys. Rev., **86**, 647 (1952).
178 J. R. Haynes, Phys. Rev., **98**, 1866 (1955).
179 E. Burstein, J. W. Davisson, E. E. Bell, W. J. Turner and H. G. Lipson, Phys. Rev., **93**, 65 (1954).
180 F. J. Morin and J. P. Maita, Phys. Rev., **90**, 337 (1953).
181 W. Kaiser and H. Y. Fan, Phys. Rev., **93**, 911, 977 (1954).
182 Roger Newman, Phys. Rev., **94**, 278 (1954).
183 E. A. Taft and F. Hubbard Horn, Phys. Rev., **94**, 1530 (1954).
184 R. Newman, Phys. Rev., **94**, 1530 (1954).
185 F. J. Morin, J. P. Maita, R. G. Schulman and N. B. Hannay, Phys. Rev., **96**, 833 (1954).
186 R. Newman, Phys. Rev., **99**, 465 (1955).
187 Melvin Lax and Elias Burstein, Phys. Rev., **100**, 592 (1955).
188 Y. F. Gross and N. A. Karryev, Dokl. Akad. Nauk SSSR, **84**, 261 (1952); Y. F. Gross and B. P. Zakharchenya, Dokl. Akad. Nauk SSSR, **90**, 745 (1953); Gross, Zakharchenya and Reinov, Dokl. Akad. Nauk SSSR, **92**, 265 (1953).
189 J. H. Apfel and L. N. Hadley, Phys. Rev., **100**, 1689 (1955).
190 A. H. Kahn, Phys. Rev., **97**, 1647 (1955).
191 W. Kaiser, R. J. Collins and H. Y. Fan, Phys. Rev., **91**, 1380 (1953).
192 H. Y. Fan, Infrared Absorption in Semiconductors, to appear in Progress in Physics, (1956).

CHAPTER VIII

THE DE HAAS-VAN ALPHEN EFFECT

BY

D. SHOENBERG

ROYAL SOCIETY MOND LABORATORY, CAMBRIDGE

CONTENTS: 1. Introduction, 226. — 2. Theory, 230. — 3. Comparison of theory with experiment, 238. — 4. Experimental methods, 245. — 5. Survey of the results for individual metals, 256.

1. Introduction

In 1930, in the course of measurements on the magnetic susceptibility of bismuth single crystals at low temperatures, de Haas and van Alphen [1] found that the susceptibility (defined as the ratio of magnetization to field) was not constant, as is usual for feebly magnetic materials, but varied in an oscillatory manner with the field (Fig. 1). The amplitude of the oscillations diminishes as the temperature is raised and the effect disappears altogether above about 30 or 40° K. Quite soon afterwards Peierls [2] laid the basis of the theory of the effect by showing that the magnetization of a free electron gas should oscillate as the field was varied because of the quantization of the free electron orbits in a magnetic field. To account for the observed oscillations quantitatively it was necessary to suppose that the effect in bismuth was caused by very few electrons — about 10^{-5} per atom — and that the effective electron mass was much smaller than the true mass.

Peierls' theory and an extension of it by Blackman [3] to take account of anisotropy were in implicit form, which complicates comparison with experimental data; an important advance was made by Landau [4], who was able to obtain an explicit formula for the magnetization as a function of the field. A new study [5] of bismuth by means of an experimental technique more suited to the problem (measurement of torque in a uniform field rather than force in a non-uniform field), showed that Landau's formula could explain many of the observed features in remarkable detail. The comparison of the data with the formula confirmed Peierls' rough estimates of the parameters char-

acterizing the electrons in bismuth which produce the effect, and yielded more precise values. The fact that the number of electrons was much smaller than one per atom could be interpreted as meaning that just a very few electrons overflowed from a nearly full Brillouin zone into the next zone, and in these circumstances anomalous effective masses are to be expected.

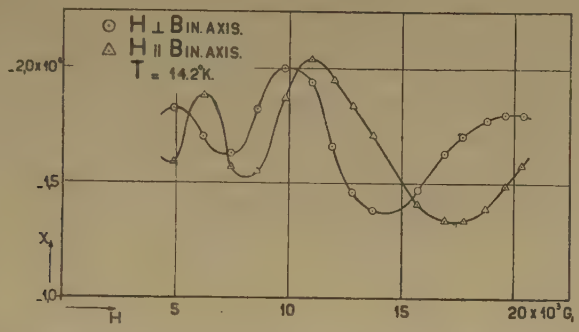

Fig. 1. The de Haas-van Alphen effect in bismuth [1]. The field H is perpendicular to the trigonal axis. χ is the ratio of magnetization per gram to H.

Such small pieces of Fermi surface of high curvature containing small numbers of electrons (or holes) should occur in any multivalent metal and a systematic investigation of the magnetic behaviour of other metals [6–13], did indeed show that the de Haas–van Alphen effect occurred in nearly every multivalent metal examined, and was not, as seemed at one time possible, an effect characteristic only of bismuth. Some of the rich variety of features found in the various metals is illustrated in Fig. 2; leaving aside for the moment any detailed discussion of the curves, the important point to be made here is that the number of electrons concerned is always small – at most 10^{-3} per atom – and the effective mass is always low. In fact it follows from Landau's formula that if the number of electrons is much higher than 10^{-3} per atom, the period of the oscillations at fields of say 20 kG would become so small that resolution would be very difficult, and also that if the effective electron mass was as great as the true electron mass, the amplitude at 20 kG would be much reduced, even at 1° K, thus making observations very difficult. Thus it is clear that measurements of de Haas–van Alphen effect at ordinary fields – say up to 20 kG – can give information only about *small* overlap regions of the Fermi surface – what might loosely be

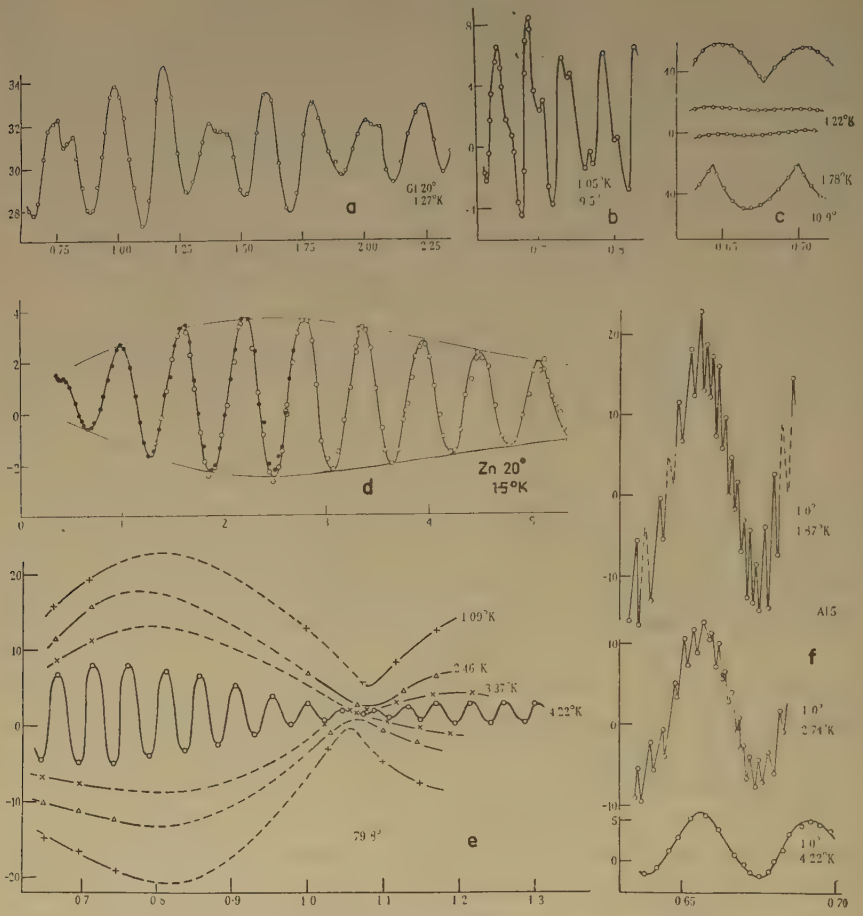

Fig. 2. Typical de Haas–van Alphen curves [7,25]. The abscissae are $10^4 \times 1/H$ (G^{-1}) and the ordinates are as explained below, where C is the couple per gram. (reproduced by courtesy of the Royal Society). The figures on each graph indicate the values of ψ and T.

(a) Graphite: ordinates $10^6 \times C/H^2 \sin\psi \cos\psi$ (ψ from hexagonal axis).

(b) and (e) Gallium, ac-plane; ordinates $10^7 \times C/H^2 \sin\psi \cos\psi$ (ψ from a-axis).

(c) Tin; ordinates $10^8 \times C/H^2 \sin\psi \cos\psi$ (ψ from tetragonal axis). The points shown are the maxima and minima of the individual oscillations; the cusp shaped envelope indicates the presence of a subsidiary period close to half of the dominant one.

(d) Zinc; ordinates $10^8 \times C/H^2$ (ψ from hexagonal axis).

(f) Aluminium; ordinates $10^8 \times C/H^2$ (ψ from a tetrad axis.) The short period oscillations are usually more complex than those illustrated here.

called the 'fine structure' of the Fermi surface. In order to get information about the larger number of electrons in monovalent metals, or contained within larger pieces of the Fermi surface in some of the multivalent metals, much larger fields are required, and special oscillographic techniques [14] have recently been developed to observe the de Haas–van Alphen effect in high fields (up to 100 kG) produced by discharging a large condenser through a coil. So far this method has been successful in detecting oscillations in lead, tin and cadmium of much shorter period than usual – corresponding to nearly 10^{-1} electrons per atom – but for reasons not yet completely understood no effect has yet been found in monovalent metals.

Landau's formula is based on the assumption that the energy surfaces in momentum space are ellipsoidal in shape. This is an assumption commonly made in the theory of metals; mathematically it is the simplest to make and it is indeed physically plausible that the energy should vary quadratically with momentum in the immediate neighbourhood of a zone boundary, but there is no reason why it should continue to vary in such a simple way further from the boundary and the de Haas–van Alphen effect offers plenty of evidence to show that the Fermi surface is not usually ellipsoidal at all. This evidence comes from the variation of the characteristic features of the oscillations – particularly the period – with the direction of the field relative to the crystal axes. If a particular form of ellipsoid (or ellipsoids) consistent with the symmetry of the crystal is assumed to represent the Fermi surface, Landau's formula makes detailed predictions as to how the period should vary with the orientation of the field. For bismuth these predictions are fulfilled remarkably closely, but for other metals considerable deviations occur and for some metals it is clear that no reasonable scheme of ellipsoids can account for the observed variations.

Recently Onsager [15] opened up an important new theoretical approach by examining what could be predicted about the magnetic behaviour of a metal with energy surfaces of arbitrary shape. He was able to show by rather general arguments that the period of the de Haas–van Alphen oscillations is inversely proportional to the extreme area of cross-section of the Fermi surface by planes normal to the field. Lifshitz and Kosevich [16] using mathematical techniques similar to those of Landau, but replacing Landau's ellipsoidal assumption by Onsager's more general formulation, have given an explicit

formula in which the effective masses which enter into Landau's formula are replaced by various geometrical features of the Fermi surface. In fact, however, the most important part of their formula is that already given by Onsager, namely the formula for the period. In principle, a knowledge of all the extreme cross-sectional areas of a surface serves to specify the surface completely (under certain simplifying assumptions) and an explicit method of calculating the radii of a centro-symmetric surface from its central cross-sectional areas has been recently given by Lifshitz and Pogorelov [17]. Since Onsager's theory enables the areas to be found from measurements of the period as a function of field direction, we see that the de Haas–van Alphen effect, from being somewhat of a scientific curiosity is thereby raised to the status of a potentially powerful tool for studying the electronic structure of metals. The first step in the application of this tool has been made by Gunnersen [18], who has worked out the shape and size of the small parts of the Fermi surface in aluminium which give rise to some of the oscillations observed in moderate fields, but much remains to be done, particularly in the domain of high field measurements, which should yield valuable information about much larger pieces of the Fermi surface.

We shall now give a rather more detailed, though still largely descriptive, account of the theory, drawing largely on Pippard's excellent exposition [19] of Onsager's idea, and indicating how it leads to the detailed general result of Lifshitz and Kosevich. Landau's formula will finally appear as a special case of the general result. This will be followed by a general account of the nature of the agreement between the theory and experiment, and of the experimental methods. Finally we shall review the results on the various individual metals from the point of view of the information they yield on the individual electronic structures. We shall not give any account of various galvano- and thermo-magnetic properties of metals, which also show an oscillatory behaviour similar to the de Haas–van Alphen effect (a recent paper by Steele [20] gives full references); the interpretation [21] of these effects is intrinsically much more complicated than that of the oscillations in magnetization.

2. Theory

The origin of the de Haas–van Alphen effect can be appreciated most simply by considering the energy levels of a two-dimensional

metal in a magnetic field applied normal to the plane of the metal. The argument was first given by Peierls [2] for a free electron gas, in which the curves of constant energy in momentum space are circles, but we shall here discuss the more general case in which the curves have the arbitrary form $E = E(\mathbf{p}')$ ($\mathbf{p}'$ is the quasi-momentum i.e. h times the wave vector). To avoid complication the effect of the magnetic moment of the electron spin will for the time being be ignored.

In a magnetic field the electrons move in curved paths and it is easily proved that the electron orbits have the same shape as the curves of constant energy in $\mathbf{p}'$-space, but are twisted through 90° and reduced in scale by the factor eH/c. This follows because a magnetic field cannot do any work on an electron, so its representative point in $\mathbf{p}'$-space must move on a curve of constant energy, and moreover with $\dot{\mathbf{p}}'$ equal to the Lorentz force $e(\mathbf{H} \times \mathbf{v})/c$, if $\mathbf{v}$ is the velocity of the electron in real space and e is the modulus of its charge in E.S.U. Quantum theory restricts the possible motions to only certain orbits, namely those that satisfy the Bohr–Sommerfeld condition

$$\int (\mathbf{p}' - e\mathbf{A}/c) \cdot \mathbf{ds} = (r + \gamma)h \tag{1}$$

where $\mathbf{A}$ is the vector potential of the field and the integration is round the orbit in real space; r is an integer and γ is a phase constant, which is $\frac{1}{2}$ for $E(\mathbf{p}') = \mathbf{p}'^2/2m$ (circular orbits). Making use of the fact that $\mathbf{p}'$, the radius vector of the constant energy curve, is just eH/c times the radius vector of the real orbit, and perpendicular to it, and of the relation

$$\int \mathbf{A} \cdot \mathbf{ds} = OH$$

where O is the area of the orbit, the quantization condition (1) becomes

$$eHO/c = (r + \gamma)h$$

or, since

$$a(E) = O(eH/c)^2$$

where $a(E)$ is the area of the curve of constant energy E in $\mathbf{p}'$-space,

$$a(E) = (r + \gamma)ehH/c. \tag{2}$$

Eq. (2), which can be regarded as an implicit equation specifying the energy levels $E_1(H)$, $E_2(H)$, ... $E_r(H)$ ... of the system, shows

that the permitted curves of constant energy are separated by equal areas ehH/c. In the absence of a magnetic field the permitted states are represented by a very close uniform distribution of points over the plane, say g per unit area, but in a magnetic field, only the states corresponding to the curves described by (2) are permitted. This means that each of the permitted energy levels must be highly degenerate, since it must contain $gehH/c$ states (i.e. the number of representative points between any two curves); the total number of states which would be occupied at absolute zero is $N = ga(E_0)$, if E_0 is the Fermi energy and N is the total number of electrons.

As the field H is increased, the curves of constant energy and also the energy levels will become more and more separated; moreover since each will be able to accommodate more and more electrons, fewer and fewer energy levels will be occupied. Consider the state of affairs at absolute zero such that the n lowest levels are fully occupied and the $(n+1)$th only partially occupied. The total energy will then be

$$U = \sum_{r=1}^{n} (gehH/c)E_r(H) + (ga(E_0) - ngeh\,H/c)E_{n+1}(H). \tag{3}$$

As soon as H is increased beyond the value for which

$$1/H = neh/ca(E_0), \tag{4}$$

the $(n+1)$th level is left completely empty and the nth level starts emptying; it is clear from the form of (3) that this will involve a discontinuity in the slope of a graph of U against H i.e. a discontinuity in the magnetization M which is $-\partial U/\partial H$. It is clear from (4) that these discontinuities must occur at equal intervals $eh/ca(E_0)$ of $1/H$, and these are just the intervals at which successive 'permitted' curves cross the Fermi curve $E = E_0$. The variation of U and M with H can be easily calculated explicitly for the special case of $\mathbf{E}(\mathbf{p}') = \mathbf{p}'^2/2m$, and the results are indicated in Fig. 3. They serve to illustrate the character of the discontinuities in U and M, and it can be seen that this simple two-dimensional model already produces some of the salient features of the observed de Haas–van Alphen effect, namely the periodic character of the fluctuations and the fact that there is a constant period in $1/H$. The amplitude of the oscillations is however much exaggerated, and this we shall see is mainly because we have ignored the third dimension of the metal.

To extend the argument to a three-dimensional metal we must regard $\mathbf{p}'$ as the component in a plane normal to H, of $\mathbf{p}$, the total quasi-momentum, and all the quantities introduced so far as referring to one particular value of p_H, the component of $\mathbf{p}$ in the direction of H; this is permissible since p_H is unaffected by H, so that all our

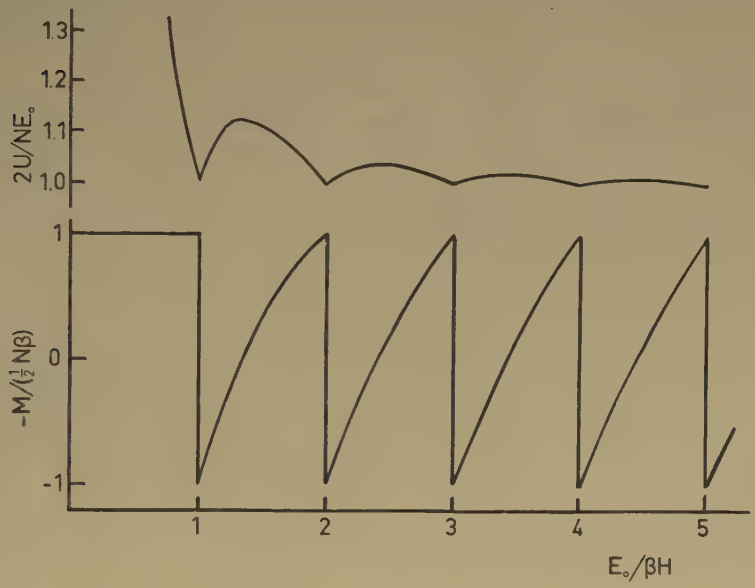

Fig. 3. Energy and magnetization of two-dimensional metal. The graphs are based on the formulae:

$$2U/NE_0 = (2r+1)\,(\beta H/E_0) - r(r+1)\,(\beta H/E_0)^2$$

$$M/(\tfrac{1}{2}N\beta) = (2r+1) - 2r(r+1)\,(\beta H/E_0)$$

These hold for $(r+1) > (E_0/\beta H) > r$, where r is any integer and β is $eh/2\pi mc$, i.e. 2 Bohr magnetons.

previous discussion of the effect on $\mathbf{p}'$ of applying a field, still holds good whatever the value of p_H. The parameter g is now to be taken as the number of states in the range $(p_H, p_H + \mathrm{d}p_H)$ i.e. $2V\mathrm{d}p_H/h^3$, if V is the volume of the metal, and we obtain

$$U = \int_{-\infty}^{\infty} \sum_{r=1}^{n} \frac{2VeH}{ch^2}\, E_r(H, p_H)\, \mathrm{d}p_H. \qquad (5)$$

The upper limit n of the summation is to be taken as the highest

value of r for which $E_r < E_0$, and n of course varies with p_H. * It will be noticed that the last two terms of (3) find no counterpart in (5); this is because there is never a partially occupied level in the sense that there was in the two-dimensional metal. In the three-dimensional metal it is the occupied range of p_H which varies with H for a given n; as H increases, this range shrinks until H is such that $E_n(H, p_H)$ just reaches E_0, and beyond this point the nth level is no longer occupied at all for the particular value of p_H concerned.

Thus with increase of field a term falls out of the integrand of (5) whenever $E_n(H, p_H) = E_0$, i.e. just as before, at intervals $eh/ca(E_0, p_H)$ of $1/H$. We can therefore think of the integrand of (5) as a periodic function of the argument $ca(E_0, p_H)/ehH$ with period unity. Since this argument (which is approximately the same as n, the number of terms in the summation) is usually $\gg 1$, the integrand undergoes many oscillations as p_H (and with it, $a(E_0, p_H)$) varies, and the only appreciable contribution to the integral comes from the region of p_H where $a(E_0, p_H)$ varies least, i.e. from the region where $a(E_0, p_H)$ assumes its extreme value $\mathscr{A}$. In fact the result of the integration is to produce an energy U which is still periodic in $1/H$, but with period $eh/c\mathscr{A}$; this essentially is Onsager's result. Owing to the fact that only a small part of the range of integration contributes effectively to the result, the oscillations of U (or of M) are much less marked than in the two-dimensional metal. Qualitatively it is evident that the amplitude will be the greater the slower the variation of $a(E_0, p_H)$ with p_H in the region of the extreme, and calculation shows that in fact the amplitude is proportional to $(\partial^2 a(E_0, p_H)/\partial p_H^2)_m^{-1/2}$, where the suffix m indicates the value at the extreme of $a(E_0, p_H)$.

So far we have considered only the behaviour at absolute zero, where the probability of occupation of a state drops sharply to zero for energies greater than E_0. At finite temperatures the probability drops to zero over an energy range of order kT around E_0 and this has the effect of still further reducing the amplitude of the oscillations, though their period is unaffected. The magnetic properties at finite temperature are indeed determined, not by U, the energy, but by F,

* It should be noticed that we are implicitly treating E_0 as constant, though strictly it should be regarded as a function of H and its value determined from the condition that N, the total number of electrons, is given. In fact, the variation with H is very slight and becomes important only at very high fields.

the free energy, which is

$$F = NE_0 - \frac{2VeHkT}{ch^2} \int_{-\infty}^{\infty} \sum_{r=1}^{\infty} dp_H \ln\left(1+\exp\left((E_0 - E_r(H, p_H))/kT\right)\right) \quad (5a)$$

(for $T \to 0$, this reduces to U, i.e. to (5)). The detailed working out of (5a) was first given by Lifshitz and Kosevich [16], following on the lines of Landau's original calculation for the special case of an ellipsoidal energy surface. Since the mathematics is complicated, we shall merely quote the final result for that part of F which is oscillatory (the remainder is responsible for the steady diamagnetism and does not concern us here). This is

$$F = \frac{2VkT}{h^3}\left(\frac{ehH}{c}\right)^{3/2}\left(\frac{\partial^2 a}{\partial p_H^2}\right)_m^{-1/2} \sum_{r=1}^{\infty} \frac{\cos\left(\frac{2\pi rc\mathscr{A}}{ehH} - 2\pi r\gamma \mp \frac{\pi}{4}\right)\cos\left(r\pi m/m_0\right)}{r^{3/2}\sinh\left(2\pi^2 rkT/\beta H\right)} \quad (6)$$

where $m = (d\mathscr{A}/dE_0)/2\pi$, and has the significance of an effective mass, β is $eh/2\pi mc$ i.e. β is an *effective* double Bohr magneton, and m_0 is the real electron mass. The $\mp$ signs apply according as $\mathscr{A}$ represents a maximum $(-)$, or a minimum $(+)$. The last cosine factor in (6) arises from a feature not included in the formulation of (5a), namely the doubling of the energy levels on account of the magnetic moment of the electron spin; its correct form was first given by Dingle [22] and it is usually nearly unity since m/m_0 is usually small.

The formula is valid only if $c\mathscr{A}/ehH \gg 1$ i.e. if the phase of the periodic variation is high; if in addition $2\pi^2 kT/\beta H \gg 1$, only the first term in the summation need be considered, and (6) reduces to

$$F = \frac{4VkT}{h^3}\left(\frac{ehH}{c}\right)^{3/2}\left(\frac{\partial^2 a}{\partial p_H^2}\right)_m^{-1/2} e^{-2\pi^2 kT/\beta H}\cos\left(\frac{2\pi c\mathscr{A}}{ehH} - 2\pi\gamma \mp \frac{\pi}{4}\right). \quad (7)$$

For simplicity, we have here also omitted the 'spin' factor $\cos(\pi m/m_0)$.

From (6) or (7) it is easy to obtain either M, the magnetization $(= -\partial F/\partial H)$, or C, the couple about any axis $(= -\partial F/\partial\psi$, if ψ is an angle specifying rotation in a plane normal to the axis). In the differentiations the main contributions come only from differentiation of the cosine term, since $c\mathscr{A}/ehH \gg 1$. Thus the simplified expressions for M and C will differ from (7) only by a change from cos to sin and an extra factor $2\pi c\mathscr{A}/ehH^2$ in M, and $-2\pi c(\partial\mathscr{A}/\partial\psi)/ehH$ in C; it should be noticed that apart from the exponential and sin factors, both M/H and C/H^2, which are convenient quantities to describe the experimental results, vary as $H^{-3/2}T$.

The amplitude of the oscillations is reduced if account is taken of a possible broadening of the energy levels due to collisions or other causes. Dingle [23] showed that on certain simplifying assumptions the effect of the broadening that would correspond to a collision time τ, is as if the temperature T in the sinh terms of (6) or the exponential of (7) were increased by x, where

$$x = h/2\pi^2 k\tau. \tag{8}$$

In the special case that the energy surfaces are ellipsoidal, the quantities entering into (6) and (7) assume simpler meanings. For this case the volume contained within the Fermi surface (now an ellipsoid) is proportional to $E_0^{3/2}$ and the area of any section, for instance the area $\mathscr{A}$, is proportional to E_0. Thus the quantity defined as $2\pi m\ (=d\mathscr{A}/dE_0)$ is independent of E_0, and we have $\mathscr{A} = 2\pi m E_0$. The period P therefore becomes

$$P = \Delta(1/H) = eh/c\mathscr{A} = \beta/E_0. \tag{9}$$

The actual value of β depends, of course, on the detailed form of the ellipsoid, and we shall give an explicit expression below [Eq. (11)], but the important point to notice here is that it is the same β as enters in the exponential in (7) (or the sinh in (6)).

If the Fermi surface is an ellipsoid, its equation with respect to rectangular Cartesian axes fixed in the crystal can be expressed as

$$\sum \alpha_{ij} p_i p_j = 2m_0 E_0 \tag{10}$$

where $\alpha_{ij} = \alpha_{ji}$, and the α's are of course dimensionless. Although crystal symmetry usually ensures that some of the coefficients α_{ij} vanish and others are equal, it is useful to consider the most general form (10) because, as will be explained later, the Fermi surface can sometimes (e.g. in bismuth and antimony) be described by a group of several identical ellipsoids arranged so that the whole group has the required crystal symmetry, though each separately has not. It is not difficult to show that the extreme area $\mathscr{A}$ of cross-section (for an ellipsoid this is the area of a central cross-section) normal to the direction $(\lambda_1\lambda_2\lambda_3)$ is given by

$$\mathscr{A} = 2\pi m_0 E_0 / X^{1/2} \tag{11}$$

where $X = \lambda_1^2(\alpha_{22}\alpha_{33} - \alpha_{23}^2) + 2\lambda_2\lambda_3\ (\alpha_{12}\alpha_{13} - \alpha_{23}\alpha_{11})$ + similar terms ob-

tained by cyclic change of suffices. It follows that β in (9) and the corresponding effective mass m, are given by

$$\beta = \beta_0 X^{1/2} \text{ and } m = m_0/X^{1/2} \tag{12}$$

and the period P by

$$P = X^{1/2}\beta_0/E_0, \tag{13}$$

where β_0 is $eh/2\pi m_0 c$, i.e. a true double Bohr magneton (numerically, $\beta_0 = 1.85 \times 10^{-20}$).

If the field direction $(\lambda_1\lambda_2\lambda_3)$ is rotated round some fixed axis through an angle ψ from some reference line in the plane of rotation, it can be shown that P^2 will vary as

$$P^2 = A + B\cos 2\psi + C\sin 2\psi \tag{14}$$

where A, B and C are constants which can be expressed in terms of the direction cosines of the axis of rotation and the reference line. The values of A, B and C are easily calculable from (11) for any particular geometry and the rather complicated general formulae need not be given. Eq. (14) serves as a useful criterion for testing the validity of the assumption that the Fermi surface is ellipsoidal.

The factor $(\partial^2 a/\partial p_H^2)_m^{-1/2}$ which enters into (6) or (7) is, of course, dimensionless and can be written down explicitly for an ellipsoid. It can be shown that for an ellipsoid

$$a = \mathscr{A}(1 - p_H^2/p_0^2) \tag{15}$$

where p_0 is the length of the perpendicular from the centre of the ellipsoid to a tangent plane normal to the field; p_0 can be most simply expressed as

$$p_0 = (2m_0 E_0 X/D)^{1/2} \tag{16}$$

where

$$D = \begin{vmatrix} \alpha_{11} & \alpha_{12} & \alpha_{13} \\ \alpha_{12} & \alpha_{22} & \alpha_{23} \\ \alpha_{13} & \alpha_{23} & \alpha_{33} \end{vmatrix}.$$

Thus

$$(\partial^2 a/\partial p_H^2)_m^{-1/2} = p_0/(2\mathscr{A})^{1/2} = (\beta/\beta_0)^{3/2}/(2\pi D)^{1/2} \tag{17}$$

(bearing in mind that $X^{1/2} = \beta/\beta_0$); for the special case of a sphere (17) reduces to $(2\pi)^{-1/2}$.

The number n of electrons per atom contained within the Fermi surface is easily deduced if the form of the surface is known; it is given by

$$n = 2Vv/\mathcal{N}h^3 \tag{18}$$

where V is the atomic volume of the metal, v is the volume of the Fermi surface in p-space and $\mathcal{N}$ is Avagadro's number. If the Fermi surface has the form of the ellipsoid (10), its volume is given by

$$v = \tfrac{4}{3}\pi(2m_0E_0)^{3/2}/D^{1/2} \tag{19}$$

so

$$n = \frac{8}{3}\pi\frac{V}{\mathcal{N}D^{1/2}}\left(\frac{2m_0E_0}{h^2}\right)^{3/2}. \tag{20}$$

An alternative expression for n which is rather more directly linked to the experimental data can be obtained by expressing v in terms of the areas $\mathscr{A}_1, \mathscr{A}_2, \mathscr{A}_3$ of the three principal cross-sections i.e. $v = \frac{4}{3}(\mathscr{A}_1\mathscr{A}_2\mathscr{A}_3/\pi)^{1/2}$; if now we introduce the periods P_1, P_2, P_3 for the field along the principal axes, we find

$$n = \frac{8V}{3\mathcal{N}}\left(\frac{e}{hc}\right)^{3/2}(P_1P_2P_3)^{-1/2}. \tag{21}$$

For the special case of a spherical surface $P_1 = P_2 = P_3 = P$ and (21), expressed numerically, becomes

$$n = 0.95\times10^{-14}\,VP^{-3/2}. \tag{22}$$

Even when the Fermi surface is not spherical, (22) is a useful formula for obtaining a rough estimate of n in the absence of a detailed study of the variation of P with field direction. It should be noticed that (20) and (21) give only the contribution from one complete ellipsoid; as we shall explain below, the Fermi surface is often built up of a number of closed surfaces and the total number of electrons per atom is then the sum of the n's for each one.

3. Comparison of Theory with Experiment

(i) Periodicity

In agreement with theory, the period of the oscillations is indeed always strictly constant if any magnetic property is plotted against $1/H$. This can be seen for instance in the graphs of Fig. 2 where C/H^2 is plotted in this way. It can be seen too that there are often several

periodic terms present simultaneously and that the values of the periods vary widely for different metals. If the periods are not very different (Fig. 2e), or if one is not very different from a multiple of the other (Fig. 2c) 'beat' effects occur; if the periods are comparable but not very nearly equal, the curves become distorted, as in Figs. 2a and b. Sometimes the periods are so well separated that each may be easily identified (as in Fig. 2f), but in general it is not a simple matter to sort out the various periods reliably; the methods of Fourier analysis are rarely applicable since the amplitude of the oscillations varies continuously and usually it is necessary to resort to trial and error methods of analysis, supported by comparison with synthetic curves.

The simultaneous occurrence of more than one periodic term in the oscillations is due fundamentally to the fact that in a multivalent metal the Fermi surface must cross the Brillouin zone boundaries in a number of regions. The overlap regions (and the corresponding empty regions in the lower zone) can in general be put together to form a number of closed surfaces, and for a given field direction, each of these closed surfaces will in general give rise to its own periodic term. The various periodic terms can in principle be classified as follows:

(a) If any closed piece of the Fermi surface has not itself the symmetry of the crystal, then it must always be accompanied by other closed surfaces which are identical in shape but differently oriented with respect to the crystal axes so that the whole group does have the crystal symmetry. Since each member of the group is in general differently oriented with respect to the field, it will give rise to its own value of $\mathscr{A}$, i.e. to its own period.

(b) There may be a number of such groups of overlap regions, the members of each group being related to each other by crystal symmetry as in (a), but the members of different groups being quite unrelated.

(c) When the number of electrons is such that it could just completely fill a Brillouin zone (as in a divalent metal), any overlap into the next higher zone should be accompanied by an empty region in the lower zone. As is well known, such empty regions can be thought of as occupied by 'holes', and the pieces of Fermi surface bounding these empty regions can be dealt with in the same way as the overlap regions discussed in (a) and (b); thus as well as the groups of periods associated with overlap electrons, as in (a) or (b), there should be groups of periods associated with holes.

(d) A closed piece of the Fermi surface might in principle have such a shape that there are several extreme areas of cross section by planes normal to the field. For instance a 'dumb-bell' shaped surface would have two maxima and a minimum for some directions but not for others. Each such extreme should give rise to a periodic term, though in practice the amplitudes might be so very different that only some of the terms could be observed. It should be noticed that owing to this possibility, even a monovalent metal (e.g. an alkali) could show a number of periodic terms, though apart from this possibility one would expect only a single period since the Fermi surface should be entirely within one zone and therefore all in one piece. In fact the de Haas–van Alphen effect has not yet been found in a monovalent metal.

A detailed analysis of the periods has been made so far for only a few metals; several cases of 'groups' of periods related by crystal symmetry as in (a) have in fact been established (e.g. bismuth, antimony, aluminium, arsenic) but a relation (such as (b), (c) or (d)) between such groups of periods and other groups or individual periods has never been unambiguously established. In principle the 'hole-electron relation' (i.e. (c)) could be established if the number of carriers per atom were found to be the same for both groups of periods, but in practice this requires more detailed data than have yet been collected for any metal. Another method of investigating whether any period is due to holes or electrons is to investigate the effect on the period of alloying a small quantity of an electro-positive or electro-negative element with the metal in question. If the added element has for instance more electrons per atom, the number of electrons in an overlap region should be increased and the corresponing period reduced, and the number of holes in an empty region decreased, and the corresponding period increased. This method has considerable possibilities but has so far been little exploited, partly because of the practical difficulty that the amplitude of the de Haas–van Alphen effect is nearly always rapidly reduced by the addition of even very small quantities (usually $< 1\ \%$) of other elements. The theory of the method is in fact a good deal more complicated than suggested by these qualitative remarks; a recent discussion has been given by Heine [24].

Once the various periods have been sorted out, it is possible from the variation of any one particular period with field direction to

deduce something about the shape of the corresponding closed piece of Fermi surface. If (14) is found to apply for all planes of rotation, the piece concerned is ellipsoidal and the values of $\alpha_{ij}/m_0 E_0$ (i.e. the shape and size of the ellipsoid) can be worked out from the values of the coefficients A, B, C for a sufficient number of different axes of rotation of H. It is however only rarely that the ellipsoidal assumption is in fact strictly applicable, (for details see § 5) and in general the theorem of Lifshitz and Pogorelov [17] must be used to determine the shape and size of the Fermi surface. This theorem gives the radius vector $\varrho(\mathbf{e})$ of a centro-symmetrical surface in the direction $\mathbf{e}$, in terms of the areas $\mathscr{A}(\boldsymbol{\xi})$ of maximum cross-section normal to the directions $\boldsymbol{\xi}$ (assuming these are central cross-sections) as

$$\varrho(\mathbf{e}) = \left(\frac{1}{\pi}\left(\chi_e(0) - \int_0^1 \left(\chi_e(u) - \chi_e(0)\right) \mathrm{d}u/u^2\right)\right)^{1/2} \tag{23}$$

where

$$\chi_e(u) = \frac{1}{2\pi}\int_0^{2\pi} \mathscr{A}(\boldsymbol{\xi})\, \mathrm{d}\varphi.$$

Here $\chi_e(u)$ is the average value of $\mathscr{A}(\boldsymbol{\xi})$ round a latitude θ, $u = \cos\theta$, θ is the angle between the unit vectors $\boldsymbol{\xi}$ and $\mathbf{e}$, and φ is the azimuthal angle. The various integrations can be carried out graphically if the variation of $\mathscr{A}(\boldsymbol{\xi})$ with direction $\boldsymbol{\xi}$ is sufficiently well established. Encouraging results have been obtained by applying this procedure to aluminium and it is hoped to apply it soon to other metals. The assumption of a centro-symmetrical surface requires some comment. In fact some of the closed pieces of Fermi surface may well lack a centre of symmetry, but if (as is usually the case) the crystal itself does have a centre of symmetry, such pieces must occur in groups (e.g. pairs) which taken together are centro-symmetrical. For instance if one piece is egg-shaped pointing in some direction it would be accompanied by a second identically shaped piece pointing the opposite way. Now the two periodic terms arising from two such complementary pieces will always be identical since the maximum areas of cross-section normal to any field direction will be unchanged if the egg is reversed. In other words the de Haas–van Alphen effect cannot distinguish between the members of such a pair, and the best that can be done is to calculate the shape of a centro-symmetrical surface which has the same maximum cross-sectional areas as either member of the pair.

(ii) Variation of amplitude with temperature

The marked increase of amplitude as the temperature is lowered can be seen in Figs. 2c, e and f. According to (7) if c is the amplitude of the oscillations (it is immaterial here whether the oscillations are in the couple or in susceptibility), a plot of $\log c/T$ against T should be linear and of slope $-2\pi^2k/\beta H$. This is always found to be true, as long as $2\pi^2kT/\beta H \gg 1$, but when $2\pi^2kT/\beta H$ approaches unity, (7) is inadequate and the more general formula (6) must be used. This is found necessary both for large β (as in bismuth and zinc) and for large H (as in the measurements at 10^5 gauss); the measurements (most thoroughly made in bismuth [25]) confirm that the observed temperature variation is indeed consistent with (6).

If the piece of Fermi surface responsible for a periodic term can be adequately represented by an ellipsoid, then the period P is β/E_0 and hence $\beta/P = E_0$, and should be the same for all field directions. Comparison of values of β/P (β being found from the temperature dependence) for different field directions thus provides a criterion of whether or not the Fermi surface can be represented by an ellipsoid, and if it can, whether or not the periodic terms observed in various directions belong to the same piece of Fermi surface (or one linked to it by crystal symmetry). In fact relatively few systematic measurements of β have as yet been made and it has rarely been possible to apply this criterion in practice. One difficulty is that if there are several periodic terms present simultaneously the determination of the β's for the different terms requires a good deal of analysis (essentially the observed curves at different temperatures must be completely separated out into their component periodic terms). For this reason β has so far usually been measured only for such field directions along which there is only a single dominant periodic term.

If it were possible to obtain a detailed knowledge of how β varied with field direction for each separate periodic term – and this could probably be done if enough trouble were taken – it should be possible to derive the electron velocity (which is $(\mathrm{grad}_p E)_{E=E_0}$) at each point of the Fermi surface. By definition, a knowledge of β is equivalent to one of $\mathrm{d}\mathscr{A}/\mathrm{d}E_0$ and it is evident that if the procedure of Lifshitz and Pogorelov (see § 3 (i)) is applied to $\mathrm{d}\mathscr{A}/\mathrm{d}E_0$ instead of to $\mathscr{A}$, we can find $\varrho(\mathbf{e})\,\mathrm{d}\varrho(\mathbf{e})/\mathrm{d}E_0$ for each direction $\mathbf{e}$. If $\varrho(\mathbf{e})$ has already been determined from the period values, $\mathrm{d}E_0/\mathrm{d}\varrho(\mathbf{e})$ is obtained, and $(\mathrm{grad}_p E)_{E=E_0}$, which is just the electron velocity, can be found if the

whole Fermi surface has been calculated, so that the angle between the normal and the radius vector is everywhere known.

(iii) Harmonic content and phase

The presence of harmonics in the oscillations is clearly shown in the observed curves whenever $2\pi^2kT/\beta H \lesssim 1$, and specially designed experiments [25] with bismuth (for which the conditions are most favourable) showed that the harmonic content of the observed curves is consistent with the predictions of (6). The presence of fairly strong harmonics sometimes increases the difficulties of identification of the basic periodic terms in an observed set of oscillations (cf. graphite). In the high field method (see below) the harmonics may be even stronger than in the torque method, both because the field is high and because it is $\mathrm{d}M/\mathrm{d}H$ that is measured; the rth harmonic in $\mathrm{d}M/\mathrm{d}H$ is relatively r times as strong as in M because of the extra differentiation.

The phase of the oscillations can be studied only if the argument of the cosine factor is not too large (for the ellipsoidal assumption, if $E_0/\beta H$ is not too large). Reliable results have been obtained for only a few metals and these indicate a different situation for each metal, and in general a lack of agreement with the prediction for the ellipsoidal assumption. Since the phase is probably particularly sensitive to various simplifying assumptions implicit in the theory, this lack of agreement need not be regarded as too worrying.

(iv) Field dependence of amplitude

Once β is known from the temperature variation of amplitude, it is possible to check the form of the theoretically predicted variation of amplitude with field. It can be shown that the presence of harmonics does not greatly effect the amplitude, even for $2\pi^2kT/\beta H \approx 1$, and if they are ignored, (6) predicts that a plot of $\log(cH^{3/2}T^{-1}\sinh 2\pi^2kT/\beta H)$ against $1/H$ should, on the simple theory of level broadening, be a straight line of slope $-2\pi^2kx/\beta$ for all temperatures (c is the amplitude of oscillation of C/H^2). This is found to be true for bismuth, but for zinc the amplitude falls off too fast at high fields (Fig. 5d) and the plot is far from linear there [25]; the cause of the discrepancy has not been explained. For most other metals the approximation (7) is quite adequate and the appropriate plot is of $\log cH^{3/2}$ against $1/H$. This

plot is usually found to be linear and with a slope which is approximately independent of temperature; by comparing the slope with the theoretical value, $-2\pi^2 k(T+x)/\beta$, x can be estimated, though in practice it is not easy to make an accurate determination.

The values of x found are usually of order 1° K, and comparison with (8) shows that this would imply a collision time τ of order 2×10^{-12} sec. or 100 times shorter than suggested by resistivity data. It is clear in fact that the level broadening in a pure metal must come mainly from some other cause than ordinary collisions; Dingle has suggested that it is connected with the periodic electric field of the lattice and the problem has recently been discussed by Harper [26] and Brailsford [27]. The fact that collisions can contribute to the level broadening has, however, been demonstrated in experiments [7] on a series of alloys of tin with up to 0.5 % indium, which showed that x varied linearly with the ratio of residual to room temperature resistance. In this way it was possible to estimate the collision time τ_0 in tin at room temperature as 1.5×10^{-14} sec., in good agreement with estimates by other methods. This method of studying the collision times in metals might have useful applications, but has so far been little exploited.

(v) Absolute value of amplitude

For various reasons the absolute value of amplitude cannot be very accurately measured and it is not usually a very reproducible feature. It may for instance be sensitive to the perfection of the crystal (since in an imperfect crystal the amplitude is that of the resultant of several periodic terms with periods which may be appreciably different because of varying orientation), to the purity (see previous §) and to field homogeneity. In principle, comparison of the amplitude with the theoretical formula should lead to a value of $(\partial^2 a/\partial p_H^2)_m$, since β and $\mathscr{A}$ can be found from the temperature dependence and period respectively, and the factor $\partial\mathscr{A}/\partial\psi$ in the expression for the couple can be found if the variation of $\mathscr{A}$ with ψ is known. If $(\partial^2 a/\partial p_H^2)_m$ were determined in this way, the theory could be checked by comparison of this value with that found from the form of the Fermi surface (as determined from the $\mathscr{A}$'s for all field directions).

Owing to the poor accuracy of amplitude measurement this programme is rather impracticable as yet, and all that has been attempted is a rough check of the theoretical formula when the Fermi surface

is treated as ellipsoidal. For tin and gallium the theoretically calculated amplitude of the oscillations in the couple does agree in order of magnitude with the observed amplitude, but it is disturbing that the discrepancy is in the wrong direction, the observed amplitude being the higher, although the various sources of inaccuracy mentioned above would all tend to *reduce* the amplitude. Possibly the discrepancy arises from the inadequacy of the ellipsoidal representation, for which inadequacy there is indeed ample evidence in the details of variation of period with field direction. For several other metals (bismuth, graphite, antimony) where the ellipsoidal representation seems to fit rather well, one of the coefficients α_{ij} proves to be either very small or very large (for details see § 5) so that its relative size cannot be found from the orientation dependence of period. This means that the absolute amplitude cannot be used as a basis of checking the theory, but rather that the missing coefficient can be determined from the amplitude if the theory is assumed correct.

In the high field method absolute amplitude measurements (of dM/dH in this case) are subject to additional inaccuracies because of uncertainties in circuit calibration. The anisotropy of the oscillations seems to be not so marked as at low fields and it is perhaps permissible to compare the observed amplitudes with those theoretically predicted for a spherical Fermi surface; this does in fact give order of magnitude agreement. When the anisotropy has been studied in greater detail it should be possible to make a more critical comparison.

4. Experimental Methods

The original results on bismuth were obtained by the conventional method of observing the force acting on a specimen in an inhomogeneous field; this method suffers from the obvious disadvantage that different parts of the specimen are in different fields and the amplitude of oscillation may consequently be much reduced if the range of fields is large compared with a period. It may nevertheless still be of value in looking for oscillations of very long period if the Fermi surface is nearly spherical so that there is little anisotropy; in these conditions both the other methods to be described will fail.

To overcome the difficulties associated with an inhomogeneous field, the torque method was tried and has proved eminently suitable for studying the de Haas–van Alphen effect in moderate fields (up to 30 kG). The specimen is suspended by means of a long quartz rod

from a short torsion element chosen of such a stiffness that the couple twists it by only a small angle (usually less than 1°); the couple is measured by the movement of a light spot reflected from a mirror attached to the suspension. Usually the whole apparatus is supported independently of the electromagnet and the direction of the field (i.e. ψ) is conveniently varied by rotating the magnet about a vertical axis. By attaching the crystal to its suspension in a variety of orientations, it is possible in this way to vary the direction of the field relative to the crystal axes over the whole solid angle.

For some metals the phase of the oscillations is so sensitive to the orientation of the crystal that even the small angular twist involved in the measurement of the couple may appreciably change the phase; this can lead to serious distortion of the form of the oscillations, and in extreme conditions to instability. To overcome this difficulty, various forms of electrical feed-back arrangements have been devised [18, 28, 44] in which the light reflected from the mirror falls on a photocell and the amplified current from the photocell passes through a small coil attached to the suspension and in the field of a small permanent magnet. The permanent magnet then exerts a couple on the coil which counteracts the couple on the suspension and can be made to reduce the angle of twist to any desired extent; the current through the coil serves as a measure of the couple. The method has the advantage that the effective sensitivity can be controlled by adjustment of the circuit constants, and is almost independent of the torsion element.

A feature of the torque method is that the torque vanishes at certain orientations determined by crystal symmetry (for instance, if the field is along an axis of crystal symmetry). The individual periodic terms arising from the separate members of a group of pieces of Fermi surface may indeed not vanish at such symmetry positions, but their sum always must. If, however, the field is only slightly off the symmetry position the separate members may get sufficiently out of phase to produce quite an appreciable resultant oscillation. This means that some care is needed in identifying these symmetry positions by the vanishing of the couple. It may be noted that the amplitude of the *individual* periodic terms is proportional to $\mathrm{d}P/\mathrm{d}\psi$ and so vanishes whenever P, the period, has a maximum or minimum as the field is rotated in a plane normal to the axis of measurement of the couple. This feature can occasionally be put to advantage [25]

if it is wished to exclude some of the periodic terms in order to study one of them in isolation.

Finally we may mention two difficulties that arise in the use of the torque method. First, there is in general a steadily varying, as well as an oscillatory, couple (except for cubic crystals and for crystals of lower symmetry suspended with a trigonal, tetragonal or hexagonal axis vertical). If the steadily varying couple, which is proportional to H^2, is large compared with the oscillatory one, as it is for instance in antimony, the oscillations may easily be missed altogether unless careful systematic measurements are made. Secondly, if the metal has high conductivity in the magnetic field, large eddy currents are induced when either the magnitude or the direction of the field is changed. Because of anisotropy of conductivity and of non-spherical shape, the magnetic field can interact with the eddy currents and produce couples which may seriously disturb the measurements in various ways. The effects are very striking with metals of high conductivity such as copper, gold and silver; if the magnet is rotated the crystal appears to be almost rigidly locked to it and returns to its equilibrium position only very slowly – as if in treacle – after the rotation is stopped; again if the magnet current is not perfectly steady the eddy currents set up by the fluctuations cause a continuous fluctuating movement of the measuring light spot. Fortunately these effects are usually much reduced in most metals because of the reduction of conductivity in a magnetic field (magneto-resistance effect).

Because of the limitations of conventional electromagnets the possibilities of observing the de Haas–van Alphen effect by the torque method are limited, particularly as regards period. In practice, even with a large electromagnet giving 30 kG, it is difficult to study any oscillations of period P much less than $10^{-7}\mathrm{G}^{-1}$. This corresponds to a field interval of only about 100 G and considerable stability of the magnet current is required to hold the couple steady with such a short period, while the field homogeneity in space must be better than 1 in 1000 over the specimen, if the amplitude of the oscillations is not to be diminished. Now $P = 10^{-7}$ corresponds in order of magnitude to only 10^{-3} to 10^{-2} electrons per atom [see Eq. (22)] so it is evident that the torque method cannot show up the rather shorter periods to be expected from larger pieces of the Fermi surface. The order of magnitude of the period to be expected for one electron per atom is

indeed only 2×10^{-9} [applying (22) to copper] i.e. the field interval would be only about 2 G at 30 kG. To overcome this limitation an entirely new type of method was devised which is particularly suitable for detecting oscillations of short period.

In this method the specimen is put inside one of a pair of balanced coils connected to an amplifier and C.R.O., and the coils are placed at the centre of a liquid-air cooled solenoid in which a field of order 100 kG is produced impulsively by discharging a 2000 μF condenser charged to 1700 volts. As the field varies, an E.M.F. is induced in the coil which, besides a smoothly varying component due to lack of balance of the coils, contains a component proportional to $\mathrm{d}M/\mathrm{d}t$ and therefore to $\mathrm{d}M/\mathrm{d}H$, if M is the oscillatory part of the magnetization. This method is particularly sensitive for detecting short period oscillations, because the amplitude of $\mathrm{d}M/\mathrm{d}H$ is higher than that of M/H by a factor $2\pi/PH$. Thus for a free electron monovalent metal with the atomic volume of copper, the amplitude of M/H (M is per unit volume here) should be about 2×10^{-5} for $H = 100$ kG and $T = 1.2°$ K, while $\mathrm{d}M/\mathrm{d}H$ should be 4×10^{4} times greater, i.e. as high as 0.8 (these estimates ignore level broadening and assume that the effective mass is equal to m_0).

In fact, although this method has shown up oscillations of short period (as low as $P = 6 \times 10^{-9}$ for tin) for various multivalent metals, which presumably are associated with major parts of the Fermi surface, it has not so far succeeded with any monovalent metal. Before discussing possible reasons for the failure of the method with monovalent metals, it will be convenient to say a little about its features when it does work.

Some typical oscillograms are reproduced in Fig. 4 and 5; with suitable electronic devices it is possible to pick out any desired part of the discharge process and thus to study any particular feature of the oscillations in detail. In the latest form of the equipment the discharge lasts about 30 ms and $\mathrm{d}H/\mathrm{d}t$ is of order 5×10^{6} G sec^{-1} at its maximum; for $H = 70$ kG and $P = 10^{-8}$, the interval ΔH for one oscillation is 50 G, and therefore occupies 10 μs. This means that the frequency of the oscillations as they appear on the C.R.O. is of order 100 kc/sec, though it becomes much smaller near the field maximum, where $\mathrm{d}H/\mathrm{d}t$ vanishes. The oscillating E.M.F.s actually observed for specimens of tin, lead and cadmium a few tenths of a mm in diameter and a few mm long, and for pick-up coils with about 10^{3} turns are of

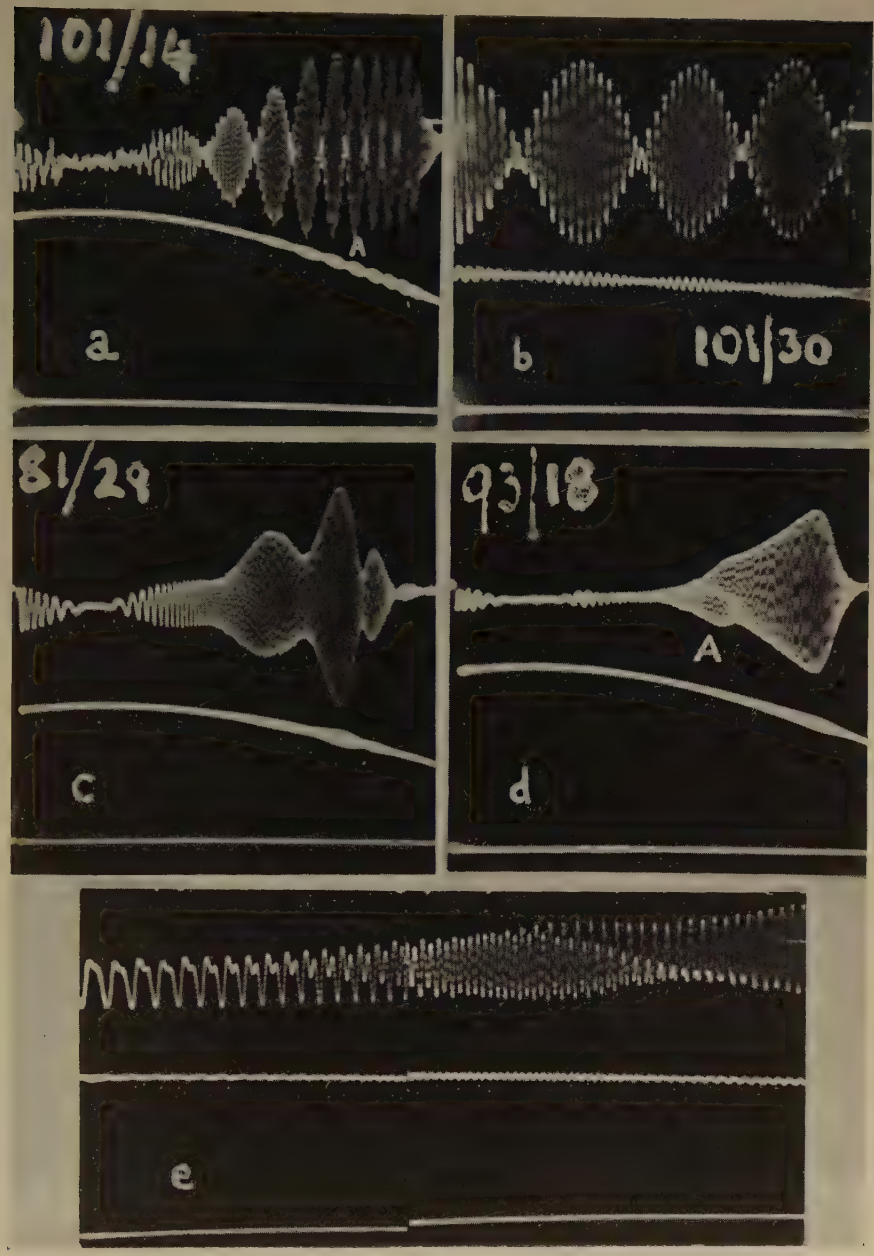

Fig. 4

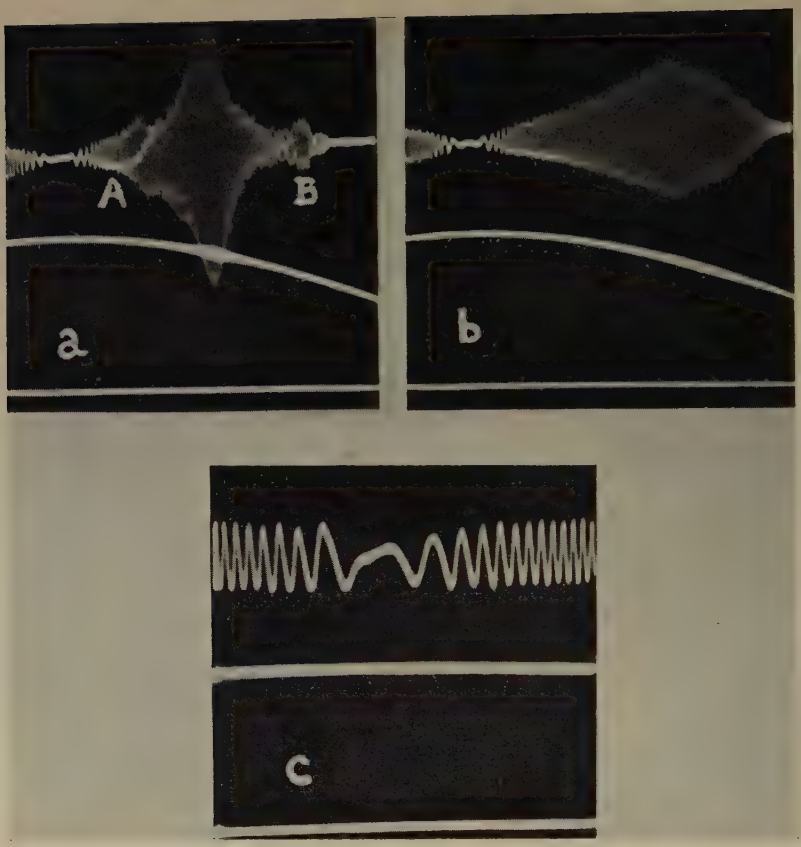

Fig. 5. Oscillograms with H along a tetrad axis in lead. The oscillations are now of appreciably shorter period ($P \sim 1.8 \times 10^{-8}\mathrm{G}^{-1}$); the peakiness and distortions (at A) of (a) are due to coil resonance and are eliminated in (b) where a cathode follower has been interposed between coil and cable. It should be noticed that the resonance enhances the long period oscillations at B in (a), where their time-frequency is right for resonance; (a) and (b) are about 3 ms across. (c) is an oscillogram obtained by the R.F. method, showing only the middle 2 ms of the discharge (note that (c) is taken with a different solenoid and a larger condenser so that the discharge is about twice as slow as in all the other illustrations).

order 10 mv or less, and this means that the amplitude of $\mathrm{d}M/\mathrm{d}H$ is of order 10^{-3} (which proves to agree reasonably with the theoretically predicted value for a spherical Fermi surface). Since the effective noise level is about 0.1 mV it can be seen that it should be possible to detect an effect of amplitude even 10^4 or 10^5 times less than that predicted for an ideal monovalent free-electron metal. It may be noted that oscillations of greater period, such as can be only just observed by the torque method (i.e. $P \approx 10^{-7}$), can also be observed by this method, but their amplitude will not in general be as great as of those of smaller period, because of the extra factor $(2\pi/PH)$ involved in $\mathrm{d}M/\mathrm{d}H$. Thus although the two methods overlap for about $P = 10^{-7}$ the overlap is not great, since for $P \approx 10^{-7}$ the amplitude of the voltage produced by the new method is approaching the noise level.

In the practical realization of the method a number of points have to be carefully watched. In the design of the solenoid care has to be taken that the field is sufficiently homogeneous over the length of the specimen. For $P = 2 \times 10^{-9}$ a homogeneity of rather better than 1 in 10^4 is required in order not to smear out the oscillations appreciably: this requirement can be met most easily by suitable disposition of auxiliary windings but considerable care is necessary in the winding of the coil to avoid any irregularity. The coil must be mechanically strong to avoid any vibrations of individual turns during the condenser discharge. Such vibrations are thought to have been the cause of a good deal of extra 'noise' observed with some of the earlier coils, and they seem to have been largely eliminated by impregnating the coil with a plastic cement. It is worthy of note that the presence of even quite small quantities of solid air in the liquid helium can cause very large disturbances on account of the strong paramagnetism of oxygen; not only is there a great deal of extra signal 'noise', but the heat of magnetization liberated during the rise of the field to its maximum is sufficient to throw up a considerable fountain of liquid helium.

In the interpretation of the oscillograms it is necessary to bear in mind that there may be considerable distortion if the time-frequency of the oscillations is close to a resonance frequency of the pick-up coil system. This is responsible for the 'peakiness' of some of the observed envelope curves and it can also cause peculiar phase effects. For instance the first harmonic of any fundamental frequency will be exaggerated as its time-frequency passes through the resonant

frequency of the system, and the wave form of the fundamental appears distorted; in passing through the resonant frequency the phase is changed by π and this can be clearly seen in Fig. 4e as a movement of the distortion from the top to the bottom of the cycle of the fundamental. These distortions can be modified and to some extent eliminated by suitable circuits (e.g. use of a cathode follower to reduce cable capacity; cf. Figs. 5a and 5b), but it is worth noticing that they might be put to advantage, if the circuit were deliberately made to resonate with a high Q. In these conditions each period (and each harmonic) would resonate sharply at a particular instant (i.e. when its time-frequency was just right) and we should have a kind of spectrum of the de Haas–van Alphen effect. In practice, although this idea can sometimes help (for instance in separating out a weak long period from a strong short one; cf. Fig. 5a), it is in principle not possible to obtain a spectrometer of very high resolution since the time-frequency varies continuously with time so that the resonant frequency is never held long enough to build up to a very sharp resonance.

Owing to the complications just mentioned, the method does not lend itself easily to absolute amplitude measurements; even its use for relative measurements (such as are required in finding β from the temperature variation of amplitude) is subject to appreciable inaccuracies, because the conditions of discharge are not quite reproducible unless a lot of care is taken. The difficulty is that the field coil takes a long time to achieve thermal equilibrium after a discharge, so that its resistance at any moment depends on its immediate previous history and the precise value of $\mathrm{d}H/\mathrm{d}t$ at a particular instant after commencement of discharge is thus not exactly reproducible.

The one feature of the oscillations which can be accurately measured, and fortunately this is an important one, is the period P. The second

Fig. 4. Typical oscillograms of the de Haas–van Alphen effect in lead. Each picture is about 3 ms across, except (b) which is 0.5 ms across and is an expanded version of the region round A in (a), and (e), about 1 ms across, which is an expanded version of the region round A in (d); (d) and (e) illustrate the distortion due to coil resonance (see text). All the pictures except (c) were made with a crystal having H approximately at 37°, 65°, 66° to the tetrad axes, and the sensitivity of the effect to exact orientation is illustrated by the difference between (a) and (d) caused merely by remounting the crystal; (c) is for a crystal with H approximately at 25°, 65° and 89° to the tetrad axes. All the pictures show only the longer period $P \approx 4 \times 10^{-8}\mathrm{G}^{-1}$.

trace of the C.R.O is used to record the current through the solenoid and in principle all that is necessary to determine P is to count the number of cycles between two points for each of which the current, and the therefore the field, is known. In practice only a poor accuracy can be achieved in this way, mainly because the field varies so little even over the largest number of cycles which can be clearly resolved (in practice not more than about 100 cycles can be resolved in any one picture, and for $P = 10^{-8}$ this means a change of H of only about 5 kG at 70 kG). Gold [29] has recently developed a much more accurate method in which most of the 'steady' level of the current trace is backed off and the variable part can therefore be greatly amplified without going off the picture. Calibration lines are automatically put on each picture to eliminate screen distortion and variation of sensitivity of the C.R.O, and the period can be measured with an accuracy of 1 or 2 %.

It will be noticed that this method suffers from the awkwardness that it is not easy to vary the direction of the field relative to the crystal axes. Recently a mechanism has been devised by means of which the crystal (and the pick up coils round it) can be rotated about a horizontal axis, providing the same degrees of freedom as in the torque method. With this mechanism, which is accommodated in a Dewar vessel of only 11 mm internal diameter, Gold is at present making a detailed study of how the short periods in lead vary with field direction (with a view to finding the shape of the Fermi surface). It is hoped to extend this study to other metals soon.

We have left to the last the main difficulty of the high field method. This is that the eddy currents induced in the specimen by the varying field make the local field in the core of the specimen lag behind that at the outside. If this inhomogeneity of field is comparable to the field interval of one period, the amplitude of the oscillations will be reduced. The inhomogeneity is least at the maximum field, where dH/dt vanishes, but just there the amplitude vanishes too, and the oscillations become very spread out. A simple calculation shows that one could not hope to observe many more than q oscillations from the point of maximum H, where

$$q_{\frac{1}{2}} = PH\varrho^2 t_{\max}^2 / 8\pi^4 a^4. \tag{24}$$

Here ϱ is the specific resistivity of the metal in the field (in E.M.U.), $t_{\max}$ the time from the start of the discharge to the maximum field,

H the maximum field, and a the radius of the cylindrical specimen. Clearly a should be made as small as possible, but it is hardly possible to reduce it much below 10^{-2} cm. In the latest design of the equipment, t_{max} has been increased to 11 ms (and this has been achieved only at a sacrifice of maximum field, H having being reduced from about 100 to 80 kG), so that for $P = 2 \times 10^{-9}$ G^{-1}, $q \approx 2 \times 10^{-3} \varrho^2$. It is evident then that there is little hope of observing many oscillations unless ϱ is at least 30 or so; in copper silver, gold and sodium the increase of resistance in a magnetic field is not very great even at liquid helium temperatures and ϱ in a pure specimen may indeed be less than 30. This then is a possible reason why no de Haas–van Alphen effect has yet been found in these metals and in sodium there is an additional complication – a phase transition at about 30° K which may break up a single crystal grown at a higher temperature.

A few experiments in which the resistivity of pure copper was deliberately increased by adding a little gold have had no success either, possibly because the increased damping of the oscillations due to alloying outweighs the reduction of eddy current effects. It is indeed possible that the absence of an effect may be due to the opposite cause – insufficient purity or insufficient perfection of the crystal, and attempts to improve the quality of copper crystals are now in progress. It may be noted that even if the resistance in zero field is thereby reduced, the eddy current effects may not necessarily be worse, since in a high magnetic field the resistivity tends to be independent of the zero-field resistance. For most multivalent metals the magneto-resistance effect raises ϱ to as much as 100 or 1000 E.M.U. (there are few precise data) and since moreover P is usually 10 or 100 times higher than the figure assumed for copper, q becomes a large number and eddy currents impose no restrictions on the observability of the oscillations, even if the radius is 2 or 3×10^{-2} cm.

Another effect of eddy currents which must be mentioned is the heating, but we shall not discuss this in detail since it can be shown that provided there is sufficiently direct access of liquid helium II to the specimen and provided the radius is not too great, the temperature rise is small, and moreover adjusts itself to the instantaneous power with a relaxation time of order 10^{-6} sec. Thus it is unlikely that this heating effect seriously impedes the observation of the de Haas–van Alphen effect.

During the last year a new radio-frequency method of measuring

differential susceptibility at high fields has been developed in the hope that the eddy current effect might be reduced sufficiently to permit observation of the de Haas–van Alphen effect in monovalent metals. This hope has not materialized, but the method has been shown to work and has interesting possibilities, so it merits a brief description. The high fields are produced in the same way as before, but detection of the magnetic behaviour is made by means of a small mutual inductance surrounding the specimen, using a small measuring current of 10 Mc/sec frequency. The amplitude of the R.F. voltage across the secondary of the mutual inductance depends on the instantaneous value of $\mathrm{d}M/\mathrm{d}H$ in the R.F. skin depth of the specimen, and is therefore modulated if there is a de Haas–van Alphen effect so that $\mathrm{d}M/\mathrm{d}H$ oscillates as the main field is varied. The frequency of the measuring current is deliberately chosen to be high compared with the time-frequency of the de Haas–van Alphen effect, which as we saw earlier is of order 100 kc/sec for typical conditions. Most of the R.F. voltage from the secondary is balanced out and the remainder amplified by a tuned amplifier, rectified and then amplified again by an amplifier which is insensitive below 5 kc/sec, and displayed on a C.R.O. The considerable variation of the general level of the rectified signal, due to the change of skin depth with field because of the magneto-resistance effect, is relatively slow and is filtered out by the last stage of amplification so that the de Haas–van Alphen effect finally appears as a well marked oscillation about a horizontal base line (Fig. 5c). A slight advantage of the R.F. method over the direct one is that the amplitude no longer vanishes at the field maximum, since the observed E.M.F. no longer derives from the $\mathrm{d}H/\mathrm{d}t$ of the main field.

The original idea behind the R.F. method was that since the skin depth for 10 Mc/sec is small ($\approx 10^{-4}$ cm for copper and $\approx 3 \times 10^{-3}$ cm for lead at 100 kG) the magnetic properties would effectively be measured only in a very thin layer, in which the main field could be regarded as sensibly uniform in spite of eddy currents. In fact this argument is probably unsound because of end effects; inevitably the specimens must be kept short, and therefore the end regions, in which eddy currents will certainly reduce the value of the main field at the specimen surface, cannot be ignored. The theoretical problem of the distribution of the lines of force in a finite cylinder showing the de Haas–van Alphen effect in conditions where the field is appreciably

less at the ends (due to eddy currents) is complicated and has not been properly discussed. However, it seems unlikely that the eddy current situation is really greatly improved in the R.F. method as compared with the direct method, in spite of the fact that only a thin surface skin is effective in the former instead of the whole cross section as in the latter. It should be noted too that surface conditions (e.g. whether the surface is etched or electro-polished) may be much more relevant in the R.F. than in the direct method.

The R.F. method (in several variants, e.g. using a self, instead of a mutual, inductance) has worked quite well with lead, tin and aluminium, but whether on account of eddy currents or for more fundamental reasons, no more success has been obtained with copper, silver and gold then with the direct method. It may be noted that (unlike the direct method), the sensitivity of the R. F. method increases with increasing skin-depth and is therefore most sensitive if the magneto-resistance effect is large. An extreme case is bismuth, where the resistance becomes so high as to make the skin depth greater than the specimen diameter; the sensitivity is thus 20 or 30 times as high as in lead and is sufficient to show up the ordinary low field de Haas–van Alphen effect (no new oscillations appear at high fields).

We have given only a very qualitative account of the theory of the R.F. method, which in fact depends on rather subtle details (e.g. the phase) of the skin effect in a high magnetic field. Although it is likely that the R. F. method has not sufficient advantage over the direct method to justify the extra complications it involves, it has interesting possibilities as a possible tool for studying the skin effect in high magnetic fields. One approach which has been tried but not developed very far, is to leave out the low frequency filter in the final stage of amplification; the main change of the rectified signal (due to magneto-resistance), which for lead and tin is much larger than the oscillations due to de Haas–van Alphen effect, then becomes apparent. Some attention has been given to the possibility of using the R.F. method at ordinary steady fields, but it turns out that the changes in the rectified signal due to change of magneto-resistance as the field is varied, mask the much smaller changes due to de Haas–van Alphen effect; it is in fact only because the field changes are fairly rapid that it is possible to separate the two effects in the impulsive field technique.

TABLE I

Metal	Effective masses m_1/m_0	m_2/m_0	m_3/m_0	m_4/m_0	Typical values of $P \times 10^7$(G^{-1})	$E_0 \times 10^{14}$ (erg)	n
Cubic							
Al	(0.09)				36 (2)	5.3	(1.5×10^{-5})
	(0.15)				3 (3)	40	3.6×10^{-3}
Pb	(0.75)				0.4 (2)	60	(2×10^{-2})
	(1.1)				0.16	100	(7×10^{-2})
Tetragonal							
Sn	0.10		≈ 2		2–6	32	1.5×10^{-3}
	0.16		1.1		2	40	2.6×10^{-3}
	(≈ 0.5)				0.4 (2)	90	(2×10^{-2})
	cf Fawcett's estimates [33]				0.07	400	(0.3)
	A 0.9		0.1			430	
	B 0.04	0.5	1.0				
In	(0.3)				2	30	(1.7×10^{-3})
Orthorhombic							
Ga	>0.2	>0.15	<0.05		20	10	$>0.3 \times 10^{-4}$
	0.1	0.3	0.03		30	11	0.4×10^{-4}
	0.2	0.02	0.4		50	6	0.7×10^{-4}
Hexagonal							
C	3.6×10^{-2}		200		220	2.3	3.4×10^{-5}
	7×10^{-2}		25 to 700		165	1.6	1.4 to 7×10^{-5}
Zn	5.7×10^{-3}	8.2×10^{-3}	0.9		50–650.	4.2	5.8×10^{-6}
	1.7	0.42	1.1×10^{-2}		2–20	7?	2×10^{-4}
	(0.4)				2	20	(10^{-3})
Cd	(0.14)				1–1.9 (2)	70	(2×10^{-3})
	(≈ 0.5)				≈ 0.15	≈ 300	$(\approx 7 \times 10^{-2})$
Tl	(0.35)				5–50	11	$(\approx 10^{-4})$
Be	(0.03)				70	8.4	(3×10^{-6})
					0.7		(3×10^{-3})
Mg					10–20 (2)		(7×10^{-5})
Rhombohedral							
Bi	2.4×10^{-3}	2.5	0.05	−0.25	200–800	2.8	1.5×10^{-5}
Sb	5×10^{-2}	1.00	0.52	−0.65	10–16	18	1.1×10^{-3}
As	3.1×10^{-2}		0.23		300	1.6	1.5×10^{-6}
	0.19	0.96	1.77	−1.33	5	29.4	1.2×10^{-3}
Hg	(0.15)				10–14	9	$(\approx 10^{-4})$

Notes

Entries under m_1/m_0 in brackets refer to an effective mass corresponding to the values of β found from the temperature dependence in some particular direction (for details see [7]), otherwise the m's are as explained in the main text. Values of n in brackets are deduced from Eq. (22) and have only a very rough significance. Where a figure occurs in brackets after a value of P, this indicates the minimum number of observed periodic terms present simultaneously; the absence of such a figure does not however necessarily mean that only a simple periodic term is observed. The values of E_0 have been obtained from experimentally observed values of β by assuming that $P = \beta/E_0$ i.e. that the Fermi surface is ellipsoidal; if this assumption is invalid, E_0 as given in the table has only an order of magnitude significance. The value of β used in the calculation can of course be found by multiplying P and E_0, and it is helpful to remember that for a free electron $\beta = 1.85 \times 10^{-20}$; the degeneracy temperature T_0 can be obtained from E_0 by dividing by 1.38×10^{-16}.

5. Survey of the Results for Individual Metals

The numerical information is collected in Table 1, and in addition some general remarks about the shape of the Fermi surface and particular features of each metal are set out as notes; where no mention is made of the high field method, no investigation has yet been made.

Aluminium [7, 18]

Two groups of oscillations have been found (see Fig. 2f); the long period ones have not yet been properly analysed, though experiments on alloys with magnesium suggest that they come from electrons rather than holes. The short period ones can be analysed into 3 periodic terms and application of Lifshitz and Pogorelov's method shows that the relevant parts of the Fermi surface are equivalent to 3 centro-symmetric surfaces approximately of the shape shown in Fig. 6.

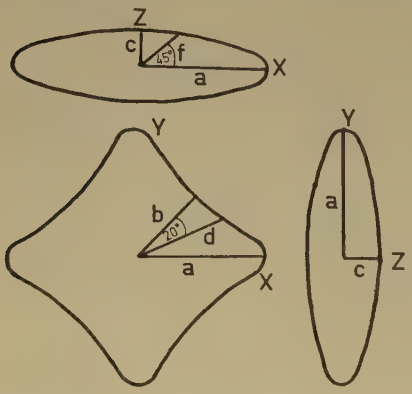

Fig. 6

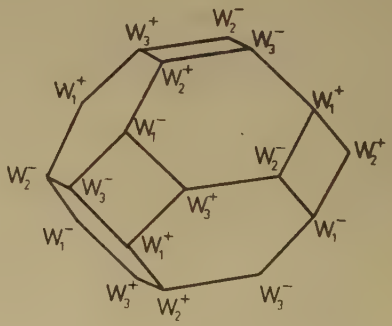

Fig. 7

Fig. 6. The diagram illustrates the relative orientations of the 3 identical cushion shaped surfaces which make up the Fermi surface in aluminium [18]. X, Y, Z are the tetrad axes. The dimensions of the surface have been calculated only for the directions indicated, and are (in units of 10^{-20} g cm sec^{-1})

$\varrho(\mathrm{a}) = 1.8$ $\varrho(\mathrm{b}) = 1.2$ $\varrho(\mathrm{c}) = 0.7$ $\varrho(\mathrm{d}) = 1.2$ $\varrho(\mathrm{f}) = 0.8$

Fig. 7. The probable locations of the holes causing the effect in aluminium are just inside the first zone at the corners W. Each group of 4 corners marked with same suffix and index (in general only 3 of each group are visible in this perspective sketch) makes up one closed surface while the + and − group for the same suffix are related by inversion symmetry. Each of the 3 ± *pairs* of surfaces correspond to *one* of the cushion surfaces of Fig. 6.

A discussion by Heine [30] suggests that these surfaces are made up of the bounding surfaces of regions of holes just inside the first Brillouin zone at the corners W (see Fig. 7). The high field method has given oscillations with $P \approx 3 \times 10^{-7}$ i.e. identical with the short period ones just discussed; no oscillations of much shorter period have been found, though Heine's discussion suggests that they should occur over a range of field directions. This negative result cannot be regarded as conclusive, since only a few field directions have been tried.

Lead [14, 25]

There seem to be two groups of oscillations (see Fig. 4 and 5) though it is not yet clear how many periods occur in each group. For many orientations, fairly long period beats are observed in the longer period group, corresponding to two nearly equal periods. The shorter period shows up most strongly for H along a [100] direction. A detailed investigation is now in progress. The longer period oscillations have also been observed by the torque method but the resolution was not good enough to obtain any accurate data.

Tin [7, 8, 9, 10, 14, 31, 32]

The low field oscillations consist mainly of two periodic terms (see Fig. 2c) and except near $\psi = 90°$ each period appears to satisfy

$$P^2 = A + B \cos 2\psi \tag{25}$$

where ψ is the angle between H and the tetragonal axis. The relevant pieces of Fermi surface appear to be approximately two ellipsoids of revolution elongated along the tetragonal axis:

$$\frac{p_x^2 + p_y^2}{2m_1} + \frac{p_z^2}{2m_3} = E_0 \tag{26}$$

where m_1, m_3 and E_0 are as shown in Table 1. This is clearly not a complete description, however, because the periods when ψ is nearly 90° no longer fit this simple scheme. If ψ is exactly 90° and the direction of H is varied relative to a binary axis, the period varies slightly, indicating clearly that at least one of the surfaces cannot be exactly a surface of revolution.

The high field effects are complicated and no detailed study has yet been made. There appear to be at least two groups of short

periods, as indicated in Table 1. From a study of the anomalous skin effect Fawcett [33] suggests that the main part of the Fermi surface in tin can be approximately represented by 3 ellipsoids, one of the same form as (25) but with masses m_1^A, m_3^A and the other two:

$$\frac{p_x^2}{2m_1^B}+\frac{p_y^2}{2m_2^B}+\frac{p_z^2}{2m_3^B}=E_0 \text{ and } \frac{p_x^2}{2m_2^B}+\frac{p_y^2}{2m_1^B}+\frac{p_z^2}{2m_3^B}=E_0, \qquad (27)$$

the values of the masses being as shown. There is a rough correspondence between Fawcett's ellipsoids and the de Haas–van Alphen periods observed for the few field directions tried, but it is not known how his ellipsoids would fit into the Brillouin zone structure of tin.

Indium [7, 9, 10]

Data obtained by the torque method are insufficient to say anything useful about the shape of the Fermi surface. No oscillations have been found at high fields, but this may be because indium has a particularly small magneto-resistance, so that eddy current inhomogeneities impede observation.

Gallium [7]

The results can be explained roughly in terms of 3 ellipsoids with the principal masses as shown, but for some orientations there are periods which do not fit into the scheme. Two typical curves are shown in Figs. 2b and 2e.

Graphite [7]

There appear to be two periods in the ratio of 4 : 3 (see Fig. 2a) and both are almost exactly proportional to $\cos\psi$ if ψ is the angle between H and the hexagonal axis. This suggests that if an ellipsoidal representation is used, each ellipsoid must be greatly elongated parallel to the hexagonal axis; the value of the long axis (i.e. of the large effective mass) is obtained rather artificially by appeal to the formula for the absolute amplitude. The estimate is particularly rough for the subsidiary oscillations and the range indicated covers extreme possible interpretations. Now the long axis of the main ellipsoid (i.e. $2(2m_3E_0)^{1/2}$), according to the figures in Table 1, is 1.8×10^{-19} g cm sec^{-1}, but the length of the Brillouin zone (a prism) in which the ellipsoid must be accommodated is h/b, where $b=6.7\times10^{-8}$ cm is the dimension of the unit cell in the direction of the hexagonal axis, and this is only

about 10^{-19} gcms^{-1}. This then supports a suggestion of Onsager [15] that the Fermi surface is really not ellipsoidal, but tubular, extending from one face of the zone to the opposite one. The two observed periods might correspond to the maximum and minimum cross sectional areas of the tube, or possibly to holes and electrons; in principle there should be at least two periodic terms for the tubes bounding the electrons and the holes, but some of these terms may be of unobservably small amplitude. A detailed discussion of the electronic structure of graphite has been given by Johnston [51], but the relation of his discussion to the de Haas–van Alphen effect data has not been worked out. In our description of the theory of the de Haas–van Alpen effect it has been implied throughout that each group of electrons or holes may be treated quite independently; in fact, interband interactions may be relevant [26], and it is possible that these may be particularly important in graphite and further complicate the interpretation.

Zinc [6, 9, 10, 25, 34, 35, 36, 37, 38, 39, 40, 41]

Verkin and Dmitrenko [40] have made the most detailed study of the variation of P with orientation and find that the main oscillations of long period (see Fig. 2d) may be represented by 3 ellipsoids of the form:

$$\frac{p_x^2}{2m_1} + \frac{p_y^2}{2m_2} + \frac{p_z^2}{2m_3} = E_0, \tag{28}$$

and two others obtained from this one by rotation of $\pm 120°$ about the p_z axis. The authors, however, do not make clear how they derive the absolute values of the masses shown; they do not appear to have made use of the temperature dependence of amplitude, and if, as seems likely, their figures are based on the field dependence (which is anomalous in zinc [25]) without any correction for level broadening, the absolute values of the m's, E_0 and n may be seriously in error. The relative values of the m's are however probably reliable and these have been combined with accurate data [25] on temperature dependence to give the figures shown. Experiments [52] on alloys with copper, suggest [24] that it is holes rather than electrons which are concerned in these long period oscillations.

Measurements in rather higher fields (up to 30 kG) show 2 further sets of oscillations of much shorter period. One of the sets of periodic terms is said by Verkin and Dmitrenko to fit a 3-ellipsoid scheme as

above, though they give no discussion of why only one period is seen for any field direction. The other has not been studied in great detail. The figures given in Table 1 must be regarded as provisional, in particular the value of E_0 is dubious (the second figure, 20×10^{-14}, is based on [25]).

A peculiarity found in zinc is that the long period value of P varies appreciably with temperature in the range above 30° K [37, 38]; this is probably connected with thermal expansion, which might well change the dimensions of the Brillouin zone enough to cause an appreciable change in the very small number of holes involved.

Cadmium [7, 9, 10, 42, 43]

The most detailed study has been made by Berlincourt [42] who finds 2 periodic terms of periods given to a fair approximation by

$$P = 1.88 \times 10^{-7} \cos(\psi \pm 28.5°)\ \mathrm{G}^{-1}$$

where ψ is the angle between H and the hexagonal axis; P does not appear to depend significantly on the angle between H and a binary axis. It has not been possible to find a sensible shape of Fermi surface which will produce this directional variation and also satisfy the hexagonal crystal symmetry. On the basis of Gunnersen's experience in studying aluminium (where a similar difficulty occurred at first), it is possible that the solution lies in the existence of other periodic terms which are of such small amplitude for most directions as to have been missed. Owing to the shortness of the period a study of cadmium is particularly difficult experimentally, so this question may remain open for some time.

Quite recently much shorter period oscillations have been found with the high field technique; no detailed investigation has yet been made.

Thallium [7]

Data obtained by the torque method are insufficient to say anything useful about the shape of the Fermi surface.

Beryllium [9, 10, 41, 44]

No detailed scheme has been worked out; the figures given for the short period oscillations are only orders of magnitude (the value of n for the short period term is given in [41] as 3×10^{-2}; this may be a misprint).

Magnesium [9, 10, 41]

The results are stated by Verkin, Dmitrenko and Mikhailov to fit the 3-ellipsoid scheme of zinc [i.e. Eq. (28)] but no details have been published.

Bismuth [1, 5, 8, 25, 43, 45]

The results fit a 3-ellipsoid scheme particularly well, but the principal axes of the ellipsoids do not coincide with those of the crystal. The ellipsoids are

$$\alpha_1 p_x^2 + \alpha_2 p_y^2 + \alpha_3 p_z^2 + 2\alpha_4 p_y p_z = 2m_0 E_0 \tag{29}$$

and two others obtained from this one by rotation of $\pm 120°$ about the p_z axis. The α's are determined in terms of effective masses $m_1 m_2 m_3$ and m_4 by the relations

$$\alpha_1 = \frac{m_0}{m_1}, \quad \alpha_2 = \frac{m_0 m_3}{m_2 m_3 - m_4^2}, \quad \alpha_3 = \frac{m_0 m_2}{m_2 m_3 - m_4^2}, \quad \alpha_4 = \frac{m_0 m_4}{m_2 m_3 - m_4^2}. \tag{30}$$

Because m_1 is very small and never enters alone into the expressions for P as a function of field direction, its relative value has to be determined by appeal to absolute amplitudes, and is therefore not very reliable. The relative values of the other masses are much more reliable but their absolute values (and that of n) depend on m_1 and are only orders of magnitude. Recent experiments on the Hall effect [46] and cyclotron resonance [47, 48] have provided some confirmation of these data.

Experiments on alloys [45] make it probable that these ellipsoids are made up of those pieces of the Fermi surface which bound electrons overlapping into the higher Brillouin zone. Heine [49] has suggested that the corresponding holes in the lower zone produce no appreciable de Haas–van Alphen effect because of their larger effective masses. Since it is probable that in bismuth the observed ellipsoids and the corresponding surface bounding the holes (probably a single ellipsoid of revolution) comprise the whole of the free Fermi surface (for a discussion see [46, 47, 48]), it is unlikely that any new oscillations will be found at high fields. None have indeed been found, although the R.F. version of the impulsive field method should have been particularly sensitive for bismuth (see § 4).

The effect of hydrostatic pressure has recently been investigated [50] (not directly on the de Haas–van Alphen effect, but on the similar

oscillations in the Hall effect); an appreciable variation of P with pressure was found.

Antimony [7, 11]

The 3-ellipsoid scheme described for bismuth fits here too, but for certain field directions there appear to be extra periods which do not fit into the scheme.

Arsenic [13]

The long period oscillations showed a variation of P with ψ in fair accord with Eq. (25), which could be interpreted as coming from a single ellipsoid of revolution of the type (26). However the absolute amplitudes are as much as 30 times greater than the theoretical ones (based on the masses as given in Table 1) and there are unexplained extra periods for some orientations. The short period oscillations fit very well into the 3-ellipsoid scheme of bismuth.

Mercury [7, 12]

No detailed study has yet been made because of the difficulty of determining the crystal orientation.

METALS AND SEMI-CONDUCTORS NOT SHOWING THE EFFECT

(a) *At fields up to* ~ 30 *kG (torque method)*

Copper [25], silver [25], gold [25], tantalum [42], molybdenum [42], titanium [42], germanium [7], tellurium [7], *n*-indium antimonide [18], *n*-gallium arsenide [18] and *n*- and *p*-lead sulphide [18].

(b) *At high fields up to* ~ 100 *kG* [14, 43] *(impulsive field method)*

Copper* [1]), silver*, gold*, sodium$^+$, titanium$^+$, uranium$^+$, nickel$^+$, silicon-iron$^+$.

It is probably not surprising that ferromagnetics show no effect in view of the high internal magnetic fields, whose local variation might well smear out any effect. It will be noticed, however, that if any oscillations occur they could be detected by the high field method

[1]) The metals marked * have been tried both by the R.F. and the direct method; those marked $^+$ have been tried only by the direct method and not in the best conditions (i.e. the crystals were of unknown quality and the technique of the method was not fully developed).

even in the presence of the high magnetization M, since the method rejects anything but an oscillatory variation of $\mathrm{d}M/\mathrm{d}H$ (I owe this remark to Dr. R. Street).

Apart from the germanium and tellurium specimens, the semi-conductors were deliberately chosen to have a sufficiently high electron density to produce a not too long period; the negative results may well be due to broadening of the energy levels because of short collision times, but it is also possible that in some of the materials examined, the Fermi surface may have been very nearly spherical so that the torque might have been unobservably small. Further experiments using the force method and a wider range of specimens are required before the negative results on semi-conductors can be accepted with confidence. In conclusion it should be noted that any negative results must be accepted with caution, since quite often in the past the de Haas–van Alphen effect has been observed in metals for which negative results had been earlier reported. Thus future improvements in the techniques of measurement and of preparation of specimens may well show up the effect in some of the metals quoted above as giving negative results.

I should like to thank Dr. R. G. Chambers and Mr. V. Heine for their valuable advice and criticism in the preparation of this article.

NOTES ADDED IN PROOF (Sept. 1956)

1. I have recently learnt that Onsager's result [15] was obtained independently by I. M. Lifshitz and reported to a meeting of the Ukrainian Academy of Sciences in January 1951.

2. Further consideration of the influence of eddy currents in the impulsive field method shows that although the amplitude of the signal should be much reduced after q oscillations (see (24)), the residual signal should still be amply large enough to observe if $\mathrm{d}M/\mathrm{d}H$ has its theoretical value for a monovalent metal. This residual signal should be approximately independent of $\mathrm{d}H/\mathrm{d}t$ and of radius.

3. It should be noted that the number of ellipsoids mentioned in § 5 as required to account for the data for each metal is merely the *minimum* number. It is assumed in fact that the ellipsoids can be considered as effectively centred at the origin and if this assumption fails, further identical ellipsoids may be required to preserve crystal symmetry; e.g. each of the 3 bismuth ellipsoids might well require duplication at an appropriate position in p-space. Such possible multiplication would, of course, involve corresponding multiplication of the values of n in Table I.

4. Since this article was written, the author has examined a number of

further metals in fields up to 80 kG by the direct method. Short period oscillations were found in magnesium (4 and 0.6), molybdentim (2 and 0.4) and tungsten (2, 0.4 and 0.07); the numbers indicate typical values of $10^7 \times P$ in G^{-1}. Beryllium and zinc showed only the moderately short period oscillations of the groups already found by the torque method (Table I). The following metals gave negative results: antimony, gallium, graphite, lithium, mercury, niobium, rhenium, tantalum, thallium and zirconium.

REFERENCES *

1 W. J. de Haas and P. M. van Alphen, Leiden Comm. 208d, 212a (1930) and 220d (1932).
2 R. Peierls, Z. Phys., **81**, (1933).
3 M. Blackman, Proc. Roy. Soc. A, **166**, 1 (1938).
4 L. D. Landau, appendix to 5.
5 D. Shoenberg, Proc. Roy. Soc. A, **170**, 341 (1939).
6 J. A. Marcus, Phys. Rev., **71**, 559 (1947).
7 D. Shoenberg, Phil. Trans. A, **245**, 1 (1952).
8 B. I. Verkin, B. G. Lazarev and N. S. Rudenko, Doklady Akad. Nauk S.S.S.R., **69**, 773 (1949).
9 B. I. Verkin, B. G. Lazarev and N. S. Rudenko, J. Exp. Th. Phys. U.S.S.R., **20**, 93 (1950).
10 B. I. Verkin, B. G. Lazarev and N. S. Rudenko, J. Exp. Th. Phys. U.S.S.R., **20**, 995 (1950).
11 B. I. Verkin, B. G. Lazarev and N. S. Rudenko, J. Exp. Th. Phys. U.S.S.R., **21**, 658 (1951).
12 B. I. Verkin, B. G. Lazarev and N. S. Rudenko, Doklady Akad. Nauk. S.S.S.R., **80**, 45 (1951).
13 T. G. Berlincourt, Phys. Rev., **99**, 1716 (1955).
14 D. Shoenberg, Physica, **19**, 791 (1953).
15 L. Onsager, Phil. Mag., **43**, 1006 (1952).
16 I. M. Lifshitz and A. M. Kosevich, J. Exp. Th. Phys. U.S.S.R., **29**, 730 (1955).
17 I. M. Lifshitz and A.V. Pogorelov, Doklady Akad. Nauk, **96**, 1143 (1954).
18 E. M. Gunnersen, Phil. Trans. A, in the press; also PhD. Thesis, Cambridge (1956).
19 A. B. Pippard, Reports 10th Solvay Congress, 1955, p. 123.
20 M. C. Steele, Phys. Rev., **99**, 1751 (1955).
21 G. E. Zilberman, J. Exp., Th. Phys. U.S.S.R., **29**, 762 (1955).
22 R. B. Dingle, Proc. Roy. Soc., A, **211**, 500 (1952).
23 R. B. Dingle, Proc. Roy. Soc. A, **211**, 517 (1952).
24 V. Heine. Proc. Phys. Soc., in the press.
25 J. S. Dhillon and D. Shoenberg, Phil. Trans. A, **248**, 1 (1955).
26 P. G. Harper, Proc. Phys. Soc. A, **68**, 874, 879 (1955).

* This is a fairly complete bibliography of experimental papers, but mentions only a selection of the theoretical papers; a fairly complete list of theoretical papers up to 1952 is given in [7].

[27] A. D. Brailsford, to be published.
[28] G. T. Croft, F. J. Donahoe and W. F. Love, Rev. Sci. Inst. **26**, 360 (1955).
[29] A. V. Gold, to be published.
[30] V. Heine, to be published.
[31] T. G. Berlincourt, Phys. Rev., **88**, 242 (1952).
[32] G. T. Croft, W. F. Love and F. C. Nix, Phys. Rev., **95**, 1403 (1954).
[33] E. Fawcett, Proc. Roy. Soc. A, **232**, 519 (1955).
[34] L. Mackinnon, Proc. Phys. Soc. B, **62**, 170 (1949).
[35] S. G. Sydoriak and J. E. Robinson, Phys. Rev., **75**, 118 (1949).
[36] B. I. Verkin, Doklady Akad. Nauk S.S.S.R., **81**, 529 (1951).
[37] B. I. Verkin and I. F. Mikhailov, J. Exp. Th. Phys. U.S.S.R., **24**, 342 (1953).
[38] T. G. Berlincourt and M. C. Steele, Phys. Rev., **95**, 1421 (1954).
[39] F. J. Dohanoe and F. C. Nix. Phys. Rev. **95**, 1395 (1954).
[40] B. I. Verkin and I. M. Dmitrenko, Izv. Akad. Nauk S.S.S.R., (Fiz. ser.) **19**, 409 (1955).
[41] B. I. Verkin, I. M. Dmitrenko and I. F. Mikhailov, Doklady Akad. Nauk S.S.S.R., **101**, 233 (1955).
[42] T. G. Berlincourt, Phys. Rev., **94**, 1172 (1954).
[43] D. Shoenberg, Report to Conference on Magnetism, Moscow (1956).
[44] B. I. Verkin and I. F. Mikhailov, J. Exp. Th. Phys. U.S.S.R., **25**, 471 (1953).
[45] D. Shoenberg and M. Z. Uddin, Proc. Roy. Soc. A, **156**, 701 (1936).
[46] B. Abeles and S. Meiboom, Phys. Rev., **101**, 544 (1956).
[47] B. Lax, K. J. Button, H. J. Zeiger and L. M. Roth, Phys. Rev., **102**, 715 (1956).
[48] M. Tinkham, Phys. Rev., **101**, 902 (1956).
[49] V. Heine, Proc. Phys. Soc., in the press.
[50] W. C. Overton and T. G. Berlincourt, Phys. Rev., **99**, 1165, (1955).
[51] D. F. Johnston, Proc. Roy. Soc. A, **227**, 349, 359 (1955).
[52] J. A. Marcus, Phys. Rev. **77**, 750 (1950).

CHAPTER IX

PARAMAGNETIC RELAXATION

BY

C. J. GORTER

KAMERLINGH ONNES LABORATORIUM, LEIDEN

CONTENTS: 1. Introduction, 266. — 2. Description of the spin-lattice relaxation with the Casimir–Du Pré formulae, 271. — 3. Relaxation at very low temperatures, 274. — 4. Relaxation in the spin system, 279.

1. Introduction

If Curie's law

$$M = \frac{CH}{T} \tag{1}$$

where M is the magnetization (per mole) of a sample, T its temperature and H the magnetic field, is valid in a good approximation it is customary to speak about "normal paramagnetism". According to Langevin [1] "normally paramagnetic" substances owe their magnetic properties to free permanent magnetic dipoles. These magnetic dipoles may have different orientations with respect to the field H and these different orientations have different energies. If a Boltzmann distribution over these orientations is realised, this leads according to Langevin, at not loo low temperatures T and not too high fields H, to Curie's law (1), in which the Curie constant C is proportional to the number of dipoles (per mole) and to the square of their magnitude. The condition under which (1) is thus derived is that the maximum value of the energy difference between two orientations is small compared to kT, where k is Boltzmann's constant. If the ratio H/T is increased more and more, deviations from (1) will occur and M will finally reach a constant saturation value. This occurs at liquid helium temperatures in fields above 10^4 ø.

According to quantum theory the state of affairs is in general somewhat more complicated [2, 3]. If we have only one occupied degenerate energy level which splits lineary into a number of Zeeman components, however, Langevin's simple description still holds true.

The magnetic dipole moment then is a diagonal matrix, which indicates that each Zeeman level has a constant moment in the direction of the field H. The Boltzmann distribution leads, for low values of H/T, to (1) with a Curie constant

$$C = \frac{N}{pk} \sum_l M_{ll}^2 \tag{2}$$

where the M_{ll}'s denote the diagonal elements of the magnetic moment, p gives the number of non-degenerate levels over which the summation takes place while N is the number of dipoles (per mole).

If, however, the energy splittings are not strictly linear in H, which may occur if we have to do with the influence of internal electric fields on the carriers of the dipoles, or with hyperfine structures, non-diagonal matrix elements of the magnetic dipole moment also come into the picture. In case the energy splittings concerned are all very small compared with the energy distances to other (groups of) energy levels the theorem of "spectroscopic stability" applies according to which $\sum_l \sum_{l'} M_{ll'}^2$, where the summation is taken over diagonal and non-diagonal combinations of the p states, is independent of the nature and magnitude of the splittings.

Both the diagonal and the non-diagonal elements of M contribute to the change of the magnetization when the field is modified, but according to very different mechanisms. If we increase the field H by ΔH, the energy of the state l changes by $-M_{ll}\Delta H$ and therefore the Boltzmann distribution, supposed to be existing originally, will be disturbed. When it is re-established the magnetization will have increased. If we suppose all the energy differences between the p levels to be very small compared to kT, the increase in magnetization will be

$$(\Delta M)_d = N \frac{\sum_l M_{ll}^2}{pkT} \Delta H \tag{3}$$

where the summation only extends over the diagonal combinations. In the derivation of (3) we have made use of $\sum_l M_{ll} = 0$.

On the other side, the magnetic moment M_{ll} of the state l increases by $\sum_{l'} 2M_{ll'}^2 \Delta H/(W_{l'} - W_l)$. Thus a non-diagonal element $M_{ll'}$ leads to an increase of the magnetic moment of the lower one of the two states l and l' and to a decrease of the same magnitude of the higher one. Since we suppose the Boltzmann distribution to apply before the introduction of ΔH, this leads to an average increase of the

magnetic moment per atom in one of the states l and l', of $M_{ll'}^2 \Delta H/kT$ and, taking the sum over all non-diagonal combinations, we obtain

$$(\Delta M)_{nd} = N \frac{\sum_l \sum_{l'} M_{ll'}^2}{pkT} \Delta H \tag{4}$$

where each $M_{ll'}^2$ appears twice in the double sum.

Van Vleck [2] has stressed that, according to the theorem of "spectroscopic stability" mentioned, the sum of (3) and (4) under the conditions stated is independent of the nature and the magnitude of the splittings, and this explains why, in spite of considerable differences in character and magnitude of the splittings, and thus of the magnetic resonance spectra, the various diluted salts of ions having the same number of electrons have practically the same static molar susceptibilities M/H at not too low temperatures.

The splittings mentioned only lead to a small contribution to the specific heat, which is inversely proportional to T^2.

Van Vleck [4] has also analysed the influence of magnetic and exchange interaction between the dipoles. For many purposes the magnetic interaction may be characterized adequately by the root mean square value H_i of the magnetic field brought about at the position of one dipole by the surrounding dipoles. When $M_{ll} H_i \ll kT$ the change of the magnetic moment per mole is still given by the invariant sum of (3) and (4) while a computable contribution to the specific heat inversely proportional to T^2 results. The same conclusions apply for sufficiently weak exchange interactions.

The three different contributions to the specific heat, which are all inversely proportional to T^2, are additive in a first approximation. We note incidentally that in other respects exchange interaction radically modifies the effects due to splittings and magnetic interaction [5].

When we study the magnetization of a paramagnetic sample in a varying magnetic field we encounter paramagnetic relaxation and paramagnetic resonance. Both of them are usually studied in an harmonically varying magnetic field superposed on a constant field H_c.

$$H = H_c + h \cos \omega t. \tag{5}$$

The resulting magnetization is then

$$M = \chi_0 H_c + \chi' h \cos \omega t + \chi'' h \sin \omega t \tag{6}$$

where the static susceptibility χ_0, as well as the real part χ' and the

imaginary part χ'' of the oscillatory susceptibility, are tensors of the second order. The components χ' and χ'' are not completely independent but are interconnected by the Kramers–Kronig relations [6, 3].

If χ' and χ'' vary rapidly in a narrow frequency range we speak of paramagnetic resonance. This resonance comes to the fore when h is perpendicular to H_c. If we focus our attention on the individual dipoles we may say that it occurs if $\hbar\omega \approx W_{l'} - W_l$, where $\hbar$ is Planck's constant h devided by 2π, and that its over-all intensity is proportional to $M^2_{ll'}$. If h is parallel to H_c and if χ' and χ'' do not vary rapidly, we speak of paramagnetic relaxation, in particular if the frequencies used are small compared to those required for the observation of resonance. We shall see in § 4 that relaxation is often in particular concerned with the diagonal elements M_{ll} of the individual dipole moments. It is not always easy to make a clear distinction between the effects of resonance and of relaxation. Historically the discovery of paramagnetic resonance by Zavoisky [7] sprang from his investigations on paramagnetic relaxation.

At relatively low frequencies χ' and χ'' are usually measured simultaneously by means of a Hartshorn bridge, such as is standard in the investigations on adiabatic demagnetization (see Vol. I, Ch. XIV). In the Leiden set-up the frequency interval now available ranges from 3 to 1200 Hz. The accuracy is of the order of 10^{-7} in the sample permeability [8, 9].

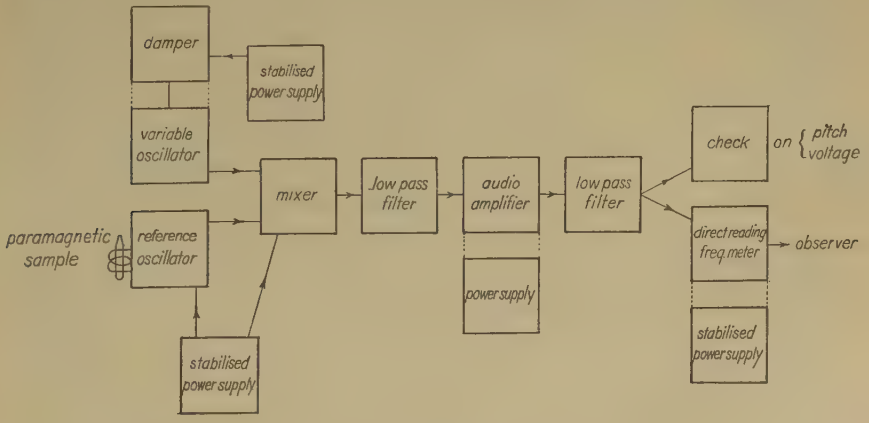

Fig. 1. Block diagram of the beat frequency apparatus used by Broer and Schering for the measurement of χ'.

At radio frequencies χ' is usually measured by means of a high frequency oscillator circuit into the coil of which the paramagnetic sample may be moved. The variation of the beat frequency with a constant oscillator is observed. This method is used from about 10^5 Hz to 2×10^7 Hz. The relative accuracy in frequency is of the order of $10^{-6} - 3 \times 10^{-8}$ which leads to an accuracy in the sample permeability of 3×10^{-5} to 10^{-7} [10]. By means of a more complicated twin T bridge, χ'' and χ' may be measured simultaneously with a comparable accuracy.

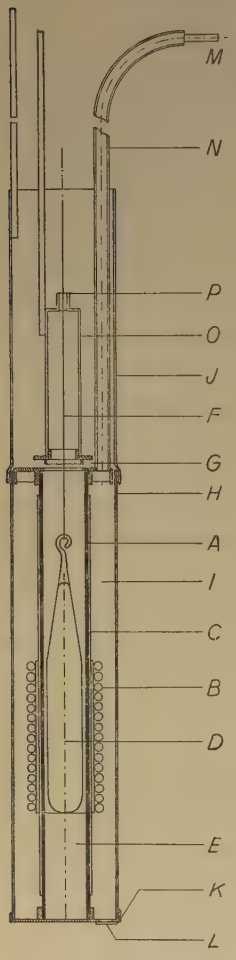

Fig. 2. Coil of the oscillator into which the paramagnetic sample is moved.

The calorimetric method [11] to measure χ'' extends from about 10^5 to 10^8 Hz. The sample is contained in a glass calorimeter-gasthermometer and subjected to a high frequency magnetic field caused by a high frequency current in a coil or a Lecher system. The heat developed in the sample is measured by the rise in pressure of the gas. Since the amplitude of the high frequency current may be taken large, the accuracy may be quite good, at liquid hydrogen temperatures of the order 10^{-8} in the sample permeability. The determination of the absolute values of χ'' requires the determination of the heat capacity of the calorimeter and of the amplitude of the high frequency field, and is thus much less accurate than are the relative values in different fields. Since the method is rather time consuming its application is at present confined to the frequencies above 10^7 Hz where no other accurate method is available.

Zavoisky and his school [12] observe variations in an oscillating high frequency circuit by carefully watching the d.c. grid current of the oscillator tube. In this way minute changes in the effective resistance of the oscillator coil may be detected. It is very remarkable that in this way an accuracy in the sample permeability of 10^{-8} has been obtained.

For a more thorough description of the theoretical background

and of the experimental methods the original literature should be consulted. For the state of affairs in this field ten years ago the author refers to his early monograph on the subject [3]. An excellent but shorter review has been published by Cooke a few years later [14].

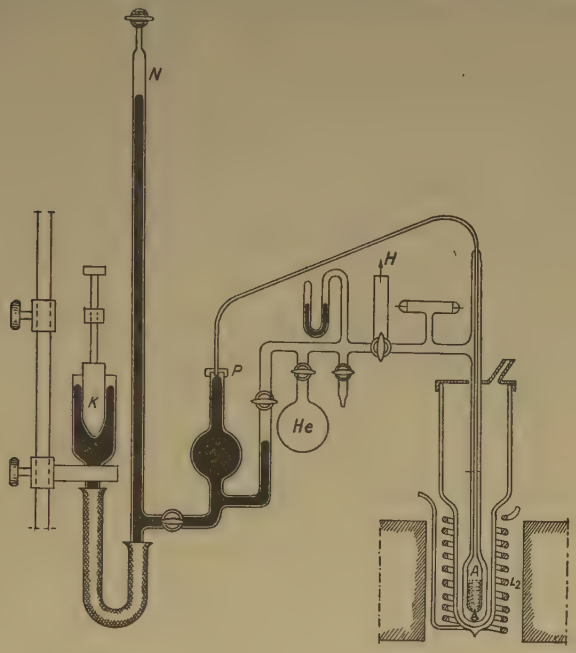

Fig. 3. Calorimetric method for the measurement of χ''.

2. Description of the Spin-Lattice Relaxation with the Casimir-Du Pré formulae

In a normally paramagnetic substance we have, according to Van Vleck, a system of almost independent magnetic dipoles, the splittings and shifts of their energy levels due to the constant parts of the internal electric fields and the external magnetic field being small compared to kT, while this also applies to the magnetic and exchange interactions between a dipole and its neighbours. This system of dipoles was called the spin system by Casimir and Du Pré [14] and they have introduced the supposition that, even in varying external magnetic fields, it is at any moment in internal equilibrium. The occupation of its energy levels would then be according to Boltzmann factors $\exp(-W/kT_s)$, in which T_s is the so-called spin temperature. The interaction with the heat motion of the surroundings,

i.e. the heat waves in the crystal lattice in which the dipoles are placed, is supposed to give rise to a transfer of energy $\alpha(T-T_s)$ per second. If the angular frequency ω of the oscillating part of the magnetic field is so high that the transfer of energy from and to the lattice is negligeable, the spin temperature T_s oscillates with the angular frequency ω. Consequently the variation of the magnetic moment is given by an adiabatic susceptibility [15].

$$\chi_{ad} = \frac{C_M}{C_H}\chi_0 \tag{7}$$

where C_M and C_H are the specific heats of the spin system at constant magnetic moment and constant external field respectively, while $\chi_0 = (\partial M/\partial H)_T$.

In a normally paramagnetic substance Curie's law (1) applies to a very high approximation in which case $C_M = b/T^2$, $C_H = (b+CH_c^2)/T^2$, where the constant b depends on the structure of the energy levels occupied by the dipoles. Consequently

$$\chi_{ad} = \frac{b}{b+CH_c^2}\chi_0 \tag{8}$$

according to which the adiabatic susceptibility decreases with increasing field, reaching half its original value at $H_c = \sqrt{b/C}$. If the angular frequency ω is decreased so far that the energy transfer to and from the surroundings plays a rôle, the susceptibility goes over into the static susceptibility χ_0 according to

$$\chi = \chi' - i\chi'' = \frac{CH_c^2\chi_0}{(b+CH_c^2)(1+i\tau\omega)} + \frac{b\chi_0}{b+CH_c^2} \tag{9}$$

with

$$\tau = C_H/\alpha = (b+CH_c^2)/\alpha T^2 \tag{10}$$

which, introducing

$$F = \frac{CH_c^2}{b+CH_c^2} \tag{11}$$

is often written as

$$\chi' = \frac{F\chi_0}{1+\tau^2\omega^2} + (1-F)\chi_0 \tag{12}$$

$$\chi'' = \frac{F\chi_0\tau\omega}{1+\tau^2\omega^2}. \tag{13}$$

In this form Casimir and Du Pré's formulae are usually compared with the experimental data which, in fact, very often give a Debije function for the absorption coefficient χ'' and a Debije function plus a constant term for the high frequency susceptibility χ', while F depends on the constant field as predicted by (11).

In nearly all researches carried out on χ' down to the temperatures of liquid oxygen and nitrogen good agreement is found with Eq. (12) and (11) and so their results can be described [3] by giving the value b/C and τ as a function of H_c and T. Often τ as a function of H_c is given by [16]

$$\tau = \tau_0 \frac{b + CH_c^2}{b + pCH_c^2} \tag{14}$$

with p independent of T, which is also in agreement with the theoretical expectation [17] for this temperature region. Then the complete data are described by giving τ_0 as a function of T and moreover the constants b/C and p.

b/C gives an accurate and valuable determination of the specific heats of the spin system which in general agrees with that quantity derived from direct specific heat measurements, magnetic resonance spectra or adiabatic demagnetization (see Vol. I, Ch. XII, XIV).

According to the theory of Waller [18], Kronig [19] and Van Vleck [17] the energy transfer between the spins and the crystalline lattice at these temperatures is due to in-elastic scattering of phonons, the so-called quasi-Raman process. This leads to the general conclusion that, if the temperature is low compared to the Debije characteristic temperature, τ_0 should be proportional to T^{-7} and if it is high compared to this characteristic temperature, it should be proportional to T^{-2}. The magnitude of the interaction is dependent on the orbital contribution to the spins. This makes it understandable that ions in which this orbital contribution is small (Cr^{+++}, Mn^{++}, Fe^{+++}, Gd^{+++}) have relatively long relaxation times. Only rough predictions on the magnitudes of τ_0 have been given. If one considers the experimental data it is striking that in hydrated salts τ_0 is not very different in different salts of the same ion. In Mn^{++}-salts it is much longer than in the isoelectronic Fe^{+++}-salts, while in different Gd^{+++}-salts τ_0 shows a peculiar anomaly at liquid air temperatures leading to a very feeble dependence of τ_0 on T in a wide range of temperatures [3]).

p is generally found to be smaller than 1 which means that τ

increases with H_c. In some cases it is nicely independent of T, but in other cases it is not. It may be, however, that the effects to be described in § 4, having to do with relaxation inside the spin system, have confused this issue somewhat.

The amount of data on χ'' is much smaller than that on χ'. It is generally found that already in zero field χ'' differs from zero and consequently it has become customary to add a second term to (13) which is proportional to ω:

$$\chi'' = \frac{F\chi_0 \tau\, \omega}{1+\tau^2\, \omega^2} + (1-F)\, \chi_0 \tau'\, \omega. \qquad (15)$$

Such a term would account for the time which the spin system requires to reach equilibrium, and thus describe a small deviation from the basic supposition of Casimir and Du Pré that the spin system is at any moment in internal equilibrium. In agreement with the theoretical treatment of Waller [18] and Broer [20] on the so-called spin-spin relaxation, τ' was in many cases found to be independent of T and to be of the order of $\hbar/\beta H_i$ where β is the Bohr magneton. In these cases $\tau'\omega$ was considerably smaller than 0.1 which means that a corresponding term in the expression (12) for χ' should be negligeable. It will be shown in § 4 that in many cases (15) is too simple an expression and the whole problem of the spin-spin relaxation in a magnetic field has to be reconsidered.

Finally we remark that the data on χ' and χ'' at liquid helium temperatures have a complicated character and were, during a long time, considered to be in flagrant disagreement with the theoretical expectations. They will be treated in § 3.

3. Relaxation at Very Low Temperatures

Quite early [21] it was observed that at liquid helium temperatures the slopes of the χ'-curves are often smaller, and the maxima of the χ''-curves flatter, than is predicted by (12) and (13). This can formally be described by introducing more than one relaxation time or even a continuous distribution of relaxation times. It is customary to introduce an average relaxation time by giving the inverse angular frequency at which χ' is equal to $\chi_0(1-F/2)$ or at which χ'' has its maximum. These two ways of defining τ_{av} seldom give widely different results. If they do, it is an indication of the existence of two very different kinds of relaxation. This may be striking in large crystals

or large pressed powder samples of non diluted salts [22], and is apparently due to the rôle of the heat transport between the inner and the outer parts of the sample.

In the cases that τ_{av} is rather short, it often varies with a high

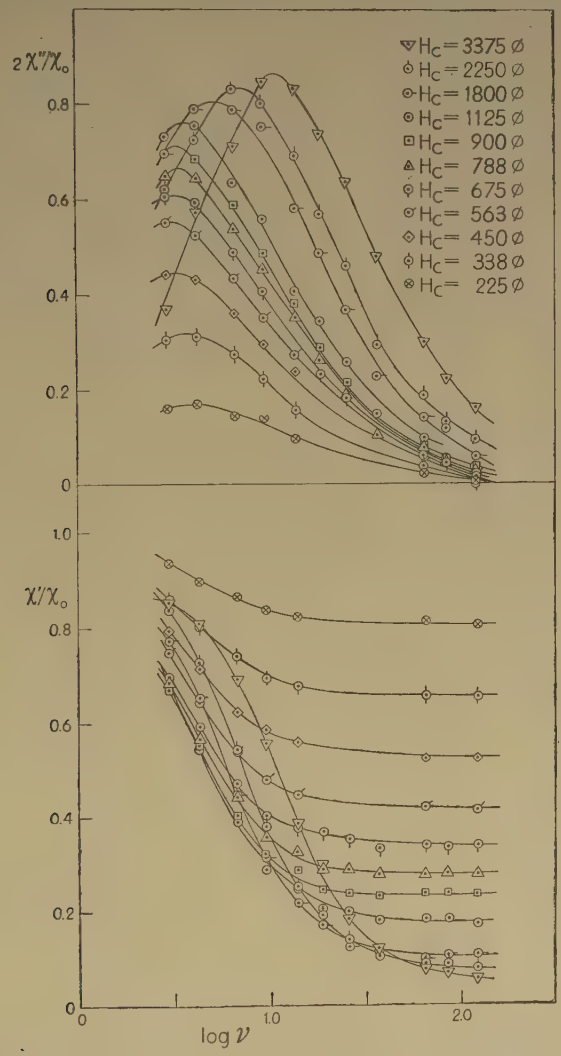

Fig. 4. $2\chi''/\chi_0$ and χ'/χ_0 as a function of log $\nu = \log(\omega/2\pi)$ for powdered $Fe_{0.016}Al_{0.984}NH_4(SO_4)_2 \cdot 12H_2O$ at $T = 2.339°$ K.

negative power of T (-3 to -5) and increases with rising H_c, while in the cases that τ_{av} is relatively long (of the order of 0.1 second or

longer), it frequently varies with a small negative power of T (-1 to -2) and decreases in large fields inversely proportional to H_c. This latter case is often encountered in salts in which the magnetic ions

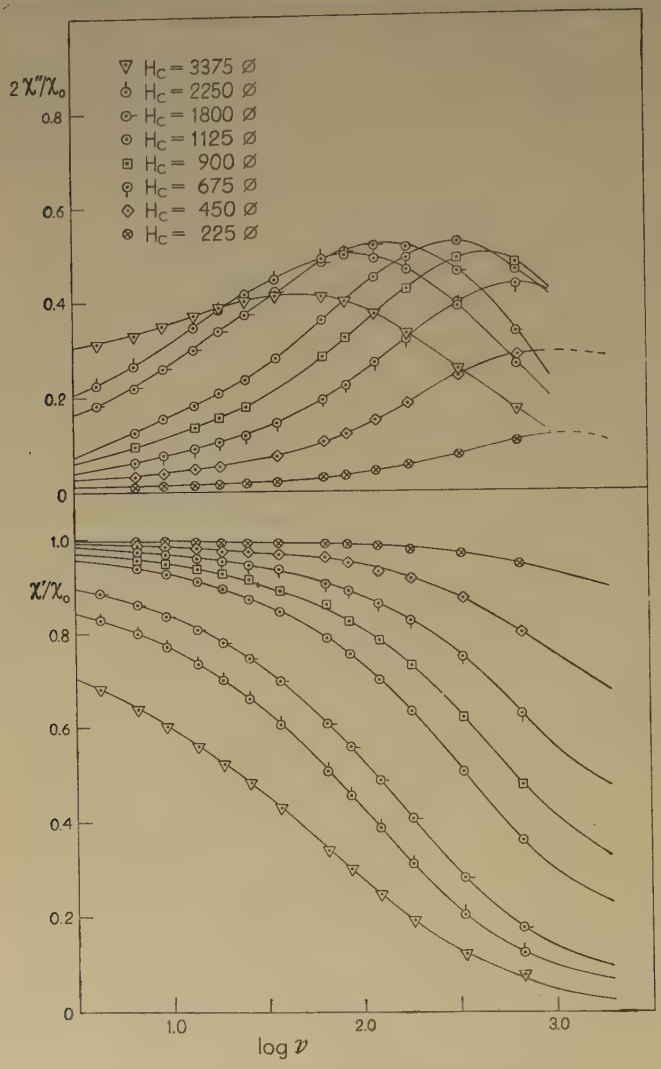

Fig. 5. $2\chi''/\chi_0$ and χ'/χ_0 as a function of $\log \nu = \log (\omega/2\pi)$ for a compressed cylinder with a diameter of 2 cm of $FeNH_4(SO_4)_2 \cdot 12H_2O$ at 2.883° K.

have been diluted with non-magnetic ions of the same valency. Another pecularity is that, even in the non diluted salts, τ_{av} may

vary considerably from sample to sample, even if no detectable chemical differences occur. It must, however, be noted that the irreproducibilities only are concerned with the frequency dependence of χ' and χ'', but do not influence χ_{ad}, observed at the high frequencies, which is invariably given by (8). The Fig. 4, 5 and 6 give a few examples of χ' and χ'' as functions of the frequency $\nu = \omega/2\pi$ and of $\varrho_{av} = 2\pi\tau_{av}$ as a function of H_c.

According to theoretical evaluations, the inelastic scattering of phonons (see § 2) is ineffective at these low temperatures and the energy transfer between the spins and the crystalline lattice should be provided for by straight forward absorption and emission of phonons. This would lead to a relaxation time τ which is proportional to T^{-1}, while it should decrease with increasing H_c. In fields larger than $(b/C)^{\frac{1}{2}}$ the relaxation time should be [17] inversely proportional to $H_c^{\,2}$. This expected behaviour is very different indeed from that found experimentally for τ_{av}.

Temperley [23] has suggested that different spins might flip simultaneously which would cause a decrease of τ in non diluted salts in small fields. Though his theoretical arguments have been contested by Van Vleck [17], it cannot be denied that the dependence of τ_{av} on H_c agrees qualitatively with his expectations.

Van Vleck [24] has called the attention to a difficulty inherent to the energy exchange by emission and absorption of phonons at very low temperatures. This absorption and emission of phonons only concerns a narrow region of lattice oscillators which are, so to say, on speaking terms with the spins. The other oscillators, which contain almost the whole thermal energy of the crystal, will only be affected secondarily e.g. through anharmonicity of the elastic forces and, in the case of low frequencies and low excitations, this will lead to a severe bottleneck for the transfer of energy to and from the spin system. In contrast to Temperley's proposal this would lead to an increase of τ. The excitation of the oscillators "on speaking terms" would then vary periodically with the spin temperature, while the real bottleneck of the observed relaxation phenomena would not be the interaction between the spins and the oscillators "on speaking terms" but the transformation of the energy of these oscillators into energy of all oscillators and thus into heat and vice versa. This transformation might be caused by the anharmonicity, already mentioned, of the elastic forces, but Van Vleck's evaluation of this possibility

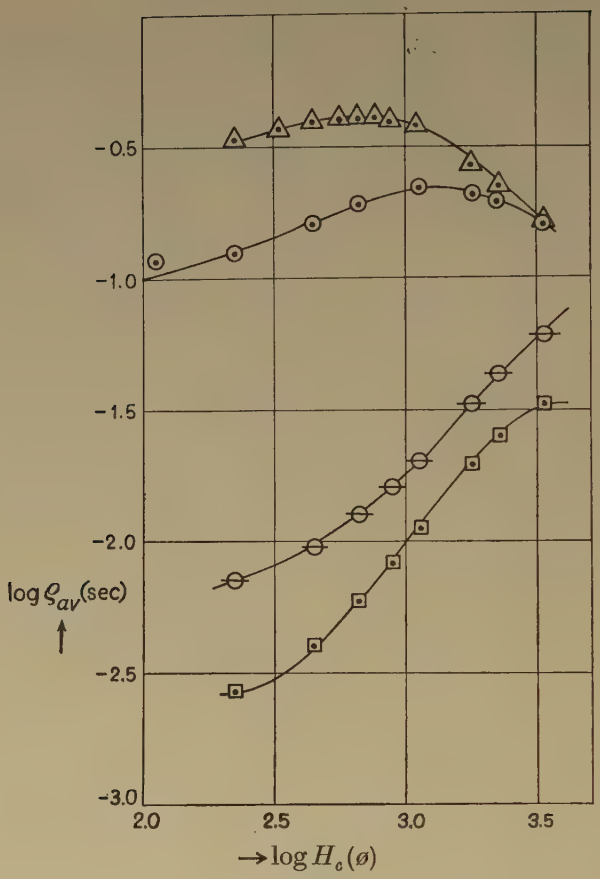

Fig. 6. $\varrho_{av} = 2\pi\,\tau_{av}$ for iron ammonium alum and a number of diluted alums as a function of the parallel field H_c

▽ Fe $NH_4(SO_4)_2 \cdot 12H_2O$; $T = 2.050°$ K
⊙ $Fe_{0.23}\,Al_{0.77}(SO_4)_2 \cdot 12H_2O$: $T = 1.645°$ K
⊖ $Fe_{0.052}\,Al_{0.948}(SO_4)_2 \cdot 12H_2O$; $T = 1.727°$ K
⊡ $Fe_{0.016}\,Al_{0.984}(SO_4)_2 \cdot 12H_2O$; $T = 1.706°$ K.

makes it plausible that at the lower temperatures other mechanisms, e.g. transport by the oscillators "on speaking terms" to crystal boundaries or defects where the transformation may be easy, must prevail.

A very provisional evaluation of this last case [25], energy transport by oscillators "on speaking terms", has led to the prediction that $\tau_{av} \infty (b+CH^2)T^{-2}c^{-3})$ for small values of H_c and $\tau_{av} \infty H_c^{-1}T^{-2}c$ for large values of H_c, where c is the concentration of the magnetic ions/

(b and C increase with rising c). These predictions account for a number of data. However, it looks as if for relatively large values of c and T a mechanism that depends more rapidly on T (e.g. the anharmonicity mentioned) may also play a rôle, while in powders of high magnetic anisotropy [26] the exchange of heat between different particles may come into the picture. The theoretical analysis of the behaviour of the oscillators "on speaking terms" is in a shockingly primitive state and it is quite possible that a more thorough theoretical consideration would immediately clarify the situation.

Eschenfelder and Weidner [27] have studied the so-called saturation of paramagnetic resonance by supplying high microwave power to certain magnetically diluted crystals. From this study, relaxation times τ could be derived which are considerably shorter than those obtained by straight forward relaxation measurements, and which are approximately inversely proportional with T^{-1} and independent of c, in agreement with the original theoretical expection for the bottleneck caused by absorption and emission of phonons. Preliminary results obtained in Leyden suggest that this, however, only applies if the spin temperature is considerably increased above the bath temperature. This would indicate that if the effective temperature of the oscillators "on speaking terms" is sufficiently high, the transformation of their energy into heat causes no difficulty so that the bottleneck again would be that between the spins and the oscillators "on speaking terms". For these cases then Temperley's explanation would have to be abandoned, which explanation also seems to be in disagreement with certain temperature dependences of τ.

4. Relaxation in the Spin System

In § 2 it was noted that in many cases at liquid air temperatures, and above, χ'' is satisfactorily described by Eq. (15), with the quantity $(1-F)\tau'$ in the last term independent of temperature. In some cases, however, deviations are found and one might try to test the formula proposed by Shaposhnikov [28] for the case that the ratio between the internal spin-spin relaxation time τ' and the spin-lattice relaxation time τ is not very small. The obvious way, however, to eliminate the influence of τ is to reduce the temperature and then to utilize angular frequencies $\omega \gg \tau^{-1}$. This is done by going to liquid hydrogen temperatures, where in many salts τ is of the order of 10^{-4} or 10^{-5} sec, which leaves the easily accessible interval between 10^5 and 10^8 Hz,

available for the study of absorption and dispersion phenomena inside the spin system. So far these phenomena are found to be independent of T but the last term is (15) is too simple to describe them [29, 30].

Let us consider the measurements on some salts of the iron group and first fix our attention on the dependence of χ'' on H_c at constant values of the frequency. The Fig. 7, 8 and 9 give a few examples of this dependence; the dotted line gives $\chi''/\chi''_{H_c=0} = 1 - F$ which should

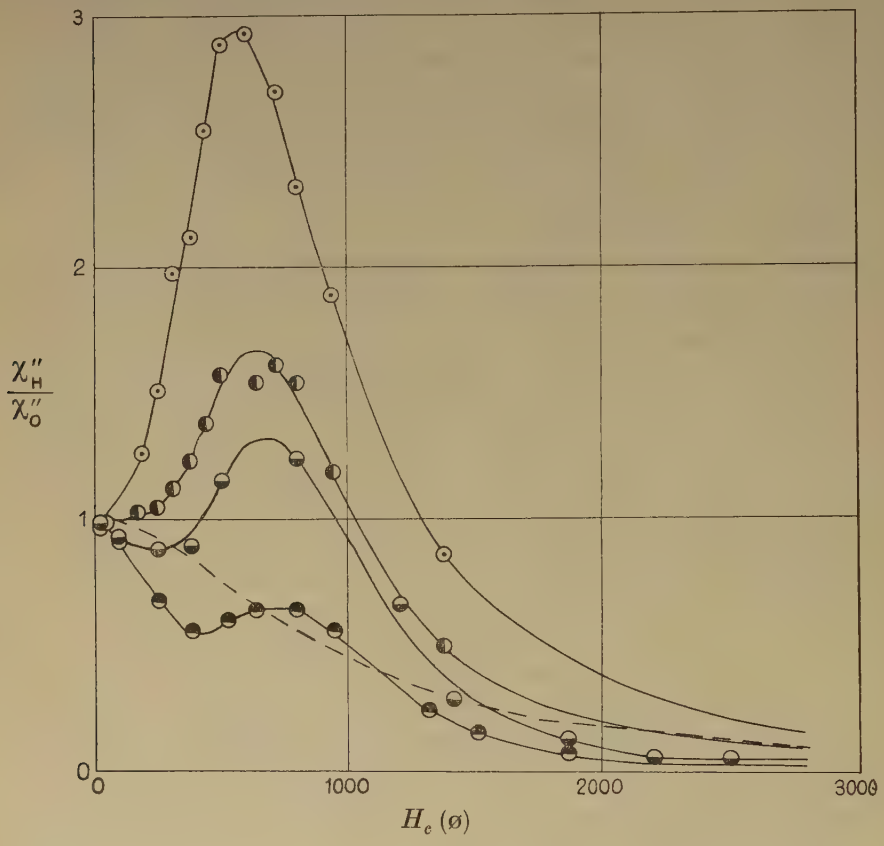

Fig. 7. χ'' relative to its value in zero field as a function of the parallel field H_c for $CrK(SO_4)_2 \cdot 12H_2O$ at 20.4° K

⊙ 23.1 MHz
◐ 35.9 MHz
◒ 44.4 MHz
◓ 83.0 MHz
– – – – $1 - F = b/(b + CH_c^2)$.

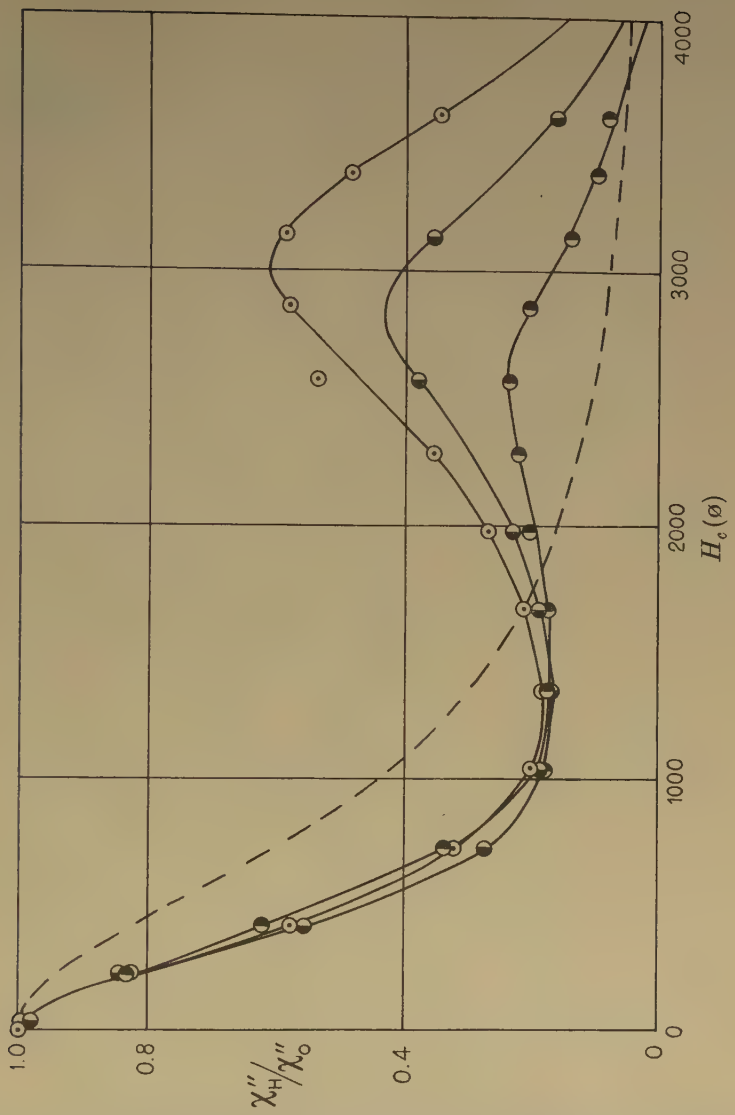

Fig. 8. χ'' relative to its value in zero field as a function of the parallel field H_c for $Mn(NH_4)_2(SO_4)_2 \cdot 6H_2O$ at 20.4° K

⊙ 11.9 MHz
◐ 20.0 MHz
◑ 40.2 MHz
---- $1 - F = b/(b + CH_c^2)$.

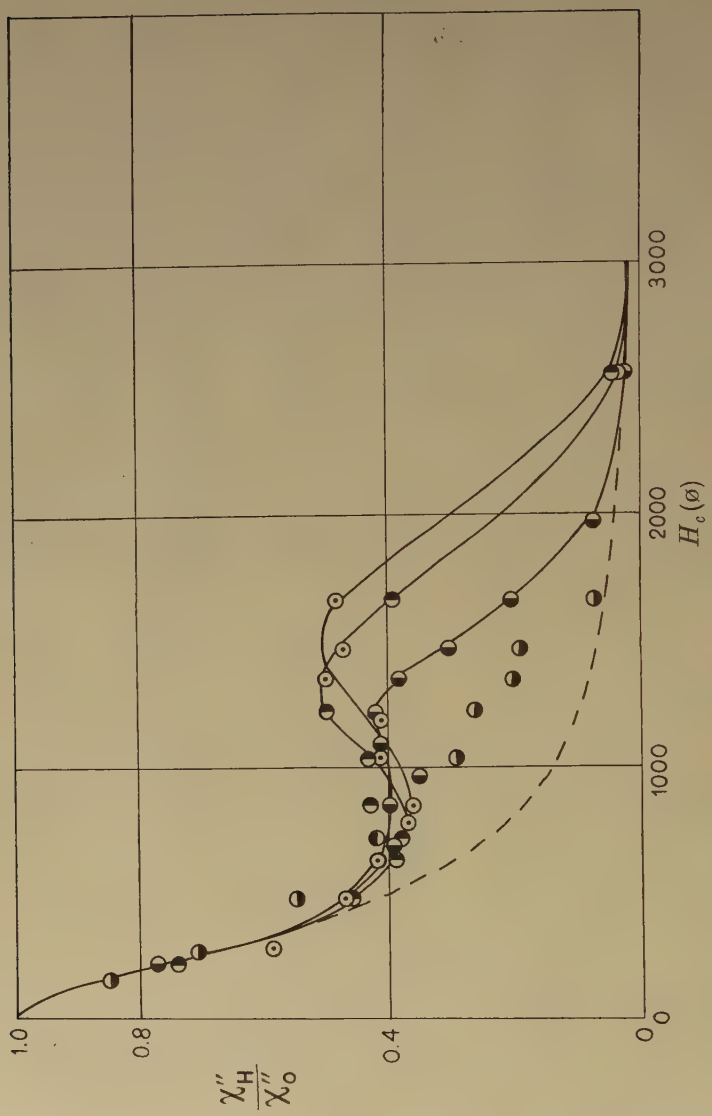

Fig. 9. χ'' relative to its value in zero field as a function of the parallel field H_c for $Cu(NH_4)_2(SO_4)_2 \cdot 6H_2O$ at 20.4° K

⊙ 12.5 MHz
◑ 18.8 MHz
◐ 34.5 MHz
◒ 92.0 MHz
---- $1 - F = b/(b + CH_c^2)$.

be followed if (15) would apply with a value of τ' which would not depend on H_c.

Considering these data one finds that the substances investigated arrange themselves in three groups viz.

A: those having an anomalously high χ'' in low fields (examples: $rCK(SO_4)_2 \cdot 12H_2O$, $CrNH_4(SO_4)_2 \cdot 12H_2O$, $CrNH_3CH_3(SO_4)_2 \cdot 12H_2O$;

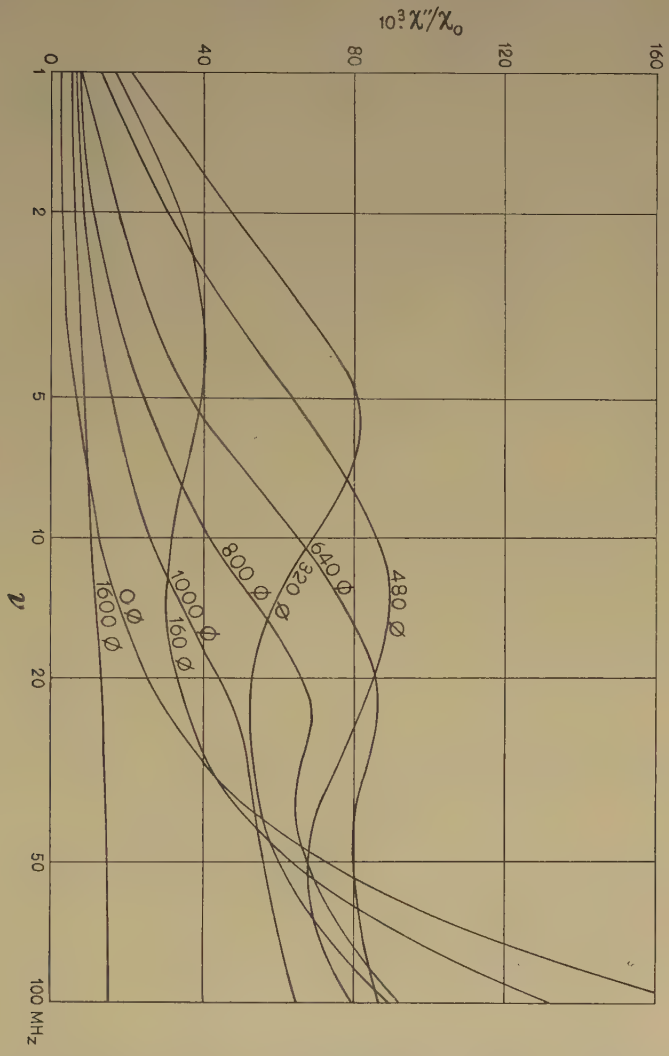

Fig. 10. χ''/χ_0 as a function of the frequency $\nu = \omega/2\pi$ for different values of H_c in $CrK(SO_4)_2 \cdot 12H_2O$ at 20.4° K.

B: those having a rather steep fall of χ'' in low fields but an extra contribution in much higher fields; examples: $FeNH_4(SO_4)_2 \cdot 12H_2O$, $Mn(NH_4)_2(SO_4)_2 \cdot 6H_2O$;

C: those behaving normally in low fields ($\chi'' \infty 1-F$) but also having an extra contribution in higher fields: $Cu(NH_4)_2(SO_4)_2 \cdot 6H_2O$.

The Fig. 10, 11 and 12 give χ'' as a function of the frequency for a number of H_c-values [27]. The extra absorption occurring in low fields in the salts of group **A** shifts to higher frequencies when the field H_c is increased. The extra absorption in **B** salts, however, occurring in high fields, shifts rapidly to lower frequencies upon increase of H_c.

The salts of the three groups **A**, **B** and **C** distinguish themselves by the ratios of the electric splittings $W_{l'} - W_l$ to the magnetic broadening of the energy levels which is of the order of $M_{ll} H_i$ (see § 1). In the salts of group **A** the electric splittings are considerably larger than the magnetic broadening. In those of the group **C** the opposite is the case while in group **B** the two are of the same order of magnitude.

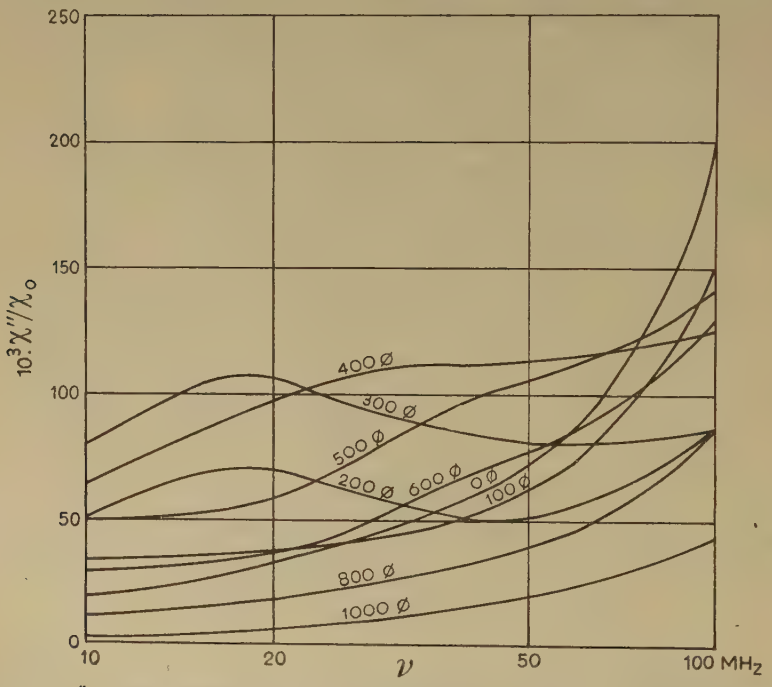

Fig. 11. χ''/χ_0 as a function of the frequency $\nu = \omega/2\pi$ for different values of H_c in $Cr(NH_3CH_3)(SO_4)_2 \cdot 12H_2O$ at 20.4° K.

This characterisation of the three groups is confirmed by observations on salts originally belonging to **B**, in which the magnetic broadening is reduced by diluting the magnetic ions by non-magnetic ions of the same valency (see Fig. 13). These diluted salts, then, range themselves in group **A**.

Fig. 14 gives a series of measurements on χ' as a function of H_c at 20.4° K in $CrNH_4(SO_4)_2 \cdot 12H_2O$, which salt belongs to group **A** while Fig. 13 refers to a series of diluted iron alums.

Bölger [31] in Leyden and the school of Kozyrev and Altschuler in Kazan [32] have measured χ'' at the microwave frequency 9.4×10^9 Hz in salts of group **B** and found that it decreases faster with H_c than $1 - F$ does. This indicates a rapid displacement of the absorption band but measurements at more frequencies are required to decide whether the displacement with rising H_c is towards higher frequencies, as has been suggested by Shaposhnikov [32], or towards lower frequencies, as would agree with the results described above.

The theory of these phenomena inside the spin system is still not

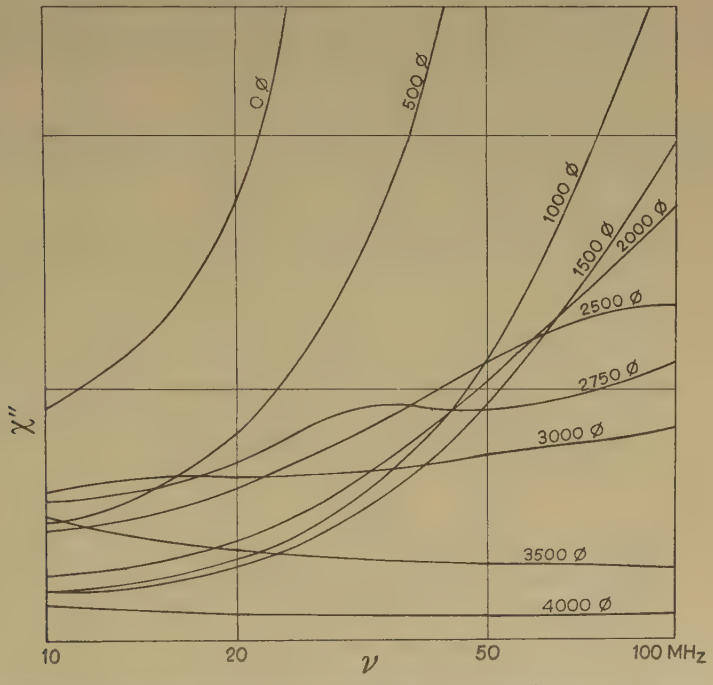

Fig. 12. χ'' in arbitrary units as a function of the frequency $\nu = \omega/2\pi$ for different values of H_c in $Mn(NH_4)_2(SO_4)_2 \cdot 6H_2O$ at 20.4° K.

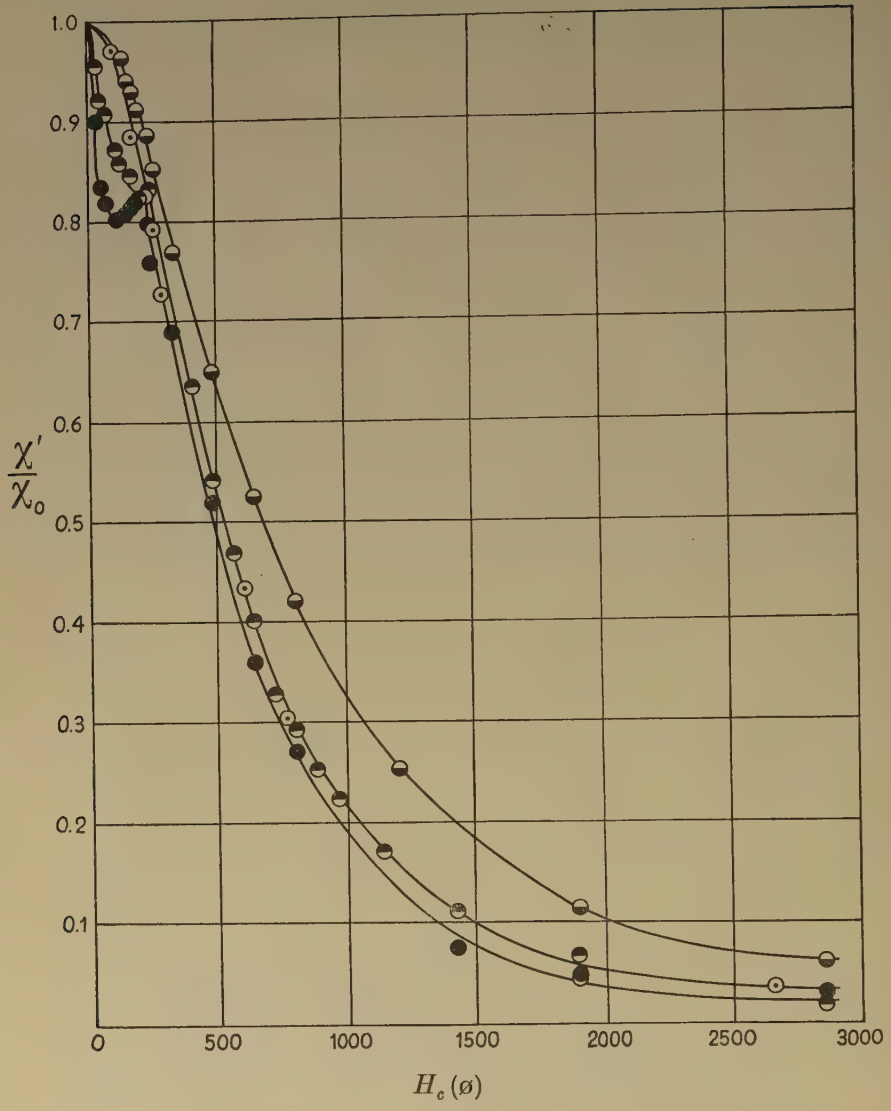

Fig. 13. χ'/χ_0 as a function of H_c for iron ammonium alum and a series of diluted alums at 20.4° K and 20 MHz

- $FeNH_4(SO_4)_2 \cdot 12H_2O$
- $Fe_{0.23}\,Al_{0.77}(SO_4)_2 \cdot 12H_2O$
- $Fe_{0.052}\,Al_{0.948}(SO_4)_2 \cdot 12H_2O$
- $Fe_{0.016}\,Al_{0.984}(SO_4)_2 \cdot 12H_2O$.

in too satisfactory a state but it has already an interesting history. In 1938 Kronig and Bouwkamp [30] considered the relaxation in the absence of an electrical field and of exchange interaction. They

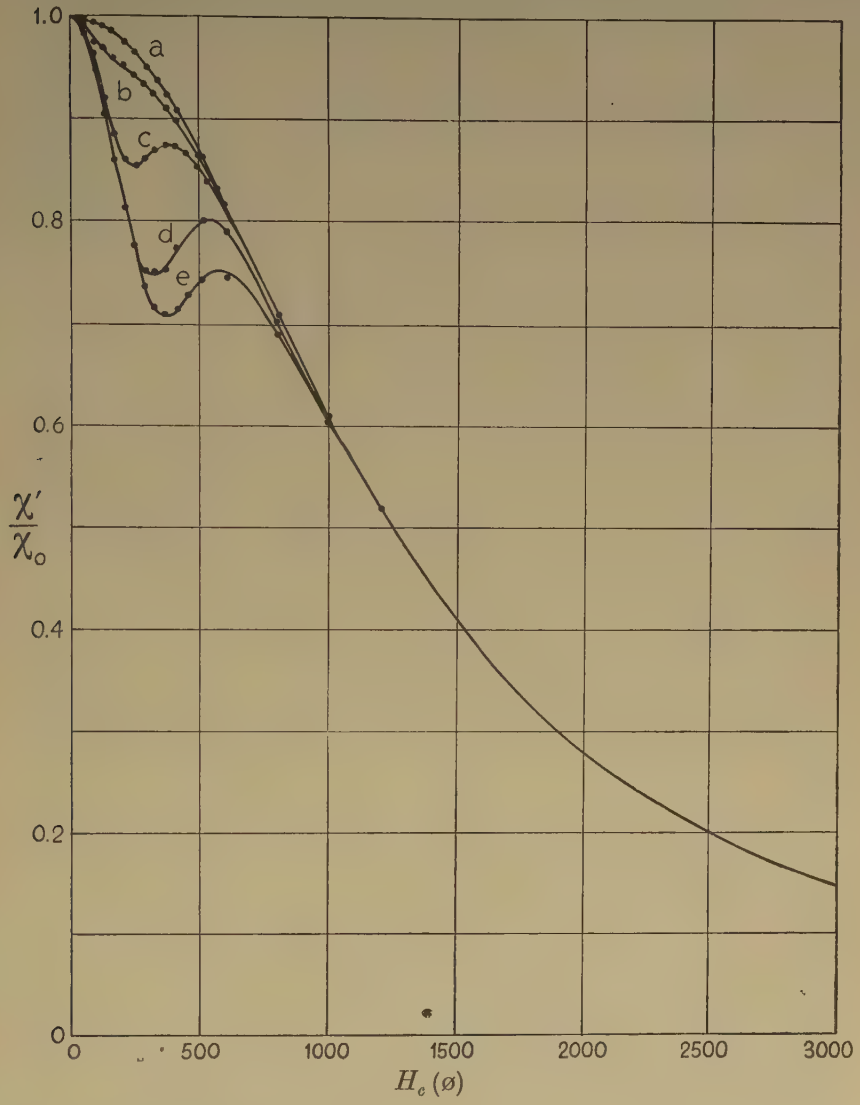

Fig. 14. χ'/χ_0 as a function of H_c for $Cr(NH_4)_2(SO_4)_2 \cdot 12H_2O$ at 20.4° K at the following frequencies
a: 0.15 MHz; b: 0.50 MHz; c: 2.00 MHz; d: 9.68 MHz and e: 19.36 MHz.
Curve a is identical with $1 - F$.

suggested that the decisive condition for the change of orientation of a spin is that the momentary vector sum of the external field and the fluctuating internal field happens to be zero. In zero external field this leads to a relaxation time calculated by Waller [18] to be of the order of $\hbar\beta^{-1}H_i^{-1}$ (see § 2), but in an external field $H_c > H_i$ the vector sum zero would be a much rarer event and this would lead to a relaxation time proportional to exp (H_c^2/H_i^2).

In 1942 Broer [34] remarked that, in the presence of an electrical splitting this reasoning would only apply to that part of the variation of the magnetization caused by a variation of the field, which was determined by the diagonal elements of the magnetic moment (see § 1). The non-diagonal moments would give rise to an immediate contribution which would not be subject to relaxation at all below the resonance frequency $(W_{l'} - W_l)/h$. For the case of a Cr^{+++}-ion in a cubic field he calculated the sum of contributions of the non-diagonal elements as a function of the H_c. Taking into account that the diagonal elements will also give a contribution to χ_{ad}, as long as H_c is not much larger H_i, Broer predicted for Cr-alum a rather complicated curve for χ_{ad} as a function of H_c, which should be observed already at a frequency of the order of 10 MHz but of which until then no indication had been observed.

Thus he concluded Kronig and Bouwkamp's reasoning not to apply and in a subsequent paper [35] he gave theoretical arguments for that, coming to the conclusion that τ' should remain of the same order of magnitude when an external field is applied and even decrease somewhat.

But it has now been found that the conclusion then drawn from the experimental data was incorrect since they were perturbed by spin-lattice relaxation. The results reproduced in Fig. 14 for the highest frequence are almost indentical with Broer's rejected prediction of 1942.

So it appears now that Kronig and Bouwkamp's treatment gives the right answer. The results observed for the substances of the groups **B** and **C** are essentially in agreement with Kronig and Bouwkamp's prediction that, when $H_c \gg H_i$, the relaxation time will shift rapidly to higher values, though perhaps the shifting is not quite so rapid as was expected. In the salts of group **A** the observed adiabatic susceptibility has—as mentioned—the expected characteristics.

The behaviour of the relaxation times in this group still under

investigation. But it is clear already that, in the presence of an electrical splitting $W_{l'} - W_l$, it is not necessary that the external field and the fluctuation field just compensate each other in order to enable a spin to change its orientation. It may even be more effective if the vector sum of the two fields causes two energy levels just to cross over so that $W_{l'} - W_l = 0$. This generally occurs at fields higher than corresponds to the maximum of $\chi_0(1-F) - \chi_{ad}$ and thus the relaxation times in salts of group A may have a tendency to decrease at an increase of H_c.

Still many data have to be collected and the theory is wanting to be brought to a more irrefutable formulation.

Finally the problem of the influence of exchange interaction on relaxation in the spin system should be mentioned. Quite early [35] it was found that in salts with strong exchange interactions (e.g. $CuCl_2 \cdot 2H_2O$; $MnSO_4$) the absorption due to relaxation in the spin system is abnormally high or – in other words – that $\tau' \gg \hbar\beta^{-1}H_c^{-1}$. This was even one of the basic facts which led to the notion of exchange narrowing [5] which later was mainly [37] but not exclusively [38] applied to the bands of paramagnetic resonance. Recent observations at angular frequencies of the order of $(\tau')^{-1}$ lead to interesting results. In a remarkable paper Bloembergen and Wang [39] showed that the increase of τ' by exchange is also observable in the so-called saturation of paramagnetic resonance by a high power microwave field. They called the attention to radicals like diphenyl trinitro phenyl hydrazine but largely overestimated the exchange interaction [40] in them. It seems that further experimental and theoretical research also about this topic is wanted.

REFERENCES

1 P. Langevin, J. de Phys., **4**, 678 (1905).

2 J. H. van Vleck, Phys. Rev., **31**, 587 (1928).
J. H. van Vleck, Theory of electric and magnetic susceptibilities, New York (1932).

3 C. J. Gorter, Paramagnetic Relaxation, Amsterdam (1947).

4 J. H. van Vleck, J. chem. Phys., **5**, 320 (1937).

5 C. J. Gorter and J. H. van Vleck, Leiden Comm. Suppl. No. 97*a*; Phys. Rev., **73**, 1229 (1947).
J. H. van Vleck, Phys. Rev., **74**, 1168 (1948).

6 R. Kronig, J. Opt. Soc. Amer., **12**, 547 (1926); Ned. T. Natuurkunde, **9**, 402 (1942).

H. A. Kramers, Atti Congr. Fis., Como, 545 (1927).
[7] E. Zavoisky, J. Phys. U.S.S.R., **10**, 197 (1946).
[8] L. C. van der Marel, J. van den Broek and C. J. Gorter, Leiden Com. No. 306*a*.
[9] C. J. Gorter, Leiden Comm. Suppl. No. 97*c*; Proc. Phys. Soc., A, **61**, 541 (1948).
[10] L. J. F. Broer and D. C. Schering, Physica, **10**, 631 (1943).
[11] C. J. Gorter, Leiden Comm. No. 241*e*; Physica **3**, 503 (1936).
L. J. Dijkstra, Thesis Amsterdam, (1943).
J. Volger, F. W. de Vrijer and C. J. Gorter, Physica **13**, 635 (1947).
J. Smits, H. E. Derksen, J. Verstelle and C. J. Gorter, Leiden Comm. No. 304*d*; Physica, **22**, 773, (1956).
[12] E. Zavoisky, J. Phys. U.S.S.R., **9**, 211 (1945).
[13] A. H. Cooke, Rep. Progr. Phys., **13**, 276 (1950).
[14] H. B. G. Casimir and F. K. Du Pré, Leiden Comm. Suppl. No. 85*a*; Physica, **5**, 507 (1938).
[15] P. Debye, Phys. Z., **39**, 616 (1938).
[16] F. Brons, Thesis Groningen (1938).
[17] J. H. van Vleck, Phys. Rev., **57**, 426 (1940).
[18] I. Waller, Z. Phys., **79**, 370 (1932).
[19] R. Kronig, Physica, **6**, 33 (1939).
[20] L. J. F. Broer, Physica, **10**, 801 (1943).
[21] H. C. Kramers, D. Bijl and C. J. Gorter, Leiden Comm. No. 280*a*; Physica, **16**, 65 (1950).
D. Bijl, Thesis Leiden (1950).
R. J. Benzie and A. H. Cooke, Proc. Phys. Soc., A, **63**, 201 (1950).
[22] R. J. Benzie, Proc. Phys. Soc., A, **64**, 507 (1951).
L. C. van der Marel, J. van den Broek and C. J. Gorter, Leiden Comm. No. 306*a*.
[23] H. N. V. Temperley, Proc. Cambr. Phil. Soc., **35**, 256 (1939).
[24] J. H. van Vleck, Phys. Rev., **59**, 724 and 730 (1941).
[25] C. J. Gorter, L. C. van der Marel and B. Bölger, Leiden Comm. Suppl. No. 109*c*; Physica, **21**, 103 (1955).
L. C. van der Marel, Conf. de Physique basses Temp., Paris, 225 (1955).
[26] T. Haseda and E. Kanda, Physica, **22**, 647 (1956).
[27] A. H. Eschenfelder and R. T. Weidner, Phys. Rev., **92**, 869 (1953).
[28] I. G. Shaposhnikov, J. Exp. Theor. Phys., U.S.S.R., **18**, 533 (1948).
[29] F. W. de Vrijer and C. J. Gorter, Leiden Comm. No. 289*b*; Physica, **14**, 617 (1949); *ibid.* **18**, 549 (1952).
F. W. de Vrijer, Thesis Leiden (1951).
[30] J. Smits, H. E. Derksen, J. Verstelle and C. J. Gorter, Leiden Comm. No. 304*d*; Physica, **22**, (1956).
J. Verstelle, Conf. de Physique basses Temp., Paris, 229 (1955).
[31] B. Bölger, Conf. de Physique basses Temp., Paris (1955), p. 244.
[32] I. G. Shaposhnikov, Conf. Phys. magn. Phen., Moscow, 101 (1956).
[33] R. Kronig and C. J. Bouwkamp, Physica, **5**, 521 (1938) and **6**, 290 (1939).
[34] L. J. F. Broer, Physica, **9**, 547 (1942).

[35] L. J. F. Broer, Physica, **10**, 801 (1943).
L. J. F. Broer, Thesis Amsterdam (1945).
[36] J. Volger, F. W. de Vrijer and C. J. Gorter, Physica, **13**, 621 (1947).
J. Volger, Thesis Leiden (1946).
[37] M. H. L. Pryce and K. W. H. Stevens, Proc. Phys. Soc., A, **63**, 36 (1950).
D. W. Anderson and P. R. Weiss, Rev. Mod. Phys., **25**, 269 (1953).
R. Kubo and K. Tomita, J. Phys. Soc. Japan, **9**, 889 (1953).
[38] A. Wright, Phys. Rev., **76**, 1826 (1949).
[39] N. Bloembergen and S. Wang, Phys. Rev., **93**, 72 (1954).
[40] H. J. Gerritsen, R. F. Okkes, H. M. Gijsman and J. van den Handel, Leiden Comm. No. 294*c*; Physica, **20**, 13 (1954).

CHAPTER X

ORIENTATION OF ATOMIC NUCLEI AT LOW TEMPERATURES

BY

M. J. STEENLAND

KAMERLINGH ONNES LABORATORIUM

AND

H. A. TOLHOEK

INSTITUUT-LORENTZ, LEIDEN

CONTENTS: 1. Theoretical results on nuclear effects with oriented nuclei, 292. — 2. Methods for orienting nuclei, 301. — 3. Description of experiments and results, 316. — 4. Discussion of possible further developments, 331.

Introduction

Atomic nuclei, which have a spin I different from zero, may be oriented, that is, the nuclear angular momentum may have preferential directions in space. The energy differences associated with such orientation are very small, because they are proportional to the very small nuclear magnetic moment or electric quadrupole moment. In order to avoid the disturbance of the nuclear orientation by the thermal motion, the majority of the methods for nuclear orientation uses very low temperatures. The possibility of utilising oriented nuclei has a number of interesting consequences for nuclear physics.

1. Theoretical Results on Nuclear effects with Oriented Nuclei

We give a short summary of the ways in which orientation may be detected by the methods of nuclear physics (for a more extensive review see ref. 26, more concise, earlier reviews are given in [4] and [8]). We further discuss the interest which these experiments have for nuclear spectroscopy.

If we have a collection of oriented nuclei (with nuclear spin I) so that the system has an axis of rotational symmetry η, the orientation of the nuclei may be characterized by the populations a_m of the different states with magnetic quantum numbers $m = -I, \ldots, +I$ with respect to the axis η. We normalize the a_m in such a way that

$\Sigma_{m=-I}^{+I} a_m = 1$, so that the orientation is characterized by $2I$ independent parameters. In the theoretical formulae, it is preferable to use certain parameters $f_k(I)$ (degree of orientation of order k) instead of the a_m in order to characterize the orientation. For $k=1, 2, 3, 4$ they are given by (for the general definition see ref. 19):

$$\left.\begin{aligned} f_1 &= (1/I)\ \Sigma_m\, m\, a_m \\ f_2 &= (1/I^2)\ [\Sigma_m\, m^2\, a_m - \tfrac{1}{3}\, I\,(I+1)] \\ f_3 &= (1/I^3)\ [\Sigma_m\, m^3\, a_m - \tfrac{1}{5}\,(3I^2+3I-1)\ \Sigma_m\, m\, a_m] \\ f_4 &= (1/I^4)\ [\Sigma_m\, m^4\, a_m - \tfrac{1}{7}\,(6I^2+6I-5)\ \Sigma_m\, m^2\, a_m + \\ &\qquad + \tfrac{3}{35}\, I\,(I-1)\,(I+1)\,(I+2)]. \end{aligned}\right\} \qquad (1.1)$$

These parameters have the property that they become zero if there is no orientation (all a_m equal); also $f_k(I)=0$ for $k>2I$.

We speak of *orientation* of a system of nuclei, if not all a_m are equal.

If the positive and negative η directions are equivalent, then all odd $f_k=0$ and we speak of *alignment*. If these directions are inequivalent, then some odd $f_k \neq 0$, and we speak of *polarization* of the nuclei.

a. Absorption of Neutrons by Polarized Nuclei [1]

The absorption cross section for polarized neutrons by polarized nuclei will depend in general on this polarization. If only a compound state with a definite nuclear spin $I_c = I \pm \frac{1}{2}$ can be formed, the polarization dependence of the cross section is given by

$$\sigma = \sigma_0 \left(1 + \frac{I}{I+1}\, f_1\, f_1^n\right), \quad \text{if } I_c = I + \tfrac{1}{2} \qquad (1.2)$$

and

$$\sigma = \sigma_0\,(1 - f_1\, f_1^n) \qquad , \text{ if } I_c = I - \tfrac{1}{2} \qquad (1.3)$$

(f_1 and f_1^n are the parameters according to (1.1) for the nuclei and neutrons respectively).

It follows from (1.2) that an effect linear in f_1 can be observed if the transmission of polarized neutrons through a sample of polarized nuclei is observed; analogously the part of an unpolarized beam of neutrons transmitted through such a sample will be partially polarized, proportional to f_1. The transmission of an unpolarized neutron beam through a thick sample of polarized nuclei depends also on the polarization, but this is only an effect in f_1^2.

If we have an (n, γ)-reaction, a polarization of the compound state

will generally result, even if we irradiate a sample of polarized nuclei with unpolarized neutrons. It follows (cf. b) that the emitted γ-radiation may show as well directional anisotropy, as linear and circular polarization.

b. Emmission of Gamma Radiation from oriented Radioactive Nuclei

If gamma radiation is emitted from oriented nuclei we may observe as well an anisotropic directional distribution as linear and circular polarization. The theory was developed by Spiers [2], Tolhoek and Cox [10, 11, 14, 19] and Steenberg [5, 9, 18]. We want to elucidate some features by giving the formulae for the *directional distribution* $W(\vartheta)$ for two simple cases: (ϑ is the angle of the direction of emission with the η-axis of rotational symmetry)

Dipole radiation; nuclear spin change from $I \to I-1$

$$\tfrac{1}{2}\, W(\vartheta) = 1 + \tfrac{3}{2}\, N_2 f_2 P_2(\cos\vartheta). \tag{1.4}$$

Quadrupole radiation; nuclear spin change from $I \to I-2$

$$\tfrac{1}{2}\, W(\vartheta) = 1 - \tfrac{1.5}{7}\, N_2 f_2 P_2(\cos\vartheta) - 5 N_4 f_4 P_4(\cos\vartheta). \tag{1.5}$$

N_2 and N_4 are given by

$$N_2 = I/(2I-1)\ ;\ N_4 = I^3/(I-1)(2I-1)(2I-3), \tag{1.6}$$

P_2 and P_4 are Legendre polynomials.

These formulae show for two simple cases that:

(1) the directional distribution depends only on $P_k(\cos\vartheta)$ of even order (equivalence of positive and negative η-direction);
(2) $W(\vartheta)$ depends only on even f_k not on odd f_k;
(3) the highest order k for f_k and $P_k(\cos\vartheta)$ which can occur for 2^L-pole radiation is $k = 2L$;
(4) the directional distribution does not depend on the magnetic or electric character of the 2^L-pole radiation.

Similarly we want to give the formulae for the *polarization of the gamma radiation* in these cases. We represent a state of polarization by a real vector ξ in a 3-dimensional polarization space (Stokes parameters [19]): the unit vectors in the positive directions of the three axes (χ_1, χ_2, χ_3) represent the two states of linear polarization (with polarization planes rotated over 45°) and the state of left circular polarization χ_c ($= \chi_3$). Opposite directions represent orthogonal states.

The state of linear polarization for which the electrical vector lies in the plane determined by η and the direction of emission $\mathbf{k}$, is represented by $\chi_{||}$ ($=\chi_1$). The magnitude $P=|\xi|$ determines the degree of polarization of the emitted radiation ($0 \leqslant P \leqslant 1$). ξ is given by the following formulae in the same cases, as were mentioned above ($W(\vartheta)$ according to (1.4) and (1.5)).

Electric dipole radiation; $(I \to I-1)$

$$W(\vartheta)\,\xi = -\tfrac{3}{2} N_2 f_2 (1-\cos^2\vartheta)\,\chi_{||} + 3N_1 f_1 (\cos\vartheta)\,\chi_c. \tag{1.7}$$

Electric quadrupole radiation; $(I \to I-2)$

$$\left.\begin{aligned} W(\vartheta)\,\xi = {} & [\tfrac{45}{7} N_2 f_2 (\cos^2\vartheta - 1) + \tfrac{25}{4} N_4 f_4 (-7\cos^4\vartheta + \cos^2\vartheta - 1)]\,\chi_{||} + \\ & + [2N_1 f_1 \cos\vartheta + 5N_3 f_3 (-5\cos^3\vartheta + 3\cos\vartheta)]\,\chi_c, \\ & N_1 = 1\,,\; N_3 = I^2/(I-1)\,(2I-1). \end{aligned}\right\} \tag{1.8}$$

We may formulate some general rules concerning the polarization effects:

(1) the plane perpendicular to η is a plane of symmetry for the linear polarization (as it is for the directional distribution);
(2) the linear polarization (coefficient of $\chi_{||}$) depends only on even f_k;
(3) the circular polarization (coefficient of χ_c) depends only on odd f_k;
(4) for the case of magnetic radiation the sign of $\chi_{||}$ must be changed relative to the corresponding formulae for the electric case, while the sign of χ_c remains unaltered.

Hence we see that circular polarization will occur for polarized nuclei, but not for aligned nuclei.

It should be noted that multipole radiation may have a mixed character, e.g., mixed magnetic dipole and electric quadrupole. Already small admixtures can have an appreciable influence on the properties of the emitted gamma radiation. (For explicit formulae for mixed radiations cf. ref. 21).

If there is a cascade of two or more gamma transitions, a *directional correlation of two gamma rays* can be observed already for unoriented nuclei. For oriented nuclei the directional correlation is changed (we obtain functions of 3 directions: the axis η and the two directions of emission $\mathbf{k}_1$ and $\mathbf{k}_2$). The theory was worked out by Cox, De Groot and Tolhoek [7, 13, 16] (See also ref. 22). The result is given by rather complicated formulae for which we refer to the original papers. It depends on parameters f_k of even order. The study of these directional correlations may have a certain interest in addition to the study of the

individual directional distributions of two gamma rays, as it depends on more parameters f_k. For example, if we have a cascade of two quadrupole transitions, the directional distributions measured independently depend only on f_2 and f_4, the directional correlation depends, however, as well on f_6 and f_8 so that the directional correlation may be more sensitive to certain features of the orientation of the initial nuclei. This may be of interest for the study of the orientation mechanism (cf. § 2) or even for spin assignments.

The influence of transitions preceding the gamma radiation [9, 14, 22, 25]. Except for the isomeric transitions (and no nuclei or at most very few nuclei showing isomeric transitions can be oriented by the present methods) the lifetimes for gamma transitions are too short to use them directly in nuclear orientation experiments. Hence the usual experimental situation will be that the gamma transition is preceded by a beta transition (or possibly an alpha transition) with a lifetime sufficient, for example, to grow a crystal including the nuclei which must be oriented. It may also be that we have a cascade of several gamma rays, so that the second gamma ray is preceded by one beta ray and one gamma ray (cf. Fig. 6 and 10). It is possible to derive formulae connecting the orientation parameters f_k for the initial and final states for beta or gamma transitions, preceding the gamma transition which is studied. This connection depends on the nuclear spins in the initial and final states and on the multipolarity of the transition in between (order of forbiddenness for a beta transition). It can be generally shown that a parameter $f_k(I_i)$ for the state with nuclear spin I_i depends only on the degree of orientation $f_k(I_0)$ for the initial state of the *same* order k. An example of a relation between $f_k(I_i)$ and $f_k(I_0)$ is:

$$N_k(I_i)\, f_k(I_i) = N_k(I_0)\, f_k(I_0). \tag{1.9}$$

This is valid if $I_0 \rightarrow I_i = I_0 - L$; $N_k(I)$ are the same numbers as used in (1.6) and (1.8). The formula is valid for a 2^L-pole gamma transition between I_0 and I_i, or for a beta transition, if the relevant matrix-element is characterized by L (roughly the order of forbiddenness), e.g., $L=1$ for an allowed beta transition determined by the nuclear matrix element $\int \boldsymbol{\sigma}$. For general formulae and explicit formulae for other special cases connecting the f_k in the states with spin I_0 and I_i we refer to ref. [14, 21].

All these formulae are derived under the assumption that no appreci-

able precession of the nuclear spins takes place in the intermediate states. It was shown experimentally that this holds very well, for the intermediate state between γ_1 and γ_2 for ^{60}Co [107]. The possible influence of precession of the nuclear spin in intermediate states was discussed in some papers [23, 27, 117] and is analogous to the influence of this effect in directional correlations [115].

c. Directional Distribution and Polarization of Beta Radiation Emitted from Oriented Nuclei [3, 6, 26]

Although no experiments have been performed on beta radiation from oriented nuclei, we want to survey the theoretical results derived by Tolhoek and de Groot.

For *allowed beta-transitions* [6] the directional distribution remains spherically symmetric for any state of nuclear orientation (at least if the β-interaction is taken to be invariant for Lorentz transformations including reflections of space). However, a polarization of the emitted beta radiation must be expected for polarized nuclei ($f_1 \neq 0$). The degree of polarization of the electrons may even be unity for completely polarized nuclei. We may characterize the polarizations of electrons by a (3-dimensional real) vector $\boldsymbol{\zeta}$ specifying the direction of the electron spin (in a coordinate system in which the electron is at rest), while the magnitude $P = |\boldsymbol{\zeta}|$ gives the degree of polarization ($0 \leqslant P \leqslant 1$). We give the result for the polarization of electrons emitted with direction $\mathbf{p}$ for the case $I_i \to I_i - 1$

$$\boldsymbol{\zeta} = f_1 \left[\boldsymbol{\eta}/E + \mathbf{p}\, p \cos\vartheta / E\,(E+1)\right] \tag{1.10}$$

($\boldsymbol{\eta}$, axis of rotational symmetry; f_1 is taken for the initial state with spin I_i; we write $\mathbf{p}\cdot\boldsymbol{\eta} = p\cos\vartheta$; E is the electron energy including its rest energy; we use units such that $\hbar = 1$, $c = 1$, $m_e = 1$). It follows from (1.10) that for emission in the direction of $\boldsymbol{\eta}$, $\boldsymbol{\zeta}$ has the direction of $\mathbf{p}$, while $P = f_1$; for emission perpendicular to $\boldsymbol{\eta}$, $\boldsymbol{\zeta}$ is perpendicular to $\mathbf{p}$ and $P = f_1/E$.

In principle measurements of the polarization of the emitted β-radiation may provide a means to decide the relative sign of the contributions of the scalar and tensor interaction in β-radioactivity [6]. Dolginov pointed out that measurements of the circular polarization of the $K_{\alpha 1}$ and $K_{\alpha 2}$ X-rays emitted after K-capture may give the same information [28a]. However, both measurements are very difficult with the present experimental technique.

For *forbidden beta-transitions* [10, 26] we may have as well a directional distribution of the beta radiation, which differs from spherical symmetry, as a polarization effect. However, this effect in the directional distribution will only occur for those forbidden beta transitions with a beta spectrum which differs from the "allowed" shape (that is for the same beta transitions for which the $\beta-\gamma$ correlation function differs from isotropy, if the β is followed by a γ). A group of first forbidden beta transitions with $\Delta I = \pm 2$ and change of parity is the best-known group with this property. As an example for a directional distribution we give the formula for the case $I_i \rightarrow I_i - 2$

$$\tfrac{1}{2}W(\vartheta) = 1 - 3\,\mu N_2 f_2 P_2\,(\cos\vartheta) \tag{1.11}$$

where $\mu = (E^2-1)/[E^2-1+(E_0-E)^2]$ is a function of E, which varies from $\mu = 0$ for $E = 1$ to $\mu = 1$ for $E = E_0$ (maximum energy of the beta spectrum). Hence we see that the anisotropy of the directional distribution is most pronounced for the electrons of the highest energy.

Recently Lee and Yang [28c] have suggested to investigate in detail the possibility for parity non-conservation for the so-called weak interactions, to which the β-interaction belongs. Their suggestion originates from the observation that the τ^+ and θ^+ mesons have the same masses of $966 \pm 2\ m_e$ and the same lifetimes of $(1.2 \pm 0.2) \times 10^{-8}$ sec, within the experimental errors. It is tempting to suppose that the τ^+ and θ^+ mesons represent only different modes of decay of the same particle, but in view of what is known of these decays, this seems only to be possible if parity is not conserved in the weak interactions which determine their decay. Lee and Yang showed that the experimental evidence for parity conservation for weak interactions is very meagre, but that the angular distribution of β-rays emitted from oriented β-emitters provides one of the most suitable experiments sensitive to a possible non-conservation of parity (which means that the laws of nature would no longer be invariant for reflections of space). The angular distribution of the β-rays may then contain a $\cos\vartheta$-term

$$W(\vartheta) \backsim \left(1 + \alpha \frac{p}{E} f_1 \cos\vartheta\right) \tag{1.11a}$$

where for an allowed $I \rightarrow I-1$ β-transition, α is given by

$$\alpha = \frac{2C_T C_T'}{C_T^2 + C_T'^2} \tag{1.11b}$$

if we assume that the β-interaction contains the tensor-interaction, but no axial vector interaction. The constants C_T and C_T' are the (real) coefficients, with which the normal tensor interaction and a non-parity conserving tensor interaction (for which the mathematical expression is obtained by adding a $\gamma_5 = \gamma_1\gamma_2\gamma_3\gamma_4$ factor to the Dirac operator combining the lepton fields) are combined as a linear combination. We notice the remarkable fact that (1.11a) does not satisfy the usual symmetry of the angular distribution for reflection at a plane perpendicular to the axis of orientation η, which symmetry follows by a simple argument, once the invariance of physical laws for reflections of space is accepted. The present experimental technique should allow in this way to check with a considerable accuracy whether parity is conserved in the β-interaction.

d. Directional Distribution of Alpha Particles Emitted from Oriented Nuclei [2, 28]

As alpha particles have spin 0 no polarization effect can exist, but the directional distribution may differ from spherical symmetry depending on the orbital angular momentum l, with which the α-particle is emitted and the initial and final nuclear spins I_i and I_f. Since the alpha particle is a boson, the possible values for l are either

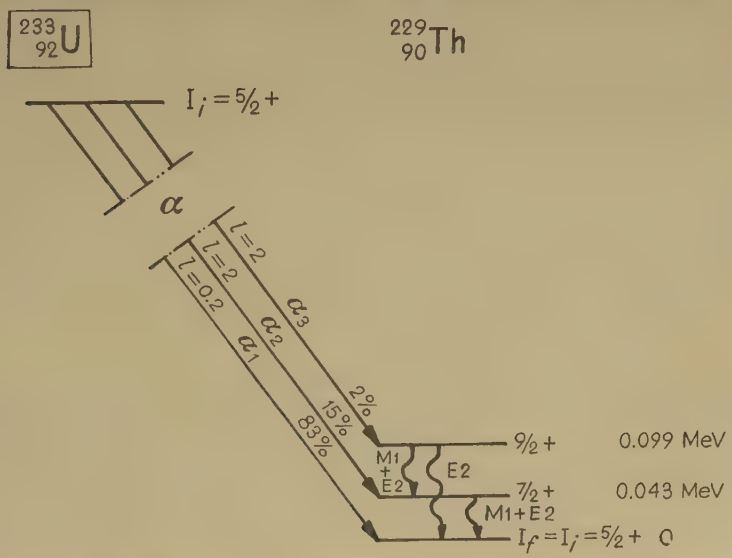

Fig. 1. Decay scheme of ^{233}U. Figure from Bohr, Fröman, Mottelson [24a].

$l=0, 2, 4, \ldots$ or $l=1, 3, 5 \ldots$ according to whether the parities of the initial and final states are the same or not.

The directional distribution of alpha particles has a special interest for the theory of alpha emission for the following reason: an interesting group of alpha emitters are the heaviest nuclei with a strong intrinsic spheroidal deformation, having rotational levels as a consequence. The alpha energies show a "fine structure" because of these rotational levels. A typical scheme is represented in Fig. 1, in which the predominant orbital angular momenta of the emitted alpha particles are given. It follows that the directional distribution of α_2 and α_3 is fixed by the value of I_i; however, the directional distribution of the ground to ground transition α_1 depends essentially on the interference of the $l=0$ and $l=2$ emissions. The directional distribution of α_1 is given by $(I=I_i=I_f)$ [23b]

$$\left.\begin{aligned}\tfrac{1}{2}W(\vartheta)=1+\left[-\sqrt{6}\sqrt{5}\left(\frac{I(I+1)}{(2I-1)(2I+3)}\right)^{\frac{1}{2}}a_0a_2+\frac{15}{7}\frac{(2I-3)(2I+5)}{(2I-1)(2I+3)}a_2^2\right]K_2f_2P_2(\cos\vartheta)+\\ +\frac{45}{(2I-1)(2I+3)}a_2^2K_4f_4P_4(\cos\vartheta)\end{aligned}\right\} \quad (1.1$$

with

$$K_2=I/(I+1), \quad K_4=I^3/(I+1) \qquad (1.13)$$

The numbers a_0 and a_2 are real $(a_0^2+a_2^2=1)$ and a_2/a_0 determines the relative importance and sign of the $l=2$ and $l=0$ waves, which is of much interest for the theory of alpha disintegration (it is related to the problem whether the alpha particles are emitted from the "tips" or the "equator" of a "cigar-shaped" nucleus [17, 20, 24]). This information can only be obtained from the directional distribution of alpha particles from oriented nuclei and not from $\alpha-\gamma$ directional correlations, as by this latter method only α_2 and α_3 can be investigated (in the scheme of Fig. 1), which do not show the interesting interference of $l=0$ and $l=2$ waves.

e. Fission of Oriented Nuclei.

If fissionable nuclei with spin $I\neq 0$ are oriented, one has to expect that the fission products formed in spontaneous fission or by slow neutron irradiation will have a directional distribution which is no longer isotropic. It is possible to make a number of theoretical predictions on this directional distribution depending on what connection is assumed between the average nuclear shape (which has already a

strong spheroidal deformation for nuclei such as U and Np) and the nuclear surface in the scission configuration. As the nuclei U and Np have al readybeen oriented, the experiment of directed fission seems quite feasible and interesting for testing some points of fission theory.

The determination of the nuclear spin of a compound nucleus formed after neutron absorption by a heavy nucleus and leading to fission might be carried out according to § 1a, and is of interest for fission theory [28d].

2. Methods for Orienting Nuclei

In this section the different proposals for orienting nuclei will be reviewed, in particular those making use of low temperatures.

a. External Field Polarization

In 1934 and 1935 Gorter [30], Kurti and Simon [31] pointed out that nuclei could be polarized at sufficiently low temperatures by the interaction of the nuclear magnetic moment with a magnetic field. In 1939 Simon [33] considered this in more detail. (Sometimes this is referred to as the "brute force method"). In thermodynamic equilibrium the populations a_m of the states with different magnetic quantum number m are given by the Boltzmann distribution

$$a_m \backsim \exp\,[-E_m/kT] \qquad (2.1)$$

where E_m follows from the part $\mu\mathbf{H}\cdot\mathbf{I}$ of the Hamiltonian describing the interaction of the magnetic moment μ of the nucleus with the external magnetic field H:

$$E_m = \mu Hm/I = g_N \mu_N Hm \qquad (2.2)$$

(I nuclear spin, g_N gyromagnetic ratio of the nucleus, μ_N nuclear magneton $= (0.505038 \pm 0.000018) \times 10^{-23}$ erg/oersted). Hence we have

$$a_m \backsim \exp\,(-\beta m) \text{ with } \beta = g_N \mu_N H/kT = \mu H/IkT. \qquad (2.3)$$

The degrees of orientation f_k may be calculated immediately from the populations a_m according to (2.3). Explicit formulae for f_1, f_2, f_3 and f_4 valid for any β and I are given by Poppema [108] (see also ref. 81), as well as graphs for f_1, f_2, f_3, f_4 for values of I up to $I = 5$ and values of β from 0 to 5. For small values of β (hence not too low temperatures) we have that $f_k \backsim \beta^k \backsim 1/T^k$.

In order to obtain an appreciable orientation with this method a combination of a high magnetic field and a low temperature is required. For example one calculates that for a polarization of 20 % ($f_1 = 0.2$) for protons ($\mu = 2.79\ \mu_N$) a value of 1.95×10^6 oersted/°K is required, hence, e.g., about 20.000 oersted at 0.01° K. The experimental difficulty in satisfying these conditions is that temperatures of the order 0.01° K are obtained by adiabatic demagnetization, while here the very low temperature and the high magnetic field are required at the same time and place (see also ref. 65). It should be possible to attain this by carrying heat away through heat conduction from the nuclear sample in a high magnetic field to the coolant paramagnetic salt, which has been demagnetized. However, the low heat conductivities of these salts and the very poor heat contacts at these low temperatures present a formidable difficulty for this method. One may hope that in the near future a cooling of a nuclear sample to about 0.02° K and a polarizing field of say 50.000 ø will be attainable.

If then one should succeed in breaking the thermal contact with the coolant salt, a demagnetization of the nuclear sample should give a further, appreciable decrease in temperature.

b. Orientation by Means of Hyperfine Structure Splittings in Solids

In 1948 it was suggested independently by Gorter [35] and Rose [36] that the magnetic h.f.s. splittings occurring in paramagnetic ions might be a suitable tool for orienting nuclei, since they correspond to a coupling of the nuclear magnetic moment with atomic magnetic fields, which may be of the order of $10^5 - 10^6$ oersted, higher than can easily be obtained in the laboratory. It results that the energy levels corresponding to different magnetic quantum numbers m of the nucleus may be farther apart than is obtainable in the "brute force method", hence causing a higher orientation at the same temperature. Since 1948 a number of different suggestions was made corresponding to different circumstances in which h.f.s. splittings in solids may occur.

We discuss:

1. Magnetic h.f.s. alignment (Bleaney)
2. Magnetic h.f.s. polarization (Gorter–Rose)

3. Electric h.f.s. alignment (Pound)
4. Magnetic h.f.s. alignment in an antiferromagnetic substance
5. Magnetic h.f.s. orientation in a ferromagnetic substance.

In order to explain these methods in more detail we make use of a discussion of h.f.s. in crystals as given by Abragam and Pryce [40] and by Bleaney [41, 42]. They show that in many cases the h.f.s. splitting for paramagnetic ions in crystals can be derived from a "phenomenological" Hamiltonian of the form

$$\left.\begin{aligned}\mathcal{H} = {} & D\,[S_z^2 - \tfrac{1}{3}S(S+1)] + g_{\|}\mu_B H_z S_z + g_{\perp}\mu_B (H_x S_x + H_y S_y) + \\ & + [A\,S_z I_z + B(S_x I_x + S_y I_y)] + \\ & + eQ\,(\partial^2 V/\partial z^2)\,[3I_z^2 - I(I+1)]/[4I(2I-1)] - g_N \mu_N \mathbf{H}\cdot\mathbf{S} + G(S,S').\end{aligned}\right\} \quad (2.4)$$

In this formula **S** is the spin angular momentum of the atomic electrons (which may sometimes be an "apparent electron spin"); Q the nuclear quadrupole moment; $\partial^2 V/\partial z^2$ is the second derivative of the potential of the intercrystalline electric field; $G(S, S')$ represents spin-spin interactions between neighbouring ions (it is often neglected; see, however, ref. 47 and 74); direct nucleus-nucleus and nucleus-neighbouring ion interactions are omitted from the Hamiltonian (D, $g_{\|}$, $g_{\perp}$, A and B are constants). The Hamiltonian (2.4) is only valid if the crystalline field has rotational symmetry about the z-axis.

In order to derive the orientation of the nuclei at a certain temperature T, the h.f.s. must first be investigated theoretically and experimentally so that one knows the values of the constants in (2.4) and the resulting energy levels. Let Ψ_n be the eigenstates of the Hamiltonian (2.4) and E_n the energy belonging to Ψ_n. In general the Hamiltonian will not be diagonal in I_z, so that the states Ψ_n will be mixtures of states with several m (magnetic quantum number belonging to I_z):

$$\Psi_n = \Sigma_m c_m^n \varphi_m^n. \quad (2.5)$$

The probability for having a state Ψ_n in thermodynamic equilibrium at temperature T, is according to Boltzmann's law:

$$w_n = \frac{1}{Z}\exp\,[-E_n/kT]; \quad Z = \Sigma_n \exp\,(-E_n/kT). \quad (2.6)$$

The probability of having a certain value of m is now given by

$$a_m = \Sigma_n w_n |c_m^n|^2. \quad (2.7)$$

The values of the degrees of orientation f_k can be calculated immediately, once the populations a_m are known.

After these general remarks we give a more detailed discussion of the methods proposed and at the same time of the meaning of the couplings represented by the different terms of (2.4).

1. *Magnetic h.f.s. Alignment (Bleaney)* [41, 42, 47, 57, 74]

No external magnetic field is used. In this case the Hamiltonian (2.4) becomes, when the quadrupole coupling and spin-spin interaction are neglected

$$\mathscr{H} = D\,[S_z^2 - \tfrac{1}{3}S(S+1)] + A S_z I_z + B(S_x I_x + S_y I_y). \qquad (2.8)$$

If $S = \frac{1}{2}$ there is no contribution of the first term. Further in some crystals $|B| \ll |A|$.

In case $B = 0$, the Hamiltonian is simply

$$\mathscr{H} = A S_z I_z. \qquad (2.9)$$

One then sees immediately that there are $2I+1$ doubly degenerate equidistant levels; the levels with $I_z = m$, $S_z = m_s$ and $I_z = -m$, $S_z = -m_s$ having the same energy. We may say for $A > 0$, that the states with **I** and **S** antiparallel – either in the positive or negative z-direction – have the lowest energy; the highest energy occurs for parallel **I** and **S** (in the positive or negative z-direction). Hence an alignment results for low temperatures connected with the preferred crystalline axis, which we call the z-axis. It follows that the populations are given by

$$a_m \backsim \tfrac{1}{2}[\exp(A/2kT)m + \exp(-A/2kT)m] = \cosh(A/2kT)m \qquad (2.10)$$

Comparing with (2.1) and (2.2), one sees that this gives the same values for the even f_k as under a, if $\beta = A/2kT$ so that the f_k can be calculated in the same way as under a. The odd f_k vanish for the population (2.10). Hence we have alignment and no polarization.

The coefficients A arise from the coupling of the nuclear magnetic moment with an internal magnetic field, so that A is proportional to the g_N-value, if one has different nuclei of equal Z in the same crystal.

Explicit formulae for the populations a_m for the case $D = 0$ and $B \ll A$ are given by Steenberg [57] with the aid of perturbation

calculus. Gray and Satchler [25] give some numerical results for f_2, $0<\beta<1$ and $B/A \neq 0$. Simon, Rose and Jauch [47] give an explicit formula for f_2 for $B\neq 0$, $D=0$, which is the first non-vanishing term of an expansion in $\beta=A/2kT$, and also a correction for the case $D\neq 0$ (see also ref. 81). As in experiments rather high values of β (of order 1) can be reached, such an expansion will often be insufficient.

2. *Magnetic h.f.s. Polarization (Gorter and Rose)* [35, 36, 47, 57]

The idea of this method is to orient S of the paramagnetic ions by means of a weak external magnetic field (a few hundred oersted) and to use such a low temperature (obtained by adiabatic demagnetization) that the $\mathbf{I}\cdot\mathbf{S}$ coupling forces the nuclear spin to follow S in its orientation. The important terms of the Hamiltonian (2.4) in a case, where this method will apply, are

$$\mathcal{H} = g_{\|}\,\mu_B S_z H_z + g_{\perp}\,\mu_B (S_x H_x + S_y H_y) + A S_z I_z + B (S_x I_x + S_y I_y). \quad (2.11)$$

Let us take as an example $B=0$ and a magnetic field $H_z=H$ in the z-direction. The Hamiltonian becomes ($G=g_{\|}\,\mu_B H$)

$$\mathcal{H} = G S_z + A S_z I_z. \quad (2.12)$$

It has as energy eigenvalues

$$E_{m_s,m} = m_s\,[G + Am]. \quad (2.13)$$

The resulting populations for $S=\frac{1}{2}$ are

$$a_m \sim e^{-\gamma-\beta m} + e^{\gamma+\beta m}\ (\gamma = G/2kT;\ \beta = A/2kT). \quad (2.14)$$

From this it follows that the degrees of orientation, as functions of γ and β are given by (see ref. 81)

$$f_k(\gamma,\beta) = \begin{cases} f_k(\gamma=0,\beta) & \text{even } k \\ (\operatorname{tgh}\gamma)\, f_k'(\gamma=0,\beta) = f_1^e\, f_k(\gamma=0,\beta) & \text{odd } k \end{cases} \quad (2.15)$$

$f_1^e = \operatorname{tgh}\gamma$ is the degree of polarization of the electron spins. The $f_k\,(\gamma=0,\beta)$ are identical with the $f_k(\beta)$ from a. We see that this method allows polarization of nuclei, not only alignment. This means that experiments such as on neutron absorption, circular polarization of emitted gamma radiation or polarization of beta rays may be done with the aid of this method, but not with method 1. In the general case ($B\neq 0$) the populations a_m are not given by the simple formula (2.14), but they follow immediately if one has a formula for the

energy levels of the h.f.s. (see Bleaney [41, 42], Trenam [58] and Steenberg [57]). Some explicit formulae for f_1 are given by Simon, Rose and Jauch [47] but they give only the first term in an expansion to powers of β. A formula for f_2 (expansion up to second order in β) is given by Van Vleck [88a].

At the present time quite a number of nuclei of the 3d-transition group and of the rare earth group have been oriented by the magnetic h.f.s. methods. From microwave studies [50, 77] several crystals are known where the constants A and B reach values of the order of some hundredths of a degree. Thus, if one cools the nuclei down to temperatures of the same order of magnitude an appreciable nuclear orientation is to be expected. It has been proved that the most suitable way for cooling is by incorporating the nuclei in a paramagnetic crystal in which nuclear and electron interactions are small so that it can be demagnetized adiabatically to temperatures well below the temperature corresponding to the overall h.f.s. splitting of the nucleus to be oriented. Only recently h.f.s. splittings of radioactive nuclei have been measured directly by the paramagnetic resonance method. Usually only the h.f.s. splittings for the stable isotopes are known. In the case that large h.f.s. splittings are to be expected an indirect cooling might be possible, but in general it is not easy to obtain temperatures below 0.05° K in this manner. When the radioactive ions are incorporated in the demagnetized crystal itself, replacing a small part of the cooling ions, one may expect such good heat contact between the radioactive ions and the cooling ions that the measurements can be interpreted assuming complete thermal equilibrium.

Suitable cooling salts. The following salts have proved to be suitable cooling substances.

Copper Tutton salts (typical formula $Cu^{++}M_2^{+}(SO_4)_2 \cdot 6H_2O$, where M^+ may stand for K^+, $(NH_4)^+$, Rb^+, ...) are useful for incorporating divalent radioactive ions of the 3d-transition group. In these salts only a single electronic doublet level is occupied at low temperatures, so that one can omit the D-term in the Hamiltonian (2.4). The stable copper isotopes have only small h.f.s. splittings. By diluting the Cu^{++} ions magnetically with Zn^{++} ions the exchange and magnetic dipole interactions are reduced, so that low temperatures (about 0.02° K) can be reached upon adiabatic demagnetization.

Several γ-radioactive Co isotopes have been investigated using Tutton salt crystals with a relative Co^{++}, Cu^{++}, Zn^{++} ratio of, for example, 1 : 20 : 79. The Tutton salts form monoclinic crystals, the unit cell contains two paramagnetic ions, each subjected to a crystalline electric field of nearly tetragonal symmetry. In the case of the cobalt Tutton salt these two tetragonal axes make an angle of about 70° [43]. The ratio A/B is large (≈ 10) so that in zero external field an alignment of the cobalt nuclei will take place along the tetragonal axes. Formula (2.9) for the Hamiltonian can be used. The intensity of the γ-radiation emitted will show the largest changes in the direction of the bisector of the tetragonal axes and perpendicular to the plane of these axes.

Another suitable cooling salt is diluted nickelfluosilicate (Ni^{++} $SiF_6 \cdot 6H_2O$) *. Here the Ni^{++}-ion has an even number of electrons, but the splitting of the lowest triplet seems to be very small. The only nickel isotope with nuclear spin is only 1 % abundant. Temperatures of about 0.01° K can be reached. Cobalt fluosilicate has a single cobalt ion in unit cell, thus here only one axis of alignment exists. In this respect the fluosilicates must be preferred over the Tutton salts for alignment of Co nuclei. The ratio A/B is 4 [43].

Crystals of the rare earth ethylsulphates $M^{+++}(C_2H_5SO_4)_3 \cdot 9H_2O$ (where M may stand for cerium, neodymium or ytterbium) prove to be useful for alignment of rare earth nuclei. They can be cooled to temperatures of about 0.02° K, while $A \gg B$ [113].

A very interesting and useful cooling substance is the double nitrate $2Ce(NO_3)_3 \cdot 3Mg(NO_3)_2 \cdot 24H_2O$. At very low temperatures only a single Kramers doublet is occupied, no h.f.s. splittings are found because the stable cerium isotopes have zero spin and the electron spin-spin interactions are small. Down to 0.006° K the temperature dependent part of the susceptibility follows Curie's law within 5 % and temperatures of about 0.003° K can easily be attained [54]. Moreover, the substance is magnetically very anisotropic, the magnetic properties being symmetrical about the trigonal crystalline axis. For the ground doublet $g_{\parallel} = 0.25$ and $g_{\perp} = 1.84$ [53], so that a field applied in the direction of the axis gives only a small rise in temperature. This makes the substance particularly suitable for h.f.s. *polarization* experiments.

* Private communication of Dr. N. Kurti, Oxford.

Divalent ions of the 3d-transition group can be included in this salt in place of part of the Mg^{++}-ions. Both Co^{++} and Mn^{++} have been used. Paramagnetic resonance measurements on the isomorphous $2Bi(NO_3)_3 \cdot 3Mg(NO_3)_2 \cdot 24H_2O$ showed in both cases two magnetically distinct types of ions in unit cell [58]. In the case of Co about 2/3 of the ions has $A \approx B$, the remaining 1/3 has $A \gg B$. The $g_{||}$-values for both types of Co-ions are high, in sharp contrast to the $g_{||}$-value of the Ce-ions, thus by applying an external magnetic field in the direction of the axis an appreciable polarization of the Co nuclei can be reached, while the temperature rise is very small. In the case of Mn the g-values for all the ions are practically isotropic and very nearly 2. Also $A \approx B$, but, in particular for 2/3 of the ions, the electric field splitting constant D is of the same order as the hyperfine constant A, for the remaining 1/3 it is somewhat bigger.

Trivalent radioactive isotopes of the rare earth group can be incorporated in place of some of the stable cerium ions. These cerium sites are characterized by $B \gg A$, thus without an external field cerium nuclei with non zero spin will tend to "align in a plane" perpendicular to the trigonal axis. The nuclear levels with $m = \pm \frac{1}{2}$ are preferentially populated.

The same is true for neodymium in neodymium magnesium nitrate, as paramagnetic resonance experiments have shown, B/A being about 6 [78a].

3. *Electric h.f.s. Alignment (Pound)* [37, 47, 67]

A magnetic h.f.s. as discussed in 1. may be changed if the nucleus has a quadrupole moment and is placed in an inhomogeneous field. For certain crystals and nuclei the h.f.s. may even be caused entirely or mainly by the quadrupole moment. The relevant term of the Hamiltonian is then:

$$\mathcal{H} = eQ(\partial^2 V/\partial z^2)\,[3I_z^2 - I(I+1)]/[4I(2I-1)]. \qquad (2.16)$$

It is immediately seen that the population $a_m = a_{-m}$ so that only alignment but no polarization can be attained. The a_m are given by

$$a_m \backsim \exp\left[-\frac{eQ\,(\partial^2 V/\partial z^2)\,[3m^2 - I(I+1)]}{4I\,(2I-1)\,kT}\right]. \qquad (2.17)$$

When developing in powers of $[eQ(\partial^2 V/\partial z^2)/kT]$ the first term for f_2 is

$$f_2 = -\frac{eQ(\partial^2 V/\partial z^2)(I+1)(2I+3)}{60 I^3 kT}. \qquad (2.18)$$

Note that f_2 is here proportional to $1/kT$, while f_2 is proportional to $(1/kT)^2$ for the methods of orientation a and b 1,2.

Nuclei suitable for a Pound alignment must have a large quadrupole moment and $I \geqslant 1$. Such nuclei are found in the regions of mass numbers between 150 and 190 and above 220. Moreover, crystals with strong electric field gradients at the place of the nucleus are required. Recently the first successful Pound alignment has been performed on ^{233}U in the hexagonal uranyl rubidium nitrate, $(UO_2)^{++}Rb(NO_3)_3$ [130]. The uranyl ion has a linear structure O–U–O, and lies in the direction of the crystalline c-axis. The distance U–O is 1.9 Å, certainly smaller than the distance between the U-atom and other neighbouring atoms. The crystalline electric field at the U-place is dominated by the axially symmetrical field arising from the uranyl ion itself.

$(UO_2)^{++}$ is diamagnetic or feebly paramagnetic depending on the direction, but $(NpO_2)^{++}$ is paramagnetic. Microwave studies of Bleaney *et al.* [61] on $^{237}NpO_2$ included in $UO_2\,Rb(NO_3)_3$ showed, except for a large magnetic h.f.s., also an electric quadrupole splitting of several hundredths of a degree. Eisenstein and Pryce [80] who made a detailed study of the electronic structure of the uranyl like ions, could explain this large quadrupole coupling by the participation of 6d-electrons to the bond. They expected that the 6d-orbitals in NpO_2 and UO_2 should be similar, so that also $UO_2Rb(NO_3)_3$ should show a large quadrupole splitting. This expectation has been confirmed experimentally (see § 3, c).

4. *Magnetic h.f.s. Alignment in an Antiferromagnetic Substance*

Daunt [44] and Gorter [45] suggested the possibility for nuclear alignment occurring in antiferromagnetic crystals.

In a number of paramagnetic substances a negative exchange interaction between nearest neighbours exists, leading to an antiferromagnetic order below a certain temperature, T_N. According to Néel [29] in this antiferromagnetic state the lattice of the magnetic ions can be divided into two sublattices in such a way that at $T = 0$ the two sublattices each are magnetized completely, but in opposite directions. From this it follows that below T_N a certain degree of

alignment of electronic moments will exist, which could lead to a nuclear alignment through magnetic h.f.s. coupling. From measurements of Garrett [92] it is known that $Co(NH_4)_2(SO_4)_2 \cdot 6H_2O$ below about 0.1° K behaves as an antiferromagnetic substance. A crystal of this salt, which can be demagnetized to about 0.05° K, seems to be very suitable to demonstrate the alignment by antiferromagnetism, if some ^{60}Co is incorporated. However, no anisotropy in the ^{60}Co γ-radiation has been detected [108].

^{141}Ce included in cerium ethylsulphate does show large anisotropies at temperatures where this salt shows an antiferromagnetic behaviour. However, it is questionable whether the antiferromagnetic ordering enhances the existing magnetic h.f.s. alignment *.

5. *Magnetic h.f.s. Orientation in a Ferromagnetic Substance* [119, 122]

Hyperfine splittings in a metal can not be observed directly, but especially in the case of the metals of the 3d-group an appreciable h.f.s. splitting can be expected because the 3d-electrons can be considered as sufficiently localized, so that the situation is more or less analogous to the paramagnetic case.

In the ferromagnetic Weiss domains all the electronic moments will be pointing parallel. If a preferred direction for the domains exists, an alignment of the nuclei with respect to this same axis can be expected at temperatures of some hundredths of a degree. In an external field, which is high enough to cause saturation, a polarization of the nuclei will occur. The ferromagnetic substance has to be cooled by thermal contact with a demagnetized paramagnetic salt. Successful experiments on a cobalt single crystal are described in § 3, b.

c. Non-Stationary Method of Polarization in Case of Long Relaxation Times (Abragam)

Recently Abragam [84] has proposed a method of orienting nuclei making use of magnetic h.f.s. of paramagnetic ions or atoms in solids in an external magnetic field, but not in thermodynamic equilibrium as under b. It is based on the relatively long nuclear relaxation times at low temperatures. The method can be explained for a h.f.s. derived from a Hamiltonian

$$\mathcal{H} = g\mu_B \mathbf{H} \cdot \mathbf{S} + \mathbf{A}\mathbf{S} \cdot \mathbf{I}. \qquad (2.19)$$

* Private communication of Dr. C. E. Johnson, Oxford.

As an example we take $I=\frac{1}{2}$ and $S=\frac{1}{2}$. In figure 2 the energy levels of the h.f.s. are represented as functions of H. The wave functions in the limiting cases of high and low magnetic fields are indicated. The state vector $|S_z, I_z\rangle$ is indicated by the signs only, as we have $S_z=\pm\frac{1}{2}$ and $I_z=\pm\frac{1}{2}$. If we have the system at a certain

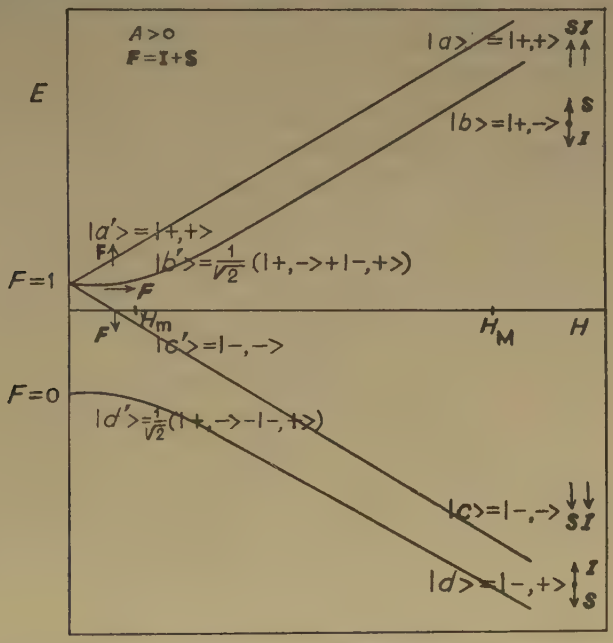

Fig. 2. Proposal for nuclear orientation of Abragam.

moment in thermodynamic equilibrium in a field H_M and at a temperature T, such that $g\mu_B H/kT \gg 1$ and $A/kT \ll 1$, the populations of the states $|a\rangle$ and $|b\rangle$ will be negligible, of $|c\rangle$ and $|d\rangle$ will both be $\frac{1}{2}$ and the polarization f_1 of the nuclei is negligible. If we then demagnetize from the field H_M to a field H_m in a time $\tau \ll T_1$ (relaxation time for the nuclear spin-lattice interaction), but slow enough so that the transition is adiabatic, the state $|c\rangle$ goes to $|c'\rangle$ and $|d\rangle$ to $|d'\rangle$. But in the state $|d'\rangle$ there is no orientation as $F=0$. One sees that a polarization $f_1=-\frac{1}{2}$ results, which goes back to 0 with the relaxation time T_1. In the general case of arbitrary I (but $S=\frac{1}{2}$) one obtains for the polarization of the nuclei after demagnetization

$$f_1=\frac{\mp 1}{2I+1}\,\mathrm{tgh}\left(\frac{g\mu_B H}{kT}\right) \quad \text{(signs according to sign of } A\text{)} \qquad (2.20)$$

and for the coefficient f_2

$$f_2 = \pm \frac{(2I-1)}{(I+1)(2I+1)} \operatorname{tgh}\left(\frac{g\mu_B H}{kT}\right). \qquad (2.21)$$

At a temperature of 1.5° K relaxation times T_1 of 1 min and 15 sec have been found for atoms of As and P introduced as impurities in Si crystals.

d. Resonance Method for Polarization (Feher)

Recently Feher [86] proposed a non-equilibrium resonance method for orienting nuclei in paramagnetic centers in crystals. The method can be explained with the aid of Fig. 3 (representing the same situation

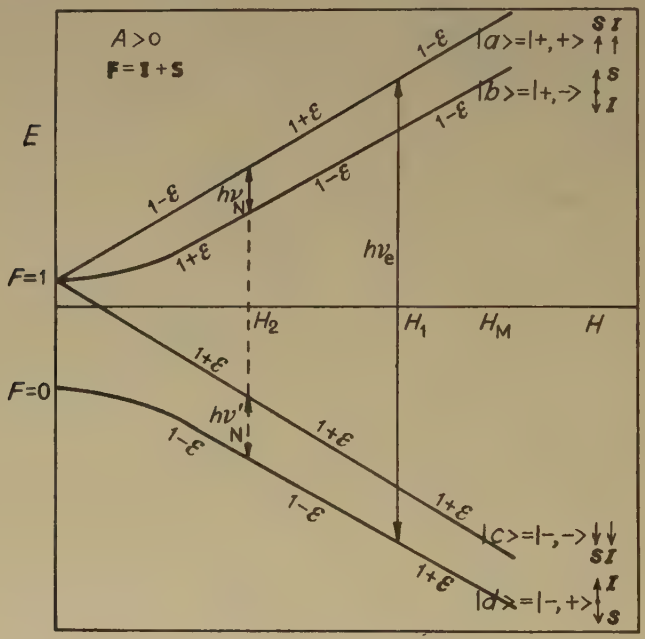

Fig. 3. Proposal for nuclear orientation of Feher.

as Fig. 2). Suppose we start from a situation at a high field H_M at a temperature, where $|a\rangle$ and $|b\rangle$ are far less populated than $|c\rangle$ and $|d\rangle$. When gradually decreasing the magnetic field and applying a microwave field the spins may be turned over 180° for a certain value of H, say for H_1; the populations of $|a\rangle$ and $|d\rangle$ are interchanged in this way by the microwave field. Lowering the magnetic field further to

a value H_2 (where the energy difference of $|a\rangle$ and $|b\rangle$ differs appreciably from $|c\rangle$ and $|d\rangle$), the populations of $|a\rangle$ and $|b\rangle$ may be interchanged by a radiofrequency field. This leaves us for values of $H < H_2$ with populations as indicated in the figure, representing an appreciable nuclear orientation, which will be maintained for a time of the order of the nuclear relaxation time T_1 as in Abragam's method. The method of Feher is more complicated than Abragam's method and further requires the same experimental conditions, but it may provide higher nuclear orientations.

The method was tested experimentally on a phosphorus doped silicon crystal and confirmed by a resonance method [87] but not yet by means of nuclear radiations.

e. Optical Method of Polarization (Kastler) [32, 34, 38, 39, 46, 48, 49, 51, 55, 59, 62, 70, 71, 78]

Since 1936 Kastler and collaborators have studied the orientation of atoms in a magnetic field with irradiation by circularly polarized light. This may also cause orientation of nuclear spins. We shall only indicate concisely the principle of the method, as it does not usually require low temperatures and as it was recently reviewed by Kastler [71]. As an example, we show in Fig. 4 the transitions possible between the sublevels (corresponding to different m_F sublevels) of two states with $F = 1$ and $F = 2$. Let a magnetic field define the axis of quantization and suppose we radiate with left circularly polarized resonance radiation in this direction. Let the magnetic field be so weak that it does not decouple **I** and **J** ($\mathbf{F} = \mathbf{I} + \mathbf{J}$). The single arrows in Fig. 4 show

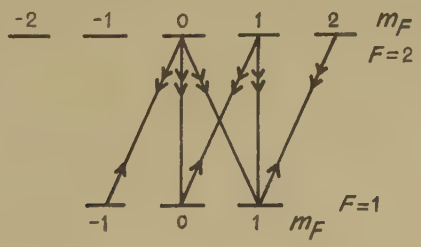

Fig. 4. Optical method for nuclear orientation of Kastler.

which transitions from the ground state are caused by the resonance radiation; the double arrows show by which transitions the atom can fall back. It is seen that the irradiation with circularly polarized light

provides an "optical pumping" from lower to higher values of m_F and may cause a polarization of the ground state as well as of the excited state. This means that an orientation of **F**, as well as of **I** and **J** is caused in this way.

This method was realized experimentally by Kastler and coworkers [49, 59, 71] and by Dicke and Hawkins [55] for Na. The degree of polarization of the nuclear spin was estimated by the latter authors to be $f_1 = 0.12$. The experiments may be performed with a beam of atoms or a gas of low pressure. A disadvantage is that only small samples of nuclei can be oriented in this way. Except for gases or atomic beams, the optical method for polarization may also be possible for solids at very low temperatures [71] containing fluorescent paramagnetic ions (ions of rare earths) for which at low temperatures the optical spectra are very well defined [79].

f. Polarization by Saturation of Electronic Resonances (Overhauser) [52, 56, 60, 63, 64, 68, 69, 72, 73, 75, 76, 76a, 80a, 82, 83, 85, 88]

The mechanism of reorientation of nuclear spins (nuclear relaxation) in solids is often such that the nuclear spin only flips together with an electronic spin (or does so preferentially). Generally speaking, this provides a means for causing a deviation of the nuclear orientation from the orientation in thermodynamic equilibrium in the following way: by saturating an electronic resonance with an applied microwave field the population of certain electronic states may be changed. But this may also entail a change in the population of the nuclear spin levels because nuclear spins "flip together with electron spins". This provides a dynamical method for obtaining nuclear orientation at temperatures, for which no orientation is observable in thermodynamic equilibrium.

A quantitative study of this effect requires separate considerations for a number of possible arrangements: nuclei in metals, or nonmetals, e.g., paramagnetic centers in crystals. As we cannot review all the different cases, which were treated in the literature [56, 63, 64, 69, 72, 73, 75, 76, 76a, 80a, 82, 83], in the scope of this article, we shall confine ourselves here to a concise discussion of this effect for nuclei with spin in paramagnetic ions contained in a crystal.

The conditions essential for the effect are as follows:

1. The part of the Hamiltonian, which can cause a flip of the nuclear spin is $\alpha \mathbf{I} \cdot \mathbf{S}$, which can be written as a sum of terms $I_z S_z$, $I_+ S_-$ and

I_-S_+ (using spherical vector components). A term such as I_+S_- has only matrix elements in which m is increased by one, if m_s is decreased by one; hence the nuclear spin can only flip together with an electron spin.

2. The interaction $\alpha \mathbf{I}\cdot\mathbf{S}$ provides only a minor part of the relaxation of the electronic spins, as this is mostly caused by the interaction of the electronic spins with the vibrations of the crystal lattice. However, $\alpha \mathbf{I}\cdot\mathbf{S}$ provides nearly the whole heat contact of the nuclear spins with the crystal.

3. For a spin-exchange between a nucleus and an electron the energy is conserved by a simultaneous absorption or emission of a lattice quantum $2\mu_0 H$ (μ_0 is an effective magnetic moment of the order of the Bohr magneton).

4. In setting up equations for detailed balancing, one must take into account that the probabilities of absorption (increase of magnetic energy of the electron) and emission are proportional to ν and $\nu+1$ respectively. ν is the number of lattice quanta of magnitude $2\mu_0 H$ at a temperature T.

In thermodynamic equilibrium (no microwave field) in an external magnetic field H, detailed balancing is expressed by

$$|M_m|^2 n_+^0 a_m^0 (\nu+1) = |M_m|^2 n_-^0 a_{m+1}^0 \nu \qquad (2.22)$$

$n_\pm^0$ are the populations of the electronic spin states with $m_s = \pm \frac{1}{2}$ (assuming effective spin $\frac{1}{2}$ for simplicity); a_m^0 represents the populations of the nuclear spin sublevels — both in thermodynamic equilibrium for which $n_+^0/n_-^0 = \exp[-2\mu_0 H/kT]$ and all a_m^0 are nearly equal (unless T is extremely low, cf. a). $|M|^2$ is the square of a matrix element.

In the steady state obtained when saturating the electronic resonance with an applied microwave field, we have instead of (2.22)

$$|M_m|^2 n_+ a_m (\nu'+1) = |M_m|^2 n_- a_{m+1} \nu' \qquad (2.23)$$

$n_\pm$, a_m are the populations for the steady state; if the lattice-lattice relaxation is sufficiently short, the number of lattice quanta in the steady state $\nu' = \nu$. For complete saturation of the electronic resonance $n_+ = n_-$. Equation (2.23) with $n_+ = n_-$ will not always be valid; we can use it, if no h.f.s. can be resolved for the electronic resonance. If the electronic transition shows a resolved h.f.s. we should use populations $a(m_s, m)$ instead of $n_\pm a_m$ and we should obtain a set of

equations more complicated than (2.23), unless all subtransitions of the electronic resonance are saturated at the same time.

Under these conditions it follows from (2.22) and (2.23) that

$$\left.\begin{aligned} &a_{m+1}/a_m = n_-^{0'}/n_+^0 = \exp\,[2\mu_0 H/kT] \\ &\text{or} \\ &a_m \backsim \exp \beta m \ \text{ with } \ \beta = 2\mu_0 H/kT. \end{aligned}\right\} \tag{2.24}$$

Hence we see that for the nuclear spins an "apparent Boltzmann" distribution may be attained not belonging to the value of the nuclear moment but to the effective electron magnetic moment μ_0! The actual polarization of the nuclei may be less than given by (2.24) for the above-mentioned ideal situation for the following reasons:

1. the electronic resonance may only be partially saturated so that $n_+ < n_-$.
2. the coupling between **I** and **S** may differ from the form **I**·**S**, so that the nuclear spin flip has not always to be accompanied by an electronic spin flip.

In the Overhauser effect it seems generally useful to go to a low temperature T of, say, 1° K for the following reasons:

1. In order to obtain a reasonable nuclear orientation β must be of order unity.
2. For lower temperatures the longitudinal relaxation time T_1 for the electronic spin becomes larger, which is favourable as it is then easier to attain saturation of the electronic resonance.

The theoretical predictions concerning nuclear orientation were verified in some experiments by resonance methods [52, 60, 85], but no experiments have yet been reported in which the orientation was confirmed with the aid of nuclear radiations.

3. Description of Experiments and Results

The first successful experiments on nuclear orientation at very low temperatures were carried out in 1951 using magnetic h.f.s. alignment. Recently also the "brute force" method (external field polarization) and the electric h.f.s. method have been applied with good success. In the following we shall review the experiments which have been done so far and discuss their results. Most attention will be paid to the cryogenic aspects of the investigations. For previous review articles see ref. 102, 112 and 123.

a. Absorption of Neutrons by Polarized Nuclei

^{115}In. Dabbs, Roberts and Bernstein [114] have performed an external field polarization of ^{115}In nuclei. The nuclear orientation was detected by measuring the absorption of a beam of polarized thermal neutrons by the indium sample. A change in transmission was found when the neutron spin orientation was reversed from the direction parallel to the external field at the nuclear sample into the antiparallel direction. ^{115}Indium is one of the most favourable substances for a "brute force" polarization. It has a large nuclear magnetic moment ($5.50\,\mu_N$), an H/T-value of 12.2×10^4 ø/degree gives already a nuclear polarization of 1 %. When used as a metal a short nuclear spin-lattice relaxation time is to be expected.

Moreover, small polarizations of ^{115}In can already be detected by a neutron transmission measurement, because the thermal neutron cross section is large and almost entirely due to one resonance level at 1.46 eV. The neutron cross sections for a compound state with nuclear spin $I_c = I \pm \frac{1}{2}$ are given in equations (1.2) and (1.3). From these formulae it follows that, using indium plates of 0.5 cm total thickness and $|f_1^n| = 0.85$ – the actual conditions of the experiment – it is possible to get a 3 % change in the transmitted intensity for a nuclear polarization of only 1 %. Thus the change in transmission is a sensitive means for the detection of the nuclear polarization. From the sign of this change the value of I_c can be derived.

The indium was cooled by adiabatically demagnetized iron ammonium alum. The thermal contact was made by 20 silver wires of 0.046 cm diameter and 12 cm length. At the upper ends of the wires 20 indium plates of $0.025 \times 1.5 \times 3.5$ cm were soldered. The lower ends were flattened and the coolant salt was crystallized around them in order to provide an intimate heat contact. The total contact surface area was about 40 cm^2.

This unit was mounted on a rigid plastic support in a silver "guard" cage, which in its turn was cooled by a second iron ammonium alum sample. The whole cage was suspended from nylon threads under spring tension to minimize vibration heating.

Both salts were demagnetized from 0.99° K and 16400 ø ($S/R = 0.40$) to a temperature of some hundredths of a degree. Then the whole assembly was lowered slowly till the indium sample came into the gap of the magnet. The magnetic field was turned on again to 11150 ø, parallel to the plane of the indium plates, the coolant salts being

magnetically shielded. The field changes have to be made slowly to reduce eddy current heating. Particularly, when the field is raised suddenly to a value above the superconducting threshold field an appreciable eddy current heating may occur.

Under steady state conditions the heat input was estimated to be 40 erg/min, of which quantity about 4 erg/min was due to nuclear reactions induced by neutron irradiation.

The neutrons were polarized by reflecting them from a magnetized single crystal of Fe_3O_4. The reflected beam having passed the sample, the transmitted intensity was measured by a BF_3-counter.

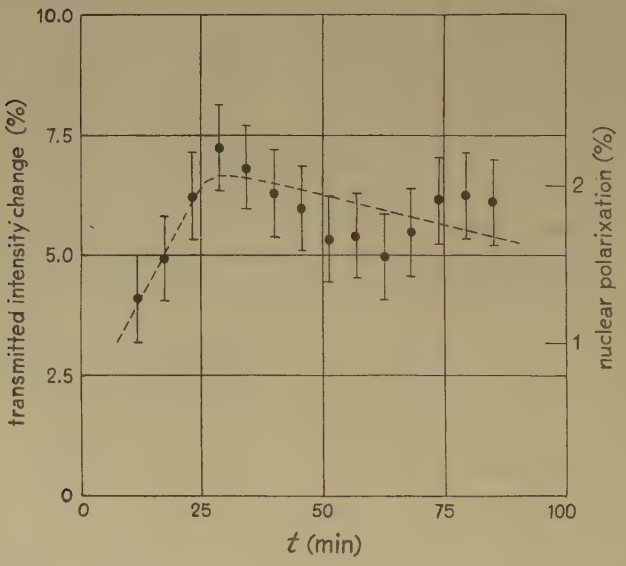

Fig. 5. Observed change in transmitted neutron intensity with reversal of relative spin orientation as a function of time. Average of four runs. Figure from Dabbs, Roberts, Bernstein [114].

Fig. 5 gives the observed change in transmitted intensity with reversal of the neutron spin orientation. An averaged effect of about 5.5 % was found, corresponding with a nuclear polarization of about 2 %. From this an average temperature of the indium nuclei of about 0.055° K is derived. The dashed curve in Fig. 5 represents a possible course with time, the maximum corresponds to a lowest temperature of 0.043° K.

From the sign of the transmitted intensity change the angular momentum of the 1.46 eV level is found to be $I_c = I + \frac{1}{2} = 5$.

^{55}Mn and ^{149}Sm. Experiments with these nuclei oriented by magnetic h.f.s. polarization have been made at Oak Ridge. They were reviewed in Vol. I, Ch. XIV, § 6 of "Progress in low temperature physics", together with earlier but inconclusive Leiden measurements [89, 90], so that in this article we will confine ourselves to a very brief survey.

$^{55}Mn(ND_4)_2(SO_4)_2 \cdot 6D_2O$ was cooled by adiabatic demagnetization to a final temperature of 0.20° K in a field of 2350 ø [66, 103]. By neutron irradiation ^{56}Mn is formed with a 2.6 hour γ-activity. This activity was found to be 3.4 % less for neutron and nuclear spin directions parallel than for the antiparallel state.

$^{149}Sm(C_2H_5SO_4)_3 \cdot 9H_2O$ was cooled indirectly in the same manner as the indium in the brute force experiments [109]. It was kept in a field of 11000 ø and used as neutron polarizer. The analyzer consisted of a magnetized Fe_3O_4 single crystal set to reflect 0.07 eV neutrons. A change in the intensity of the reflected beam was found when the neutron polarization produced by the Sm-sample was destroyed. From the results it followed that neutrons with spin parallel to the spins of the ^{149}Sm nuclei were captured preferably. This means that the 0.094 eV resonance level of ^{149}Sm has $I_c = I + \frac{1}{2}$.

The sample temperature was estimated to be about 0.13° K. The rather large difference with the temperature of the coolant salt (0.06 – 0.07° K) could be explained by an appreciable heat leak [114].

b. Gamma-Radiation from Oriented Radioactive Nuclei

General description of the experiments [105, 108, 125]

In general, a stack of a few single crystals is used with parallel axes, the total weight being of the order of 10 g. Adiabatic demagnetizations are carried out in the usual way. Susceptibility determinations are made by measuring the change in a mutual inductance formed by two coils surrounding the sample. From the susceptibility χ the "magnetic temperature", T^*, can be calculated, using Curie's law $\chi = C/T^*$. For the salts mentioned in § 2.b T^* is almost equal to the thermodynamic temperature T over a wide temperature range. Only at the lowest temperatures considerable deviations may occur, which sometimes can be evaluated theoretically. An experimental establish-

ment of the $T-T^*$ relation usually involves much labour while an accuracy better than 10 % seldom can be reached [123].

The γ-ray intensity measurements are made with scintillation counters; in the case that energy discrimination is needed NaI(Tl) crystals are used. The accuracy of the intensity measurements is of a statistical nature. It cannot be much affected by varying the amount of radioactive material in the sample. Only those γ-radioactive isotopes can be investigated with this method which have rather long halflives (e.g. a week or longer). Such isotopes first emit a β-particle. This β-radiation is almost completely absorbed in the sample itself giving rise to an appreciable heat generation. For a given mass of crystal both the counting rate and the heat generation are proportional to the total activity. Thus, increasing the source strength increases the counting rate but decreases the time available for observation in the same proportion. Usually an activity between 10 and 100 μC is chosen. A cut down of the heat influx from outside is very important. For this reason often "guard" salts like described in part a are used (see also Fig. 7). Under favourable conditions they reduce the heatleak to a value of some erg/min.

The course of the measurements is as follows. After demagnetization both the γ-ray intensity and the susceptibility are measured as functions of time. By eliminating the time the γ-ray intensity is found as a function of T^*. It should be noticed that it is important to check the shape of the warming up curves thus found by performing demagnetizations from different initial conditions, because considerable temperature inhomogeneities may arise in the sample during the warming up.

The results of the directional distribution measurements are often expressed by the maximum anisotropy, measured in two perpendicular directions,

$$\varepsilon=[R(\pi/2)-R(0)]/R(\pi/2),$$

where R denotes the counting rate. In the case that there exists in the crystals one axis of symmetry $R(\vartheta)$ is proportional to $W(\vartheta)$ of § 1, b, ϑ being the angle with the symmetry axis (z-axis). If there are two ions in unit cell with different symmetry axes, $R(0)$ is proportional to $W(\vartheta_0)$, ϑ_0 being the half angle between these two axes, $R(\pi/2)$ remains proportional to $W(\pi/2)$.

Experimental results

^{60}Co. This isotope has been studied most extensively. As its decay scheme was fairly well known, it was often used for testing a new experimental technique.

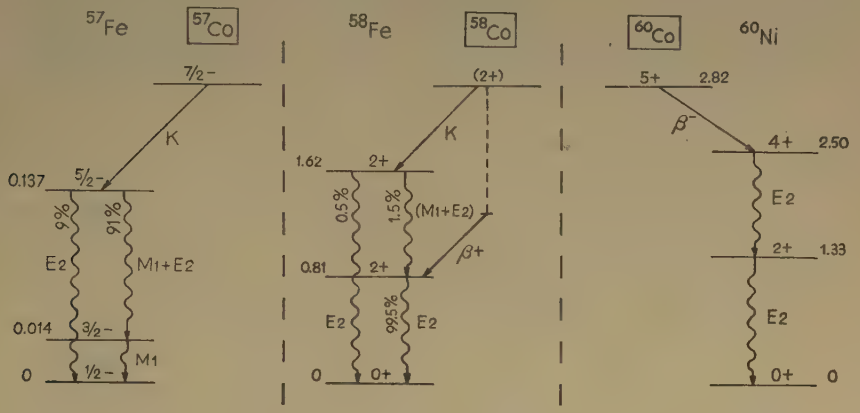

Fig. 6. Decay schemes of ^{57}Co, ^{58}Co and ^{60}Co as far as of interest for the description of the nuclear orientation work. Energies in MeV.

The first alignment experiments in 1951 were made as well in Oxford [91] as in Leiden [93] with ^{60}Co included in a Tutton salt (see Vol. I, Ch. XIV). From the shape of the directional distribution the decay scheme was confirmed. An estimate of the nuclear magnetic moment μ could be given. The Oxford results gave 3.5 μ_N by fitting theoretical and experimental curves at $T = 0.022°$ K [95, 96, 98]. The Leiden measurements yielded 4.3 μ_N obtained from a high temperature extrapolation [97, 99, 125]. Recently paramagnetic resonance measurements on ^{60}Co in cobalt ammonium Tutton salt were published [132], which gave $\mu(^{60}\text{Co}) = 3.800 \pm 0.007\ \mu_N$. The reasonable agreement with the nuclear alignment values shows that the interpretation of the alignment experiments is essentially correct. The nuclear magnetic moment once being well known the directional distribution of γ-radiation might be a useful thermometer under certain circumstances.

From measurements on the state of linear polarization of the emitted radiation using a γ-ray polarimeter the electric character of the transitions was confirmed [94].

Also the first h.f.s. polarization experiments were made on ^{60}Co included in cerium magnesium nitrate [100].

The γ-radiation emitted by polarized nuclei in the direction of the axis of polarization has a high degree of circular polarization. This was experimentally demonstrated in Leiden by measuring the change of the Compton scattering from magnetized iron when the direction of polarization of the nuclei was reversed [127] (see Fig. 7). The observed fractional change in counting rate amounted to at most 3 %. The sign of the effect proved, that ^{60}Co has a positive magnetic moment.

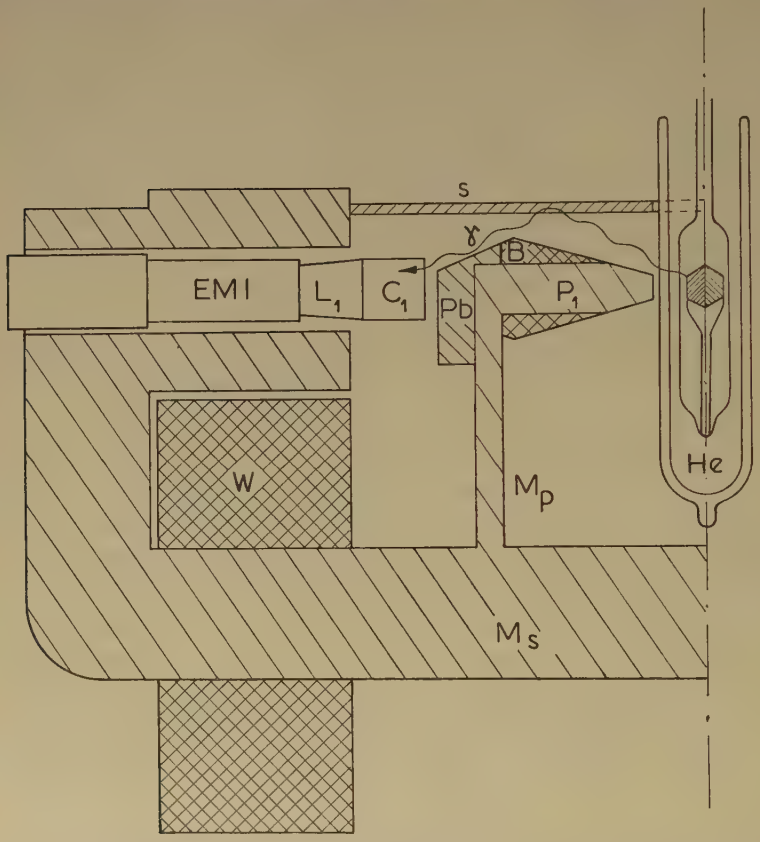

Fig. 7. Schematic diagram of the apparatus for producing and measuring circularly polarized gamma rays. 1/5 of natural size.
S : scattering iron plates,
M_s: saturating magnet with magnetizing coil W,
M_p: polarizing magnet with magnetizing coil B.
The gamma ray detectors consist of NaI(Tl) crystal C, lightpipe L and photomultiplier EMI. Figure from Wheatley, Huiskamp, Diddens, Steenland, Tolhoek [127].

The change in directional correlation between the cascaded gamma rays of ^{60}Co nuclei by nuclear orientation was determined in Columbus, Ohio [121]. The results, shown in Fig. 8, confirmed the theoretical predictions of Cox and Tolhoek [7]. An explicit knowledge of the temperature was not necessary. It is, however, questionable whether these technically complex correlation measurements will in practice be able to give more nuclear information than the directional distribution observations (see also § 1, b).

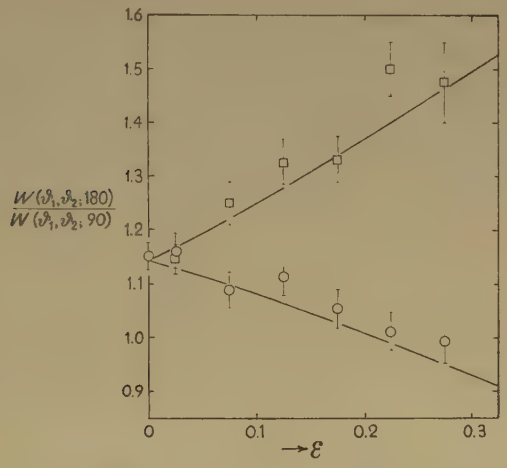

Fig. 8. Measured directional correlation of ^{60}Co gamma rays *versus* anisotropy. Orienting field of 200 oersted along cerium magnesium nitrate crystal axis.
$W(\vartheta_1, \vartheta_2; \vartheta)$: directional correlation function.
ϑ : angle between emission directions of the two photons,
ϑ_1: angle between emission direction of photon 1 and orientation axis,
ϑ_2: angle between emission direction of photon 2 and orientation axis.
$\odot$: $\vartheta_1 = 0°$ $\quad\quad$ $\boxdot$: $\vartheta_1 = 90°$.
Curves computed from Cox and Tolhoek [7] assuming equally spaced nuclear magnetic levels.
Figure from Jastram, Sapp, Daunt [121].

Measurements on metallic cobalt containing some ^{60}Co reported by Kurti, Oxford [119] and by Khutsishvili [122] have shown the possibility of nuclear orientation in a ferromagnetic. In Oxford an annealed single crystal of cobalt was cooled by thermal contact with chrome alum. In a cobalt crystal the magnetizations of the Weiss' domains are mainly oriented along the hexagonal axis. A measured ε of 0.16 demonstrated that also the nuclei were aligned along the same axis.

From comparison it follows that the h.f.s. splitting in the metal is about equal to that in the Tutton salts *. In the measurements of Khutsishvili a large external magnetic field was applied so that saturation magnetization of the electron spins was reached. A somewhat larger anisotropy of $0.10-0.15$ was found at temperatures of the order of $0.05-0.08°$ K.

As mentioned already in § 2, b Leiden measurements on undiluted cobalt ammonium Tutton salt in the antiferromagnetic state did not show any anisotropy within the statistical acccuracy (better than 1 %) [45, 108].

The paramagnetic crystals in use for nuclear orientation work are always grown from a solution containing the radioactive material. In Oxford measurements were made on a cobalt ammonium Tutton salt crystal in which ^{60}Co had been produced by neutron irradiation of the crystal itself [118]. The results showed (Fig. 9) that the anisotropy

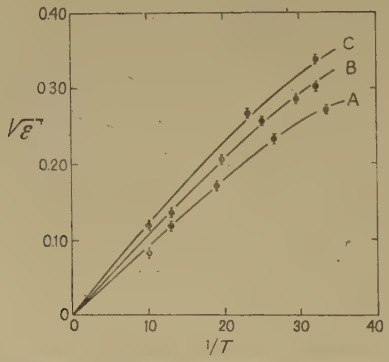

Fig. 9. Anisotropy of gamma rays of ^{60}Co included in cobalt ammonium Tutton salt crystal. Figure from Grace, Johnson, Kurti, Scurlock, Taylor [118].

A: crystal activated in chain reactor,
B: same crystal as A after annealing at 65° C during 10 days,
C: crystal grown from radioactive solution.

in the γ-radiation was 40 % less than in a similar crystal grown from a radioactive solution, even though the irradiated crystal had stood at room temperature for quite a time before cooling. After being kept at 65° C during 10 days the anisotropy had increased considerably. When ^{59}Co absorbs a slow neutron an excited state of ^{60}Co is formed,

* Private communication of Dr. M. A. Grace, Oxford.

which decays to the ground state by γ-emission. It is very likely that the 60 eV recoil of the ^{60}Co nucleus during this γ-transition may cause a displacement of the nucleus, which can be annulled by annealing.

^{58}Co. Measurements of the directional distribution of the γ-radiation were made in Oxford, some ^{58}Co being incorporated in copper rubidium Tutton salt [96, 98, 120]. Assuming a decay consisting of 85 % K-capture, 15 % β^+-radiation followed by a single 0.81 MeV γ-ray [134] the best agreement between experiment and theory was found for the case:

$$I_0 = 2 \overset{L_\beta=1}{\rightarrow} I_i = 2 \overset{L_\gamma=2}{\rightarrow} I_f = 0.$$

A nuclear magnetic moment of $3.5 \pm 0.3\ \mu_N$ was derived. From the state of linear polarization of the γ-radiation the electric character of the transition was established [94].

Dobrowolski and Jeffries [131] determined $\mu(^{58}\text{Co})$ by microwave measurements. They found a value of $4.05\ \mu_N$.

Wheatley, Griffing and Hill [128] determined the ratio of $\mu(^{58}\text{Co})$ and $\mu(^{60}\text{Co})$ by incorporating both isotopes in the same Tutton salt crystal and measuring the γ-ray intensities simultaneously. The result is rather strongly dependent upon the type of β-interaction assumed. For pure Gamow–Teller interaction a value of

$$|\mu(^{58}\text{Co})|/|\mu(^{60}\text{Co})| = 1.10 \pm 0.03$$

was found, which is very near to the ratio derived from the microwave data. This shows that the spin assignment concluded from the Oxford directional distribution measurements is essentially correct.

Lately the decay of ^{58}Co has been investigated in more detail; a second 0.81 MeV γ-transition together with a cross over transition of 1.62 MeV was discovered [133, 139, 141] (see Fig. 6). Since the intensities of these new lines are small, the above mentioned results on nuclear alignment will be only slightly affected. Recently Griffing and Wheatley [135] studied the directional distribution of both, the 0.81 MeV and the 1.62 MeV, γ-transitions in detail. About 100 μC ^{58}Co was included in 2.7 g diluted copper potassium Tutton salt crystals. This sample was demagnetized in two stages. In the first stage 5 g manganese ammonium Tutton salt, used as a thermal reservoir, was cooled to about $0.2 - 0.3°$ K. A lead tape formed the thermal link between reservoir and sample. While this tape is in a field above the threshold value, the sample is magnetized in a field of 7500 ø. After turning

off this field the sample reaches a temperature of about 0.012° K and the lead is in the superconducting state where its thermal conductivity is very low (see also ref. 123, § 5, d).

The accuracy of the directional distribution measurements enabled to determine the parameter λ, which is proportional to a ratio of nuclear matrixelements of the beta transition:

$$(1-\lambda)/\lambda=[(C_T^2+C_A^2)/(C_S^2+C_V^2)]\left|\int \boldsymbol{\sigma}\right|^2/\left|\int 1\right|^2$$

(C_T, C_A, C_S, C_V are proportional to the coupling constant for the tensor, axial vector, scalar and vector parts of the beta interaction resp.). For the β-transition to the 0.81 MeV level a λ of 0.12 ± 0.04 could be determined by making use of internal consistency arguments only. If this value is used to compute the ratio $|\mu(^{58}\mathrm{Co})|/|\mu(^{60}\mathrm{Co})|$ from the experiments with both isotopes in the same crystal as mentioned above [128] the result is in agreement with the microwave data.

From the 1.62 MeV data it followed that this radiation very likely must be quadrupole and the λ for the β-transition to this level was found to be 0.45 ± 0.11.

^{57}Co. Measurements on aligned ^{57}Co nuclei included in copper rubidium Tutton salt showed the absence of any anisotropy in the 123 keV γ-radiation down to the lowest temperatures attainable (0.01° K) [117], although the nuclear magnetic moment was known to be of the same order as that of the other cobalt isotopes (4.6 μ_N) [101]. It appeared, however, that the γ-radiation had a finite plane polarization [111]. This can be explained by assuming that the γ-transition instead of being pure M1 is a mixture of 96.4 % M1 and 3.6 % E2.

The degree of plane polarization was much smaller than expected. From this it is concluded that a disorientation of the nucleus takes place, probably in consequence of the K-capture process preceding the γ-transition.

^{56}Co. This isotope was aligned in Leiden by incorporating it in diluted copper ammonium Tutton salt [116]. Its decay scheme is rather complex, there are six γ-transitions [126] (see Fig. 10). For each of the γ-rays the anisotropy ε was determined. A theoretical discussion taking into consideration further existing experimental data leads to the spin values as indicated in Fig. 10 [124]. An estimate of the

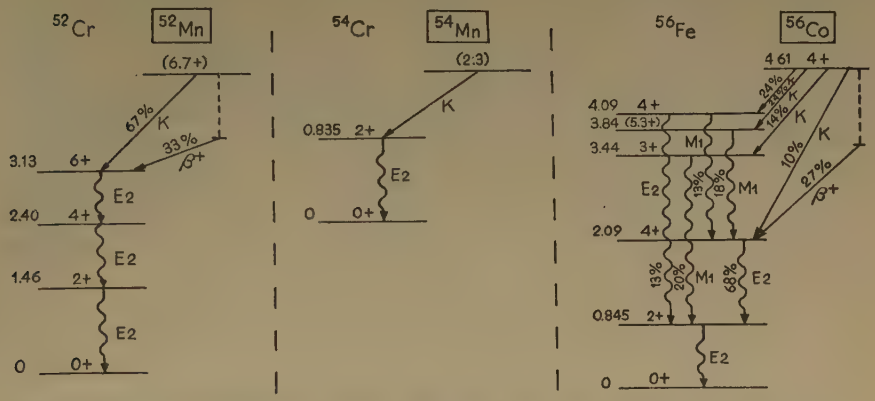

Fig. 10. Decay schemes of ^{52}Mn, ^{54}Mn and ^{56}Co as far as of interest for the description of the nuclear orientation work. Energies in MeV.

magnetic moment yielded $2.8 \pm 0.9\ \mu_N$. Jastram, Sapp and Schroeder [140] reported measurements on the polarization of ^{56}Co in cerium magnesium nitrate. They found a magnetic moment of $2.64 \pm 0.16\ \mu_N$. Recent paramagnetic resonance experiments of Baker *et al.* [129] and Jones *et al.* [137] gave $\mu\ (^{56}\text{Co}) = 3.85\ \mu_N$, $I\ (^{56}\text{Co}) = 4$.

In Leiden measurements are in progress on the states of linear polarization of the different γ-rays. The preliminary results show that all the ^{56}Fe levels must have even parity.

^{54}Mn. In Oxford alignment and polarization of ^{54}Mn were measured [104, 106]. The ^{54}Mn was included in cerium magnesium nitrate. A polarizing field of 1000 ø was used to swamp the effects of internal and crystalline fields. From the results it followed that the first excited state of ^{54}Cr has spin 2 and even parity. However, quantitative agreement between experiment and theory could not be obtained. In the case of alignment the course of the anisotropy ε with temperature was even very peculiar, it passed through a maximum at 0.01° K. New measurements with ^{54}Mn included in nickel fluosilicate showed no maximum in the ε versus $1/T$ curve and gave a nuclear moment of about $2\ \mu_N$ *.

^{52}Mn. In Leiden experiments on ^{52}Mn were made similar to the ^{54}Mn measurements mentioned above [136]. An additional experimental

* Private communication of Dr. C. E. Johnson, Oxford.

difficulty is the short half life (5.7 day). All the three cascaded γ-radiations appeared to be quadrupole radiations with $\Delta I = -2$. The alignment measurement gave more or less analogous results as for ^{54}Mn. Also in this case they cannot be explained from the paramagnetic resonance h.f.s. data obtained on bismuth magnesium manganese nitrate [58]. Recent measurements on the states of polarization of the emitted γ-radiations showed that the transitions have all electric character and that the magnetic moment is positive.

^{139}Ce, ^{141}Ce, ^{147}Nd. The first measurements on aligned nuclei of the rare earth group were made by Ambler, Hudson and Temmer [110] by incorporating γ-radioactive cerium and neodymium in $^{137}Ce_2Mg_3(NO_3)_{12} \cdot 24H_2O$. In § 2, b we saw already that in this case an "alignment in a plane" is to be expected. The anisotropy in the directional distribution of the γ-radiation was measured.

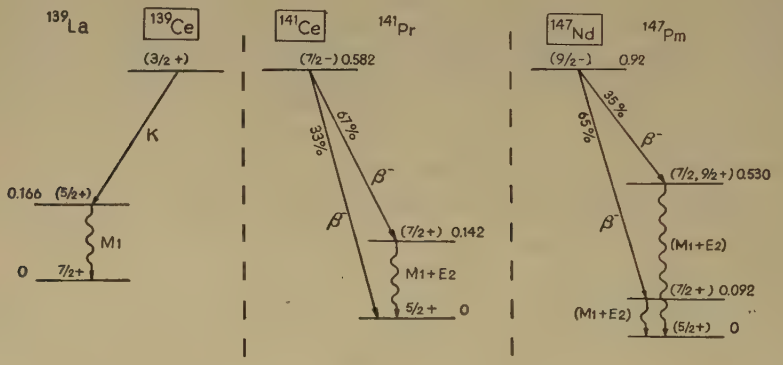

Fig. 11. Decay schemes of ^{139}Ce, ^{141}Ce and ^{147}Nd as far as of interest for the description of the nuclear orientation work. Energies in MeV.

The results were rather different from what had to be expected. For the 92 keV transition even no ε greater than 0.05 was measured. The authors point out that reorientation effects in the intermediate states are unlikely to be significant, but that two other factors may influence the anisotropy considerably. Electron spin spin interactions can be expected to cause an overlap of the lowest h.f.s. levels especially in the case $B \gg A$ and small admixtures of coherent E2 radiation to the M1 radiation can alter the directional distribution radically (see § 1, b).

In Oxford measurements were performed on ^{139}Ce, ^{141}Ce and ^{147}Nd aligned in neodymium ethylsulphate [113]. In this salt $A \gg B$. Both, the anisotropy and the plane polarization of the γ-radiations were measured so that admixtures of dipole and quadrupole radiations could be determined accurately. The ^{139}Ce radiation proved to be almost pure M1. The nuclear moment is 0.73 μ_N. The Washington results can be fitted to the Oxford ones. The 145 keV radiation of ^{141}Ce showed an E2 admixture of about 1 %. A nuclear moment of about 0.7 μ_N was evaluated. The ^{147}Nd results are in disagreement with the Washington ones, especially on the 92 keV transition an anisotropy of about 0.10 was measured, whereas Ambler *et al.* found no ε greater than 0.05. For the 530 keV transition a large mixing ratio E2/M1 was derived. The nuclear moment is $0.44 \pm 0.06\ \mu_N$.

^{169}Yb and ^{175}Yb have recently been aligned in ytterbium ethylsulphate in Oxford. The 282 keV γ-radiation of ^{175}Yb showed a positive ε, the 396 keV γ-ray a small negative ε. From the results it can be concluded that the 396 keV level has spin 7/2. Both γ-rays are mixtures of E1 and M2. The nuclear moment of ^{175}Yb is about 0.2 μ_N *.

In general one may conclude that experiments on γ-radiation of oriented nuclei can provide useful additional information concerning the decay schemes of these nuclei, especially in the case that directional correlation measurements are impossible. Usually only an estimate of the nuclear magnetic moment can be given. For producing nuclear polarization cerium magnesium nitrate has proved to be a very suitable substance, although more data on the electron spin spin interactions in this salt are required in order to make quantitative interpretations possible.

c. Alpha Radiation from Oriented Nuclei

^{237}Np. Roberts *et al.* [138], Oak Ridge, observed the directional distribution of the intensities of α-particle emission from ^{237}Np. A single crystal of $UO_2Rb(NO_3)_3$ was coated with a layer of $NpO_2Rb(NO_3)_3$. This sample was placed at the bottom of the cryostat and could be rotated over 90°. The α-particles were detected by a scintillation counter consisting of a ZnS screen closely above the sample and a phototube at room temperature. The apparatus is shown in Fig. 12.

* Private communication of Dr. C. E. Johnson, Oxford.

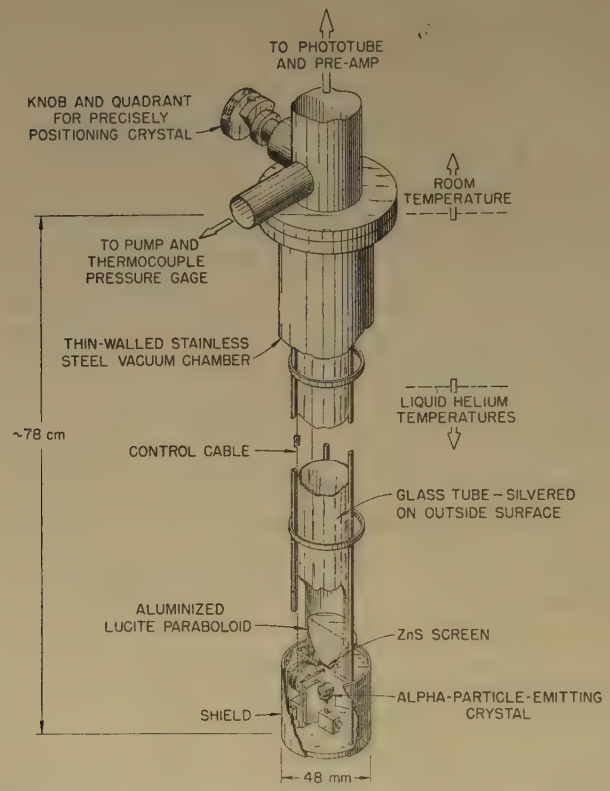

Fig. 12. Apparatus for observing anisotropic alpha-particle emission. Figure from Roberts, Dabbs, Parker, Ellison [138].

At helium temperatures an appreciable anisotropy was already found with a maximum intensity in the direction perpendicular to the crystalline c-axis, along which axis the Np spins are aligned. In the helium range ε changed approximately proportionally with $1/T$. It was mentioned already in § 2, c, that in this case the alignment is partly due to electric quadrupole coupling.

^{233}U. A pure electric h.f.s. alignment was observed in $^{233}UO_2Rb(NO_3)_3$ by Dabbs *et al.*, Oak Ridge [130]. The experiment itself was much analogous to that described for Np. A single crystal of $^{238}UO_2Rb(NO_3)_3$ was coated with a layer of ^{233}U-rich material. The shape of the directional distribution of the α-particle intensity and its temperature dependence were found to be similar to those observed for ^{237}Np, ε being about 0.09 at 1.1° K.

A special precaution was taken to ensure a magnetic nuclear spin-lattice relaxation mechanism by adding 0.2 % ^{237}Np to the sample. This method of avoiding too long nuclear spin-lattice relaxation times by adding small quantities of paramagnetic impurities is very essential in the Pound method (see ref. 67).

The alpha-emitting nuclei ^{233}U and ^{237}Np must be expected to have a strong spheriodal deformation according to the unified model [20], probably with a large positive quadrupole moment. From the sign of the observed anisotropy Roberts *et al.* conclude that the alpha particles are emitted preferentially at the "equator" and not at the "tips" of the prolate spheroid. However, the Coulomb-barrier for the outgoing alpha particles is lowest at the "tips" [17]. Hence these experiments appear to indicate that the preformation of the alpha particles within the nucleus occurs preferentially near the equator, even overcompensating the higher penetrability of the Coulomb barrier at the tips [24]. This information is very important for the theory of alpha disintegration.

4. Discussion of Possible further Developments

If we overlook the work which has been done on nuclear orientation and which is now in progress, we notice that much experimental work was published recently, especially in 1955. The new successful experiments with external field polarization and electric h.f.s. alignment have demonstrated the possibility for orientation of nuclei of non-paramagnetic ions. Moreover, there is quite a number of recent suggestions which look promising for extending the number of nuclei for which orientation is feasible (as discussed in § 2).

In this way the method of nuclear orientation will gain in importance for nuclear spectroscopy. We summarize which information may be obtained with the method:

1. The multipole character of gamma radiation can be determined. For distinguishing between the magnetic or electric character of radiation a measurement of the linear polarization is required; this can also lead to spin and parity determinations in nuclear disintegration schemes [15].
2. In case of neutron absorption by polarized nuclei, the nuclear spin of the compound state may be determined.
3. Nuclear magnetic moments of radioactive nuclei may be deter-

mined. This is possible from a measurement of the temperature and the anisotropy of the radiation if the orientation mechanism is known. This method is not too accurate (cf. § 3, b). Higher accuracies could be obtained if the method of nuclear orientation could be combined with a radio frequency resonance method as was suggested by Tolhoek and de Groot [6] and later discussed in more detail by Bloembergen and Temmer [12], Abragam [84] and Jeffries [88]. However, this was not yet realized in experiments.

The experimental determination of the sign of the magnetic moment requires the determination of the sign of the circular polarization of emitted gamma radiation.

4. Information on the relative magnitude of beta nuclear matrix elements such as $|\int \boldsymbol{\sigma}|^2$ and $|\int 1|^2$ for a beta transition without spin change, can be obtained in principle as well from the study of gamma radiation which follows the beta transition [15] as from the polarization of the emitted beta rays.

The directional distribution of beta rays of a forbidden transition may give information on the character of this transition.

Measurements of the polarization of beta rays can decide on the change of nuclear spin in the beta transition.

The polarization of beta rays depends on the relative sign of the S and T parts of the beta interaction so that it might be used for the determination of this sign.

5. Measurements of the directional distribution of alpha particles of oriented nuclei may give valuable information on the mechanism of alpha decay as explained in § 1, d and § 3, c.

6. Measurements on the directional distribution of fission products coming from oriented heavy nuclei irradiated with slow neutrons are of interest in connection with fission theory (see § 1, e).

7. Measurements of the directional distribution of the beta radiation of oriented nuclei can check the recent suggestion of Lee and Yang that there might be non-conservation of parity in the beta interaction, which would be as well a revolutionary as fundamental thing for the principles of physics.

8. The study of the orientation mechanism can give information on solid state physics in which the measurements on nuclear radiation serve as a tool. The more recent suggestions for nuclear orientation may establish an even closer connection with the field of nuclear resonance and paramagnetic h.f.s. investigations.

9. Measurements of the anisotropy of emitted radiations may provide a useful thermometer if the orientation mechanism is known.

One of the authors (H.A.T.) of this review is a member of the scientific staff of the "Stichting voor Fundamenteel Onderzoek der Materie", which is financially supported by the Netherlands organization for pure scientific research (Z.W.O.).

REFERENCES

I. Theoretical Results on Nuclear Effects with Oriented Nuclei

[1] M. E. Rose, Nucleonics, 3, 23 (1948); Phys. Rev., 75, 213 (1948); Report AECD, 2183 (1948).
[2] J. A. Spiers, Nature, 161, 807 (1948); Thesis, Oxford (1948).
[3] H. A. Tolhoek and S. R. de Groot, C. R. Paris, 230, 1580 (1950).
[4] M. H. L. Pryce, Proc. int. Conf. low temp. Phys. Oxford, 155–157 (1951).
[5] N. R. Steenberg, Phys. Rev., 84, 1051 (1951).
[6] H. A. Tolhoek and S. R. de Groot, Physica, 17, 81 (1951).
[7] J. A. M. Cox, Physica, 18, 1262 (1952); J. A. M. Cox and H. A. Tolhoek, Physica, 18, 359 (1952).
[8] S. R. de Groot, Physica, 18, 1201 (1952).
[9] N. R. Steenberg, Proc. Phys. Soc. A, 65, 791 (1952).
[10] H. A. Tolhoek, Physica, 18, 1257 (1952).
[11] H. A. Tolhoek and J. A. M. Cox, Physica, 18, 357 (1952).
[12] N. Bloembergen and G. M. Temmer, Phys. Rev., 89, 883 (1953).
[13] J. A. M. Cox and S. R. de Groot, Physica, 19, 683 (1953).
[14] J. A. M. Cox and H. A. Tolhoek, Physica, 19, 673 (1953).
[15] J. A. M. Cox, S. R. de Groot and Chr. D. Hartogh, Physica, 19, 1119 and 1123 (1953).
[16] J. A. M. Cox and H. A. Tolhoek, Physica, 19, 1178 (1953).
[17] D. L. Hill and J. A. Wheeler, Phys. Rev., 89, 1102 (1953).
[18] N. R. Steenberg, Proc. Phys. Soc. A, 66, 391 (1953).
[19] H. A. Tolhoek and J. A. M. Cox, Physica, 19, 101 (1953).
[20] A. Bohr, Diss. Copenhagen (1954).
[21] Chr. D. Hartogh, H. A. Tolhoek and S. R. de Groot, Physica, 20, 1310 (1954).
[22] G. R. Satchler, Phys. Rev., 94, 1304 (1954); Proc. Phys. Soc. A, 66, 1081 (1954); App. IV.
[23] N. R. Steenberg, P. R., 95, 982 (1954).
[24] J. A. Wheeler, Proc. Int. Conf. Glasgow 1954; Nuovo Cim. (Ser. X) 2, Suppl. no. 3, 909 (1955).
[24a] A. Bohr, P. O. Fröman and B. R. Mottelson, Dan. Mat. Fys. Medd., 29, no. 10 (1955).
[25] T. P. Gray and G. R. Satchler, Proc. Phys. Soc. A, 68, 349 (1955).
[26] S. R. de Groot and H. A. Tolhoek, Beta- and Gamma-ray spectroscopy edited by K. Siegbahn, North-Holland Publ. Co., A'dam (1955), pp. 613–623.

[27] H. A. Tolhoek, Chr. D. Hartogh and S. R. de Groot, J. Phys. Rad., **16**, 615 (1955).
[28] M. E. Rose, L. D. Roberts and J. W. T. Dabbs, BAPS (II) **1**, 207 (1956).
[28a] A. Z. Dolginov, J. exp. theor. Phys., (in the press).
[28b] P. J. Brussaard and H. A. Tolhoek, Physica, (in course of publication).
[28c] T. D. Lee and C. N. Yang, Phys. Rev., (in course of publication).
[28d] J. A. Wheeler, Physica, 22 (1956) (in course of publication).

II. Methods for Orienting Nuclei (including some data on h.f.s. in crystals)

[29] L. Néel, Ann. Physique, (10) **18**, 5 (1932); (11) **5**, 232 (1936); (12) **3**, 137 (1948).
[30] C. J. Gorter, Phys. Z., **35**, 923 (1934).
[31] N. Kurti and F. E. Simon, Proc. Roy. Soc. London A, **149**, 152 (1935).
[32] A. Kastler, Ann. Physique, **6**, 663 (1936).
[33] F. Simon, C. R. Conf. Magnétisme Strasbourg, **3**, I (1939).
[34] A. Kastler, Physica, **12**, 619 (1946).
[35] C. J. Gorter, Physica, **14**, 504 (1948).
[36] M. E. Rose, Report AECD, 2119 (1948); Phys. Rev., **75**, 213 (1949).
[37] R. V. Pound, Phys. Rev., **76**, 1410 (1949).
[38] J. Brossel and A. Kastler, C. R. Paris, **229**, 1213 (1949).
[39] A. Kastler, J. Phys. Rad., **11**, 255 (1950).
[40] A. Abragam and M. H. L. Pryce, Proc. Roy. Soc. London A, **205**, 135 (1951).
[41] B. Bleaney, Proc. Phys. Soc. A, **64**, 315 (1951).
[42] B. Bleaney, Phil. Mag., **42**, 441 (1951).
[43] B. Bleaney and D. J. E. Ingram, Proc. Roy. Soc. London A, **208**, 143 (1951).
[44] J. G. Daunt, Proc. int. Conf. low temp. Phys. Oxford, (1951), p. 157.
[45] C. J. Gorter, Proc. int. Conf. low temp. Phys. Oxford, (1951), p. 158.
[46] A. Kastler, Physica, **17**, 191 (1951); C. R. Paris, **233**, 1444 (1951).
[47] A. Simon, M. E. Rose and J. M. Jauch, Phys. Rev., **84**, 1155 (1951).
[48] F. Bitter and J. Brossel, Phys. Rev., **85**, 1051 (1952).
J. Brossel, Ann. Phys. Paris, **7**, 622 (1952).
J. Brossel and F. Bitter, Phys. Rev., **86**, 308 (1952).
[49] J. Brossel, A. Kastler and J. Winter, J. Phys. Rad., **13**, 668 (1952).
[50] B. Bleaney and K. W. H. Stevens, Rep. Progr. Phys., **16**, 108 (1953).
[51] F. Bitter, R. F. Lacey and B. Richter, Rev. Mod. Phys., **25**, 174 (1953).
[52] T. R. Carver and C. P. Slichter, Phys. Rev., **92**, 212 (1953).
[53] A. H. Cooke, H. J. Duffus and W. P. Wolf, Phil. Mag., **44**, 623 (1953).
[54] J. M. Daniels and F. N. H. Robinson, Phil. Mag., **44**, 630 (1953).
[55] W. B. Hawkins and R. H. Dicke, Phys. Rev., **91**, 1008 (1953).
W. B. Hawkins, Phys. Rev., **96**, 532 (1954) and **98**, 478 (1955).
[56] A. W. Overhauser, Phys. Rev., **92**, 411 (1953).
[57] N. R. Steenberg, Proc. Phys. Soc. A, **66**, 399 (1953).
[58] R. S. Trenam, Proc. Phys. Soc. A, **66**, 118 (1953).
[59] J.-P. Barrat, J. Brossel and A. Kastler, C. R. Paris, **239**, 1196 (1954).
[60] H. G. Beljers, L. van der Kint and J. S. van Wieringen, Phys. Rev., **95**, 1683 (1954).

[61] B. Bleaney, P. M. Llewellyn, M. H. L. Pryce and G. R. Hall, Phil. Mag., **45**, 992 (1954).
[62] J. Brossel, B. Cagnac and A. Kastler, J. Phys. Rad., **15**, 6 (1954).
[63] P. Brovetto and G. Cini, Nuovo Cim., **11**, 618 (1954) and **12**, 899 (1954).
[64] P. Brovetto and S. Ferroni, Nuovo Cim., **12**, 90 (1954).
[65] J. W. T. Dabbs and L. D. Roberts, Phys. Rev., **95**, 307 (1954).
[66] J. W. T. Dabbs and L. D. Roberts, Phys. Rev., **95**, 970 (1954).
[67] J. M. Daniels, Can. J. Phys., **32**, 662 (1954).
J. M. Daniels and J. L. G. Lamarche, Comm. Conf. phys. basses temp. Paris, (1955), p. 313.
[68] A. Honig, Phys. Rev., **96**, 234 (1954) and A. Honig and J. Combrisson, Phys. Rev., **102**, 917 (1956).
[69] J. I. Kaplan, Phys. Rev., **96**, 238 (1954).
[70] A. Kastler, J. Phys. Rad., **15**, 300 (1954).
[71] A. Kastler, Proc. Phys. Soc. A, **67**, 853 (1954).
[72] C. Kittel, Phys. Rev., **95**, 589 (1954).
[73] J. Korringa, Phys. Rev., **94**, 1388, 1389 (1954).
[74] N. R. Steenberg, Phys. Rev., **93**, 678 (1954).
[75] A. Abragam, Phys. Rev., **98**, 1729 (1955).
[76] W. A. Barker and A. Mencher, Phys. Rev., **98**, 1868 (1955); **100**, 1224 (1955); **102**, 1023 (1956).
[76a] C. Bloch and A. Messiah, J. Phys. Rad., **16**, 785 (1955).
[77] K. D. Bowers and J. Owen, Rep. Progr. Phys., **18**, 304 (1955).
[78] J. Brossel, J. Margerie and A. Kastler, C. R. Paris, **241**, 474 and 865 (1955).
[78a] A. H. Cooke and H. J. Duffus, Proc. Roy. Soc. London A, **229**, 407 (1955).
[79] G. H. Dicke and L. Heroux, Phys. Rev., **100**, 965 (1955).
[80] J. C. Eisenstein and M. H. L. Pryce, Proc. Roy. Soc. London A, **229**, 20 (1955).
[80a] J. I. Kaplan, Phys. Rev., **99**, 1322 (1955).
[81] G. P. Khutsishvili, J. exp. theor. Phys. USSR, **28**, 496 (1955) (Sovjet Physics, Vol. 1, 390 (1955)).
[82] M. J. Klein, Phys. Rev., **98**, 1736 (1955).
[83] C. P. Slichter, Phys. Rev., **99**, 1822 (1955).
[84] A. Abragam, C. R. Paris, **242**, 1720 (1956).
[85] T. R. Carver and C. P. Slichter, Phys. Rev., **102**, 975 (1956).
[86] G. Feher, Phys. Rev., **103**, 500 (1956).
[87] G. Feher and E. A. Gere, Phys. Rev., **103**, 501 (1956).
[88] C. D. Jeffries, Phys. Rev. (in course of publication).
[88a] J. H. Van Vleck, BAPS (II), **1**, 11 (1956).

III. Description of Experiments (including some related data on disintegration schemes and magnetic moments)

[89] C. J. Gorter, D. de Klerk, O. J. Poppema, M. J. Steenland and Hl. de Vries, Physica, **15**, 679 (1949).
[90] O. J. Poppema, Helv. Phys. Acta, **23**, Suppl. III p. 187 (1950).
[91] J. M. Daniels, M. A. Grace and F. N. H. Robinson, Nature, **168**, 780 (1951).

92 C. G. B. Garrett, Proc. Roy. Soc. London A, 206, 242 (1951).
93 C. J. Gorter, O. J. Poppema, M. J. Steenland and J. A. Beun, Communications Kamerlingh Onnes Lab., Leiden, no. 287b; Physica, 17, 1050 (1951).
94 G. R. Bishop, J. M. Daniels, G. Goldschmidt, H. Halban, N. Kurti and F. N. H. Robinson, Phys. Rev., 88, 1432 (1952).
95 B. Bleaney, J. M. Daniels, M. A. Grace, H. Halban, N. Kurti and F. N. H. Robinson, Phys. Rev., 85, 688 (1952).
96 J. M. Daniels, M. A. Grace, H. Halban, N. Kurti and F. N. H. Robinson, Phil. Mag., 43, 1297 (1952).
97 C. J. Gorter, H. A. Tolhoek, O. J. Poppema, M. J. Steenland and J. A. Beun, Commun. Leiden, Suppl. no. 104a; Physica, 18, 135 (1952).
98 M. A. Grace and H. Halban, Physica, 18, 1227 (1952).
99 O. J. Poppema, J. A. Beun, M. J. Steenland and C. J. Gorter, Commun. Leiden, no. 291a; Physica, 18, 1235 (1952).
100 E. Ambler, M. A. Grace, H. Halban, N. Kurti, H. Durand, C. E. Johnson and H. R. Lemmer, Phil. Mag., 44, 216 (1953).
101 J. M. Baker, B. Bleaney, K. D. Bowers, P. F. D. Shaw and R. S. Trenam, Proc. Phys. Soc. A, 66, 305 (1953).
102 R. J. Blin–Stoyle, M. A. Grace and H. Halban, Progr. Nucl. Phys., vol. 3, Pergamon Press, London (1953), pp. 63–83.
103 S. Bernstein, L. D. Roberts, C. P. Stanford, J. W. T. Dabbs and T. E. Stephenson, Phys. Rev., 94, 1243 (1954).
104 G. R. Bishop, J. M. Daniels, H. Durand, C. E. Johnson and J. Perez y Jorba, Phil. Mag., 45, 1197 (1954).
105 B. Bleaney, J. M. Daniels, M. A. Grace, H. Halban, N. Kurti, F. N. H. Robinson and F. E. Simon, Proc. Roy. Soc. London A, 221, 170 (1954).
106 M. A. Grace, C. E. Johnson, N. Kurti, H. R. Lemmer and F. N. H. Robinson, Phil. Mag., 45, 1192 (1954).
107 H. R. Lemmer and M. A. Grace, Proc. Phys. Soc. A, 67, 1051 (1954).
108 O. J. Poppema, Nuclear orientation in solids, Ph. D. thesis Groningen (1954).
109 L. D. Roberts, S. Bernstein, J. W. T. Dabbs and C. P. Stanford, Phys. Rev., 95, 105 (1954).
110 E. Ambler, R. P. Hudson and G. M. Temmer, Phys. Rev., 97, 1212 (1955); *ibid* 101, 196 (1956); Comm. Conf. phys. basses temp. Paris, (1955) p. 255.
111 G. R. Bishop, M. A. Grace, C. E. Johnson, A. C. Knipper, H. R. Lemmer, J. Perez y Jorba and R. G. Scurlock, Phil. Mag., 46, 951 (1955); Comm. Conf. phys. basses temp. Paris, (1955) p. 259.
112 R. J. Blin–Stoyle, M. A. Grace and H. Halban, Beta- and Gamma-ray spectroscopy, edited by K. Siegbahn, North-Holland Publ. Co., Amsterdam, (1955), pp. 600–612.
113 C. F. M. Cacho, M. A. Grace, C. E. Johnson, A. C. Knipper, R. G. Scurlock and R. T. Taylor, Phil. Mag., 46, 1287 (1955) and private communications of H. J. M. Meyer and C. E. Johnson, Oxford.
114 J. W. T. Dabbs, Thesis, University of Tennessee (1955).
J. W. T. Dabbs, L. D. Roberts and S. Bernstein, Phys. Rev., 98, 1512 (1955); Comm. Conf. phys. basses temp. Paris, (1955), p. 274.

115 H. Frauenfelder, Beta- and Gamma-ray spectroscopy, edited by K. Siegbahn, North-Holland Publ. Co., Amsterdam, (1955), pp. 572–595.
116 L. J. Gallaher, Ch. Whittle, J. A. Beun, A. N. Diddens, C. J. Gorter and M. J. Steenland, Commun. Leiden, no. 298c; Physica, 21, 117 (1955).
117 M. A. Grace, J. Phys. Rad., 16, 622 (1955).
118 M. A. Grace, C. E. Johnson, N. Kurti, R. G. Scurlock and R. T. Taylor, Comm. Conf. phys. basses temp. Paris, (1955), p. 261.
119 M. A. Grace, C. E. Johnson, N. Kurti, R. G. Scurlock and R. T. Taylor, Comm. Conf. phys. basses temp. Paris, (1955), p. 263.
120 H. Halban, J. Phys. Rad., 16, 609 (1955).
121 P. S. Jastram, R. C. Sapp, C. M. Schroeder and J. G. Daunt, Comm. Conf. phys. basses temp. Paris, (1955), p. 270; Phys. Rev., 101, 1381 (1956).
122 G. R. Khutsishvili, J. exp. theor. Phys. USSR, 29, 894 (1955).
123 D. de Klerk and M. J. Steenland, Progress in low temp. Phys. Vol. I, North–Holl. Publ. Co., Amsterdam, (1955), pp. 321–335.
124 O. J. Poppema, J. G. Siekman, R. van Wageningen and H. A. Tolhoek, Commun. Leiden, Suppl. no. 109b; Physica, 21, 223 (1955).
125 O. J. Poppema, M. J. Steenland, J. A. Beun and C. J. Gorter, Commun. Leiden, no. 298b; Physica, 21, 233 (1955).
126 M. Sakai, J. Phys. Soc. Japan, 10, 729 (1955).
M. Sakai, J. L. Dick, W. S. Anderson and J. D. Kurbatov, Phys. Rev., 95, 101 (1954).
127 J. C. Wheatley, W. J. Huiskamp, A. N. Diddens, M. J. Steenland and H. A. Tolhoek, Commun. Leiden, no. 301b; Physica, 21, 841 (1955).
128 J. C. Wheatley, D. F. Griffing and R. D. Hill, Phys. Rev., 99, 334 (1955).
129 J. M. Baker, B. Bleaney, P. M. Llewellyn and P. F. D. Shaw, Proc. Phys. Soc. A, 69, 353 (1956).
130 J. W. T. Dabbs, L. D. Roberts and G. W. Parker, BAPS (II), 1, 207 (1956).
131 W. Dobrolowski and C. D. Jeffries, (in course of publication).
132 W. Dobrolowski, R. V. Jones and C. D. Jeffries, Phys. Rev., 101, 1001 (1956).
133 H. Frauenfelder, N. Levine, A. Rossi and S. Singer, Phys. Rev., 103, 352 (1956).
134 M. A. Grace, G. A. Jones and J. O. Newton, Phil. Mag., (8) 1, 363 (1956).
135 D. F. Griffing and J. C. Wheatley, Phys. Rev. (in course of publication) and D. F. Griffing, Thesis, University of Illinois, 1956.
136 W. J. Huiskamp, M. J. Steenland, A. R. Miedema, H. A. Tolhoek and C. J. Gorter, Commun. Leiden, no. 304c; Physica, 22, 587 (1956).
137 R. V. Jones, W. Dobrowolski and C. D. Jeffries, Phys. Rev., 102, 738 (1956).
138 L. D. Roberts, J. W. T. Dabbs, G. W. Parker and R. D. Ellison, BAPS (II), 1, 207 (1956).
139 B. L. Robinson and R. W. Fink, BAPS (II), 1, 40 (1956).
140 R. C. Sapp and C. M. Schroeder, BAPS (II), 1, 91 (1956).
P. S. Jastram, C. M. Schroeder and R. C. Sapp, BAPS (II), 1, 172 (1956).
141 C. S. Cook and F. M. Tomnovec, BAPS (II), 1, 253 (1956).

CHAPTER XI

SOLID HELIUM

BY

C. DOMB

King's College, University of London

AND

J. S. DUGDALE

Division of Pure Physics, National Research Council, Ottawa

Contents: *Part I*, 338. — 1. Introduction, 338. — 2. General Thermodynamic Properties of Solid He^4, 340. — 3. Thermal Conductivity of Solid Helium, 346. — 4. Melting Curve and Melting Parameters of He^4, 349. — 5. Melting Parameters and General Properties of Solid He^3, 355. — *Part II*, 356. — Theoretical Aspects, 356.

I. EXPERIMENTAL ASPECTS

1. Introduction

Before the last war, the thermodynamic properties of solid helium had been investigated only in the temperature region 1.5 to 4° K and under pressures up to about 140 atmospheres [1]. The melting characteristics of solid helium had been more extensively studied: the latent heat of melting had been measured at several temperatures [1, 2] and the melting curve had been determined by Simon and his coworkers up to a temperature of about 43° K, corresponding to more than 8 times the liquid-gas critical temperature. The melting curve for helium is shown in Fig. 1.

The unique importance of solid helium in the study of melting has been stressed by Simon [5, 51], whose argument may be summarized in the following way. Experiments on many substances show that their melting curves may all be represented by an equation of the form [6]

$$\frac{p}{a} = \left(\frac{T}{T_0}\right)^c - 1. \tag{1}$$

For a given class of substance (e.g. the solidified gases, the alkali metals, etc.) c has approximately the same value, so that there exists

for each class a reduced melting curve in which a and T_0, the characteristic temperature and pressure, are the reducing parameters. Of all substances helium has the lowest value of a and of T_0 and so, for given laboratory resources, is capable of yielding the most extensive information about the behaviour of the melting curve of a typical substance at 'high' temperatures and pressures.

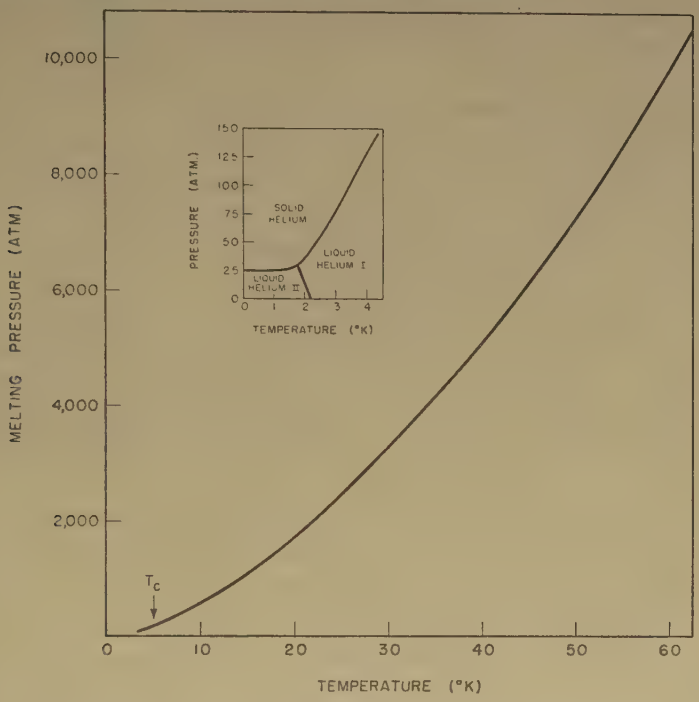

Fig. 1. The melting curve of He^4; T_c is the critical temperature. The inset shows the low temperature phase diagram of He^4.

Of great practical importance is the fact that the melting properties of helium can be studied in the region of low temperatures where the heat capacities of the necessary pressure vessels are conveniently small. This of course applies equally to other thermal measurements on solid helium under pressure. The effect on these properties of quite modest pressures is drastic. For example, by applying to solid helium pressures of only a few thousand atmospheres, its volume can be halved and its Debye temperature changed by a factor of 5.

From a more detailed theoretical point of view, the properties of the solid have a double interest: the helium atom, having central

additive short-range forces, makes the solid a suitable substance for theoretical treatment, while the small mass of the helium atom and its relatively weak binding force make manifest, in a remarkable way, the effects of the zero-point motions of the atoms in the solid.

All these considerations which are true of solid He^4 apply even more strongly to solid He^3, and they have formed the basis of much of the recent work on solid helium. This work we shall now discuss in more detail.

2. The General Thermodynamic Properties of Solid He^4

2.1. Specific heats

Keesom and Keesom [1] in 1936 measured the heat capacity of solid helium at low densities in the temperature range from 1.5° to 4° K. The more recent work has, therefore, been concentrated on the temperature regions above and below this.

Webb, Wilkinson and Wilks [7] were primarily interested in the thermal conductivity of solid helium and wished to correlate their conductivity measurements with the characteristic temperature of the lattice. In order to do so, they measured the specific heat of the solid at temperatures between 0.6 and 1.5° K at three different densities.

Their method was to enclose both the paramagnetic salt (which was used as the cooling agent) and the solid helium in a calorimeter and to measure the total heat capacity. The salt was used as a thermometer and heat was supplied electrically. The heat capacity of the helium was obtained by subtracting from the total the estimated heat capacity of the calorimeter and salt. Their results are shown in Fig. 2.

Dugdale and Simon [8] measured the heat capacity of solid helium in the higher range of temperatures and densities, covering the region from 5° K to the melting temperature at molar volumes between 16 and 10.6 ccs. They used a vacuum calorimeter designed to stand pressures up to 3000 atmospheres, and measured temperatures with a constantan thermometer. Their results at four densities are shown in Fig. 3.

The measurements of Keesom and Keesom may be compared directly with those of Webb, Wilkinson and Wilks. The two sets of results are in reasonable agreement and indicate that the Debye temperature at these densities rises with falling temperature. In Fig. 4 the Debye temperatures for the two lowest densities are derived

from the measurements of Keesom and Keesom. At the still lower temperatures reached in the experiments of Webb *et al.* the θ_D reaches a maximum and begins to fall. The Debye temperatures, calculated from Dugdale and Simon's measurements, are also shown in Fig. 4: they are almost constant although falling somewhat as the melting point is approached.

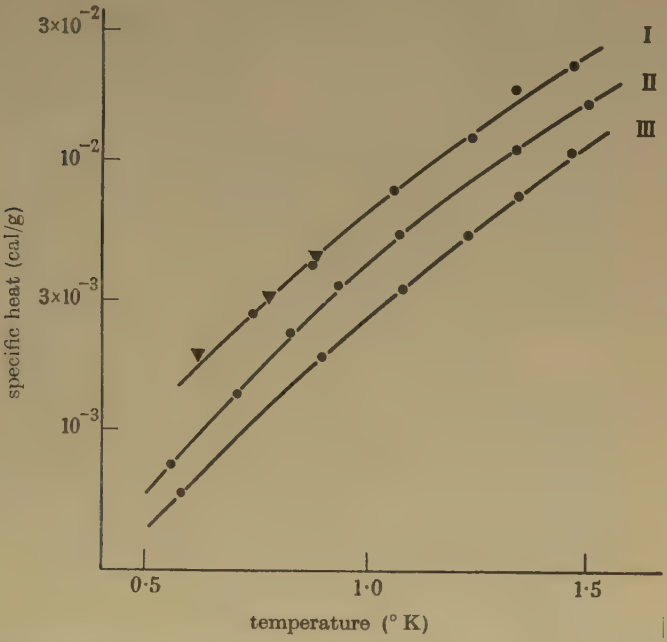

Fig. 2. The specific heat at constant volume of solid He^4 at three different densities.
I. 0.194 g/cm³; II. 0.205 g/cm³; III. 0.214 g/cm³.

Unfortunately the low temperature measurements of Keesom and Keesom and of Webb *et al.* on the one hand and the higher temperature measurements of Dugdale and Simon on the other do not sufficiently overlap in density and temperature range to allow a very close comparison and more measurements would be valuable, particularly at high densities in the liquid helium temperature range.

2.2. The equation of state of the solid

Dugdale and Simon found that their results could be adequately represented by a Grüneisen equation of state. That is, the specific

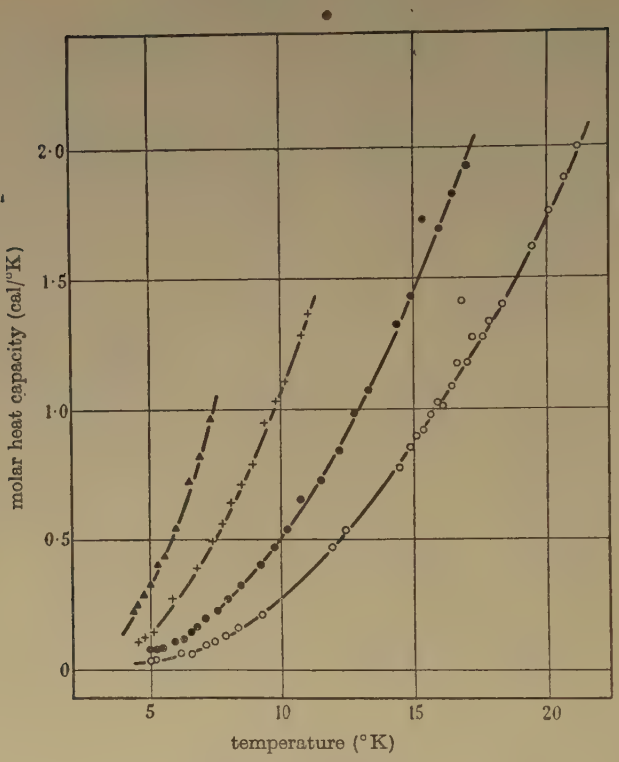

Fig. 3. The heat capacity of solid He^4 at four molar volumes. o, 10.6 cm³; ●, 11.7 cm³; +, 13.0 cm³; ▲, 14.4 cm³.

heat at constant volume was found to be a function of T/φ where φ is a characteristic temperature depending only on the volume. Furthermore, for the purpose of calculating certain thermodynamic properties of the solid from the specific heats, the results of Keesom and Keesom could also, though less closely, be represented in this way. The values of φ calculated from their results are shown in table I as a function of volume.

TABLE I

Smoothed values of the parameter φ as a function of volume

V (cm³)	φ	V (cm³)	φ
10.5	113	15	48.5
11	101.5	16	41.4
12	83.2	17	35.7
13	68.7	18	31.1
14	57.4	19	27.2
		20	24.2

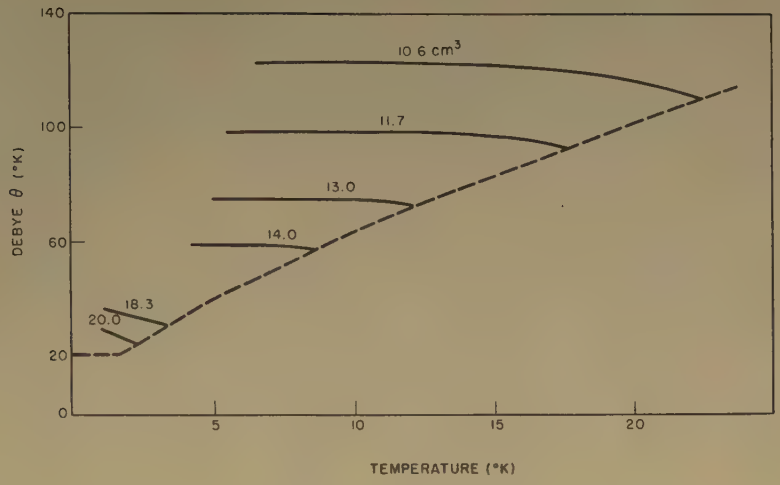

Fig. 4. The Debye θ's of solid He^4 at six molar volumes.

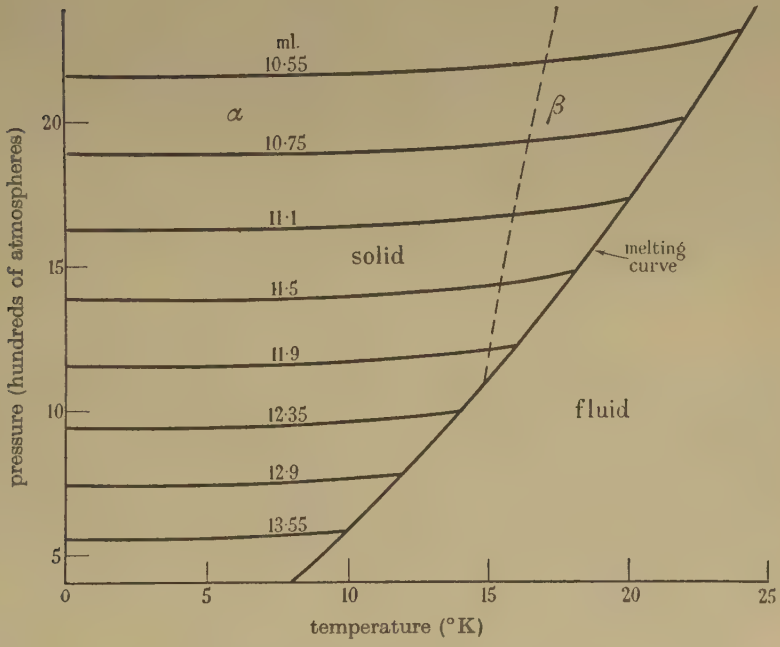

Fig. 5. The isochores of solid He^4 at eight molar volumes.
– – – – – transition line in the solid.

From the specific heats it is then possible to calculate the entropy, S, and the thermal contribution to the internal energy, $U-U_0$. Here U is the internal energy at temperature T and volume V, and U_0 the internal energy at the same volume and at absolute zero. Table II gives C_v, S and $(U-U_0)/T$ as functions of T/φ derived in this way.

TABLE II

C_v, S and $(U-U_0)/T$ as a function of T/φ. (All in cal/° C per mole)

T/φ	C_v	S	$(U-U_0)/T$
0.04	0.02	0.008	0.010
0.06	0.08	0.023	0.017
0.08	0.19	0.060	0.043
0.10	0.38	0.121	0.091
0.12	0.64	0.213	0.158
0.14	0.96	0.333	0.248
0.16	1.33	0.483	0.359
0.18	1.73	0.662	0.491
0.20	2.21	0.870	0.645

The specific heats as a function of temperature and volume do not by themselves form a thermodynamically *complete* set of data. For completeness one p, V, T relationship which traverses the same range of temperature and volume is needed and the melting curve together with the volume of the solid on melting provides this additional information (see § 4.1 below).

On this basis it is now possible to calculate the isochores of the solid by integrating the relationship

$$\left(\frac{\partial p}{\partial T}\right)_v = \frac{\gamma C_v}{V} \qquad \text{where } \gamma = \frac{\mathrm{d}\ln\varphi}{\mathrm{d}\ln V} \tag{2}$$

which is valid if C_v is a function of T/φ and φ depends only on volume. The isochores at eight densities are shown in Fig. 4 together with the equilibrium line between the two solid modifications (§ 2.3). This figure shows that the isochores are only very slightly temperature dependent: indeed, as a first approximation, it might be said that the pressure in the solid is independent of temperature and dependent only on the volume *.

* It is partly for this reason that solid helium can be a useful pressure transmitting medium at low temperatures. The pressure can be applied at such a temperature that the helium is fluid. Thereafter the system may be cooled at constant volume to the working temperature without serious loss of pressure.

From the data in Fig. 5, the compressibility, β, at 0° K can be derived and by using Eq. (2) the thermal expansion coefficient, α, can be calculated. These quantities are listed in tables III and IV. On the same basis the internal energy at 0° K can be found and hence, by subtracting from this the zero point energy, the lattice energy can be deduced [8].

TABLE III

The compressibility of solid helium at 0° K

volume (cm^3)	pressure (atm)	$10^5\ \beta$ (atm^{-1})	volume (cm^3)	pressure (atm)	$10^5\ \beta$ (atm^{-1})
10.5	2170	10	15.0	295	54
11.0	1660	12	16.0	200	76
12.0	1070	17	17.0	136	103
13.0	695	26	18.0	88	140
14.0	460	38	19.0	50	190

TABLE IV

The thermal expansion of solid helium; the volume expansion coefficient as a function of temperature

T (°K)	10.6 cm^3 $10^4\ \alpha$	12 cm^3 $10^4\ \alpha$	15 cm^3 $10^4\ \alpha$
0	0	0	0
2	–	–	1.05
4	0.09	0.48	10.2
8	0.93	4.9	–
12	3.4	14.6	–
16	7.3	–	–
20	12.6	–	–

2.3. Lattice structure and transition

Dugdale and Simon in the course of their investigation of the heat capacity of solid helium found an anomaly in the specific heats between 15 and 17° K, the actual temperature depending on the volume. They concluded from their experiments that this was a first order, reversible transition involving an entropy change of about 5×10^{-3} cals/° K per mole *. Furthermore, since substances with short-range forces of the van der Waals type are stable only in close-packed

* Since all such quantities associated with the transition are small (e.g. the volume change is estimated at 4×10^{-4} ccs/Mole) their contribution to the general thermodynamic properties of the solid has been neglected.

lattices, they also concluded that the transition was due to a change from the close-packed hexagonal structure stable at the lower temperatures [9] (i.e. the so-called α-phase) to the close-packed cubic structure stable at the higher temperatures (the β-phase).

3. The Thermal Conductivity of Solid Helium

3.1. Experimental results

3.1.1. *Introduction*

In discussing the thermal conductivity, $\varkappa$, of a dielectric it is convenient to define a mean free path, λ, by the relationship

$$\varkappa = \tfrac{1}{3} C \cdot v \cdot \lambda$$

where C is the lattice heat capacity per unit volume and v the velocity of the lattice waves. At sufficiently low temperatures, the thermal conductivity of a chemically pure and physically perfect dielectric is limited only by the dimensions of the specimen. If, for example, the specimen has the form of a long, narrow cylinder then the mean free path is under these conditions approximately equal to the diameter of the cylinder. Consequently the thermal conductivity varies directly with the heat capacity, C, which means in general that $\varkappa$ is proportional to the cube of the absolute temperature at very low temperatures.

The growth of thermal conductivity in an ideal crystal with rising temperature is ultimately arrested by so-called 'Umklapp' processes, a concept introduced by Peierls [10, 11]. In an Umklapp process, two normal modes interact to produce a resultant whose wave number lies outside the basic cell of the reciprocal lattice. This means that its wave number is opposite in direction to that of its components. According to Peierls it is just these Umklapp processes which give rise to thermal resistivity in ideal insulators, and he estimates that the rate at which they occur at low temperatures is proportional to $\exp(-\theta/bT)$; here θ is the characteristic Debye temperature of the lattice and b is a numerical factor greater than 1 [12]. It thus seems reasonable to assume that the mean free path at such temperatures should be given by

$$\lambda = A \exp(\theta/bT) \tag{3}$$

where A is a parameter which depends on the coupling of the lattice waves and may indeed include a temperature factor.

3.1.2. *The Measurements*

Measurements of the thermal conductivity of solid helium have been made by Webb, Wilkinson and Wilks [7, 13] and by Webb and Wilks [14]. The conductivity was measured at densities between 0.345 and 0.194 gms/cc in the helium temperature range; at the lowest density, the measurements were extended down to 0.3° K. This change of density altered the Debye temperature of the lattice from about 25° K to about 90° K and increased the thermal conductivity at 2° K by a factor of over 300.

Webb, Wilkinson and Wilks made the measurements at the lower densities (0.194 to 0.218 gms/cc). For most of the experiments the specimen holder was a German silver tube of internal diameter 6 mm: for the measurements below 1° K the holder had a diameter of 0.5 mm. Their results at three densities are shown in Table V.

TABLE V

The thermal conductivity of solid helium

Density	Temperature in °K							
(gms/cm³)	0.25	0.50	1.0	1.2	1.4	1.7	2.0	2.3
0.194	20 *	85 *	107 *	24 *	11	5	–	–
0.208	–	–	–	–	58	19	8	–
0.218	–	–	–	–	160	52	22	11

* These size-dependent values were obtained with specimens of 0.5 mm diameter.

At the higher densities, the measurements were made by Webb and Wilks using two experimental arrangements which were essentially modifications of the previous apparatus. Up to a density of 0.28 gms/cc the results of this work were self-consistent and consistent with the earlier measurements. These results and some from the earlier work are shown in Fig. 6.

For densities above 0.28 gms/cc however the two apparatuses gave different results. These differences were not simply attributable to specimen size effects and moreover the results from each apparatus singly were somewhat irregular. It is therefore difficult to make any deductions from these measurements.

3.1.3. *Comparison with Theory*

The experimental values of thermal conductivity and specific heat enable the mean free path of lattice waves, λ, to be calculated (the

velocity of sound may be deduced from the appropriate value of θ). The mean free paths so deduced are shown plotted as a function of θ/T at various densities up to 0.218 gms/cc in Fig. 7 [7].

Two conclusions can be drawn. In the first place, provided that size effects are absent, log λ is proportional to θ/T as the theory

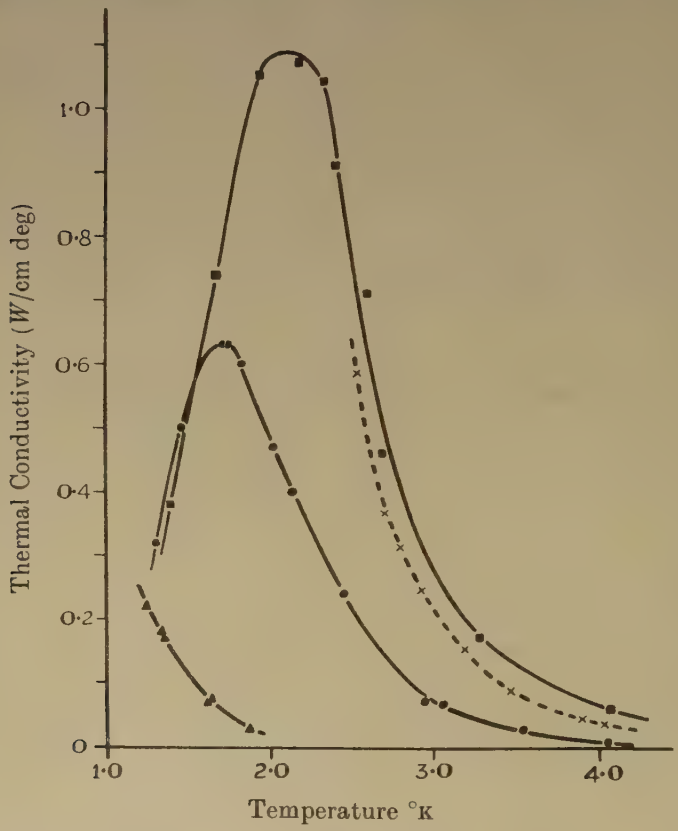

Fig. 6. The thermal conductivity of solid He^4 at four densities. ▲, 0.218 g/cm³; ●, 0.262 g/cm³; ×, 0.276 g/cm³; ■, 0.282 g/cm³.

demands. The constant b of Eq. (3) has the value 2.3 and the parameter, A, of the same equation appears to be independent of density, having the value 6×10^{-8} cms.

In the second place, size effects become evident at very low temperatures (large values of θ/T) and λ becomes almost constant, although even at the lowest temperature it is only about half of the theoretically

expected value, 5×10^{-2} cms., which is the diameter of the specimen. It should also be noted that the thermal conductivity, in the temperature range where λ is limited by size, varies as $T^{2.3}$ and not T^3 as theory predicts.

In a recent paper [55] Leibfreid and Schlömann have attempted for the first time to calculate the absolute value of the thermal conductivity of dielectric crystals. The anharmonic terms in the expansion of the lattice potential energy are taken account of by means of Gruneisen's γ. The authors find that the thermal conductivity is given by $\varkappa_0 f(\theta/T)$ where f is a universal function, and $\varkappa_0$ is proportional to $\delta\theta^2/\gamma^2$, δ being the lattice spacing of nearest neighbours in the crystal. When detailed values are substituted for solid helium reasonable agreement in absolute values is obtained over a considerable range of pressures.

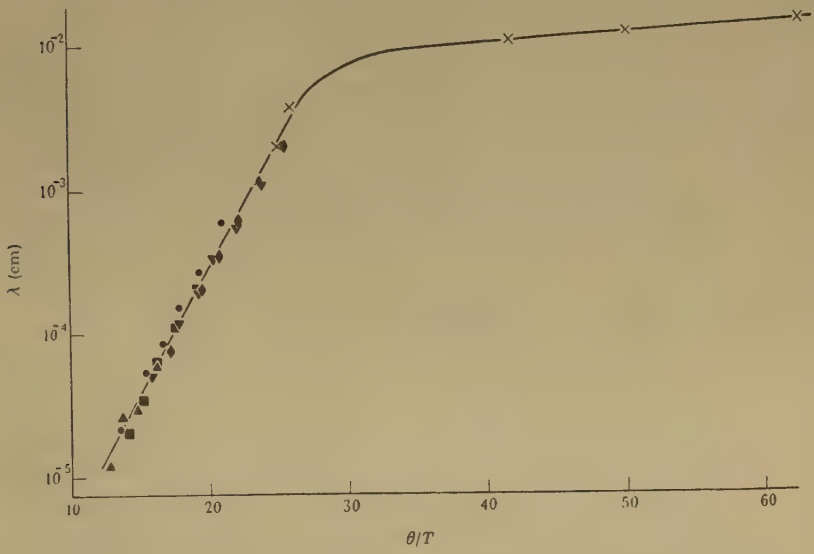

Fig. 7. The mean free path of lattice waves in solid He^4.

4. The Melting Curve and Melting Parameters of He^4

4.1. Experimental results

4.1.1. *The Melting Curve*

Because helium can remain liquid down to the lowest temperatures, the melting curve of solid helium does not join the vapour pressure

TABLE VI

Measurements of the melting curve of He^4

Author	Date	Temperature Range	Pressure Range	Estimated Accuracy	Method used
Keesom [15]	1926	1.2° to 4.2° K	25–140 ats.	0.1° K, 0.1 ats.	Blocked capillary.
Simon, Ruhemann and Edwards [3]	1929	12.2° to 20.2° K	800 to 1800 ats.	0.1° K, 1 % of pressure	Heating curve method.
Simon, Ruhemann and Edwards [4]	1929	20° to 42° K	1800 to 5500 ats.	0.1° K, 1 % of pressure	Blocked capillary.
Keesom and Keesom [16]	1933	1.15° to 1.8° K	26–30 ats.	0.01° K, 0.01 ats.	Density measurements.
Holland, Huggill, Jones and Simon [17, 18]	1950	35° K to 50° K	4000 to 7500 ats.	0.1° K ± 100 ats.	Blocked capillary
Simon and Swenson [19, 20]	1950	1.0° to 1.8° K	25.0 to 27.0 ats.	.01° K, 0.01 ats.	Blocked capillary.
Swenson [21]	1952	1.6° to 4° K	27 to 130 ats.	.01° K, 0.1 % of pressure	Piston displacement *.
Swenson [22]	1953	1.5° to 4° K	26 to 130 ats.	.01° K, 0.1 % of pressure	Blocked capillary *.
Dugdale and Simon [8]	1953	4.2° to 12° K	140 to 800 ats.	0.1° K, ± 3 ats.	Blocked capillary.
Robinson [23]	1953	20° to 55° K	9,000 ats.	± 0.5° K, ± 5 % of pressure	Moving pellet.
Mills and Grilly [24]	1955	2° to 30° K	35–3,500 ats.	.01° K, .05 % of pressure	Blocked capillary.

* Swenson [22] has discussed in detail the relative merits of the blocked capillary and piston displacement methods of measuring melting curves.

curve at a triple point. Instead the melting pressure at very low temperatures tends to become constant, its slope vanishing in accordance with the third law of thermodynamics.

There have been many measurements made on the melting curve of He^4 and these are summarized in Table VI, which shows the range of measurements in temperature and pressure, the method used and the estimated accuracy achieved.

According to Swenson [20], the melting pressure between 1.0 and 1.4° K can be represented by $P = 25.00 + 0.053\,T^8$ ats; and between 2.1 and 4° K by $P + 5.6 = 13.458\,T^{1.66074}$ ats [21]. Values of P up to 6° K are given in Table VII. All workers agree that their results above 4° K can be represented by a Simon-type expression as given in Eq. (1). The Oxford workers have found that the melting curve can be expressed in the form

$$\frac{P}{16.45} = \left(\frac{T}{.992}\right)^{1.5544} - 1 \tag{4}$$

where P is measured in atmospheres, and T in degrees Kelvin. Mills and Grilly gave their results as

$$P + 17.80 = 17.315\,T^{1.5554} \tag{5}$$

with P in Kg/cm^2, which may be re-written in the same form and units as Eq. (4)

$$\frac{P}{17.23} = \left(\frac{T}{1.0179}\right)^{1.5554} - 1 \tag{6}$$

4.1.2. *The Melting Parameters*

Swenson [22] has made very accurate measurements of the melting parameters of He^4 between 1 and 4° K. A free piston gauge was used to measure the melting pressure, and the volume change on melting was measured by the displacement of the piston. Dugdale and Simon, using the apparatus already described for measuring specific heats under pressure, measured also the melting parameters of solid helium at higher temperatures. The combined results of these experiments and those of Swenson are given in Table VII, and shown in Fig. 8 and 9.

The melting parameters, ΔS, ΔU and ΔV at very low temperatures are of particular interest [19]. The application of the Clausius–Clapeyron Equation to the melting curve enables us to determine $\Delta S/\Delta V$, and according to the measurements of Simon and Swenson [19] previously

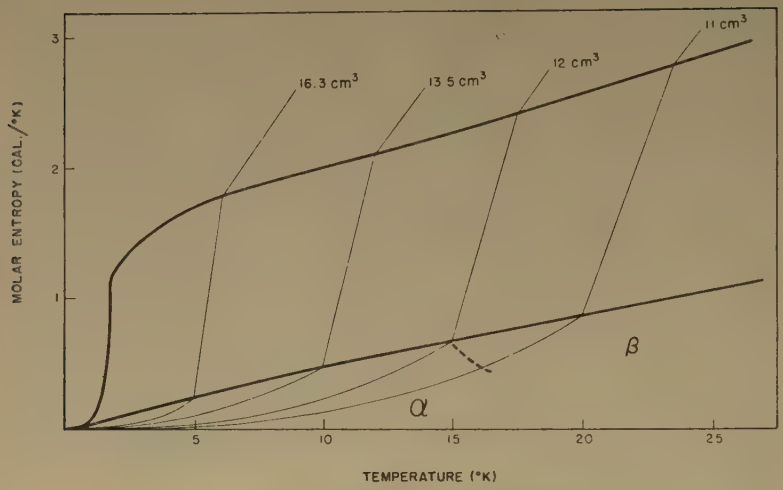

Fig. 8. The entropy of He^4 on melting and solidification. The fine lines are lines of constant volume; – – – – – transition line in the solid.

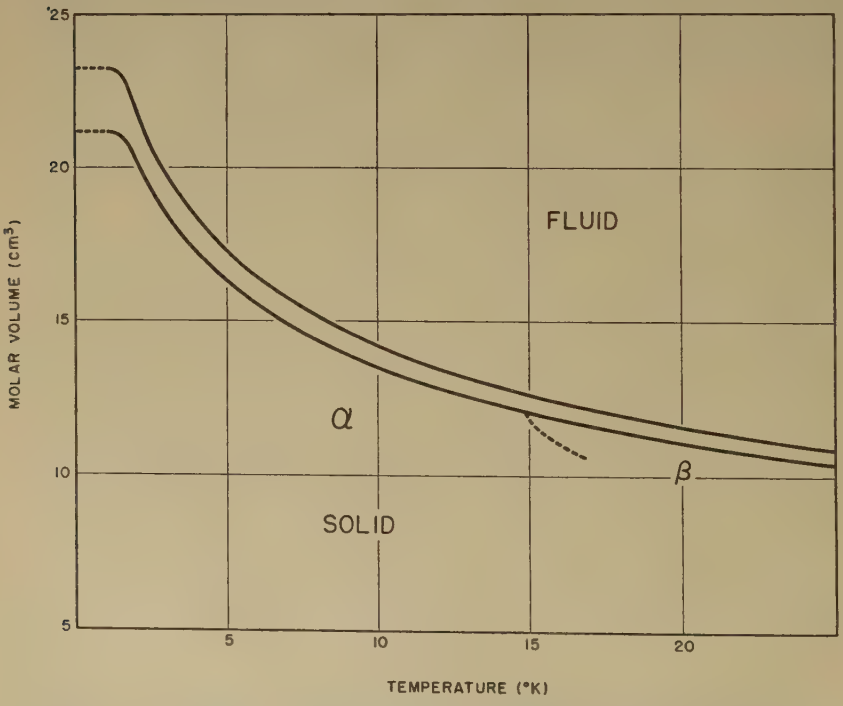

Fig. 9. The molar volume of He^4 on melting and solidification. – – – – – transition line in the solid.

TABLE VII

The entropy and molar volume of He^4 along the melting line. Entropies (S) in cals/°K per mole, volumes (V) in cm^3/mole. (The volumes above 4° K are specified more accurately than is warranted by the experiments in order to give V correctly)

T °K	P (ats.)	S_{Solid}*	S_{Fluid}	V_{Solid}	V_{Fluid}*
0	25.00	0	0	21.18	23.25
1.0	25.05	0.03	0.05_1	21.17	23.24
1.2	25.22	0.04	0.11_5	21.15	23.22
1.4	25.81	0.05	0.26	21.05	23.11
1.6	26.99	0.06	0.50	20.95	22.84
2.0	37.08	0.07	1.24	20.26	21.66
2.5	56.3	0.10	1.37	19.32	20.60
3.0	78.1	0.13	1.47	18.52	19.72
4.0	128.6	0.18	1.59	17.37	18.40
6.0	255	0.29	1.79	15.53	16.42
10.0		0.48	2.00	13.45	14.13
14.0		0.63	2.21	12.30	12.88
18.0		0.78	2.42	11.42	11.95
22.0		0.94	2.66	10.75	11.24
26.0		1.08	2.88	10.10	10.57

* Below 4° K S_{Solid} and V_{Fluid} are from the measurements of Keesom and Keesom [1, 16].

referred to, this is of order T^7 for small T. From the third law of thermodynamics, ΔS, the entropy difference between the solid and liquid phase, must vanish as the temperature approaches the absolute zero; in fact these experimental results on solid helium provide a striking confirmation of the third law. (The latent heat of melting ($\varrho = T\Delta S$) must vanish even more rapidly.) Since $T\Delta S = \Delta U + p\Delta V$, two possibilities exist, remembering that p does not vanish. Either ΔU and ΔV must both tend to zero with ΔS so that the two phases become identical, or else $\Delta U = -p\Delta V$ in the limit as $T\Delta S$ vanishes. It is the second alternative which is found experimentally (see Fig. 10) implying that the phase with the larger volume has the smaller energy. Since liquid helium has always a greater volume than the solid, the liquid ultimately has the lower energy and so becomes the only known example of a liquid having an internal energy lower than that of the solid with which it is in equilibrium.

The high-temperature trends of the melting parameters are of interest also, because they may give an answer to the general problem

of whether or not a solid-fluid critical point exists. It is seen that although the volume difference between the phases decreases with rising temperature, the entropy difference continues slowly to *increase* and one must conclude that there is certainly no evidence here for the existence of such a critical point.

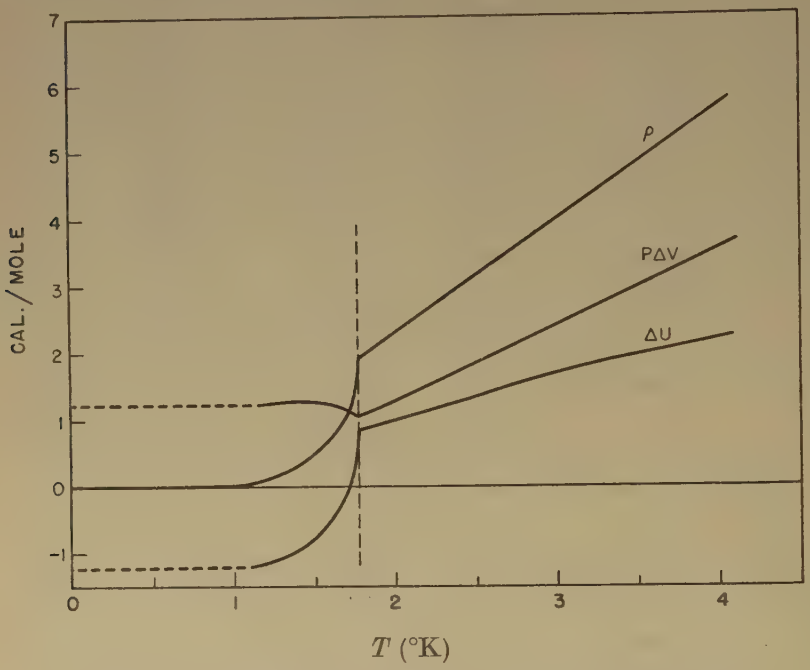

Fig. 10. The melting parameters of solid He^4 below 4° K.
ϱ is the latent heat of melting.
P is the pressure.
ΔV is the change of volume on melting.
ΔU is the internal energy change.

Another feature to which Simon has drawn attention is the increase in entropy of solid helium along the melting line, a behaviour which characterizes all other substances for which this entropy trend can be estimated. If it is true of *all* solids at sufficiently high pressures that the entropy at the melting point increases with temperature then it is impossible to melt a substance by adiabatic reversible compression, a fact that may be of significance in geophysics and atrophysics.

4.1.3. *The Lindemann Melting Formula Applied to* He^4

According to the Lindemann melting formula,

$$\theta = c\sqrt{\frac{T_m}{MV^{2/3}}}$$

where θ is the characteristic temperature of the lattice at volume V and T_m is the melting temperature; M is the molecular weight of the substance and c is a constant. The measurements on solid He^4 provide, for the first time, the data necessary to test this formula over a substantial region of the melting curve of *one single* substance.

Table VIII gives the values of c calculated for He^4 at several different temperatures and it is seen that they are indeed very nearly constant. The value of c for He^4 is however considerably smaller than for the heavier inert gases for which c is approximately 160. Some further comments on the Lindemann melting formula are made in § 6.4 below.

TABLE VIII

Application of the Lindemann Melting Formula to He^4

θ_D (°K)	T_m (°K)	V (cm³)	c
110	23.3	10.6	101
92	17.3	11.6	100
72	11.3	13.1	102
55	7.9	14.4	95
32	3.1	18.3	96

5. The Melting Parameters and General Properties of Solid He^3

As yet there is no detailed knowledge of the thermodynamic properties of solid He^3. Its melting curve, however, has been measured from 0.2 to 35° K. Abraham, Osborne and Weinstock have measured the curve in the low temperature region [25, 26] and Mills and Grilly at high temperatures [27, 28]. Both used the blocked-capillary technique. The data can be represented by the following equations

$$P = 26.8 + 13.1\,T^2 \text{ atm. between } 0.5 \text{ and } 1.5° \text{ K}$$

and

$$P - 25.16 = 20.082\,T^{1.5171} \text{ kg/cm}^2 \text{ between } 2 \text{ and } 35° \text{ K}.$$

The second of these expressions may be compared with Eq. (5) above which represents the melting curve of He^4 over similar temperature and pressure range (see also §§ 6.2 and 6.5 below).

The low temperature end of the melting curve is again, as with He^4, of particular interest but for a different reason. The He^3 nucleus, unlike that of He^4, has a nuclear spin and magnetic susceptibility experiments have shown that in the liquid state the nuclear spins are already partially aligned at 0.4° K [29, 30, 31]. Pomeranchuk [32] pointed out that if the nuclear spins were aligned in the liquid but remained randomly oriented in the solid until dipole-dipole interaction produced alignment then below a certain temperature the liquid would have a lower entropy than the solid. Consequently assuming no dramatic change in the volume relationship, the slope of the melting curve would vanish at this temperature and become negative below it *. Before finally vanishing it might even become positive again when the nuclear spins became aligned in the solid. Pomeranchuk suggested that this alignment should occur at about 10^{-7} °K, but Primakoff [52] has pointed out that the special properties of solid helium would make this temperature in the neighbourhood of 10^{-3} °K.

Experimental evidence on whether the melting curve does in fact change sign is still lacking. Indeed it has been pointed out that the blocked capillary technique could not record such a change since it will always block at the minimum pressure [33]. If, however, the melting curve does indeed have a minimum we shall then have the surprising instance of a liquid which freezes as it is heated at constant pressure!

II. THEORETICAL ASPECTS

6.1. Introduction

The behaviour of solid helium is dominated by the effect of zero point energy [53]. In detailed character zero point energy consists of random fluctuations of the atoms about their equilibrium positions in the lattice, and these fluctuations are responsible for the fact that helium is a liquid at the absolute zero. As another consequence of the zero point energy the volume of the solid which forms when liquid helium is subjected to a pressure of 25 atmospheres is well over twice the volume corresponding to the minimum of the potential energy

* If this assumption is correct, one may estimate from the entropy diagram [31] of He^3 that the pressure rise on the low temperature side of the minimum should be about 4 atmospheres, assuming that the volume difference between the phases is comparable with that found in He^4.

of the lattice. Thus even in the solid at absolute zero the atoms execute vibrations of relatively large amplitude about their equilibrium positions, and the normal approximation of lattice dynamics which expands the potential up to terms of the second order about static equilibrium ceases to be valid. The first theoretical problem posed by solid helium is therefore to find a modified treatment which can be applied to a system with large zero point vibrations.

As mentioned in the experimental section the high compressibility of solid helium has enabled measurement of melting properties and thermodynamic functions to be made over a range corresponding to a factor of two in volume. This is a far greater range than can be achieved with any other substance, and the data can be used to cast some light on the general properties of substances under pressure. Because of the zero point effects helium cannot be regarded as a perfect model substance. Nevertheless, for some purposes it may be possible to take these effects into account and draw general conclusions; and in other cases an analysis of the differences between the behaviour of classical substances and helium can be illuminating. In particular the data on the melting of solid helium over such a wide range of volumes provide considerable insight into the general properties of the melting curve at high pressures.

The polymorphic transition discovered by Dugdale and Simon has also stimulated theoretical work on the cubic and hexagonal packed lattices and their relative stability at different volumes and temperatures.

Many of the theoretical developments to be described in the following sections cannot be regarded as complete, but do seem to indicate the possibility of accounting adequately for the experimentally observed properties of solid helium.

6.2. The static lattice at absolute zero

If a negative pressure could be applied to a solid at absolute zero so that its volume expanded, the solid would cease to be elastically stable at a volume for which $\partial p/\partial v$ becomes zero. For solids consisting of the heavier inert gases, where the effect of zero point energy is small, this volume corresponds to about 1.4 times the normal equilibrium volume. Now zero point energy has the same effect as a negative pressure, and expands the solid at absolute zero to a larger equilibrium volume; for helium this volume is more than twice the volume corresponding to the minimum of the potential energy of the lattice,

and yet the solid is perfectly stable elastically. This is because zero point energy does not correspond to a static negative pressure but to a dynamic negative pressure arising from the motions of the atoms, and its value is volume dependent, decreasing with increasing volume of the solid.

This point can be more clearly illustrated if a theoretical attempt is made to calculate Debye θ values for solid helium from the data on intermolecular forces. The detailed calculation of the frequency spectrum of normal vibrations of a crystal lattice is a problem of some complexity which has engaged the attention of many authors. However from these calculations we may draw the general conclusion that deviations from the Debye theory do not usually amount to more than a few per cent, and if we confine our attention to the high temperature expansion of the specific heat, we can readily and simply obtain a formula for θ [34]. Thus if $\varphi(r)$ is the static lattice energy per particle, the limiting value of θ at high temperatures is given by

$$\theta_\infty = 0.4109 \frac{h}{k} \sqrt{\frac{\varphi''(r)}{m}} \qquad (7)$$

where m is the mass of an atom of the crystal. When the solid is subjected to pressure we assume that vibrations take place about the new equilibrium position with a changed force constant, and this is accounted for by the term $\varphi''(r)$. Eq. (7) thus represents the variation of θ with volume.

When we substitute the values of the lattice energy corresponding to helium in Eq. (7) the lowest curve in Fig. 11 results, and this is clearly in serious disagreement with the experimental values represented by the upper curve. The calculated θ-values become zero at a molar volume of 14.9 cm^3 whereas finite experimental values are observed right up to the melting volume of 21.18 cm^3.

This discrepancy provides a confirmation of Born's contention [35, 36] that classical lattice dynamics, based on vibrations about a position of static equilibrium, has only a restricted region of validity. Born has indicated that one should rather consider vibrations about dynamic (or more generally thermodynamic) equilibrium, and has suggested this as a basis for a modified lattice dynamics which has subsequently been developed by Hooton [37, 38, 39]. We can take account of Born's suggestion in an approximate manner by replacing the lattice energy

in Eq. (7) by the free energy, which at absolute zero reduces to $\varphi(r)+\frac{9}{8}k\theta_\infty$. We thus obtain for θ_∞ the equation

$$\theta_\infty = 0.4109\sqrt{\frac{\varphi''(r)}{m}+\frac{9}{8}\frac{k}{m}\frac{\mathrm{d}^2\theta_\infty}{\mathrm{d}r^2}}. \tag{8}$$

This is a non-linear differential equation whose detailed properties are quite complex. But to test whether the correction is in the right direction we have substituted the experimental value of

$$\gamma\,(=-V\frac{\partial}{\partial V}\ln\theta_\infty)$$

into the right hand side of (8). The result is again shown in Fig. 11 (upper dotted curve) and it will be seen that the calculated values are now much closer to the experimental values.

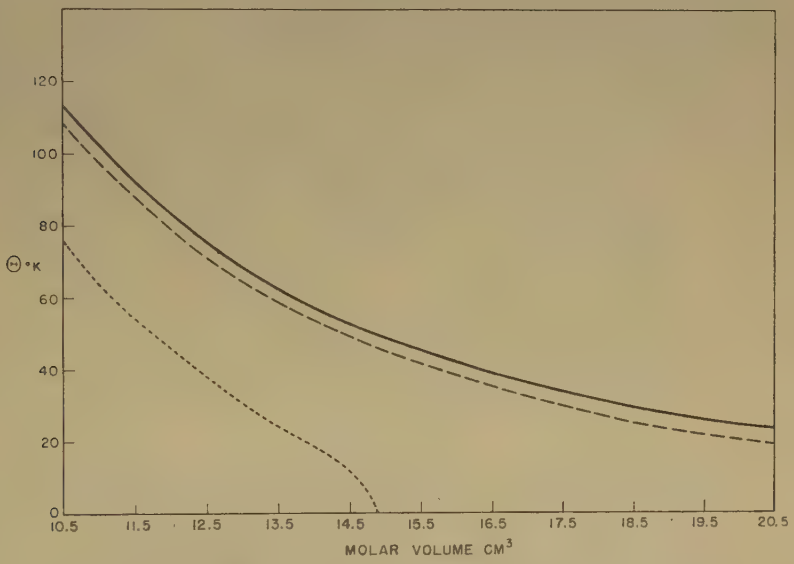

Fig. 11. The Debye θ as a function of volume in solid He^4.
——— experimental values.

We now discuss briefly some of the properties of the differential Eq. (8). As it is a second order equation we might at first expect two arbitrary constants to appear; in fact however we are looking for a singular solution, and this is determined by the physical property that for sufficiently small volumes the effect of zero point energy is

negligible. This property of the physical solution makes a numerical approach at integration rather difficult.

The equation may alternatively be regarded as determining the internal energy, E_0, at absolute zero, as a function of volume, and following Dugdale and MacDonald [40] we can write it in the form

$$E_0 = \varphi(r) + a\left(\frac{\mathrm{d}^2 E_0}{\mathrm{d}r^2}\right)^{1/2} \tag{9}$$

where a is a constant. Dugdale and MacDonald consider the particular case when $\varphi(r)$ is a Mie–Lennard Jones function

$$\varphi(r) = \frac{A}{r^{10}} - \frac{B}{r^6}.$$

They are then able to derive a solution in the form of a series expansion in powers of r. However, the series is only of use for small a, corresponding to small zero point effects, and cannot be applied to helium. They alternatively suggest an approximate solution in closed form which agrees with the initial terms of the series expansion, and can be applied over a much wider range. An important feature of this solution is the disappearance of the minimum in E_0 at a particular value of a (Fig. 12). This seems to correspond to an interesting dif-

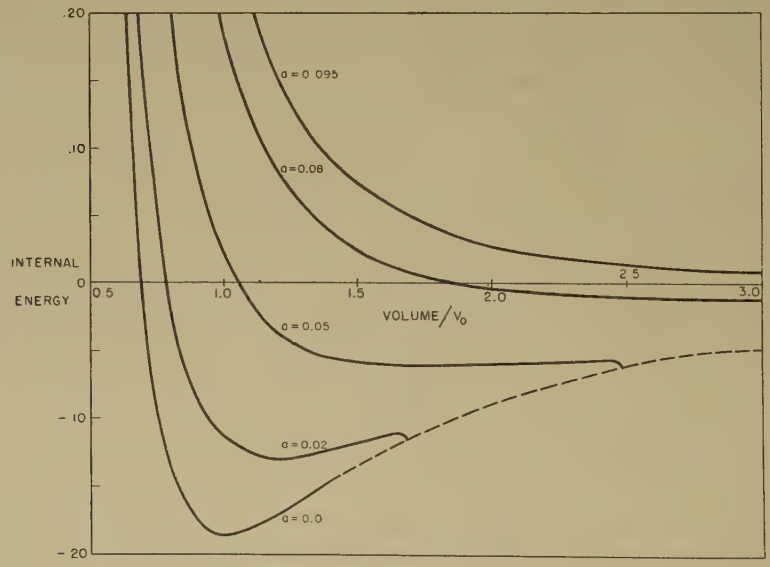

Fig. 12. The internal energy as a function of volume for various values of the parameter a.

ference between the solid phases of He^4 and He^3: the internal pressure of the former as determined from the Simon melting equation (see §§ 4 and 5) is positive as for all normal substances whereas the internal pressure of the latter is negative.

As mentioned above a more fundamental approach to a modified lattice dynamics when anharmonic effects are large was initiated by Born and developed by Hooton. The nature of Born's approach can be illustrated by the following simple example. In the problem of the vibrations of a simple diatomic molecule one has to solve the Schrödinger Equation for a potential well of shape Fig. 13(a). For small vibrations (energy level as shown) only the bottom of the well is relevant, and a harmonic approximation is reasonable. If however the well is of a different shape Fig. 13(b), such as is experienced by an atom in the interior of a crystal with a large atomic spacing, the harmonic approximation breaks down completely. Nevertheless a pseudo-harmonic approximation is still possible, using a harmonic oscillator wave function and fitting the frequency parameter by the variation principle.

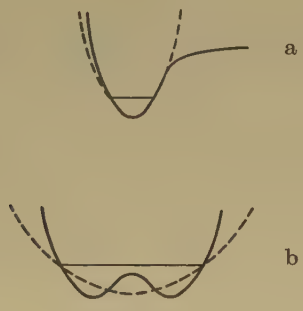

Fig. 13

Hooton develops a lattice dynamics in this manner, the equilibrium positions of atoms, normal frequencies, and normal co-ordinates being parameters which are fitted so as to give a minimum value to the thermodynamic free energy. These parameters are then dependent on temperature as well as volume, although the temperature dependence is small and can be neglected to a first approximation. In principle the method is capable of determining the complete vibration spectrum (including its volume and temperature dependence) of a lattice with large anharmonic vibrations; in practice, however, the equations become extremely complicated. By using an approx-

imation of Debye type Hooton is led to an equation similar to (8), although he suggests that the use of Debye functions in standard manner is no longer appropriate.

A simple and direct approach, which is nevertheless capable of providing useful information, is to consider how the shape of the potential well in which each atom finds itself changes as the volume of the solid is varied. This method was used by Henkel [41] to account for the temperature dependence of the elastic constants of solids, and is really a development of the Einstein approximation. Although it would not be expected to account correctly for the thermal behaviour at low temperatures, it should provide a reasonable approximation to the volume dependence of the lowest energy state. Thus as the volume increases, the shape of the potential curve becomes rather similar to a three-dimensional square well, and this can be used as a first approximation. This approach is being further investigated by I. J. Zucker at King's College, London.

6.3. The transition in solid helium

As mentioned in § 2.3 Dugdale and Simon discovered a polymorphic transition in solid helium which they conjectured to be a transition from hexagonal close packed to cubic close packed structure. It is of interest to consider the relative stability of these two structures when the interatomic forces are central forces of van der Waals type.

For the static lattices at absolute zero calculations have been made independently by several authors [42, 43, 44]. The general conclusion is that for all reasonable forms of potential the hexagonal structure is more stable, the difference in energy, however, being only about 0.01 %. Under very high pressures, corresponding to a reduction of a factor of 2 in volume, the cubic structure becomes the more stable.

Barron and Domb [44] then considered the properties of the two lattices at elevated temperatures. The equivalent Debye θ at the absolute zero is smaller for the cubic lattice, the difference being about 1 %. Hence, ignoring zero point energy, we should expect a transition to occur from hexagonal to cubic at an elevated temperature. The estimated temperature and energy of the transition are of the same order of magnitude as those observed experimentally in solid helium. However the calculations can only be regarded as indicating the possibility of an explanation, since lattice dynamics based on a

harmonic approximation is not adequate to deal with the large anharmonic vibrations occurring in solid helium.

6.4. Zero point energy and melting

The experimental values of θ determined by Dugdale and Simon [8] enable us to estimate vibration amplitudes and various related properties for a considerable length of the melting curve. Assuming a Debye model the mean square vibration amplitude is given by

$$\left.\begin{aligned} \overline{u^2} &= \frac{9h^2}{4\pi^2 m}\frac{T}{k\theta^2} \qquad T \gg \theta \\ \overline{u^2} &= \frac{9h^2}{16\pi^2 mk\theta}\left[1+\frac{2\pi^2T^2}{3\theta^2}-4\left(\frac{T}{\theta}+\frac{T^2}{\theta^2}\right)e^{-\theta/T}+\ldots\right] \qquad T \ll \theta. \end{aligned}\right\} \tag{10}$$

The results are shown in Table IX. The 4th column, T_m/θ, represents the degree of degeneracy at the melting point, and it will be observed that melting becomes steadily less degenerate as the melting tem-

TABLE IX

Molar Volume in cm³	Melting Temp. °K	θ °K	T_m/θ	Zero point energy Cals/Mole	Thermal energy Cals/Mole	Ratio $\sigma=\sqrt{\overline{u^2}}/a$	Ratio σ'
*21.18	0	21	.0	46.9	0	.310	0
20.0	2.12	24	.088	53.6	0.17	.303	.067
18.0	3.40	31.5	.108	70.4	0.49	.277	.074
16.0	5.35	42.5	.126	95.0	1.19	.251	.077
14.0	8.65	57.0	.152	127.0	3.18	.228	.083
12.5	13.10	76.3	.172	170.0	6.43	.212	.086
11.5	17.65	92.5	.191	207.0	11.2	.201	.088
10.5	23.55	114	.207	255.0	17.8	.190	.089

* This value corresponds to the liquid phase He II, the remaining values correspond to He I.

perature rises. In the 5th and 6th columns we have tabulated the zero point energy and thermal energy, and a comparison of their magnitudes illustrates strikingly a fact first pointed out by Simon [54]. The zero point energy is much larger than the thermal energy, and if we consider, for example, the heating of helium at a constant molar volume of 14.0 cm³ from the absolute zero, we find that 127 calories of zero point energy are incapable of melting the solid, whereas an additional 3.18 calories of thermal energy are sufficient to induce melting.

In the 7th column we have tabulated the ratio σ of the r.m.s. vibration amplitude of the atoms, $\sqrt{\overline{u^2}}$, to the distance between nearest neighbours in the lattice. According to the Lindemann melting formula, which is well satisfied experimentally by classical substances, this ratio should nearly always be in the neighbourhood of 1/10. However, it will be seen that for solid helium this ratio varies continuously along the melting curve from three times to twice the classical value. If we consider the vibrational energy, the difference from classical behaviour is still more striking. The molar volume in the last line of Table IX corresponds to a nearest neighbour spacing about equal to the distance of the minimum in the potential energy curve. By analogy with the heavy inert gases we can estimate that if the melting of helium were purely classical, about 25 calories of thermal energy would then be necessary to produce melting at this volume; in fact the actual vibrational energy at the melting point is more than ten times this quantity.

In the final column we have tabulated the corresponding ratio σ', taking account only of thermal vibrational energy. It will be seen that the values rapidly increase at first and steadily approach the classical value of 1/10.

The experimental data thus demonstrate clearly that zero point energy is much less effective than thermal energy at producing melting. The two types of energy differ from one another only in spectral distribution, the former being proportional to ν^3 (on the Debye model) and the latter to $\nu^3/(e^{h\nu/kT}-1)$. However small T is, the denominator in the thermal energy term becomes equal to $h\nu/kT$ for sufficiently small ν, and hence the thermal energy is proportional to ν^2 for small ν. On general physical grounds we might expect that it is long waves which are responsible for melting; for example it is known that sufficiently short transverse waves can be propagated in liquids, and it is long waves which destroy long range order in two dimensional lattices [11]. The ineffectiveness of zero point energy seems thus to be due to the fact that it is concentrated in the short wave region of the spectrum, whereas thermal energy has a larger proportion concentrated in the long wave region.

These results also demonstrate that it is not vibrational amplitude which should be correlated with melting, and hence that the derivation of the Lindemann melting formula by means of vibration amplitudes cannot be regarded as satisfactory even empirically. An alternative

approach is needed to account for the wide range of agreement of this formula with experiment.

6.5. The Simon melting equation

Perhaps the most important aspect of the experimental work on solid helium is the light which it throws on the general properties of the melting curve, and its confirmation of the Simon melting formula (1) over an extensive range. Although we are still far from an adequate theory of melting, even crude approximations have begun to provide evidence of theoretical justification for the formula. Thus Domb [45] and de Boer [46], using the theory of Lennard Jones and Devonshire, were able to derive a formula of type (1), the constant c being related to the repulsive power in the intermolecular potential energy. By making the assumptions of the Grüneisen theory of solids, Salter [47] was able to show that the Simon formula was equivalent to the Lindemann melting formula, the constant c being related to Grüneisen's constant. Finally I. Z. Fisher [48, 49, 50] in considering the limits of stability of the solid phase has obtained a theoretical derivation of the formula (1).

There is still a good deal of controversy regarding the possibility of a solid-fluid critical point, but there seem to be strong theoretical reasons for rejecting the idea [45]. It is therefore interesting to note that the experimental results also show no evidence of an approach to a critical point.

The recent extensive experimental work on solid He^3 by Mills and Grilly [28] is also of considerable theoretical interest. We have seen that for He^4 the degeneracy decreases steadily along the melting curve. At a sufficiently high temperature along the melting curve we might therefore expect the behaviour to become classical, so that the isotopic masses would have no relevance and the melting curves of He^4 and He^3 would become identical. It is perhaps significant in this connection that although the melting curves of He^4 and He^3 run almost parallel for a large range, the formulae of Mills and Grilly indicate that they approach one another at higher temperatures. The Simon melting formulae to which Mills and Grilly fitted their experimental results would intersect at a much higher temperature.

We have seen that as a result of quantum effects helium cannot be regarded as a model substance in the completely rigorous sense. Nevertheless it may fairly be claimed that these quantum effects

do not mask the general conclusions which can be drawn, and that the experiments on solid helium have provided great insight into the properties of matter at high pressures and densities.

The authors are very grateful to Sir Francis Simon for his interest and for helpful correspondence. They also wish to express their thanks to Dr. T. H. K. Barron and Dr. D. K. C. MacDonald for reading the manuscript.

REFERENCES

1 W. H. Keesom and A. P. Keesom, Physica, **3**, 105 (1936); Comm. Leiden 240b.
2 F. Simon and F. Steckel, Z. Phys. Chem., Bodenstein-Festband, 737 (1931).
3 F. Simon, M. Ruhemann and W. A. M. Edwards, Z. Phys. Chem. B, **2**, 340 (1929).
4 F. Simon, M. Ruhemann and W. A. M. Edwards, Z. Phys. Chem. B, **6**, 62 (1929).
5 F. Simon, Trans. Farad. Soc., **33**, 65 (1937).
6 F. Simon and G. Glatzel, Z. anorg. Chem., **178**, 309 (1929).
7 F. J. Webb, K. R. Wilkinson and J. Wilks, Proc. Roy. Soc. A, **214**, 546 (1952).
8 J. S. Dugdale and F. E. Simon, Proc. Roy. Soc. A, **218**, 291 (1953).
9 W. H. Keesom and K. W. Taconis, Physica, **5**, 161 (1938); Comm. Leiden 250e.
10 R. E. Peierls, Ann. Phys. Lpz., **3**, 1055 (1929).
11 R. E. Peierls, Ann. Inst. Poincare, **5**, 177 (1935).
12 R. E. Peierls, Quantum Theory of Solids, p. 43 (1955).
13 K. R. Wilkinson and J. Wilks, Proc. Phys. Soc. **64A**, 89 (1951).
14 F. J. Webb and J. Wilks, Phil. Mag., **44**, 663 (1953).
15 W. H. Keesom, Comm. Leiden 184b (1926).
16 W. H. Keesom and A. P. Keesom, Proc. Roy. Acad. Amsterdam, **36**, 612 (1933); Comm. Leiden 224.
17 F. A. Holland, J. A. W. Huggill, G. O. Jones and F. E. Simon, Nature, **165**, 147 (1950).
18 F. A. Holland, J. A. W. Huggill and G. O. Jones, Proc. Roy. Soc. A, **207**, 268 (1951).
19 F. E. Simon and C. A. Swenson, Nature, **165**, 829 (1950).
20 C. A. Swenson, Phys. Rev., **79**, 626 (1950).
21 C. A. Swenson, Phys. Rev., **86**, 870 (1952).
22 C. A. Swenson, Phys. Rev., **89**, 538 (1953).
23 D. W. Robinson, Thesis, University of Oxford (1952).
24 R. L. Mills and E. R. Grilly, Phys. Rev., **99**, 480 (1955).
25 D. W. Osborne, B. M. Abraham and B. Weinstock, Phys. Rev., **82**, 263 (1951).
26 B. M. Abraham, B. Weinstock and D. W. Osborne, Proc. Internat. Conf. on Low Temp. Phys., p. 29, Oxford (1951).

[27] R. L. Mills and E. R. Grilly, Proc. Internat. Conf. on Low Temp. Phys., p. 350, Paris (1955).
[28] R. L. Mills and E. R. Grilly, Phys. Rev., **99**, 480 (1955).
[29] W. M. Fairbank, W. Gordy and S. R. Williams, Phys. Rev., **92**, 208 (1953).
[30] W. M. Fairbank, W. B. Ard and G. K. Walters, Phys. Rev., **95**, 566 (1954).
[31] B. M. Abraham, D. W. Osborne and B. Weinstock, Phys. Rev., **98**, 551 (1955).
[32] I. Pomeranchuk, J. Exp. and Theor. U.S.S.R., **19**, 42 (1950).
[33] T. R. Roberts and S. G. Sydoriak, Phys. Rev., **93**, 1418 (1954).
[34] C. Domb and L. S. Salter, Phil. Mag., **43**, 1083 (1952).
[35] M. Born, Changements de Phases, p. 334, Paris (1952).
[36] C. Domb, Changements de Phases, p. 338.
[37] D. J. Hooton, Phil. Mag., **46**, 422 (1955).
[38] D. J. Hooton, Phil. Mag., **46**, 433 (1955).
[39] D. J. Hooton, Phil. Mag., **46**, 485 (1955).
[40] J. S. Dugdale and D. K. C. MacDonald, Phil. Mag., **45**, 811 (1954).
[41] J. H. Henkel, J. Chem. Phys., **23**, 681 (1955).
[42] T. Kihara and S. Koba, J. Phys. Soc. Japan, **7**, 348 (1952).
[43] J. A. Prins, J. M. Dumaré and L. T. Tjoan, Physica, **18**, 307 (1952).
[44] T. H. K. Barron and C. Domb, Proc. Roy, Soc., **227**, 447 (1955).
[45] C. Domb, Phil. Mag., **42**, 1316 (1951).
[46] J. de Boer, Proc. Roy. Soc. A, **215**, 4 (1952).
[47] L. Salter, Phil. Mag., **45**, 369 (1954).
[48] I. Z. Fisher, Soviet Physics, **1**, 154 (1954).
[49] I. Z. Fisher, Soviet Physics, **1**, 273 (1955).
[50] I. Z. Fisher, Soviet Physics, **1**, 280 (1955).
[51] F. E. Simon, Proc. American Acad. of Arts and Sciences, **82**, 319 (1953).
[52] H. Primakoff, Private Communication.
[53] F. E. Simon, Nature, **133**, 529 (1934).
[54] F. E. Simon, Changements de Phase, p. 329.
[55] G. Leibfried and E. Schlömann, Göttingen Nachrichten, p. 41 (1954).

CHAPTER XII

SOME PHYSICAL PROPERTIES OF THE RARE EARTH METALS

BY

F. H. SPEDDING, S. LEGVOLD,

A. H. DAANE AND L. D. JENNINGS

CONTENTS: 1. Introduction, 368. — 2. Lanthanum, 373. — 3. Cerium, 375. — 4. Praseodymium, 378. — 5. Neodymium, 378. — 6. Samarium, 380. — 7. Europium, 380. — 8. Gadolinium, 382. — 9. Terbium, 382. — 10. Dysprosium, 383. — 11. Holmium, 385. — 12. Erbium, 387. — 13. Thulium, 389. — 14. Ytterbium, 391. — 15. Lutetium, 391. — 16. Summary, 391.

1. Introduction

The rare earth elements offer one of the most attractive series of metals for studying the relationships between electronic structure and the physical and chemical properties of metals. As a corollary, these metals make an excellent series to relate one physical property to another. The elements in this group generally have three electrons in the valence shell or the conduction band of the metal and as the atomic number increases, electrons appear in the inner, incomplete 4f shell. Most of the physical properties of these metals, to a first approximation, are determined by the interaction of the outer electrons of the metal atom with those of neighboring atoms, although some properties such as magnetism are primarily determined by the inner electrons in the incomplete shell.

The elements scandium, yttrium, lanthanum and actinium are not true rare earths but they have the same external electronic structures as the rare earths. Yttrium and lanthanum are always found in nature associated with the rare earths, and their chemical properties are so similar to the rare earths that it is extremely difficult to separate these elements from the members of the rare earth series. The elements cerium, praseodymium, samarium, europium, terbium and ytterbium have 4f and conduction electron energy bands so close to each other that a 4f electron may move to the conduction band or vice versa. As illustrations, we may cite the cases of europium and ytterbium

which have two conduction electrons, and the case of cerium which can exist as a metal with either three or four conduction electrons.

Due to the great difficulty of separating the rare earths in the pure form, these elements were not generally available prior to 1944, and much of the work reported in the literature was carried out using impure samples. Our experience has shown that many of the properties are sensitive to small amounts of impurities and to previous history of the sample (work hardening, annealing, etc.). In view of this sensitivity, some of the early work shows remarkably good qualitative agreement with the most recent measurements.

With the development of the ion-exchange method for separating rare earths [1] and the development of methods for preparing pure rare earth metals [2] in quantity, it has become possible to make much more extensive measurements on the properties of these metals. Some of these measurements are refinements of previous measurements and some are new. Since considerable quantities of the rare earths have been available at Ames, most of the figures show the Ames measurements. Direct references are given in the text to latest reported data where helpful. In addition, an index of workers in the field is appended.

We have not been able to get quantitative agreement with the predictions of the present theories of metals. However, we feel that considerably more data of the type outlined in this paper are needed before we would wish to draw a critical comparison with existing theories. For this reason, we will not attempt in this paper to do more than to point out the interesting properties and the obvious correlations between the properties which the various elements show.

In Table I, many of the physical constants of the rare earth metals are given as now known or estimated. While most of the experimental data listed were obtained using rare earth metals of very high purity with regard to other rare earths and metallic impurities, this is not true with regard to non-metallic impurities such as oxygen, nitrogen, hydrogen, and carbon. It is very difficult to prepare these metals free from small amounts of these elements. Even when prepared pure, it is very difficult to keep the rare earth metals pure, since they are among the world's best 'getters', particularly at high temperatures. Traces of water vapor, carbon dioxide, oxygen and nitrogen in the measuring apparatus, whether in the inert gases surrounding the specimens or adsorbed on the walls of the apparatus, almost inevitably end up in the metal. When this occurs, the sensitive properties such

TABLE I

Physical and Chemical Constants of the Rare Earth Metals (1956)

Element	M.P. °K	B.P. °K	Transition Temp. °K	ΔH vap. Kcal/mole	ΔH fusion Kcal/mole	Crystal Structure (Room Temp. form)	Lattice Constants Å a_0	c_0
Sc	1820–1870	2750	—	73*	3.8*	h.c.p.	3.3090	5.2733
Y	≈1820	3300	—	80*	4.1*	h.c.p.	3.6474	5.7306
La	1193†	4500	573–623 1141†	81	2.4*	hex f.c.c.	3.770 5.302Å	12.159
Ce	1077†	3200	1027†	79	2.2*	f.c.c.	5.1612	—
Pr	1208†	3290	1071†	79	2.4*	hex	3.6725	11.835
Nd	1297†	3450	1141†	69	2.6*	hex	3.6579	11.799
Pm	1570*	3000*	—	70*	3.0*	—	—	—
Sm	1325†	1900*	1190*	46*	2.6*	Rhom	8.996	$\alpha=23°1$
Eu	<1170	1700*	—	≈40	2.5*	b.c.c.	4.606	—
Gd	≈1520	3000*	—	72*	3.7*	h.c.p.	3.6360	5.7826
Tb	1638†	2800*	1583†	70	3.9*	h.c.p.	3.6010	5.6936
Dy	≈1670	2600	—	67	4.1*	h.c.p.	3.5903	5.6457
Ho	≈1770	2600*	—	67*	4.1*	h.c.p.	3.5773	5.6158
Er	1770–1820	2900*	—	70*	4.1*	h.c.p.	3.5588	5.5874
Tm	1820–1920	2400	—	56*	4.4*	h.c.p.	3.5375	5.5546
Yb	1097†	1800*	1071†	40	2.2*	f.c.c.	5.4862	—
Lu	1920–2020	2200*	—	59*	4.6*	h.c.p.	3.5031	5.5509

† Determined by thermal analysis

* Best estimated values from Ames Laboratory experience, and literature.

Density g/cm³	Compressibility Room Temp. [3] cm²/Kg × 10⁶	Results from Sound Velocity Measurements				Spectrogr. states for trivalent ion	Experimental Entropy, 300° K
		Debye Temperature	Young's Modulus Kg/cm² × 10⁻⁵	Shear Modulus Kg/cm² × 10⁻⁵	Poisson's Ratio		
3.016	—	—	—	—	—	—	—
4.472	2.96	—	8.33	3.29	0.265	—	—
6.162	4.06	162	3.66	1.42	0.288	$^1S_0$	13.64
6.190							
6.768	3.87	118	3.11	1.26	0.235	$^2F_{5/2}$	16.68
6.769	3.67	143	3.58	1.38	0.301	$^3H_4$	17.49
7.007	3.19	148	.386	1.48	0.310	$^4I_{9/2}$	17.54
—	—	—	—	—	—	—	—
7.540	3.71	—	—	—	—	$^6H_{5/2}$	—
5.166	—	—	—	—	—	—	—
7.868	2.58	176	5.78	2.29	0.259	$^8S_{7/2}$	15.83
8.253	—	175	5.91	2.34	0.264	$^7F_6$	—
8.556	2.74	182	6.45	2.60	0.243	$^6H_{15/2}$	17.91
8.799	2.66	—	—	—	—	$^5I_8$	17.91
9.058	2.63	192	7.65	3.06	0.238	$^4I_{15/2}$	17.52
9.318	2.72	—	—	—	—	$^3H_6$	—
6.959	8.00	—	—	—	—	—	—
9.849	2.32	—	—	—	—	$^1S_0$	—

as electrical resistivity, etc., may be markedly affected. During the past two years, our Laboratory has learned a great deal about preparing metals where these impurities are kept to a minimum. Therefore, the more recent measurements are likely to be more accurate than the earlier ones. We have also found that, when the metal can exist in two different crystalline forms, the impurities may influence which form will be obtained. The presence of impurities frequently makes the transition temperature between solid phases sluggish, and, when the metal is cooled from a high temperature, the polycrystalline metal obtained frequently consists of mixtures of two crystalline forms or of peculiarly stacked atomic layers. Therefore, the properties of the metals may be sensitive to the previous treatment of the particular specimens.

It is evident that as metals of increased purity are obtained, and more is learned concerning the heat treatment, more accurate physical constants will be obtained, but the values given in the table are the best known as of the date of writing. We hope, in the not-too-distant future, to be able to measure some of these properties with single crystals; we have succeeded in growing a few at the present time. However, the growing of single crystals is made somewhat difficult by a characteristic high temperature crystalline transformation which has been found in these metals in all cases examined.

The magnetic susceptibility measurements for the elements lanthanum, ytterbium and lutetium are not of the relative accuracy we would desire. The measurements were made using equipment designed primarily for the rare earths with higher moments, and further, we have not given the attention to obtaining extremely pure lanthanum, ytterbium and lutetium that we have given to a number of the other metals, although the amounts of the paramagnetic impurities were so low that there was considerable question as to whether they could be determined by spectrographic analysis. Therefore the samples of these metals are likely to have a trace of paramagnetic impurity so that our values may be high, yet they are considerably lower than those previously reported in the literature.

In the figures, we give plots of the temperature dependence of the specific heats, electrical resistivities, and magnetic properties. These properties will be discussed under the heading of the various elements along with other properties such as X-ray data, coefficients of expansion, Hall coefficient measurements, and superconductivity.

No attempt has been made to list all the known properties of the rare earth metals.

2. Lanthanum

It has been the experience of most investigators that it is difficult to obtain lanthanum metal in a single crystalline form [4, 5]. Usually the metal appears in the modified hexagonal close-packed form with a double c axis, although it may have the face-centered cubic form. Indeed, many cast samples have contained a mixture of both forms. Only recently has it been possible at Ames to get a sample which is entirely of the cubic form. Because of these difficulties, some of the data available on the properties of the metal will be superceded when the data on the pure crystallographic forms become available.

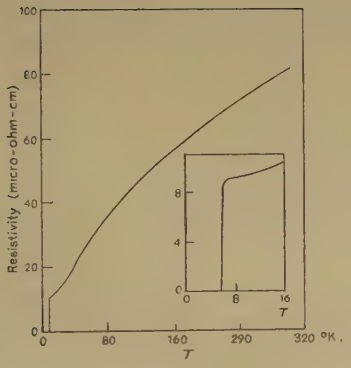

Fig. 1

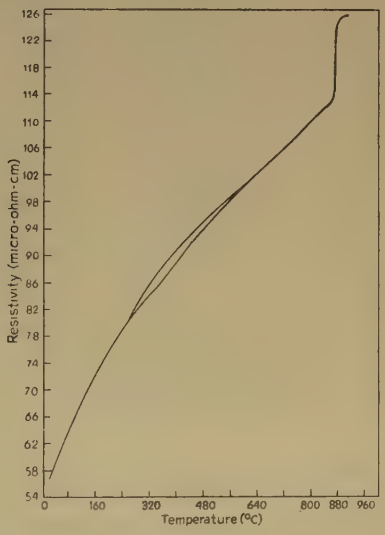

Fig. 2

Lanthanum is a superconductor with a transition temperature variously reported from 3.9° K to 5.8° K [4]. Our data [6, 7] on the electrical resistivity are shown in Figs. 1 and 2. Here the superconducting transition, as shown in the insert of Fig. 1, occurs at 5.8° K. Above the superconducting transition, the resistivity, though relatively high, has normal behavior for a metal. There are, however, two phase transitions at the higher temperatures. One occurs at

1141° K and is relatively sharp. This transition occurs just 52° below the melting point and is particularly interesting. About half the entropy of order disappears at this temperature according to cooling rate data collected on samples cooled from the molten state. Attempts to get X-ray data above the transition have not been successful. Dilatometric studies have likewise met with little success because of a high plastic deformation rate in samples heated to near this temperature. Although the samples appear to be solids above the transition, they behave as though no crystal structure were present. The lower temperature transition occurs somewhere between 550° K—900° K, and is very sluggish, requiring long annealing times at the most favorable temperature to obtain one of the pure forms.

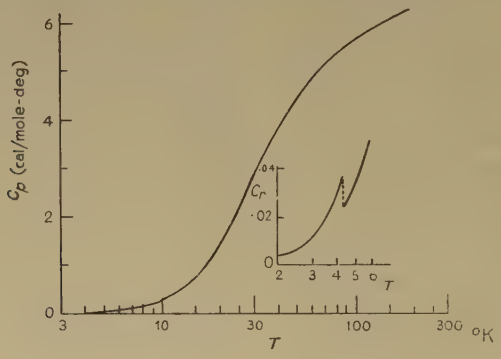

Fig. 3

Measurements of the magnetic susceptibility give a room temperature χ_{at} of 115×10^{-6} within 3 % and a 20.4° K χ_{at} of 220×10^{-6} within 7 %.

Fig. 3 shows that the heat capacity [8] has only one anomaly, that caused by the superconducting transition. Above the temperature of this transition, the heat capacity resembles that of lead, and may be characterized by a Debye temperature which varies between limits of 123° K and 137° K. The insert in Fig. 3 shows the region of the superconducting transition, which occurs at 4.37° K for the sample of Parkinson, Simon and Spedding [8]. X-ray data showed that their sample contained both hexagonal and cubic phases. More recently, on a somewhat purer sample, Berman, Zemansky, and Boorse [9] have found two distinct transitions; one at 5.8° K is associated with the cubic phase and one at 4.8° K is associated with the hexagonal phase.

Berman, *et al.*[9], have also measured the heat capacity down to 1.6° K in a large magnetic field and tentatively find that $\gamma = 21 \times 10^{-4}$ cal/mole-deg and that $\theta = 133°$ K. A re-evaluation of the work of Parkinson, *et al.*[8], shows that their data are not inconsistent with this value of γ, but they favor a higher value of θ.

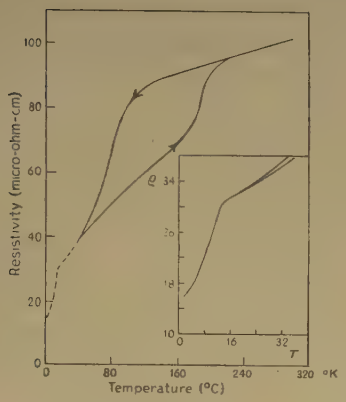

Fig. 4

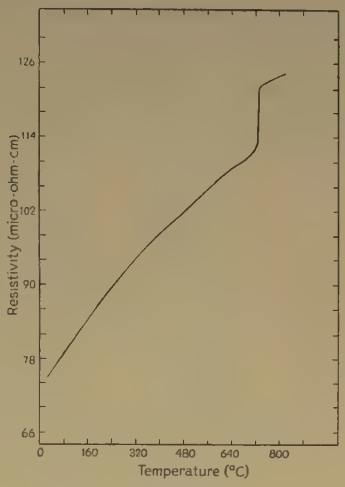

Fig. 5

3. Cerium

Cerium metal at room temperature appears to have a face-centered cubic structure, although some samples have been observed which contain both a face-centered cubic and a hexagonal close-packed form of the metal[5]. Cerium, when cooled below 85° K[10] or placed under a pressure of 15,000 atmospheres at room temperature[11], transforms more or less completely to a face-centered cubic structure with a lattice constant 6 % smaller than the room temperature form. This transition to the condensed form has been shown to be the result of the shifting of the 4f electron to the conduction band. At 1027° K, cerium undergoes a transformation from the face-centered cubic structure to an unknown structure. This transformation, like the corresponding transformation of lanthanum, is very sharp and involves a considerable amount of energy.

Fig. 4 shows the low temperature resistivity of a cast sample of cerium which was found to contain both cubic and hexagonal forms of the metal[6]. As the temperature is lowered, a sharp decrease in

the electrical resistivity is observed as the metal experiences the cubic-to-condensed-cubic transformation below 100° K; another break is apparent near 14° K (see insert of Fig. 4). Whether this latter break is due to a crystal field phenomenon or the typical onset of a magnetic transformation (which might be related to the crystal field) in the non-condensed hexagonal fraction is still an open question. As the temperature is raised, the resistivity rises in a reversible way up to about 50° K and then remains lower than the data taken on cooling the sample. At 180° K the resistivity rises sharply as an electron moves from the conduction band back into the 4f shell.

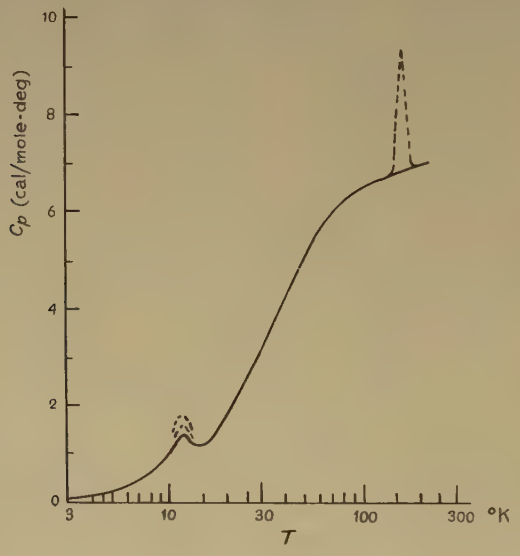

Fig. 6

This same type of temperature hysteresis has been observed in magnetic susceptibility studies [12], in dilatometric studies [13] and in measurements of the Hall effect [14]. As shown in Fig. 5, the high temperature transformation in cerium at 1027° K produces a marked disconstinuity in the resistivity [7]. This transformation has also been observed in the magnetic susceptibility by Gaume–Mahn [15].

The solid curve in Fig. 6 represents the most reproduceable heat capacity data for cerium [8]; these data were taken on a sample that contained both cubic and hexagonal forms of the metal. The dashed lines represent two alternative ways of removing the room temperature

entropy. The peak at 165° K is obtained if the sample has previously been cooled slowly below 85° K, while the solid line through this region is obtained if the sample has not previously been cooled below 135° K. This behavior is associated with the cubic-to-condensed cubic transformation. The dashed peaks at 12° K are obtained when the sample is cooled rapidly to the lowest temperature; the solid line is the result after slow cooling. As the cubic-to-condensed cubic transformation is not complete at the higher temperature region, it is supposed that the peak at 12° K represents the magnetic contribution of the untransformed 4f electrons.

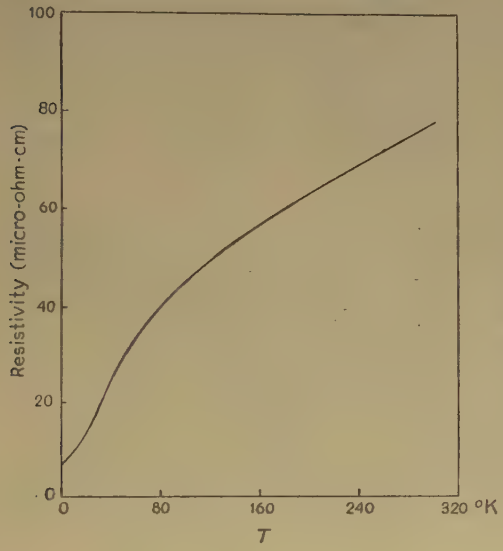

Fig. 7

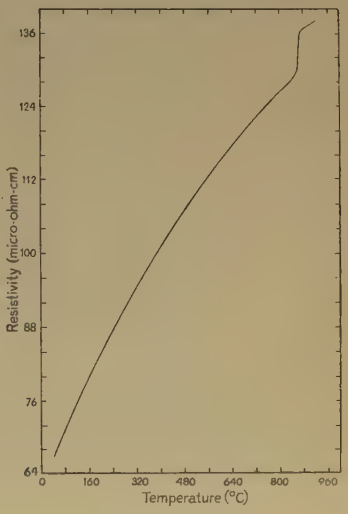

Fig. 8

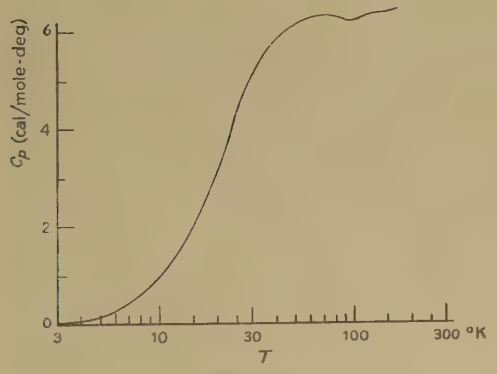

Fig. 9

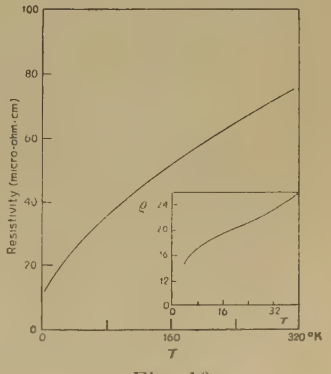

Fig. 10

4. Praseodymium

Praseodymium with two electrons in the 4f shell exhibits the double c axis hexagonal structure as in the case of lanthanum [5]. A cubic form has occasionally been reported in the literature, but it has not yet been established that such a form can exist when the metal is free of impurities. In the low temperature region, there are no outstanding anomalies in the electrical resistivity [6] of this metal as can be seen in Fig. 7. A high temperature transformation in praseodymium at 1070° K is apparent as a sharp discontinuity in the electrical resistivity measurements [7] as shown in Fig. 8.

In a study of the magnetic susceptibility, La Blanchatais [16] found that from 77° K to 500° K praseodymium obeys the Curie–Weiss law $\chi_{at}=\frac{1.58}{T+21^\circ}$. Her room temperature value for the atomic susceptibility is 4920×10^{-6}, while in our Laboratory, we get the considerably higher value of 5470×10^{-6}.

The heat capacity data [8], as shown in the plot of Fig. 9, obey Debye's law well up to 20° K with $\theta = 74^\circ$ K, if the conduction electron contribution is assumed to be the same as in lanthanum [9]. Although sound velocity measurements [17] show that the Debye temperature is lower for praseodymium than for lanthanum, such a low value as 74° K seems untenable. If, on the other hand, one assumes that the lattice contribution for praseodymium is about the same as for lanthanum, the 4f contribution to the heat capacity rises about as T^2 at low temperatures and reaches a rounded maximum at about 30° K. This behavior is not understood.

5. Neodymium

Neodymium at room temperature has the same modified hexagonal close-packed structure as lanthanum and praseodymium, and as in the case of these metals it undergoes a high temperature phase transition, at 1065° K. The low temperature electrical resistivity of neodymium [6] (three electrons in the 4f shell) is shown in Fig. 10; a slight knee at about 16° K is best seen in the insert. This behavior correlates well with the fact that neodymium apparently goes through a magnetic transformation as the temperature is lowered below 20° K, and with the fact that the heat capacity [8] (Fig. 11) shows two rounded maxima at 7° K and at 19° K. The high temperature transformation in neodymium at 1065° K may be observed in resistivity measure-

ments [7] as shown in Fig. 12. Dilatometric observations have shown recently that there is a 0.2 % increase in volume as the metal is heated through this transition.

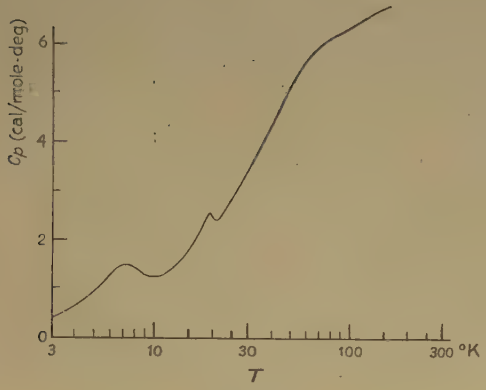

Fig. 11

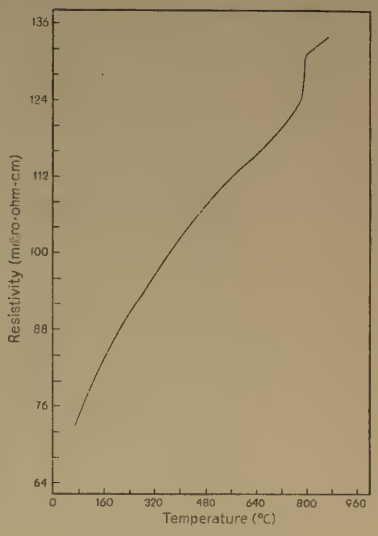

Fig. 12

Between 30° K and 145° K, our magnetic susceptibility data [18] on a polycrystalline sample fit the Curie–Weiss law $\chi_{at}=\frac{1.51}{T-1^\circ}$ and above 145° K the law $\chi_{at}=\frac{1.70}{T+16^\circ}$. We have also made magnetization studies at hydrogen and helium temperatures on this sample. The data obtained are shown in Fig. 13. The 4.2° K isotherm shows a field dependence of the magnetic moment of the type encountered in the antiferromagnetic temperature range of some of the heavier metals described later in this chapter.

Recently, we have determined the magnetic susceptibility of a small single crystal of neodymium metal and find that from 120° K to 270° K, $\chi_{at_\perp}=\frac{1.73}{T+11^\circ}$, $\chi_{at_\parallel}=\frac{1.71}{T+17^\circ}$, and from 40° K to 120° K $\chi_{at_\perp}=\frac{1.53}{T-5^\circ}$, $\chi_{at_\parallel}=\frac{1.52}{T}$. Here $\chi_{at_\parallel}$ indicates the susceptibility with the field parallel to the c axis and $\chi_{at_\perp}$ indicates the susceptibility perpendicular to the c axis. These data indicate the type of anisotropy

that is likely to exist in many of the metals. Here the data imply a tendency for the magnetic moment to line up perpendicular to the c axis.

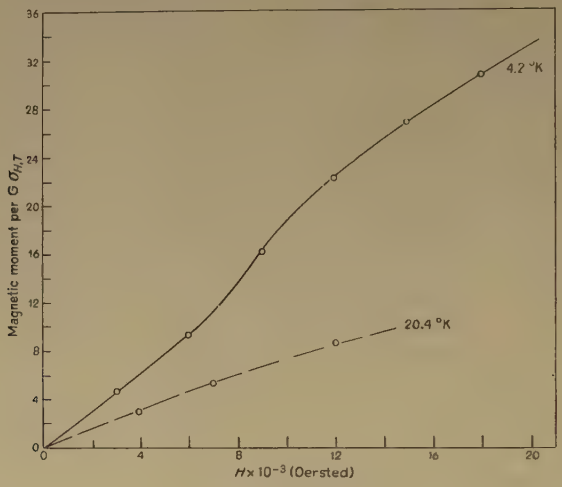

Fig. 13

6. Samarium

Samarium with five electrons in the 4f shell has a very strange crystal stacking [19] with layers of atoms in planes perpendicular to the c axis arranged in the order ababcbcac, giving a cell with four and one-half times the normal hexagonal close-packed c axis. From magnetic studies, Klemm and Bommer [20] report $\chi_{at} = 1820 \times 10^{-6}$ at room temperature. Measurements at this Laboratory indicate a much lower value of 1320×10^{-6}.

7. Europium

With regard to its physical properties, europium metal does not really belong to the rare earth series. It has a much lower density and obviously has only two electrons in the conduction band. It-more properly belongs in the calcium-strontium-barium series, since it is a soft metal having a relatively low boiling point and corrodes very rapidly in air.

From studies of the magnetic susceptibility, Klemm and Bommer [20] report that the $1/\chi$ vs T plot departs from linearity at 140° K and that the paramagnetic Curie temperature is 15° K. We have not

investigated the magnetic properties of the metal at low temperatures but would expect gadolinium-like behavior with a considerably lower Curie temperature than that for gadolinium.

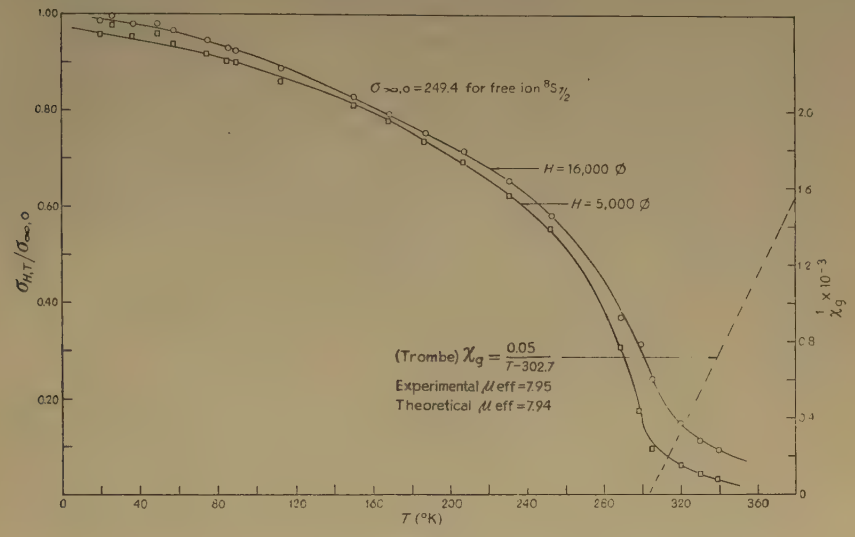

Fig. 14

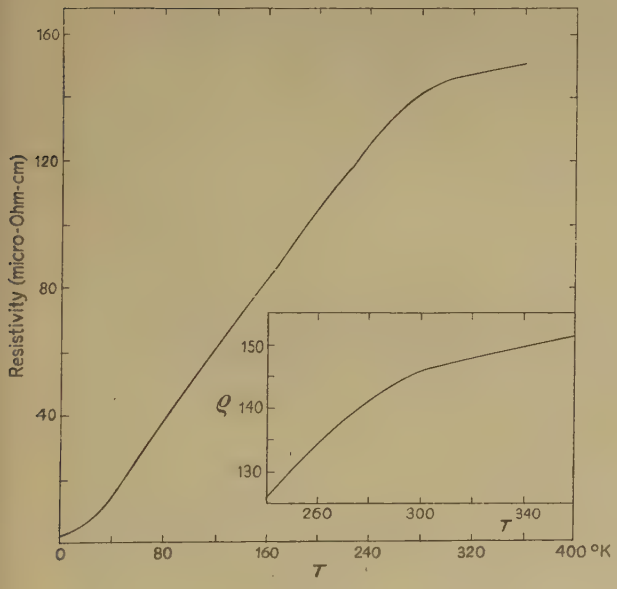

Fig. 15

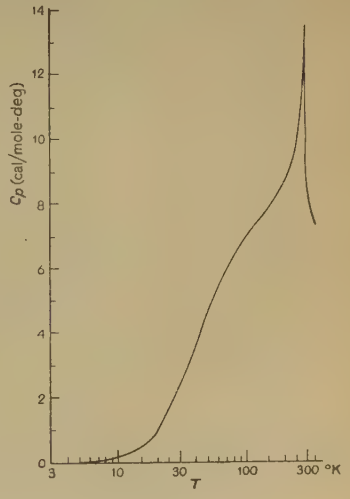

Fig. 16

8. Gadolinium

The rare earth metals from gadolinium to the end of the series, except for ytterbium, all exhibit simple hexagonal close-packed structures at room temperatures and below [5, 21].

The seven electrons of gadolinium in the 4f shell require that the shell be half full and that all the electron spins be alligned according to Hund's rule as applied to the free ion. The metal becomes ferromagnetic at 289° K. The dependence of the magnetic moment at constant field (iso-field data) on the temperature appears in Fig. 14 [22]. Extrapolations of the magnetic moment data to saturation at different temperatures yield saturation moments which fit very well the $T^{3/2}$ law predicted by the spin wave theory of ferromagnetism. The saturation moment at absolute zero agrees well with the value calculated for the free ion.

The electrical resistivity of gadolinium metal [23] is shown in Fig. 15. There is a sharp change in the slope of the curve (a knee) at the Curie temperature (see insert) with nearly linear dependence of the resistivity on temperature both above and below this point.

The coefficient of expansion is extremely small [24] below the Curie temperature. This comes about because the c axis expands slightly as the temperature is lowered [21].

The heat capacity [25] of Fig. 16 shows a single λ-type anomaly at 291.8° K. The measurements extended only down to 15° K, and at this temperature there was still an appreciable magnetic contribution to the heat capacity. It was not possible, therefore, to determine a value for the Debye temperature, but the value of 152° K obtained from the lowest experimental point may be taken as a lower limit.

9. Terbium

Only preliminary measurements have been made on the magnetic properties of terbium metal. The dependence of the magnetic moment on temperature (isofield plot) for a relatively impure sample (3 % impurity) is shown in Fig. 17. Here, it appears that the metal becomes ferromagnetic below about 230° K.

Klemm and Bommer [20] found terbium to obey a Curie–Weiss law of $\chi_{at} = 10.1/T - 205$. They report a room temperature atomic susceptibility of 115×10^{-3}. Our recent measurements on a good metal sample indicate an atomic susceptibility of 172×10^{-3} for the pure metal.

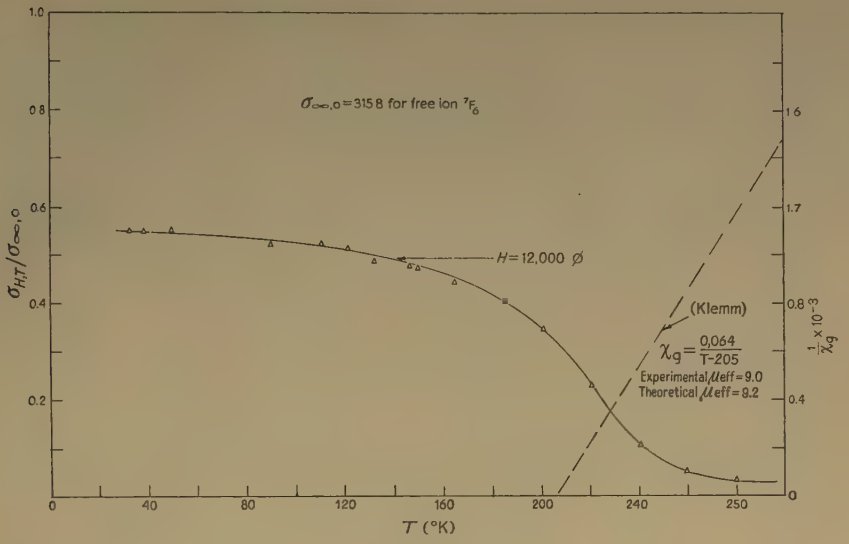

Fig. 17

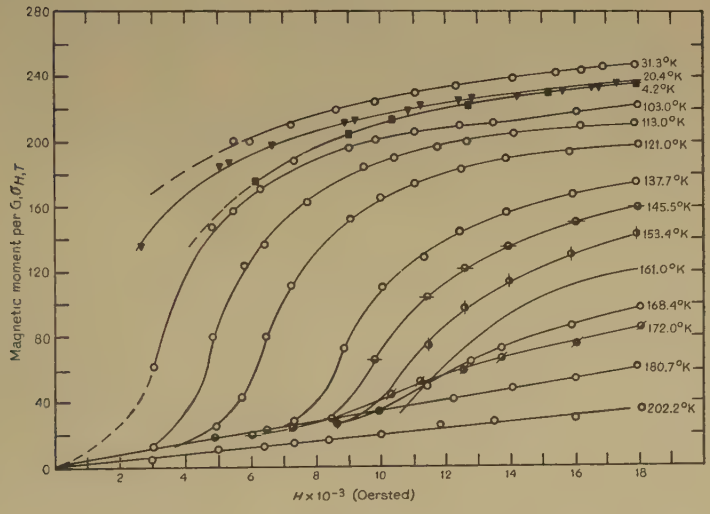

Fig. 18

10. Dysprosium

Magnetization curves (isotherms) for dysprosium [26] over the temperature range from 4.2° K to 200° K are shown in Fig. 18. However, it is easier to follow the magnetic transitions on an isofield plot of

the dependence of the magnetic moment per gram on temperature as shown in Fig. 19. Here it can be seen that the behavior is paramagnetic down to 175° K. It is interesting to note that the experimental μ_{eff} of 10.2 is very close to the calculated μ_{eff} of 10.6 for the free ion. At 175° K there is a cusp in the data which has the appearance of a Neel point as suggested by Trombe [27]. The metal apparently becomes antiferromagnetic below 175° K. It does not remain in this state all

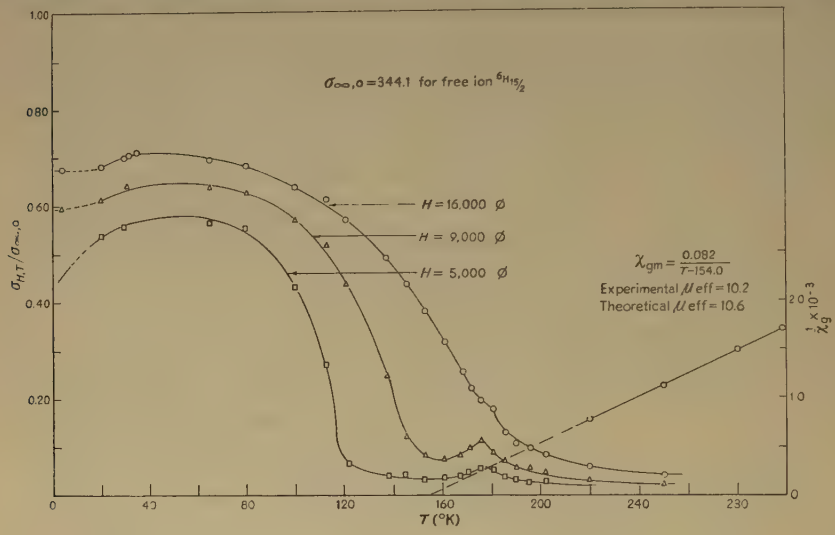

Fig. 19

the way down to absolute zero, however, but undergoes a transformation to the ferromagnetic state at 85° K. Magnetic remanance was observed below 85° K if the sample was not heated above the Neel point prior to each magnetization run. At temperatures below 30° K, there is a decrease in the observed magnetic moment with decreasing temperature. Although the metal is magnetically hard, it does not seem that this could account for this dropping off of the moment. Rather it seems more plausible that either the antiferromagnetic form again becomes competitive or that some lower moment electronic state is becoming populated as the temperature decreases, or both, assuming the lower lying state favors antiferromagnetism.

The electrical resistivity of dysprosium [23] (Fig. 20) exhibits anomalies at the temperatues of the magnetic transformations described above. As the temperature is lowered through 175° K, there is a leveling off

of the resistivity indicating that this transformation is certainly not from paramagnetism to ferromagnetism as in the case of gadolinium. This information corroborates qualitatively the proposal that the transition is one from the paramagnetic to an antiferromagnetic state. There is also a small change in the slope of the resistivity curve at 85° K, which is near the antiferromagnetic-ferromagnetic transformation.

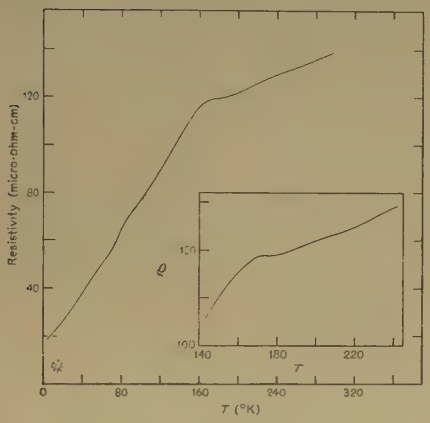

Fig. 20

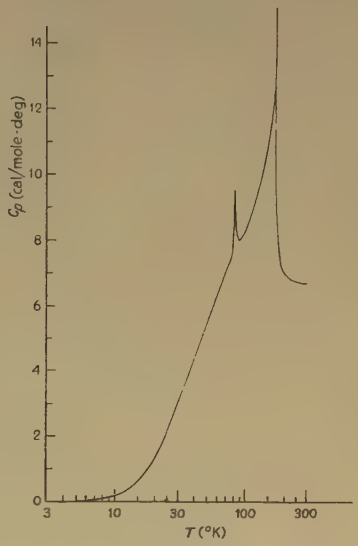

Fig. 21

The heat capacity [28] of Fig. 21 shows these two transitions. The one at 174° K is of the λ-type, and is associated with the antiferromagnetic transition. The lower temperature anomaly, associated with the ferromagnetic transition, is centered at 83.5° K, and is nearly symmetrical. The transition taking place in this temperature region shows thermal hysteresis; the entire entropy is not removed unless the sample is cooled well below the temperature of the anomaly. The measurements extended down to 15° K, and the magnetic contribution to the heat capacity was still appreciable at this temperature.

11. Holmium

The magnetization isotherms for holmium are shown in Fig. 22 and the isofield curves have the form shown in Fig. 23. The latter curves are very much the same as those for dysprosium. Assuming a

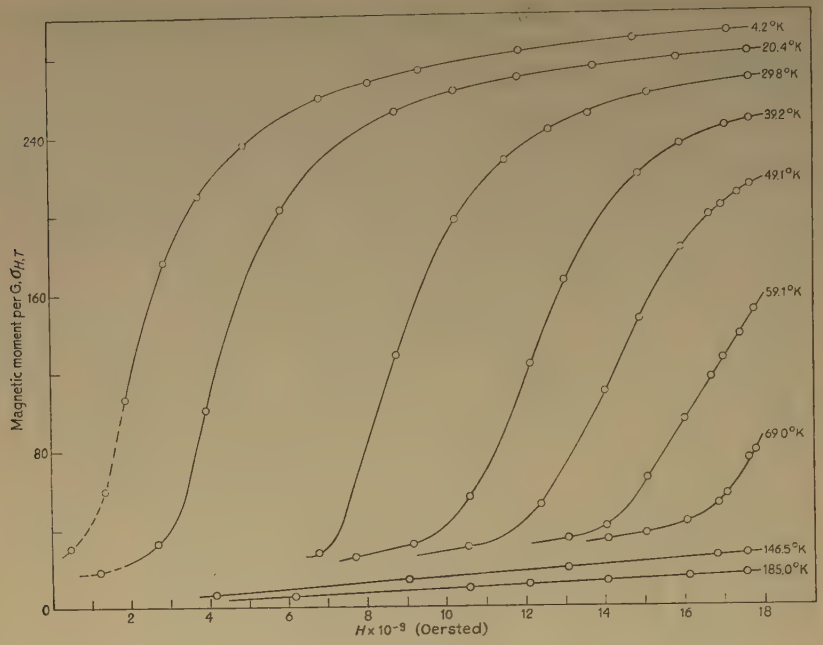
4.2°K
20.4°K
29.8°K
39.2°K
49.1°K
59.1°K
69.0°K
146.5°K
185.0°K
Magnetic moment per G, $\sigma_{H,T}$
$H \times 10^{-3}$ (Oersted)

Fig. 22

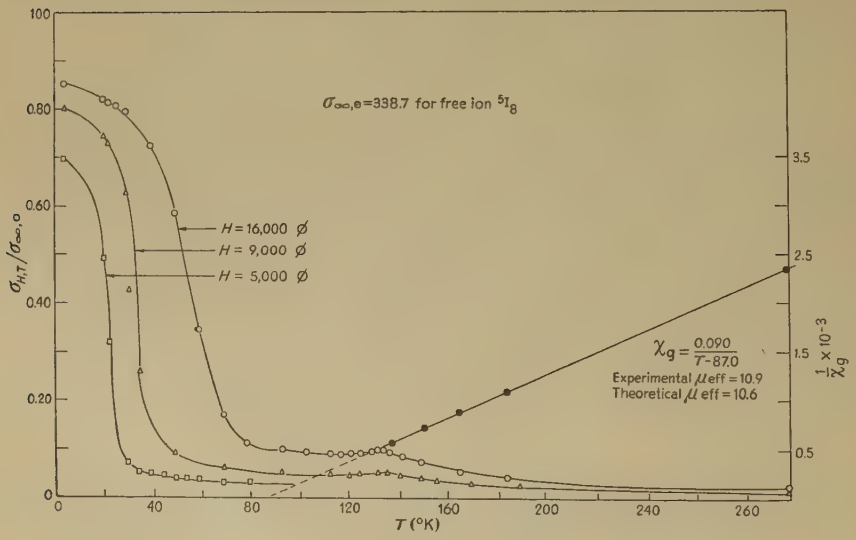
$\sigma_{\infty,0}$=338.7 for free ion $^5I_8$
H = 16,000 Ø
H = 9,000 Ø
H = 5,000 Ø
$\chi_g = \frac{0.090}{T-87.0}$
Experimental μ eff = 10.9
Theoretical μ eff = 10.6
$\sigma_{H,T}/\sigma_{\infty,0}$
$\frac{1}{\chi_g} \times 10^{-3}$
T (°K)

Fig. 23

similar interpretation of the data, there is a Neel point at 132° K, and a ferromagnetic Curie temperature at about 20° K. This means that holium is ferromagnetic below 20° K and is antiferromagnetic from 20° K to 132° K. Above 132° K, it is paramagnetic with an experimental μ_{eff} of 10.9 compared to the calculated value of 10.6 for the free ion. As in the case for dysprosium, data taken with decreasing fields at 4.2° K fell above the data for increasing fields

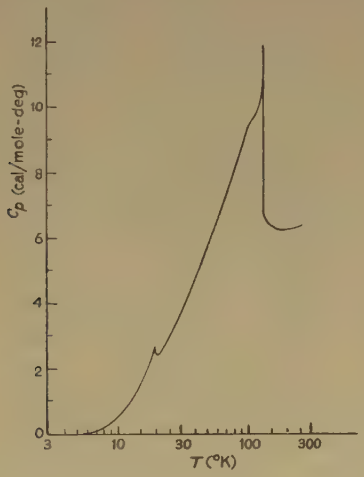

Fig. 24

giving part of a typical hysteresis loop. These data gave an indication of considerable remanence. There is no apparent dropping off of the saturation magnetization below 20° K as in the case of dysprosium.

The heat capacity of Fig. 24 shows a behavior which is very like that of dysprosium. The λ-type antiferromagnetic transition is at 131.6° K; the symmetrical, ferromagnetic transition is at 19.4° K and shows thermal hysteresis. The curve shows two points of inflection between the two transitions, however, while that for dysprosium shows none.

12. Erbium

Magnetically, erbium does not exhibit clean-cut transitions as do dysprosium and holmium. The magnetization isotherms [29] are shown in Fig. 25 and some isofield data appear in Fig. 26. From the latter, it is apparent that the very weakly developed rise and fall of

magnetization with temperature near 78° K could correspond to a Neel point. Near 20° K, likewise there appears to be a tendency for the metal to become ferromagnetic. Kohler [30] has made neutron diffraction observations on erbium and has been able to ascertain that

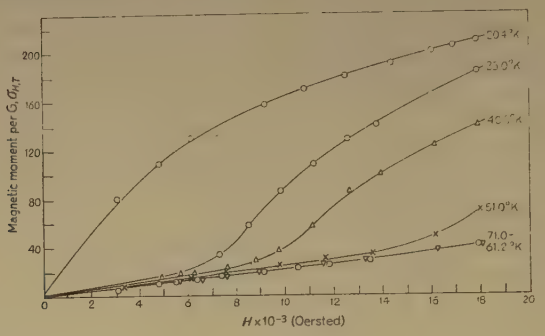

Fig. 25

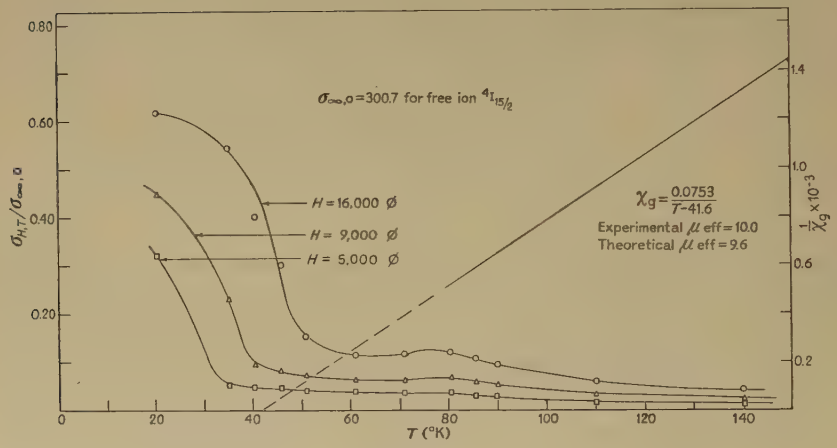

Fig. 26

it is ferromagnetic at helium temperatures. In the higher temperature regions, magnetic ordering is detected but the magnetic lattice has not been determined. It should be pointed out that the liquid hydrogen isotherm shown in Fig. 25 has not been repeatable although several attempts on different samples have been made. In most instances, the needle-like samples of ten to one aspect ratio turn crosswise in the magnetic field at this temperature indicating the presence of fairly

sizable crystallites and strong anisotropy. It is quite clear that single crystal data are needed to clarify the picture.

The electrical resistivity of erbium [23] appears in Fig. 27 and shows a slight break at the 78° K magnetic anomaly. The resistivity of this metal is very high, approaching that of bismuth in its poorly conducting direction.

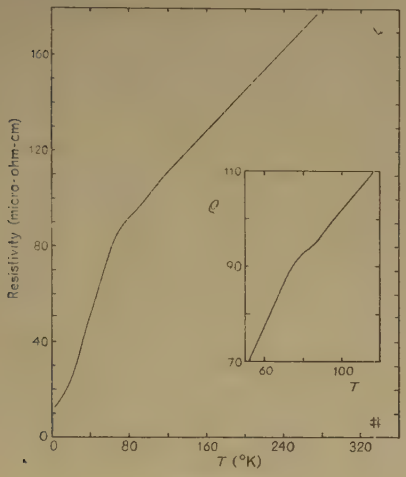

Fig. 27

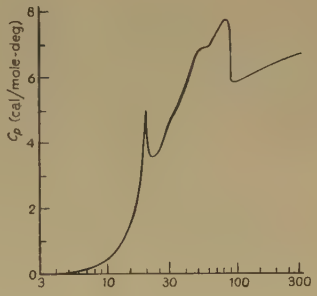

Fig. 28

There are three anomalies in the heat capacity [31] as shown in Fig. 28. The low temperature peak at 19.9° K is symmetrical and shows thermal hysteresis, apparently corresponding to the ferromagnetic transitions in holmium and dysprosium. The rounded maximum at 53.5° K also shows thermal hysteresis and does not correspond to an anomaly in any other data available at present. The heat capacity near 84° K is quite reproducible and does not display hysteresis; it is almost flat over a region of about one degree at the very maximum and then drops off very rapidly with temperature. This anomaly is near the temperature where the susceptibility shows its weak maximum.

13. Thulium

In Figs. 29 and 30 are shown the magnetization isotherms and the isofield data for thulium metal. From the latter it is apparent that thulium undergoes a magnetic transformation from the paramagnetic

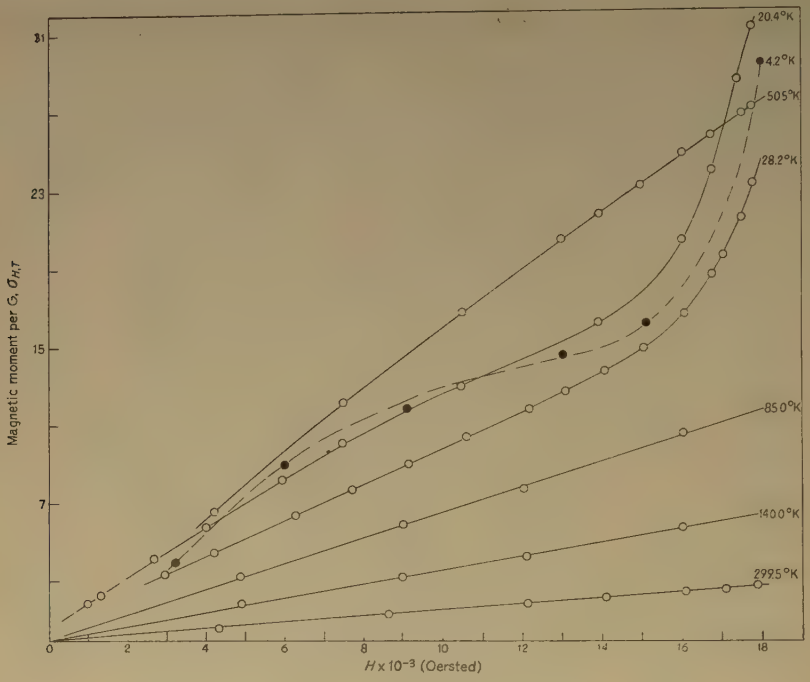

Fig. 29

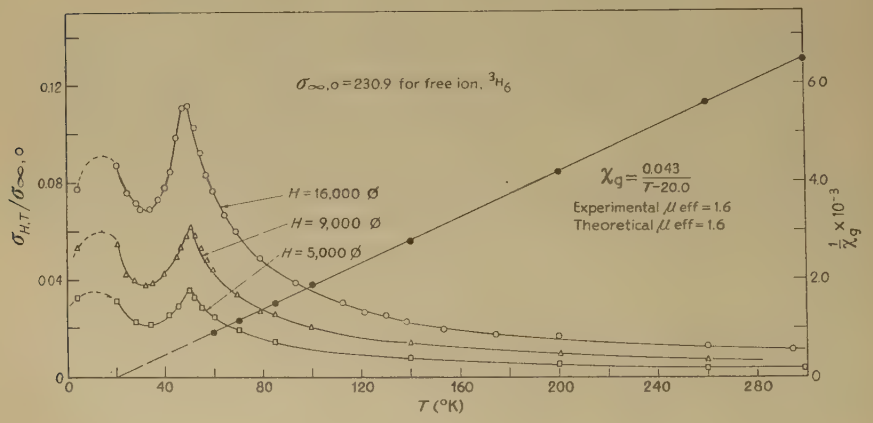

Fig. 30

state to the antiferromagnetic state at 51° K. The fact that the 4.2° K isotherm falls below the 20.4° K curve indicates that the metal does not become ferromagnetic.

14. Ytterbium

The 4f shell is filled in ytterbium metal and this leaves just two conduction electrons, making its properties unlike those of the other rare earth metals. It is not superconducting down to 2.2° K. The atomic magnetic susceptibility measured at room temperature is 81×10^{-6}.

15. Lutetium

Lutetium, the last of the rare earth series, has the 4f shell full and has three conduction electrons. We find the magnetic susceptibility at room temperature $\chi_{at} = 179 \times 10^{-7}$. It is not superconducting down to 2.2° K.

16. Summary

We are able to draw some general conclusions from the data which are now available. The rare earth metals are soft and have a low Debye temperature. On the other hand, they have low coefficients of expansion, comparable to those of glasses. In addition, the room temperature resistivities are high.

The behavior of the 4f electrons is well predicted at room temperatures by the assumption that their behavior is the same as in the free trivalent ion. This assumption is substantiated by the values of the Curie constants. It is also substantiated by the values of the entropy at room temperature, which may be explained as the sum of contributions from the 4f electrons, from the conduction electrons, and from the lattice. Making reasonable estimates of the latter two contributions, based on the data for lanthanum and on the measurements of sound velocity, we find that the contribution of the 4f electrons is $R \ln (2J+1)$, where the J value is that for the tripositive free ion. Until low temperature measurements establish the lattice and conduction electron contribution for each element, we may regard the agreement with the predicted contribution of the 4f electrons as established only within about 20 %.

The cooperative magnetic interactions which give rise to the ferromagnetic and antiferromagnetic states must be explained in terms other than the simple Heisenberg exchange, because of insufficient overlap of the 4f electrons. Looking to super-exchange by way of the conduction electrons may be fruitful. In any event, the available neutron diffraction data indicate that the nature of the antiferromagnetic ordering is complex.

Hall effect measurements are best interpreted in terms of a two-band model. The Hall voltage is positive for some of the rare earth metals and negative for others. It is interesting to note that the antiferromagnetic transition gives rise to a knee in the electrical resistivity versus temperature curve, as best seen in the case of dysprosium.

APPENDIX

The workers mentioned below are among the many who have worked with the rare earth metals in the following fields:

1. Heat Capacity.
2. Electrical Conductivity.
3. Magnetic Susceptibility.
4. Hall Coefficient.
5. Melting Point and Vapor Pressure.
6. Structure.
7. Thermal Expansion.
8. Miscellaneous Physical Properties.
9. Preparation of Metals.

Ahmann, D. H., 5, 8, 9
Allen, J. F., 2
Banister, J. R., 6, 7
Barson, F., 2, 3, 4
Bates, L. F., 3
Behrendt, D., 6
Benedicks, C., 2
Bommer, H., 3, 5, 6, 8, 9
Bottema, J. A., 2, 7
Bowman, M. G., 6
Bridgman, P. W., 2, 8
Daane, A. H., 2, 5, 6, 8, 9
Daunt, J. G., 2
De Haas, W. J., 2
Dennison, D. H., 5, 8, 9
Ellinger, F. H., 6
Elliott, J. F., 2, 3, 4
Ericson, R. P., 9
Farr, J. D., 6
Floyd, A. L., Jr., 6
Foex, M., 7
Gaume–Mahn, F., 3, 9
Giorgi, A. L., 6
Griffel, M., 1
Hach, C. C., 9
Herrmann, K. W., 2, 6, 8
Heumann, T., 8
Hopkins, B. S., 8, 9
Hull, A. W., 6
Jaeger, F. M., 2, 7
Kaufmann, A. R., 3
Keller, W. H., 9
Kevane, C. J., 4
Koehler, W. C., 3
Klemm, W., 3, 5, 6, 8, 9
Klose, H., 8, 9
Kremers, H. C., 9
La Blanchetais, C., 3
Lawson, A. W., 6
Leach, S. J., 3
Legvold, S., 2, 3, 4, 6, 7, 8
Loasby, R. G., 3
Loriers, J., 8
Lucas, F. F., 6
McKay, R. W., 6
McLennan, J. C., 6
Meisel, K., 6, 9
Mendelssohn, K., 2

Messenhausen, W., 8
Monkman, R. J., 6
Muthmann, W., 5, 9
Neumayr, S., 6, 9
Onstott, E. I., 9
Owen, M., 3
Parkinson, D. H., 1
Quill, L. L., 5, 6, 8, 9
Rosenbohm, E., 2, 7
Rossi, A., 6
Rundle, R. E., 6
Schuch, A. F., 6
Schumacher, E. E., 6
Shoenberg, D., 2
Simon, F. E., 1
Skochdopole, R. E., 1
Smith, A. W., 4
Smith, H. G., 6
Spedding, F. H., 1, 2, 3, 4, 5, 6, 7, 8, 9
Starr, C., 3
Stevens, K. W. H., 3
Sturdivant, J. H., 6
Tang, T., 6
Trombe, F., 3, 5, 6, 7, 8, 9
Urbain, G., 3
Vogel, R., 8, 9
Voogd, J., 2
Weiss, L., 5, 9
Weiss, P., 3
Wilhelm, H. A., 9
Wilhelm, J. O., 2
Wollan, E. D., 3
Young, R. A., 6
Zachariasen, W. H., 6
Ziegler, W. T., 6
Zintl, E., 6, 9

REFERENCES

1 F. H. Spedding and J. E. Powell, J. Metals, **6**, 1131 (1954).
2 F. H. Spedding and A. H. Daane, J. Metals, **6**, 504 (1954).
3 P. W. Bridgman, Proc. Am. Acad., **83**, 1 (1954).
4 W. T. Ziegler, R. A. Young and A. L. Floyd, J. Am. Chem. Soc., **75**, 1215 (1953).
5 F. H. Spedding, A. H. Daane and K. W. Herrmann, Acta Cryst., **9**, 559 (1956).
6 N. R. James, S. Legvold and F. H. Spedding, Phys. Rev., **88**, 1092 (1952).
7 F. H. Spedding, A. H. Daane and K. W. Herrmann, J. Metals, (to be published).
8 D. H. Parkinson, F. E. Simon and F. H. Spedding, Proc. Roy. Soc. A, **207**, 137 (1951).
9 A. Berman, M. W. Zemansky, and H. A. Boorse, Conference on Low Temperature, Louisiana State University (1955).
10 A. F. Schuch and J. H. Sturdivant, J. Chem. Phys., **18**, 145 (1950).
11 A. W. Lawson and T. Tang, Phys. Rev., **76**, 301 (1949).
12 C. la Blanchetais, Compt. Rend., **220**, 392 (1945).
13 F. Trombe and M. Foex, Compt. Rend., **217**, 501 (1943).
14 C. J. Kevane, S. Legvold and F. H. Spedding, Phys. Rev., **91**, 1372 (1953).
15 F. Gaume–Mahn, Compt. Rend., **241**, 286 (1955).
16 C. la Blanchetais, Compt. Rend., **234**, 1353 (1952).
17 J. F. Smith, Private Communication, Iowa State College.
18 J. F. Elliott, S. Legvold and F. H. Spedding, Phys. Rev., **94**, 50 (1954).
19 A. H. Daane, R. E. Rundle, H. G. Smith and F. H. Spedding, Acta Cryst., **7**, 532 (1954).

[20] W. Klemm and H. Bommer, Z. Anorg. u. Allgem. Chem., **231**, 138 (1937).
[21] J. R. Bannister, S. Legvold and F. H. Spedding, Phys. Rev., **94**, 1140 (1954).
[22] J. F. Elliott, S. Legvold and F. H. Spedding, Phys. Rev., **91**, 28 (1953).
[23] S. Legvold, F. H. Spedding, F. Barson and J. F. Elliott, Rev. Mod. Phys., **25**, 129 (1953).
[24] F. Trombe and M. Foex, Compt. Rend., **235**, 42 (1952).
[25] M. Griffel, R. E. Skochdopole and F. H. Spedding, Phys. Rev., **93**, 675 (1954).
[26] J. F. Elliott, S. Legvold and F. H. Spedding, Phys. Rev., **94**, 1143 (1954).
[27] F. Trombe, J. Phys. Radium, **12**, 222 (1951).
[28] M. Griffel, R. E. Skochdopole and F. H. Spedding, Submitted to J. Chem. Phys.
[29] J. F. Elliott, S. Legvold and F. H. Spedding, Phys. Rev., **100**, 1595 (1955).
[30] W. C. Koehler and R. O. Wollan, Phys. Rev., **97**, 1177 (1955).
[31] R. E. Skochdopole, M. Griffel and F. H. Spedding, J. Chem. Phys., **23**, 2258 (1955).

CHAPTER XIII

THE REPRESENTATION OF SPECIFIC HEAT AND THERMAL EXPANSION DATA OF SIMPLE SOLIDS

BY

D. BIJL

St. Salvator's College, St. Andrews, Scotland

Contents: 1. Introduction, 395. — 2. Solids at low temperatures, 397. — 3. The continuum (Debye) model, 399. — 4. Solids at high temperatures, 400. — 5. Methods of representing specific heat data, 403. — 6. Experimental data on the specific heat, 410. — 7. Discussion, 418. — 8. The representation of thermal expansion data, 422. — 9. Discussion, 426.

1. Introduction

The experimental study of the specific heat of solids has been for many years one of the foci of attention of low temperature research. The reasons for this are easy to indicate. From a purely thermodynamic point of view the specific heat (whether at constant pressure or at constant volume) is an important quantity at any temperature. Furthermore, specific heat data provide a crucial check of certain predictions of the quantum theory of the thermal properties of solids, in particular at low temperatures. These properties depend strongly on the thermal vibrations of the constituent atoms or molecules, which in their turn are determined by the interatomic forces between the constituents.

Nevertheless, it is possible to describe the vibrational contribution to the specific heat surprisingly well without entering into any detail of the interatomic forces as has been shown as long ago as 1912 by Debye [2]. In fact, Debye's theory is so successful, that ever since its introduction it has been used as a standard of reference in discussing experimental data. One of the purposes of this paper is to analyse various possible methods of representing specific heat data in terms of the Debye theory and to show that the usual method is inferior to a proposed new method in describing the relation between the predictions of the Debye theory, the actual behaviour of solids and

the predictions of the much more rigorous lattice dynamical theories of Born and von Karman [4], Blackman and others [3, 8, 78]. This comparison is largely based on recent specific heat measurements. It may be remarked already at this stage, that the use of low temperature techniques often imposes an unfortunate limitation on the temperature range in which measurements are carried out on a particular sample. Very few, if any, measurements on samples used in low temperature research extend to temperatures considerably above room temperature. This limitation is completely arbitrary from a physical point of view and often makes the connection between low temperature and high temperature data sufficiently uncertain to prevent a check of the theory at higher temperatures to be made.

Much the same remarks can be made with respect to properties related to the equations of state (in particular the thermal expansion), although the amount of available experimental data is regrettably small. The general features of the thermal expansion at low temperatures are described remarkably well by the theories of the equation of state of Debye [12] and Grüneisen [1], which both are essentially based on the physical picture underlying Debye's theory of the specific heat. Both theories predict an intimate relation between the specific heat and the thermal expansion. The experimental check of this relation is more involved than often has been supposed and, as Hume–Rothery pointed out [18], considerable confusion has been the result. In this paper we will discuss this situation in some detail, in particular in relation to recent experimental results. These results indicate that the Debye–Grüneisen theory is too much simplified and has to be replaced (as in the case of specific heats) by a more rigorous lattice dynamical theory [23].

Before proceeding to the main part of the discussion it will be useful to give a brief survey of the relevant theory. We shall assume that the temperature dependent part of the free energy of a solid of particles can be represented by the free energy of a system of $3N$ harmonic oscillators (the lattice waves) with frequencies ν which may depend on the volume. Hence we shall write for the Helmholtz free energy F [11] of the lattice

$$F = \Phi + 3NkT \int_0^{\nu_m} g(\nu) \ln \{1 - \exp(-h\nu/kT)\} \, d\nu. \qquad (1)$$

The second term describes the temperature dependent part of F. It is

assumed that the temperature is sufficiently high to describe the frequency spectrum by a continuous distribution function $g(\nu)$ [7], where $g(\nu)$ is normalised by the relation $\int_0^{\nu_m} g(\nu)\mathrm{d}\nu = 1$. The first term in Eq. (1) depends on the volume only and describes the potential energy and the energy of the zero-point motion. The use of Eq. (1) necessarily restricts the discussion to certain types of solids (see § 5) and furthermore implies that the anharmonicity of the thermal vibrations is small [6]. The entropy S, the internal energy U, specific heat C_v and the ratio between the volume coefficient of thermal expansion α and the isothermal compressibility $\varkappa$ can be found from F by the well-known thermodynamic relations

$$S = -\frac{\partial F}{\partial T},\ U = \frac{\partial (F/T)}{\partial (1/T)},\ C_v = \frac{\partial U}{\partial T},\ \frac{\alpha}{\varkappa} = \frac{\partial S}{\partial v}. \tag{2}$$

All thermodynamic quantities in Eq. (2) depend essentially on the frequency spectrum $g(\nu)$. The frequency spectra of different solids are so widely different, however, that no general treatment is possible, except in the limiting cases of high and low temperatures, which will be outlined in the following three sections.

2. Solids at Low Temperatures

At sufficiently low temperatures ($T < \theta_0/50$ [3]) only lattice waves with a wavelength long compared with the interatomic distances are excited. These waves are identical with elastic waves and hence the velocities of propagation are determined by the elastic constants. In each direction (characterised by an element of solid angle $\mathrm{d}\Omega$) there are three independent elastic waves with in general different velocities of propagation $v_s (s = 1, 2, 3)$; the velocities v_s depend on the direction. The frequency spectrum of these waves is given by

$$g(\nu) = 3\left(\frac{h}{k\theta_0}\right)^3 \nu^2 \tag{3}$$

and hence is characterised by the (volume dependent) 'characteristic temperature' θ_0 of the dimension of a temperature. It can be shown that [8]

$$\theta_0 = \frac{h}{k}\left(\frac{9N}{V}\right)^{1/3}\left(\sum_{s=1}^{3}\int\int \frac{\mathrm{d}\Omega}{v_s^3}\right)^{-1/3}, \tag{4}$$

where the integration has to be carried out over all directions. For an isotropic solid we have:

$$g(\nu) = 3\left(\frac{4\pi N}{V}\right)\left(\frac{1}{v_l^3} + \frac{2}{v_t^3}\right), \tag{3a}$$

where v_l and v_t are the velocities of propagation of the longitudinal and transverse waves respectively. θ_0 is a function of the velocities of the elastic waves and can be calculated from the elastic constants measured at low temperatures. In all cases where this theoretical value of θ_0 could be compared with an experimental value the agreement is excellent.

With the aid of Eq. (3) we can express F, S, U and $C_l(=C_v)$ * in terms of T and θ_0 only. We find (assuming $V=V_0$, where V_0 is the volume at $T=0$)

$$F_l=\Phi_0-(\pi^4/5)\,NkT(T/\theta_0)^3 \tag{5}$$

$$S_l=(4\pi^4/5)\,Nk(T/\theta_0)^3 \tag{6}$$

$$U_l=\Phi_0+(3\pi^4/5)\,NkT(T/\theta_0)^3 \tag{7}$$

$$C_l=(12\pi^4/5)\,Nk(T/\theta_0)^3. \tag{8}$$

The thermal expansion is determined by

$$\alpha/\varkappa_{00}=(1/V_0)\gamma_0 C_l, \tag{9}$$

where we have introduced the dimensionless Grüneisen factor defined by

$$\gamma_0=-\mathrm{d}\ln\theta_0/\mathrm{d}\ln V \tag{10}$$

and where C_l is given by Eq. (8). γ_0 can be calculated if the volume dependence of the elastic constants is known or alternately from the interatomic potential [24]; $\varkappa_{00}$ (compressibility at $T=0$, $V=V_0$) is related to $\Phi(V)$ by $1/\varkappa_{00}=V_0\Phi''(V_0)$.

The experimental specific heat at sufficiently low temperatures is always found to be proportional to T^3 and hence Eq. (8) can be used to determine and 'effective' value of θ_0 from experimental data. According to Eq. (9) α and C_l are proportional to each other. This proportionality is often called the Grüneisen rule. For reasons which will become clear in § 8 we take here the Grüneisen rule to imply that γ_0 is exactly constant.

It is important to note that a change of volume only affects the value of θ_0 in Eq. (3); the distribution function remains a quadratic function of the frequency, or in other words, all lattice frequencies

* The subscript $_l$ refers throughout the paper to contributions due to the lattice waves, calculated at $V=V_0$.

are altered in the same proportion. This cannot be expected to be so in general and hence deviations from the Grüneisen rule may occur.

3. The Continuum (Debye) Model

A simple but powerful model of the thermal properties of a solid was introduced by Debye [2, 12] by assuming that the frequency spectrum is determined by Eq. (3) not only at low frequencies, but at all frequencies. The maximum frequency is determined by the normalising condition for $g(\nu)$ and is given by $\nu_m = k\theta_0/h$. The use of Eq. (4) implies that the spectrum is completely determined by the long wave properties of the solid or, in other words, the discrete structure of a solid is not taken into account except for the introduction of the finite maximum frequency ν_m.

We now have

$$S_l^D = 12\,NkT\left(\frac{T}{\theta_0}\right)^3 \int_0^{\theta_0/T} \frac{x^3}{e^x - 1}\,dx - 3\,Nk\log\left(1 - e^{-\theta_0/T}\right) \tag{11}$$

$$C_l^D = 9\,Nk\left(\frac{T}{\theta_0}\right)^3 \int_0^{\theta_0/T} \frac{x^4 e^x}{(e^x - 1)^2}\,dx \tag{12}$$

$$\alpha/\varkappa_{00} = (\gamma_0/V_0)\,C_l^D; \tag{13}$$

the index ^{D} refers to the Debye model. In Eq. (12) γ_0 is given by Eq. (10) and C_l^D is given by Eq. (12). As before Φ, θ_0 and γ_0 have to be taken at $V = V_0$, which should be remembered when comparing experimental data with this theory. According to Eq. (13) the Debye theory predicts the validity of the Grüneisen rule at *all* temperatures.

At low temperatures ($T < 0.1\,\theta_0$) S_l^D, C_l^D and $\alpha/\varkappa_{00}$ are given by the corresponding relations in § 2. At high temperatures ($T > \theta_0$) we have [11, 12]

$$S_l^D = 4\,Nk + 3\,Nk\ln(T/\theta_0) \tag{14}$$

$$C_l^D = 3\,Nk\left(1 - \frac{1}{20}\frac{\theta_0^2}{T^2} + \frac{1}{560}\frac{\theta_0^4}{T^4} - \ldots\right) \tag{15}$$

$$\alpha/\varkappa_{00} = (\gamma_0/V_0)\,C_l^D.$$

Obviously γ_0 is still given by Eq. (10), but C_l^D now is given by Eq. (15). At intermediate temperatures only numerical evaluation of the integrals in Eq. (11), (12) and (13) is possible; tables of the corresponding values of S_l^D and C_l^D as a function of T/θ_0 can be found in several works [9, 108].

According to Eq. (11) and (12) S_l^D and C_l^D are functions of the 'reduced' temperature T/θ_0 only and hence these equations express a law of corresponding states for S_l^D and C_l^D. In view of the approximate character of the Debye theory the experimental values of S_l and C_l satisfy these laws of corresponding states surprisingly well. So well in fact, that deviations from the predictions of the Debye theory sometimes were regarded as anomalies which could only be explained by ad hoc assumptions; and moreover, that the much more fundamental theory of Born and von Kármán [4] did not receive the attention it deserved. This situation has completely altered, largely due to Blackman's work. On the other hand, the Debye theory is so useful for a first orientation and its heuristic value (in particular of the characteristic temperature θ_0) is so great, that it is still justifiable to use it as a reference standard for experimental work. Also in the present article we will adhere to this, although the actual comparison between the Debye theory and the experimental results will be carried out in a way which differs from the usual method found in the literature.

4. Solids at High Temperatures

The specific heat C_l at any temperature can be written in the form

$$C_l = 3Nk \int_0^{\nu_m} c(\nu, T)\, g(\nu)\, \mathrm{d}\nu \qquad c(\nu, T) = \frac{\left(\frac{h\nu}{kT}\right)^2 \exp\left(\frac{h\nu}{kT}\right)}{\left(\exp\left(\frac{h\nu}{kT}\right) - 1\right)^2}, \tag{16}$$

which becomes at high temperatures [14]

$$C_l = 3Nk\left(1 - \frac{1}{12}\left(\frac{h}{k}\right)^2 \frac{\overline{\nu^2}}{T^2} + \frac{1}{240}\left(\frac{h}{k}\right)^4 \frac{\overline{\nu^4}}{T^4} - \ldots\right), \tag{17}$$

where

$$\overline{\nu^{2n}} = \int_0^{\nu_m} \nu^{2n}\, g(\nu)\, \mathrm{d}\nu;$$

and $c(\nu, T)$ is the contribution to the specific heat of an oscillator with frequency ν. It is important to note that Eq. (15) and (17) both describe the specific heat as a power series in $1/T$. Formal equivalence between these equations can be established by introducing (retaining terms to the 4th power of $1/T$ only) [13]

$$\theta_\infty^{(c)^2} = \frac{5}{3}\left(\frac{h}{k}\right)\overline{\nu^2} - \frac{1}{28}\left(\frac{h}{k}\right)^4 \frac{1}{T^2}\left(\frac{7}{3}\,\overline{\nu^4} - \left(\frac{5}{3}\,\overline{\nu^2}\right)^2\right).$$

Then Eq. (17) becomes

$$C_l = 3Nk\left(1 - \frac{1}{20}\frac{\theta_\infty^{(c)2}}{T^2} + \frac{1}{560}\frac{\theta_\infty^{(c)4}}{T^4} - \cdots\right). \tag{18}$$

At high temperatures therefore the specific heat should be equal to that of a Debye solid with characteristic temperature $\theta_\infty^{(c)}$. In general there is no reason to expect $\theta_\infty^{(c)}$ (which is determined by all lattice frequencies) and θ_0 (which is determined by the elastic constants) to be equal. Only in the Debye case we should expect $\theta_0 = \theta_\infty^{(c)}$.

An experimental determination of $\theta_\infty^{(c)}$ using Eq. (18) is very difficult to carry out accurately because of the sensitivity of an experimental value of $\theta_\infty^{(c)}$ for small errors in C_l. But the existing data are certainly consistent with a formula of the type (18) and generally lead to value of $\theta_\infty^{(c)}$ different from the value of θ_0. However, if experimentally $C_l > 3Nk$ the concept of a characteristic temperature as defined by (18) loses its meaning.

The thermal expansion at any temperature is given by

$$\frac{\alpha}{\varkappa} = \frac{3Nk}{V}\int_0^{\nu_m} \gamma(\nu)\, c(\nu, T)\, g(\nu)\, \mathrm{d}\nu \qquad (\gamma(\nu) = -\mathrm{d}\ln\nu/\mathrm{d}\ln V),$$

if we ignore the difference between C_v and C_l. This can be written in a form similar to Eq. (9)

$$\frac{\alpha}{\varkappa} = \frac{1}{V}\gamma_T C_l, \tag{19}$$

if we introduce an 'effective Grüneisen factor' γ_T defined by

$$\gamma_T = \frac{3Nk}{C_l}\int_0^{\nu_m} \gamma(\nu)\, c(\nu, T)\, g(\nu)\, \mathrm{d}\gamma; \tag{20}$$

C_l is given by Eq. (16). If $V = V_0$, γ_T will depend on the temperature only. At high temperatures $c(\nu, T) \to 1$ and then

$$\gamma_T \to \gamma_\infty = \int_0^{\nu_m} \gamma(\nu)\, g(\nu)\, \mathrm{d}\nu = \overline{\gamma(\nu)}, \tag{21}$$

which is independent of temperature. At high temperatures therefore the Grüneisen rule must be satisfied (at any rate in the harmonic approximation, according to which the specific heat approaches a constant value for high temperatures).

The limiting value γ_∞ can be related more directly to the properties

of the frequency spectrum in the following way. At high temperatures we have

$$F_l = \Phi_0 + 3NkT \int_0^{\nu_m} g(\nu) \ln (h\nu/kT)\, d\nu$$

and hence it can be shown that

$$S_l = 4Nk + 3Nk \ln (T/\theta_\infty^{(s)}),$$

where

$$\theta_\infty^{(s)} = e^{1/3} \frac{h}{k} \left(\Pi(\nu)\right)^{1/3N}$$

with

$$\log \Pi(\nu) = \int_0^{\nu_m} g(\nu) \ln (\nu)\, d\nu = \overline{\ln (\nu)}.$$

For the thermal expansion we find

$$\frac{\alpha}{\varkappa} = \frac{\partial s}{\partial V} = \frac{3Nk}{V} \left(-\frac{d \ln \theta_\infty^{(s)}}{d \ln v}\right) = \frac{1}{V} \gamma_\infty C_l,$$

so that

$$\gamma_\infty = \overline{\gamma(\nu)} = -d \ln \theta_\infty^{(s)} / d \ln V.$$

In general θ_0 and $\theta_\infty^{(s)}$ must be expected to be different. This implies that at intermediate temperatures deviations from the Grüneisen rule may occur. Furthermore we must expect that $\theta_\infty^{(c)} \neq \theta_\infty^{(s)}$. It will be obvious that $\theta_\infty^{(s)}$ retains its meaning, even if $C_l > 3Nk$.

The preceding discussion shows, that several thermal properties show a temperature dependence at low and high temperatures which can be described in terms of the Debye model, provided the characteristic temperatures involved are suitably chosen. In the Debye case, one value of characteristic temperature is sufficient to describe the thermal properties at all temperatures. If, however, the experimental data indicate the need to use different values of the characteristic temperature in the above limiting cases, then this is an indication that a more elaborate model than the Debye model is needed. This turns out to be so practically always.

It is not possible to give a general discussion of the thermal behaviour of solids at intermediate temperatures. In fact, just at these temperatures the influence of the individual features of the lattice spectrum are most pronounced. Before discussing the intermediate range, however, we will give a review of the experimental data relevant to the present article.

5. Methods of Representing Specific Heat Data

For a comparison with the predictions of the Debye theory we require experimental values of the contribution of the lattice vibrations to the specific heat for the volume $V = V_0$. This limits the consideration to substances for which possible other contributions to the specific heat can satisfactorily be accounted for. Hence we will omit from the discussion

(a) solids showing phase transitions of any kind, such as martensitic transitions, higher order transitions, etc.,
(b) solids possessing other degrees of freedom (e.g. electronic excitation) not falling under (a) and for which no reliable correction is possible,
(c) solids in which anharmonicity effects are important (such as solid helium, which is treated elsewhere in this volume [6, 22].

The reduction of experimental values of C_p to values of C_v has to take place in various steps, which will briefly be described.

1. Reduction of C_p to C_v at Volume $V = V_0$

This reduction is carried out in two steps.

(a) The reduction of C_p to C_v at the actual volume by means of the thermodynamic formula

$$C_p - C_v = \alpha^2 V T / \varkappa. \tag{22}$$

If not all quantities in Eq. (22) are known, often the (approximate) formula of Nernst–Lindemann,

$$C_p - C_v = A C_p^2 T$$

can be used; the constant A has to be determined at one temperature for which the thermodynamic relation (22) can be used. Even this is not always possible and then recourse has to be taken to the more approximate formula

$$C_p - C_v = 0.0214\, C_p^2 T / T_s,$$

where T_s is the melting temperature.

(b) The next step should be the reduction of C_v at the actual volume to C_{V_0}, the value of C_v at the volume at the absolute zero. An estimate of the magnitude of this correction can be obtained in the following

way. From Eq. (19), assuming γ_T to be constant, and the thermodynamic relation $(\partial C_v/\partial V)_T = T(\partial(\alpha/\varkappa)/\partial T)_V$ it is easily found that

$$\frac{\Delta C_{V_0}}{C_{V_0}} = -\frac{T\gamma_T}{C_{V_0}}\left(\frac{\partial C_v}{\partial T}\right)\frac{\Delta V}{V_0},$$

where $\Delta V = V - V_0$. This correction is negligible at low temperatures ($\Delta V/C_{V_0} \to 0$) and at high temperatures ($\partial C_v/\partial T \to 0$). At $T \approx \theta_0$ we have for a metal such as copper $\theta_0 \approx 300$, $C_v \approx 3R$, $\Delta V/V_0 \approx 0.01$, $\partial C_v/\partial T = 0.3R\theta^2/T^3$ and consequently $\Delta C_v/C_{V_0} \approx -2.10^{-3}$; at $T \approx \theta_0/2$ we find $\Delta C_v/C_{V_0} \approx -4.10^{-3}$. For substances with a small thermal expansion $\Delta C_v/C_{V_0}$ is often much smaller than the values given for copper [25]. The uncertainty involved in the determination of θ_0 in our representation of the specific heat (see § 5.4) is usually larger than $\Delta C_v/C_{V_0}$ and hence for our purpose we can neglect this correction.

2. The Calculation of the Lattice Specific Heat

In many solids the specific heat contains contributions from causes other than the lattice vibrations. An example are metals; in which (to a first approximation) the conduction electrons give an additive contribution to F and hence to C_v. Another example is ferromagnetic materials in which the change of spontaneous magnetisation with temperature gives an additive contribution to C_v.

For metals we would expect theoretically at sufficiently low temperatures

$$C_{V_0} = AT^3 + aT, \tag{23}$$

where the first term gives the lattice contribution and the second term the contribution of the conduction electrons; A and a are constants. If therefore the experimental values of C_{V_0} at low temperatures satisfy Eq. (23), the first term is interpreted as the contribution C_l of the lattice waves and hence is used to calculate an experimental value of θ_0 [compare Eq. (8)]; the second term is interpreted as the contribution of the conduction electrons. It is customary to assume that also at higher temperatures the electronic contribution is given by aT, so that the calculation of C^{exp} is simple. This is often a reasonable assumption, but can lead to difficulties if a is exceptionally large, such as in Pd [47]. Then the correction to be applied in calculating C_l^{exp} from C_{V_0} becomes much more involved and may be impossible to carry out.

The change of spontaneous magnetisation in a ferromagnetic

substance should theoretically give a contribution proportional to $T^{3/2}$. Except possibly in the case of iron this effect must be expected to be negligible below room temperature [40, 41].

5.3. The Customary Representation of Values of C_l^{exp}

The mentioned difference in value between θ_0 and $\theta_\infty^{(c)}$ suggests the possibility of representing specific heat data at all temperatures by an effective characteristic temperature θ_{eff} which can be defined at each temperature as the value of θ in the Debye expression for the specific heat C_l^D which satisfies the relation

$$C_l^D(\theta/T) \equiv C_l^{\text{exp}},$$

where C_l^{exp} is the experimental value of C_l; θ_0 and $\theta_\infty^{(c)}$ then appear as the limiting values of θ_{eff} at low and high temperatures respectively. This, in fact, is the usual representation of specific heat data in terms of the Debye theory, which can easily be worked out with the existing tables of C_l^D as a function of θ/T.

Normally θ_{eff} is found to depend on temperature, approaching a constant value at low temperature, while at high temperatures the experimental evidence is not inconsistent with a constant value of θ_{eff} (which usually differs from the value at low temperatures). Curves of θ_{eff} as a function of temperature can be found in many places in the literature (for instance [5, 26]) and need not be reproduced here. For the purpose of comparing different substances sometimes reduced representations are used, such as a plot of $\theta_{\text{eff}}/\theta_0$ against T/θ_0 [27], and $\theta_{\text{eff}}/\theta_\infty^{(c)}$ against $T/\theta_\infty^{(c)}$ [28]. The first of these two representations certainly has to be preferred, as $\theta_\infty^{(c)}$ cannot be determined accurately as a rule and furthermore has a less simple physical meaning than θ_0.

Notwithstanding the widespread use of θ_{eff} for representing specific heat data, this method has serious disadvantages.

(a) The representation cannot be used at all at temperatures for which C_l^{exp} is larger than the equipartition value $3Nk$. This admittedly may not effect the discussion of the substances in the temperature range considered in particular in this paper, but it nevertheless seriously restricts the applicability of the usual representation in other cases.

(b) At temperatures of the order $T \approx \theta_0$ and higher, θ_{eff} becomes

very sensitive to small uncertainties in C_l^{exp}. We have in fact [compare Eq. (18)]

$$\frac{\delta\theta_\infty^{(c)}}{\theta_\infty^{(c)}} \approx -10\left(\frac{T}{\theta_\infty^{(c)}}\right)^2 \frac{\delta C_l^{\text{exp}}}{C_l^{\text{exp}}},$$

so that at $T=\theta_\infty^{(c)}$ an error of 1 % in C_l^{exp} causes a 10 % error in $\theta_\infty^{(c)}$. The situation becomes rapidly worse at higher temperatures, and therefore an accurate determination of $\theta_{(c)}^{\infty}$ is virtually impossible.

(c) In a sense the choice of C_l for determining θ_{eff} is arbitrary, because any other thermodynamic function could be chosen [29, 104].

(d) If the actual frequency density $g(\nu)$ rises in a certain frequency range above the Debye spectrum fitted to the actual spectrum at low frequencies (as is very often the case), the specific heat C_l rises above the value of $C_l^D(\theta_0/T)$ in a limited temperature range. The corresponding values of θ_{eff}, however, are then *lower* than θ_0. Conversely, if the specific heat C_l falls below C_l^D, the corresponding values of θ_{eff} are *larger* than θ_0. Therefore the relation between $g(\nu)$ and θ_{eff} is of a more complex nature than the relation between $g(\nu)$ and C_l.

It would be possible to remove the first two objections to the usual representation by using another thermodynamic function (such as the entropy [104] or the internal energy) to calculate θ_{eff}. The best choice of function is, however, often by no means clear. Further, the obtained values of θ_{eff} vary much less with temperature than the corresponding values obtained from C_l [29]. This is certainly no advantage if one is interested in studying the detailed relation between the theoretical frequency spectrum and the experimental data on thermodynamic quantities. It may be added that this situation does not constitute an argument in favour of the applicability of the Debye theory, but merely indicates that the chosen function is even less sensitive to details of the frequency spectrum than the specific heat. It seems therefore reasonable to look for a representation using the specific heat itself in a more satisfactory manner than in the usual representation.

5.4. An Improved Representation of Specific Heat Data

An improved representation based on the direct use of C_l^{exp} should not only meet at least some of the objections raised in § 5.3, but should also retain the favourable features of the usual representation,

viz. the new representation should be capable of being brought in a reduced form and indicate clearly the low temperature range in which the Debye approximation is valid.

One such procedure has been used by Hwang [15], who plotted $C_l^{\exp}/(T/\theta_0)^3$ against T/θ_0. Kapadnis and Hartmans [16, 17] (following a suggestion by C. J. Gorter) plotted $C_l^{\exp}/T^3$ as a function of T. These representations are admirably suited for illustrating the behaviour at low temperatures ($T \ll \theta_0$), but at high temperatures $C_l^{\exp}/T^3$ approaches zero. This makes the comparison in a wide temperature range of different substances difficult to carry out by using one graph at all temperatures.

In this paper we adopt another and (as far as we are aware) new procedure by plotting $C_r = C_l^{\exp}/C_l^D(\theta_0/T)$ against T/θ_0; θ_0 is determined from low temperature data and is used in the calculation of C_l^D. A wide temperature range is covered by using a logarithmic scale for T/θ_0.

Before discussing experimental data we will consider the general features of this representation in terms of some characteristic frequency spectra. If $g(\nu)$ is given by Eq. (3) for all frequencies (Debye case) the result is trivial: $C_r = 1$ at all temperatures. In all other cases C_r approaches the value one at sufficiently low temperatures and also at high temperatures, provided $C_l^{\exp}$ approaches the equipartition value. This we will assume here, and we then have at high temperatures

$$C_r = \frac{1 - \frac{1}{12}\frac{h^2}{k^2}\frac{\overline{\nu^2}}{T^2}}{1 - \frac{1}{12}\frac{h^2}{k^2}\frac{\overline{\nu^2}^D}{T^2}} = 1 + \frac{1}{12}\frac{h^2}{k^2}\frac{\overline{\nu^2}^D}{T^2}\left(1 - \frac{\overline{\nu^2}}{\overline{\nu^2}^D}\right) = 1 + \frac{1}{20}\frac{\theta_0^2}{T^2}\left(1 - \frac{\theta_\infty^{(c)2}}{\theta_0^2}\right),$$

where $\overline{\nu^2}^D$ is calculated using the Debye spectrum with characteristic temperature θ_0. Apart from the trivial case mentioned we have two possibilities; (a) $\overline{\nu^2}^D > \overline{\nu^2}$ or $\theta_0 > \theta_\infty^{(c)}$, and hence $C_r > 1$; (b) $\overline{\nu^2}^D < \overline{\nu^2}$ or $\theta_0 < \theta_\infty^{(c)}$, and $C_r < 1$. Case (a) is much more common than (b). At intermediate temperatures we can only tentatively conclude that if in a suitable frequency range $g(\nu) > g(\nu)^D$, there may be a range of T for which $C_r > 1$. If, however, in a suitable range $g(\nu) < g(\nu)^D$ we can have $C_r < 1$.

These various possibilities can be illustrated by considering the typical frequency spectra sketched in Fig. 1, together with the Debye spectrum, $g(\nu)^D$, obtained by extrapolation of the low frequency part

of the spectra. (Other examples can be found in the literature [76, 79]). The scales along the frequency axis have been chosen in such a way for the different spectra, that the same Debye curve can be used in all cases. A spectrum of type *I* is characteristic for many cubic face

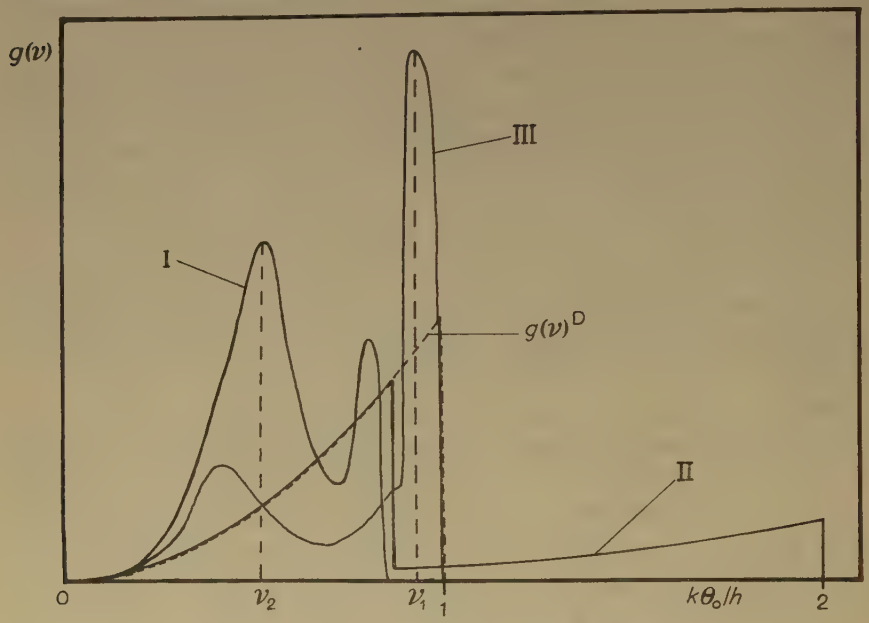

Fig. 1. Some examples of frequency spectra.

centred and body centred metals such as copper and tungsten. Here we have $\overline{\nu^{2D}} > \overline{\nu^2}$ and hence at high temperatures we find $C_r > 1$. At intermediate frequencies the spectrum rises well above the Debye spectrum and we would expect at average temperatures also $C_r > 1$. At low temperatures we must have $C_r = 1$ and hence a maximum in the curve of C_r as a function of T/θ_0 seems probable. The case of copper (Fig. 2) fits into this picture.

An example for which $g(\nu) < g(\nu)^D$ at all frequencies is spectrum II in Fig. 1, which represents the Brillouin spectrum for an isotropic solid. It is assumed here that both the transverse and longitudinal waves have a Debye spectrum with the same cut off wavelength, which as a consequence of the different velocity of propagation leads to a different cut off frequency for the two types of waves. We find in this case that $C_r < 1$ at all temperatures as is illustrated in Fig. 2, assuming that $(\nu_m)_{\text{trans}} \approx \frac{1}{2}(\nu_m)_{\text{long}}$. A more realistic spectrum for which

$\overline{\nu^2} > \overline{\nu^{2D}}$ is spectrum III in Fig. 1, which is characteristic for cubic elements with a diamond structure [62]. At high temperatures we would expect $C_r < 1$, while at intermediate temperatures the hump in the frequency curve at intermediate frequencies would lead us to expect

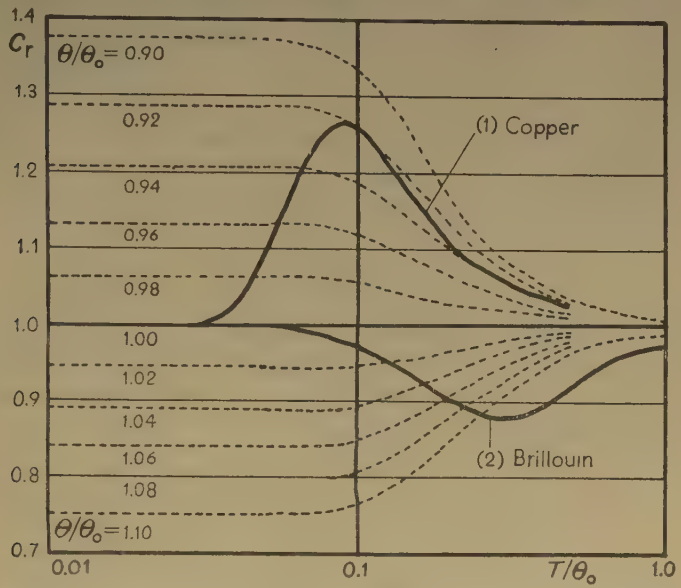

Fig. 2. The relation between C_r and θ_{eff}. Curves of constant θ/θ_0 are shown dashed.

$C_r > 1$. This is in fact the behaviour found for the elements silicon and germanium (compare Fig. 4).

The simple qualitative relation between the frequency spectrum and the general features of the present representation can be used with advantage in the discussion of experimental specific heat data.

We finally have to discuss the relation between the usual and the present representation. For this purpose we have drawn in Fig. 2 curves of the ratio of two Debye functions, $C_l^D(\theta)/C_l^D(\theta_0)$, against T/θ_0, for different values of the ratio of characteristic temperatures. These curves represent curves of constant θ/θ_0 in our representation. The general shape of these curves can easily be understood from the general behaviour of a Debye function. At very low temperatures the ratio of two Debye functions is constant, the value of the ratio depends on the ratio of the characteristic temperatures. At high temperatures $C_l^D(\theta)/C_l^D(\theta_0) \to 1$. Our curve for copper can now be

interpreted in terms of θ_{eff} in the following way. At low temperatures up to $T/\theta_0 \approx 0.03$, θ_{eff} is constant, then θ_{eff} decreases and reaches a minimum value for $T/\theta_0 \approx 0.1$. Finally at $T/\theta_0 \approx 0.2$, θ_{eff} reaches a constant value which is, however, lower than the value of θ_0. It must further be noted that the maximum of C_r for copper does not exactly correspond to the minimum value of θ_{eff}. This would be the case only if the maximum in appeared at a temperature for which $T/\theta_0 < 0.05$. The crowding together of the curves $\theta/\theta_0 = \text{constant}$ at temperatures above $T/\theta_0 \approx 0.2$ illustrates the sensitiveness of the value of θ_{eff} for small uncertainties in the value of C_l^{exp}.

The uncertainty in the values of C_r is given by

$$\frac{\delta C_r}{C_r} = \frac{\delta C_l^{\text{exp}}}{C_l^{\text{exp}}} - \frac{\delta C_l^D}{C_l^D},$$

where the first term describes the uncertainty in the experimental data and the second term the uncertainty of the fit of the Debye function to the low temperature part of the experimental data. Expressed in terms of θ_0 we have

$$T > \theta_0 \quad \frac{\delta C_l^D}{C_l^D} = -0.1 \left(\frac{\theta_0}{T}\right) \frac{\delta\theta_0}{\theta_0},$$

$$T \ll \theta_0 \quad \frac{\delta C_l^D}{C_l^D} = -3 \frac{\delta\theta_0}{\theta_0}.$$

Clearly at high temperatures the uncertainty in C_r is caused mainly by the uncertainty in the experimental data at high temperatures, whereas at low temperatures the uncertainty in θ_0 can play an important role; this should be considered in each case individually. At intermediate temperatures a numerical estimate of $\delta C_l^D/C_l^D$ is possible; the value of this quantity lies between the limiting values just given.

6. Experimental Data on the Lattice Specific Heat

In this § we give a survey of experimental results on the lattice specific heat, C_l^{exp}, for which consistent data are available in a wide temperature range (between $T \approx 0.01\,\theta_0$ and $T \approx \theta_0$). We confine ourselves to substances of simple crystal structure, for which some comparison with theory is possible, viz. substances with cubic and hexagonal close-packed structures (ideal and distorted), cubic body centred structure and diamond structure.

The arrangement of the elements is based on their place in the periodic table. This seems to be the simplest way of illustrating some

general features in their behaviour, although several exceptions do occur. A classification according to their crystal structure seems to have no advantages over the arrangement chosen here. A survey of the elements discussed is given in Table I.

The data themselves are represented in the form of plots of C_r against T/θ_0, whereas a survey of the crystal structure, value of θ_0,

TABLE I
Elements discussed

Column *	II, II*b*	III	IV, IV*b*	IV*a*	V*a*	VIII *a*	VIII *b*	VIII *c*	VIII *d*
	Be	—	C (diam)	—	—	—	—	—	—
	Mg	Al	Si	—	—	—	—	—	—
	Zn	—	Ge	Ti	—	Fe	Co	Ni	Cu
	Cd	—	Sn	—	—	—	Rh	Pd	Ag
	—	—	—	—	Ta	—	Ir	Pt	Au
	—	—	—	Th	—	—	—	—	—
Fig.	3	9	4	5	9	9	6	7	8
Table	II	VI	III	IV	VI	VI	V	V	V

* Periodic Table

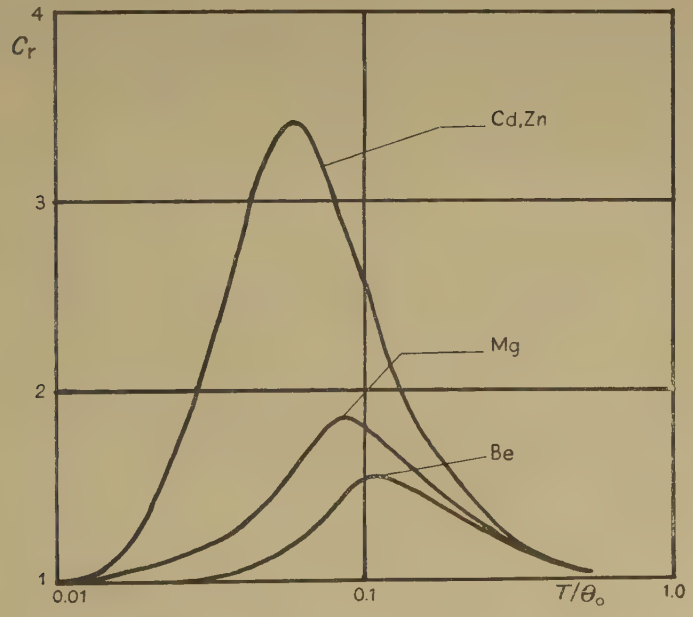

Fig. 3. Elements of Column II, II*b*.

value of a is given in tables. No attempt is made to indicate the accuracy; for this the original papers should be consulted. References are usually restricted to recent work; many references to work prior to 1952 can be found in Schifman's report [21]. Three unsatisfactory examples have been included, viz. platinum, tantalum and iron. Several similar cases have been omitted: chromium [32, 67, 68], vanadium [35, 44, 69, 70], hafnium [35, 44, 71], thallium [72, 73], tungsten [35, 44, 74, 75], molybdenum [35, 44, 94, 95], zirconium [35, 44, 96, 97], rhenium [55, 44, 93, 98] and lead [52, 100, 101, 102].

TABLE II

Elements from Columns II, IIb (Fig. 3)

Element	Structure	c/a	θ_0 (°K)	Range (°K)	$10^4 \times a$ (cal/°)	References
Beryllium	hcp *	1.58	1160	4–300	0.54	Hill and Smith [55]
				273–1173		Ginnings, Douglas and Ball [56]
Magnesium	hcp	1.62[5]	406±10	1–20	3.15	Smith [57]
				12–320		Graig *et al.*[58]
Zinc	hcp	1.86	306	1.5–4	1.5	Daunt and Silvidi [59]
				4–20		Smith [57]
				12–200		Clusius and Harteck [60]
Cadmium	hcp	1.88	188	1–20		Wolcott [35]
				1–20	1.50	Smith [61]
				12–320		Craig *et al.* [58]

* hexagonal close packed.

Remarks Table II

Magnesium: The values of C_v have been calculated from the table of θ_{eff} in Smith's paper [57]. *Zinc and Cadmium*: Within the experimental accuracy the curves of zinc and cadmium (Fig. 3) coincide.

Remarks Table III

Diamond: The chosen value of θ_0 has been calculated from elastic data by Smith [62]. Pitzer's [63] values of the specific heat would seem to be more reliable than the values of Desorbo [64]. Evidently new measurements are highly desirable. *Silicon*: According to P. H. Keesom (private communication) measurements in progress suggest a lower value of θ_{eff}, ($\theta_0 \approx 630°$ K). This would bring the curve for silicon below the curve of germanium against theoretical expectation. For the time being we can only use the value chosen. *Germanium*:

There is a slight discrepancy (maximally 3 % at $T/\theta_0 \approx 0.25$) between Hill and Parkinson's [27] and Esterman and Weertman's [99] values for temperatures above $T \approx 0.18\,\theta_0$. Otherwise the agreement in the common temperature range is very good.

TABLE III
Elements from Columns IV, IV*b* (Fig. 4)

Elements	Structure	θ_0 (°K)	Range (°K)	References
Diamond	Diamond	930 [62]	70–300	Pitzer [63]
			20–300	De Sorbo [64]
Silicon	Diamond	658	1–100	Pearlman and Keesom [65]
			60–300	Anderson [66]
Germanium	Diamond		5–160	Hill and Parkinson [27]
		360	2–4	Keesom and Pearlman [28]
			20–200	Esterman and Weertman [99]
Grey Tin	Diamond		7–160	Hill and Parkinson [28]
		216	1.5–4	Webb and Wilks [84]

TABLE IV
Elements from Column IV*a* (Fig. 5)

Element	Structure	c/a	θ_0 (°K)	Range (°K)	$10^4 \times a$ (cal/°)	References
Titanium	hcp	1.60	430	1.2–20	8.5	Wolcott [35, 44]
				15–305		Johnston and Kothen [86]
Thorium	cfc*	—	170	1–20	11.2	Smith and Wolcott [87]
				20–300		Griffel and Skochdople [88]

* cubic face centered.

Remarks Table IV

Titanium: Wolcott's [35, 44] and Johnston and Kothen's [86] values connect smoothly, except for J. and K's value at 15° K.

Remarks Table V

Cobalt: The agreement between the measurements of Clusius and Schachinger [40] and Duyckaerts [41] is excellent in the region of overlap. The influence of the spontaneous magnetisation is negligible [40, 41].

Nickel: Only fairly old measurements are available below 20° K [46]. It cannot be excluded that the values $C_r < 1$ are fortuitouts. *Palladium*: The representation of the electronic specific heat by aT is probably

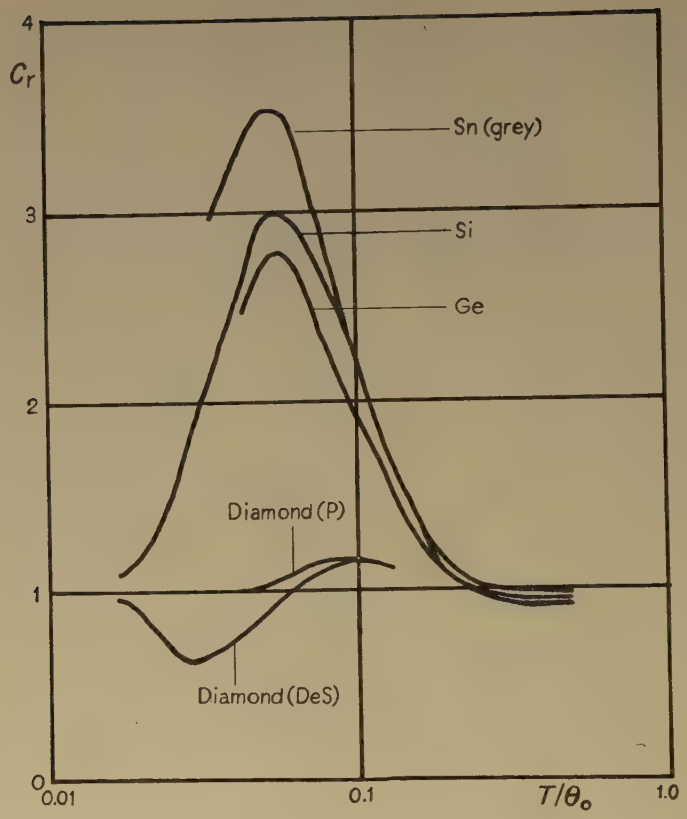

Fig. 4. Elements of Column IV, IV*b*.

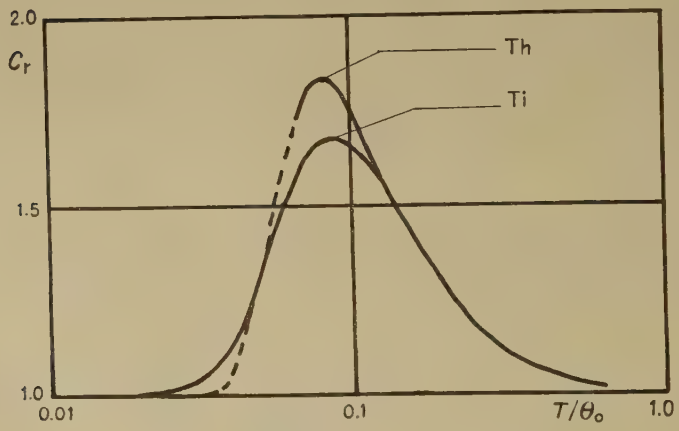

Fig. 5. Elements of Column IV*a*.

incorrect for the higher temperatures [47]. Taken Clusius's values of C_v [47]. *Platinum*: Example of bad agreement between different sets of experiments. New measurements above 1° K in a wide temperature range are very much needed.

TABLE V

Elements from Column VIII (Fig. 6, 7, 8)

Element	Structure	c/a	θ_0 (°K)	Range (°K)	$10^4 \times a$ (cal/°)	References
Cobalt	hcp	1.633	443	2–18	12.0	Duyckearts [41]
(Fig. 6)				15–270		Clusius and Schachinger [40]
Rhodium	cfc	—	478	1.2–20	11.7	Wolcott [35, 44]
(Fig. 6)				10–273		Clusius and Losa [43]
Iridium	cfc	—	420	1.2–20	7.5	Wolcott [35, 44]
(Fig. 6)				10–273		Clusius and Losa [43]
Nickel	cfc	—	413	1–19	17.4	Keesom and Clark [46]
(Fig. 7)				15–300		Busey and Giauque [45]
Palladium	cfc	—	275	1–22	(31.0)	Pickard and Simon [48]
(Fig. 7)				13–269		Clusius and Schachinger [47]
				< 1		Rayne [33]
Platinum	cfc	—	233	2–20	16.1	Kok and Keesom [50]
(Fig. 7)				17–300		Simon and Zeidler [49]
				< 1		Rayne [33]
Copper	cfc	—	335	1.8–4.2	1.80	Esterman *et al.*[32]
(Fig. 8)				1–5		Corak *et al.*[31]
				1.5–20		Wolcott [35]
				< 1		Rayne [33]
				15–300		Meads *et al.*[30]
Silver	cfc	—	225	1–4	1.58	Keesom and Pearlman [37]
(Fig. 8)				1–5		Corak *et al.*[31]
				< 1		Rayne [33]
				15–300		Meads *et al.*[36]
Gold	cfc	—	165	1–5	1.78	Corak *et al.*[31]
(Fig. 8)				1.5–20		Wolcott [35]
				15–300		Geballe and Giauque [39]

Remarks Table V (continued)

Copper: A table of values of θ_0 can be found in Corak *et al's* paper [31]. Esterman's [32] and Kok and Keesom's [34] value of θ_0 are the same.

TABLE VI

Miscellaneous elements (Fig. 9)

Element	Col.	Structure	θ_0 (°K)	Range (°K)	$10^4 \times a$ (cal/°)	References
Aluminium	III	cfc	419	1–20	3.48	Kok and Keesom [51]
				15–300		Meads *et al.*[30]
Tantalum	V*a*	cbc*	245	1.2–20	14.0	Wolcott [35, 44]
				1–4.5		Keesom and Desirant [89]
				10–273		Clusius and Losa [90]
Iron (*a*)	VIII*a*	cbc	462	1.5–20	12	Keesom and Kurrelmeyer [91]
				16–206		Eucken and Werth [92]
				54–296		Kelly [93]

* cubic body centered.

TABLE VII

	Diamond	Silicon	Germanium
v_2/v_1	0.58	0.26	0.34
h_2/h_1	0.22	0.75	0.61

TABLE VIII

	Copper	Silver	Gold
S	3.21	2.89	2.86
σ	0.434	0.426	0.455
v_l/v_s	2.93	2.78	3.47

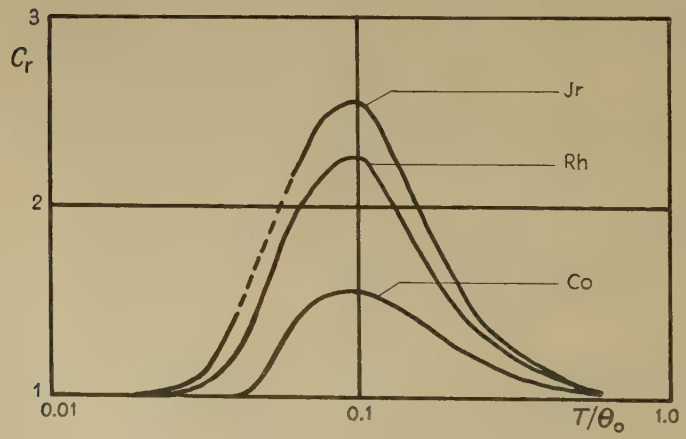

Fig. 6. Elements of Column VIII*b*.

According to Wolcott [44] the specific follows heat a Debye curve until $T/\theta_0 \approx 0.03$. *Silver*: The values of θ_0 given by Keesom and Kok [38], and Keesom and Pearlman [37] agree very well. *Gold*: A Debye curve is followed until $T/\theta_0 = 0.11$ ($T = 18°$ K) [35]. There is excellent agreement between the values of θ_0 given by Corak *et al.* [31] and Wolcott [35].

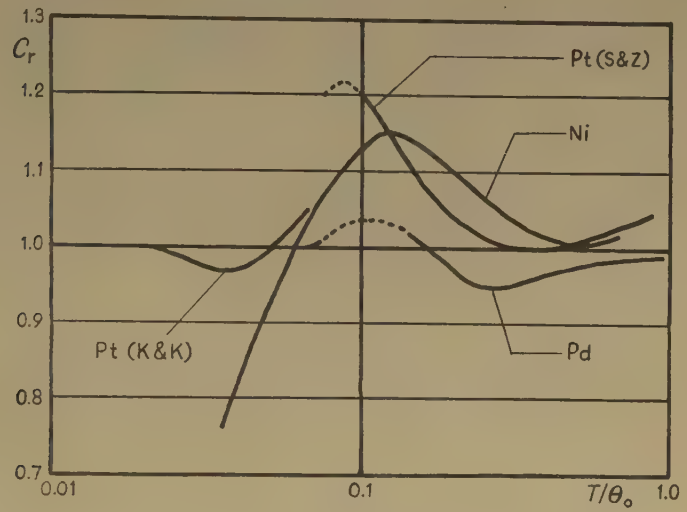

Fig. 7. Elements of Column VIIIc.

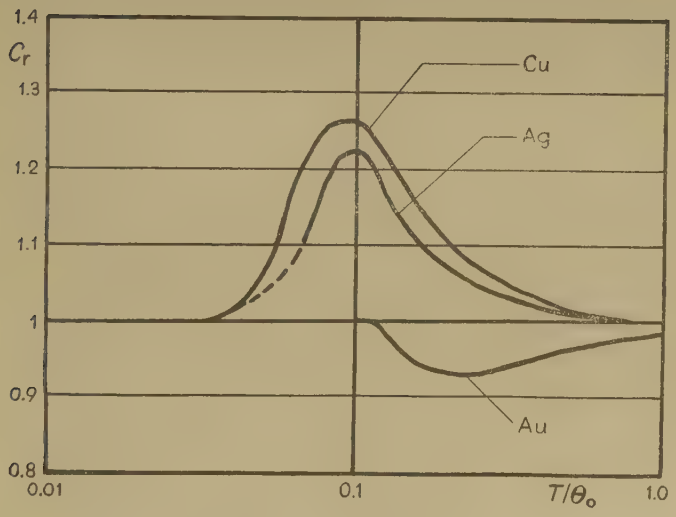

Fig. 8. Elements of Column VIIId (or Ib).

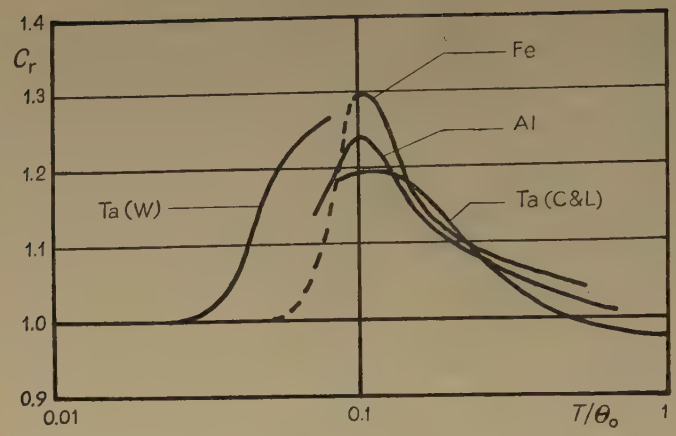

Fig. 9. Miscelaneous elements.

7. Discussion

In this § we will discuss the experimental results presented in § 6 n terms of theoretical conclusions based on lattice dynamics. A qualitative discussion is sufficient for the purpose of this article; details of the theory can be found elsewhere [76, 77, 78].

7.1. It is simplest to treat a solid as an elastic, isotropic continuum, taking into account the atomicity of a (finite) piece of solid by the introduction of a finite maximum frequency. In the Debye theory the two possible types of elastic wave (for a given direction one longitudinal wave and two transverse waves) are assumed to have the same maximum frequency (compare § 3). This theory, however, contains an inconsistency [76, 78], as can be seen by considering Eq. (3a). In this case the number of longitudinal waves and the number of transverse waves are in the ratio $1/v_l^3 : 2/v_t^3$. For most metals we have $v_l \approx 2v_t$ so that in the Debye spectrum the longitudinal waves are largely suppressed. It is more consistent to treat the two types of waves separately and to require that the numbers of longitudinal and transverse waves are in the ratio of 1 : 2, while the maximum frequencies are determined by the same (minimum) cut-off wavelength (Brillouin model [78]). The resulting spectrum for $v_l \approx 2v_t$ (and hence $(\nu_m)_l \approx 2(\nu_m)_t$) is given in Fig. 1. A comparison between curve (2) in Fig. 2 and the large majority of the other curves in § 6 indicates, that the Brillouin model is hardly, if at all, better than the Debye

model for explaining specific heats. No noticeable improvement results if the continuum model of Brillouin is extended by taking into account the elastic anisotropy.

The development of lattice dynamics has shown unambiguously that it is essential to take the lattice structure of solids into account. In particular, for the high frequencies, or in other words, for wave lengths which are comparable with the interatomic distances, the influence of the lattice is very marked and causes the frequencies to be smaller than the values predicted by the elastic theory for the same wavelength. This dispersion of the lattice waves causes the spectrum to be compressed towards smaller frequencies, in such a way that the higher frequencies are shifted more than the lower frequencies. The details of the resulting spectrum can only be found by considering each case separately and depend on the crystal structure and the characteristics of the interatomic forces. Often the calculations are carried out taking into account only forces between an atom and its neighbours and next nearest neighbours. The corresponding force constants are usually fitted to elastic data and hence elastic anisotropy is automatically taken into account.

As in the Brillouin case, the lattice dynamically estimated spectra are characterised broadly speaking by two maxima, which are usually much more pronounced and (as discussed above) displaced to lower frequencies. In the case of all elements of simple structure discussed theoretically (silver [80], tungsten [81], lithium [13], diamond [62], silicon [82], germanium [82]) the low-frequency maximum rises above the low-frequency Debye spectrum and hence should cause a maximum in a C_τ versus T/θ_0 curve. The shape, height and position of the high-frequency maximum has an important influence on $\overline{\nu^2}$ and may cause either $\overline{\nu^2} < \overline{\nu^2}^D$ or $\overline{\nu^2} > \overline{\nu^2}^D$. Examples of this first case are silver[80], tungsten [81]; examples of the second case are: silicon and germanium [82].

7.2. We will now consider the experimental results given in § 6 against this background. With the exceptions of the diamond structure elements, gold and palladium, (which will be discussed separately) all elements show a maximum of C_τ at a temperature of about $0.1\,\theta_0$ or lower, whereas at higher temperatures ($T \approx \theta_0$), $C_\tau > 1$. Clearly the vibration spectra of such elements rise above the low-frequency Debye spectrum and furthermore we find $\overline{\nu^2} < \overline{\nu^2}^D$. Quite likely therefore the spectra are of the type 1 in Fig. 1.

No systematic influence of the crystal structure is obvious for the cubic closed packed, ideally hexagonal closed packed ($c/a = 1.633$) and cubic body centred elements. The maximum in C_v occurs always very near $T/\theta_0 = 0.1$; the height varies considerably, but not in any way clearly related to the crystal structure. In the case of the diamond structure elements the maximum occurs at temperatures as low as $T/\theta_0 \approx 0.05$. This may be primarily a consequence of the crystal structure, although the characteristics of the interatomic forces no doubt have an important influence (see below). The metals in the sequence Be, Mg, Zn, Cd have structures which deviate progressively from the ideal hexagonal close packing, as can be seen from their c/a values. This is accompanied by a shift of the maximum of C_v to lower temperatures and it seems possible that this shift is primarily caused by the change in crystal structure. There is, however, other evidence, that also the elastic anisotropy (in particular for zinc and cadmium) may play an important role.

7.3. In general, however, the importance of elastic anisotropy has been over-emphasised and over-simplified [78]. It must, in fact, be expected that the elastic anisotropy (which is measured for long waves) has not a simple relation with properties of solids which are largely determined (except at very low temperatures) by the short waves; these waves deviate considerably from the elastic waves in a continuum. That no such relation exists in many cases follows from a scrutiny of the anisotropy factor $S = 2C_{44}/(C_{11} - C_{12})$ (compare Table IX) and the Fig. 4 and 8. On the other hand, for Zn and Cd the (macroscopic) elastic anisotropy is so large, that it can be treated as an overriding influence on various thermal properties, such as the thermal expansion [1]. Apparently waves in the direction parallel to the hexagonal axis are very much easier excited than in the perpendicular direction. The frequency spectrum of such a crystal would presumably be characterised by a large concentration of frequencies for low values of the frequency. This then could explain a large maximum of C_v at low temperatures ($T/\theta_0 \approx 0.05$), such as is found for zinc and cadmium.

7.4. It will be noted that in several of the figures the height of the maximum of C_v increases with the atomic number, whereas there is also a simultaneous tendency for the maximum to shift to lower

temperatures (excluding gold and palladium). The only available theoretical calculations of the frequency spectra of elements in one column of the periodic table have been carried out for diamond [62], silicon [82] and germanium [82]. The salient features of the very similar spectra are given in Table 7, where ν_2/ν_1 is the ratio of the frequencies of the low frequency and the high frequency maximum of the spectrum respectively (see Fig. 1) and h_2/h_1 is the ratio of the corresponding heights. Taking these figures at their face value, one might expect the maxima of C_τ to shift to higher temperature in the sequens silicon, germanium, diamond (with the larger shift between germanium and diamond), whereas the height of the maximum in C_τ should increase in the order diamond, germanium, silicon (with the largest difference in height between diamond and germanium). The experimental data given in Fig. 4 are in qualitative agreement with this. It should be remembered, however, that the experimental results are not entirely satisfactory (compare § 6), consequently we cannot exclude the possibility of a fortuitous agreement. In any case it would seem, however, that the chosen representation of the lattice specific heat is able to reveal several details of the frequency spectrum which do not become apparent in the representation by a temperature dependent θ_{eff}.

7.5. The data represented in Fig. 3, 5, 6 and (possibly) 7 indicate that the maximum in C_τ becomes progressively higher for the heavier elements in each column of the periodic table. In Fig. 3, 5, 6 and perhaps (excluding Pd) 7 there is a simultaneous tendency of shift to lower temperatures. Thus it seems likely that the low frequency maximum in the spectra becomes progressively higher and shifts to lower frequencies.

There are some theoretical indications that this may be caused by a relative increase in next neighbour interaction. For instance, the next neighbour interaction is stronger in silicon than in germanium. Further, an increase of next neighbour interaction causes an increase of height and a shift towards lower frequency of the lower frequency maximum [82]. Montroll [83] found a similar behaviour in the case of a cubic body centred substance; in the case of a simple cubic lattice, the low frequency maximum increases in height, but shifts to higher frequencies. Further theoretical calculations may clarify the situation.

7.6. The metals gold and palladium clearly must have a frequency spectrum, which deviates considerably from that of the other elements. This can certainly not be explained in terms of elastic anisotropy; copper, for instance, is considerably more anisotropic than gold. It may be revealing however, to consider the Poisson ratio σ in the direction of a cubic axis of copper, silver and gold (Table 8). Treating the solid simply as a continuum we find for gold $v_l/v_t = 3.5$, for copper $v_l/v_t = 2.9$ and for silver $v_l/v_t = 2.8$. A Brillouin type frequency spectrum for gold should therefore extend relatively much further beyond the Debye limit than in the cases of copper and silver. Presumably the dispersion of the lattice waves in gold is not large enough to cause the spectrum of gold to rise above the low temperature Debye spectrum, whereas in copper and silver the usual situation exists. A similar situation may occur in palladium.

7.8. No attempt has been made to represent data at temperatures above $T = \theta_0$. A discussion of the specific heat at higher temperatures would certainly be of interest, but cannot be carried out unless very accurate experimental data are available, which is not so at present (compare § 1).

8. The Representation of Thermal Expansion Data

In §§ 2, 3, 4 we gave a general discussion of the relations between the thermal expansion coefficient and the specific heat. Characteristic for the Debye theory is a constant value of $\gamma_T (= \gamma_0)$. Here we will discuss the representations of thermal expansion data allowing a check of the Debye result. For a proper understanding it will be useful to give first an outline of Grüneisen's theory [1].

8.1. Grüneisen's first Formula

For simplicity we will write Eq. (1) in the form

$$F = \Phi + F_t(V, T).$$

The volume at any temperature is supposed to be given by

$$P = -\partial F/\partial V = 0,$$

or by

$$\Phi' = \partial F_t/\partial V (= P_t); \tag{23}$$

P_t can be called the thermal pressure. Following Grüneisen we now expand both sides of Eq. (23) in powers of $\delta(=(V-V_0)/V_0)$, we have $\Phi'(V_0)=0$)

$$\Phi''\delta+\tfrac{1}{2}V_0\Phi'''\delta^2+\ \ldots\ =(P_t/V_0)+(\partial P/\partial V)\delta+\ \ldots, \tag{24}$$

in which Φ'', Φ''', P_t and $\partial P/\partial V$ must be taken at $V=V_0$.

Retaining only terms up to δ^2 we find

$$\delta=\frac{P_t}{V_0\Phi''\left(1+\frac{\Phi'''}{2(\Phi'')^2}P_t-\frac{1}{\Phi''}\frac{\partial P_t}{\partial V}\right)}. \tag{25}$$

This is a generalised form of Grüneisen's first equation, in which Eq. (25) can be transformed by assuming

$$P_tV=\Gamma_tE_T, \tag{26}$$

where Γ_T only depends on T and E_T is the thermal energy, $E_T=\int_0^T C_v dT$. It is not difficult to show that Eq. (26) is satisfied in the Debye theory. From Eq. (26) we find (valid for any volume)

$$\frac{\partial P_t}{\partial V}=-\frac{\Gamma_T(\Gamma_T+1)}{V^2}E_T+\frac{\Gamma_T^2}{V^2}TC_V.$$

At constant volume, $V=V_0$, we have at low temperature $E_T\infty T^4$ and at high temperatures $E_T\infty T$ so that in these limiting cases $\partial P_t/\partial V\infty E_T$. We shall assume this to be so at all temperatures. We can now write instead of Eq. (25)

$$\delta=\frac{\varkappa_{00}\Gamma_T}{V_0}\frac{E_T}{1-bE_T}, \tag{27}$$

where b is a small constant. This is Grüneisen's first equation which is valid under the mentioned assumptions as long as $bE_T\ll 1$. Grüneisen [1] only considered the Debye case, for which Γ_T constant. Then we would have (neglecting bE_T in the denominator) $\delta\infty E_T$, which is often called Grüneisen's first rule. The conclusion $\Gamma_T=$ constant, however, is characteristic for the Debye theory and the Grüneisen theory alike and hence is considered here as the first Grüneisen rule. If $F_t(V,T)$ is only due to lattice vibrations, which we will assume unless stated otherwise, also E_T refers to the *lattice waves*.

8.2. Grüneisen's Second Formula

The expansion coefficient at $P=0$ is found by differentiation of Eq. (27) with respect to T. We find

$$\alpha = \frac{\varkappa_{00}}{V_0}\,\gamma_T\,\frac{C_l}{(1-bE_T)^2}, \tag{28}$$

where

$$\gamma_T = \Gamma_T + (1/C_l)\,(1-bE_T)\,E_T\,(\mathrm{d}\Gamma_T/\mathrm{d}T). \tag{29}$$

If γ_T is independent of T, Eq. (28) is Grüneisen's second formula. Then we have (neglecting as in § 8.1) bE_T in the denominator) $\alpha \propto C_l$ which is often called Grüneisen's second rule, or briefly: Grüneisen's rule. For the reasons given near the end of § 8.1, however, we take the Grüneisen rule to imply γ_T is independent of T.

It is important to note [see Eq. (29)] that in general $\gamma_T \neq \Gamma_T$. Only if $\Gamma_T'=0$ we have $\Gamma_T=\gamma_T$; this is so if the Grüneisen rule is valid. Furthermore, then Eq. (19) and (28) are identical; hence we have

$$\frac{\varkappa}{V} = \frac{\varkappa_{00}}{V_0}\,(1-bE_T)^{-2} \simeq \frac{\varkappa_{00}}{V_0}\,(1+2\,bE_T). \tag{30}$$

This relation is useful when carrying out a check of the Grüneisen rule.

8.3. The Use of Grüneisen's First Formula

A check of the constancy of γ_T or Γ_T involves a check of Eq. (28) and (27), but not necessarily a calculation of γ_T or Γ_T. Several checks have been carried out in the literature; some have been discussed by Hume–Rothery [18].

The most straight forward check of Eq. (27) would appear to be to rewrite Eq. (27) in the form

$$\frac{1}{\delta} = \frac{V_0}{\varkappa_{00}\,\Gamma_T}\left(\frac{1}{E_T} - b\right). \tag{31}$$

A linear relation between $1/\delta$ and $1/E_T$ (E_T should be calculated from experimental data) would indicate a constant value of $V_0/\varkappa_{00}\Gamma_T$ and hence of Γ_T; $V_0/\varkappa_{00}\Gamma_T$ and b could then be obtained from a plot of $1/\delta$ as a function of $1/E_T$. Γ_T could then be calculated using Eq. (30) and the experimental value of $\varkappa/V$ obtained at room temperature. This method, however, does not seem to have been used in literature.

Hume–Rothery [18] carried out a check of Eq. (27) by taking values of b from Grüneisen's work [1] and by determining $Q_0(=V_0/\varkappa_{00}\Gamma_T)$ by trial and error; Q_0 is assumed to be constant. In this way good

agreement was found for the volume as a function of temperature (obtained from X-ray data) of a number of cubic metals, e.g. copper, silver and aluminium between 20° K and about 900° K.

The actual determination of Q_0 has given rise to a certain amount of confusion. Assuming $\gamma_T = \Gamma_T$ several authors calculated Q_0 from the equation defining Q_0, using for γ_T the value obtained from Eq. (19) by taking experimental values for α, $\varkappa$, V and C_l. Then in Eq. (27), E_T was represented by a Debye function, in which θ was appropriately chosen. By this procedure Q_0 could easily be 5–20 % in error and hence often the used value of θ deviated considerably from the (roughly constant) value giving a reasonable representation of the specific heat (e.g. [103]). As Hume–Rothery rightly points out, this check of the first Grüneisen relation cannot be considered as satisfactory.

A more satisfactory way of calculating follows from Eq. (19) and (30). We easily find

$$Q_0 = \frac{C_l}{\alpha}(1 + 2\,bE_T). \tag{32}$$

This relation was used by Simon and Vohsen [105], who however replaced C_l by an experimental value of C_p. By doing this, Q_0 appears to depend on the temperature at which α, C_p and E_T have been taken. It would seem, that Hume–Rothery's method, or the use of Eq. (31) is preferable for a check of the constancy of Γ_T.

It should be pointed out however, that for work at low temperatures a treatment based on Eq. (27) has a serious practical disadvantage not related to the previous discussion. If T_0 is the lowest temperature of measurement of the volume, then we can derive from experiment

$$\frac{V - V_{T_0}}{V_{T_0}} \simeq \frac{V - V_0}{V_0} - \frac{V_{T_0} - V}{V_0} = \delta - \delta_{T_0};$$

similarly we can only observe differences in thermal energy. So there are two possibilities: (a) δ and E_T are calculated by an extrapolation of δ_{T_0} and E_{T_0} * to 0° K, or, (b) δ_{T_0} and E_{T_0} are neglected. Both procedures are allowed if $T \gg T_0$, but become meaningless if $T \simeq T_0$. In the last case therefore Eq. (27) cannot be used, and it is better to take recourse to Eq. (28).

---

* The extrapolation of E_T can be carried out if the specific heat is measured down to the range where $C_l \infty T^3$.

8.4. The use of Grüneisen's Second Formula

A straightforward check can be based on Eq. (28) written in the form

$$(C_l/\alpha)^{1/2} = (V_0/\varkappa_{00}\,\gamma_T)^{1/2}\,(1-bE_T), \tag{33}$$

or (if $bE_T \ll 1$)

$$\alpha/C_l = (\varkappa_{00}\,\gamma_T/V_0)\,(1+2\,bE_T)\,. \tag{33a}$$

If $\gamma_T = \Gamma_T =$ constant, Eq. (32) and (33a) are identical.

If $\gamma_T =$ constant, $(C_l/\alpha)^{1/2}$ or α/C_l (if $bE_T \ll 1$) should be a linear function of E_T. Eq. (33) has been used by Zemansky [106] and Rubin *et al.* [107] taking C_v for C_l. Eq. (33a) has been used by Rubin *et al.* replacing C_l by C_p. No attempt was made by these authors to calculate γ_T.

Grüneisen [1] applied Eq. (28) to average coefficients of thermal expansion and obtained values of $V_0/\varkappa_{00}\gamma_T$ and b, assuming $V_0/\varkappa_{00}\gamma_T$ and b to be constant. If b is known, the calculation of γ_T can be carried out, using room temperature values (indicated by subscript $_{RT}$) for $\varkappa$ and V by means of the relation

$$\alpha = \frac{\varkappa_{RT}}{V_{RT}}\,(1-2\,bE_{RT})\,(1+2\,bE_T)\,\gamma_T\,C_l \text{ [85]},$$

which is easily derived from Eq. (28) and (30).

9. Discussion

9.1. Rigorous checks of the constancy of Γ_T and γ_T have been carried out by a few investigators [18, 20, 106, 107, 85]. The Grüneisen rule ($\gamma_T =$ constant) appears to be valid for several cubic substances (copper [18, 20, 107], silver [18, 20], iron [18, 20], aluminium [18, 20], potassium bromide [20] at temperatures between $T \approx 0.4\,\theta_0$ and (maximally) $T \simeq 1.5\,\theta_0$. However, in a number of cubic substances (copper [20, 85], silver [20], iron [20], aluminium [20, 85], potassium bromide [20]) γ_T decreases with decreasing temperature below $T \approx 0.3\,\theta_0$. Although the experiments have not been extended to sufficiently low temperatures to show another constant value of γ_T viz. γ_0, the results clearly indicate that γ_∞ and γ_0 are different. This could be expected on general grounds (compare § 4).

The physical implication of this is easily seen by considering Eq. (20). Only if $\gamma(\nu)$ is independent of ν we would have $\gamma_T =$ constant. A temperature dependent γ_T implies according to Eq. (20) different values of $\gamma(\nu)$ for different frequencies; γ_T then appears to be a weighted

average of the $\gamma(\nu)$. It further implies, that the shape of the lattice spectrum is affected by a volume change. A theoretical calculation of γ_T as a function of T requires a lattice dynamical treatment, such as has been given by Born [10] (for alkali halides) and Barron [23] (cubic face centred lattice). The results of this theoretical work are in qualitative agreement with the experimental decrease of γ_T with decreasing temperature.

9.2. The previous discussion applies only to the lattice contribution to the thermal expansion. For metals the effect of the conduction electrons must be considered. This can be done to a first approximation by adding a corresponding term to the free energy. It then follows that the effect is negligible if the electronic heat is very much smaller than the lattice specific heat. This applies to all metals, at average temperatures. At very low temperatures, however, the electronic specific heat becomes comparable to the lattice specific heat. If $C_l \propto T^3$, however, the two effects might be separated[85].

REFERENCES

1 E. Grüneisen, Hb. d. Physik, X, 1 (1926).
2 P. Debye, Ann. Physik, **39**, 789 (1912).
3 M. Blackman, Zs. Physik, **86**, 421 (1933); Proc. Roy. Soc., **148**, 384 (1935); *ibid.*, **159**, 416 (1937).
4 M. Born, Th. von Kármán, Physik. Z., **13**, 297 (1912); *ibid.*, **14**, 15 (1913).
5 M. Blackman, Rep. Progr. Physics, **8**, 11 (1941).
6 D. J. Hooton, Phil. Mag., **46**, 422, 433, 485 (1955); Zs. f. Phys., **142**, 42 (1955).
7 D. Bijl, Phil. Mag., **43**, 1342 (1952).
8 M. Born, K. Huang, The dynamical theory of crystal lattices, Oxford (1954).
9 F. Simon, Landolt–Börnstein, Phys. Chem. Tabelle, 3rd ed., 1st Erg. Band, 702 (1927).
10 M. Born, Atomtheorie des festen Zustandes, Leipzig (1923)
11 R. C. Tolman, The principles of statistical mechanics, Oxford (1938).
12 P. Debye, Wolfskehl Vorträge, Göttingen, 17 (1914).
13 G. Leibfied, W. Brenig, Zs. f. Phys., **134**, 451 (1953).
14 H. Thirring, Phys. Z., **14**, 867 (1913).
15 J. L. Hwang, J. Chem. Phys., **21**, 168 (1953).
16 D. G. Kapadnis, Physica, **22**, 159 (1956).
17 D. G. Kapadnis, R. Hartmans, Physica, **22**, 173, 181 (1956).
18 W. Hume–Rothery, Proc. Phys. Soc., **57**, 209 (1945).
19 D. Bijl, H. Pullan, Physica, **21**, 185 (1955),

[20] D. Bijl, Congrès de physique des bass temp. Paris, 445 (1955).
[21] C. Schifman, The heat capacities of the elements below room temperature G.E.C., New York (1952).
[22] C. Domb and J. S. Dugdale, Progr. low temp. Phys., II, Ch. XI, Amsterdam, (1956).
[23] H. Barron, Phil. Mag., **46**, 720 (1955).
[24] J. de Boer *et al.*, Physica, **14**, 139, 149, 520 (1948).
[25] K. Clusius, H. H. Bühler, Zs. f. Naturf., **10a**, 930 (1955).
[26] M. Blackman, Hb. d. Physik, **VII** (1), 325 (1955).
[27] R. W. Hill and D. H. Parkinson, Phil. Mag., **43**, 309 (1952).
[28] N. Pearlman and P. H. Keesom, Phys. Rev., **88**, 398 (1952).
[29] F. M. Kelly and D. K. C. MacDonald, Can. J. Phys., **31**, 147 (1953).
[30] P. F. Meads, W. R. Forsythe and W. F. Giauque, J. Am. Chem. Soc., **63**, 1897 (1941).
[31] W. S. Corak, M. P. Garfunkel, C. B. Satterthwaite and A. Wexler, Phys. Rev., **98**, 1699 (1955).
[32] I. Esterman, S. A. Friedberg and J. E. Goldman, Phys. Rev., **87**, 582 (1952).
[33] J. Rayne, Phys. Rev., **95**, 1428 (1954).
[34] J. A. Kok and W. H. Keesom, Leiden Comm. 245a.
[35] N. M. Wolcott, Thesis, Oxford (1955).
[36] P. F. Meads, W. R. Forsythe and W. F. Giauque, J. Am. Chem. Soc., **63**, 1902 (1941).
[37] P. H. Keesom and N. Pearlman, Phys. Rev., **98**, 548 (1955).
[38] W. H. Keesom and J. A. Kok, Leiden Comm., 219d (1932), 232d (1933).
[39] T. H. Geballe and W. F. Giauque, J. Am. Chem. Soc., **74**, 2368 (1952).
[40] K. Clusius and L. Schachinger, Zs. f. Naturf., **7a**, 185 (1952).
[41] G. Duyckaerts, Physica, **6**, 817 (1939).
[42] G. Duyckaerts, Mem. Soc. Roy. Sci. Liège, **6**, 193 (1945).
[43] K. Clusius and C. G. Losa, Zs. f. Naturf., **10a**, 545 (1955).
[44] N. M. Wolcott, Conf. d. Phys. d. Basses Temp. Paris, (1955), p. 286.
[45] R. H. Busey and W. F. Giauque, J. Am. Chem. Soc., **74**, 3157 (1952).
[46] W. H. Keesom and C. W. Clark, Physica, **2**, 513 (1935).
[47] K. Clusius and L. Schachinger, Zs. f. Naturf., **2a**, 90 (1947).
[48] G. L. Pickard and F. E. Simon, Proc. Phys. Soc. London, **61**, 1 (1948).
[49] F. Simon and W. Zeidler, Zs. f. phys. Chem., **123**, 383 (1926).
[50] J. A. Kok and W. H. Keesom, Physica, **3**, 1035 (1936).
[51] J. A. Kok and W. H. Keesom, Physica, **4**, 835 (1937).
[52] M. Horowitz, A. A. Silvidi, S. F. Malaker and J. G. Daunt, Phys. Rev., **88**, 1182 (1952).
[53] J. R. Clement and E. H. Quinnell, Phys. Rev., **85**, 502 (1952).
[54] W. H. Keesom and J. N. v. d. Ende, Leiden Comm., 203d, 213c.
[55] R. W. Hill and P. L. Smith, Phil. Mag., **7**, **49**, 636 (1953).
[56] D. C. Ginnings, T. B. Douglas and A. F. Ball, J. Am. Chem. Soc., **73**, 1236 (1951).
[57] P. L. Smith, Phil. Mag., **46**, 744 (1955).
[58] R. S. Craig, C. A. Krier, L. W. Coffer, E. A. Bates and W. E. Wallace, J. Am. Chem. Soc., **76**, 283 (1955).

[59] J. G. Daunt and A. A. Silvidi, Phys. Rev., **77**, 125 (1950).
[60] K. Clusius and P. Harteck, Zs. phys. Chem., **134**, 243 (1928).
[61] P. L. Smith, Conf. d. Phys. d. Basses Temp. Paris, (1955), p. 286.
[62] H. Smith, Phil. Trans. Roy. Soc., A, **241**, 105 (1949).
[63] K. Pitzer, J. Chem. Phys., **6**, 68 (1938).
[64] W. Desorbo, J. Chem. Phys., **21**, 876 (1953).
[65] N. Pearlman and P. H. Keesom, Phys. Rev., **88**, 398 (1952).
[66] C. T. Anderson, J. Am. Chem. Soc., **52**, 2301 (1930).
[67] C. T. Anderson, J. Am. Chem. Soc., **59**, 488 (1937).
[68] J. R. Weertman, D. Burk and J. E. Goldman, Paper ZA5, Am. Phys. Soc. meeting, Jan. 31–Feb. 2 (1952).
[69] C. T. Anderson, J. Am. Chem. Soc., **58**, 564 (1936).
[70] W. S. Corak, B. B. Goodman, C. B. Satterthwaite and A. Wexler, Phys. Rev., **102**, 656 (1956).
[71] D. Burk and F. Darnell, Paper ZA6, Am. Phys. Soc. meeting, Jan. 31–Feb. 2 (1952).
[72] W. H. Keesom and J. A. Kok, Physica, **1**, 167, 324, 595 (1934).
[73] J. F. G. Hicks Jr., J. Am. Chem. Soc., **60**, 1000 (1938).
[74] C. Zwikker and G. Schmidt, Phys. Zs., **52**, 668 (1928).
[75] F. Lange, Zs. phys. Chem., **110**, 343 (1924).
[76] G. Leibfried and W. Brenig, Fortschr. d. Phys., 1, 187 (1953).
[77] G. Leibfried, Encycl. Physics, **7** (1), 104 (1955).
[78] M. Blackman, Encycl. Physics, **7** (1), 325 (1955).
[78] L. Brillouin, Wave propagation in periodic structures, New York (1943).
[79] G. Leibfried and Landolt–Börnstein, I (4), 756 (1955).
[80] R. B. Leighton, Rev. Mod. Phys., **20**, 165 (1948).
[81] P. C. Fine, Phys. Rev., **56**, 355 (1939).
[82] Yü–Chang Hsieh, J. Chem. Phys., **22**, 306 (1954).
[83] E. W. Montroll and D. Paeslee, J. Chem. Phys., 12, 98 (1944); *ibid.*, **11**, 481 (1943).
[84] F. J. Webb and J. Wilks, Proc. Roy. Soc., A, **230**, 549 (1955).
[85] D. Bijl and H. Pullan, Physica, **21**, 285 (1955).
[86] H. L. Johnston and C. W. Kothen, J. Am. Chem. Soc., **75**, 3101 (1953).
[87] P. L. Smith and N. M. Wolcott, Conf. d. Basses Temp. Paris, (1955).
[88] M. Griffel and R. E. Skochdople, J. Am. Chem. Soc., **75**, 5250 (1953).
[89] W. H. Keesom and M. Desirant, Physica, **8**, 273 (1941).
[90] K. Clusius and C. G. Losa, Zs. f. Naturf., **10a**, 939 (1955).
[91] W. H. Keesom and B. Kurrelmeyer, Physica, **6**, 364, 633 (1939).
[92] A. Eucken and H. Werth, Zs. Anorg. Allgem. Chem., 188, 152 (1930).
[93] K. K. Kelly, J. Chem. Phys., **11**, 16 (1943).
[94] F. Simon and W. Zeidler, Zs. phys. Chem., **123**, 383 (1926).
[95] M. Horowitz and J. G. Daunt, Phys. Rev., **91**, 1099 (1953).
[96] G. B. Skinner and H. L. Johnston, J. Am. Chem. Soc., **73**, 4549 (1951).
[97] I. Esterman and S. A. Friedberg, Phys. Rev., **87**, 582 (1952).
[98] W. T. Smith, G. D. Oliver and J. W. Cobble, J. Am. Chem. Soc., **75**, 5785 (1953).
[99] I. Esterman and J. R. Weertman, J. Chem. Phys., **20**, 472 (1952).

100 W. H. Keesom and J. N. v. d. Ende, Leyden Comm., 203d, 203c.
101 P. F. Meads, *et al.*, J. Am. Chem. Soc., **63**, 1902 (1945).
102 J. R. Clement and E. H. Quinnell, Phys. Rev., **85**, 502 (1952).
103 F. C. Nix and D. McNair, Phys. Rev., **60**, 597 (1941); *ibid.*, **61**, 74 (1942).
104 E. A. Guggenheim, Thermodynamics, Amsterdam (1949).
105 F. E. Simon and E. Vohsen, Zs. phys. Chem., **133**, 165 (1928).
106 M. Zemansky, Heat and thermodynamics, McGraw–Hill, London (1951).
107 T. Rubin, H. W. Altman and H. L. Johnston, J. Am. Chem. Soc., **76**, 5289 (1954).
108 Beattie, Journ. Math. and Phys. (Mass. Inst. Techn.), **6**, 1 (1926).

CHAPTER XIV

THE TEMPERATURE SCALE IN THE LIQUID HELIUM REGION

BY

H. VAN DIJK AND M. DURIEUX

KAMERLINGH ONNES LABORATORY, LEIDEN

CONTENTS: 1. Introduction, 431. — 2. Thermodynamic pT-relation, 432. — 3. First Measurements with the Gas Thermometer, 1908–1915, 433. — 4. The 1924-Scale, 435. — 5. Use of the Hot-wire Manometer, 435. — 6. Measurements of 1927, 1928 and 1929, 437. — 7. Measurements of 1937, 440. — 8. The 1929- and the 1932-Scale, 443. — 9. The 1937- and the 1939-Scale, 443. — 10. The 1948-Scale, 445. — 11. Measurements of Kistemaker and Keesom, 445. — 12. Magnetic Temperatures, 446. — 13. Confirmation of Kistemaker's Results, 447. — 14. Measurements of Keller on Helium Isotherms, 451. — 15. pT-relation of Clement, Logan and Gaffney, 452. — 16. The Temperature Scale above 4.2° K, 452. — 17. Modification of the pT-relation of Clement *et al.*, 453. — 18. Accurate Vapour Pressure Measurements of Ambler and Hudson, 454. — 19. Thermodynamic pT-relation. Historical Remarks, 456. — 20. Numerical Calculation of the Different Terms in the pT-relation, 456. — 21. Calculation of the Heat of Vaporization, 458. — 22. Extension of the Scale to the Critical Point, 460. — 23. The T_{L55}-Scale, 462.

1. Introduction

Between 1.0 and 5.2° K temperatures are usually determined from the saturated vapour pressure of the liquid helium bath. To convert pressures into temperatures the pT-relation is required. The fundamental measurements to determine this relation were made with the gas thermometer. They could be completed with measurements on isotherms, measurements of the temperature dependence of the susceptibility of paramagnetic salts, and with some secondary temperature measurements based on resistance measurements on alloys and semiconductors, or on the specific heat of metals.

For the calculation of several corrections on the measurements with the gas thermometer it was necessary to determine accurately the thermo-molecular pressure effect, the adsorption of helium, the expansion of glass and copper and the capillary depression of mercury.

As the determination of the equilibrium pressure is less complicated

and more accurate than measurements with the gas thermometer, in practice vapour pressure measurements are nearly always used for temperature measurements and for calibrations of secondary thermometers.

2. Thermodynamic pT-relation

The pT-relation for the liquid-vapour equilibrium is a thermodynamic equation that in principle can be calculated exactly [1]:

$$\ln p = i - \frac{L_0}{RT} + \tfrac{5}{2} \ln T - \frac{1}{RT} \left(\int_0^T S_l \, \mathrm{d}T - \int_0^p V \, \mathrm{d}p \right) + \varepsilon \qquad (1)$$

where

$$\varepsilon = \ln \{(pV_g)/(RT)\} - (2B/V_g) - (3C/V_g^2)$$

and

$$pV_g = RT \{1 + (B/V_g) + (C/V_g^2)\}.$$

For practical use the following numerical data are required: (*a*) i, the chemical constant; (*b*) L_0, the heat of vaporization at $T = 0°$ K; (*c*) the specific heat of the liquid (for the calculation of the entropy S_l); (*d*) V_l, the molar volume of the liquid; (*e*) B and C, the virial coefficients of the gas. Moreover a preliminary temperature scale is indispensable.

In the beginning it was necessary to use interpolation formulae of a form expected from the thermodynamic pT-relation. The constants were determined from measurements with the gas thermometer. In this way Kamerlingh Onnes and Weber [2] described in 1915 the results of their first vapour pressure measurements [cf. Eq. (5)].

After the vapour pressure at low temperatures had been measured Verschaffelt [3] could provide a purely thermodynamic equation containing only one unknown constant (L_0) which had been determined from measurements with the gas thermometer. For low temperatures (1) can be reduced to

$$\ln p = i - L_0/(RT) + \tfrac{5}{2} \ln T. \qquad (2)$$

When p has been measured with the gas thermometer for sufficiently low temperatures, L_0 can be calculated using Eq. (2).

Since for low temperatures $L = L_0 + \frac{5}{2}RT$, where L is the heat of vaporization it follows that L can also be calculated. Verschaffelt found $L = (14 + 5T)$ cal mole^{-1}. The values of L calculated in this way join smoothly to those measured by Dana and Kamerlingh

Onnes [4]. This has been a check for the value of L_0 used by Verschaffelt in his pT-relation:

$$^{10}\log p_{\text{cm Hg},0^\circ\text{C}} = 1.19 - (3.1/T) + \tfrac{5}{2}\,{}^{10}\log T, \quad (T < 1.475^\circ \text{ K}). \qquad (3)$$

Only after thirty-one years, in 1955, could the general pT-relation (1) be calculated numerically with sufficient accuracy up to 4.2° K and put into use as T_{L55}. Before considering that scale, we will give a historical survey of the vapour pressure measurements performed on helium, and of the temperature scales in this temperature region. In this survey we shall use T_{L55} to compare the different scales.

3. First Measurements with the Gas Thermometer, 1908-1915

The first vapour pressure measurement with the gas thermometer was made by Kamerlingh Onnes [5] on the day he liquified helium for

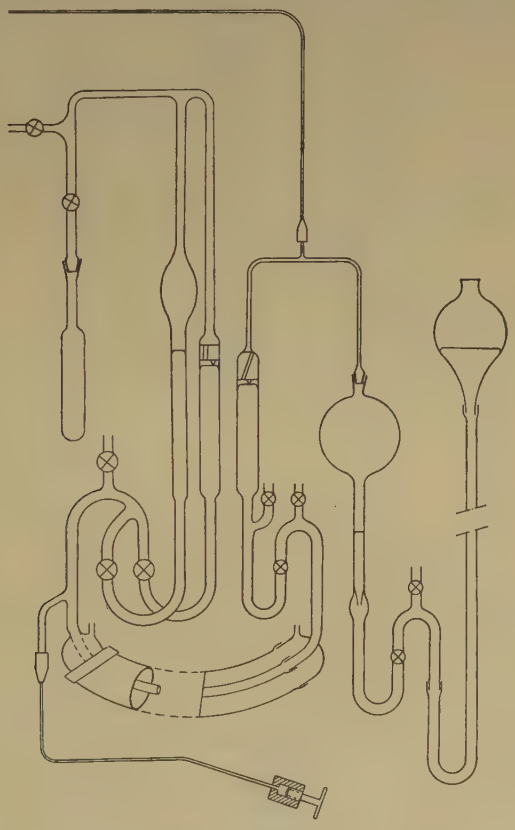

Fig. 1. Gas thermometer used by Kamerlingh Onnes. [7]

the first time (July 10, 1908). He found 4.3° K for the normal boiling point.

In 1910 and 1911 the vapour pressure was measured by Kamerlingh Onnes [6,7] from about 1.5 to 5.2° K. In 1913 these measurements were completed by Kamerlingh Onnes and Weber [2]. A summary of the results is given in Table I. The correction for the thermo-molecular

TABLE I

Vapour pressure of helium measured with the gas thermometer, early results. p_0 is the ice point pressure of the gas thermometer and p the vapour pressure of helium. The temperature T has been corrected for thermo-molecular pressure effect and for non-ideality of the gas

Year and series	p_0 mm Hg, 0° C	p mm Hg, 0° C	T °K	T_{L55} °K	$T-T_{L55}$ deg
1910/1911	145	760	4.223	4.216	+ 0.007
I		565	3.903	3.918	− 0.015
		197	3.183	3.053	+ 0.130
		51	2.253	2.298	− 0.045
		3	1.363	1.461	− 0.098
II	145	760	4.213	4.216	− 0.003
		197	3.123	3.053	+ 0.070
		51	2.313	2.298	+ 0.015
		3	1.383	1.461	− 0.028
1911	300	767	4.226	4.226	0.000
		1329	4.916	4.863	+ 0.053
		1520	5.056	5.039	+ 0.017
		1569	5.106	5.081	+ 0.025
		1668	5.176	5.165	+ 0.011
		1718	5.206	5.206	+ 0.000
1913	257.4	756.6	4.200	4.211	− 0.011
		359.5	3.525	3.510	+ 0.015
		4.4	1.455	1.541	− 0.086
1913	253.6	757.5	4.210	4.213	− 0.003
		4.15	1.486	1.528	− 0.042
		756.5	4.214	4.211	+ 0.003

pressure difference could not be calculated until 1915 [2]. The correction for the deviation from the ideal gas law amounts to only a few millidegrees. The underlined pT-values were considered by the authors to be the most accurate ones. They do not differ much from T_{L55}.

It is remarkable that the normal boiling point, derived from the data of Kamerlingh Onnes and Weber [2], agrees very well with the value 4.216° K which was found by Schmidt and Keesom [8] and which is still considered to be the best one.

4. The 1924-Scale

In 1915 Kamerlingh Onnes and Weber [2] described their results with the following pT-relation:

$$[10]\log p_{\text{cm Hg},0°\text{C}} = 3.7290 - (7.9780/T) - (0.13628/T^2) + (4.3634/T^3). \quad (4)$$

This relation was used afterwards for the definition of the 1924-scale of temperatures between 1.475 and 5.2° K. For temperatures

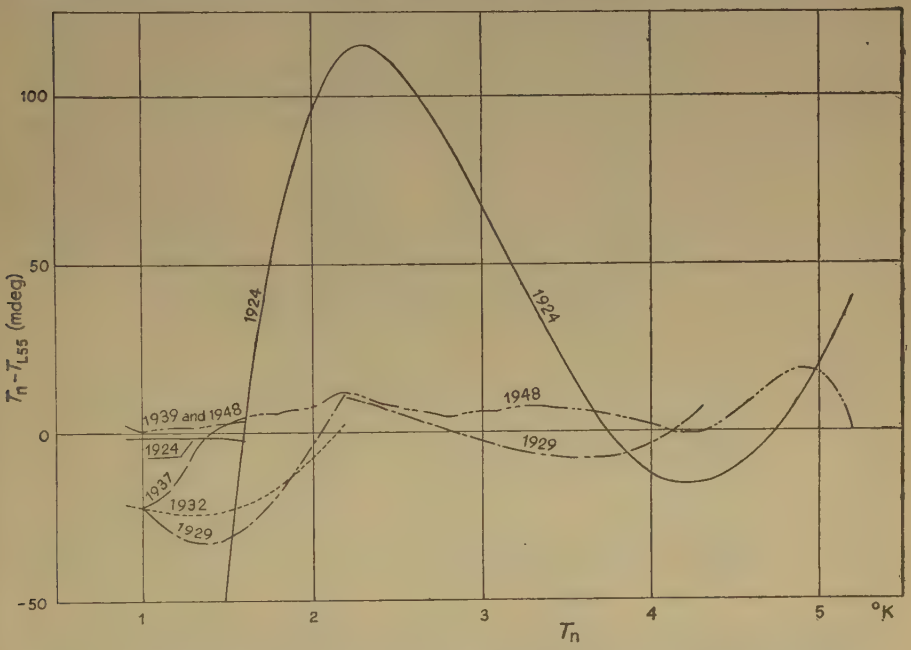

Fig. 2. Several temperature scales for the liquid helium region compared with T_{L55}. T_n is T_{1924} to T_{1948} as indicated in the figure.

lower than 1.475° K this scale was defined by Verschaffelt's formula mentioned above [Eq. (3)].

5. Use of the Hot-wire Manometer

In all these experiments of Kamerlingh Onnes and Weber, the

TABLE II

Deviations from the T_{L55} scale. T_n in °K, $\Delta T_n = T_n - T_{L55}$ in milli degree

T_n	ΔT_{1924}	ΔT_{1929}	ΔT_{1932}	ΔT_{1937}	ΔT_{1939}	ΔT_{1948}
0.9	− 1		− 21			+ 3.0
1.0	− 1	− 22.4	− 22	− 22	+ 1	+ 1.0
1.1	− 1	− 26.9	− 23	− 20	+ 2	+ 1.7
1.2	− 1	− 30.4	− 24	− 14	+ 2	+ 2.0
1.3	− 1	− 32.3	− 24	− 6	+ 3	+ 1.9
1.4	− 1	− 32.6	− 24	+ 1	+ 2	+ 2.8
1.5	− 1.5	− 31.2	− 23	+ 3	+ 3	+ 3.1
1.6	+ 2.2	− 28.3	− 21	+ 4		+ 5.0
1.7	+ 35	− 23.8	− 19	+ 5		+ 6.0
1.8	+ 61	− 18.0	− 16	+ 5		+ 6.0
1.9	+ 81	− 11.1	− 12	+ 6		+ 7.4
2.0	+ 96	− 3.4	− 7.5	+ 8		+ 8.0
2.1	+ 107	+ 4.6	− 2.3	+ 9		+ 10.8
2.18				+ 10		
2.19		+ 11.4	+ 2.5	+ 12		
2.2	+ 113	+ 10.3		+ 12		+ 11.6
2.3	+ 115	+ 9.1		+ 9		+ 10.7
2.4	+ 113	+ 7.5		+ 7		+ 9.0
2.6	+ 103	+ 3.9		+ 5		+ 6.7
2.8	+ 87	+ 0.4		+ 4		+ 4.6
3.0	+ 68	− 2.8		+ 5		+ 6.3
3.2	+ 48	− 5.5		+ 6		+ 7.5
3.4	+ 28	− 7.3		+ 6		+ 7.4
3.6	+ 11	− 8.0		+ 6		+ 6.3
3.8	− 3.3	− 7.0		+ 5		+ 4.5
4.0	− 12.6	− 3.9		+ 2		+ 2.1
4.2	− 15.5	+ 2.5		− 3		− 0.7
4.4	− 13.5					+ 2
4.6	− 7.1					+ 10
4.8	+ 3.9					+ 17
5.0	+ 19.9					+ 17
5.2	+ 39.8					− 0

ice point pressure p_0 in the gas thermometer was kept low. This made it possible to obtain good accuracy without corrections for the deviations from the ideal gas law and also enabled them to measure at low pressures of the helium bath with the same filling of the gas thermometer without condensation of the helium gas. The pressure in the gas thermometer at the boiling point of helium was only a few millimeters of mercury.

To be able to measure at still lower temperatures and to reach a

higher accuracy, it was necessary to use another method of pressure measurement and to determine accurately the thermo-molecular pressure differences. Kamerlingh Onnes and Weber chose the hot-wire

Fig. 3. Gas thermometer with hot-wire manometer [9].

manometer and Weber made extensive calculations of the thermo-molecular pressure effect. The first measurements with the hot-wire manometer were carried out in 1913 [2]. The results were not very accurate.

6. Measurements of 1927, 1928 and 1929

In 1927, 1928 and 1929 the vapour pressure was measured with the gas thermometer once more. This time the pressure in the gas thermometer was measured with the hot-wire manometer only.

By taking larger diameters of the capillaries of the gas thermometers (2.0 and 3.7 mm) and by using higher ice point pressures for the measurements above 1.7° K (about 100 and 50 mm Hg) the

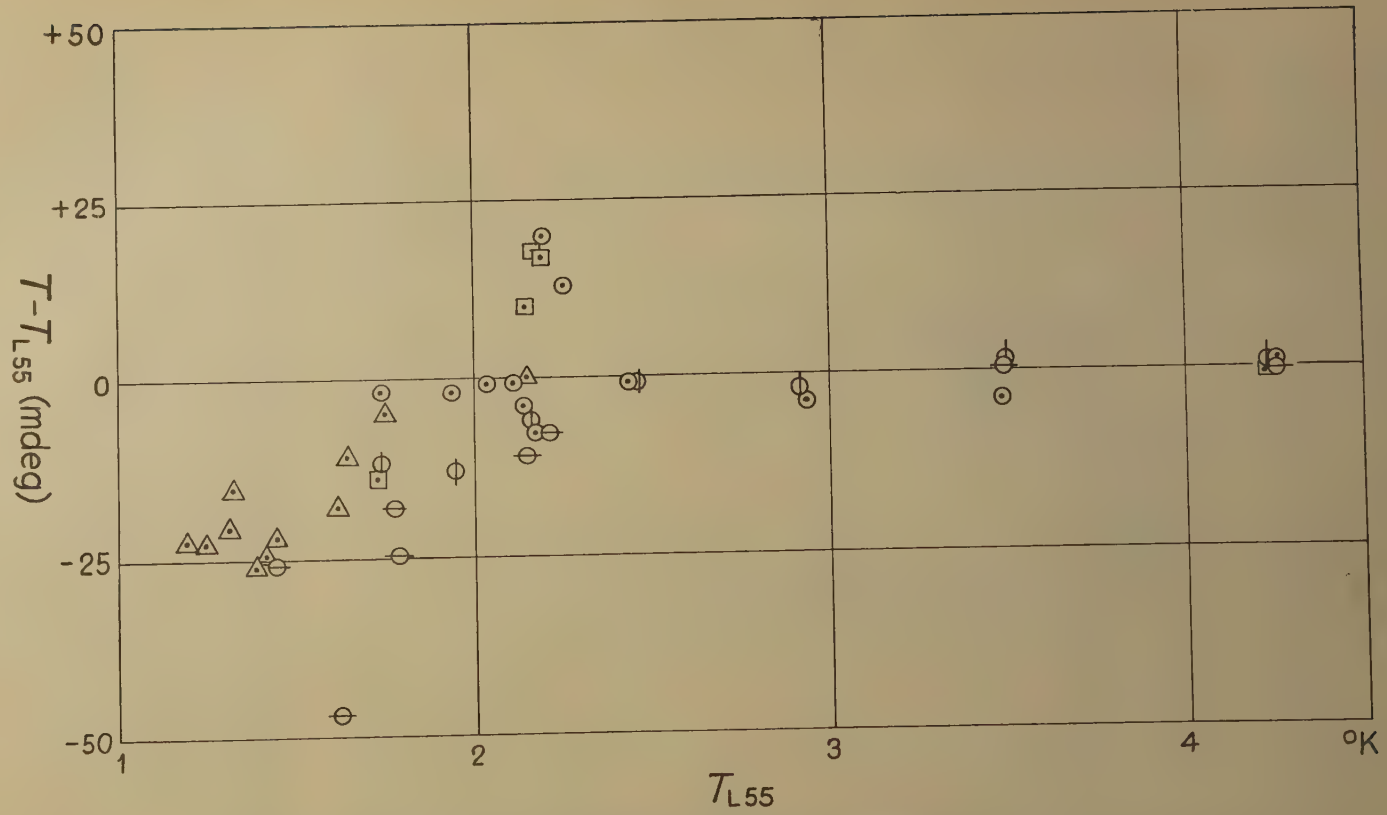

Fig. 4. Measurements with the gas thermometer of Keesom *et al.* in 1927–1929 compared with T_{L55}.

⊙: 16–12–1927
⊡: 21–12–1927
◐: 20– 1–1928
⊖: 1–2–1929
△: 7–2–1929 (normalized at $T_{L55} = 2.114°$ K)

corrections of the thermo-molecular pressure effect could be reduced considerably. The results obtained in this way by Keesom, Weber and Nørgaard [9] agree, after correction according to the method described by Weber and Schmidt [10], well with T_{L55} as appears from Fig. 4 and Table III.

In the experiments of 1927–1929 the normal boiling point was not determined again but taken equal to 4.22° K, the result of Kamerlingh Onnes and Weber. The measurements made by Keesom, Weber and

TABLE III

Results of the measurements of 1927–1929, T_1 and T_2 are the temperatures measured with two different gas thermometers $T_{12} = (T_1 + T_2)/2$

p mm Hg, 0° C	T_1 °K	T_2 °K	$T_{12}-T_{L55}$ m deg
16-12-1927, $p_0 = 99.55$ mm			
784.7	4.250	4.250	0
350.0	3.484	3.485	− 4
164.7	2.929	2.929	− 4
69.50	2.447	2.438	− 1
46.33	2.260	2.276	+ 13
40.61	2.206	2.232	+ 20
37.63	2.167	2.153	− 8
34.94	2.141	2.121	− 4
31.92	2.107	2.098	− 1
26.55	2.041	2.029	− 1
19.74	1.942	1.926	− 2
10.20	1.747	1.735	− 2
21-12-1927, $p_0 = 99.55$ mm			
768.5	4.228	4.228	0
39.82	2.189	2.227	+ 17
37.46	2.155	2.214	+ 18
36.68	2.145	2.191	+ 10
9.94	1.728	1.716	− 14
20-1-1928, $p_0 = 54.62$ mm			
782.2	4.246	4.246	0
351.3	3.496	3.487	+ 1
161.0	2.922	2.910	− 2
70.95	2.456	2.449	− 1
36.45	2.155	2.143	− 6
20.06	1.931	1.924	− 13
10.06	1.734	1.720	− 12
1-2-1929, $p_0 = 55.75$ mm			
772.7	4.233	4.233	0
351.2	3.497	3.487	+ 1
41.30	2.201	2.195	− 8
35.57	2.139	2.131	− 11
11.77	1.765	1.749	− 25
11.52	1.765	1.752	− 18
6.59	1.611	1.560	− 48
2.82	1.432	1.415	− 26
7-2-1929, $p_0 = 55.75$ mm			
35.68	2.123	2.105	0
10.81	1.735	1.716	− 5
7.04	1.613	1.613	− 11
6.19	1.586	1.568	− 18
2.78	1.404	1.400	− 22
2.53	1.394	1.372	− 25
2.01	1.350	1.327	− 26
1.40	1.283	1.287	− 15
1.32	1.275	1.272	− 21
0.920	1.212	1.214	− 23
0.595	1.148	1.152	− 23

Schmidt [11] in 1929 below the λ-point differ from T_{L55}: there is a constant deviation of about 0.035 degree with respect to the T_{L55}-scale. This deviation can be reduced considerably by normalization with the aid of the results obtained for temperatures just below the λ-point in 1927–28 in stead of normalization with the aid of measurements at the boiling point as done by Keesom, Weber and Schmidt [11]. The corrections for the data of ref. 11 were recalculated by us in accordance with the method mentioned above. The results obtained in this way are compared with T_{L55} in Fig. 4; Table III gives the numerical values. For the low ice point pressures the correction for the thermo-molecular pressure difference was so large, that no accurate results could be expected.

7. Measurements of 1937

After an extensive investigation of the thermo-molecular pressure effect [10, 12] new measurements of the vapour pressure were carried out by Schmidt and Keesom [13] in 1937.

The principal improvements of the method of measurement were: the hot-wire manometer was kept at a constant temperature of about 76.5° K instead of 0° C, more precautions were taken against contamination of the hot-wire, and the calibration of the hot-wire manometer was carried out no longer at 0° C but at the boiling point of hydrogen or helium. Just as in earlier investigations the volume of the gas thermometer and the amount of gas within were kept constant when temperatures were measured. During the calibration small amounts of gas were added by means of a gas pipet (volume 0.5 ml). See Fig. 5. In this way thé indication of the hot-wire manometer was measured as a function of the density of the gas at the calibration temperature; at these low densities the pressure can be calculated from the density with sufficient accuracy. Therefore the pressure in the bulb can be calculated as a function of the indication of the hot-wire manometer. This relation is very nearly independent of the temperatures of the gas in the bulb if this temperature is low enough ($<4.25°$ K) and it can also be used to calculate the pressure (and temperature) of the gas in the bulb if the amount of gas in the bulb is left unchanged but the temperature is made different from the temperature of calibration.

The principal results of the vapour pressure measurements of 1937 are:

(a) The ratio of the normal boiling points of liquid helium and liquid hydrogen was measured accurately. From the known value of

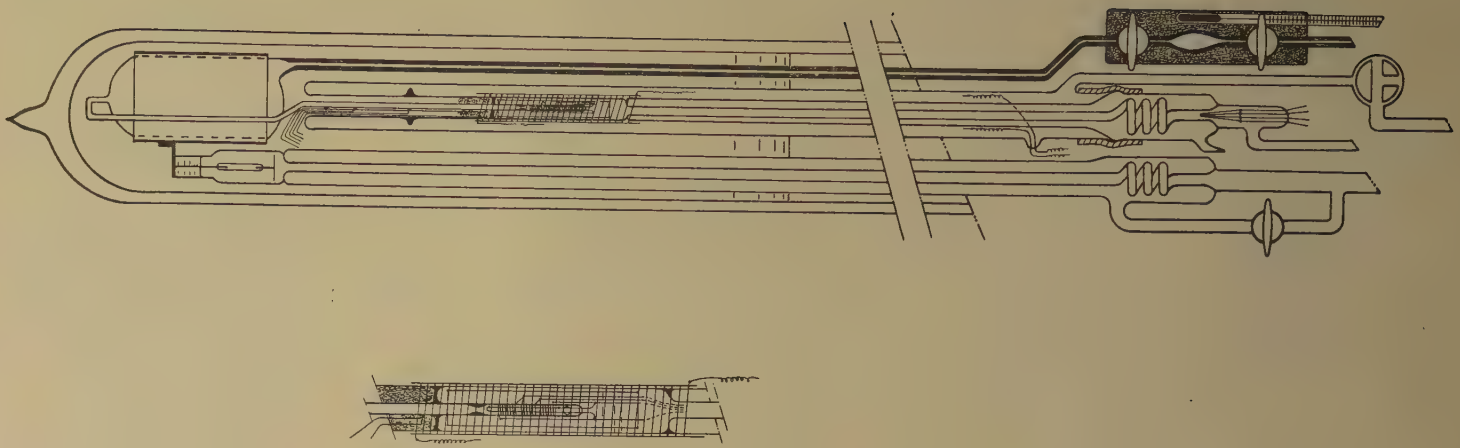

Fig. 5. Gas thermometer of Schmidt and Keesom in 1937 [13].

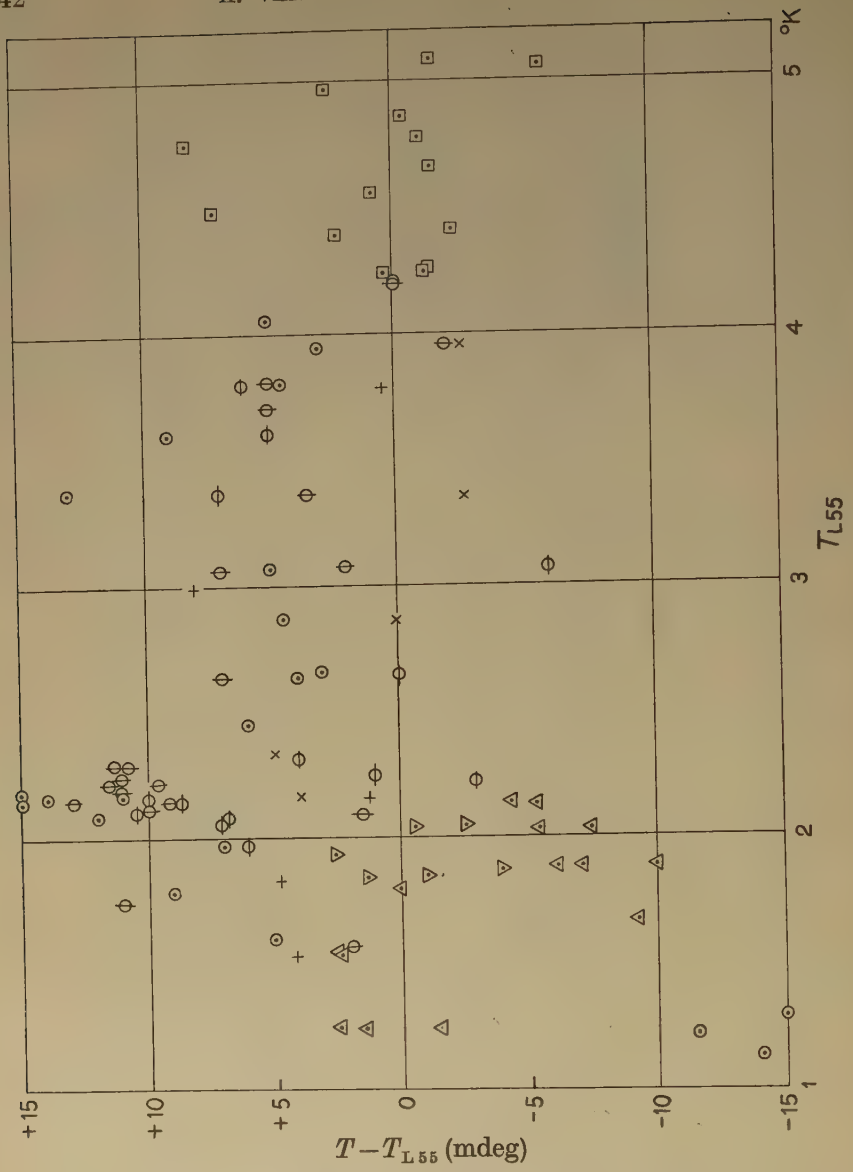

Fig. 6. Several measurements compared with T_{L55}.

⊙ ⊖ ⊖: Measurements of Schmidt and Keesom (gas thermometer).
△: ,, ,, Kistemaker (gas thermometer).
▽: ,, ,, Kistemaker (^{4}He-isotherms).
+: ,, ,, Keller (^{3}He-isotherms).
×: ,, ,, Keller (^{4}He-isotherms).
⊡: ,, ,, Berman and Swenson (gas thermometer).

the boiling point of hydrogen (20.381° K) a value for the boiling point of helium of 4.216° K was found. This is in good agreement with earlier measurements with the gas thermometer making use of a mercury manometer to compare directly the boiling point of helium with the ice point.

(b) In the neighbourhood of 1.5° K p was measured as a function of T with a greater accuracy than before.

(c) In the temperature region between 4.2 and 2.0° K new data were obtained which completed the results of 1927–28 but did not exceed the latter is accuracy.

(d) The vapour pressure at the λ-point was measured more accurately than before. A value of 38.3 mm was found. The deviation of the experimental data of 1937 with respect to the T_{L55}-scale are plotted in Fig. 6.

8. The 1929- and the 1932-Scale

With the aid of the results obtained in 1927–29, the following pT-relations were introduced as the "1929-scale" [11].

$$^{10}\log p_{\text{cm Hg},0°\text{C}} = 1.217 - (3.024/T) + 2.208\ ^{10}\log T \quad (T > 2.190° \text{ K}) \qquad (5)$$

$$^{10}\log p_{\text{cm Hg},0°\text{C}} = 2.035 - (3.859/T) + 0.922\ ^{10}\log T \quad (T < 2.190° \text{ K}). \qquad (6)$$

The differences between this scale and T_{L55} are given in Table II and Fig. 2.

In 1932, Keesom [14] replaced (6) by:

$$^{10}\log p_{\text{cm Hg},0°\text{C}} = 1.197 + (3.018/T) + 2.484\ ^{10}\log T - 0.00297\ T^4. \qquad (7)$$

The reason was that (6) was not suitable for extrapolation to lower temperatures. Eq. (7) agrees more closely with what can be expected from thermodynamics [14]. The relations (5) and (7) define the 1932-scale.

9. The 1937- and the 1939-Scale

After the measurements of 1937 Schmidt and Keesom [13] published corrections on the 1932-scale in the form of a deviation curve and a table. These corrections, together with (5) and (7) defined the 1937-scale.

Later on Keesom [15] gave the 1937-scale in the form of a table. We used this table to calculate the data for Fig. 2 and Table II.

Shortly after its introduction the 1937-scale was found to be

unsatisfactory at temperatures below 1.5° K, as it led to thermodynamic conclusions that are unacceptable [16, 17].

With the aid of two different formulae for the heat of vaporization Bleaney and Simon [16] calculated the following pT-relation for $T < 1.6°$ K in a thermodynamic way:

$$^{10}\log p_{\text{cm Hg},0°\text{C}} = 1.196 - (3.117/T) + 2.5\ ^{10}\log T - 0.00227\ T^3 + \Delta \quad (8)$$

where Δ represents a small correction term which amounts to only 0.003 degree at 1.6° K. This relation together with the 1937-scale for $T \geqslant 1.6°$ K, defines the 1939-scale.

By comparing (3) and (8) and also from Fig. 2 it appears that there is only a small difference between the pT-relation of Bleaney and Simon and the relation of Verschaffelt.

The pT-relation of Bleaney and Simon was confirmed by measurements of the temperature dependence of the susceptibility of paramagnetic salts at Oxford by Bleaney and Hull [18] and at Leiden by Casimir, De Klerk and Polder [19] (see Fig. 7).

For a further definition of the 1937- and 1939-scales Lignac

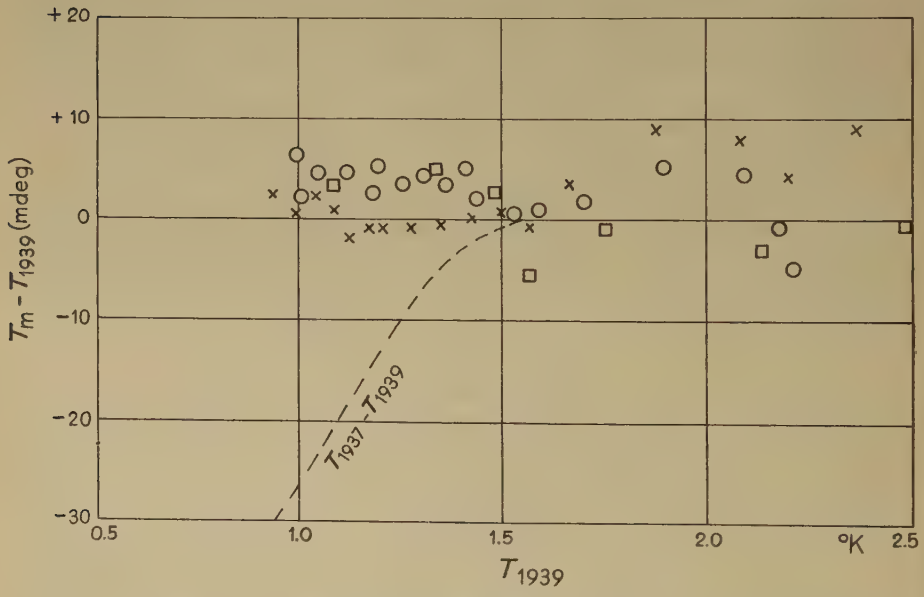

Fig. 7. Deviations of the magnetic temperature, T_m, according to measurements of Bleaney and Hull from T_{1939} [18].

calculated two formulae [20]:

$$^{10}\log p_{\text{cm Hg},0°\text{C}} = 2.6730 - (4.7921/T) + 0.00783\,T + 0.017601\,T^2 \quad (9)$$

for $2.19 \leqslant T \leqslant 4.20°$ K, and

$$^{10}\log p_{\text{cm Hg},0°\text{C}} = 1.1916 - (3.1189/T) + \tfrac{5}{2}\,{}^{10}\log T - 5.981 \times 10^{-5} T^8 \quad (10)$$

for $T < 2.19°$ K.

The formulae agree (according to his calculation) within a few millidegree with the 1939-scale as defined above.

10. The 1948-Scale

Shortly after 1939 a pT-table came into use at Leiden which replaced the scale defined by formulae and deviation curves. This table was later extended to higher and lower temperatures. The extension to lower temperatures was based on Bleaney and Simon's formulae, to higher temperatures on the experimental data of Kamerlingh Onnes and Weber now represented by an equation deduced in Cambridge:

$$T = 2.967 + 1.905 \times 10^{-3}\, p_{\text{mm Hg},20°\text{C}} - 3.52 \times 10^{-7}\, p^2_{\text{mm Hg},20°\text{C}}. \quad (11)$$

From the Leiden table, which gave p as a function of T, a more detailed table was calculated at Cambridge giving T as a function of p. All this came in use as 1948-scale [21]. The differences between several scales and T_{L55} are given in Table II and in Fig. 2.

11. Measurements of Kistemaker and Keesom

In 1948 there were indications that temperatures calculated with the 1948-scale were about 0.01 degree too high in the neighbourhood of the λ-point. From their measurements on isotherms between 1.8 and 2.1° K Kistemaker and Keesom [22] calculated from the limiting value of pV for $p = 0$ a little lower temperatures than those obtained from the measured vapour pressure of the liquid helium bath with the 1937-scale. (In this region there is no difference between the 1937- and 1948-scale.)

As he had an apparatus suitable for very accurate measurements of small pressures with a mercury manometer by means of X-ray shadow graphs, Kistemaker decided to make measurements once more of the vapour pressure with the gas thermometer between 1.4 and 2.2° K. These measurements confirmed the 1937-scale at 1.5° K. In the

neighbourhood of 2° K deviations were found that were somewhat larger than those found from the isotherms and in the same direction. To his measurements Kistemaker [23] added a thermodynamic calculation. The results of Kistemaker's measurements are given in Figs. 6 and 8 and in Table IV.

Today it is clear that adoption of Kistemaker's scale or rather of

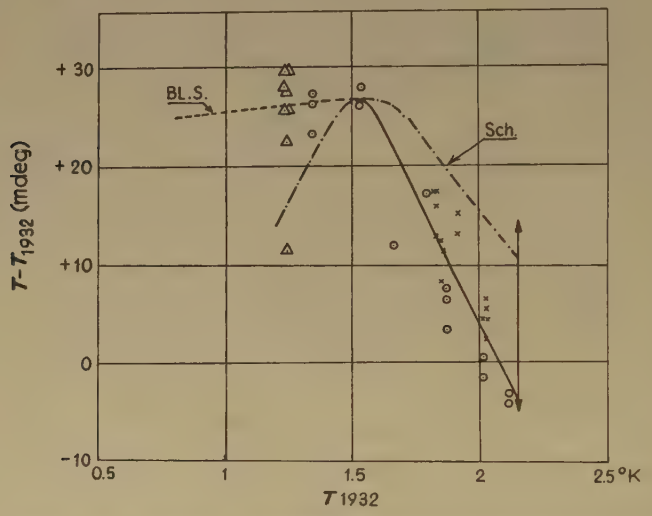

Fig. 8. Deviations from the 1932-scale below the λ-point according to Kistemaker [22].

⊙: Measurements with the gas thermometer of Kistemaker.
×: „ on isotherms of Kistemaker.
△: Magnetic measurements of Casimir, De Klerk and Polder [19].
Sch. is the 1937-scale.
Bl.S. is the 1939-scale.
The full line was considered by Kistemaker in 1945 to be the best scale.

a scale based on accurate thermodynamic calculations would have given a considerable improvement over the 1939-scale. But several uncertainties in Kistemaker's data and calculations made it advisable in 1948 not to change the scale until Kistemaker's results had been confirmed.

12. Magnetic Temperature

The susceptibility of suitable paramagnetic salts is between 1.0 and 4.25° K very nearly a linear function of $(T-\Delta)^{-1}$, where Δ is a small correction, that can be calculated rather accurately. Small

TABLE IV

Results of Kistemaker and of Keller compared with T_{L55}, T_g and T_{is} are the temperatures obtained from measurements with the gas thermometer and from measurements on isotherms respectively; T_{4is} and T_{3is} are temperatures from ^{4}He-isotherms and ^{3}He-isotherms

Kistemaker				Keller			
T_g °K	T_{is} °K	T_g-T_{L55} m deg	$T_{is}-T_{L55}$ m deg	T_{4is} °K	T_{3is} °K	$T_{4is}-T_{L55}$ m deg	$T_{3is}-T_{L55}$ m deg
2.133		− 5.4		3.961		− 2.6	
2.134		− 4.4			3.786		+ 0.5
	2.043		− 2.5	3.348		− 2.7	
	2.036		− 0.5		2.991		+ 8.0
2.031		− 7.5		2.862		+ 0.1	
2.033		− 5.5		2.324		+ 4.9	
	1.930		+ 2.6		2.1605		+ 1.2
1.878		− 6.1		2.154		+ 3.9	
1.877		− 7.1			1.818		+ 4.8
1.879		− 10.0			1.5156		+ 4.1
	1.861		− 4.0				
	1.844		− 1.0				
	1.832		+ 1.3				
1.792		0.0					
1.667		− 9.2					
1.543		+ 2.4					
1.546		+ 2.5					
1.350		+ 2.5					
1.347		+ 1.5					
1.341		− 1.4					

deviations from the linear relation can also be calculated. A quantity related linearly to the susceptibility is also a linear function of $(T-\Delta)^{-1}$. The quantity may be the selfinductance or the mutual inductance of one or of two coils surrounding the paramagnetic sample. This linear relation between the mentioned quantity and $(T-\Delta)^{-1}$ can be used to obtain temperatures from measurements of this quantity after calibrations at two temperatures; such a temperature is usually called magnetic temperature. The normal boiling point of helium and a temperature near 1.5° K are often chosen as calibration points.

13. Confirmation of Kistemaker's Results

A first confirmation of Kistemaker's results was obtained at Leiden in 1949 from accurate measurements of the temperature dependence

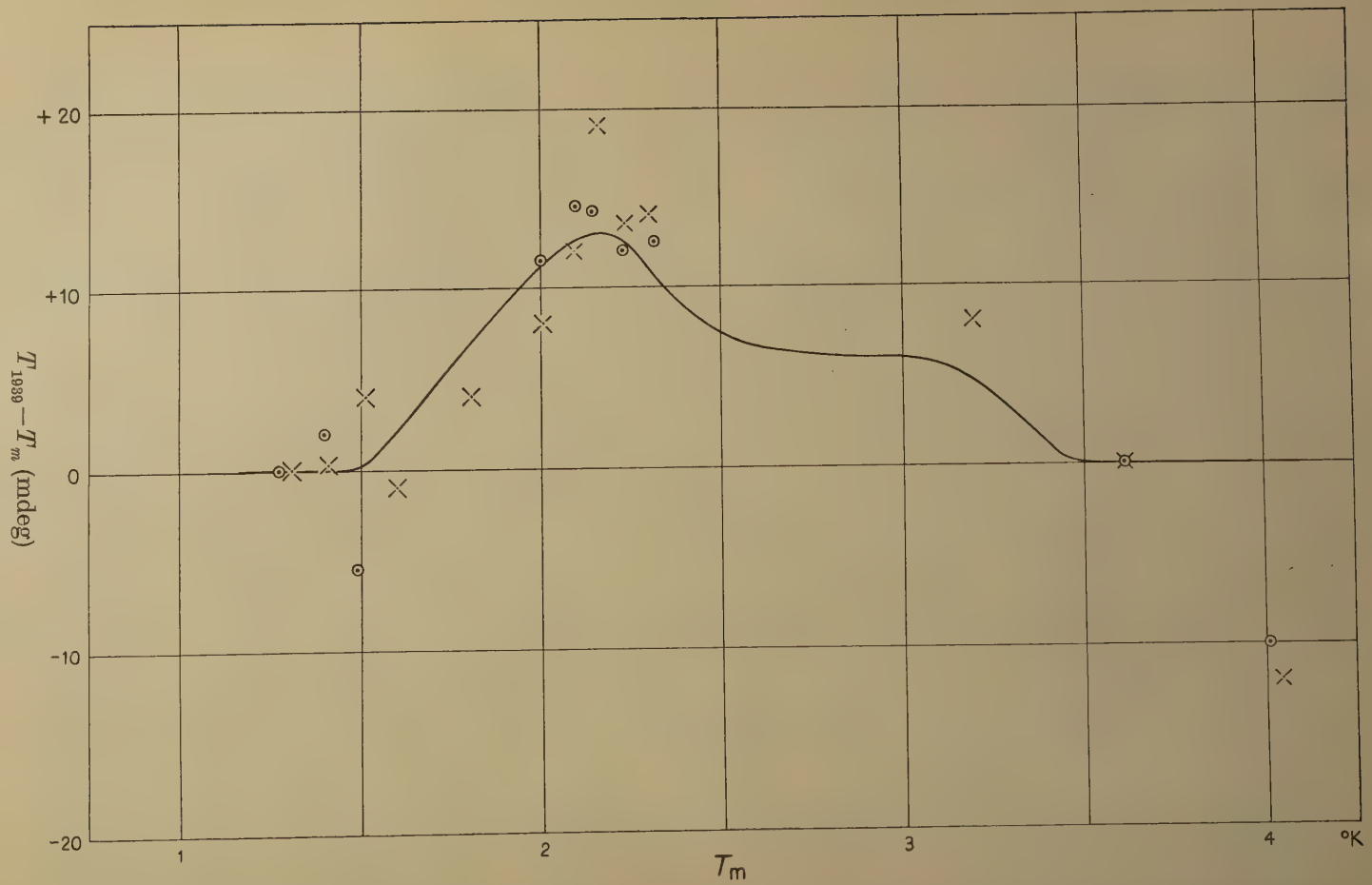

Fig. 9. Deviations from the 1939-scale proposed by Kistemaker (full line) and found at Leiden from magnetic measurements on potassium chromium alum in 1949 (⊙ and ×). The magnetic thermometer had been calibrated at 1.5 and 3.6° K.

of the susceptibility of potassium chromium alum (see Fig. 9). Other accurate and more complete data from magnetic measurements were communicated by Erickson and Roberts (U.S.A.) and by Van Dijk and Durieux (Leiden) at the conference of Physics at low temperatures

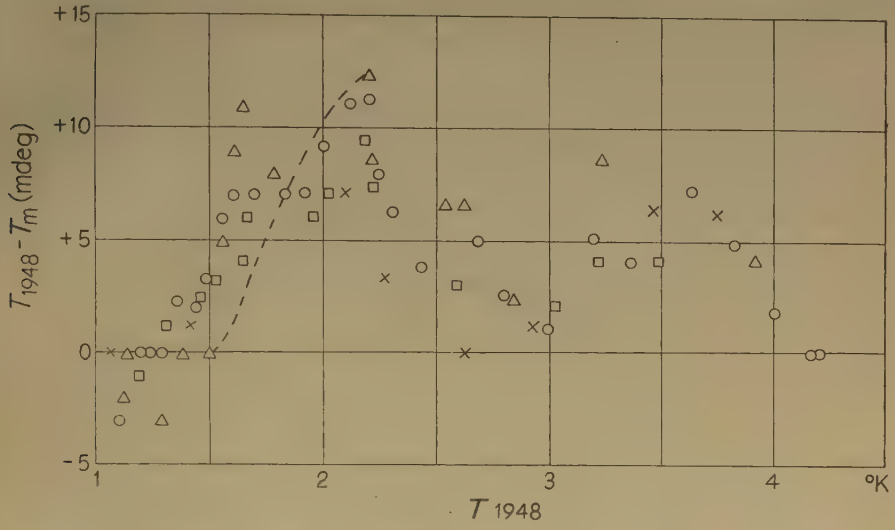

Fig. 10. Deviations of the 1948-scale from the magnetic temperature, T_m, according to Erickson and Roberts [24]. Kistemaker's proposed correction is shown by the broken line.

in Houston (Dec. 1953). Erickson and Roberts [24] published their results in 1954. Their data were obtained from measurements on Fe- and Mn-salts. Fig. 10 shows their deviations from the 1948-scale. The results of the Leiden measurements [25], completed with results of measurements made in 1954, were presented on the third symposion on temperature measurements held in Washington D.C., Oct. 28–30, 1954 (see Fig. 11).

Though there is a rather good agreement between the results obtained in the U.S.A. and at Leiden, some uncertainties still remained mainly between the λ-point and 3.5° K. These results were completed and extended with other data obtained in the U.S.A. Clement, Logan and Gaffney [26] made measurements of the resistance of carbon thermometers as a function of the vapour pressure between 1.5 and 4.3° K and gave an experimental relation between resistance and temperature. When the 1948-scale was used the resistance showed an anomaly,

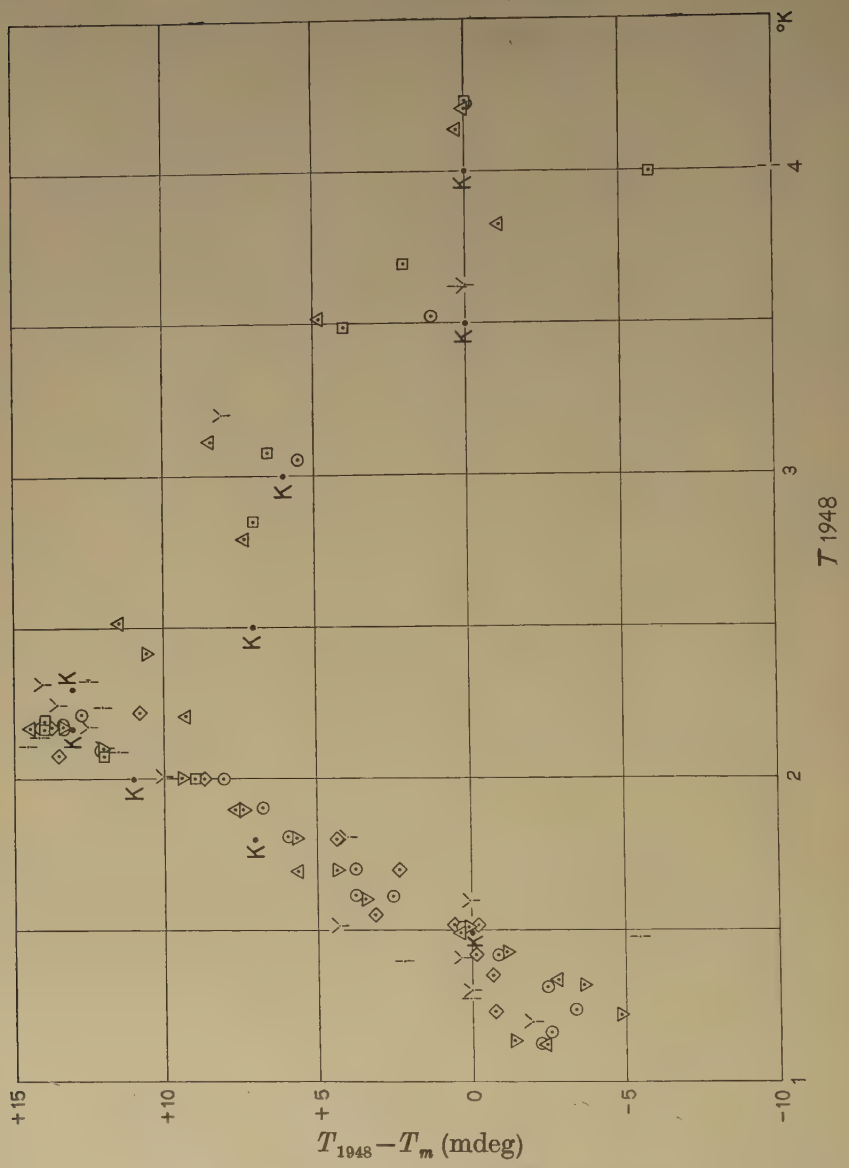

Fig. 11. Deviations of the 1948-scale from the magnetic temperature, T_m, according to the measurements at Leiden.

┆, Y: chromium potassium alum (1949).
▽, △, ⊡, ⊙: „ „ „ (1952).
◇: chromium methylamine alum (1954).
K: Kistemaker's proposed scale (1945).

that could be removed by correcting the 1948-scale according to Kistemaker, Erickson and Roberts, and Keller [27].

14. Measurements of Keller on Helium Isotherms

Keller [27, 28] measured isotherms of ^{4}He and ^{3}He, and vapour pressures of ^{4}He.

A reservoir of accurately known volume (low temperature cell) was kept at the temperature of the isotherm to be measured. This temperature was controlled and measured by means of a vapour pressure tube within the low temperature cell. The pressure of the helium gas in the cell was measured as a function of the amount of gas in it. A correction for the dead space was avoided by closing the cell at low temperature after each measurement of the pressure within

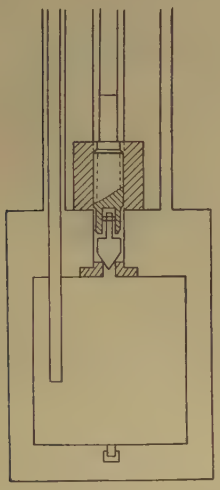

Fig. 12. Low-temperature cell of Keller's gas thermometer.

the cell and by pumping off the gas in the connecting tubes; this amount of gas was measured accurately in a volume manometer.

For each point of the isotherm Keller measured three pressures accurately: the pressure in the cell, in the vapour pressure tube and in the volume manometer after an amount of gas had been pumped off.

Pressures within the cell smaller than 40 mm Hg were measured with a manometer filled with dibutyl sebacate; the higher pressures were measured with a mercury manometer. Keller obtained a good temperature equilibrium by surrounding the low-temperature cell with a vacuum space. The cell itself had a small heat capacity and a good

heat conductivity so temperature equilibrium was reached quickly (see Fig. 12).

For each isotherm the temperature could be calculated from the limit of the ratio between pressure and density for zero pressure. This temperature was compared by Keller with the temperature computed from the vapour pressure. The differences between the temperatures obtained by Keller and T_{L55} are given in Table IV. They are plotted against T_{L55} in Fig. 6.

15. pT-relation of Clement, Logan and Gaffney

Clement, Logan and Gaffney [29] gave the following empirical pT-relation for the saturated vapour pressure of ^{4}He:

$$\left.\begin{aligned}\ln p_{\text{mm Hg, 20° C}} &= I - \frac{A}{T} + B \ln T + \\ &+ \frac{C}{2} T^2 - D\left(\frac{\alpha\beta}{\beta^2+1} - \frac{1}{T}\right) \tan^{-1}(\alpha T - \beta) - \frac{\alpha D}{2(\beta^2+1)} \ln \frac{T^2}{1+(\alpha T-\beta)^2},\end{aligned}\right\} \quad (12)$$

where: $I = 4.62025$, $A = 6.399$, $B = 2.541$, $C = 0.00612$, $D = 0.5197$, $\alpha = 7.00$ and $\beta = 2.541$; $g = 980.665$ cm sec^{-2}.

From this relation p was calculated as a function of T for temperatures between 0.6 and 5.38° K in steps of 0.005 degree. The temperature scale thus obtained was a considerable improvement over the 1948-scale. It was not only in reasonable agreement with the above mentioned measurements but certain anomalies in the specific heat of pure metals found by Keesom and Pearlman [30] and by Corak, Garfunkel, Satterthwaite and Wexler [31] using the 1948-scale disappeared when this new scale was used.

16. The Temperature Scale Above 4.2° K

Above the normal boiling point, Clement, Logan and Gaffney adjusted their scale to give good agreement with the results of Berman and Swenson [32]. Above 4.2° K the 1948-scale was still based on the measurements of Kamerlingh Onnes published in 1911 and corrected by Kamerlingh Onnes and Weber in 1915. As a result of their measurements on carbon thermometers of Allen and Bradley, the suggestion was made by Worley, Zemansky and Boorse [33] that temperatures calculated with the 1948-scale are to high. They supposed that the temperature scale above 4.2° K could be defined better by extrapolation of the formula of Keesom and Lignac [Eq. (5)] than by

(11). These formulae give considerably different values of dp/dT, a quantity which Berman and Swenson wished to know accurately for corrections to apply to the measurements of the heat of vaporization of Berman and Poulter [34]. Therefore Berman and Swenson carried out measurements of the vapour pressure with a gas thermometer. Starting from the same value of the normal boiling point of hydrogen (20.381° K) as used by Keesom and Schmidt, they found deviations in the same direction as found by Worley, Zemansky and Boorse, although appreciably smaller. Moreover Berman and Swenson could verify the normal boiling point of He found by Keesom and Schmidt (4.216° K) within 0.002 degree and the critical temperature found by Kamerlingh Onnes and Weber [2] (5.20° K) within a few hundredths of a degree.

The density of the saturated vapour (ϱ_g) at 4.2° K as calculated by Berman and Swenson from their pT-relation and Berman and Poulter's measured apparent heat of vaporization (L^*) using the equation $\varrho_g = (T/L^*)\,(\mathrm{d}p/\mathrm{d}T)$ is in good agreement with the density calculated from the virial coefficients measured at Leiden [35] or by Keller [27].

As a result of their measurements Berman and Swenson gave the following pT-relation:

$$^{10}\log p_{\mathrm{cm\,Hg},\,20^\circ\mathrm{C}} = 0.97864 - (2.77708/T) + \tfrac{5}{2}\,{}^{10}\log T. \qquad (13)$$

The difference between the temperature calculated from this relation and T_{L55} is shown in Fig. 13.

17. Modification of the pT-relation of Clement *et al.*

Further experimental information about the deviations in the 1948-scale led Clement [36] to tabulate and issue a new pT-relation This pT-relation differs below 4.2° K a maximum of 0.004 degree from (12) (see Fig. 13 and Table V).

Clement denoted this scale by T_{55E}.

Meanwhile it was clear by the end of 1954 that there was not complete agreement between the deviations from the 1948-scale found in U.S.A. and at Leiden.

On the one hand it was desirable to improve the technique of vapour pressure measurements, on the other hand to reach a decision by accurate thermodynamic calculation of the pT-relation.

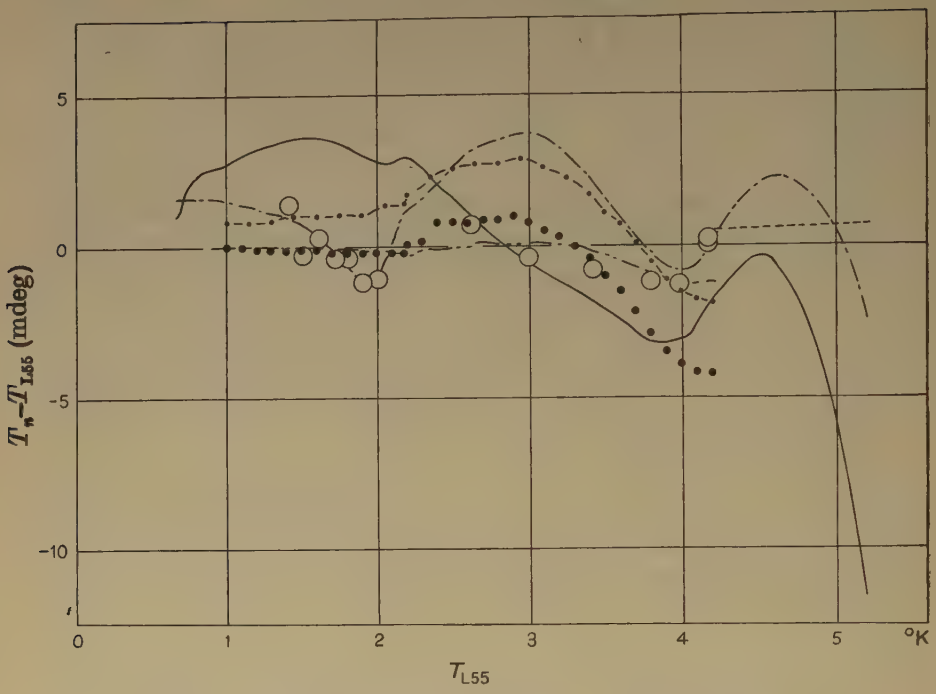

Fig. 13. Deviations of several scales from the T_{L55}-scale.

– – – – – – – – – – – : T_n is temperature according to Berman and Swenson [32].

– – – – – – – – – – – : T_n is the provisional scale of Van Dijk and Durieux [40].

– – – – – – – – – – – : T_n is the temperature according to Clement *et al.* (first scale) [29].

————————— : T_n is the temperature according to Clement *et al.* (second scale) [36].

— • — • — • — • : T_n is the thermodynamic temperature according to Erickson's calculation using formula (1) and (12). The latter for a preliminary definition of the scale [39].

• • • • • • • • • • • : T_n is temperature according to Erickson [39] recalculated with $L_0 = 59.50$ joule mole^{-1}.

○ : T_n is the magnetic temperature according to Ambler and Hudson (August 17, 1955) [37].

18. Accurate Vapour Pressure Measurements of Ambler and Hudson

The main difficulty in obtaining accurate results from susceptibility measurements combined with vapour pressure measurements lies in determining the exact value of the pressure corresponding to the average temperature of the paramagnetic sample. The sample itself must have practically the same temperature over its whole volume.

The best way to realize this condition is to place the sample in a

TABLE V

Deviations from the T_{L55}scale. T_n in °K, $\Delta T_n = T_n - T_{L55}$ in milli degrees.
T_{BS} means scale for $T > 4.2$ according to Berman and Swenson's formula.
T_{L55p} means provisional Leiden 1955 scale issued in August 1955.
T_{CI} means scale of Clement, Logan and Gaffney issued in May 1955.
T_{CII} means scale of Clement issued in December 1955 (T_{55E}).
T_E means scale according to the thermodynamic pT-relation calculated by Erickson and communicated to us in August 1955.
T_m means magnetic temperature according to the results of measurements of Ambler and Hudson obtained in August 1955.

T_n	ΔT_{1948}	ΔT_{BS}	ΔT_{L55p}	ΔT_{CI}	ΔT_{CII}	ΔT_E	T_m	ΔT_m
0.9	+ 3.0		− 0.02	+ 1.6	+ 2.6			
1.0	+ 1.0		0.00	+ 1.5	+ 2.7	+ 0.8		
1.1	+ 1.7		0.00	+ 1.4	3.0	0.8		
1.2	+ 2.0		0.00	+ 1.3	3.2	0.8		
1.3	+ 1.9		0.00	+ 1.1	3.4	0.9		
1.4	+ 2.8		0.00	+ 1.0	3.5	0.9	1.4155	+ 1.4
1.5	+ 3.1		0.00	+ 0.7	3.6	1.0	1.5066	− 0.3
1.6	+ 5.0		− 0.03	+ 0.4	3.6	1.0	1.6152	+ 0.3
1.7	+ 6.0		− 0.05	− 0.1	3.5	1.0	1.7189	− 0.4
1.8	+ 6.0		− 0.09	− 0.6	3.3	1.0	1.8111	− 0.4
1.9	+ 7.4		− 0.11	− 1.2	3.0	1.1	1.9011	− 1.2
2.0	+ 8.0		− 0.14	− 1.0	2.8	1.1	2.0072	− 1.1
2.1	+ 10.8		− 0.17	+ 0.2	2.8	1.2		
2.17				+ 1.1	3.0	1.2		
2.2	+ 11.6		− 0.29	+ 1.2	2.9	1.6		
2.3	+ 10.7		− 0.12	+ 1.6	2.6	1.7		
2.4	+ 9.0		− 0.11	+ 2.1	2.0	2.3		
2.5	+ 7.6		− 0.10	+ 2.6	1.6	2.4		
2.6	+ 6.7		− 0.03	+ 3.1	1.1	2.4	2.6104	+ 0.7
2.8	+ 4.6		+ 0.06	+ 3.5	+ 0.2	2.7		
3.0	+ 6.3		+ 0.06	+ 3.7	− 0.6	2.5	2.9953	− 0.4
3.2	+ 7.5		− 0.01	+ 3.2	− 1.2	2.1		
3.4	+ 7.4		− 0.20	+ 2.2	− 1.8	1.4	3.4118	− 0.8
3.6	+ 6.3		− 0.55	+ 0.9	− 2.5	0.4		
3.8	+ 4.5		− 0.94	− 0.3	− 3.2	− 1.0	3.7898	− 1.2
4.0	+ 2.1		− 1.24	− 0.9	− 3.1	− 2.0	3.9770	− 1.3
4.2	− 0.7	+ 0.5	− 1.23	+ 0.2	− 1.8	− 2.3	4.1656	+ 0.2
4.4	+ 2	+ 0.5		+ 1.6	− 0.7		4.1649	+ 0.0
4.6	+ 10	+ 0.5		+ 2.2	− 0.6			
4.8	+ 17	+ 0.5[6]		+ 1.8	− 2.3			
5.0	+ 17	+ 0.6		+ 0.4	− 5.8			
5.2	− 0	+ 0.6		− 2.4	− 11.6			

small vessel filled with a little liquid helium separated from the bulk helium in the cryostat. It is necessary to prevent heat influx to this inner bath through the tube connecting it with the manometer, while at the same time this tube may not have a temperature lower than the temperature of the liquid helium in the inner bath, as this would give rise to condensation of the helium in the tube and to a temperature gradient in the liquid surrounding the paramagnetic salt.

In their opinion Ambler and Hudson [37] best succeeded in realizing this in their most accurate measurements of August 17, 1955. Their results are compared in Fig. 13 with T_{L55}, they are also given in Table V. There is an agreement with the thermodynamically calculated T_{L55}-scale within 1.5 millidegree. *

19. Thermodynamic pT-relation. Historical Remarks

Of all scales used before 1955 in the liquid helium region the thermodynamic scales were the most accurate ones. As mentioned before the first purely thermodynamic scale for practical use was calculated by Verschaffelt as early as 1924. It was limited to temperatures below 1.475° K. The pT-relation of Bleaney and Simon for $T \leqslant 1.6°$ K also was essentially a thermodynamic scale.

Kistemaker [38], in 1945, and Erickson and Roberts [24] in 1954, published thermodynamic pT-relations derived from the general Eq. (1). These were only valid below the λ-point. Kistemaker's equation was:

$$^{10}\log p_{\mathrm{mm\,Hg},0°\mathrm{C}} = 2.198 - (3.115/T) + \tfrac{5}{2}\,{}^{10}\log T - 0.00046\,T^6 + \left.\begin{array}{r} \\ +0.42\,T^{\frac{1}{2}} \exp(-7.2/T) + \Phi(T) \end{array}\right\} \quad (14)$$

where $\Phi(T) = 1.6 \times 10^{-2}\,\{1-(1.6/T)\}$ between 2.17 and 1.6° K, and $\Phi(T) = 0$ for $T < 1.6°$ K.

Erickson and Robert's equation was:

$$\left.\begin{array}{l} {}^{10}\log p_{\mathrm{mm\,Hg},20°\mathrm{C}} = 2.1940 - (3.1071/T) + \tfrac{5}{2}\,{}^{10}\log T - 0.000500\,T^6 + \\ +0.448\,T^{\frac{1}{2}} \exp(-7.15/T) + (0.0522/T)\int_0^T \exp\{-20(2.20-T)^2\}\mathrm{d}T. \end{array}\right\} \quad (15)$$

20. Numerical Calculation of the Different Terms in the pT-relation

Again the starting point of the calculations is the relation.

$$\ln p = i - \{L_0/(RT)\} + \tfrac{5}{2}\ln T - \{1/V(RT)\}\left(\int_0^T S_l\,\mathrm{d}T - \int_0^p V_l\,\mathrm{d}p\right) + \varepsilon \quad (1)$$

* Note added in proof: In a second paper (J. Res. Nat. Bur. Stand., Wash., 57, 22 (1956)) Ambler and Hudson published new measurements and reanalyzed their older ones, the results are not as close in agreement with T_{L55} as according to their first paper.

where $\varepsilon = \ln\{(pV_g)/(RT)\} - (2B/V_g) - (3C/V_g^2)$

and $pV_g = RT\{1 + (B/V_g) + (C/V_g^2)\}$.

On substituting the numerical values of the constants, the following equation is obtained:

$$^{10}\log p_{\text{mm Hg},0°\text{C}} = 2.19260 - (3.10710/T) + \tfrac{5}{2}\,{}^{10}\log T - (0.052220/T) \left\{ \left[\left(\int_0^T S_l\,dT - \int_0^p V_l\,dp\right) + 0.4342945\,\varepsilon\right] \right. \quad (16)$$

here $g = 980.665$ cm sec^{-2} and $S_l\,dT$ and $V_l\,dp$ are taken in joule mole^{-1}.

The chemical constant i is given by the formula

$$i = \ln\{(2\pi m)^{3/2} k^{5/2} h^{-3}\}.$$

The numerical value is 12.2440 c.g.s. units. It can be calculated with great accuracy, since the constants are all accurately known. The best way to calculate L_0, the heat of vaporization at $T = 0°$ K is from Eq. (1) itself, by substituting in it the best experimental values of the vapour pressure. This gives the most reliable results between 1.5 and 2.5° K. At temperatures below 1.5° K the measurements with the gas thermometer are less accurate and at temperatures above 2.5° K the correction terms in (1) become more important, in particular $\int_0^T S_l\,dT$. In this way the value 59.50 ± 0.03 joule mole^{-1} for L_0 is obtained.

Of the other terms $\{1/(RT)\}\int_0^p V_l\,dp$ is the smallest one. V_l has been measured accurately as a function of the equilibrium pressure by Kamerlingh Onnes and Boks [41] and thus $\int_0^p V_l\,dp$ can be calculated with sufficient accuracy. To calculate $\{1/(RT)\}\int_0^p V_l\,dp$ as a function of T it is then still necessary to know p as a function of T with reasonable accuracy. The accuracy of the 1948-scale is more than sufficient.

For the calculation of ε a provisional pT-relation and accurate values of the virial coefficients or at least of B/V and C/V^2 are required. Erickson and Roberts [24] calculated ε from the Leiden values of the virial coefficients. Afterwards Erickson [39] used the table of Kilpatrick, Keller and Hammel [42]. The two calculations gave nearly the same result. Moreover the value of V_g at 4.2° K found by Erickson is equal to that calculated by Berman and Swenson from entirely other data (see § 16). All this gives good evidence that the virial coefficients below 4.216° K are known with sufficient accuracy to calculate ε. Van Dijk and Durieux used in their calculations the table of Kilpatrick *et al.*

One of the main difficulties in the computation of the pT-relation arises from the term $\int_0^T S_l \mathrm{d}T$. The measured values of the specific heat of the liquid above 2.5° K are not as accurate as at lower temperatures. The value of $\int_0^T S_l \mathrm{d}T$ at 4.2° K is about 5 times as large as at 2.5° K. In fact, at 4.2° K this integral is 38 % of L_0. When the integral is not calculated with a sufficient accuracy, Eq. (1) gives a boiling point that is too high or too low.

To overcome the difficulty of finding accurate values of the specific heat, c_l, from experimental data we used the relation:

$$c_l = \tfrac{5}{2} R - V_l \frac{\mathrm{d}p}{\mathrm{d}T} + \frac{\mathrm{d}}{\mathrm{d}T}\left\{RT\left(\frac{B}{V_g} + \frac{C}{V_g^2}\right) - \frac{T}{V_g}\frac{dB}{dT} - \frac{T}{2V_g^2}\frac{\mathrm{d}C}{\mathrm{d}T}\right) - L_{\mathrm{exp}}\right\} \quad (17)$$

which can be obtained by differentiation from:

$$L = L_0 + \tfrac{5}{2} RT + RT\left(\frac{B}{V_g} + \frac{C}{V_g^2} - \frac{T}{V_g}\frac{\mathrm{d}B}{\mathrm{d}T} - \frac{T}{2V_g^2}\frac{\mathrm{d}C}{\mathrm{d}T}\right) - \left. - \int_0^T c_l \,\mathrm{d}T - \int_0^p V_l \,\mathrm{d}p. \right\} \quad (18)$$

Eq. (17) enables one to calculate c_l from the experimental values of L [4, 34]. It appeared that the values of c_l thus obtained are nearly the average of the experimental values of Dana and Kamerlingh Onnes [43] and those of Keesom and Clusius [44]. The calculation of the pT-relation with the specific heat of the liquid obtained for $T > 2.5°$ K from (17) resulted in a value of the normal boiling point of 4.215° K. This is only 0.001 degree below the normal boiling point given by Schmidt and Keesom and this difference is within experimental error.

Erickson's [39] result for $\int_0^T S_l \mathrm{d}T$ agrees for $T < 3.20°$ K, within the equivalent of 0.0005 degree with our calculation.

21. Calculation of the Heat of Vaporization

We have calculated L from thermal quantities using (18). In Table VI this calculated L is compared with experimental data. There is agreement within experimental accuracy. This means that there is a good consistency between measured values of L and the thermal quantities c_l, B, V_l and L_0 and thus also between L and the pT-relation.

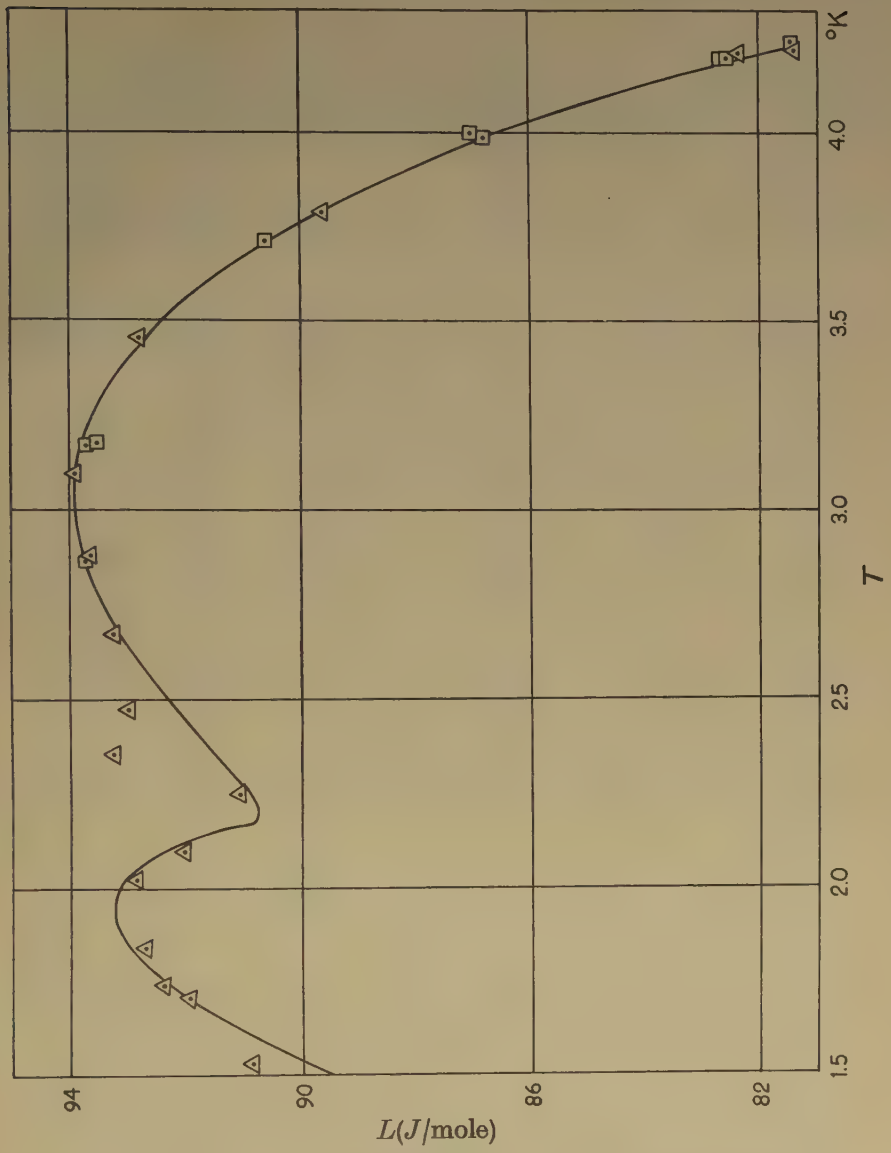

Fig. 14. The heat of vaporization of helium *versus* temperature.
△: Measurements of Dana and Kamerlingh Onnes [43].
⊡: „ „ Berman and Poulter [34].
Full line: calculated from Eq. (18).

TABLE VI

Heat of vaporization of ^{4}He. L_{exp}, has been obtained by graphical interpolation from the experimental data of Dana and Kamerlingh Onnes [4], Berman and Poulter [34] and the smoothed values of Keesom [15].

T_{L55} °K	L_{calc} joule mole^{-1}	L_{exp} joule mole^{-1}	T_{L55} °K	L_{calc} joule mole^{-1}	L_{exp} joule mole^{-1}
1.000	80.22		2.400	91.73	91.91
1.100	82.22		2.500	92.92	92.46
1.200	84.17		2.600	92.80	92.95
1.300	86.03		2.700	93.25	93.31
1.400	87.76		2.800	93.58	93.59
1.500	89.36	89.70	2.900	93.81	93.81
1.600	90.74	90.86	3.000	93.91	93.90
1.700	91.88	91.92	3.100	93.90	93.90
1.800	92.72	92.72	3.200	93.75	93.78
1.900	93.17	93.13	3.300	93.44	93.50
2.000	93.13	93.01	3.400	92.99	93.06
2.100	92.32	92.03	3.500	92.42	92.46
2.150	91.47	91.16	3.600	91.64	91.67
2.160	91.21	90.98	3.700	90.71	90.71
2.170	90.86	90.79	3.800	89.53	89.55
2.190	90.75	90.71	3.900	88.17	88.22
2.200	90.75	90.77	4.000	86.56	86.62
2.250	90.91	91.05	4.100	84.59	84.76
2.300	91.16	91.34	4.200	82.34	82.46

L_{calc} has been obtained from Eq. (18).

22. Extension of the Scale to the Critical Point

The data for the thermodynamic calculation of the pT-relation up to the critical point (5.2° K) are not yet available. For this reason it is a very happy circumstance that the results of Berman and Swenson's measurements with the gas thermometer can be used for the extension of the scale above 4.2° K.

By changing Berman and Swenson's formula slightly, but in such a way that it still represents their experimental data as accurately as the original formula [Eq. (13)], and by modifying the c_l *versus* T curve somewhat, it appeared to be possible to get a smooth junction of the Berman and Swenson-scale with the thermodynamic scale. At the same time Keesom and Schmidt's value of the normal boiling point (4.216° K) could be kept unchanged. As this boiling point was always confirmed by measurements of other investigators there is in

TABLE VII

Vapour pressure of ^4He according to scale T_{L55} in mm Hg at 0° C ($g = 980.665$ cm sec^{-2})

T(°K)	.00	.01	.02	.03	.04	.05	.06	.07	.08	.09
0.9	0.04224	0.04738	0.05304	0.05924	0.06604	0.07346	0.08157	0.09039	0.09999	0.11041
1.0	0.12170	0.13393	0.14714	0.16140	0.17676	0.19330	0.21108	0.23016	0.25062	0.27253
1.1	0.29597	0.32101	0.34774	0.37623	0.40657	0.43885	0.47316	0.50958	0.54822	0.58917
1.2	0.63253	0.67840	0.72688	0.77808	0.83211	0.88907	0.94909	1.01226	1.07872	1.14858
1.3	1.22196	1.29899	1.37979	1.46448	1.55321	1.64609	1.74326	1.84487	1.95103	2.06190
1.4	2.17762	2.29833	2.42416	2.55528	2.69183	2.83395	2.98180	3.13553	3.29529	3.46124
1.5	3.63354	3.81234	3.99780	4.19008	4.38934	4.59575	4.80946	5.03064	5.25946	5.49607
1.6	5.74065	5.99336	6.25438	6.52385	6.80196	7.08887	7.38474	7.68975	8.00406	8.32783
1.7	8.66124	9.00445	9.35762	9.72093	10.0945	10.4786	10.8733	11.2788	11.6952	12.1227
1.8	12.5614	13.0116	13.4733	13.9467	14.4320	14.9293	15.4388	15.9606	16.4948	17.0415
1.9	17.6010	18.1734	18.7587	19.3570	19.9685	20.5933	21.2316	21.8833	22.5485	23.2274
2.0	23.9199	24.6264	25.3467	26.0809	26.8289	27.5909	28.3670	29.1571	29.9610	30.7789
2.1	31.6106	32.4565	33.3161	34.1894	35.0762	35.9764	36.8896	37.8152	38.7536	39.7069
2.2	40.6754	41.6597	42.6597	43.6757	44.7078	45.7564	46.8217	47.9038	49.0030	50.1193
2.3	51.2531	52.4041	53.5728	54.7591	55.9634	57.1858	58.4264	59.6854	60.9628	62.2590
2.4	63.5739	64.9077	66.2607	67.6328	69.0244	70.4354	71.8661	73.3166	74.7871	76.2776
2.5	77.7884	79.3196	80.8713	82.4436	84.0368	85.6509	87.2861	88.9425	90.6203	92.3197
2.6	94.0407	95.7837	97.5486	99.3356	101.145	102.977	104.831	106.707	108.607	110.529
2.7	112.474	114.443	116.435	118.450	120.489	122.552	124.639	126.749	128.884	131.043
2.8	133.227	135.435	137.668	139.926	142.208	144.516	146.849	149.208	151.592	154.001
2.9	156.437	158.899	161.386	163.900	166.440	169.007	171.600	174.220	176.867	179.541
3.0	182.242	184.971	187.727	190.511	193.322	196.162	199.029	201.925	204.849	207.801
3.1	210.782	213.792	216.830	219.898	222.994	226.120	229.275	232.460	235.674	238.918
3.2	242.192	245.496	248.830	252.195	255.590	259.016	262.473	265.960	269.479	273.029
3.3	276.610	280.222	283.866	287.542	291.249	294.989	298.761	302.565	306.402	310.272
3.4	314.174	318.109	322.077	326.078	330.113	334.181	338.283	342.418	346.588	350.792
3.5	355.030	359.303	363.610	367.952	372.329	376.741	381.188	385.671	390.189	394.744
3.6	399.334	403.960	408.623	413.323	418.059	422.832	427.642	432.490	437.375	442.297
3.7	447.258	452.257	457.293	462.368	467.482	472.635	477.827	483.058	488.328	493.638
3.8	498.988	504.378	509.808	515.279	520.790	526.342	531.935	537.570	543.246	548.963
3.9	554.723	560.524	566.368	572.254	578.183	584.156	590.172	596.233	602.337	608.486
4.0	614.680	620.919	627.203	633.533	639.909	646.332	652.801	659.317	665.881	672.492
4.1	679.152	685.860	692.617	699.424	706.281	713.188	720.146	727.156	734.212	741.313
4.2	748.459	755.649	762.886	770.167	777.494	784.867	792.285	799.749	807.259	814.816
4.3	822.418	830.067	837.762	845.504	853.293	861.129	869.011	876.941	884.918	892.942
4.4	901.013	909.132	917.299	925.514	933.777	942.087	950.446	958.853	967.309	975.813
4.5	984.366	992.967	1001.62	1010.32	1019.07	1027.86	1036.71	1045.61	1054.55	1063.55
4.6	1072.60	1081.69	1090.84	1100.03	1109.28	1118.57	1127.92	1137.32	1146.77	1156.27
4.7	1165.82	1175.42	1185.07	1194.78	1204.53	1214.34	1224.20	1234.11	1244.07	1254.08
4.8	1264.15	1274.27	1284.44	1294.66	1304.94	1315.27	1325.65	1336.09	1346.57	1357.11
4.9	1367.71	1378.36	1389.06	1399.81	1410.62	1421.48	1432.40	1443.37	1454.39	1465.47
5.0	1476.60	1487.79	1499.03	1510.33	1521.68	1533.08	1544.54	1556.06	1567.63	1579.26
5.1	1590.94	1602.68	1614.47	1626.32	1638.23	1650.19	1662.21	1674.28	1686.41	1698.59
5.2	1710.84	1723.14	1735.49							

our opinion no sufficient reason to change it now. Nevertheless the value 4.215° K would fit more closely to our thermodynamic calculations, moreover there is some indication [45] that the normal boiling point of hydrogen has a somewhat lower value than that used by Schmidt and Keesom, this would also be a reason for preferring 4.215° K.

23. The T_{L55}-scale

Using Eq. (1) we calculated p in intervals of 0.05 degree. Near the λ-point the steps were narrowed to 0.01 degree. The numerical data were carefully smoothed to avoid irregularities and to enable correct interpolation and accurate calculation of dp/dT in a simple way. The subtabulation has been carried out by the Mathematical Centre of the University of Amsterdam in intervals of 0.001 degree from $T=0.9$ up to 5.25° K. From $T=0$ up to 0.5° K p has been calculated in steps of 0.1 degree and from $T=0.5$ up to 0.9° K in steps of 0.01 degree. Copies of these tables including a list of the basic data used in the calculation can be obtained from the thermometry section of the Kamerlingh Onnes Laboratory. An abstract of the pT-table is appended to this article as Table VII.

REFERENCES

1 J. E. Mayer and M. G. Mayer, Statistical Mechanics, John Wiley and Sons New York, (1940), p. 292.

2 H. Kamerlingh Onnes and Sophus Weber, Leiden Comm. 147*b*; Proc. Roy. Acad. Amsterdam, 18, 493 (1915).

3 J. E. Verschaffelt, Leiden Comm. Suppl. 49; Rapp. et Commun. 4e Congr. int. du Froid, London, (1924).

4 L. I. Dana and H. Kamerlingh Onnes, Leiden Comm. 179*c*; Proc. Roy. Acad. Amsterdam, 29, 1051 (1926).

5 H. Kamerlingh Onnes, Leiden Comm. 108; Proc. Roy. Acad. Amsterdam, 11, 168 (1908).

6 H. Kamerlingh Onnes, Leiden Comm. 119; Proc. Roy. Acad. Amsterdam, 13, 1093 (1911).

7 H. Kamerling Onnes, Leiden Comm. 124*b*; Proc. Roy. Acad. Amsterdam, 14, 678 (1911).

8 G. Schmidt and W. H. Keesom, Leiden Comm. 250*b*; Physica, 4, 963 (1937).

9 W. H. Keesom, Sophus Weber and G. Nørgaard, Leiden Comm. 202*b*; Proc. Roy. Acad. Amsterdam, 32, 864 (1929).

10 Sophus Weber and G. Schmidt, Leiden Comm. 246*c*; Rapp. et Commun. 7e Congr. int. du Froid, la Haye – Amsterdam, (1936).

[11] W. H. Keesom, Sophus Weber and G. Schmidt, Leiden Comm. 202*c*; Proc. Roy. Acad. Amsterdam, 32, 1314 (1929).
[12] Sophus Weber, W. H. Keesom and G. Schmidt, Leiden Comm. 246*a*; Rapp. et Commun. 7e Congr. int. du Froid, la Haye – Amsterdam, (1936).
Sophus Weber, Leiden Comm. 246*b*.
Sophus Weber, Leiden Comm. 246*d*; Rapp. et Commun. 7e Congr. int. du Froid, la Haye – Amsterdam, (1936).
[13] G. Schmidt and W. H. Keesom, Leiden Comm. 250*b* and *c*; Physica, 4, 963 and 971 (1937).
[14] W. H. Keesom, Leiden Comm. 219*a*; Proc. Roy. Acad. Amsterdam, 35, 136 (1932).
[15] W. H. Keesom, Helium, Elsevier, Amsterdam, (1942).
[16] B. Bleaney and F. Simon, Trans. Faraday Soc., 35, 1205 (1939).
R. P. Hudson, in Temperature Its Measurement and Control, 2, Reinhold Publish. Corp., New York, (1955), p. 187.
[17] W. H. Keesom and W. P. J. Lignac, in Temperature Its Measurement and Control, 1, Reinhold Publish. Corp., New York, (1939); Leiden Comm. Suppl. 90*c*.
[18] B. Bleaney and R. A. Hull, Proc. Roy. Soc., London, 178, 74 (1941).
[19] H. B. G. Casimir, D. de Klerk and D. Polder, Leiden Comm. 261*a*; Physica, 7, 737 (1940).
[20] W. P. J. Lignac, Ned. Tijdschrift voor Natuurkunde, 7, 14 (1940), also ref. 17.
H. van Dijk, Proc. Int. Conf. on the Physics of very low Temperatures M.I.T., 1949, p. 118.
[21] H. van Dijk and D. Shoenberg, Nature, 164, 151 (1949); Procès Verbaux du Comité Consultatif de Thermométrie auprès du Comité International des Poids et Mesures, Session de 1952 p. T 151 (Gautiers–Villars, Paris).
[22] J. Kistemaker and W. H. Keesom, Leiden Comm. 269*b* and *c*; Physica, 12, 227 and 272 (1946).
[23] J. Kistemaker, Leiden Comm. Suppl. 95*a*, Physica, 12, 281 (1946).
[24] R. A. Erickson and L. D. Roberts, Phys. Rev., 93, 957 (1954).
[25] H. van Dijk, in Temperature Its Measurement and Control, 2, Reinhold Publish. Corp., New York, (1955).
[26] J. R. Clement, J. K. Logan and J. Gaffney, Naval Research Laboratory Report 4542, Washington D.C., U.S.A., (May 1955).
[27] W. E. Keller, Phys. Rev., 97, 1 (1955) and 100, 1790 (1955).
[28] W. E. Keller, Phys. Rev., 98, 1571 (1955).
[29] J. R. Clement, J. K. Logan and J. Gaffney, Phys. Rev., 100, 743 (1955).
[30] P. H. Keesom and V. Pearlman, Phys. Rev., 96, 897 (1954).
[31] W. S. Corak, M. P. Garfunkel, C. B. Satterthwaite and A. Wexler, Phys. Rev., 98, 1699 (1955).
[32] R. Berman and C. A. Swenson, Phys. Rev., 95, 311 (1954).
[33] R. D. Worley, M. W. Zemansky and H. A. Boorse, Phys. Rev., 93, 45 (1954).
[34] R. Berman and J. Poulter, Phil. Mag., (7), 43, 1047 (1952).
[35] W. H. Keesom and W. K. Walstra, Leiden Comm. 260*c*; Physica, 7, 985 (1940).

[36] See ref. [29]; note added in proof.
[37] E. Ambler and R. P. Hudson, J. Res. Nat. Bur. Stand., Wash., **56**, 99 (1956).
[38] J. Kistemaker, Thesis, Leiden (1945).
[39] R. A. Erickson, Private Communication Aug. 1955.
[40] H. van Dijk and M. Durieux, Commun. Conférence de Physique des basses températures, Paris, (1955), p. 595.
[41] H. Kamerlingh Onnes and J. D. A. Boks, Leiden Comm. 170*b*; Rapp. et Commun. 4e Congr. int. du Froid, London, (1924).
[42] J. E. Kilpatrick, W. E. Keller and E. F. Hammel, Phys. Rev., **97**, 9 (1955).
[43] L. I. Dana and H. Kamerlingh Onnes, Leiden Comm. 179*d*; Proc. Roy. Acad. Amsterdam, **29**, 1061 (1926).
[44] W. H. Keesom and K. Clusius, Leiden Comm. 219*e*; Proc. Roy. Acad. Amsterdam, **35**, 307 (1932).
[45] G. W. Moessen, J. G. Aston and R. G. Ascah, J. chem. Phys., **22**, 2096 (1954).
G. W. Moessen, Thesis, Penn. State Univ., (1955).
A. S. Borovik–Romanov and P. G. Stralkov, Procès Verbaux du Comité Consultatif de Thermometrie auprès du Comité International des Poids et Mesures, Session de 1952, p. T 32 (Gautiers–Villars, Paris).
H. van Dijk, Procès Verbaux du Comité Consultatif de Thermometrie, Session de 1952, p. T 37.

AUTHOR INDEX

Abeles, B., 261, *265*
Abragam, A., 303, 310, 314, 332, *334*, *335*
Abraham, B. M., 9, *57*, 93, *104*, 355, 356, *366*, 367
Abrahams, E., 168, *184*
Ahmann, D. H., 392
Aigrain, P., 203, *223*
Alers, P. B., 181, *185*
Allen, J. F., 84, 85, 91, 99, 101, *103*, *104*, 392
Altman, H. W., 426, *430*
Ambler, E., 80, *82*, 125, *136*, 321, *336*, 454, 456, *464*
Anderson, C. T., 412, 413, *429*
Anderson, D. W., 289, *291*
Anderson, W. S., 326, *337*
Andrews, F. A., 160, 177, *184*
Andronikashvili, E., 100, *104*
Apfel, J. H., 219, 220, *225*
Ard, W. B., 356, *367*
Ascah, R. G., 462, *464*
Aston, J. G., 114, 115, *136*, 462, *464*
Atkins, K. R., 10, 26, 27, 28, *57*, 60, 65, 66, 67, 68, 69, *81*, *82*, 91, 101, 102, *103*, 108, 112, 115, 119, 120, 121, 124, 131, 133, *135*, *136*, *137*
Azbel, M. Ya., 183, *186*

Baker, J. M., 326, 327, *336*, *337*
Ball, A. F., 412, *428*
Baltensperger, W., *223*
Band, W., 117, *136*
Bannister, J. R., 382, 392, *394*
Bardeen, J., 165, 168, *184*, 216, *225*
Barker, W. A., 314, *335*
Barnes, C. B., *81*
Barrat, J. P., 313, 314, *334*
Barrett, C. S., 156, *183*
Barron, H., 396, 427, *428*
Barron, T. H. K., 362, *367*
Barson, F., 382, 384, 389, 392, *394*
Bastin, J. A., 200, *222*
Bates, E. A., 412, *428*
Bates, L. F., 392
Beattie, *430*
Beaumont, C. F. A., 14, *57*
Becker, J. H., 217, *225*
Becker, M., 216, *225*
Beenakker, J. J. M., 88, *103*
Behrendt, D., 392
Beljers, H. G., 314, 316, *334*
Bell, E. E., 218, 219, *225*
Benedicks, C., 392
Benedict, T. S., 207, *223*
Benzie, R. J., 274, 275, *290*
Bergenlid, U., 213, *224*
Berlincourt, T. G., 227, 257, 259, 260, 261, 262, *264*, *265*
Berman, A., 374, 375, 378, *393*
Berman, R., 160, 161, 177, *184*, 214, *224*, 452, 453, 454, 458, 459, 460, *463*
Bernstein, 317, 318, 319, *336*
Beun, J. A., 319, 321, 326, *336*, *337*
Bhatia, A. B., 178, *185*
Biermasz, Th., 174, 175, *185*
Bishop, G. R., 321, 325, 326, 327, *336*
Bitter, F., 313, *334*
Blackman, M., 157, 169, *183*, 211, *224*, 226, *264*, 396, 405, *427*, *428*, *429*
Blakewood, 109, *136*
Blatt, F. J., 168, *184*, 216, *225*
Blatt, J. M., *58*
Bleaney, B., 303, 304, 306, 307, 309, 319, 321, 326, 327, *334*, *335*, *336*, *337*, 444, *463*
Blewitt, T. H., 177, *185*
Blin-Stoyle, R. J., 316, *336*
Bloch, C., 314, *335*
Bloch, F., 152, *183*
Bloembergen, N., 289, *291*, 332, *333*
Blunt, R. F., 216, 217, *225*
Bohm, D., 168, *184*
Bohr, A., 299, 300, 331, *333*
Bölger, B., 278, 285, *290*
Bommer, H., 380, 382, 392, *394*
Bond, W. L., 211, 212, *224*
Boorse, H. A., 121, 124, 125, *136*, *137*,

374, 375, 378, *393*, *452*, *463*
Borelius, G., 162, *184*
Born, M., 41, 42, 43, 44, *58*, 358, *367*, 396, 400, 427, *427*
Borovik–Romanov, A. S., 462, *464*
Bots, G. J. C., 67, *81*
Bottema, J. A., 392
Bouwkamp, C. J. 287, *290*
Bowen, D. H., 141, *150*
Bowers, K. O., 306, 326, *335*, *336*
Bowers, R., 86, 92, 95, 96, *103*, *104*, 108, 112, 114, 115, 124, 127, 133, *135*, *136*, *137*
Bowman, M. G., 392
Brailsford, A. D., 244, *265*
Brattain, W. H., 195, 196, *221*
Bray, R., 205, *223*
Breckenridge, R. G., 217, *225*
Brenig, W., 400, 408, 418, 419, *427*, *429*
Brewer, D. F., 89, *103*, 109, 115, 127, *136*, *137*
Bridgman, P. W., 392
Briggs, H. B., 218, *225*
Brillouin, L., 37, *58*, 418, 420, *429*
Broer, L. J. F., 270, 274, 288, 289, *290*, *291*
Broese van Groenou, A., 95, 99, 102, *104*
Brons, F., 273, *290*
Bronstein, M., 208, *223*
Brooks, H., 199, 213, 215, *222*, *224*
Brossel, J., 313, 314, *334*, *335*
Brovetto, P., 314, *335*
Brown, S. C., 207, *223*
Brunauer, 115, *136*
Brussaard, P. J., 300, *334*
Buckel, W., 150, *150*
Buehler, E., 212, *224*
Bühler, H., 404, *428*
Bühler, H. H., *428*
Burge, E. J., 110, *136*
Burk, D., 412, *429*
Burstein, E., 218, 219, *220*, *225*
Busch, G., 203, 204, *220*, *222*
Busey, R. H., 415, *428*
Busse, C. A., 165, *184*
Butler, S. T., 14, *57*, *58*
Button, K. J., 261, *265*
Bijl, A., 132, *137*
Bijl, D., 274, *290*, 397, 426, 427, *427*, *428*, *429*

Cacho, C. F. M., 307, 329, *336*
Cagnac, B., 313, *335*
Callaway, J., *221*
Carlson, R. C., 198, 201, *222*
Carver, T. R., 314, 316, *334*, *335*
Casimir, H. B. G., 214, *224*, 271, *296*, 444, 446, *463*
Chandrasekhar, B. S., 85, 92, 95, *103*, *104*, 121, 122, 124, *136*
Chase, C. E., 26, *57*, 60, 65, 75, 76, *81*, *82*
Chester, G. V., 14, *57*
Chester, P. F., 142, *150*
Cini, G., 314, *335*
Clark, C. W., 413, 415, *428*
Clement, J. R., 212, *224*, 412, *428*, *430*, 449, 452, 453, *454*, *463*
Clusius, K., 404, 405, 412, 413, 415, 416, *428*, 429, 458, *464*
Cobble, J. W., 412, *429*
Cobble, L. W., 143, *150*
Coffer, L. W., 412, *428*
Cohen, E. G. D., 28, 36, 40, *58*
Cohen, M., 54, 56, *58*
Collins, R. J., 220, *225*
Coltman, R. R., 177, *185*
Combrisson, J., 195, *221*, 314, *335*
Conwell, E. M., 198, 199, 200, *222*
Cook, C. S., 325, *337*
Cooke, A. H., 271, 274, *290*, 307, 308, *334*, *335*
Corak, W. S., 412, 415, 417, *428*, *429*, 452, *463*
Corenzwit, E., 146, *150*
Cornish, F. H., 169, *185*
Cox, J. A. M., 292, 294, 295, 296, 323, 331, *333*
Craig, R. S., 412, *428*
Cristescu, S., 209, *223*
Croft, G. T., 246, 257, *265*

Daane, A. H., 369, 373, 375, 378, 380, 382, 392, *393*

Dabbs, J. W. T., 299, 302, 309, 317, 318, 319, 329, 330, *334*, *335*, *336*, *337*
d'Altroy, F. A., 206, 207, *223*
Dana, L. I., 432, 458, 459, 460, *462*, *464*
Daniels, J. M., 307, 308, 319, 321, 325, 327, 331, *334*, *335*, *336*
Darnell, F., 412, *428*
Dash, J. C., 19, *58*
Dash, J. G., 95, 101, *104*, 105, 124, *136*
Daunt, J. C., 15, *57*
Daunt, J. G., 9, 28, *57*, *58*, 61, *81*, 118, 121, *135*, *136*, 309, 323, *334*, *337*, 392, 412, *428*, *429*
Daunt, L. G., 143, 145, *150*
Davisson, J. W., 218, 219, *225*
De Boer, J., 4, 7, 28, 36, 40, *57*, *58*, 132, *137*, 158, 177, *184*, *185*, 365, *367*, 398, *428*
Debye, P., 198, 199, 200, 214, *222*, *224*, 272, 290, 395, 396, 399, 427
De Greeve, L., 205, *223*
De Groot, S. R., 84, *103*, 209, *223*, 292, 295, 296, 297, 298, 331, 332, *333*, *334*
De Haas, W. J., 108, 124, *135*, 145, *150*, 158, 174, 175, 177, *184*, *185*, 226, 227, 261, 262, *264*, 392
De Klerk, D., 60, 68, *81*, 316, 319, 320, 326, *335*, *337*, 444, 446, *463*
De Launay, J., 211, 212, *224*
Delsing, A. M. G., 86, 95, 96, 97, 100, *103*, *104*
Dennison, D. H., 392
Derksen, H. E., 270, 280, *290*
Désirant, M., 416, *429*
De Sorbo, W., 213, *224*, 412, 413, *428*
De Troyer, A., 100, *104*
Devonshire, A. F., 29, *58*
De Vries, G., 9, *57*
De Vries, Hl., 319, *335*
De Vrijer, F. W., 270, 280, *290*, *291*
Dexter, R. N., 190, 191, 192, 198, 199, *221*, *222*
Dhillon, J. S., 228, 242, 243, 246, 259, 260, 261, 262, *264*
Dick, J. L., 326, *337*
Dicke, G. H., 314, *335*
Dicke, R. H., 313, 314, *334*
Diddens, A. N., 322, 326, *337*
Dillinger, J. R., 126, *137*
Dingle, R. B., 28, *58*, 189, 199, *221*, *222*, 235, 236, *264*
Dmitrenko, I. M., 259, 260, 261, *265*
Dobrolowski, W., 321, 325, 327, *337*
Dokoupil, Z., 9, *57*, 61, *81*, 89, 95, *103*
Dolginov, A. Z., 297, *334*
Domb, C., 358, 362, 365, *367*, 403, *428*
Donahoe, F. J., 246, 259, *265*
Dorfman, J. D., 189, *221*
Douglas, T. B., 412, *428*
Dresselhaus, G., 190, 191, 192, 194, 196, *221*
Duchateau, W., 205, *223*
Duffus, H. J., 307, 308, *334*, *335*
Dugdale, J. S., 6, 9, 10, 21, 22, *57*, 340, 345, 350, 360, 363, *366*, *367*, 403, *428*
Dumaré, J. M., 362, *367*
Dunajew, J. A., 188, 196, *221*
Dunlap, Jr., W. C., 198, 201, 219, *222*
Du Pré, F. K., 201, *222*, 271, *290*
Durand, H., 321, *327*
Durieux, M., 454, *464*
Duyckaerts, G., 99, *104*, 405, 413, 415, *428*
Dyba, 109, *136*
Dijkstra, L. J., 270, *290*

Edwards, D. O., 89, *103*
Edwards, M. H., 28, *57*, 60, 66, 67, *81*
Edwards, W. A. M., 350, *366*
Egelstaff, P. A., 19, *58*
Egli, P. H., *220*
Eisenstein, J. C., 109, 134, *135*, 309, *335*
Ellinger, F. H., 392
Elliot, J. F., 382, 383, 384, 387, 389, 392, *393*, *394*
Elliot, R. J., 195, *221*
Ellison, R. D., 329, 330, *337*
Emmett, 115, *136*
Englman, R., 183, *186*
Erginsoy, C., *223*

Erickson, R. A., 449, 454, 456, 457, *463*, *464*
Ericson, R. P., 392
Eschenfelder, A. H., 279, 284, *290*
Eselsohn, B. N., 119, 121, 124, *136*
Estermann, I., 195, 210, *222*, *223*, 412, 413, 415, *428*, *429*
Eucken, A., 416, *429*

Fagen, E., 215, *224*
Fairbank, H. A., 61, 77, 80, *81*, *82*, 95, *104*
Fairbank, W. M., 356, *367*
Fan, H. Y., 196, 206, 207, 216, 217, 218, 219, 220, *220*, *222*, *223*, *225*
Farr, J. D., 392
Fawcett, E., 183, *186*, 258, *265*
Feher, G., 195, 196, *221*, 312, *335*
Ferroni, S., 314, *335*
Feynman, R. P., 1, 14, 28, 38, 54, 55, 56, *57*, *58*, 126, 134, *137*
Fine, P. C., 419, *429*
Fink, R. W., 325, *337*
Fisher, I. Z., 365, *367*
Fletcher, R. C., 190, 191, 192, 195, 196, *221*
Floyd, A. L., 373, 392, *393*
Foex, M., 376, 382, 392, *393*
Foner, A., 195, *222*
Forrez, G., 26, *57*
Forsythe, W. R., 415, 416, *428*
Fowler, R. H., 208, *223*
Franchetti, S., 134, *137*
Franz, H., 145, *150*
Frauenfelder, H., 297, 317, 325, *337*
Frederikse, H. P. R., 114, 117, *136*, 208, 209, 216, 217, *223*, *225*
Frenkel, J., 124, 130, *136*, *137*
Friedberg, S. A., 412, 415, *428*, *429*
Friedman, M. H., 14, *57*
Fritzsche, H., 198, 200, 201, 202, 204, 205, 206, *222*
Fröhlich, H., 13, 28, 29, *57*, 168, *184*
Fröman, P. O., 299, *333*

Gaffney, J., 449, 452, 453, 454, *463*
Gallaher, L. J., 326, *337*
Ganme–Mahn, F., 376, 392, *393*
Garfunkel, M. P., 415, 417, *428*, 452, *463*
Garrett, C. G. B., 310, *336*
Geballe, T. H., 198, 199, 200, 201, 204, 208, 209, 215, *222*, *223*, *226*, 415, *428*
Gere, E. A., 195, 196, *221*, *335*
Gerritsen, A. N., 177, 178, 181, *185*, *186*, 201, *222*
Gerritsen, H. J., 289, *291*
Giauque, W. F., 415, 416, *428*
Ginnings, D. C., 412, *428*
Ginsburg, V. L., 168, *184*
Giorgi, A. L., 392
Ginzbarg, A. S., 203, 204, *222*
Glatzel, G., 338, *366*
Gliessman, J. R., 200, 201, 204, *222*
Goff, J., 215, *224*
Gold, A. V., 251, *265*
Goldey, J. M., 207, *223*
Goldman, J. E., 412, 415, *428*
Goldschmidt, G., 321, 325, *336*
Goldstein, L., 19, *58*
Goldstein, M., 19, *58*
Goodman, B. B., 412, *428*
Gordon, W. L., 15, *57*
Gordy, W., 356, *367*
Gorter, C. J., 9, 27, *57*, 60, 65, 67, 68, 69, 71, 72, 73, 78, *81*, *82*, 83, 84, 85, 89, 92, 95, 97, 99, 101, 102, *103*, *104*, 114, 117, *136*, 266, 268, 269, 270, 271, 273, 274, 275, 278, 280, 289, *289*, *290*, *291*, 301, 302, 305, 309, 319, 321, 324, 326, 327, *334*, *335*, *336*, *337*
Grace, M. A., 297, 307, 310, 316, 319, 321, 323, 324, 325, 326, 327, 329, *335*, *336*, *337*
Gray, T. P., 296, 305, *333*
Griffel, M., 382, 384, 389, 392, *394*, 413, *429*
Griffing, D. F., 325, 326, *337*
Grilly, E. R., 350, 355, 365, *366*, *367*
Gross, E. F., *220*
Gross, Y. F., 219, *225*
Grüneisen, E., 157, *183*, 396, 422, 423, 424, 426, *427*

Gudden, B., 204, *223*
Guggenheim, E. A., 406, *430*
Gunnersen, E. M., 230, 246, 256, 262, *264*
Gurevich, L., 172, *185*, 206, *223*
Gurney, R. W., 213, *224*
Gijsman, H. M., 289, *291*

Hach, C. C., 392
Hadley, L. N., 219, 220, *225*
Hägg, G., 148, *150*
Halban, H., 316, 319, 321, 325, *336*, *337*
Hall, G. R., 309, *335*
Hall, L. H., 216, *225*
Ham, A. C., 110, 111, 122, 124, *136*
Ham, F. S., 169, 183, *184*, *186*
Hammel, E. F., 93, *104*, 457, *464*
Hanna, I. I., 170, *185*
Hannay, N. B., 219, *225*
Han-Ying Ku, 192, *221*
Hardy, G. F., 147, 148, *150*
Harper, P. G., 244, 259, *264*
Harteck, P., 412, *429*
Hartogh, Chr. D., 295, 296, 297, 331, *333*, *334*
Harvey Brooks, *220*
Haseda, T., 279, *290*
Hatton, J., 201, *222*
Hawkins, W. B., 313, 314, *334*
Haynes, J. R., 218, *225*
Heer, C. V., 61, *81*
Heikkila, 74, *82*, 100, *104*
Heine, V., 240, 257, 259, 261, *264*, *265*
Henkel, J. H., 362, *367*
Henshaw, D. G., 15, *57*, 110, 115, 122, *136*
Herlin, M. A., 60, 75, 76, 80, *81*, *82*
Herman, F., 187, 193, 194, 195, *221*
Hermann, K. W., 373, 375, 378, 382, 392, *393*
Heroux, L., 314, *335*
Herring, C., 197, 199, 209, 214, *222*, *223*
Heumann, T., 392
Hicks, J. F. G., 412, *429*
Hill, D. L., 300, 331, *333*
Hill, R. D., 325, 326, *337*
Hill, R. W., 210, 213, *223*, *224*, 405, 412, 413, *428*
Hill, T. L., 131, *137*
Hilsch, R., 142, 150, *150*
Holden, A. N., 195, *221*, *222*
Holland, F. A., 350, *366*
Hollis Hallett, A. C., 74, *82*, 83, 100, 102, *103*, *104*
Honig, A., 195, *221*, 314, *335*
Hooftman, 115, *137*
Hooton, D. J., 358, *367*, 396, 403, *427*
Hopkins, B. S., 392
Horowitz, M., 412, *428*, *429*
Hosler, W. R., 217, *225*
Hrostowski, H. J., 200, 201, *222*
Hsieh, Y. C., 210, 213, *224*
Huang, K., 41, 42, 43, 44, *58*, 396, *427*
Hubbard Horn, F., 219, *225*
Hudson, R. P., 60, 68, *81*, 328, *336*, 444, 454, *464*
Huggill, J. A. W., 350, *366*
Huiskamp, W. J., 322, 327, *337*
Hull, A. W., 392
Hull, G. W., 204, 208, 209, 215, *223*, *225*
Hull, R. A., 61, *81*, 89, *103*, *444*, *463*
Hulm, J. K., 146, 147, 148, *150*, 160, 177, *184*
Hume–Rothery, W., 396, 424, 426, *427*
Hung, C. S., 95, 97, 99, *104*, 200, 201, 203, 204, *222*
Hunt, B., 60, *81*, 95, 97, 99, *104*
Hunter, S. C., 165, *184*
Hurst, D. G., 15, *57*
Hutchison, T. S., 14, *57*
Hutner, R. A., 201, *222*
Hwang, J. L., 407, *427*

Ingram, D. J. E., 307, *334*

Jackson, L. C., 110, 111, 115, 122, 124, *136*
Jaeger, F. M., 392
James, H.M., 198, 203, 204, *222*
James, N. R., 147, *150*, 373, 375, 378, *393*

Jansen, L., 84, *103*
Jastram, P. S., 323, 327, *337*
Jauch, J. M., 303, 304, 305, 306, 308, *334*
Jeffries, C. D., 314, 321, 325, 327, 332, *335*, *337*
Johnson, C. E., 307, 310, 321, 323, 324, 326, 327, 329, *336*, *337*
Johnson, V. A., 199, 200, 201, *222*
Johnston, D. F., 259, *265*
Johnston, H. L., 412, 413, 426, *429*, *430*
Jones, G. A., 325, *337*
Jones, G. O., 141, 142, *150*, 350, *366*
Jones, H., 28, 29, *57*, 84, *103*, 165, 169, *184*, *185*, 199, *222*
Jones, R. V., 321, 327, *337*
Justi, E., 188, *221*

Kaganov, M. I., 183, *186*
Kahn, A. H., 220, *225*
Kaiser, W., 217, 218, 219, 220, *225*
Kamerlingh Onnes, H., 105, *135*, 432, 434, 435, 437, 458, 459, 460, *462*, *464*
Kanda, E., 279, *290*
Kapadnis, D. G., 9, *57*, 61, *81*, 89, 95, *103*, 407, *427*
Kapitza, P. L., 85, 88, 89, 91, 95, 99, *103*
Kaplan, J. I., 314, *335*
Karryev, N. A., 219, *225*
Kastler, A., 313, 314, *334*, *335*
Kasuya, T., 163, *184*
Kaufmann, A. R., 392
Keesom, Miss A. P., 338, 340, 350, 353, *366*
Keesom, P. H., 210, 211, 212, 213, *223*, *224*, 405, 413, 415, 417, *428*, *429*, 452, *463*
Keesom, W. H., 9, 10, 14, 31, *57*, *58*, 99, *104*, 177, *185*, 338, 340, 346, 350, 353, *366*, 412, 413, 415, 416, 417, *428*, *429*, *430*, 435, 437, 439, 440, 441, 443, 444, 445, 453, 458, 460, *462*, *463*, *464*
Keller, W. E., 451, 453, 457, *463*, *464*
Keller, W. H., 392
Kelly, F. M., 158, *183*, 406, *428*
Kelly, K. K., 412, 416, *429*
Kemp, W. R. G., 158, 160, 176, 177, *184*, *185*
Kevane, C. J., 376, 392, *393*
Khalatnikov, I., 14, *57*, 62, 70, 71, 72, 74, *81*, *82*
Khalilov, A., 200, *222*
Khutsishvili, G. P., 305, 310, 323, *335*, *337*
Kieffer, R., 147, *150*
Kihara, T., 362, *367*
Kikoin, A. K., 106, *135*
Kilpatrick, J. E., 457, *464*
King, J. C., 80, *82*, 95, *104*
Kip, A. F., 190, 191, 192, 194, 195, 196, *221*
Kistemaker, J., 445, 446, 456, *463*, *464*
Kitano, Y., 213, *224*
Kittel, C., 187, 190, 191, 192, 194, 195, 196, *220*, *221*, *222*, 314, *335*
Klein, M. J., 314, *335*
Klemens, P. G., 99, *104*, 158, 160, 163, 169, 172, 173, 174, 175, 176, 177, *184*, *185*, 213, 214, *224*
Klemm, W., 380, 382, 393, *394*
Klose, H., 392
Knipper, A. C., 307, 326, 329, *336*
Koba, S., 362, *367*
Koehler, W. C., 388, 393, *394*
Kohler, M., 159, 181, *184*, *185*
Kohn, W., 192, *221*
Kok, J. A., 412, 415, 416, 417, *428*, *429*
Komatsu, K., 213, *224*
Korenblit, L. L., 170, *185*
Korringa, J., 178, *185*, 314, *335*
Kosevich, A. M., 229, 235, *264*
Koshino, S., 205, *223*
Kothen, C. W., 413, *429*
Kramers, H. A., 14, 39, *57*, 269, *290*
Kramers, H. C., 9, 27, *57*, 60, 65, 66, 67, 68, 69, 71, 72, 73, 78, 80, 81, 82, 89, *103*, 274, *290*
Krautz, E., 159, *184*
Kremers, H. C., 392

Krier, C. A., 412, *428*
Kroger, F. A., 198, 200, 201, 204, *222*
Krumshansl, J., 213, 215, *224*
Kubo, R., 289, *291*
Kurbatov, J. D., 326, *337*
Kurrelmeyer, B., 416, *429*
Kurti, N., 60, 80, *81*, *82*, 106, *135*, *136*, 301, 310, 319, 321, 323, 324, 325, 327, *334*, *336*, *337*

Labhardt, H., 203, 204, *222*
La Blanchetait, C., 376, 378, 392, *393*
Lacey, R. F., 313, *334*
Lamarche, J. L. G., 308, 331, *335*
Landau, L. D., 13, 39, 40, *58*, 64, 65, 68, 70, *81*, *82*, 226, *264*
Landolt–Börnstein, 408, *427*, *429*
Lane, C. T., 109, *136*
Lange, F., 412, *429*
Langevin, P., 266, *289*
Lark-Horovitz, K., 196, 198, 199, 200, 201, 202, 204, 205, 206, *220*, *222*
Lautz, G., 205, *223*
Lawson, A. W., 375, 392, *393*
Lax, B., 190, 191, 192, 193, 198, 199, *221*, *222*, 261, *265*
Lax, M., 219, *225*
Lazarev, B. G., 106, 119, 121, 124, *135*, *136*, 227, 257, 258, 259. 260, 261, 262, *264*
Leach, S. J., 392
Lee, T. D., 298, *334*
Legvold, S., 147, *150*, 373, 375, 376, 378, 382, 383, 384, 387, 389, 392, *393*, *394*
Lehman, G. W., 198, *222*
Leibfrid, 214, *224*, 349, *367*, 400, 408, 418, 419, *427*, *429*
Leifer, H. N., 198, *222*
Leighton, R. B., 419, *429*
Lemmer, H. R., 297, 321, 326, 327, *336*
Lennard–Jones, J. E., 29, *58*
Lesensky, L., 125, *137*
Levine, N., 325, *337*
Lifshitz, I. M., 229, 230, 235, 241, *264*
Lignac, W. P. J., 444, 445, *463*
Linde, J. O., 177, 181, *185*, *186*
Lipson, H., 218, 219, *225*
Llewellyn, P. M., 309, 327, *335*, *337*
Loasby, R. G., 392
Logan, J. K., 449, 452, 453, 454, *463*
London, H., 19, 21, *57*, *58*, 65, *81*, 84, *103*
Long, E., 114, 115, 126, 129, *136*, *137*
Loriers, J. 392
Losa, C. G., 415, 416, *428*
Love, W. F., 246, 257, *265*
Lucas, F. F., 392
Lunbeck, R. J., 7, *57*
Luttinger, J. M., 192, *221*

MacDonald, D. K. C., 157, 158, 160, 161, 162, 163, 166, 169, 172, 173, 177, 178, 179, 180, 182, *183*, *184*, *185*, 360, *367*, 406, *428*
Macfarlane, G. G., 217, 218, *225*
Mackinnon, L., 259, *265*
Mackintosh, I. M., 205, *223*
Madelung, O., *220*
Maita, J. P., 198, 199, 200, 201, 218, 219, *222*, *225*
Makinson, R. E. B., 163, 169, 170, 172, 173, 175, 176, *184*, *185*
Malaker, S. F., 412, *428*
Marcus, J. A., 227, 259, *265*
Margerie, J., 313, *335*
Maslekovitz, J. P., 188, 196, *221*
Mason, W. P., 211, *224*
Mastrangelo, S. V. R., 114, 115, *136*
Matthias, B. T., 138, 146, *150*
Mattis, D., 183, *186*
Mayer, J. E., 432, *462*
Mayer, M. G., 432, *462*
Mayper, R. D., 80, *82*
Mazur, P., 84, *103*
McCrum, N. G., 109, 114, 134, *135*, *136*
McKay, R. W., 392
McLennan, J. C., 392
McMillan, W. G., 115, *136*
McNair, D., 425, *430*
McSkimin, H. J., 211, 212, *224*
Meads, P. F., 412, 415, 416, *428*, *430*
Meiboom, S., 261, *265*
Meisel, K., 392

Meissner, W. H., 145, 146, *150*
Mellink, J. H., 85, 88, 92, 95, 99, 101, *103*, *104*
Mencher, A., 314, *335*
Mendelssohn, K., 86, 89, 92, 95, 96, *103*, *104*, 108, 109, 114, 115, 118, 121, 122, 124, 127, *135*, *136*, *137*, 157, 158, 160, 166, 177, 181, *183*, *184*, *185*, 392.
Mendoza, E., 177, *185*.
Mercus, G. R., 9, *57*
Merritt, F. R., 190, 191, 192, 195, 196, *221*, *222*
Messenhausen, W., 393
Messiah, A., 314, *335*
Meyer, H. J. M., 307, 329, *336*
Meyer, L., 88, 95, 99, *103*, *104*, 109, 114, 115, 126, 129, *136*, *137*
Michels, A., 132, *137*
Miedema, A. R., 327, *337*
Mikhailov, I. F., 246, 259, 260, 261, *265*
Miller, C. E., 146, *150*
Mills, R. L., 350, 355, 365, *366*, *367*
Misener, A. D., 85, 91, *103*
Moessen, G. W., 462, *464*
Monkman, R. J., 393
Montgomery, C. G., 207, *223*
Montvoll, E. W., 421, *429*
Mooser, E., 208, 209, *223*
Morin, F. J., 198, 199, 200, 201, 218, 219, *222*, *225*
Moss, T. S., 216, *225*
Mott, N. F., 133, *137*, 165, *184*
Mottelson, B. R., 299, *333*
Muthman, W., 393

Neumayr, S., 393
Nabarro, F. R. N., 165, *184*
Nagamiya, T., 213, *224*
Nakhimovich, N. M., 181, *185*
Nasledov, D. N., 200, *222*
Neaves, A., 170, *185*, 209, *223*
Néel, L., 309, *334*
Newell, G. F., 213, *224*
Newman, R., 219, *225*
Newton, J. O., 325, *337*
Niels-Hakkenberg, C. G., 65, *82*
Nisenoff, M., 196, *222*
Nix, F. C., 257, 259, *265*, 425, *430*
Nørgaard, G., 439, *462*

Okkes, R. F., 289, *291*
Oliver, G. D., 412, *429*
Olsen, J. L., 160, 177, *184*
Olsen, K. M., 211, *224*
Onsager, L., 209, *223*, 229, 259, 263, *264*
Onstott, E., 393
Osborne, D. V., 68, 69, 74, *81*
Osborne, D. W., 9, *57*, 60, 93, 104, 355, 356, *366*, *367*
Oshinsky, W., 217, *225*
Overhauser, A. W., 314, *334*
Overton, W. C., 261, *265*
Owen, J., 306, *335*
Owen, M., 393

Paesly, D., 421, *429*
Parker, G. W., 309, 329, 330, *337*
Parkinson, D. H., 210, 212, *223*, 374, 375, 376, 378, 393, *394*, 405, 413, *428*
Pearlman, N., 210, 211, 212, 213, 215, *223*, *224*, 405, 413, 415, 417, *428*, *429*, 452, *463*
Pearson, G. L., 195, 196, *221*
Pearson, W. B., 162, 163, 173, 177, 178, 179, *184*, *185*
Peierls, R., 165, 168, 174, 180, 181, *184*, *185*, 214, 224, 226, 231, *264*, 346, 364, *366*
Pellam, J., 60, 68, 69, *81*
Perez y Jorba, J., 326, 327, *336*
Peshkov, V. P., 60, 67, 68, 69, 73, *81*, *82*
Petford, A. D., 198, 201, *222*
Philippot, J., 35, *57*
Pickard, G. L., 415, *428*
Picus, G. S., 119, *136*
Pikus, G. E., 208, *223*
Pines, D., 168, *184*
Pippard, A. B., 182, 183, *186*, 230, *264*
Pitzer, K., 412, 413, *429*

Pogorelov, A. V., 230, 241, *264*
Polder, D., 444, 446, *463*
Poll, J. D., 86, 95, 96, 100, *103*
Pomeranchuk, I., 214, *224*, 356, *367*
Poppema, O. J., 301, 310, 319, 321, 324, 326, *335*, *336*, *337*
Portis, A. M., 195, 196, *221*
Poulter, J., 453, 458, 459, 460, *463*
Pound, R. V., 308, *334*
Powell, J. E., 369, *393*
Price, P. J., 28, 36, 53, *58*
Prigogine, I., 1, 28, 35, *57*
Primakoff, H., 356, *367*
Prins, J. A., 362, *367*
Pryce, M. H. L., 289, *291*, 292, 303, 309, *333*, *334*, *335*
Pullan, G. T., 162, *184*
Pullan, H., 426, 427, *427*, *429*

Quarrington, J. E., 217, *225*
Quill, L. L., 393
Quinnell, E. H., 412, *428*, *430*

Raub, E., 143, *150*
Rayne, J., 415, *428*
Read, W. T., 195, *221*
Redman, J. K., 177, *185*
Reekie, J., 14, 15, *57*, 85, 99, 101, *103*, *104*
Reinov, 219, *225*
Reitz, J. R., 169, *184*
Rhodes, P., 163, *184*
Rice, O. K., 28, 36, 53, *58*
Richter, B., 313, *334*
Rittner, E. S., 201, *222*
Roberts, L. D., 299, 302, 309, 317, 318, 319, 329, 330, *334*, *335*, *336*, *337*, 449, *463*
Roberts, T. R., 9, *57*, 356, *367*
Roberts, V., 217, 218, *225*
Robinson, B. L., 325, *337*
Robinson, D. W., 350, *366*
Robinson, F. N. H., 307, 319, 321, 325, 327, *334*, *335*, *336*
Robinson, J. E., 259, *265*
Rohrschach Jr., H. E., 92, 101, *104*
Rollin, B. V., 106, *135*, 198, 201, *222*
Rose, M. E., 292, 299, 302, 303, 304, 305, 306, 308, *333*, *334*
Rosenberg, H. M., 160, 164, 177, 178, 179, 181, *184*, *185*, 214, 215, *224*, *225*
Rosenblum, E. S., 190, *221*
Rosenbohm, E., 393
Rosenstock, H. B., 213, *224*
Rossi, A., 325, *337*, 393
Roth, L. M., 193, *221*, 261, *265*
Rubin, T., 426, *430*
Rudenko, N. S., 227, 257, 258, 259, 260, 261, 262, *264*
Ruhemann, M., 350, *366*
Rundle, R. E., 380, 393, *393*
Ruppel, W., 205, *223*

Sakai, M., 326, 327, *337*
Salter, L. S., 358, 365, *367*
Samoylovich, A. G., 170, 185
Sapp, R. C., 323, *337*
Sarginson, K., 180, 182, *185*
Saris, B. F., 99, *104*
Satchler, G. R., 295, 296, 305, *333*
Satterthwaite, C. B., 412, 415, 417, *428*, *429*, 452, *463*
Sauter, F., 165, *184*
Schachinger, L., 404, 405, 413, 415, *428*
Schaeffer, W. D., 114, *136*
Schafroth, R., 58
Schering, D. C., *290*
Schiff, L., 130, 131, *137*
Schifman, C., 412, *428*
Schlömann, E., 214, *224*, 349, *367*
Schmidt, G., 412, *429*, 435, 439, 440, 441, 442, *462*, *463*
Schönberg, N., 148, *150*
Schottky, W., 201, 204, *223*
Schroeder, C. M., 323, 327, *337*
Schuch, A. F., 93, *104*, 375, 393, *393*
Schuhmacher, E. E., 393
Schulman, R. G., 219, *225*
Schultz, H., 159, *184*
Schulz, H., 188, *221*
Schulz–DuBois, E., 196, *222*
Schuyler, M. C., 192, *221*
Schwarzkopf, P., 147, *150*

Scott, R. B., 68, 69, *81*
Scurlock, R. G., 307, 310, 323, 324, 326, 329, *336*, *337*
Seide., G., 212, *224*
Serova, F. G., 165, *184*
Shaposhnikov, I. G., 279, 285, *290*
Shaw, C. H., 15, *57*
Shaw, P. F. D., 326, 327, *336*, *337*
Shepherd, M., 217, *225*
Shifrin, K. C., 200, *222*
Shockley, W., 187, 189, 191, 195, 196, 207, *220*, *221*, *223*
Shoenberg, D., 138, 139, 142, 145, *150*, 226, 227, 228, 229, 242, 243, 246, 255, 256, 257, 258, 259, 260, 261, 262, *264*, *265*, 393, 445, *463*
Sidoriak, S. G., 9, *57*, 259, *265*
Siekman, J. G., 326, *337*
Silin, V. P., 168, *184*
Silvidi, A. A., 412, *428*, *429*
Simon, A., 303, 304, 305, 306, 308, *334*
Simon, F. E., 6, 9, 10, 21, 22, 57, 106, *135*, 209, 214, *223*, *224*, 301, 319, *334*, *336*, 338, 340, 345, 350, 351, 356, 363, *366*, *367*, 374, 375, 376, 378, 393, *393*, 412, 415, 425, *427*, *428*, *429*, *430*, 444, *463*
Singer, S., 325, *337*
Skinner, G. B., 412, *429*
Skochdopole, R. E., 382, 384, 389, 394, *399*, 413, *429*
Sladek, R. J., 177, *185*
Slater, J. C., 178, *185*
Slichter, C. P., 196, *222*, 314, 316, *334*, *335*
Smith, A. W., 393
Smith, B., 121, 124, 125, *136*
Smith, H., 409, 412, 419, 421, *429*
Smith, H. G., 380, 393, *393*
Smith, H. M. J., 210, 212, *224*
Smith, J. F., 378, *393*
Smith, P. L., 412, 413, *428*, *429*
Smith, R. W., 28, *58*
Smith, W. R., 114, *136*
Smith, W. T., 412, *429*
Smits, J., 270, 280, *290*
Somers, H. S., 19, *58*
Sommerfeld, A., 162, *184*
Sondheimer, E. H., 159, 163, 170, 182, 183, *184*, *185*, *186*, 209, *223*
Spedding, F. H., 147, *150*, 369, 373, 374, 375, 376, 378, 380, 382, 383, 384, 387, 389, 393, *393*, *394*
Spenke, E., *220*
Spiers, J. A., 292, 299, *333*
Spitzer, W., 217, *225*
Spohr, D. A., 160, 177, *184*
Sreedhar, A. K., 158, 160, 176, 177, *184*, *185*
Stanford, C. P., 319, *336*
Starr, C., 393
Stasior, R. A., 27, *57*, 66, *81*
Staver, T., 168, *184*
Steckel, F., 338, *366*
Steele, M. C., 181, 182, *186*, 230, 259, 260, *264*, *265*
Steenberg, N. R., 294, 296, 297, 303, 304, 305, 306, *333*, *334*, *335*
Steenland, M. J., 316, 319, 320, 321, 322, 326, 327, *335*, *336*, *337*
Stephenson, T. E., 319, *336*
Stern, F., 203, *223*
Stevens, K. W. H., 205, *223*, 289, *291*, 306, *334*, 393
Stralkov, P. G., 462, *464*
Strauss, A. J., 114, 115, 130, *136*
Sturdivant, J. H., 375, 393, *393*
Sweeney, D., 19, *58*
Swenson, C. A., 350, 351, *366*, 452, 454, *463*
Swim, R., 92, 101, *104*
Sydoriak, S. G., 356, *367*

Taconis, K. W., 14, 31, 88, 93, 97, 98, *103*, *104*, 346, *366*
Taft, E. A., 219, *225*
Talley, R. M., 203, *223*
Tang, T., 375, 393, *393*
Tarassov., V. V., 213, *224*
Taylor, R. D., 95, *104*
Taylor, R. T., 307, 310, 323, 324, 329, *336*, *337*
Teal., G. K., 211, 212, *224*
Teller, E., 115, *136*

Temmer, G. M., 328, 332, *333*, *336*
Temperley, H. N. V., 28, 36, 53, *58*, 277, *290*
Ter Haar, D., 170, *185*, 209, *223*
Thellung, A., 63, *81*
Thirring, H., *427*
Thomas, J. G., 177, *185*
Tinkham, M., 261, *265*
Tisza, L., 68, *82*
Tjerkstra, 115, *137*
Tjoan, L. T., 362, *367*
Tolhoek, H. A., 292, 293, 294, 295, 296, 297, 298, 300, 321, 322, 323, 326, 327, 332, *333*, *334*, *336*, *337*
Tolman, R. C., 399, *427*
Tomita, K., 289, 291
Tomnovec, F. M., 325, *337*
Townes, C. H., 195, *222*
Trenam, R. S., 306, 308, 326, 328, *334*, *336*
Trombe, F., 376, 382, 384, 393, *393*, *394*
Turkevich, J., 195, *222*
Turner, W. J., 218, 219, *225*
Tyler, W. W., 213, *224*

Uddin, M. Z., 261, *265*
Urbain, G., 393
Usui, T., 84, *103*

Van Alphen, P. M., 226, 227, 261, 262, *264*
Van den Berg, G. J., 100, *104*, 108, 124, *135*, 177, *185*
Van den Broek, J., 269, 275, *290*
Van den Burg, F. A., 9, *57*, 68, 69, 71, 72, 73, 78, 80, *82*
Van den Ende, J. N., 412, *430*
Van den Handel, J., 289, *291*
Van der Kint, L., 314, 316, *334*
Van der Marel, L. C., 269, 275, 278, *290*
Van den Meijdenberg, C. J. N., 88, *103*, 115, *137*
Van Dijk, H., 445, 449, 462, *463*, *464*
Van Itterbeek, A. F., 26, *57*, 77, *82*, 100, *104*, 205, *223*
Van Peski-Tinbergen, T., 9, *57*, 68, 69, 72, 73, 78, 80, *82*
Van Soest, G., 9, *57*, 61, *81*, 89, 95, *103*
Van Vleck, J. H., 266, 268, 273, 277, 289, *289*, *290*, 306, *335*
Van Wageningen, R., 326, *337*
Van Wieringen, J. S., 168, *184*, 314, 316, *334*
Verkin, B. I., 227, 246, 257, 258, 259, 260, 261, 262, *264*, *265*
Verschaffelt, J. E., 432, *462*
Verstelle, J., 270, 280, *290*
Vink, H. J., 198, 200, 201, 204, *222*
Vogel, R., 393
Vohsen, E., 425, *430*
Volger, J., 198, 200, 201, 204, *222*, 270, *290*, *291*
Von Katman, T., 396, 400, *427*
Vonsovskii, S. V., 168, *184*
Voogd, J., 393

Wagoner, G., 192, *221*
Wallace, W. E., 412, *428*
Waller, I., 273, 274, 288, *290*
Walstra, W. K., 453, *463*
Walters, G. K., 356, *367*
Wang, S., 289, *291*
Wansink, D. H. N., 9, *57*, 61, *81*, 88, 89, 93, 95, 97, 98, *103*, *104*
Waring, R. K., 81, *82*, 125, *137*
Wasscher, J. D., 9, 27, *57*, 60, 65, 67, *81*, 89, *103*
Webb, F. J., 9, *57*, 213, *224*, 340, 347, 348, *366*, 413, *429*
Webber, R. T., 160, 177, *184*
Weber, S., 432, 434, 435, 437, 439, 440, 443, *462*, *463*
Weertmann, J. R., 210, *223*, 412, 413, *429*
Weidner, R. T., 279, 284, *290*
Weinstock, B., 9, *57*, 93, *104*, 355, 356, *366*, *367*
Weiss, L., 393
Weiss, P., 289, *291*, 393
Weisskopf, V. F., 199, *222*
Wendell, C. B., 114, *136*

Werth, H., 416, *429*
Wertz, J. E., *220*
Westerhoff, H., 145, *150*
Wexler, A., 412, 415, 417, *428*, *429*, 452, *463*
Wheatley, G. H., 200, 201, *222*
Wheatley, J. C., 322, 325, 326, *337*
Wheeler, J. A., 300, 301, 331, *333*, *334*
White, G. K., 92, 95, *104*, 124, *136*, 158, 160, 164, 175, 176, 177, *184*, *185*
Whitworth, R. W., 73, 77, *82*
Wiebes, J., 9, *57*, 65, 68, 69, 71, 72, 73, 78, 80, *82*
Wilhelm, H. A., 393
Wilhelm, J. O., 393
Wilkinson, K. R., 9, *57*, 60, *81*, 89, *103*, 340, 347, 348, *366*
Wilks, J., 9, 28, *57*, *58*, 60, 77, 80, *81*, 89, *103*, 213, *224*, 340, 347, 348, *366*, 413, *429*
Williams, S. R., 356, *367*
Wilson, A. H., 152, 158, 159, *183*, *184*, 187, *220*, *221*
Winkel, P., 86, 87, 95, 96, 97, 99, 100, 101, 102, *103*, *104*
Winkler, U., *220*
Winter, J., 313, 314, *334*
Wittle, Ch., 326, *337*
Wolcott, N. M., 412, 413, 415, 416, 417, *428*, *429*
Woldringh, H. H., 63, *81*
Wolf, W. P., 307, *334*
Wollan, R. O., 388, 393, *394*
Woods, S. B., 158, 175, 176, 177, *184*, *185*, 208, 209, *223*
Worley, A. D., 452, *463*
Wright, A., 289, *291*
Wright, R. W., 200, *222*

Yager, W. A., 190, 191, 192, 195, 196, *221*, *222*
Yang, C. N., 298, *334*
Yoshimori, A., 213, *224*
Young, R. A., 373, 393, *393*
Yü-Chang Hsieh, 419, 421, *429*

Zachariasen, W. H., 393
Zakharchenya, B. P., 219, *225*
Zavoisky, E., 269, 270, *290*
Zeidler, W., 412, 415, *428*, *429*
Zeiger, H. J., 190, 191, 198, 199, *221*, *222*, 261, *265*
Zemansky, M. W., 374, 375, 378, *393*, 426, *430*, 452, *463*
Ziegler, W. T., 373, 393, *393*
Zilberman, G. E., 230, *264*
Ziman, J. M., 152, 166, 168, 175, *183*, *184*, 214, *224*
Zinovieva, K. N., 72, 73, *82*
Zintl, E., 393
Zwikker, C., 412, *429*

SUBJECT INDEX

Absorption of sound in liquid Helium 75
absorption of second sound 64, 71
adsorption of Helium 105
alignment of atomic nuclei 293
Allen & Reekies' rule 99, 102
alpha particles emitted from oriented nuclei 299, 329
Aluminium 256
Aluminium Antimonide 217
anomalous impurity scattering of electrons 177ff
Antimony 262
Arsenic 262

Bardeen scattering function 167
Beryllium 260
beta radiation from oriented nuclei 297
beta-W structure in superconductivity 148
Bismuth 261
Bloch theory of electron transport 152ff
brute force method 301

Cadmium 260
Carbon thermometers 449
cell theory for liquid Helium 35
Cerium 375
coefficient of expansion of liquid Helium 66
compressibility of solid Helium 345
critical temperatures of inert gases 7
critical velocity in liquid Helium II 85, 100
cyclotron resonance in semiconductors 189

Debye temperature of inert gases 9
—of solid Helium, 340
Debye theory of lattice vibrations 395ff, 399ff
Degeneracy effects in semiconductors 201
De Haas-van Alphen effect 226
— theory 230
— experiment 238ff
diffraction experiments on liquid Helium 14
dissipative effects in liquid Helium 70
drag of electrons by phonons 208
droplets out of the Helium film 122
Dysprosium 383

Electrical conductivity of impurity bands, in semiconductors 203
— of metals 155ff
— of rare earth metals 372ff
— of semiconductors 198
electric hyperfine structure alignment 208
electron phonon scattering 164
electron transport in metals 151
energy band structure in semiconductors 194
energy gap in semiconductor energy-levels 187
energy-volume relationships for liquid and solid Helium 19
effective mass of electrons in semiconductors 189, 199
Erbium 387
Europium 380
excitations in liquid Helium II 59ff, 25ff
external field polarization 301

Fermi surface and De Haas-van Alphen effect 227ff

film flow in liquid Helium, below 1°K 80
— saturated 118
— unsaturated 126
film in liquid Helium, static and dynamic 109
fission of oriented nuclei 300
fluctuation theory for liquid Helium 35
fountain effect 62, 67, 84, 87ff
frequency spectra of lattice vibrations 407ff
frictional forces in liquid Helium II 90ff

Gadolineum 382
Gallium 258
Gallium-Antimonide 217
gamma radiation from oriented radioactive nuclei 294, 319
gas thermometer 433ff
Germanium, n- and p-type 190
— optical properties 217
— specific heat 209
— thermal conductivity 215
graphite 213, 258
grey Tin, specific heat 213
Grüneisen equation for solid Helium 341
Grüneisen theory 398ff, 422ff
Gurevich effect in semiconductors 208

Hall coefficient in semiconductors 197
heat conduction in liquid Helium II 77, 99
heat conduction in the normal fluid 63, 72
heat pulses in liquid Helium 68, 78, 80
heat of vaporization 458
Helium films 105
— saturated 107
— unsaturated 107
Helium three: influence on heat pulses in ^{4}He 80
Holmium 385
hot wire manometer 435
hyperfine splitting in paramagnetic substances 267
— in semiconductors 195

impurity effects in semiconductors 201, 218
Indium 258
Indium Antimonide 192, 217
intermolecular forces in liquid Helium 1
internal energy of inert gases 5
irreversible effects in Helium below 1°K 62ff

Kapitza thermal resistance 80

Lambda transition 8, 53
Landau formula for the De Haas-van Alphen effect 229ff
Lanthanum 373
lattice influence in electric transport phenomena 169ff
lattice specific heat 404, 410
Lead 257
Lindemann melting formula 355
Luthetium 391

Magnesium 261
Magnesium Stannide 217
magnetic effects in electron transport phenomena 180ff
— hyperfine structure alignment 304, 309ff
— hyperfine structure polarization 305
— properties of rare earth metals 372ff, 391
— temperature 446
magneto-resistive anomalous ratio in semiconductors 205
Matthiesen's rule 157,159
mean free path effects in electron transport phenomena 182ff

mean free path of excitations in liquid Helium 73, 77
mechano-caloric effect 62, 85, 87ff
melting curve of ^{4}He 349
— ^{3}He 355
Mercury 262
microwave absorption in semiconductors 206
mixtures of ^{3}He and ^{4}He 93ff

Neodymium 378
neutron absorption by polarized nuclei 293, 317
neutron irradiation upon semiconductors 196

Optical properties of semiconductors 216
orientation of atomic nuclei 292ff
oscillators on speaking terms 278

Paramagnetic relaxation 268
— resonance in semiconductors 194
periodic system of the elements 138
phonons, in liquid Helium 26, 61ff, 70ff
phonondrag 208
polarization of atomic nuclei 293
— by saturation of electron resonances 314
Praseodymium 378
principle of corresponding states 4

Quantummechanical principle of corresponding states 4
quasi Raman process 273

Rare earth metals 368ff, 391
relaxation in the spin system 279
resonance phenomena in paramagnetic substances 269
— semiconductors 189
rotons 61ff, 70ff
rotonspectrum values 70
Rutile, specific heat 213

Samarium 380
scattering of conduction electrons 171ff
— phonons in metals 171ff
saturation of paramagnetic resonance 279, 289
second sound 61ff, 68
second viscosity of liquid Helium 63
Silicon 192, 212, 217
specific heat of Germanium 209
— Graphite 213
— grey Tin 213
— liquid ^{4}He 8, 62
— liquid ^{3}He 9
— absorbed Helium 117
— solid Helium 340
— rare earth metals 372ff
— Rutile 213
— Silicon 212
— simple solids 395ff
spin lattice relaxation 271
static helium film 109
structure of liquid Helium 14
superconducting alloys 141ff
— compounds 141, 145ff
— elements 138
superconductivity and crystal structure 150
— in the periodic system 138
surface tension effects in Helium film 108
symmetry effects in liquid Helium 12ff

Temperature scale, in the liquid Helium region, 461
Terbium 382
Thallium 260
theory of the Helium film 130
thermal conductivity of electrons 155, 159ff, 214
— of solid Helium 346
— of lattice 169

thermal expansion of liquid and solid Helium 11, 27
— of simple solids 395, 422
thermoelectric power 156, 161ff, 208
thermomolecular pressure 434
thickness of the saturated film 110
Thulium 389
Tin 257
transition in the structure of solid Helium 345, 362
— temperatures of superconductivity 138ff
transport phenomena of liquid Helium II 83ff
two-fluid model for liquid Helium II 61ff, 83ff

Umklapp collisions 165, 347
unsaturated films in liquid Helium 113

Vapor-pressure table 461
viscosity of the normal part of liquid Helium II 100

Wiedemann-Franz law 155, 159

Ytterbium 391

Zero point energy in Helium 22, 23, 356, 363
Zinc 259

149773
AUTHOR Gorter
TITLE Progress in low temperature physics
DATE DUE
[redacted]
QC278
G6
v.2

149773

[redacted]
QC278
G6
v.2

Gorter

Progress in low temperature physics

Date Due

APR 24 1978